SAINT PETERSBURG STATE UNIVERSITY (SPbSU)

VERNADSKY INSTITUTE OF GEOCHEMISTRY AND ANALYTICAL CHEMISTRY OF RUSSIAN ACADEMY OF SCIENCES (GEOKHI RAS)

Magmatism of the Earth and related strategic metal deposits

Proceedings of XXXVI International Conference

23-26 May 2019, Saint Petersburg

Supported by Saint Petersburg State University, OPTEC (ZEISS Group) and LIMS (Raw Materials Research Laboratory)

"Magmatism of the Earth and related strategic metal deposits". Proceedings of International Conference. Saint Petersburg State University, 23-23 May 2019**.** M.: GEOKHI RAS, 2019. 378 p. ISSN - 2618-835X.

The mineral deposits of strategic metals are vulnerable to political and economic changes, and their availability is essential for high-technology, green energy, and other applications. The most of they are related to the deep-seated alkaline magmas. This book offers a collection of papers presented at the 36th International Conference on "Magmatism of the Earth and Related Strategic Metal Deposits" held from May 23th to 26th 2019 in Saint Petersburg State University, Saint Petersburg, Russia. The conference articles are focused on the understanding of the geological processes that produce high concentrations of critical metals in geological systems such as the metal transport in the mantle and crust and enrichment processes, hydrothermal and metasomatic processes leading to the formation of such significant deposits. Papers in this book give a representative overview including mineralogy, geochemistry and origin of strategic metals deposits.

Supported by Saint Petersburg State University, OPTEC (ZEISS Group) and LIMS (Raw Materials Research Laboratory)

ISSN-2618-835X

The cover pictures – View down the Neva to the river between the Winter house of its Imperial Majesty and Academy of Sciences. G.A. Kachalov's engraving according to M.I. Makhayev's drawing (approx. 1750-1752).

Content

WOLFRAMOIXIOLITE IN SUBALKALINE LITHIUM-FLUORIC GRANITES OF THE ARGA-YNNAKH-KHAYSKY MASSIF, YAKUTIA

Alekseev V.I.[1], Galankina O.L.[2], Alekseev I.V.[1]

[1]Saint-Petersburg Mining University, Saint-Petersburg, Russia, alekseev_vi@pers.spmi.ru

[2]Institute of Precambrian Geology and Geochronology, Russian Academy of Sciences, Saint Petersburg, Russia, galankinaol@mail.ru

One of the unity features of East Asian tin-tungsten zone identified in the Russian Far East by an academician S.S. Smirnov (1946) is a wide-spread occurrence in subalkaline lithium-fluoric granite (LFG) of tungsten-containing accessory minerals – wolframite, scheelite, russellite, ishikawaite, columbite, etc. Wolframoixiolite is of considerable significance for this mineral association. It has been described in LFG and ongonite from various massifs – the Severniy on Chukotka, the Tigriniy in Primorye, the Omchikandinsky in Yakutia, Laiziling and Dajishan in China (Zhang et al, 2003; Alekseev, 2014; Xie et al., 2018). The report presents a new finding of wolframoixiolite in LFG and ongonite of Arga-Ynnakh-Khaysky massif in Eastern Yakutia. These rocks being a part of kesterskiy complex of subalkaline rare-metal granites control the Kester rare-metal-tin deposit.

LFG of the Arga-Ynnakh-Khaysky massif constitutes a white sugary grained rock with following mineral composition (vol. %): albite N. 2-7 (28-41), microcline (13-29), quartz (23-41), light mica (8-13), topaz (0.5-3), montebrasite (0.1-3). Accessory minerals include cassiterite, fluorapatite, columbite-(Mn), tantalite-(Mn), niobium wolframite, wolframoixiolite, uranium-hafnium zircon, struverite, microlite, ilmenite, spodumene, monazite-(Ce), xenotime-(Y), uraninite, etc. Ongonite is a light grey aphanitic rock with a «snowball» structure and a fluidal texture. It differs from LFG by higher content of quartz, topaz and montebrasite.

Our study of LFG from the Arga-Ynnakh-Khaysky massif has allowed to establish earlier unrevealed association of accessory tantalic-niobates, containing tungsten (WO_3, weight. %): columbite-(Fe) 1.59-7.12; columbite-(Mn) 0-6.07; tantalite-(Mn) 0-4.72; uranmicrolite 0-3.64; microlite 0-1.98; struverite 0-3.39. In LFG and ongonite has been repeatedly noticed a mineral which by its main components corresponds to wolframoixiolite, – ixiolite, enriched isomorphic W, Nb, Fe and depleted Ta, Mn, Sn (Černý et al., 2007; Alekseev, 2014). Findings of wolframoixiolite were made in lepidolitic-topaze facie of LFG (on depth more than 90 m), where it associates with tungsten columbite-(Mn), uranium-hafnium zircon and cassiterite. In ongonite prevails paragenesis with tantalic-niobium wolframite, hafnium zircon and uraninite.

Yakut wolframoixiolite is represented by inclusions in topaz and light mica in form of highly elongated lamellar crystals with length 10-300 μm, and thickness less than 10 μm. In their form, crystals are similar to those of columbite. Along with scattered single crystals there are subparallel and radial fibrous aggregates. Electron scanning has shown rather stable composition of wolframoixiolite from LFG. The main components of the mineral are (weight. %): Nb_2O_5 59.1-62.5; Ta_2O_5 6.6-9.4; FeO 7.4-14.4; WO_3 7.5-13.9; MnO 4.9-11.3. Characteristic impurity – TiO_2 0.9-1.8 %. W, Fe and Mn are subject to the largest fluctuations in concentration. Mn/(Mn+Fe) ranges from 0.24 to 0.61. The empirical formula of wolframoixiolite: $(Fe_{0.41}Mn_{0.14}Nb_{0.42})_{0.97}(Nb_{0.67}W_{0.11}Ta_{0.08}Ti_{0.04})_{1.00}O_{4.00}$.

Wolframoixiolite from ongonite is characterized by large variations in Ta, Nb, W (weight. %): Nb_2O_5 21.4-59.2; Ta_2O_5 10.4-29.2; FeO 6.4-15.6; WO_3 7.8-44.0; MnO 4.2-11.5. The mineral contains a substantial impurity of TiO_2 1.5-3.5 %, as well as of Sn, Ca, Sc, Zr. It is different from the LFG analogue by a higher value of relationship Ta/(Nb+Ta) (respectively 0.19 и 0.07) and Mn/(Mn+Fe) (respectively 0.37 и 0.32). The empirical formula:
$(Fe_{0.46}Mn_{0.21}Nb_{0.22}Ca_{0.02}Sc_{0.004})_{0.92}(Nb_{0.61}W_{0.11}Ta_{0.19}Ti_{0.07}Zr_{0.01}Sn_{0.005})_{1.00}O_{4.00}$.

Wolframoixiolite discovered by A.I. Ginzburg in 1969, at the moment is not recognized as a mineral specie and is considered as a variation of ixiolite (Updated list of IMA-approved minerals (March 2018)). It has long been considered that wolframoixiolite is typical only of rare-metal pegmatites. However, in the course of new rare-metal ore provinces development the quantity of its

findings steadily grows, and in the last decades the mineral is repeatedly noted as an accessory mineral of LFG and ongonites in Europe, Africa and Asia (Zhang et al, 2003; Černý et al., 2007; Breiter et al., 2017; Melcher et al., 2017; Xie et al., 2018), including the Far East of Russia (Alekseev, 2014). "Avalanche" of wolframoixiolite findings indirectly confirms its individuality as mineral specie and allows considering it as a typomorphic mineral of subalkaline LFG.

The composition of Yakut wolframoixiolite is close to that of analogues from LFG, ongonite and rare-metal pegmatites in other world regions: ferriferous varieties are prevailing; only in 15 % of samples Mn content exceeds 50 %. The balance between Nb, W and Ta in *B* position is highly variable – 50-90, 5-50 and 5-25 % respectively. Wolframoixiolite from ongonite is rather enriched by tantalum and tungsten: Ta/(Nb+Ta) = 0.19; W/(Ta+Nb) = 0.20. Deficiency of iron, tantalum and tungsten and excess of niobium are common to wolframoixiolite from LFG: Ta/(Nb+Ta) = 0.07; W/(Ta+Nb) = 0.09. Considerable part (63 %) of niobium cations in wolframoixiolite composition takes the position *A* (apfu 0.42) (fig.).

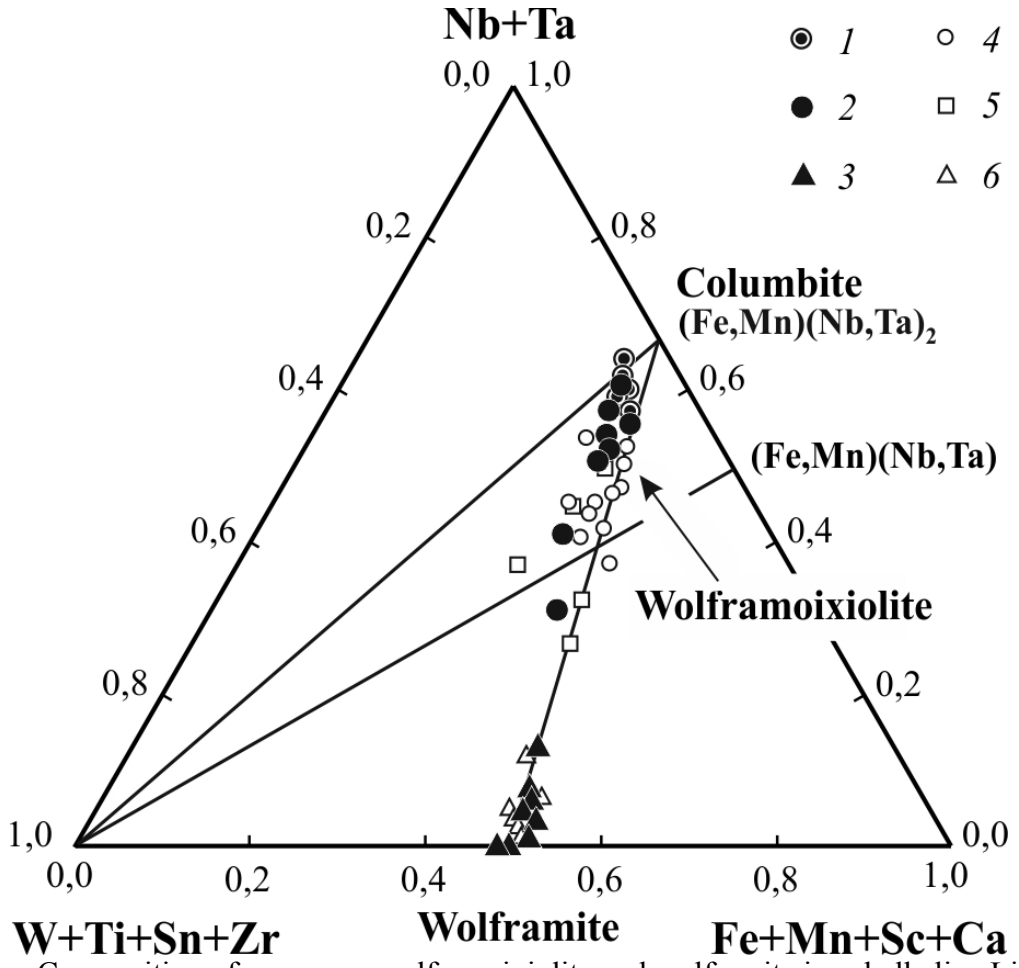

Figure. Composition of accessory wolframoixiolite and wolframite in subalkaline Li-F granites from Arga-Ynnakh-Khaysky massif and from other massifs across the globe.
1 – wolframoixiolite of Li-F granite, 2 – wolframoixiolite of ongonite, 3 – wolframite of ongonite; 4-6 – accessory minerals from all over the world: wolframoixiolite of Li-F granites and ongonite (4), wolframoixiolite of rare-metal pegmatites (5), wolframite of Li-F granites and ongonites from Asia, Europe and Africa (6) (Zhang et al, 2003; Černý et al., 2007; Alekseev, 2014; Breiter et al., 2017; Melcher et al., 2017; Xie et al., 2018).

The formation of wolframoixiolite is related to a late-magmatic stage of subalkaline fluoric-phosphorous granite magma crystallization under the influence of alkaline mantle fluids. The ratio in the mineral of main cations, such as Nb, Ta, W, Fe, Mn, is defined by transformation of columbitic structures into wolframitic structure (Černý et al., 2007; Alekseev, 2014). On the triplot of tantalic-

niobates composition imaging points of wolframoixiolite, as well as points of its analogues from other areas, are situated on a trend line «columbite - wolframite» (fig.). Similarity in morphology of wolframoixiolite and columbite and their close relationship in the Yakut LFG are accounted for the fact, that the mineral studied is a product of polymorphic transition {columbite $FeNb_2O_6$ → ixiolite $3(Fe,Nb)O_2$} and a result of crystal superstructure formation via replacement of Nb by Ta, W and Sn. Crystals of wolframoixiolite from the Arga-Ynnakh-Khaysky massif are pseudomorphoses on columbite-(Fe). Replacement of minerals from the columbite group by wolframoixiolite is a marker of subalkaline rare-metal granites shifting from a magmatic stage of primary crystallization to a pneumatolytic stage of metasomatic minerogenesis (Breiter et al., 2017; Xie et al., 2018).

Tungsten-tin ore deposits of the Far East in the areas of LFG occurrence are defined by a rare-metal mineralization (Zhang et al., 2003; Alekseev, 2014; Xie et al., 2018). The Kester deposit, where wolframoixiolite has been found, is a medium-sized tin deposit, which is currently considerably depleted, but according to prognostic resources it promises to be a large deposit of lithium, rubidium, tantalum and niobium. Wolframoixiolite is a typomorphic accessory mineral of lithium-fluoric granite that serves as an indicator of subalkaline rare-metal granite magmatism with accompanying tin-rare-metal ore mineralization.

This work was supported by the Saint-Petersburg Mining University and the Institute of Precambrian Geology and Geochronology, Russian Academy of Sciences, Russia.

References

Alekseev V.I. Lithium-fluoric granites of the Far East. SPb.: Saint-Petersburg Mining university. 2014. pp. 1-244.

Breiter K., Korbelová Z., Chládek Š., Uher P., Knésl I., Rambousek P., Honig S., Šešulka V. Diversity of Ti-Sn-W-Nb-Ta oxide minerals in the classic granite related magmatic-hydrothermal Cínovec/Zinnwald Sn-W-Li deposit (Czech Republic) // European Journal Mineralogy. 2017. Vol. 29. N. 4. p. 727-738.

Černý P., Novák M., Chapman R., Ferreira K.J. Subsolidus behavior of niobian rutile from the Písek region, Czech Republic: a model for exsolution in W- and Fe2+>>Fe3+-rich phases // Journal of Geosciences. 2007. Vol. 52. N. 1-2. p. 143-159.

Melcher F., Graupner T., Gabler H.E., Sitnikova M., Oberthur T., Gerdes A., Badanina E., Chudy T. Mineralogical and chemical evolution of tantalum-(niobium-tin) mineralisation in pegmatites and granites. Part 2: Worldwide examples (excluding Africa) and an overview of global metallogenetic patterns // Ore geology reviews. 2017. Vol. 89. p. 946-987.

Xie L., Wang Z.J., Wang R.C., Zhu J.C., Che X.D., Gao J.F., Zhao X. Mineralogical constraints on the genesis of W-Nb-Ta mineralization in the Laiziling granite (Xianghualing district, south China) // Ore geology reviews. 2018. Vol. 95. p. 695-712.

Zhang W.L., Hua R.M., Wang R.C. Intergrowth of Wolframoixiolite and W-rich Manganocolumbite in Dajishan Tungsten Deposit, Jiangxi Province, South China // Mineral Deposits. 2003. Vol. 22. N. 2. p. 158-165.

EVOLUTION OF THE COMENDITE MELTS OF THE SANT BIMODAL VOLCANIC ASSOCIATION, CENTRAL MONGOLIA: EVDENCE FROM MELT INCLUSIONS

Andreeva I.A.

Institute of Geology of Ore Deposits, Petrography, Mineralogy and Geochemistry, Russia, andreeva@igem.ru

Using various methods of melt inclusion investigation, including electron and ion microprobe techniques, we estimated the composition, evolution, and formation conditions of melts producing the comendites of the bimodal volcanic association in the Sant area (Central Mongolia), and considers the magmatic processes responsible for the accumulation of rare elements in them.

Rocks of a bimodal basalt–comendite association were found as large fields in the North Gobi Depression in central Mongolia. The association is spatially constrained to the North Gobi array of northeast-trending faults and occurs within a linear zone more than 180 km long. The bimodal association is located in the eastern part of Sant region and composes a volcanic field 20 X12 km in area. The volcanic rocks of the bimodal series are basaltoids, trachytes, comendites, pantellerites, tuffs, and ignimbrites. The rock complex also contains alkali porphyric granites. The U–Pb zircon age of the massif is 206 ± 1 Ma. By their chemistry and mineral composition, the alkalic–salic rocks correspond to felsic members of alkalic K–Na series with an agpaite index close to or above 1 and enriched in Zr, Rb, and REEs.

Petrographically comendites are a porphyric rocks with up to 20% of phenocrysts of K□Na feldspar, quartz, and aegirine. Its micro-felsic groundmass comprises microliths of K–Na feldspar, quartz, alkalic amphibole, aegirine, Ti–magnetite, and ilmenite. Accessory minerals are zircon and monazite.

The primary melt inclusions were detected in quartz from the comendites (samples SNT-2/13, SNT-2/9 and SNT-2/8), collected from various parts of the volcanic sequence. By their phase composition, they are subdivided into (1) two-phase inclusions composed of glass and gas bubble (sample SNT-2/8) and (2) multiphase inclusions containing glass, gas bubble, and daughter minerals (samples SNT-2/13 and SNT-2/9). Mica, fluorite, and villiaumite were identified among the daughter minerals. The mica composition corresponds to polylithionite with (wt %) SiO_2 - 59.7; Al_2O_3 - 11.2; FeO - 5; K_2O - 11.3, and F - 10. The deficit in the total components is 5.7 wt %. It allowed us to suggest a considerable Li_2O content.

The glasses of unheated melt inclusions of the examined samples have typically high K_2O + Na_2O, up to 10–13 wt %. SiO_2 concentrations varies in the range of 66–73 wt %, Al_2O_3 – 11.5 –14.6 wt %. Also remarkable are different F contents. The latter in glasses of melt inclusions – from samples SNT-2/13 and SNT-2/9 reaches 0.76–1.05 wt %, while in glasses of melt inclusions from sample SNT-2/8 it does not exceed 0.13 wt %. Thermometric experiments with quartz-hosted melt inclusions in the comendites (samples SNT-2/13 and SNT-2/9) showed that their homogenization temperatures are 880–960^{o}C. Complete homogenization of melt inclusions from the sample SNT-2/8 was not achieved, the gas bubble in them preserved until the temperature of 1200^{o}C.

Microprobe analysis of glasses of the homogenized melt inclusions allowed us to estimate the composition of melts responsible for comendite formation. These glasses in all the examined samples correspond to trachydacite and rhyolite with (wt %): SiO_2 – 68 –73; Al_2O_3 - 11.7 – 13.5; FeO - 2.3 – 4.8; K_2O + Na_2O – 10 – 13. An agpaite index = 1–1.3.

The analysis of trace elements in the homogeneous glasses of melt inclusions in quartz of all examined samples showed that they have similar primitive mantle - normalized trace element patterns (Fig. 1). It is clearly seen in the spidergrams that the melts are strongly enriched relative to the chondrite composition in many rare elements and REEs. The LREEs are somewhat dominate over HREEs (La_N/Yb_N = 1.8–2.6). The trace element concentrations in glasses of the melt inclusions have the following ranges (ppm): Zr – 1780 – 3200, Rb – 309 – 525, Nb – 104 – 187, Y – 167 – 348, Th – 33 – 70, and Ce – 159 – 306. The total REE contents in the glasses of quartz-hosted melt inclusions from the comendites are 408 - 830 ppm.

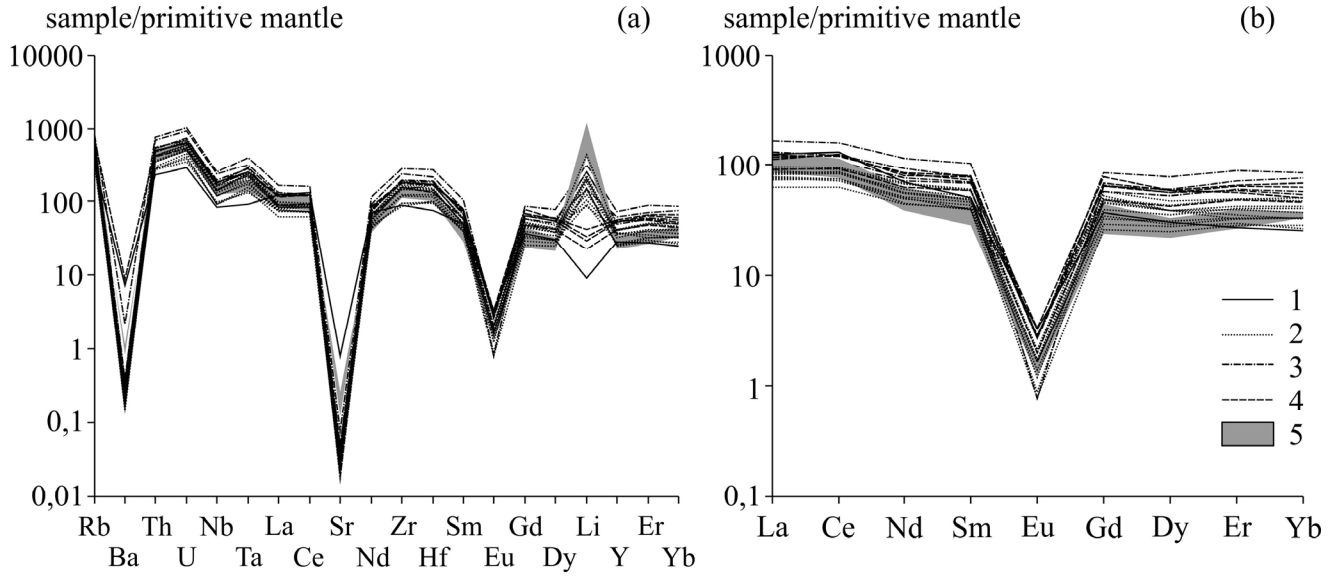

Figure 1. Primitive mantle-normalized distribution patterns of trace and rare earth elements in comendite (1) and homogenous glasses of melt inclusions in quartz Sant comendite (2–4) and Dzarta–Khuduk pantellerite (5).

The glasses of melt inclusions are significantly depleted in Ba, Sr, and Eu, which is evidently related to the scavenging of these elements by feldspars during the earlier stages of magma differentiation. Comparison of the bulk compositions of rocks with those of the glasses of the homogenized melt inclusions demonstrates enrichment of the latter in many trace elements and REEs.

The behavior of Li and volatile components (F and H_2O) in the studied melts should be specifically considered. The maximum Li concentrations of 500–700 ppm were determined in the glasses of melt inclusions in quartz from the comendites (samples SNT-2/13 and SNT-2/9), while those in the glasses from melt inclusions in quartz from the comendite (sample SNT-2/8) are substantially lower, in the range of 47 – 69 ppm. In addition, low Li concentrations of 16 – 28 ppm are typical for the bulk rock, which is distinctly manifested as a negative anomaly in the spidergram (Fig. 1). Similar tendency was established for F and H_2O. The glasses of melt inclusions in quartz from the comendite of samples SNT- 2/13 and SNT-2/9 contain 0.8 – 1.1 wt % F and 0.8 – 2.2 wt % H_2O, while those in the glasses of melt inclusions in quartz from the comendites of sample SNT- 2/8 are no higher than 0.13 and 0.3 wt % respectively.

The dependences of the concentrations of various incompatible elements in glasses of the homogenized melt inclusions and bulk rocks of the Sant bimodal association, including mafic varieties, were identified. Niobium was chosen as a differentiation index, because the partition coefficient of Nb between crystals and melt approaches zero.

Positive correlation of Nb vs. Zr and Nb vs. Hf over the entire range of the melt and rock compositions was defined. Similar relations with Nb were observed for Rb, Ta, Th, U, Hf, Y, Be and B. The concentrations of rare earth elements in the melt inclusions and rocks are also positively correlated with Nb, which is most clearly seen for the middle and heavy REEs.

Thus, the existence of common trends between melts and rocks of different compositions allowed us to suppose a genetic link between basic and acid rocks of the Sant bimodal association. Moreover, the process of crystallization differentiation of the magma was responsible for the accumulation of trace elements and REEs in the melts. As was noted above, the glasses of the homogenized melt inclusions from the comendite phenocrysts of samples SNT-2/13 and SNT-2/9 are enriched in Li and F. The melts enriched in these elements were found by us earlier in melt inclusions from trachydacite and pantellerite of the Dzarta–Khuduk bimodal association (Andreeva, Kovalenko, 2011). Both these bimodal associations occur within Mongolia–Transbaikalia Early Mesozoic zoned magmatic area and are close in age (210 Ma for Sant, 208 Ma for Dzarta–Khuduk). They also are characterized by similar specifics of the rock composition. The primitive mantle-normalized REE

patterns of glasses from melt inclusions in phenocrysts of alkalic-salic rocks of both associations are similar (Fig. 1) with the Li maximum being one of the main features.

An extremely important result of the studies of the melt inclusions in phenocrysts from the pantellerites of Dzarta–Khuduk complex was finding Li-enriched fluoride melts along with the silicate melts. This suggests the principal possibility of generation of a salt melts that extracts significant amounts of Li at the final stages of alkali melt evolution. Such salt melt could subsequently escape from the silicate magma, becoming a source of rare–metal mineralization. Evidence of the coexistence of a fluoride melt with a silicate one have was obtained experimentally (Veksler et al., 2005) and by melt inclusions studies (Solovova et al., 2010).

As can be seen in Fig. 1 compositions of glasses of melt inclusions in quartz from the comendites (sample SNT-8) does not obey the general trend with respect to Li. They, as well as the bulk rock compositions, are characterized by a negative Li anomaly. In addition they have the lowest F (<0.2 wt %) and H_2O (<0.3 wt %) contents. Probably, these melts are residual magmas after separation of the salt (fluoride) component from them, and low Li and volatile component (F and H_2O) concentrations can be explained by the partition of these components into the salt melt.

Thus, the revealed general patterns of the melt evolution of the Sant and Dzarta-Khuduk massifs in the Mongolia-Transbaikalia zoned magmatic area, close ages and compositions of the rocks, suggest a similar formation mechanism for them associated with the dominant role of the process of crystallization differentiation. The high potential of alkalis and volatile components (F and H_2O) in the melts resulted in the significant concentrations of many rare elements in them. During the final stages of differentiation fluoride melts were separated from silicate magma and extracted considerable amounts of Li.

The obtained data allow us to estimate the ore-generating potential of magmatic melts at different evolution stages, as well as the role of the processes leading to the accumulation of ore components in them. Zr, Nb, Rb, Y, Th, REE are concentrated in residual alkali-salic melts, while Li and, possibly, some other ore metals are extracted by salt fluoride melts. In general, the bimodal magmatic associations of the Mongolia-Transbaikalia zoned magmatic area can be considered as perspective objects for rare metal mineralization.

This work was supported by the Russian Foundation for Basic Research, project no. 17–05–00767.

References

Andreeva I.A., Kovalenko V.I. Evolution of the trachydacite and pantellerite magmas of the bimodal volcanic association of Dzarta_Khuduk, Central Mongolia: investigation of inclusions in minerals // Petrology, 2011, Vol. 19., No. 4, p. 348–369.

Veksler, I.V., Dorfman, A.M., Kamenetsky, M., Dulski, P., and Dingwell, D.B., Partitioning of Lanthanides and Y between Immisible Silicate and Fluoride Melts, Fluorite and Cryolite and the Origin of the Lanthanide Tetrad Effect in Igneous Rocks, Geochim. Cosmochim. Acta, 2005, Vol. 69, p. 2847–2860.

Solovova, I.P., Girnis, A.V., and Kovalenko, V.I., Fluoride and Chloride Melts Included in Phenocrysts of Agpaitic Acid Volcanic Rocks from Pantelleria Island, Dokl. Akad.Nauk, 2010, vol. 433, no. 3, pp. 390–393 [Dokl. Earth Sci.(Engl. Transl.), Vol. 433, No. 1, p. 978–981].

BASIC MAGMATISM OF THE CRATER HIGHLANDS AND GREGORY RIFT, TANZANIA: CASE STUDY OF OGOL LAVAS

Arzamastsev A.A.[1,2], Braunger S.[3], Ivashchenkova O.V.[2], Markl G.[3], Marks M.[3], Zaitsev A.N.[2]

[1]Institute of Precambrian Geology and Geochronology, Saint-Petersburg, Russia, arzamas@ipgg.ru

[2]Saint-Petersburg State University, Saint-Petersburg, Russia

[3]Universität Tübingen, Tübingen, Germany

The Neogene-Quaternary Tanzania volcanic province developed on the southern part of the Kenya rift system in the Archaean rocks of the Tanzania Craton and the north–south trending Mozambique orogenic fold belt (Fig.). B.H.Baker (Baker, 1987) reviewed the complexity of magmatic associations in the Kenya-Tanzania Rift, stressing that there is a continuum of mafic compositions from nephelinites and phonolites through basanites and alkali olivine basalts to hypersthene-normative basalts. Whereas alkaline magmatism and associated carbonatites were in the focus of recent multidisciplinary studies, basaltic volcanics were beyond the scope of the main petrological interests.

Geochronological data obtained during previous decades summarized by J.B. Dawson (Dawson, 2008) suppose the contemporaneity of the basaltic and the alkaline rocks in some neighboring volcanoes. However, recent $^{40}Ar/^{39}Ar$ age determinations (Mollel et al., 2011; 2012; Mana et al., 2015) provide evidence for the single pulse of basaltic magmatism which occurred from ~ 2.4 Ma till ~ 1.58 Ma. The basaltic igneous activity at 2.4 Ma followed the voluminous eruptions of undersaturated picrite-nephelinite-phonolite lava series of Essimingor volcano commencing about 5.76 Ma ago (Mana et al., 2012) and was dominantly peralkaline in volcanic centers of Crater Highlands and adjacent Gregory Rift till ~ 3.53 Ma (Manega, 1993). Major extrusions of the basalts typify the activity at the large shield volcanoes and calderas (Lemagrut, Shira and Mawenzi centers of Kilimanjaro, Ngorongoro, Oldeani, Monduli and others). Lava flows and tuff layers of highly evolved andesibasalt, andesite, trachybasalt-trachyte association dominate in the above volcanoes. The most primitive basalts which corresponds characteristics of primary magma composition were not found yet. In order to solve the problem of primary basalt magma we investigated so called "Ogol" lavas outcropped 25 km west of Ngorongoro crater (Wirth and Adelsberger, 2002).

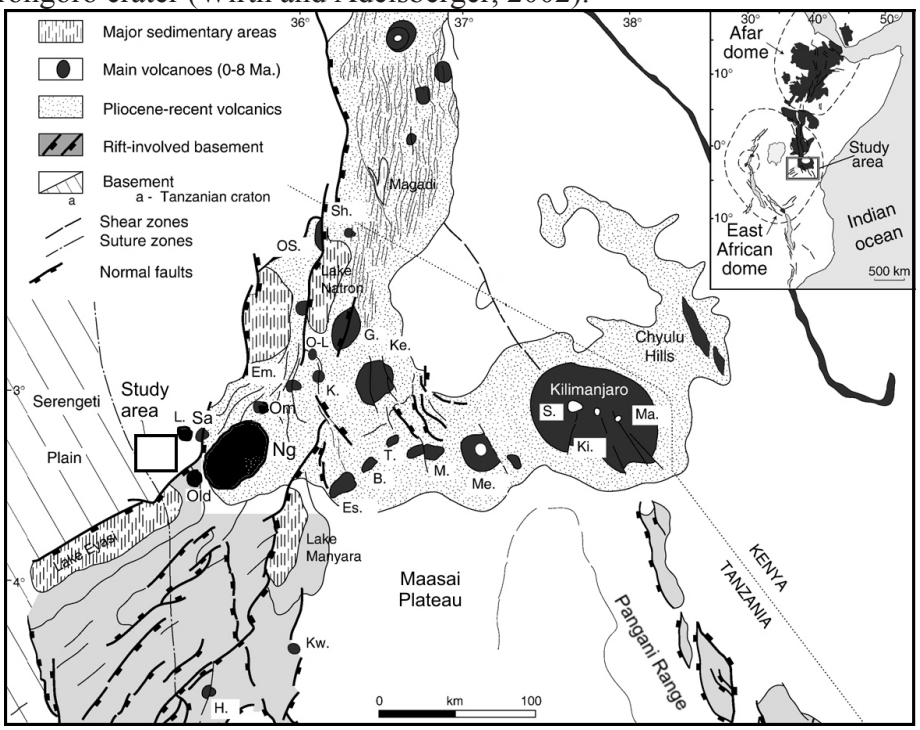

Fig. Main structural and magmatic features in the South Kenya and Northern Tanzania rift system (LeGall et al., 2008). Volcanoes: B. - Burko; Em. - Embagai; Es. - Essimingor; G. - Gelai; H. - Hanang; K. - Kerimasi; Ke. - Ketumbeine; Ki. - Kibo; Kw. - Kwaraha; L. - Lemagrut; M. -Monduli; Ma. - Mawenzi; Me. - Meru; Ng. - Ngorongoro; O-L – Oldoinyo Lengai; Old – Oldeani; Om – Olmoti; OS. - Oldonyo Sambu; S., Shira; Sa – Sadiman; Sh. - Shombole; T. - Tarosero.

The Ogol lavas have erupted from several feeder cones ranging from 0.5 to 1.5 km in diameter and 50 to 150 m in height. The eastern part of the flows is partly overlain by basalts and andesibasalts of Lemagrut volcano. Ogol lavas are partly overlain by Naibadad beds (2.15 Ma) and conformably overlie the Ndolanya (2.66 Ma) and Laetoli beds (Hay, 1987; Dawson, 2008). The latter were thoroughly studied due to findings of footprints of *Australopithecus afarensis*, the 3.66 Ma old paranthropus. $^{40}Ar/^{39}Ar$ isotope data suggest that Ogol lavas erupted between 2.31 ± 0.01 Ma and 2.27 ± 0.05 Ma (Mollel, 2007).

Basalt, the dominant rock type of Ogol lavas, is highly variable in texture, grade of crystallization and mineral composition. Chilled margins made of fine-grained porphyres with vitrophyric matrix, lamprophyric-type olivine-bearing varieties with chromium diopside in fine-grained clinopyroxene-plagioclase-magnetite matrix, are common rock types forming the lava flows. Evidently, such variations may be the result of undistinguished interlayering of lavas of different age or varying pulses of complementary derivatives erupted from the single magma chamber, or the both above processes.

Silica-saturated hypersthene-normative Ogol lavas plot in the mafic part of the TAS diagram with $45 < SiO_2 < 49\%$, $7 < MgO < 11\%$, and $(Na_2O + K_2O) < 5$ %. Lavas are broadly enriched in highly incompatible trace elements with respect to the primitive mantle. All of the samples are characterized by positive Ba and negative Pb, P anomalies; selected samples display marked positive Zr and Hf anomalies. Another major and diagnostic characteristic of Ogol magmas is that they have significant negative K anomalies (depletion in K relative to adjacent Nb, Th or La) when normalised to primitive mantle values. This feature is suggested to reflect conditions during partial melting in the presence of K-bearing phase (amphibole, phlogopite). Ogol lavas have high La/Nb–Ba/Nb values similar to basalts from Lemagrut and Ngorongoro that are characteristic of enriched mantle or mantle lithosphere sources (EM). Ba/Rb–Rb/Sr variations in Ogol, Lemagrut and Ngorongoro basalts indicate a limited role for amphibole (elevated Ba/Rb) and either phlogopite or carbonatite metasomatism (elevated Rb/Sr). The high values of $(Gd/Yb)_N$ observed in lavas and other portions of the basalts with moderately thick Archean crust suggest melting of enriched lithosphere in the presence of residual garnet (or clinopyroxene rich in Ca-Tschermak component; Blundy et al., 1998).

The Sr and Nd isotope ratios of Ogol basalts are considered to be similar to those that existed at the time of formation of the melt because of the relatively young age of the lavas. They show a restricted range in Sr and Nd isotopic composition ($^{87}Sr/^{86}Sr$ – 0.70390 - 0.70499; $^{143}Nd/^{144}Nd$ = 0.512412 – 0.512577) and plot on the general array defined by OIB. Their compositions in terms of Sr-Nd space are remarkably similar to the nearby Lemagrut lavas and lie on the East African Carbonatite Line (EACL; Bell and Blenkinsop, 1989).

The above characteristics of Ogol lavas provide evidence for the mantle origin of basaltic lavas whose features are very close to that in primary basaltic magmas erupted during 2/35 -1.55 Ma. Presence of mantle xenocrysts, high $(Gd/Yb)_N$ ratio and other geochemical features like Sr and Nd isotope characteristics argue for the metasomatized source generated from the garnet lherzolite mantle facies level.

This research is supported by the Alexander von Humboldt-Stiftung, St. Petersburg State University and Russian Foundation for Basic Research (grant 18-05-00835).

References

Baker B. H. Outline of the petrology of the Kenya rift alkaline province. In Fitton J. G. & Upton B. G. J. (eds) Alkaline Igneous Rocks, Geological Society, London, Special Publication 1987. V.27. P.293-311.

Bell K, Blenkinsop J Neodymium and strontium isotope geochemistry of carbonatites. In: Bell K. (ed) Carbonatites: genesis and evolution. Unwin Hyman, London. 1989. P.278-300.

Blundy J. D., Robinson J. A. C., Wood B. Heavy REE are compatible in clinopyroxene on the spinel lherzolite solidus // Earth and Planetary Science Letters. 1998. V.160. P.493–504.

Dawson J.B. (ed.) The Gregory Rift Valley and Neogene–Recent Volcanoes of Northern Tanzania. Geological Society, London, Memoirs, 2008. V.33. 102 p.

Hay, R. L. Geology of Laetoli area: Laetoli a Pliocene site in northern Tanzania. In: Leakey, M. D., and Harris, J. M. (ed.), A Pliocene site in northern Tanzania. Clarendon Press, Oxford. 1987. P. 23-47.

Le Gall B., Nonnotte P., Rolet J., Benoit M., Guillou H., Mousseau-Nonnotte M., Albaric J., Deverchère J. Rift propagation at craton margin. Distribution of faulting and volcanism in the North Tanzanian Divergence (East Africa) during Neogene times // Tectonophysics. 2008. V. 448. P. 1–19.

Mana S., Furman T., Carr M.J., Mollel G.F., Mortlock R.A., Feigenson M.D., Turrin B.D., Swisher III C.C. Geochronology and geochemistry of the Essimingor volcano: Melting of metasomatized lithospheric mantle beneath the North Tanzanian Divergence zone (East African Rift) // Lithos. 2012. V.155, P.310–325.

Mana S., Furman T., Turrin B.D., Feigenson M.D., Swisher III C.C. Magmatic activity across the East African North Tanzanian Divergence Zone // Journal of the Geological Society. V.172. P.368-389.

Manega, P. C. Geochronology, geochemistry and isotopic study of the Plio- Pleistocene hominid sites and the Ngorongoro volcanic highlands in northern Tanzania. Ph.D. dissertation. University of Colorado, Boulder. 1993. 194 p.

Mollel G.F., Swisher III, C.C., Feigenson M.D., Carr M.J. Petrology, geochemistry, and age of Satiman, Lemagurut and Oldeani: sources of the volcanic deposits of the Laetoli area. In: Harrison, T. (Ed.), Paleontology and Geology of Laetoli: Human Evolution in Context 1. Springer, Dordrecht. 2011. P. 99-120.

Mollel G. F., Swisher III C.C. The Ngorongoro Volcanic Highland and its relationships to volcanic deposits at Olduvai Gorge and East African Rift volcanism // Journal of Human Evolution. 2012. V.63. P. 274-283.

Wirth, K. R. and Adelsberger, K. A. Mantle source and magmatic evolution of the late Pliocene Ogol lavas of Laetoli, Tanzania. Geological Society of America, Abstracts with Programs. 2002. V.34. P. 363.

COEFFICIENT DISTRIBUTION Zr, Hf, REE MELILITE-MELT BY EXPERIMENTAL AND NATURAL DATA

Asavin A.M., Senin V.G.

V. I. Vernadsky Institute of Geochemistry and Analytical Chemistry RAS, Moscow. aalex06@inbox.ru

One of fundamental problems of geochemistry is genesis and formation conditions larnite-normative magmas. Interest to this type of magmas is caused by that of large-scale deposits is closely connected with them (Kovdor, Guli, Afrikanda). Subvolcanic rocks of such type quite rare. The most known regions where they are widespread it the African province central rift and Maymecha Kotuiy province, the Kola (Turiy Peninsula) province, the Rhine graben. The assessment of coefficient distribution (Kd) of trace elements for these liquids represents considerable interest as for understanding of processes of a fractionation of trace elements.

We investigated several natural samples porhyritic melilitites minerals: olivine (Ol), melilite (Mell), ± pyroxene (Cpx) as porphyric crystal (African and Maimecha Kotuyi province), and spent several isothermal experiments, with the melt close to turyaite and melilitite (sample 11073). For isothermal experiments used a tube furnace design L.D. Krigman. Powders of the samples put in a platinum capsule with a diameter of 0.05 mm. Duration of exposure at a given temperature the equilibrium of experience ranged from 24 to 57 hours depending on temperature. Since the experiments were conducted at uncontrolled oxygen fugacity - the air, we evaluate it on up to buffer NNO+1 (buffer $Ni+O_2 = NiO$). In rock substance added Zr and Hf and other trace element in the form of aqueous solutions of a given concentration. The concentrations of trace elements have changed from 0.002 to 5 wt.%.

These mixtures were melted at temperatures above the liquidus to the complete melting of the charge (incubated for one hour) and then decrease to the temperature of the isothermal sections and incubated for an equilibrium mineral-melt. Exposure time was sufficient to achieve an equilibrium concentration between minerals and liquid. Our measurement of concentration profiles of Zr, Hf, Ca, Si, Al, Mg, Fe in the glasses showed a homogeneous distribution of crystals around the phenocrysts. In the experience of the products were available for analysis of Mell, Ol, Cpx, magnetite (Mt) and glass (Liq).

The results of experiments were analyzed by microprobe, including those used in our specially designed technique for the analysis of low contents of Zr and Hf (Senin et al., 1989). Analysis of the contents of REE in melilite from experiments with turiyte was carried out with a laser and spark mass spectrometry (SMS) (Ramendik et al 1989).

Experiments have shown that in dry oxidizing conditions in the melilitic-nephelenite melts melilite does not crystallize. Only in the more undersaturated melts such as turiyte melilite crystallize. As the temperature falls the melt gets in the area of peretektic reaction - melilite is disappears, remains pyroxene.

Clinopyroxene–melt equilibria.

We found very high values Kd for Zr and Hf for the pyroxene-melt equilibria in the experiments with the nephelinites (Fig.1). Experimentally, Kd pyroxene- melilitite-rich melts virtually not been investigated. From the experimental data, we can mention the work (Gaetani & Grove 1995, Hill et al. 2000) that show Kd increases with increasing REE content in the pyroxene end-member Chermak in high calcium melts. The values Kd of Zr and Hf obtained in (Hill et al. 2000) is also very high, and remains a big difference in the values of (almost an order of magnitude) between them. Also published several papers on the study of equilibria in the silica-undersaturated melts. For example, in (Green et al. 1992, Sweeney et al. 1995, Klemme et al. 1995, Blundy & Dalton 2000, Adam & Green 2001) surveyed the distribution of trace elements in pyroxene carbonatite melts, which can also be viewed as an analogue of high-calcium alkaline magmas. In (Hill et al. 2000) studied a model kimberlitic melt. With the exception of (Klemme et al. 1995) in these equilibria also seen a big difference between Kd of Zr and Hf values and also Kd value is higher than in the melts of normal alkalinity. It is also very limited data on the Kd pyroxene of the in natural melilitic melts. We identified Kp for pyroxene in natural melilite-nepheline for sample 11073. At Fig.2 presents data on Kd in similar high-calcium

melts with melilite, and our data. It is seen that the data on Kd vary widely. In addition, there are a number of data for Kd in the natural lamproitic melts (Foley et al. 1996, Foley & Jenner 2004). Although the that melts usually have a specific composition - relatively high content of SiO2 and alkalis at low CaO.

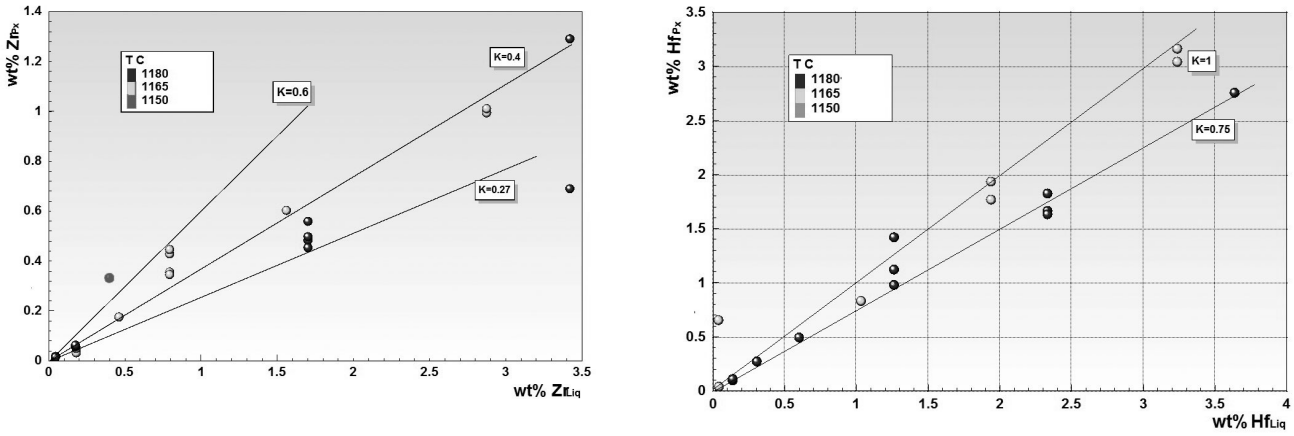

Fig. 1. Kd pyroxene-melt of Zr (a) and Hf (b) in the different equilibrium temperatures.

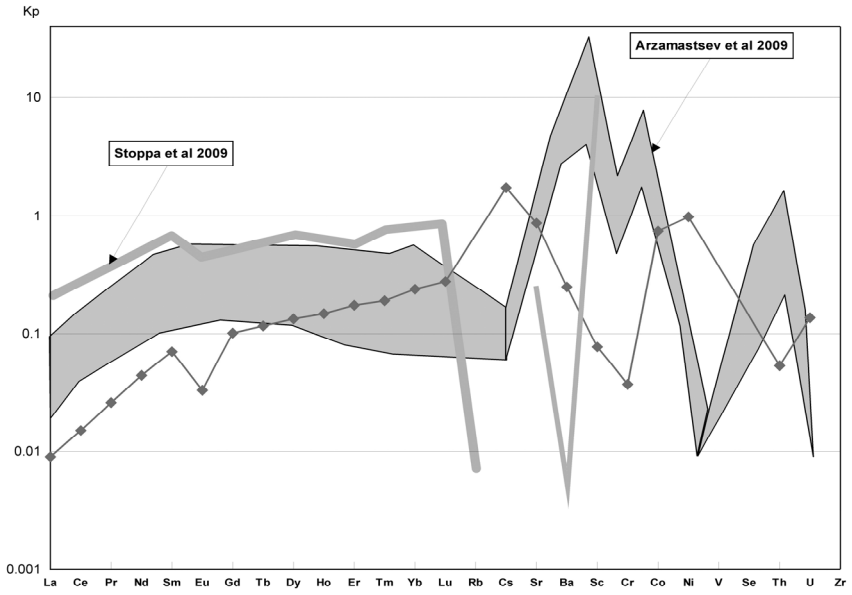

Fig. 2. Kd pyroxene measured by us for sample 11073 (line with diamonds) and literature data: (Stoppa et al 2009) for a range of Kd values for melilitic nephelinites - the wide gray line; (Arzamastsev et al. 2009) of the Turiy cape and melilite from the Kaiserstuhl - gray area

The data on the natural volcanic rocks are quite different from those obtained in experimental conditions. First the estimated Kd REE have the lowest values available in literature experimental Kd, second Kd heavy rare earths relatively light monotonically increases (the slope of the curve on the graph Kd is constant), in contrast to published data where from La to Sm Kd value increases the slope and then disappears, and for the Er–Lu may decrease the value of Kd.

In the third for our sample is characterized by a very minimum for Kd europium. Most similar to the results obtained for Kd kimberlite obtained at high pressure (6 GPa) (Keshav et al. 2005). However, these experiments were conducted at high temperatures (decrease values of Kd), and in our case, we would expect higher value of Kd REE. Very big difference in the values Kd of Cr, Co, Ni. Our values are less than 1, and the literature contains a similar and much higher than 1 value.

Lithophile elements are also characterized by a very wide interval of Kd values. And often reveals a large difference between the paired trace elements. Basically Kd Hf > Zr >> Nb, Th > U. All this creates a great opportunity to change the relationship pair of trace elements during the fractionation process. Interestingly, in experiments (Gaetani & Grove 1995, Hill et al. 2000) with pyroxenes that contain a high proportion of Chermak-component, obtained very high values Kd Zr and

Hf greater than 1. Under such circumstances, perhaps even melt depletion of lithophile trace elements the last portion of the melt.

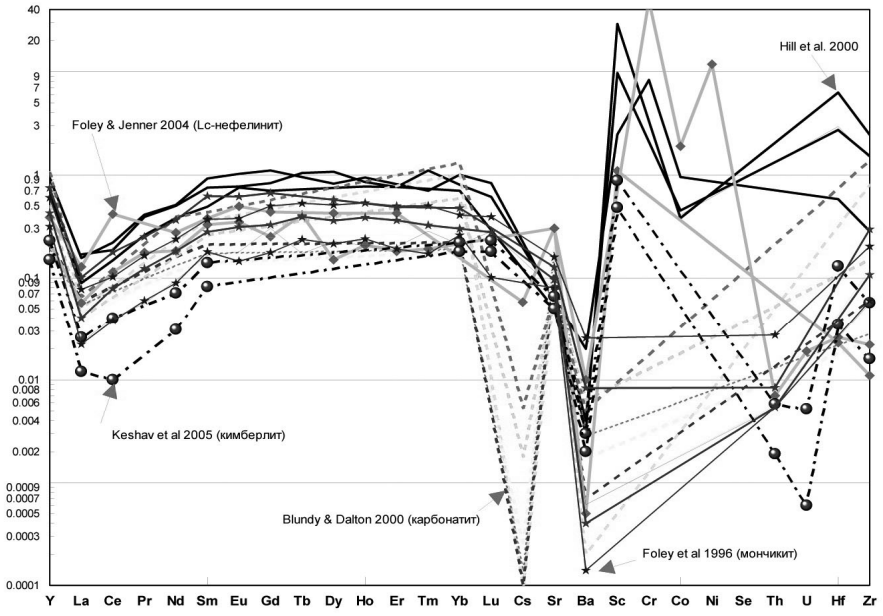

Fig. 3. Kd pyroxene from the literature: thin dashed lines – carbonatites (*Blundy & Dalton 2000*), the black solid line – with a high content in pyroxene end-Chermak minal (*Hill et al. 2000*), black dash dotted line with a ball marker – an experiment with an analog kimberlite melt at a pressure of 6 GPa (*Keshav et al. 2005*); line with asterisk markers, natural leucite nephelinite (*Foley & Jenner 2004*)

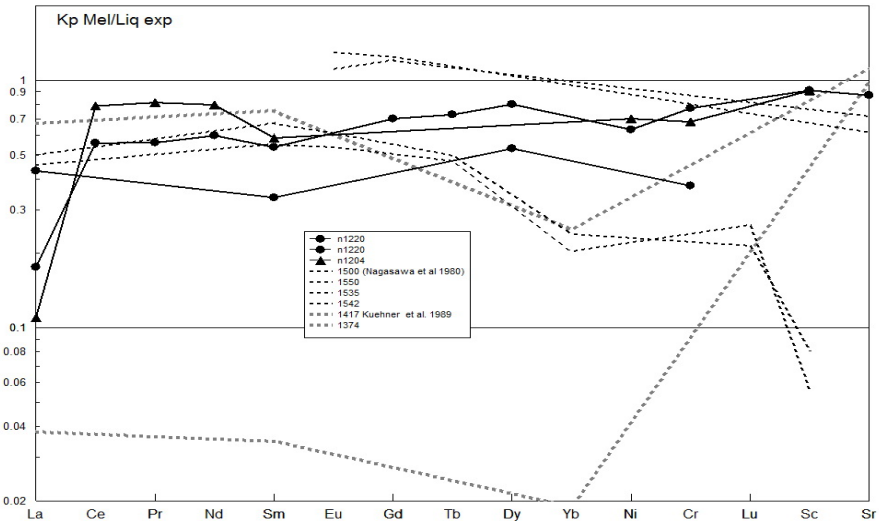

Fig. 4. Kd melilite in experiments on melting turiyte (black lines) measured by the SMS analysis. Addition experimental data (*Nagasawa et al 1980, Kuehner et al. 1989*).

Melilite–melt equilibria

Of great interest are the data we obtained for Kd melilite as the information on the quantities of this mineral Kd in natural melts is extremely small. Fig. 4 shows the measured by us in the turiyte Kd and a number of experimental data in the literature. Our data are consistent with the highest values of Kd. They are close to the Kd rare earth elements from ugandite (Onuma et al 1981) and they are approaching the magnitude of the Kd melilitite lappily tuff (Stoppa et al 2009). It is also interesting negative Eu anomalies and positive Rb. The high level of Kd values of the sample studied is shown in the considerably greater than 1 Kd Sr and high Kd Pb. Our results are similar to the Kd from turiyte studied by (Arzamastsev et al. 2009). It is interesting to note the relatively high (but low 1) the value Kd of Co, Ni, Zr. Significant difference between the Kd Th and U.

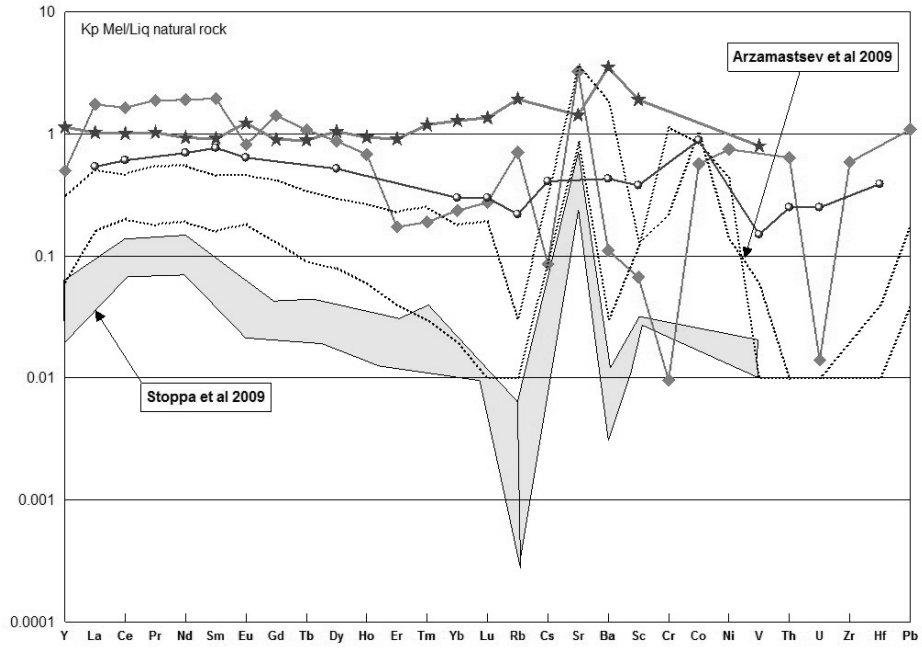

Fig. 5. Kd melilite measured us for sample 8748 (black line with diamonds) and literature data: (Stoppa et al 2009) gray box - a range of values for Kd melilitic nephelinites; and the line with the Stars - Kd melilite for melilitite-carbonatite lappilly; (Arzamastsev et al. 2009) point black lines - for turyaita Turego of the Cape and from the Kaiserstuhl melilitites; (Onuma et al 1981) line with circular dots - Kd in Uganda from Zaire

Conclusion

Our investigation of Kd pyroxene and melilite in the high-calcium melts and analysis of data in the literature, above all, shows the poor knowledge of the distribution of trace elements in the crystal-melt equilibria in these magmas.

For quite certain established patterns can be attributed - a slight difference between the LTR and HTR Kd for clinopyroxene and an inverse relationship to melilite.

High Kd melilite REE and probably high Kd clinopyroxene (due to the increase in the concentration Chermak minal) in general reduce the rate of accumulation of incompatible elements in the evolution of these magmas.

A very important feature is the significant difference in Kd lithophile elements. For melilite and pyroxene set a big difference between Th and U, Zr and Hf.

References

Adam, J., Green, T. Experimentally determined partition coefficients for minor and trace elements in peridotite minerals and carbonatitic melt, and their relevance to natural carbonatites //European Journal of Mineralogy 2001, Vol.13 (5), P.815-827.

Arzamastsev, A.A., Arzamastseva, L.V., Bea, F., Montero, P. Trace elements in minerals as indicators of the evolution of alkaline ultrabasic dike series: LA-ICP-MS data for the magmatic provinces of northeastern Fennoscandia and Germany //Petrologiya 2009, Vol.17, N.1, P.51–78.

Blundy, J. and Dalton, J. Experimental comparison of trace element partitioning between clinopyroxene and melt in carbonate and silicate systems, and implications for mantle metasomatism. //Contributions to Mineralogy and Petrology 2000, Vol.139, P.356-371.

Foley, S. and Jenner, G. Trace element partitioning in lamproitic magmas - the Gaussberg olivine leucitite. //Lithos 2004, Vol.75, P.19-38.

Foley, S.F., Jackson, S.E., Fryer, B.J., Greenough, J.D. and Jenner, G.A. Trace element partition coefficients for clinopyroxene and phlogopite in an alkaline lamprophyre from Newfoundland by LAM-ICP-MS. //Geochimica et Cosmochimica Acta 1996, Vol.60 (4), P.629-638.

Gaetani, G.A. and Grove, T.L. Partitioning of rare earth elements between clinopyroxene and silicate melt Crystal-chemical controls //Geochimica et Cosmochimica Acta, 1995, Vol.59, (10), P.1951-1962

Green, T.H., Adam, J., Siel, S.H. Trace element partitioning between silicate minerals and carbonatite at 25 kbar and application to mantle metasomatism //Mineralogy and Petrology 1992, Vol.46 (3), P.179-184.

Hill, E., Wood, B. and Blundy, J. The effect of Ca-Tschermaks component on trace element partitioning between clinopyroxene and silicate melt. //Lithos 2000, Vol.53 (3-4), P.203-215.

Keshav Shantanu, Alexandre Corgne, Gudmundur H. Gudfinnsson, Michael Bizimis, William F. Mcdonough and Yingwei Fei Kimberlite petrogenesis: Insights from clinopyroxene-melt partitioning experiments at 6GPa in the CaO-MgO-Al2O3-SiO2-CO2 system //Geochimica et Cosmochimica Acta, 2005, Vol.69, N.11, P.2829–2845,

Klemme, S., van der Laan, S.R., Foley, S.F., Günther, D. Experimentally Determined Trace and Minor Element Partitioning between Clinopyroxene and Carbonatite Melt under Upper-Mantle Conditions. //Earth and Planetary Science Letters 1995, Vol.133 (3-4), P.439-448

Kuehner, S.M., Laughlin, J.R., Grossman, L., Johnson, M.L. and Burnett, D.S. Determination of trace element mineral/liquid partition coefficients in melilite and diopside by ion and electron microprobe techniques //Geochimica et Cosmochimica Acta 1989, Vol.53, Issue 12, P 3115-3131

Nagasawa Hiroshi, Henry D. Schreiber, v.Morris Richard Experimental mineral/liquid partition coefficients of the rare earth elements (REE), Sc and Sr for perovskite, spinel and melilite // Earth and Planetary Science Letters 1980. Vol.46, Issue 3 pp.431–437

Onuma Naoki , Ninomiya Shuji and Nagasawa Hiroshi. Mineral/groundmass partition coefficients for nepheline, melilite, clinopyroxene and perovskite in melilite–nepheline basalt, Nyiragongo, Zaire //Geochemical Journal. 1980, Vol.15, pp.221–228

Ramendik G. I., B.M. Manson, D.A. Turin Quasi–equilibrium model for the formation of ions in the spark and laser mass spectrometry .//Cyrillic, Journal of Analytical Chemistry, Vol.44 pp. 996–1007

Senin V.G., A.M.Asavin, L.N.Lasutkina, N.V. Korsakova Measurement Zr and Hf in geological samples by the method of X–ray micro–probe analysis Cyrillic, //Journal of Analytical Chemistry. 1989, № 9.P.1671.

Stoppa Francesco., Adrian P.Jones, Victor V. Sharygin Nyerereite from carbonatite rocks at Vulture volcano:implications for mantle metasomatism and petrogenesis of alkali carbonate melts.// Cent. Eur. J. Geosci, Vol.1 (2) P.131–151.

Sweeney, R.J., Prozesky, V., Przybylowicz, W. Selected trace and minor element partitioning between peridotite minerals and carbonatite melts at 18-46 kb pressure //Geochimica et Cosmochimica Acta. 1995, Vol.59 (18), P.3671-3683.

CRYSTALLIZATION CONDITIONS AND FLUID REGIME OF PYROXENITE-NEFELINE MAGMATIC SUB-PHASES OF THE GULI PLUTON (MAIMECHA-KOTUI PROVINCE, RUSSIA)

Asavin A.M.[1], Serova L.D.[1,2], Kononkova N.N.[1], Buikin A.I.[1]

[1]Vernadsky Institute of Geochemistry and Analytical Chemistry RAS, Moscow, Russia, aalex06@iinbox.ru

[2]Moscow State University, Moscow, Russia. serova-larisa@mail.ru

There is an important problem of the genesis of multiphase alkaline-ultrabasic pluton that consists of different series of alkaline rocks within a single igneous chamber. This question remains open due to the lack of appropriate petrological and geochemical models for the formation of independent sub-phases during multiphase intrusion. In the published literature there are both supporters of these sub-phases formation as some sequence of differentiates from a single primary ultrabasic magma, and supporters of series completely independent mantle melts which served as the initial melt for the formation of each type of rocks sequence.

One of the most interesting types of rock sequence that is very typical for ultrabasic alkaline intrusions are the pyroxene-nepheline rocks series: jacupirangite-melteigite-ijolite-urtite-nepheline syenite. This sequence of rocks is defined by gradual transitions between each term of the series, close spatial and genetic geological relations and common mineralogy and type of ore's specialization. Massifs with a predominance of such rocks are often specialized in apatite deposits (Khibiny massif, Magan massif), perovskite mineralization (Lovoozersky massif). These problems make the study of the genesis of these ore-bearing rocks very relevant.

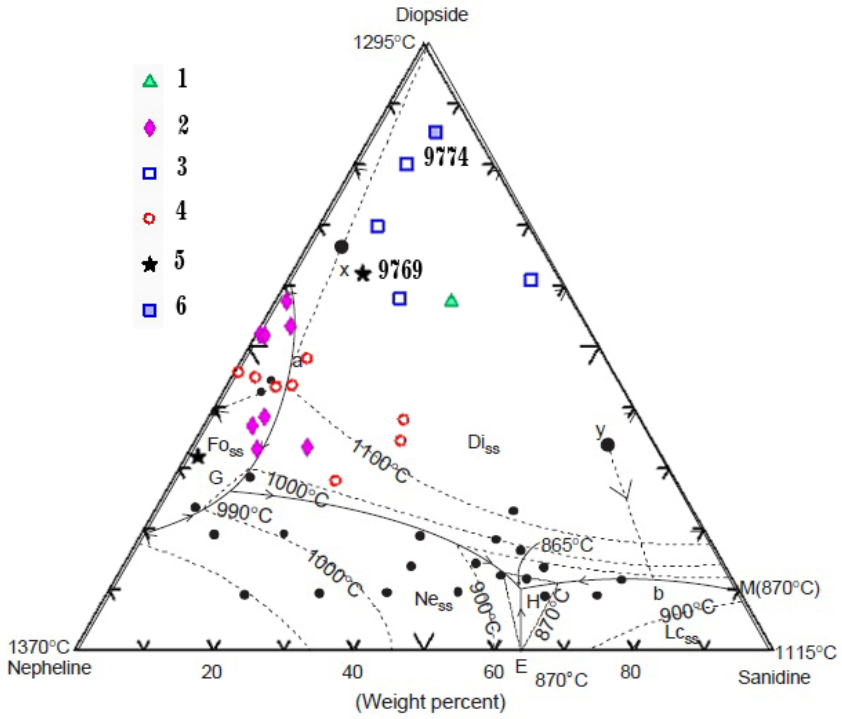

Fig.1. Legend: 1 – sample 9769, 2 – melteigite and olivine-melteigite, 3 – jacupirangites, 4 – compositions of inclusions in melteigites (Isakova et al., 2015), 5 – nepheline picrite, 6 – jacupirangite sample 9774

Unfortunately, there are very few works dedicated to genesis of this igneous phase and they mainly touch upon more differentiated rocks of this series – agpaitic nepheline syenites, urtites (Schairer, Yoder, 1960; Kogarko, 1977; Gupta et al., 2006; Giehl et al., 2013). Therefore, obtaining new data on the crystallization parameters of jacupirangite and nepheline syenites in such arrays is a rather important and urgent task.

We have studied the mineral compositions of the Guli massif rocks: jacupirangite (sample 9774), nepheline syenite (sample 660) and nepheline picrite (sample 9769). The main rock-forming minerals

of these rocks are clinopyroxene and magnetite; titanite is also found in all of them. For comparison with the rocks of the melilitic phase, we also studied pyroxenes from melilititolites (sample GH3) and uncompahgrite (GH44). The composition of rocks is typical for ultrabasic alkaline massifs and can be represented on the triangle Px-Ol-Lc + Ne (Fig. 1), on which the composition points are plotted according to the CIPW regulatory recalculation. The points of compositions of similar rocks from the works by (Egorov, 1991; Bogatikov, 1983) are also shown. In fact, this figure demonstrates the principal features of the crystallization of jacupirangite and their interrelations with more alkaline melteigite and olivine-melteigite melts of the initial stages of primary melts evolution.

For the first time, our petrographic investigations have revealed structures of solid phase decomposition in clinopyroxenes and magnetites from jacupirangite. These facts are evidence of a long history of rocks crystallization. Table 1 shows the calculation results (according to procedures published in (Lepage, 2003)), which show a fairly wide range of equilibrium temperatures of 600-700 °C for jacupirangite and 600-1000 °C for syenite. The two-stage solid-phase decay is reflected in the appearance, along with large lamella of ilmenite (dark in Fig. 2a), of small lamellae in magnetite in the intervals between these large lamellae.

Table 1. Estimates of temperature (°C) and oxygen fugacity relative to NNO buffer by Mt-Ilm equlibria.

Ilm-Mgt geothermometer	9774		660			
mineral pairs (point numbers)	2-4	3-4	2-1	1-4	5-4	3-4
Powell & Powell 1977 (T)	616	616	831	581	774	648
Anderson & Lindsly 1985 (T)	653	653	1002	702	981	819
Spensor & Lindsly 1982 (T)	630	630	1038	685	969	791
Spensor & Lindsly 1982 (NNO)logfO_2)	-18	-18	-18	-22	-18	-21
Andersen & Lindsley 1985 (NNO)logfO_2)	-20	-20	-33	-27	-33	-35
Sauerzapf et al., 2008 (T)	723	643	963	703	963	963
Sauerzapf et al., 2008 (NNO)logfO_2)	-5.1	-5.8	-5.2	-6	-5.6	-6

Temperature calculation using a geothermometer (Alvaro et al., 2015)

	9774 (jacupirangite)								
N point	5	2	11	1	1	12	3	9	13_74
	center	center	center	center	center	rim	rim	rim	rim
T(C)	1314	1246	1228	1193	1145	944	832	675	523
	660 (Ne-syenite)				GX44 (uncompahgrite)				
N point	13	12	8	10	28	29	34	35	
	center	center	center	rim	center	center	center	rim	
T(C)	1130	984	866	540	1129	988	954	933	
	9769 (Ne-picrite, bg – pyroxene form background								
N point	24_69	25	14	22	20	17	30	21	15	27	16	16
	rim	center	center (bg)	rim	center	rim (bg)	center	center	rim (bg)	rim		center (bg)
T(C)	979	941	798	795	779	750	716	607	597	565	565	533

The small size of light oriented inclusions in pyroxene did not allow us so far to evaluate the composition of these phases by microprobe analysis. However, the very fact of the decomposition of solid solutions in monoclinic pyroxene is quite illustrative. Using the mono-mineral pyroxene geothermometer based on the intra-crystalline redistribution of Mg-Fe between the M1-M2 positions (Dal Negro et al., 1982, 1986; Douce et al., 1993; Alvaro et al., 2015), we estimated the crystallization temperatures of pyroxenes.

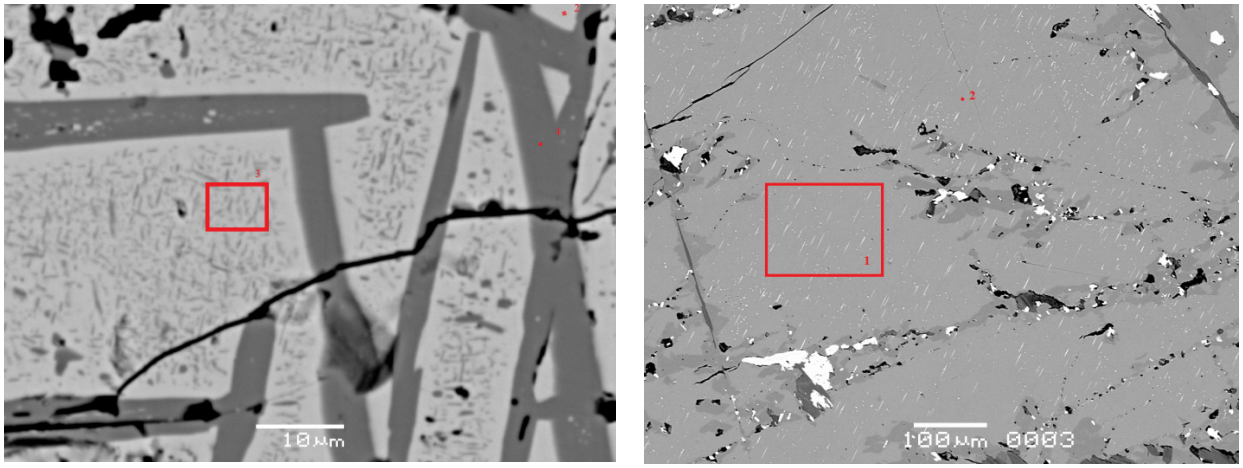

A – two-stage solid-phase decay of Mt-Ilm B – decay in clinepyroxene solid-structure

Fig. 2. Structures of solid phase decomposition in minerals from jacupirangite (sample 9774) (a) dark – Ilm, light – Ti-Mt; (b) clinopyroxene – the main grey area with light oriented inclusions of phase with unknown composition.

The result of the calculations also indicates a long crystallization path. Temperatures vary from 1250 to 550 °C. In the zonal pyroxene crystals, the edge zones differ from the central ones by temperatures of 50-100 degrees. The highest initial temperatures were obtained for the initial stages of crystallization in jacupirangite and syenite. The temperature for the pyroxene from the melilititolite is lower. Interestingly, the temperature of pyroxene (1130 °C) is close to the level of the temperature barrier (Ab-Di peritectic) – 1140 °C, which separates melilite-pyroxene melts from nepheline-pyroxene melts. It is fundamentally important for us that, depending on the conditions and the primary component of the melt, differentiation of alkaline magma can go in different directions towards more high-calcium and potassium melts with wollastonite and melilite, or towards less alkaline phonolitic derivatives with a feldspar ending.

The calculated temperature ranges for the crystallization of pyroxene from jacupirangite are well explained if we consider this rock as pyroxene cumulate, formed as a result of differentiation in the magmatic chamber. In this case, the edge zones of low-temperature pyroxene and phlogopite crystals and titanomagnetite are formed from the interstitial melt. The composition of the interstitial melt obviously changed greatly during crystallization. However, its temperature in the final stages was obviously quite low, which was reflected in the low crystallization temperatures of the marginal zones of pyroxenes and the magnetite-ilmenite equilibrium.

There is a problem of how to explain the high magnesia of the interstitial melt and at the same time its low crystallization temperature. Our study of the fluid regime allows us to solve this paradox. The data on jacupirangite indicates a high content of primary magmatic water (will be published elsewhere), and therefore, due to this, the melting point of the melt could be greatly reduced.

With a sharp decrease of pressure and the rapid removal of free fluid from the system, super cooled melts could appear which led to the rapid crystallization of pyroxene (jacupirangite). The picrite we studied (9769) can be an example of the crystallization of such melts.

According to our data, it is characterized by low equilibrium pyroxene crystallization temperatures and at the same time by a high content of MgO (16 wt. %) and alkalis and a very low content of the H_2O-fluid. The point of its composition in the diagram (green triangle in Fig. 1) in the field of crystallization of pyroxene is located very far from the olivine-pyroxene cotectic. It can be considered as a starting point for the formation of pure pyroxene cumulus followed by the addition of nepheline with a decrease in temperature.

Thus, the petrologic model of the formation of the pyroxene-nepheline phase consists of a specific fluid (H_2O) mode of highly magnesian melts. Prolonged preservation of high levels of water content in the magmatic chamber complementary to the formation of monomineral pyroxene cumulus firstly ensures the formation of jacupirangite-melteigite rocks, and secondly allows us to overcome the barrier peritectic to move from the second intrusive phase of the Guli pluton to nepheline-pyroxene melt.

A special regime of crystallization in a chamber saturated with fluids leads to the formation of highly titanium phases – titanite and ilmenite. However, a high level of silicon in the melt leads to the fact that such an ore mineral as perovskite (characteristic of melilitic species of rocks) does not crystallize in the jacupirangite of the Guli pluton. Apatite ores with titanite become the ore specialization of the jacupirangite-ijolite intrusions. A vivid example of such geological process is the Khibiny massif.

This model explains the formation of the Jacupirangite-Melteigite phase instead of melilitites, their ore specialization and a wide temperature regime combined with high water content during the crystallization of intrusive derivatives.

This work was supported by RFBR grant №19-05-00681.

References

Alvaro, M., Domeneghetti, M.C., Fioretti, A.M., Cámara, F., Marinangeli, L.A new calibration to determine the closure temperatures of Fe□Mg ordering in augite from nakhlites. // Meteoritics & Planetary Science. 2015. Vol. 50(3). P. 499-507.

Andersen, D.J., Lindsley, D.H. New (and final!) models for the Ti-magnetite/ilmenite geothermometer and oxygen barometer. // Abstract AGU 1985 Spring Meeting Eos Transactions. American Geophysical Union. 1985. Vol. 66 (18). P. 416.

Dal Negro A., Carbonin S., Molin G.M., Cundari A., Piccirillo E.M. Intracrystalline cation distribution in natural clinopyroxenes of tholeiitic, transitional, and alkaline basaltic rocks. // In Advances in physical geochemistry Springer, New York, NY. 1982. P. 117-150

Dal Negro A., Cundari A., Piccirillo E.M., Molin G.M., Uliana D. Distinctive crystal chemistry and site configuration of the clinopyroxene from alkali basaltic rocks. // Contributions to Mineralogy and Petrology. 1986. Vol. 92(1). P. 35-43.

Douce A.E.P. Titanium substitution in biotite: an empirical model with applications to thermometry, O_2 and H_2O barometries, and consequences for biotite stability. // Chemical Geology. 1993. Vol. 108(1-4). P. 133-162.

Giehl C., Marks M., Nowak M. Phase relations and liquid lines of descent of an iron-rich peralkaline phonolitic melt: an experimental study. // Contributions to Mineralogy and Petrology. 2013. Vol. 165.2. P. 283-304.

Gupta A.K., Chattopadhyay S., Chattopadhyay B., Arima M. Experimental study of the system diopside-nepheline-sanidine at 0.1, 1 and 2 GPa [$P(H_2O)=P(Total)$]: Its significance in the genesis of alkali-rich basic and ultrabasic rocks // Lithos. 2006. Vol. 86 (1-2). P. 91-109.

Lepage L. D. ILMAT: an Excel worksheet for ilmenite–magnetite geothermometry and geobarometry. // Computers & Geosciences. 2003. Vol. 29(5). P. 673–678

Powell R., Powell M. Geothermometry and oxygen barometry using coexisting iron-titanium oxides: a reappraisal // Mineralogical Magazine. 1977. Vol. 41 (318). P. 257–263.

Sauerzapf Ursula, Dominique Lattard, Michael Burchard,Ralf Engelmann. The titanomagnetite-ilmenite equilibrium: new experimental data and thermo-oxybarometric application to the crystallization of basic to intermediate rocks // Journal of Petrology. 2008. Vol. 49(6). P. 1161-1185

Schairer J. F., H. S. Yoder Jr. The nature of residual liquids from crystallization, with data on the system nepheline-diopside-silica. // Am. J. Sci.. 1960. Vol.258-A. P. 273-283

Bogatikov O.A. (Chief Ed.) Magmatic rocks. M.: Nauka. 1983. 365 pp.

Egorov L.S. Ijolite–Carbonatite Plutonism: Maimecha–Kotui Complex of the Polar Siberia. Nedra, 1991. Leningrad. [in Russian].

Isakova A.T., Panina L.I., Rokosova, E.Yu. Carbonatite melts and genesis of apatite mineralization in the Guli pluton (Northern East Siberia). // Russian Geology and Geophysics. 2015. Vol. 56(3). P. 466-475.

Kogarko L.N. The problems of genesis of agpaitic magmas. M.: Nauka. 1977. 150 pp.

MANTLE METASOMATISM AND GEOCHEMISTRY OF MINERALS IN MANTLE XENOLITHS FROM BASALTS, SVALBARD ARCHIPELAGO

***Ashikhmin D.S.*[1,2], *Skublov S.G.*[3,1]**

[1]*Saint-Petersburg Mining University, Saint-Petersburg, Russia, ashihmin-dmitriy@mail.ru*
[2]*A.P. Karpinsky Russian Geological Research Institute (VSEGEI), Saint-Petersburg, Russia*
[3]*Institute of Precambrian Geology and Geochronology (IPGG RAS), Russian Academy of Sciences, Saint-Petersburg, Russia, skublov@yandex.ru*

The paper reports the results of SIMS and EDS-EMPA study of rock-forming minerals from melt pockets in the central part of a spinel peridotite xenolith taken from Quaternary alkaline basalts of Sverre Volcano in the northwestern part of West Spitsbergen Island. Olivine and clinopyroxene are analyzed to trace changes related to the metasomatic interaction between spinel lherzolite and a carbonate melt with formation of corresponding secondary minerals and silicate glass. It is established that the metasomatic interaction of the carbonate melt with minerals of host spinel lherzolite is accompanied by partial recrystallization of olivine and clinopyroxene, or crystallization of the second generation of these minerals. Percolating carbonate melt caused significant changes in the major, trace, and rare-earth element composition of the considered minerals, thus placing constraints on the use of the composition of these minerals for calculation of P–T parameters, estimating equilibrium, and modeling petrological processes in mantle.

The geochemical analysis of peridotites and constituent minerals provides insight into composition of lithospheric mantle, as well as mechanism and physicochemical conditions of melting, composition of melts and mantle protolith. Variations and average contents of trace elements for different types of mantle rocks are compiled in published summaries. However, generalization and averaging of a great body of the data set obliterate anomalous geochemical characteristics deviating from typical ranges of contents. Nevertheless, precisely these geochemical features that are inconsistent with general tendencies require through study and interpretation. This paper analyzes compositional changes of olivine and clinopyroxene in melt pockets in the central part of mantle xenolith in response to the metasomatic interaction of spinel lherzolite with a carbonate melt.

During past decades, concepts of the nature of glasses in mantle xenoliths have been significantly modified. Previously, they were interpreted as an infiltration melt of host rocks, for instance, basalts. Since 1990s, the presence of glass as inclusions in rock forming minerals and as melt pockets was considered to be related to mantle metasomatism (Kogarko et al., 1995; Coltorti, Gregoire, 1998; Kogarko et al., 2001). At present, the formation of glasses in mantle xenoliths is regarded as a result of interaction of primary mantle mineral assemblage with hypothetical metasomatizing melts of different composition and genesis (Coltorti et al., 2000); in situ melting of mantle minerals (Chazot et al., 1996), decompression melting of pyroxenes (Francis, 1987; Yaxley, Kamenetsky, 1999), or partial melting of mantle rocks (Draper, Green, 1997). Melt pockets up to 200 μm in size consisting of diverse Ca–Mg silicate glass and carbonates (dolomite and magnesian calcite) were found and described for the first time in mantle peridotite xenoliths from alkaline basalts of the Spitsbergen Archipelago (Ionov et al., 1996, 2002). Glass in these melt pockets occurs as aggregates with bubbles of fluid inclusions at the contact of olivine and pyroxenes, and in fractures of variable width (from tenths of mm to 1–2 mm). Such melt pockets were found by us in the central part of the peridotite xenolith and studied in detail. The xenolith sample 13 x 13 cm in size (given by A.N. Sirotkin) was collected from Quaternary alkaline basalts of Sverre Volcano in northwestern West Spitsbergen. The xenolith is represented by spinel lherozlite consisting of olivine (74%), orthopyroxene (13%), clinopyroxene (7%), and spinel (4%). There are also subordinate ore mineral and carbonate associated with melt pockets.

The distribution of trace and rare-earth elements in rock-forming olivine and clinopyroxene was analyzed in the immediate vicinity and at the contact with melt pocket in order to determine the effect of the melt on geochemistry of minerals of mantle xenoliths. Melt pockets in the studied sample are irregularly shaped and up to 2 x 3 mm in size. The central part and the main volume of the pocket are usually occupied by the carbonate aggregate of variable composition. The melt pocket contains newly

formed (with respect to primary lherzolite minerals) small euhedral grains of clinopyroxene, spinel, and more rarely, olivine, which are usually separated from carbonate and pocket walls by a 20-μm rim of silicate glass. At the contact of the carbonate-bearing melt pocket with host unaltered lherzolite, spinel, olivine, and clinopyroxene grains acquire euhedral habit and heterogeneous structure, changing their composition at the contact with pocket matter, which is caused by either overgrowing of initially melted grains by corresponding newly formed minerals or their partial recrystallization accompanied by compositional change. The relicts of primary olivine, clinopyroxene, and spinel are also retained in the central parts of relatively large grains within carbonate-bearing pockets.

The formation of such melt pockets is caused by metasomatic interaction of percolating carbonate melt (genesis of carbonate melts requires separate detailed consideration and is not discussed in this paper) with host minerals of lherzolite, which resulted in the formation of carbonate, silicate glass, and newly formed clinopyroxene, olivine and spinel (Ionov et al., 1996). As shown in (Ionov et al., 1996), these carbonate-bearing melt pockets in spinel lherzolites from the alkaline basalts of Sverre volcano were formed during short time prior to the ascent of xenoliths to the surface, within upper mantle; interaction of a carbonate melt with lherzolite was mainly controlled by the following reaction (Dalton, Wood, 1993; Ionov et al., 1996):

$$CaCO_3 + MgCO_3 + MgSiO_3 = CaMgSi_2O_6 + Mg_2SiO_4 + CO_2$$
carbonate melt *Opx* *Cpx* *Ol* fluid

Clinopyroxene in general is characterized by weakly differentiated REE pattern with the average total REE content around 74 ppm. Secondary clinopyroxene frequently observed in contact with silicate glass shows relative LREE depletion within a single grain, for instance, from 64 ppm in unaltered (relict) part to 34 ppm at the contact in the altered part of the grain (Table 1). The Lu_N/La_N ratio in the secondary clinopyroxene (indicator of REE fractionation) is on average 1.2, being much lower in all other points (on average, 0.3). Eu anomaly is practically absent. The examination of the behavior of other trace elements in the clinopyroxene established that the newly formed clinopyroxene, in addition to Al, Cr, and Ti, are also significantly enriched (by 1.5–2 times) in V, Y, and Nb (Table 1). In contrast, the Sr and Zr contents in the secondary clinopyroxene decrease by approximately two times (Table 1). The Hf, Ta, and Li contents show sufficiently homogenous distribution in analyzed clinopyroxenes of both types.

The strongest difference was found between olivines surrounded by silicate glass in contact with melt pocket, on the one hand, and the central unaltered parts of large grains of primary lherzolite olivine far from glass, on the other hand. In terms of the degree of alteration correlated with the distance from the melt pocket, olivines can be subdivided into three groups: unaltered, weakly altered, and strongly altered.

The unaltered olivine contains insignificant amounts of both LREE and HREE, within tenths and hundredths of ppm (Table 1). Weakly altered olivine differs from unaltered one in the elevated (by 5–10 times) LREE contents (11 ppm). This group reveals insignificant positive Eu anomaly. The REE content in strongly altered olivine, unlike two other groups, has the elevated REE content (Table 1). An increase of REE contents is primarily caused by the increase of LREE content, whereas the HREE growth is an order of magnitude lower (112 and 12 ppm respectively). The strongly altered olivine also shows positive Eu anomaly ($Eu/Eu^* > 3$ for both groups). Other elements also demonstrate a subsequent increase from unaltered to strongly altered olivine ,for instance: Ti 18.2, 122, and 3126; V 20.8, 26.3, and 122 ppm, and Sr 1.53, 6.04, and 472 ppm, respectively. The Cr content exhibits less distinct variations, showing only 1.3 times increase from unaltered to strongly altered olivine (Table 1). Three of four points of strongly altered olivine have elevated Cr content (up to 858 ppm), which however decreases to 26.5 ppm in point 7 having extremely high LREE content. The contents of high-field strength Y and Zr reveals almost 60 times increase in strongly altered olivine as compared to unaltered grains. It is noteworthy that Ba varies within each olivine group. However, in general, the Ba content is no more than 1 ppm in unaltered olivine, within 1–10 ppm in weakly altered olivine, and reaches 12–55 ppm in strongly altered olivine, except for anomalous point 7, where the Ba content is as high as 1170 ppm. The Li, Hf, and Ta contents are practically unchangeable in all three groups and show no significant variations.

Table 1. Content trace elements (ppm) in minerals and glass from melt pocket in xenolith.

	Cpx		Glass		Olivine		
	primary n=5	secondary n=4	contact with Ol n=4	contact with Cpx n=3	unaltered n=4	weakly altered n=6	strongly altered n=4
La	11.6	3.56	36.2	22.0	0.01	0.08	8.39
Ce	28.7	14.4	75.6	48.0	0.02	0.15	16.7
Pr	3.74	2.64	8.57	5.91	b.d.l.	0.02	1.92
Nd	17.5	17.1	34.9	26.0	0.03	0.07	8.13
Sm	3.79	4.70	5.70	4.84	0.02	0.02	1.19
Eu	1.27	1.77	1.78	1.60	0.01	0.04	0.48
Gd	3.56	5.38	5.46	5.11	0.01	0.03	1.29
Dy	3.46	5.48	5.15	4.62	0.01	0.03	1.06
Er	2.18	3.62	3.58	2.86	0.02	0.05	0.82
Yb	2.30	3.15	3.50	2.78	0.03	0.08	0.69
Lu	0.30	0.43	0.53	0.42	0.01	0.01	0.11
Li	0.44	0.33	3.39	2.93	1.21	0.72	1.81
Ti	1933	7843	12242	10455	18.2	122	3126
V	271	437	490	447	20.8	26.3	122
Cr	4259	8493	109	7210	448	577	527
Sr	307	159	1907	1260	1.53	6.04	472
Y	19.2	29.7	30.1	25.8	0.09	0.23	6.64
Zr	28.9	17.0	54.5	35.7	0.54	0.66	12.4
Nb	0.77	0.92	70.6	40.8	0.05	0.31	15.7
Ba	5.28	0.27	1551	907	0.42	4.95	323
Hf	1.25	1.39	2.34	1.66	0.02	0.05	0.43
Ta	0.28	0.38	2.01	1.22	0.03	0.03	0.37
Zr/Hf	23.1	12.3	23.1	22.6	14.8	18.5	21.6
Nb/Ta	2.70	2.45	36.1	32.2	1.37	8.98	35.4

Glass from the studied melt pockets has basic composition (on average, 52.6 wt % SiO_2). Its major element composition is sufficiently homogenous. The REE distribution in glass shows differentiated pattern with decrease of contents from LREE to HREE (LuN/LaN ratio on average is 0.18). Eu anomaly is either absent or weakly-expressed of variable sign (Eu/Eu* varies from 0.8 to 1.3). The contents of trace elements in the glass show weak variations, except for Cr. The Cr content varies from 109 to 7210 ppm (Table 1). However, the contents of other elements in this point are similar to those of other glass analyses.. To sum up, the major-element composition of the glass is practically unchangeable and does not depend on the composition of adjacent mineral (Table 1). Variations are noted only for Ca content, which is elevated in points located near olivine (on average, 7.9 wt %). CaO content in glass at the contact with clinopyroxene on average is 6.5 wt %. This is likely related to the structural specifics of olivine and its extremely low isomorphic capacity relative to Ca. Therefore, glass in contact with olivine is enriched in Ca.

Similarly, such trace elements as Ti, V, Sr, Y, Ba, and Ta are not typical of olivine and, correspondingly, are accumulated at the melt–olivine contact. At the same time, glass in contact with clinopyroxene has elevated Cr content, which indicates the low degree of melt differentiation, thus confirming conclusion concerning a short-term duration of this process (Ionov et al., 1996).

It was established that the metasomatic interaction between a carbonate melt and minerals of host spinel lherzolite leads to the partial recrystallization of olivines and clinopyroxenes, or crystallization of the second generation of these minerals. The melt percolation causes significant change in contents of major, trace, and rare-earth elements, thus placing constraints on the use of these minerals for calculation of PT parameters, estimating equilibrium, and modeling of petrological processes in mantle.

We are grateful to O.L. Galankina, A.E. Melnik (IPGG RAS), S.G. Simakin, and E.V. Potapov (Valiev IPT RAS, Yaroslavl branch) for the performance of analytical works.

This study was supported by the Russian Foundation for Basic Research (project no. 19-35-50014).

References

Chazot G., Menzies M.A., Harte B. Determination of partition coefficients between apatite, clinopyroxene, amphibole, and melt in natural spinel lherzolites from Yemen: implications for wet melting of the lithospheric mantle // Geochimica et Cosmochimica Acta. 1996. Vol. 60. p. 423-437.

Coltorti M., Grégoire M. Metasomatism in oceanic and continental lithospheric mantle: introduction // In Metasomatism in Oceanic and Continental Lithospheric Mantle, Edited by M. Coltorti and M. Grégoire. Geological Society, London, Sp. Publ. 293, 1998, pp. 1-9.

Coltorti M., Beccaluva L., Bonadiman C., Salvini L., Siena F. Glasses in mantle xenoliths as geochemical indicators of metasomatic agents // Earth and Planetary Science Letters. 2000. Vol. 183. p. 303-320.

Dalton J.A., Wood B.J. The partitioning of Fe and Mg between olivine and carbonate and the stability of carbonate under mantle conditions // Contributions to Mineralogy and Petrology. 1993. Vol. 114. p. 501-509.

Draper D.S., Green T.H. Phase relations of silicic, alkaline, aluminous mantle-xenolith glasses under anhydrous and C-O-H fluid-saturated conditions // Journal of Petrology. 1997. Vol. 38. p. 1187-1224.

Francis D. Mantle-melt interaction recorded in spinel lherzolite xenoliths from the Alligator Lake volcanic complex, Yukon, Canada // Journal of Petrology. 1987. Vol. 28. P. 569-597.

Ionov D.A., O'Reilli S.Y., Genshaft Y.S., Kopylova M.G. Carbonate-bearing mantle peridotite xenoliths from Spitsbergen: phase relationships, mineral compositions and trace-element residence // Contributions to Mineralogy and Petrology. 1996. Vol. 125. p. 375-392.

Ionov D.A., Bodinier J.-L., Mukasa S.B., Zanetti A. Mechanisms and sources of mantle metasomatism: major and trace element compositions of peridotite xenoliths from Spitsbergen in the context of numerical modeling // Journal of Petrology. 2002. Vol. 43. p. 2219-2259.

Kogarko L.N., Henderson C.M.B., Pacheco H. Primary Ca-rich carbonatite magma and carbonate-silicate-sulphide liquid immiscibility in the upper mantle // Contributions to Mineralogy and Petrology. 1995. Vol. 121. p. 267-274.

Kogarko L.N., Kurat G., Ntaflos T. Carbonate metasomatism of the oceanic mantle beneath Fernando de Noronha Island, Brasil // Contributions to Mineralogy and Petrology. 2001. Vol. 140. p. 577-587.

Yaxley G.M., Kamenetsky V. In situ origin for glass in mantle xenoliths from southeastern Australia: insights from trace element compositions of glasses and metasomatic phases // Earth and Planetary Science Letters. 1999. Vol. 172. p. 97-109.

SHRIMP U-Pb ZIRCON GEOCHRONOLOGY OF VOLCANIC ROCKS HOSTING WORLD CLASS Be-U MINERALIZATION AT SPOR MOUNTAIN, UTAH, USA

Ayuso R.A., Foley N.K.

U.S. Geological Survey, Reston, Virginia, 20192 USA, rayuso@usgs.gov

The Spor Mountain Formation of Utah, U.S.A., hosts the largest deposit of volcanogenic-epithermal beryllium in the world. The Spor Mountain beryllium deposit is located in the eastern Basin and Range province, approximately 60 kilometers west of the city of Delta in Juab County, Utah. The deposit has a mineral resource estimate of 9.6 million metric tons grading 0.7 weight percent beryllium oxide (BeO) (Materion Corporation, 2016) and is the only mine of its type in the United States. Ores produced at Spor Mountain are the main reason that the U.S. has been the dominant global supplier of this commodity since the mine opened in 1969.

We report here U-Pb data for zircon and the age of rocks hosting the super-large beryllium deposit at Spor Mountain, Utah, obtained by Sensitive High-Resolution Ion Microprobe-Reverse Geometry (SHRIMP-RG). The deposit occurs in an area containing Oligocene and Eocene calderas and extensive alkalic rhyolitic ash-flow tuffs. Country rocks consist of Paleozoic limestone, dolomite, shale, and quartzite. Establishing the age of rocks hosting the beryllium deposit is critical for improving the recognition of exploration targets that may contain similar beryllium deposits.

The Spor Mountain Formation was described by Lindsey (1977). The formation consists of a lower beryllium tuff member that is overlain by the upper porphyritic Rhyolite Member (Figure). The beryllium tuff consists of fluorite-bearing, stratified, tan to pink, vitric tuffs, and tuffaceous breccias, which contain abundant clasts of carbonate rocks and minor quartzite and volcanic rocks. Bentonite and thin beds of ash-flow tuff are also present. The beryllium tuff exposed in the pits is pervasively altered to clay (represented originally by ~60% glassy matrix (Lindsey, 1977). The tuff contains locally abundant dipyramidal quartz phenocrysts. Most magmatic minerals (sanidine, plagioclase, biotite, and Fe-Ti oxides) are strongly altered (Lindsey, 1977; Foley et al., 2012).

Zircon from the crystal and lithic-rich alkaline beryllium tuff of the Spor Mountain Formation produced two populations with a predominant group yielding a weighted average $^{238}U/^{206}Pb$ age of 25.59 +0.29/-0.45 Ma (±2 sigma errors; 41 spots that form a coherent age group) and a separate younger age group at 20.84 +1.29/-0.64 Ma (16 spots). The spot analyses for each group include cores and rims. There is no evidence that younger rims systematically envelop older cores that may have been inherited from the coherent group or xenocrystic grains. The best estimate of the age of crystallization of the beryllium tuff is thus taken as 25.59 +0.29/-0.45 Ma. Younger spot analyses (not part of the coherent group) reflect Pb loss from thermal events and renewed influx of hydrothermal fluids into the beryllium tuff. Zircon from the overlying, altered, capping rhyolite yields weighted mean $^{238}U/^{206}Pb$ crystallization ages between ca. 25.1 Ma and 26.2 Ma. The fluorite- and bertrandite-rich beryllium tuff and the capping topaz-rich rhyolite of the Spor Mountain Formation thus have overlapping crystallization ages.

Apparent zircon temperatures from the beryllium tuff range from ~600 ºC to 1200 ºC and in the porphyritic rhyolite from ~525 ºC to 1000 ºC. Zircons from the beryllium tuff and rhyolite overlap in Be contents (~1 to 300 ppm). Be concentrations are uncorrelated to U-Pb dates, and contents of Hf, Ti, and most other trace element abundances and ratios. REE contents of zircon (normalized to chondritic values) are depleted in the light REE and enriched in the heavy REE and show prominent positive Ce and negative Eu anomalies. Relative enrichments in light REE have been suggested to indicate fluid-mediated alteration (Ayuso et al., 2018). Overall REE variations thus result in “V-shaped” patterns that trend toward smaller Ce positive anomalies and smaller Eu negative anomalies. V-shaped patterns are found commonly in zircons that yielded SHRIMP age data that are not part of the coherent age group. Whole rock trace element ratios of tuff and rhyolite, such as Th/U (>0.1) are typical of igneous zircons, plot in the field of continental settings (e.g., U/Yb ~ 0.8-6, Hf ~10,000-26,000 ppm), and are consistent with an origin from sources relatively enriched in Pb and generally depleted in Nb in mantle-normalized multielement diagrams.

Figure. The Spor Mountain Formation consists of two units: Massive gray volcanic rocks of the upper Rhyolite Member overlie beige-gray-pink and white tuff layers of the beryllium tuff unit. Photo showing close-up of tuffaceous layers of the main ore host, the beryllium tuff.

The apparent uniqueness of the Spor Mountain beryllium deposit reflects the interplay of an origin from alkaline (A-type) trachytic to rhyolitic magma enriched in uranium, beryllium, and fluorine and a protracted history of fractional crystallization. The magma was enriched in beryllium since its origin according to inherently high beryllium contents of zircons from both the beryllium tuff and the barren rhyolite cap (up to ~150 ppm). A key step in the evolution of the magma chamber and genesis of the mineralization is that buoyant magmas and reactive fluids produced by extensive fractionation were concentrated in apophyses at the top of an assumed magma chamber underlying the deposit. Magmatic hydrothermal fluids tapped the magma chamber, invaded the beryllium tuff starting at 25.59 Ma, reacted with the glassy matrix, removed beryllium, and precipitated bertrandite (and fluorite) at <250 ºC. Hydrothermal fluids also reacted with carbonate nodules dispersed in the tuff and precipitated fluorite, bertrandite, and uraniferous opal.

Zircon ages of the Spor Mountain Formation and apparent ages of peak deposition of Be-rich opal do not clearly correspond to any currently recognized periods of volcanic activity in the area. Thus, rocks hosting the beryllium deposit are unlikely to be cogenetic with regional volcanic rocks linked to the Mt. Laird Tuff (39 Ma), Joy Tuff (38 Ma), Drum Mountains (36 Ma), or the Dell Tuff (32 Ma). All are older than the Spor Mountain Formation, and all lie below the partially erosional and angular unconformity (as evidenced from abundant detritus of older volcanic rocks in the beryllium tuff member) that underlies the formation (Lindsey, 1982). The Spor Mountain Formation is also not cogenetic with younger alkali rhyolitic rocks from the Topaz Mountain Formation (ca. 6-7 Ma), which lie above an erosional unconformity that overlies the Spor Mountain Formation (Lindsey, 1982). Other beryllium occurrences near Spor Mountain are known in the region that highlight the extremely prospective potential for additional resources of beryllium (Lindsey, 1977). Among the most significant are related to igneous rocks in the Deep Creek Mountains, Honeycomb Hills, and Sheeprock Mountains (all within 80 km from Spor Mountain) (Burt and Sheridan, 1981 and references therein; Christiansen et al., 1983; Foley et al., 2012, 2017). New age and geochemical information is

being acquired for these occurrences. Together with Spor Mountain, they highlight the region's economic potential for beryllium.

This work was supported by the U.S. Geological Survey, Mineral Resources Program. Access and logistic support were provided by Materion Natural Resources, Utah, U.S.A.

References

Ayuso, R.A., Foley, N.K., Vazquez, J.A., Lederer, G.W, Jaskula, B.W. (2018) SHRIMP U-Pb Geochronology of zircon and geochemistry of the world-class volcanic-related beryllium deposit at Spor Mountain, Utah, USA [abs]: Resources for Future Generations, Vancouver, Canada.

Burt, D.M., and Sheridan, M.F., 1981, Model for the formation of uranium/lithophile element deposits in fluorine-rich volcanic rocks: American Association of Petroleum Geologists, Studies in Geology, v. 13, p. 99-109.

Christiansen, E.H., Burt, D.M., Sheridan, M.F., and Wilson, R.T., 1983, The petrogenesis of topaz rhyolites from the western United States: Contributions to Mineralogy and Petrology, v. 83, p. 223-236.

Foley, N.K., Hofstra, A.H., Lindsey, D.A., Seal, R.R., Jaskula, B., and Piatak, N.M., 2012, Occurrence model for volcanogenic beryllium deposits, Ch. F of Mineral deposit models for resource assessment: U.S. Geological Survey Scientific Investigations Report 2010-5070-F, 43 p.

Foley, N.K., Jaskula, B.W., Piatak, N.M., and Schulte, R.F., 2017, Beryllium, chap. E of Schulz, K.J, DeYoung, J.H., Jr., Seal, R.R., and Bradley, D.C., eds., Critical Mineral Resources of the United States—Economic and environmental geology and prospects for future supply: U.S. Geological Survey Professional Paper 1802, p. E1-E32.

Lindsey, D.A.,1977, Epithermal beryllium deposits in water-laid tuff, western Utah: Economic Geology, v. 72, p. 219-232.

Lindsey, D.A., 1982, Tertiary volcanic rocks and uranium in the Thomas Range and Northern Drum Mountains, Juab County, Utah: U.S. Geological Survey Professional Paper 1221, 71p.

Materion Corporation, 2016, Annual report—Mayfield Heights, Ohio, Materion Corporation, 98 p.

Zr-CONTAINING SILICATES IN KIMBERLITE PIPE SEITAPERÄ (KUHMO CLUSTER, FINLAND)

Azarova N.S.[1], Bovkun A.V.[1], Varlamov D.A.[2], Garanin V.K.[1]

[1]Lomonosov Moscow State University, Moscow, Russia, nadiya-azarova@mail.ru

[2]Institute of Experimental Mineralogy RAS, Chernogolovka,

The largest (6.9 ha) of diamond-containing body in Finland is pipe Seitaperä at present, which is located in the Kuhmo-Lentiira area (Eastern Finland). The body was made by orangeites (kimberlites of group II) (O'Brien, 2015). The age of rock formation was 1202±3 million years ($^{40}Ar/^{39}Ar$ phlogopite analysis) (Phillips et al., 2017).

The studied rocks are composed of phenocrysts (up to 0.5-0.8 sm) of phlogopite (8,6-10,5 wt.% FeO*, 3,1-5,8 wt.% TiO_2), less often − clinopyroxene (Mg#=81-85,8; Ca#=53,3-54,8) and completely modified olivine, immersed in a fine-grained binder mass of phlogopite, carbonate, serpentine, diopside, numerous small (up to 70-100 microns) grains of oxide minerals and Sr-containing apatite (1,3-1,4 wt.% SrO), as well as rare selections Ba-Ca-carbonate phases.

Among oxide minerals prevail: zonal perovskite, usually enriched with rare-earth elements (up to 1,2-5,1 wt.% REE_2O_3 in grain centers), and titanomagnetite (up to 15 wt.% TiO_2, 5.2 wt.% MnO), rarely zoned grains of chrome spinel. The cores of the latter contain 39.7-46.0 wt.% Cr_2O_3, and 8.4-9.7 wt.% Al_2O_3, 4,9-6,1 wt.% TiO_2, 7,4-11,6 wt.% MgO (Cr# = 74,0-77,7), boundary (rim) zones are composed by titanomagnetite. There are rare grains of Mn-containing magnesium ilmenite (6,0-6,7 wt.% MgO, and 2.3-2.5 wt.% MnO, up to 0.6 wt.% Cr_2O_3 and 4,5 wt.% Fe_2O_3).

Rare grains of Zr-silicates up to 120 μm in size were found in the bonding mass of the rock. Grains are idiomorphic, pseudohexagonal, heterogeneous in composition and in all cases partially or almost completely changed.

For pic. 1 the BSE image of one of the least modified grains of Zr-silicates containing the inclusions of perovskite and apatite of 10-15 μm size is presented.

For the main unchanged part of the grain (an. 5-6 in figure. and table.) relatively constant SiO_2 content (41.6-42.6 wt. %) and ZrO_2 (30.8-31.5 wt. %) at variable CaO contents (7.7-12 wt. %), Na_2O (1-4 wt. %), TiO_2 (0-1, 4 wt. %) and FeO_Σ (0.4-1.8 wt. %). The chemical composition of such sites and results of calculation of crystal chemical formulas testify to belonging of the mineral composing them to Ca-catapleite $(Ca,Na)_{1+x}ZrSi_3O_9 \cdot 2H_2O$.

Table 1. Composition of Zr-containing silicate (mineral diagnostics is a preliminary).

oxide	Ca-catapleite		Wadeite	Mixture of primary Ca-catapleite, Mg-hydrosilicates and Fe-containing minerals		NaCa-Zr- and K-Zr silicate			
%	**5**	**6**	**7**	**4**	**8**	**38**	**39**	**40**	**46**
SiO2	34,2	21,7	20,2	34,6	35,0	42,6	41,6	44,5	32,8
TiO2	0,7	0,9	0,7	0,5	n.d	n.d	1,4	1,0	1,8
ZrO2	32,5	44,2	51,0	30,2	31,9	30,8	31,5	32,7	45,0
Al2O3	1,0	0,7	1,1	1,2	1,0	n.d	n.d	n.d	0,7
FeO*	3,6	3,8	3,6	3,8	5,6	1,8	0,4	n.d	2,4
MnO	n.d	0,7	0,6	0,2	n.d	n.d	n.d	n.d	n.d
MgO	13,3	9,3	9,8	13,8	12,0	n.d	n.d	n.d	3,6
CaO	1,7	7,4	4,3	1,6	1,5	7,7	12,0	3,2	3,0
Ce2O3	n.d	n.d	n.d	n.d	n.d	n.d	n.d	n.d	1,2
Na2O	n.d	n.d	n.d	n.d	n.d	4,0	1,0	n.d	0,2
K2O	n.d	n.d	n.d	n.d	n.d	n.d	n.d	11,3	n.d

n.d - not detected; EN. 4-8 – grain in Fig. 1 (> 100 μm), other – grains 40-60 μm.

Figure 1. The formation of Zr-silicate in serpentine-carbonate binder weight orangeite pipe Seitaperä. The image in the back scattered electrons (figures indicate the points of analysis in table. 1).

More bright in BSE image areas (an. 7 in Fig. and table.) with blurred boundaries contain about 44.5 wt.% SiO_2 and 32.7 wt.% ZrO_2, but high in K_2O (up to 11.3 wt.%), low in CaO (up to 3.2 wt.%) and the absence of sodium. Perhaps they are wadeite $K_2ZrSi_3O_9$, while lower concentrations of K_2O and the amount of analysis may be due to underdeterminate amount of K_2O.

The changed areas along the grain edge with clear boundaries are composed by a micro grain porous aggregate of spongy appearance. Its composition (an. 4 and 8 in Fig. and table.) also characterized by a high content of ZrO_2 (31, 9-45 wt. %), stands out by the presence of varying amounts of MgO (from 4.8 to 12 wt. %), low contents of SiO_2 (a 32.8-35.0, wt. %) and CaO (1.5-3.0 wt. %). In the altered areas is increasing the content of FeO_Σ (2,4-5,6 wt.%), sometimes − Ce_2O_3 (1,2 wt.%) and TiO_2 (1.8 wt.%). It is possible that a mixture of primary Ca-catapleite, Mg-hydrosilicates and Fe-containing minerals in different proportions, represents the aggregate of the changed sites. Thus, within the described grain there are several zones with more or less similar contents of Zr and Si, but contrasting contents of Na, K, Mg and Ca.

In the sample, there are pseudohexagonal grains, composed of micrograin aggregates, similar in composition to the above-described modified areas of grain in Fig. 1, but more widely varying in contents of Zr, Si, Mg and Ca (Ah. 38-40, 46 in table.). They are probably formed because of complete replacement of earlier NaCa-Zr and K-Zr silicates.

It is known that zirconium silicates are relatively common as late-stage groundmass minerals in orangeites (Mitchell, 1995). However, compositional and paragenetic data are few for them, especially for calcium zirconium silicate. Presence of grains of a calcium zirconium silicate (Ca-catapleite?) orangeit (Group II kimberlites) Seitaperä pipe (Pipe no. 16) it was assumed earlier (O'Brien and Tuni, 1999), but the composition of the mineral in the mentioned work was not cited and the features of its association were not discussed.

The data obtained by us is the first description of the grains of zirconium silicates found in the rocks of the pipe Seitaperä, indicating their complex structure and diversity of compositions. These preliminary data require further more detailed study, including an accurate diagnosis of minerals and clarify the conditions of their formation.

References

Mitchell R.H. Kimberlites, orangeites and related rocks. Springer Science+Business Media New York, 1995

O'Brien H. Kimberlite-hosted diamonds in Finland. In: W.D. Maier, R. Lahtinen and H O'Brien. Mineral Deposits of Finland. Elsevier, 2015.P. 345-375

O'Brien H.E., Tyni M. Mineralogy and Geochemistry of Kimberlites and Related Rocks from Finland. In: J.J. Gurney, J.L. Gurney, M.D. Pascoe and S.H. Richardson (Eds.), Proceedings of the 7th International Kimberlite Conference, Cape Town. 1999. P. 625-636.

Phillips D., Zhong D., Matchan E.L. et al. A Comparison of Geochronology Methods Applied to Kimberlites and Related Rocks from the Karelian Craton, Finland // 11th International Kimberlite Conference Extended Abstract No. 11IKC-4480, 2017.

DIAMOND IN THE NEWLY DISCOVERED KIMBERLITE AND RELATED ROCKS, CENTRAL EASTERN DESERT EGYPT

***Barakat A.A.*[1]*, Kandil S.M.*[2,3]**

[1]*Sukari Gold Mines, Email <alybarakat20000@gmail.com>*

[2]*The Egyptian Mineral Resource Authority (EMRA) (Geological Survey of Egypt)*

[3]*Salah Salem Road, Abbassyia, Cairo Egypt*

Barakat et al., 2017, report kimberlite and related rocks within the Central Eastern Desert. The site occurs ~2-km south Wadi Zediun in the central part of the Eastern Desert of Egypt, between latitudes 25 36 51- 25 37 56 N and longitudes 33 53 30- 33 54 00 E. Barakat, (2018) indicates that there are seven kimberlitic pipes and main kimberlite dyke intruding the country rocks of the area. Individual one of these pipes is in the form of small tadpole. In the meantime, the whole pipes occur in the form of large tadpole, which its head in the form of wide crater (~500 m diameter) in the southwest and its tail extends northwest (Fig. 1). The site, according to Barakat, (op.cit.) has definite criteria, which candidate it of being one of the ideal sites of kimberlite and related rocks emplacement, and refers to minor phases within the rocks including moissanite and possible micro-diamond grains. According to the microscopical studies aided with backscatter imaging, the present study introduces preliminary evidence of the occurrence of micro-diamond in the studied xenoliths of the kimberlite and related rocks of the site.

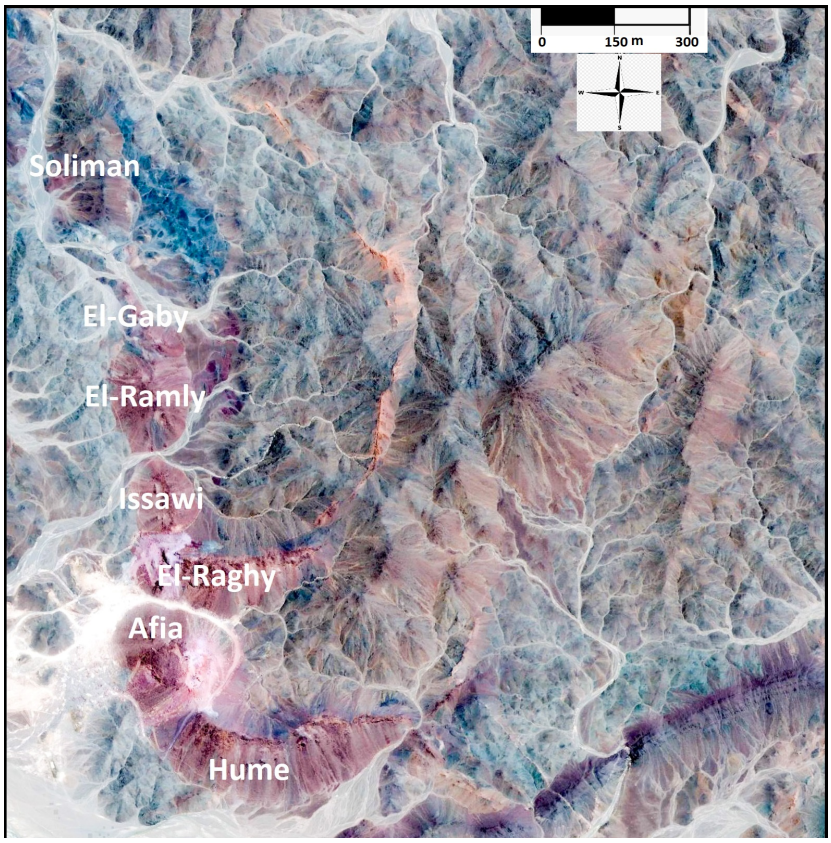

Fig. 1. Google Earth image of the site showing the main pipes.

GEOLOGICAL SETTING. The area surrounding the considered site is made up of metasediments, metavolcanics and serpentinites of Precambrian age. Francis et al., (1971) refer to the considered kimberlite and associating rock masses as carbonate veins cutting the Precambrian rocks of the site. Careful examination of the carbonate along the lateral extension of the main kimberlite pipe indicates the preservation of typical kimberlite texture indicating that the carbonate replaced ideal kimberlite rock. Despite this, there are two main features in the mentioned study worthy of interest here, i) the older age of these bodies (older than any other dykes or veins in the area as a whole) and ii)

their different trend than the other carbonates bodies. According to Barakat (op.cit.) the kimberlite and associating rocks appear via Google Earth as concentric oval shape, with the main one trending NW to attach Jebel Hadarba (the prominent topographic feature close to the site ~ 585 above sea level). Jebel Hadarba itself is a mass of serpentinite (Hathout, 1983) intruded, according to Francis, (et al. 1971) by nepheline microsyenite. The third interesting observation of Francis et al., (op cit) their referring to the nepheline microsyenite of Jebel Hadarba as elliptical mass (~500-m diameter) of dyke-like extension toward SE. This observation comes in line with our indication that the kimberlite masses extend northwest to attach Jebel Hadarab, which it needs more detailed study because it seems as kimberlitic diatreme? In the meantime, the nepheline syenite, kimberlites and carbonatites, typically occur in belts or linear arrays following the sharp Vs gradients around the cratons, and their distribution indicating the role of craton margins in channeling fluids from sublithospheric depths, (Begg, et al., 2009). In addition, Francis et al., (op.cit.) refer to lamprophyre dikes in Wadi Zeidun area, consisting of brown hornblende and plagioclase feldspar. No following studies mention these lamprophyre dykes and the bearing of their occurrence on the possibility of locating diamond within themselves (Lefebvre, et al., 2005) or their possible association of lamproites and kimberlites (Windom and Boettcher, 1980). The present study do not locate the sites of that dykes because their sites obliterated from the map and the reported lamrophyric rocks in association of the kimberlitic masses are from the observations of one of the present authors (Barakat, op.cit.).

The site occurs on the western flanks of the Arabo-Nubian Shield (~870–550 Ma ago), within or close to the suggested Paleoproterozoic–Archean age cratonic segments which occur on the edges of the Arabian-Nubian Shield (Shlevin, et al., 2009) and/or crops out in gneiss domes underneath overthrusted Pan-African island arc volcanic and volcaniclastics and associated ophiolites within the ANS itself, El-Gaby (1983). These segments may consider being the source of the detected older rocks (~0.9–3.0 Ga old) entrapped within the ANS rocks (Shlevin, et al. op. cit). In the meantime, it occurs in the heart of the newly reported East Mediterranean–Nubian diamondiferous belt (Eppelbaum, and Katz, 2012).

FIELD OCCURRENCE OF THE DIAMOND HOLDING ROCKS. Diamond has been traced within xenoliths of different rock types occurring within Afia pipe and from grey-black tuffusitic xenoliths within the silicified carbonated branches projecting from the lateral extension of El-Raghy kimberlitic pipe within the inner wall of the crater (Fig. 2). The green xenoliths are of different appearance and composition. They are fine-grained to coarse-grained. These green xenoliths acquire the general characters of lamprophyric rocks. However, the green xenoliths within the upper parts of Afia pipe are highly deformed and occur as highly sheared streaks within the holding altered rocks.

The silicified-carbonated bodies show, in some parts, parallel and intercalated macro linear strips (orbicular structures) similar to that described from carbonated kimberlite dike at Mukorob Namebia (e,g, Haggerty and Fung, 2006). Segments of these bodies hold centimeter-seized xenoliths of dull-grey fine-grained rock of different general characters than the green-rock xenoliths, which occur within the upper parts of the pipes. These xenoliths may occur as large masses of bluish-green color along the extension of these branches in the foot of the crater wall to join the main kimberlitic dyke in the western side of the crater bottom.

The green-xenoliths in the upper parts of the pipes acquire the general characters of the lamprohyric rocks as well eclogite. They consist of chlorite as alteration products of clinopyroxene with leucite, secondary quartz and calcite. Rocks of the carbonated segments show clear variations in textures and mineral constituents. They show heterogeneous appearance in thin sections under the microscope, which may indicate that they inherited the texture of a heterogeneous original rocks. The linear strips, which observed as macrostructure in the carbonated segments of the dyke can be observed in thin sections as alternate thin strips of fine-grained unresolved mineral constituents intercalated with carbonate and silica minerals stained with reddish-iron oxides. Some of the mineral constituents occur in concentric shape as well as irregular, indicating replacement of previously occurred protolith xenoliths. Relics of these protliths can be traced in the studied rocks as well defined material from the other constituents. These protoliths are of various mineral constituents. Some of these protoliths may represent fine-grained unresolved mineral constituents, which are partially or

completely replaced by fine-grained secondary quartz and invaded by secondary calcite veinlets. The feature worthy of interest in this regards is the occurrence of irregular zoned isoptropic material of majorite composition. The outer outlines of these objects are intercalated with nearly obliterated symplectic structure.

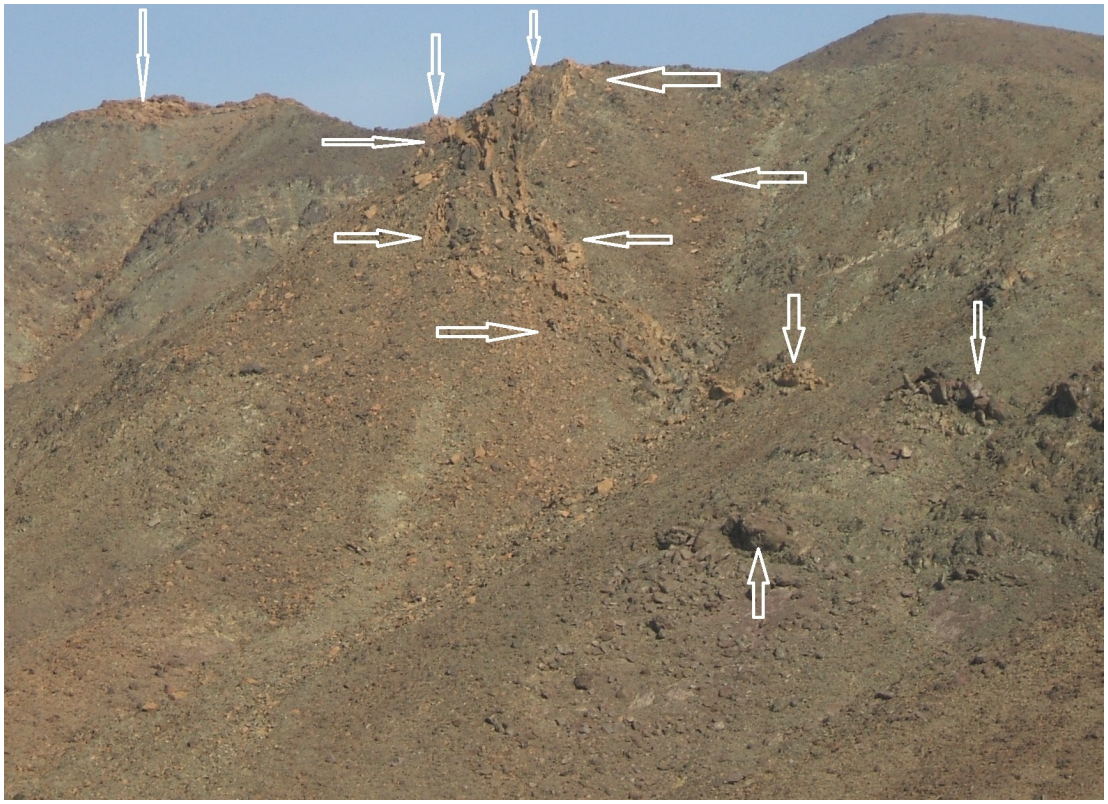

Fig. 2. Field image of the silicified carbonated branches projecting from the lateral extension of El-Raghy kimberlitic pipe within the inner wall of the crater.

The tuffusitic masses consist of very fine-grained greenish chamosite, serpentine (antigorite) which is slightly anisotropic and nearly isotropic, calcite, quartz and patches of crypto-microcrystalline silica. The chamosite is intercalated with the quartz and the antigorite. Glassy veinlets occur in the groundmass. They are slightly devitrified to antigorite and other unidentified dark brownish material. Relics of nearly steatitized olivine may occur. No obvious olivine grains have been detected. However, authors e.g., Skinner and Marsh (2004) refer to antigorite crystallization from devitrivication of quenched kimberlite glass. Skinner and Clement (1979) indicate that primary calcite and antigorite constitute at least 50% of the groundmass of hypabassal facies kimberlite (HFK). Secondary calcite and quartz occur as veinlets crosscutting the whole rock. This is normal because the studied rock has been recovered from carbonated segments of the dyke.

THE DETECTED DIAMOND. Diamonds occurs in two different forms, i) micro grains ~20 micron and ii) crypto crystalline aggregates. The micro grains (~20-50 microns) of diamond show different habits and colors. Few of these grains are colorless and transparent, while most of the micro grains are of translucent and coloured. The majority of the diamond micro grains are grey-black in colour. The ambiguous feature worthy of interest in this concern, the reddish diamond micro grains, which occur within the crypto-crystalline red aggregates, which traced as small veinlets or as individual patches. The detected micro grains of diamond have different shapes, from irregular to perfect octahedron (Fig. 3). They occur as individual grain or as aggregates of grains (Fig. 4). Some of the traced transparent grain show halos around them under plain polarized reflected light and complex halo under cross polar. This feature indicate that they undergo deformation. Inclusions are common feature in the traced diamonds. This reflects the relatively appreciable concentration of the other elements, shown in the EDX analyses of these diamond grains.

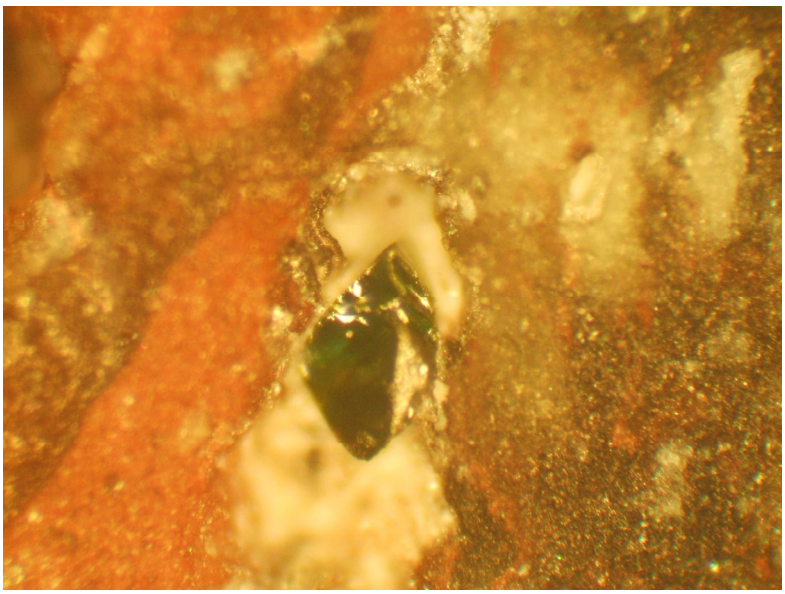

Fig. 3. Green octahedron grain of diamond (reflected PPL, F.W. 0.15 mm).

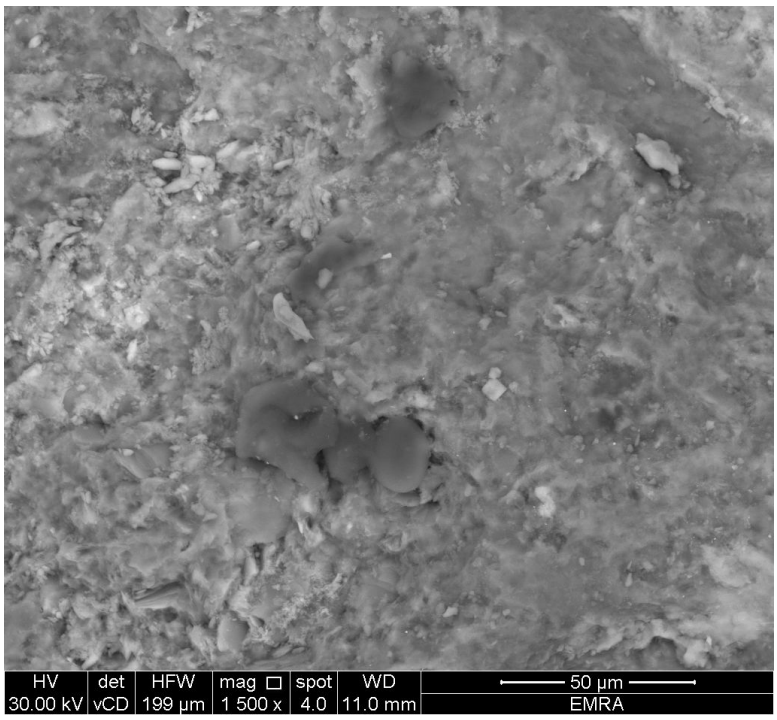

Fig. 4. SEM backscatter image of individual diamond grain or aggregates.

Abnormally sparkling calcite grains in white light occur in some of the studied samples. Microscopical investigation of extracted millimeter-seized grains indicates the presence of tiny grains of diamonds along the cleavage plains or randomly distributed. The population of these grains differs from grain to other and the higher population of diamond micrograins links with the sparkling strength. In the meantime, examination of relatively large grains (~ 2-mm diameter) of calcite in thin sections by the transmitted light confirms the occurrence of micro grains of diamond.

CONCLUSION. Reporting the economic value of the newly discovered diamond in the site depends on the detailed studies, which will carry on the site. This discovery, which lies in the heart of the newly reported East Mediterranean–Nubian diamondiferous belt (Eppelbaum, and Katz, op. cit.), may lead to the discovery of macro diamonds, which will shed light on the historical writings, which refer to the utilization of diamonds from the Eastern Desert as well as Upper Egypt (Barakat and Kandil, 2018). In the meantime, the discovery of diamond in the sand of the area northwest Aswan, Upper Egypt (Kaminsky, 2014) may connects with the southern extension of the diamondiferous belt.

In the meantime, it will reopen the discussion on the hard material used by Ancient Egyptians in wittings on the hard rocks like the breccia Verdi and other hard stones.

References

Barakat, A.A. Kandil, S. MR. The sources of the recently discovered diamonds in Egypt. 15 th Arab International Mineral Resources Conference, Cairo 26-28 November 2018.

Barakat, A.A., Soliman, Kh. A., Basal, A.K., Kandel, S.MR. Abdesalam, K. A preliminary report on the occurrence of kimberlitic and related rocks in the Central Eastern Desert of Egypt. 9th International Conference on the Geology of Africa, 7–9 November, 2017, Assiut University, Egypt.

Barakat, A.A. New Insights Into the newly discovered kimberlite and related rocks in the Central Eastern Desert of Egypt. Magmatism of the earth and related strategic minerals. Proceedings of XXXV International Conference, Moscow, 3-7 September 2018, pp.36-42.

Begg, G.C., Griffin, W.L., Natapov, L.M., O'Reilly, S. Y., Grand, S., O'Neill, C. J., Hronsky, J.M.A, Poudjom Djomani, Y., Deen, T. Bowden, P. The lithospheric architecture of Africa: Seismic tomography, mantle petrology and tectonic evolution. Geosphere, 2009, Vol. 5, p. 23-50.

El-Gaby, S. Architecture of the Egyptian basement complex. Proceedings of 5th International Conference on Basement Tectonics, Edited by Riad, S. and Baars, D. L. Cairo University, Cairo, Egypt, 1983, pp. 1-8.

Eppelbaum, L.V. and Katz, Y.I. Mineral deposits in Israel: A contemporary view. Editors Ya□ari, A. and Zahavi. Israel: Social, Economic and Political Developments, Nova Science Publishers, N.Y., USA, 2012, pp. 1-41.

Francis, M.H., Qusa, M.E., Abd El Naby, A. and Phillips, P.W. The Geology of Wadi Zeidun Area. Unpublished Report, Egyptian Geological Survey and Mining Authority, Cairo, 1971, pp. 34.

Haggerty, S.E. Fung, A. Orbicular oxides in carbonatitic kimbelites. American Mineralogist, 2006, Vol. 91, p. 1461.1472.

Hathout, M.H. Rare-earth and other trace-element geochemistry of some ultramafic rocks from the central Eastern Desert, Egypt. Chemical Geolology, 1983. Vol. 39, p. 65-80.

Kaminsky, F. Arabian diamonds: From North Africa to the Arabian Peninsula. Prospectors and Developers Association of Canada Toronto, March 3, 2014.

Lefebvre, N. Kopylova, M., Kivi, K. Archean calc-alkaline lamprophyres of Wawa, Ontario, Canada: Unconventional diamondiferous volcaniclastic rocks. Precambrian Research, 2005, Vol. 138, p. 57–87

Shlevin, Y.B., Katzir, Y., Whitehouse, M.J. Kleinhanns, I.C. Contribution of pre Pan-African crust to formation of the Arabian Nubian Shield: New secondary ionization mass spectrometry U-Pb and O studies of zircon. Geology, 2009, Vol. 37 (10), p. 899–902.

Skinner, E.M.W., Clement, C. Mineralogical classification of southern African kimberlites. Proceeding of 2nd International. Kimberlites Conference. Editors, Boyd, F.R., Meyer, H.O.A. Kimberlites, Diatremes and Diamonds: Their Geology, Petrology and Geochemistry. Transactions of the Geological Society of South Africa, Marshalltown, South Africa, 1979, pp. 129-139.

Skinner, E.M.W., Marsh, J.S. Distinct kimberlite pipe classes with contrasting eruption processes. Lithos, 2004, Vol. 76, p. 183-200

Windom, K.E. Boettcher, A.L. Mantle Metasomatism and the Kimberlite-Lamprophyre Association: Evidence from an Eclogite Nodule from Roberts Victor Mine, South Africa. Journal of Geology, 1980, Vol. 88 (6), p. 705-712.

ROLE OF SALT-CARBONATE CONTAMINATION OF MANTLE MAGMAS IN FORMATION OF ALKALINE CARBONATITE COMPLEXES

Belenitskaya G.A.

Russian Geological Research Institute (VSEGEI), St. Petersburg, Russia, gab_2212@ mail.ru

Presented peviously results of a comparative analysis of regional and global material characterizing correlations in matter and spatial-temporal correlations between natural salts and alkaline igneous complexes revealed ***geological prerequisites*** for discussing the issue of the role of salts in the formation of alkaline magma, with special regard to them as a source of alkali metals and volatiles (Belenitskaya, 2017, 2018a, 2018b;). The most significant prerequisites are as follows: 1) similarity between the sets of specific and typomorphic components and microcomponents in the composition of salt (***halophilic***) and alkaline (***foidaphilic***, according to (Lazarenkov, 1988)) complexes (Na, K, Cl, as well as Mg, Ca, SO_4, CO_3 and a wide range of microcomponents – Rb, Br, B, Cs, Sr, F, etc.), and in a wider scope – similarity between salt-carbonate and alkali-carbonatite parageneses of their formation; 2) quite common proximity of these complexes, including potassic varieties of salt and alkali rocks, when their temporal correlations are regular; 3) similarity between a number of important regularities in their location (geotectonic position, stratigraphic distribution, inherited cyclic location, etc.). General results of the previous studies as well as the subsequent ones are presented below.

Common occurrence of salt-bearing and alkaline complexes provided a basis for distinguishing ***salt-alkaline associations***, as well as ***salt-alkaline provinces and belts*** (Belenitskaya, 2017, 2018a). The associations include: alkaline igneous complexes and buried in their substrate more ancient salts, forming the main dominant pair; "young" salt strata subsynchronous to magmatism, often associated with the recycling of more ancient salts; as well as more ancient alkaline and salt strata. Depending on the geotectonic settings of the location of salt-alkaline formations, their three major ***tectonic types*** can be distinguished: 1) fold-nappe, 2) rift and 3) activated passive margins. The fold-nappe type, which is the widest spread, conventionally includes folded areas of different age (with the adjacent cover-overthrust structures overlapping the platforms' margins and middle massifs), in particular those which were formed in the basement of young and ancient platforms, including shields.

Standard alkaline-salt provinces of each tectonic type have been identified: the Italian (fold-nappe type), the Upper Rhine (rift type) and the Northwest-African (passive margins type) ones. Their most significant tectonic, kinematic, lithological and petrological features have been described (Alkaline..., 1974; Borodin, 1974; Kogarko, 1977; Kogarko, Asavin, 2009; Mazarovich et al., 1990; Peccerillo, Martinotti, 2006; Purtov et al., 2002; Ziegler et al., 1996; et al.). Spatial-temporal correlations between alkaline igneous complexes and the salts occurring in their substrate in the course of their formation, as well as the "young" salt strata of supposedly regeneration nature, subsynchronous to alkaline magmatism, have been reconstructed.

Analogues of standard associations can be identified with high confidence in ***neogeodynamic*** alkaline provinces, where alkaline complexes are often accompanied by more ancient salts in the geostructures of all three tectonic types. In ***paleogeodynamic*** provinces (especially the Precambrian ones), common occurrence of alkaline complexes and more ancient than them salts is identified less confidently. The main reason is that the state of the surviving salts is not good enough. When interpreting such common occurrences, it is necessary to comprehensively examine the alkali-salt associations as a whole, taking into consideration all features, and to compare them with the standard sites. Effective are regional paleotectonic, paleogeographic and kinematic reconstructions whose main objective is to reconstruct the original distribution boundaries of salt-bearing complexes and especially their location patterns for the period of manifestation of alkaline magmatism.

The geological-genetic model of "halo-contamination of magma" and the role of components of halophilic complexes in alkaline magmatism. The analysis findings showed that salt-bearing rocks commonly occur in the way of ascending deep-seated magmas associated with tectomagmatic activation and this is a fairly regular geological phenomenon. Salt-bearing levels intersected by hot aluminosilicate magma are favorable for its injective intrusion entailing the

formation of intermediate chambers — centers (nodes), where magma assimilates salt-bearing (carbonate-sulphate-salt) complexes and being contaminated by their components, interacts with them inducing the formation of alkaline rocks. In the course of ***chemical interaction*** between hot magmas and assimilated components of halophilic complexes, various non-equilibrium salt-melt systems are formed, greatly enriched (oversaturated) with alkali metals and volatiles.

Under such conditions, salts and their paragenous macro- and microcomponents of salt-bearing strata can be a rich source of sodium and potassium, as well as various volatiles can provide characteristic features of alkaline rocks formation. Contributions of these very components to alkaline magmatism are usually discussed in Petrology works (Aiuppa et al., 2009; Kogarko, 1977; Kogarko, Ryabchikov, 1978; Purtov et al., 2002; et al.), but with no regard for natural salts. In accordance with the dominant influence on the processes of alkaline petrogenesis, a wide range of halophilic components located in salt-bearing complexes can be divided into two groups: 1) matter ("donor") ones – Na, K, etc. (major rock-forming salt cations) and a number of small and microcomponents; 2) initiating and catalytic, mostly volatile ones – CO_2, SO_3, Cl, F, etc. (in the composition of salt anions and paragenous sulfate-carbonate rocks). Most components of halophilic complexes perform both functions. High portion of both alkali metals and volatile components in salt-bearing complexes influence the compositional characteristics of alkaline igneous rocks and hydrothermal-metasomatic formations accompanying them, and also their structural, textural and spatial features, including common occurrence of agpaitic structures, pegmatoid formations, as well as rock morphology and spatial relationships. The predominant geochemical type of salt strata (halitite or potassium-bearing) has influence on the composition of alkaline complexes that are being formed, including the type of alkalinity — mainly sodium or sodium-potassium. Thus, high portion of a number of halophilic components in salt-bearing complexes can be a rich source of both matter and agents initiating many processes, providing for a variety of the most important specific features of alkaline magmatic and associated with them metasomatic bodies. Many macro- and micro-specific features of the composition, structure, and location of alkaline complexes, including those recognized for igneous rocks as unusual and even unique, receive a satisfactory explanation.

Signs of the participation of salt-bearing complexes' components in alkaline magmatism. The concrete matter, structural and morphological features of alkaline igneous rocks can prove that components of salt-bearing complexes do participate in alkaline magmatism and reflect it (Aiuppa et al., 2009; Alkaline..., 1974; Borodin, 1974; Carbonatites, 1969; Faure, 1989; Kogarko, 1977; Kogarko, Ryabchikov, 1978; Lazarenkov, 1988; Marakushev et al., 1997; Pokrovsky, 2000; Purtov et al., 2002; Safonov et al., 2007; and many oths). The most characteristic of these features are: significant enrichment of many varieties of alkaline rock with chlorine, sulfate ion, carbonate ion, in addition to sodium and potassium, common occurrence and extreme diversity of minerals containing these ions; frequent contrast changes in the chemical and mineral composition of alkaline rocks; proximity of distributive provinces of alkaline potassium complexes and potassium salts; their enrichment with Br, Rb, Cs; identification of Cl, Br in solid and liquid inclusions in alkaline rocks, in volcanic gases; presence of salts and sulfur in volcanic emissions and craters; observable variations in isotope indexes of C, O, Sr, etc.

Thus, considering the geological data as a whole one can reasonably suggest that salts are likely to participate in alkaline magmatism and accept the ideas, which were put forward, as a draft version of the geological model ***"halo-contamination of magma"*** as a notable process of alkaline magma genesis.

An important aspect and consequence of this model is that magma is very likely to ***assimilate*** not only salts, but also ***their paragenous rocks***. This is particularly true for carbonates (primarily dolomites), anhydrites and high carbon deposits, often ore-bearing ones. Their paragenesis with salts is very stable, and their survival potential in the course of tectonic and kinematic transformations of salt-bearing complexes is significantly higher than that of salts. (Phosphate-bearing deposits and ferruginous quartzites are also important macrocomponents of

many sequences most typical for early Precambrian sections (Salop, 1982; et al.)). So, involvement of salts in their interaction with magma is reasonably predictable.

It is known that alkaline magmatic complexes are commonly accompanied by alkaline metasomatite, pegmatite, pegmatoid, hydrothermalite and often carbonatite areas, which commonly occur at the front of the ascending fluid/melt flows (Alkaline ..., 1974; Borodin, 1974; Frolov et al., 2003; et al.). Together, they form large-scale, multilevels magmatogenic-metasomatic ***alkaline-carbonatite systems*** overlying the deeper relatively "pure" derivatives from mantle magmas. The major macro-components of these systems are: alkaline igneous complexes as such, K- and Na-type alkaline metasomatites, pegmatite rocks, alkaline volcanites of explosive type, carbonatites (calcium, magnesium, sodium) and fluidogenic weathering crusts.

There are reasons for comparing and joint consideration of two larger ***alkaline (foidaphilic) and salt (halophilic) macroassociations***. One of them are "hot" magmatogenic-metasomatic alkaline-carbonatite; the others are "cold" injection-sedimentary salt-carbonate. The first are represented by the magmatogenic-metasomatic parageneses of macro-components of alkaline, sodium and potassium rocks with calcium and dolomite carbonatites; the second are represented by injection-sedimentary parageneses of halitite and potassium salts with dolomite and limestone. For the compared parageneses, the similarity of geochemical varieties of macrocomponents is characteristic. For natural salts and alkaline rocks they are sodium and potassium, for sedimentary carbonates and carbonatites they are calcium, mainly magnesium, less often sodium (calcite, dolomite, soda). All this can be a justification for discussing the issue of whether genetic relationships between salt-carbonate (sedimentary and injection-sedimentary) and alkaline-carbonatite (magmatogenic-metasomatic) parageneses are likely to exist, and whether halophilic (salt-carbonate) parageneses are likely to contribute to the formation of magmatogenic-metasomatic macro-parageneses of foidaphilic (alkaline-carbonatite) type.

Experimental studies of the interaction between aluminosilicate melts and natural salts as well as highly concentrated brines are still fairly limited, but the available data (For ex., A.A. Marakushev, V.G. Butvina, A.R. Kotelnikov, I.F. Kravchuk, J.A. Litvin, L.L. Perchuk, V.K. Purtov, O.G. Safonov, N.I. Suk, V.G. Senin, V.Yu. Chevychelov, etc.) substantiate the geological model under consideration in many aspects.

Comparison of the proposed model with those discussed in the literature shows that it has something in common with the widely known concepts of ***magma assimilating carbonate rocks*** (Alkaline..., 1974; Borodin, 1974; Rittmann, 1962; et al.), but "supplemented" with the data on the sections intersected by magma as salt-bearing ones (although, at present they are often only residual-carbonate). Many facts suggest that it is the joint involvement of the components of stable carbonate-sulphate-salt sedimentary parageneses in the assimilation by magma that to a large extent determines the outcome of the interaction processes between them. And their comprehensive analysis is a promising strand of further research. Unlike the model of A. Hofmann (Hofmann, 1997), which suggests ***mantle recycling*** of the oceanic crust material (and the overlying oceanic sediments), the proposed model is focused on ***crustal (cover-crustal) recycling, with magmatism involving salt-bearing (carbonate-sulphate-salt) components*** (not typical of the oceanic crust).

The model under consideration is not opposed to the existing ideas; it does not deny the possibility that highly alkaline magmas are produced already in the mantle, nor does it deny the involvement of other mechanism which increase alkaline in the course of magma evolution. The occurrence of different alkaline magma geneses as well as the presence (and even combination) of alkaline rocks of different genesis, dependent on different geological factors, is highly probable. We consider their study to be one of further research objectives.

One of the ***advantages*** of the proposed "halo-contamination of magma" model is that salt-bearing (and carbonate-salt-bearing) complexes are large-scale and localized sources of alkaline and volatile components. The portion of these components in any mantle supply is limited not only by their concentrations in the composition of fluids, but also by the possible total mass of the supplying fluids themselves, even with regard to their relatively long supply time. Moreover, the

considered model provides an opportunity to discuss the processes of salt contamination of magma as an important factor of fractionation, it also reveals its new mechanisms and why it takes place. The model offers an adequate explanation as to why K- and Na- type alkaline complexes occur separately, the inconsistency in their accumulation. Many specific and even "incomprehensible" features of the composition and structure of alkaline rocks that have been repeatedly noted by researchers receive a new interpretation.

Prognostic capabilities of the model can be used in studies of both alkaline and salt-bearing complexes. Salt-bearing manifestations in sections in the areas of present or past tectonic and magmatic activation can be a prerequisite for the evolution of alkaline magmatism in them, whereas the distribution of alkaline complexes can be responsible for the presence of buried salts. Occurrence of *ancient (premagmatic*) buried salts (at present there are often their relics only), widespread deep down the sections is the most important prerequisite for the evolution of alkaline magmatism. An important indirect indicator is the presence of *"young"* (syn-and post-magmatic) salts of regenerative nature, which are not involved in alkaline magmatism. "Young" salts and alkaline complexes are considered to be different kinds of derivatives from the ancient (parent) salts: the magmatogenic "hot" and injection-sedimentary "cold" ones, respectively. They have common roots (buried more ancient salts) and a common control (tectonic and magmatic activity). In specific regions, zones of intersection between the areas of ascending mantle magma intrusions and the levels of more ancient salt-bearing complexes are promising for the formation of alkaline bodies. It is expected that the proposed model will help to draw more serious attention to studying salt-bearing sections including studies of highly alkaline hydrothermal, metasomatic and other endogenous processes, which are fairly often ore-bearing. Analysis of salt contamination of magmas processes and interaction between them might be a clue to understanding the nature of these formations and discovering why they are ore-bearing.

The work was supported by the Ministry of Natural Resources of the Russian Federation and the Russian Foundation for Basic Research (projects 10-05-00555-a, 12-05-00513-D-c, 16-15-20048-D-c).

References

Aiuppa A., Baker D.R., Webster J. (2009) Halogenes in Volcanic Systems and Their Environmental Impacts. Special Issue. Chemical Geology. 263 (1-4). 163 p.

Alkaline rocks (1974) Ed. H. Serensen. John Wiley and Son. New York. 400 p.

Belenitskaya G.A. (2017) Salt in the Earth's crust: distribution and kinematic history. Litosfera, 17(3), 5-28.

Belenitskaya G.A. (2018a) On the participation of natural salts in alkaline magmatism. Article 1. Natural salt-alkaline associations. Litosfera, 18(2), 153-176. DOI: 10.24930/1681-9004-2018-18-2-153-176.

Belenitskaya G. (2018b) Salt Systems of the Earth*:* Distribution, Tectonic and Kinematic History, Salt-Naphthids Interrelations, Discharge Foci*,* Recycling. Wiley and Son. 714 p.

Borodin L.S. (Ed.) (1974) Major provinces and formations of alkaline rocks. Moscow: Science. 376 p.

Carbonatites (1969) Ed. O. Tuttle and J. Gittins. Trans. from English. Moscow: Mir. 487 p.

Faure G. (1986) Principles of isotope geology. 2nd ed.New York: Wiley. 589 p.

Frolov A.A., Tolstov A.V., Belov S.V. (2003) Carbonatite deposits of Russia. Moscow, NIA-Priroda Publ., 494 p.

Hofmann A.W. (1997) Mantle geochemistry: the message from oceanic volcanism. Nature. 385, pp. 219-229.

Kogarko L.N. (1977) Problems of agpaitic magma genesis. Moscow: Science. 294 p.

Kogarko L.N., Asavin A.M. (2009) Potassium magmatism of the World's ocean (case study of the Atlantic). Geochemistry international (9), pp. 899-909.

Kogarko L.N., Ryabchikov I.D. (1978) Volatiles in magmatic processes. Geochemistry (9), pp. 1293-1321. (In Russian).

Lazarenkov V.G. (1988) Formation analysis of alkaline rocks of continents and oceans. Leningrad: Nedra. 236 p.

Marakushev A.A., Suk N.I., Novikov M.P. (1997) Chloride extraction of metals and problem of their migration from magmatic chambers. DAN RAS. 352 (1), pp. 83-86.

Mazarovich A.O., Frikh-Khar D.I., Kogarko L.N. (1990) Tectonics and magmatism of Cape Verde Islands. *Trudy GIN*. (451). Moscow: Science. 246 p.

Peccerillo A., Martinotti G. (2006) TheWestern Mediterranean lamproitic magmatism: origin and geodynamic significance. Terra Nova, 18, pp. 109–117.

Pokrovsky B.G. (2000) Crustal contamination of mantle magmas on evidence of isotope geochemistry. Moscow: Science: MAIK "Science: Interperiodica". 225 p.

Purtov V.K., Anfilogov V.N., Egorova L.G. (2002) Interaction of basalt with chloride solutions and mechanism of acid melt formation. Geochemistry international, (10), pp. 1084-1097.

Rittmann A. (1962) Volcanoes and Their Activity. New York: Interscience (Wiley). 305 p.

Safonov O.G., Perchuk L.L., Litvin Yu.A. (2007) Interaction of Diopside and Jadeite with Potassium Chloride at 5 Gpa. DAN RAS. 415 (5), pp. 789–793.

Salop L.I. (1982) Geological evolution of the Earth during the Precambrian. Leningrad, Nedra Publ., 343 p.

Ziegler P.A., Horvath F. (Eds). (1996) Peri-Tethys. Memoir 2: Structure and Prospects of Alpine Basins and Forelands. Mem. Mus. Natn. Hist. nat. Paris. 170. 511 p.

CRUST–MANTLE INTERACTION AND THE FORMATION OF HYDROUS PHASES IN THE UPPERMOST LOWER MANTLE (EXPERIMENTS AT 24 GPa AND 1400°C)

***Bobrov A.V.*[1,2,3], *Bendeliani A.A.*[1,2], *Bindi L.*[4], *Irifune T.*[5]**

[1]*Moscow State University, Moscow, Russia, archi@geol.msu.ru*

[2]*Vernadsky Institute of Geochemistry and Analytical Chemistry RAS, Moscow, Russia*

[3]*Korzhinsky Institute of Experimental Mineralogy, Chernogolovka, Russia*

[4]*Università di Firenze, Florence, Italy*

[5]*Geodynamics Research Center, Ehime University, Matsuyama, Japan*

The modern heterogeneities in the Earth's mantle are mostly provided by subducting slabs, which can drag down material of oceanic crust, terrigenous sediments, and altered basalt to various mantle depths (Stern, 2002). As is evident from the experimental data (Poli et al., 2009; Wu et al., 2009; Brey et al., 2015), hydrous and CO_2-bearing sediments (e.g. pelites) can be transported without melting to depths greater than 300 km, i.e., to the lowermost upper mantle, transition zone, and lower mantle. From the geochemical point, this process may be an important mechanism for recycling of volatiles and incompatible elements into the mantle and for the formation of metasomatizing fluids and melts. Because of this, subsolidus transformations and melting of hydrous and carbonated pelites at mantle pressures have been a focus of a number of experimental studies. Most of the runs have been performed at pressures up to 12 GPa (Bulatov et al., 2014; Brey et al., 2015), whereas the experimental data on the behavior of the crustal material under the lower-mantle conditions is rather limited being restricted to the simplified model systems (e.g., Kakizawa et al., 2018).

It is known that subduction at mantle temperatures and pressures upon interaction of mantle peridotite and subducted crustal material (GLOSS) may result in the formation of melts enriched in Na, K, Al, Ti, REEs, and other elements, which may be parental for many deep-seated rocks. In addition, participation of the crustal material may affect significantly on the major solid-state reactions under the conditions of the Earth's mantle. Study of phase transformations upon partial melting of the crust-mantle material under the conditions of the uppermost lower mantle is an important and actual problem.

The main objective of our research is experimental study of the interaction between the model sediment GLOSS (Global Ocean Subducting Sediment) (Plank, Langmuir, 1998) and peridotite (with the composition of garnet lherzolite and weight proportions of $Ol_{60}Opx_{16}Cpx_{12}Grt_{12}$). Experiments were also focused on the study of partitioning of such elements as Al, Cr, Na, Ti, and others between the GLOSS and peridotite zones of the samples. The experiments were performed under the subsolidus conditions, at a pressure of 24 GPa and temperature of 1400°C using a 3000-t Kawai-type multi-anvil high-pressure apparatus installed at the Geodynamics Research Center, Ehime University (Matsuyama, Japan). To model the crust–mantle interaction, the starting materials were loaded into Re ampoule in 1:1 weight proportion with peridotite in the hot zone of an ampoule. Temperature during the experiment was controlled by a $W_{97}Re_3$-$W_{75}Re_{25}$ thermocouple, 0.1 mm in diameter. The pressure was calibrated at room temperature using the semiconductor-metal transitions of Bi, ZnS, and GaAs (Irifune et al., 2004). The effect of temperature on pressure was further corrected using the α-β and β-γ phase transitions of olivine (Katsura, Ito 1989). The duration of run was 4 h.

The sample after run demonstrate clear zoned structure with the peridotite, GLOSS, and intermediate zones. Bridgmanite is characterized by a strong predomination in GLOSS and peridotite zones and is almost absent in an intermediate zone. In both zones, this mineral associates with ferropericlase, $CaSiO_3$-perovskite, and minor Mg-rich carbonate. Bridgmanite shows wide compositional variations with typomorphic features in each zone (Table 1). Bridgmanite from the GLOSS zone is characterized by the higher concentrations of Al_2O_3 (up to 8 wt %) and presence of titanium (~0.7 wt % TiO_2). Bridgmanite from the peridotite zone is Cr-rich (>1 wt % Cr_2O_3), whereas the concentration of Al_2O_3 does not exceed 5 wt %. This fact indicates that bridgmanite may inherit the minor-element composition of a protolith, so that its composition may be applied for subdivision of associations of inclusions in lower-mantle diamonds into the UHP 'peridotitic' and 'eclogitic' types (Kaminsky, 2012).

Table 1. Composition of the phases produced by the GLOSS–peridotite interaction at 24 GPa and 1400°C.

Phase	*Brd* (pd)	*Brd* (GLOSS)	*SuB* (RZ)	*CaPrv* (pd)	*Phase Egg* (RZ)
SiO_2	51.82	48.75	45.86	54.69	14
TiO_2	0.19	0.54		0.25	0.19
Al_2O_3	3.87	7.92	17.43	0.12	55.42
FeO	10.63	9.48	2.36	0.7	5.15
MgO	32.34	32.8	19.85	0.83	7.66
CaO	0.08	0.06		42.12	-
Cr_2O_3	0.79	-	0.49	-	0.28
Total	99.72	99.55	85.99	98.71	82.7

Detailed study of the samples was carried out at the Laboratory of Local Methods of Matter Study, Geological Faculty, Moscow State University (Moscow), on a Jeol JSM-6480LV scanning electron microscope (Japan) equipped with an INCA Energy-350 energy-dispersive spectrometer and an INCA Wave-500 wavelength diffraction spectrometer (Oxford Instrument Ltd., United Kingdom). BSE images were obtained at an accelerating voltage of 15 kV. Quantitative microanalysis was performed by individual programs for optimization and standardization of the profiles of analyzed elements at an accelerating voltage of ~15 kV and a beam current of ~15 nA. The size of the analytical spot was ~2 μm.

The interaction zone is composed of Al-rich superhydrous phase B, Mg-rich phase Egg (Table 1), and minor carbonate. According to the single-crystal XRD data, superhydrous phase B has the following orthorhombic unit-cell parameters: a = 4.840(1), b = 13.841(7), and c = 9.875(3) Å. This phase is formed via the mechanism $2Mg^{2+} + Si^{4+} \rightarrow 2Al^{3+} + 2H^{+} + V_{Mg}$, which stimulates increase in both Al_2O_3 (up to 30 wt %) and H_2O (>10 wt %).

Phase Egg (Table 1) has a simplified formula of $Al_xMg_{1-x}SiO_3(OH)_x(H_2O)_{1-x}$, where x = 0.65. By means of high-quality single-crystal X-ray diffraction and FTIR data, we demonstrate that there exists a solid solution between $AlSiO_3OH$ and a new hypothetical $MgSiO_3{\cdot}H_2O$ endmember, according to the reaction $Mg + H_2O \Leftrightarrow Al + OH^-$. Beside the fact that $MgSiO_3{\cdot}H_2O$ is a polymorph of phase H ($MgSiO_4H_2$), it represents the first dense hydrous magnesium silicate having molecular water, which may be delivered from the mantle transition zone to the Earth's lower mantle.

As is evident from our study, the formation of Al-rich hydrous phases proceeds via the peridotite-GLOSS interaction. Although the bulk Al content in the GLOSS part of the sample is high (11.91 wt % Al_2O_3), bridgmantite in the GLOSS zone is Al-depleted, because high-Al bridgmanite is not stable under the hydrous conditions (Ohira et al., 2014) and decomposes to form high-Al hydrous phases in the reaction zone.

The results of our research, as well as the data of abovementioned studies, show that the oceanic crust subducted into the mantle could deliver significant contents of water to a depth greater than 300 km. The stability of hydrous phases at the base of the transition zone and in the uppermost lower mantle is questioned; however, recent studies (e.g., Kakizawa et al. 2018) showed that water could be transported to the lower mantle by superhydrous phase B and D in the cold slab. Their stability expands to higher temperatures with incorporation of Al_2O_3. Phase Egg (Eggelton et al. 1979) is stable in the transition zone and in the lower mantle as well, and its discovery as an inclusion in diamond (Wirth et al. 2007) provides direct mineralogical support for existence of water in the transition zone and uppermost lower mantle.

This work was supported by the Russian Science Foundation, project no. 17-17-01169.

References

Brey G.P., Girnis A.V., Bulatov V.K., Höfer H.E., Gerdes A., Woodland·A.B. Reduced sediment melting at 7.5–12 GPa: phase relations, geochemical signals and diamond nucleation // Contributions to Mineralogy and Petrology. 2015. Vol. 170. No. 18.

Bulatov V.K., Brey G.P., Girnis A.V., Gerdes A., Höfer H.E. Carbonated sediment–peridotite interaction and melting at 7.5–12 GPa // Lithos. 2014. Vol. 200–201. P. 368–385.

Eggelton R.A., Boland N.J., Ringwood A.E. High pressure synthesis of a new aluminum silicate: $Al_5Si_5O_{17}(OH)$ // Geochemical Journal. 1979. Vol. 12. P. 191–194.

Irifune, T., Kurio, A., Sakamoto, S., Inoue, T., Sumiya. H., and Funakoshi, K. Formation of pure polycrystalline diamond by direct conversion of graphite at high pressure and high temperature // Physics of the Earth and Planetary Interiors. 2004. Vol. 143-144. P. 593–600.

Kakizawa S., Inoue T., Nakano H., Kuroda M., Sakamoto N., Yurimoto H. Stability of Al-bearing superhydrous phase B at the mantle transition zone and the uppermost lower mantle // American Mineralogist. 2018. Vol. 103. P. 1121–1127.

Kaminsky F. Mineralogy of the lower mantle: a review of super-deep mineral inclusions in diamond // Earth-Science Reviews. 2012. Vol. 110. P. 127–147.

Katsura T., Ito E. The system Mg_2SiO_4-Fe_2SiO_4 at high pressure and temperatures: precise determination of stabilities of olivine, modified spinel, and spinel // Journal of Geophysical Research. 1989. Vol. 94. P. 15663–15670.

Ohira I., Ohtani E., Sakai T., Miyahara M., Hirao N., Ohishi Y., Nishijima M. Stability of a hydrous-phase, AlOOH-$MgSiO_2(OH)_2$, and a mechanism for water transport into the base of lower mantle // Earth and Planetary Science Letters. 2014. Vol. 401. P. 12–17.

Plank T., Langmuir C.H. The chemical composition of subducting sediment and its consequences for the crust and mantle // Chemical Geology. 1998. Vol. 145. P. 325–394.

Poli S., Franzolin E., Fumagalli P., Crottini A. The transport of carbon and hydrogen in subducted oceanic crust: an experimental study to 5 GPa. Earth and Planetary Science Letters. 2009. Vol. 278. P. 350–360.

Stern R.J. Subduction zones // Reviews of Geophysics. Vol. 40(4). No. 1012.

Wirth R., Vollmer C., Brenker F., Matsyuk S., Kaminsky F. Inclusions of nanocrystalline hydrous aluminium silicate “Phase Egg” in superdeep diamonds from Juina (Mato Grosso State, Brazil) // Earth and Planetary Science Letters. 2007. Vol. 259. P. 384–399.

Wu Y., Fei Y., Jin Z., Liu X. The fate of subducted upper continental crust: an experimental study // Earth and Planetary Science Letters. 2009. Vol. 282. P. 275–284.

ZIRCON SOLUBILITY IN SILICATE MELTS: NEW EXPERIMENTS, A NEW MODEL AND NEW CONSEQUENCES

Borisov A.A., Aranovich L.Y.

Institute of Geology of Ore Deposits, Petrography, Mineralogy and Geochemistry Russian Academy of Sciences, Russia, aborisov@igem.ru

Experiments on zircon (Zrn) solubility in synthetic melts have been made at 1 atm total pressure in a wide range of melt compositions and temperature range 1150-1500°C (Borisov, Aranovich, 2019). Concentration of Zr in experimental glasses, measured with EMPA varied from 4540 to 61370 ppm. Separate effects of TiO_2, Fe oxides and SiO_2 on the Zrn solubility have been evaluated. It was demonstrated that at fixed T the addition of TiO_2, FeO and Fe_2O_3 results in moderate increase of Zrn solubility, but the addition of SiO_2 results in moderate decrease of Zrn solubility in silicate melts.

We combined our data with 41 experiments from Boehnke et al., 2013 (750-1020°C and 1.2-25 kbar), 14 experiments from Gervasoni et al., 2016 (1000 or 1200°C and 7 kbar) and 7 experiments from Ellison and Hess, 1986 (1400°C and 1 bar) to obtain in total 129 experimental glasses covering Zrn solubility range from 155 to 61370 ppm Zr. All these data can be very well described ($R^2 = 0.980$) with a single empirical equation:

$\log Zr\ (ppm) = 4.322 \cdot B - 4338.8/T(K) + 6.456,$

where B is the following ratio of the oxide mole fractions in the melts:

$B=0.14(X_{TiO2}/X_{SiO2})+1.3(X_{CaO}/X_{SiO2})+1.5(X_{Na2O}/X_{SiO2})-4.5(X_{K2O}/X_{SiO2})-2.7(X_{Al2O3}/X_{SiO2})^2+(X_{MgO}/X_{SiO2})^2-3.7(X_{CaO}/X_{SiO2})^2+75(X_{K2O}/X_{SiO2})^2.$

The new equation predicts log (Zr, ppm) with a standard error of 0.104, which is equivalent to ca 24% error for the entire Zr concentration range covered by experiments (see Figure) and performs much better on the dataset than the previously published equations.

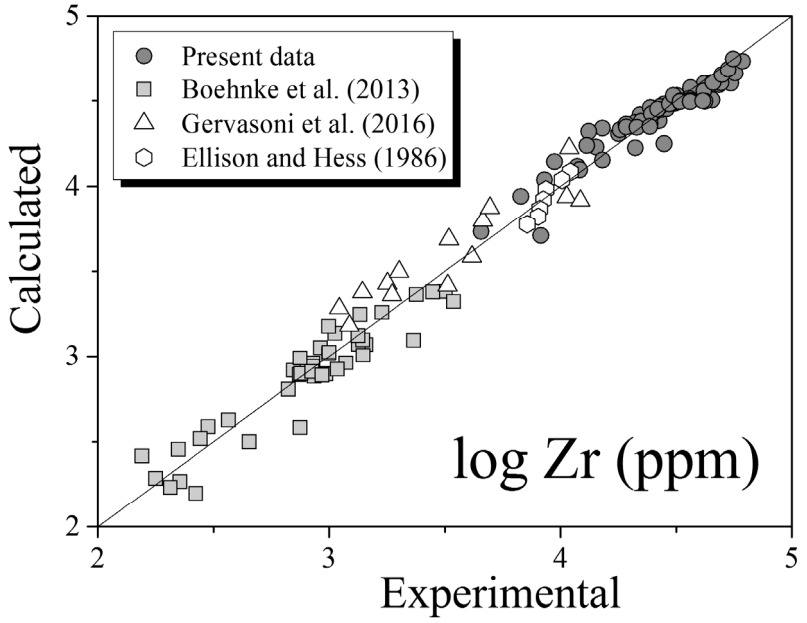

Figure. Comparison of experimental values of zircon solubility (all published literature data and this work) with those calculated according to our new model.

The new model is particularly suited for evaluating a likelihood of zircon crystallization from evolving basaltic magmas. Such evaluation done on the well constrained experiments from the literature (Grove et al., 1992; Sisson and Kelemen, 2018; Nandedkar et al., 2014) indicates that even near-solidus crystallization of zircon in deeply evolved initially basaltic melts is highly unlikely in dry

liquids although cannot be completely ruled out and may even be quite plausible in the water-containing ones.

Our results indicate that caution must be exerted while interpreting age and saturation temperature of zircon populations separated from mafic rocks.

This work was supported by the RSF grant 18-17-00126.

References

Boehnke P., Watson E.B., Trail D., Harrison T.M., Schmitt A.K., 2013. Zircon saturation re-revisited. // Chem. Geol. 351, 324–334.

Borisov A., Aranovich L. (2019) Zircon solubility in silicate melts: New experiments and probability of zircon crystallization in deeply evolved basic melts. // Chem. Geol. 510, 103-112.

Ellison A.J, Hess P.C., 1986. Solution behavior of +4 cations in high-silica melts: petrological and geochemical implications. // Contrib. Mineral. Petrol. 94, 343-351.

Gervasoni F., Klemme S., Rocha-Júnior E.R.V., Berndt J., 2016. Zircon saturation in silicate melts: a new and improved model for aluminous and alkaline melts. // Contrib. Mineral. Petrol. 171, Article 21.

Grove T.L., Kinzler R.J, Bryan W.B., 1992. Fractionation of Mid-Ocean Ridge Basalt (MORB). // Geophys. Monograph Series 71, 281–310.

Nandedkar R.H., Ulmer P, Müntener O., 2014. Fractional crystallization of primitive, hydrous arc magmas: an experimental study at 0.7 GPa. // Contrib. Mineral. Petrol. 167, Article 1015.

Sisson T.W.,·Kelemen P.B., 2018. Near-solidus melts of MORB+4 wt% H2O at 0.8–2.8 GPa applied to issues of subduction magmatism and continent formation. // Contrib. Mineral Petrol. 173, Article 70.

SAMARSKITE REVISITED, $YFe^{3+}Nb_2O_8$: THE HISTORY, MINERALOGY AND CRYSTAL CHEMISTRY OF THE LEGENDARY RARE EARTH MINERAL

Britvin S.N.[1,2], Pekov I.V.[3], Krzhizhanovskaya M.G.[1], Agakhanov A.A.[4], Ternes B.[5], Schüller W.[6], Chukanov N.V.[7]

[1]Saint-Petersburg State University, Saint-Petersburg, Russia, sergei.britvin@spbu.ru
[2]Kola Science Center, Russian Academy of Sciences, Apatity, Russia
[3]Moscow State University, Moscow, Russia
[4]Fersman Mineralogical Museum, Russian Academy of Sciences, Moscow, Russia
[5]Mayen, Germany
[6]Adenau, Germany
[7]Institute of Problems of Chemical Physics, Russian Academy of Sciences, Chernogolovka, Russia

Samarskite-(Y) is one of the earliest known rare-earth minerals, and a parent mineral for three new elements: samarium, gadolinium and europium (Britvin et al., 2019, and references therein). The mineral was first described in 1839 by Gustav Rose from the Blyumovskaya Pit at the Ilmeny Mountains, South Urals, Russia, and was named in honor of V.E. Samarsky-Bykhovets, a chief of Russian Corps of Mining Engineers (Rose, 1839). The history of samarskite-(Y) was reviewed in detail by Pekov (1998) and Polyakov (2000).

Samarskite-(Y) is a typical accessory mineral in NYF (niobium-yttrium-fluorine) pegmatites and their parent granites; hence its chemical composition was a subject to thorough studies (Ercit, 2005). However, its crystal structure remained unsolved due to metamict, X-ray amorphous state of the mineral always containing admixed U and sometimes also Th. Because of that, the chemical formula of samarskite-(Y) was so far accepted by International Mineralogical Association in the form of ABO_4 where A = (Y,Ln,Ca,Fe,U) and B = (Nb,Ti,Ta) (Hanson et al., 1999).

In the course of mineralogical research of the Eifel volcanic region (Rhineland-Palatinate, Germany), the authors of this paper (W.S. and B.T.) have found well formed samarskite-(Y) crystals in voids of nosean sanidinite of the Laacher See paleovolcano. The mineral from Laacher See is non-metamict due to its very young, Pleistocene geological age and possesses crystal structure derived from that of wolframite $(Fe,Mn)WO_4$ (Britvin et al., 2019). Samarskite-(Y) is the first example of cation ordered niobate related to the structural family of layered double tungstates (double wolframites) AMW_2O_8 (Fig. 1) It is noteworthy that reliable data on the mineral from the type locality, the Blyumovskaya Pit are rather limited. We undertook a revision of samarskite-(Y) from the type locality, including electron microprobe, thermal and powder X-ray diffraction (XRD) studies. Like the non-metamict crystal from Laacher See, the fully metamict mineral from the type locality demonstrates the same species-defining constituents and perfectly corresponds to the stoichiometry of cation ordered samarskite with the end-member formula $YFe^{3+}Nb_2O_8$.

The structure of samarskite-(Y) (Fig. 1) exhibits a specific type of cation ordering previously unreported for both natural and synthetic niobates and tantalates. It can be derived from the crystal structure of wolframite (ferberite) $Fe^{2+}W^{6+}O_4$ by imposing the following changes: (1) flat layers of corner-sharing zigzag chains of $[WO_6]$ octahedra in wolframite are replaced by topologically identical layers of $[NbO_6]$ octahedra; (2) each second $[NbO_6]$ layer is mirrored on (001) relative to the preceding one; (3) each second layer composed of zigzag chains of $[FeO_6]$ octahedra is replaced by the infinite perforated layer of corner-sharing $[YO_8]$ square antiprisms. The appeared layer sequence can be expressed as -$[AO_8]$-$[BO_6]$-$[MO_6]$-$[BO_6]$- leading to the general formula AMB_2O_8 in which A = **Y**, *Ln*, Th, U^{4+}, Ca; M = **Fe^{3+}**, Mn^{2+}; B = **Nb**, Ta, Ti, W, Zr (the species-defining constituents are highlighted in bold). Herein we propose AMB_2O_8 lettering for the general formula of samarskite-group minerals, in order to keep consistency with site designations accepted for other groups of tantalo-niobates (Ercit, 2005). As a result of the layer alternation, the unit cell of samarskite-(Y) becomes doubled along the *a* axis as compared to that of the wolframite structure archetype. The alternation of layers appeared in samarskite-(Y) was not reported for niobates and tantalates but is well represented in structurally related layered tungstates and molybdates. The observed cation ordering in samarskite-(Y) is explainable on the basis of the crystal chemical criteria: the $[AO_8]$ layer accommodates large-radius

cations favoring eight-fold coordination whereas the octahedral [MO_6] layer accumulates smaller Fe and Mn. The major substitution schemes in samarskite-(Y) can be represented as follows: $^{B}Nb^{5+} \leftrightarrow {}^{B}Ta^{5+}$; $^{A}Y^{3+} \leftrightarrow {}^{A}HREE^{3+}$; $^{A}Ca^{2+} + {}^{A}U^{4+} \leftrightarrow 2^{A}(Y,Ln)^{3+}$; $^{A}U^{4+} + {}^{B}Ti^{4+} \leftrightarrow {}^{A}(Y,Ln)^{3+} + {}^{B}Nb^{5+}$; and probably, $^{A}U^{4+} + {}^{M}(Fe,Mn)^{2+} \leftrightarrow {}^{A}(Y,Ln)^{3+} + {}^{M}Fe^{3+}$.

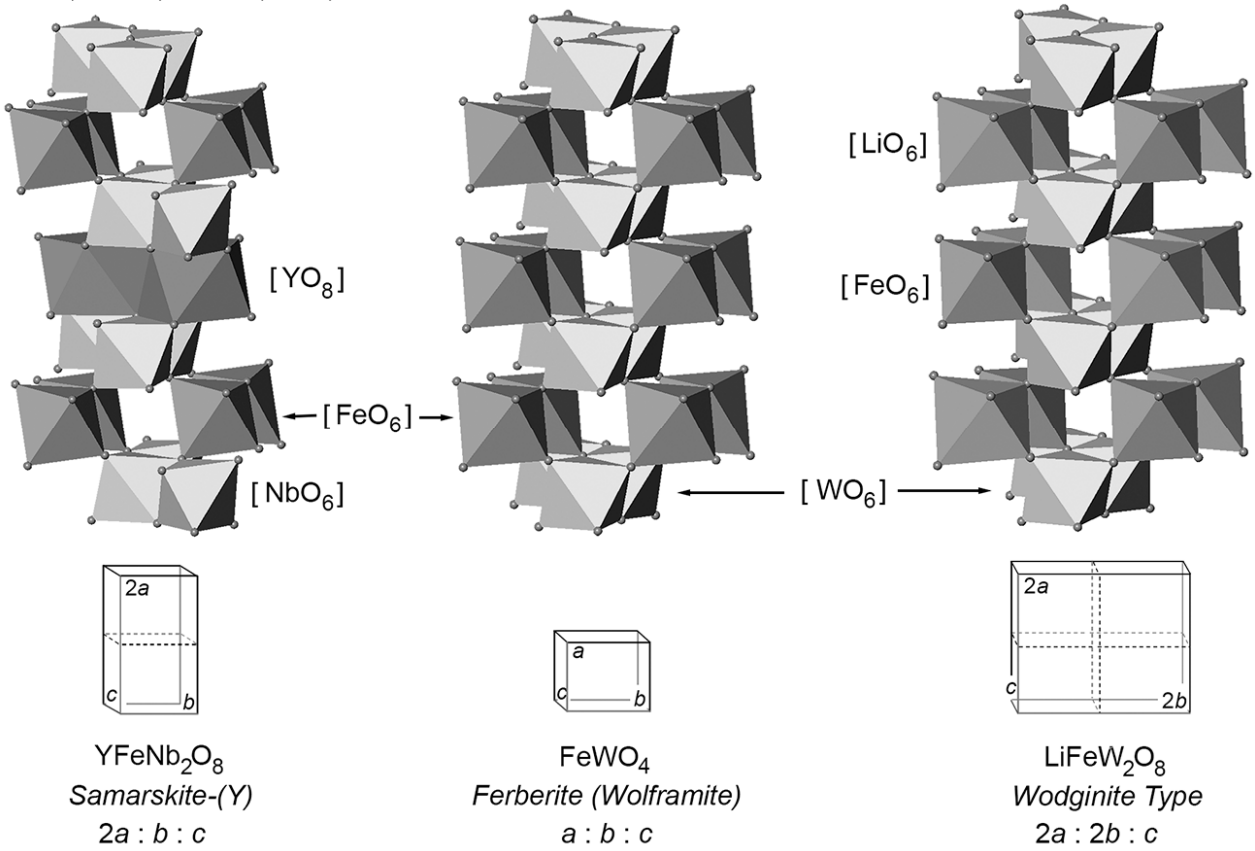

Figure 1. Wolframite structure (in the center) and its derivatives – samarskite-(Y) (left) and wodginite (right) (Britvin et al., 2019).

The ideal, end-member formula of samarskite-(Y) can be expressed as $YFe^{3+}Nb_2O_8$. For the four other minerals related to the samarskite group, the simplified formulae could be derived by analogy (Table 1). The recently discovered mineral ekebergite, $ThFeNb_2O_8$ (Kjellman et al., 2018), is herein ascribed to the samarskite group as well, on the basis of its reported chemical formula and unit cell parameters. Samarskite-(Y) resisted the attempts to reveal its original, pre-metamict structural state for 180 years. The obtained results could provide new insights on the mineralogy and petrology of the samarskite group in general. The crystal chemical criteria unambiguously explain well known trends in preferable accumulation of Th, U and *REE* in samarskite but not in chemically similar wolframite- and wodginite-group minerals (Ercit, 2005). The present work, along with the recently reported statistical data on the samarskite-group minerals (Kjellman, 2017), could provide the basement for the new nomenclature of the samarskite group, based on the formula AMB_2O_8 with focus on the ordered distribution of large (*A*) and medium-sized tri- or bivalent (*M*) cations.

Table 1. Proposed nomenclature scheme for samarskite-group minerals

Mineral	Simplified formula	Reference
Samarskite-(Y)	$YFe^{3+}Nb_2O_8$	Rose, 1839; Britvin et al., 2019
Samarskite-(Yb)	$YbFe^{3+}Nb_2O_8$	Simmons et al., 2006
Yttrotantalite-(Y)	$YFe^{3+}Ta_2O_8$	Palache et al., 1944
Ishikawaite	$U^{4+}Fe^{2+}Nb_2O_8$	Kimura, 1922
Ekebergite	$ThFe^{2+}Nb_2O_8$	Kjellman et al., 2018
Calciosamarskite	$(Ca_{1/2}U^{4+}{}_{1/2})Fe^{3+}Nb_2O_8$	Ellsworth, 1928

The results of this work have been approved by the Commission on New Minerals, Nomenclature and Classification, International Mineralogical Association (voting proposal 18-J; Memorandum 90-FH/18 of 05 December 2018).

The authors thank the X-ray Diffraction Center of SPSU for providing instrumental and computational resources.

References

Britvin S.N., Pekov I.V., Krzhizhanovskaya M.G., Agakhanov A., Ternes B., Schüller W., Chukanov N.V. Redefinition and crystal chemistry of samarskite-(Y), $YFe^{3+}Nb_2O_8$: cation-ordered niobate structurally related to layered double tungstates // Physics and Chemistry of Minerals. 2019. DOI: 10.1007/s00269-019-01034-0.

Ellsworth H.V. A mineral related to samarskite from the Woodcox Mine, Hybla, Ontario. American Mineralogist. 1928. Vol. 13. p. 63-65.

Ercit T.S. Identification and alteration trends of granitic-pegmatite-hosted (Y,REE,U,Th)-(Nb,Ta,Ti) oxide minerals: a statistical approach // Canadian Mineralogist. 2005. Vol. 43. p. 1291-1303.

Hanson S.L., Simmons W.B., Falster A.U., Foord E.E., Lichte F.E. Proposed nomenclature for samarskite-group minerals: new data on ishikawaite and calciosamarskite // Mineralogical Magazine. 1999. Vol. 63. p. 27-36.

Kimura, K. Ishikawaite: a new mineral from Ishikawa, Iwaki // Journal of the Geological Society (Tokyo). 1922. Vol. 29. p. 316-320.

Kjellman, J. ABC_2O_8 – a new look on the crystal chemistry and classification of samarskite group minerals // PEG2017: Proceedings of 8th International Symposium on Granitic Pegmatites. 2017. p. 64-67.

Kjellman, J., Pay Gómez, C., Lazor, P., Majka, J., Stanley, C., Najorka, J. Ekebergite, IMA 2018-088. IMA CNMNC Newsletter 46 // European Journal of Mineralogy. 2018. Vol. 30. p. 1181-1189.

Palache C., Berman H., Frondel C. The System of Mineralogy, Volume I. 7th ed. John Wiley and Sons, New York, 1944.

Pekov I.V. Minerals First Discovered on the Territory of the Former Soviet Union. OP: Moscow, 1998.

Polyakov V.O. Samarskite. In: Yushkin, N.P, Ed. Mineralogy of Urals. Oxides and Hydroxides. Part. I. Ural Branch of Russian Academy of Sciences: Miass-Yekaterinburg, 2000 (in Russian).

Rose G. Beschreibung einiger neuen Mineralien des Urals // Annalen der Physik. 1839. Vol. 124. s. 551-573.

Simmons W.B., Hanson S.L., Falster A.U. Samarskite-(Yb): A new species of the samarskite group from the Little Patsy pegmatite, Jefferson County, Colorado // Canadian Mineralogist. 2006. Vol. 44. p. 1119-1125.

ARGON-NITROGEN ISOTOPE SYSTEMATICS OF GULI MASSIF ULTRAMAFIC ROCKS, MAIMECHA-KOTUI PROVINCE, RUSSIA

Buikin A.I.[1], Verchovsky A.B.[2], Asavin A.M.[1]

[1]Vernadsky Institute of Geochemistry and Analytical Chemistry RAS, Moscow, Russia, bouikine@mail.ru

[2]The Open University, Milton Keynes, UK

The Guli massif is the largest alkaline-ultramafic, intrusive-volcanic complex in the world and occupies an area between the Maymecha and Kotuy Rivers at the Noth boundary of the Siberian platform with the Khatanga paleorift (northern part of the Heta-Yenisei faults-extension global system (Allen et al., 2006). The Guli massif, like many of the other alkaline-ultrabasic intrusions, is a complex, multi-stage pluton (Egorov, 1991). The complex polyphase evolution of the massif had started with formation of ultrabasic rocks (dunites, kosvites), continuing with rocks of melilite series, melteigites, jacupirangite-melteigites, picrites, going to the rocks of ijolite and then syenite series and finished with formation of sequences of veins and stocks of rocks of phoscorite and carbonatite groups (Egorov 1991). Previously, we have studied samples representing all different stages of the carbonatite formation (Buikin et al., 2016; Buikin et al., 2017). These investigations have shown that the subcontinental lithospheric mantle (SCLM) was a primary source of the fluid phase in Guli carbonatites. The early carbonatite differs significantly from the later ones in the concentration of highly volatile components, as well as in the isotopic compositions of carbon (CO_2), argon, and hydrogen (H_2O). The mantle component dominated in fluids at the early formation stages of the Guli massif carbonatites, whereas the late stages were characterized by an additional fluid source, which introduced atmospheric argon and neon, and most likely a high portion of CO_2 with isotopically heavy carbon. The carbon-argon-hydrogen isotope systematic suggests that the most likely these late stage fluids are associated with high temperature paleometeoric waters (Buikin et al., 2016). The nitrogen isotope composition is surprisingly homogeneous in the early and late carbonatites: the total $\delta^{15}N$ values are the same within the analytical error. The absence of a plume signature was explained in terms of formation of the Guli carbonatites at the waning stage of plume magmatic activity with an essential input of SCLM components (Buikin et al., 2017). To better understand the sources and evolution of the fluid phase during early formation stages of the Guli massif we have started the investigation of whole rock and mineral separates from the ultramafic and alkaline-ultramafic rocks of the massif. Here we present the first argon and nitrogen isotopic data obtained by stepwise crushing.

Analytical procedures were as follows. The whole rock and monomineral fractions (separated by picking under a binocular) were washed in ethanol in an ultrasonic bath to get rid of possible surface contamination and then placed into a drying box for 2–3 hours. Afterwards the samples were loaded into the crushing tubes connected to a vacuum line. The system was evacuated to high vacuum (10^{-8} torr) and heated to ~120°C during one day to remove gases adsorbed on the surface. The crushing tube was connected to the vacuum system of the Finesse complex (Verchovsky et al. 2002). The gases released during each crushing step were cryogenically separated and expanded into the chamber of the mass spectrometer for analysis of their isotopic compositions. Ar was additionally purified on Zr–Al getters. To get rid of possible interfering masses (first of all, CO), the nitrogen was additionally purified on CuO at 800°C. The CO_2 thus generated was trapped on a cold finger at a temperature of –170°C. The amounts of carbon were determined using pressure measurements on a high precision baratron. The blanks were 0.4–0.6 × 10^{-8} cm^3 STP, and 0.2–0.8 ng for ^{40}Ar, and N, respectively. The analytical errors for $\delta^{15}N$ are ±(0.2 – 0.6) ‰ in crushing steps and ±(0.2 – 0.3) ‰ for total values; for $^{40}Ar/^{36}Ar$ – mostly less then 2-5%.

We have studied pyroxenite (97-74, Px-separate), Ne-picrite (97-69, WR), melilitite (Gh-3, Melilite and Mt separates), and meimechite (30-46, Olv+Mt).

Nitrogen concentrations vary from 62 to 398 ng/g with the overall trend in decreasing from the earlier to the later stages rocks. ^{40}Ar concentrations also higher in pyroxenite (832×10^{-8} cm^3/g) and picrite (789×10^{-8} cm^3/g) and decrease to around 200×10^{-8} cm^3/g in melilitite, down to 30×10^{-8} cm^3/g in

meimechite. The considerably lower amounts of nitrogen and especially Ar in meimechite could be explained by loss of the gases at the eruption.

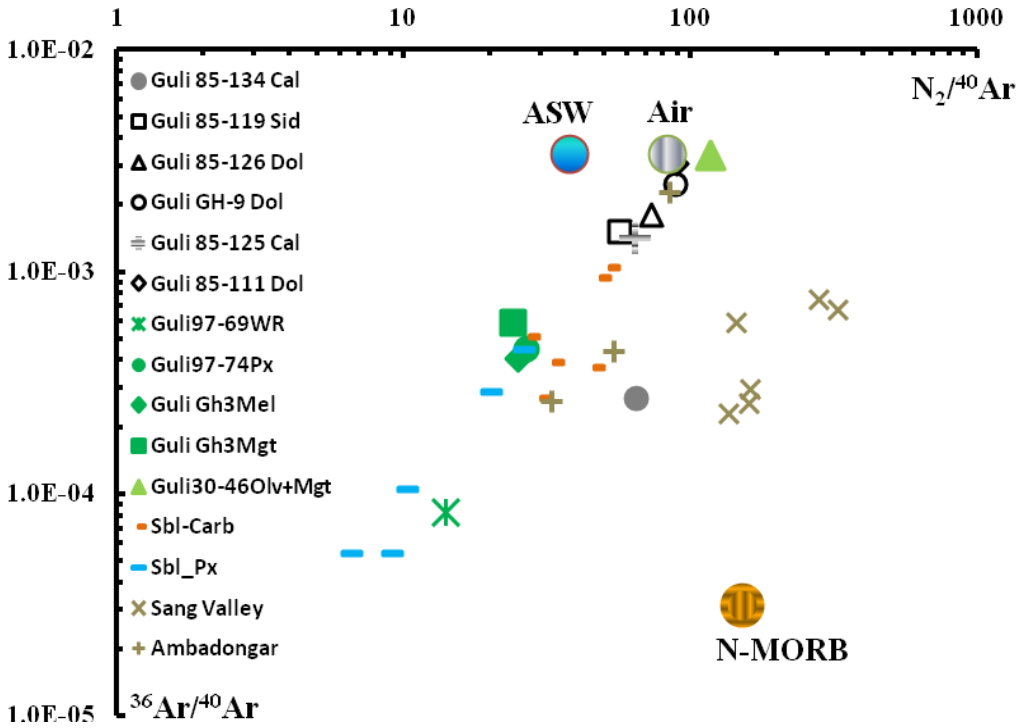

Figure. Argon isotopic compositions vs nitrogen to argon ratios in Guli carbonatites (Buikin et al., 2016) and ultramafic rocks (this work). For comparison the data for Seblyavr carbonatites and pyroxenites (Buikin et al., 2014), for Ambadongar and Sang Valley carbonatites (Basu, Murty, 2015) as well as for reference points of air, air saturated water and mantle are also shown.

Nitrogen isotopic composition in crushing steps varies from +6.7 ‰ in pyroxenite (Guli97-74) to -15.4 ‰ in meimechite (Guli30-46). The largest variations within crushing steps are observed in pyroxenite – from -8.1 to +6.7 ‰. The most homogeneous sample in this respect is the picrite Guli97-69 (-1.3 to +1.0 ‰). The total nitrogen isotopic composition in the samples varies between -5.9 ‰ in meimechite to +1.3 ‰ in pyroxenite, and shows a dependence on the total nitrogen concentration in the sample. If compare with nitrogen isotopic composition in Guli carbonatites (Buikin et al., 2016), Seblyavr carbonatites and ultramafic rocks (Buikin et al., 2014) or Indian carbonatites (Basu, Murti, 2015) the studied Guli massif ultramafic rocks contain mostly isotopically lighter nitrogen and some of them demonstrate compositions close to N-MORB one (-5±3 ‰, Fisher et al., 2009).

The argon isotopic composition in crushing steps of meimechite varies from air-like value ($^{40}Ar/^{36}Ar = 296$) to 410 thus demonstrating strong atmospheric contamination – most probably during eruption. The other samples contain argon with elevated $^{40}Ar/^{36}Ar$, higher than 1600 (bulk values), pointing to a high contribution of mantle argon component. In the last three crushing steps of picrite (97-69) the $^{40}Ar/^{36}Ar$ ratios are increased from 3207 to 12704 and 28240 with increasing ^{40}Ar concentration and simultaneous decreasing of nitrogen content. All these along with elevated K content in this sample suggest a strong contribution of *in situ* radiogenic argon at these extractions as it was previously observed in some Seblyavr samples (Buikin et al., 2018).

At the $^{36}Ar/^{40}Ar$ vs $N_2/^{40}Ar$ diagram (Figure) the data for Guli carbonatites and ultramafic rocks, Seblyavr carbonatites and pyroxenites and Ambadongar samples form a common trend from air-like compositions to the end-member with low $N_2/^{40}Ar$ and $^{36}Ar/^{40}Ar$ ratios. The lowest values are characteristic for some of Seblyavr pyroxenites and picrite from Guli massif, and reflect a significant addition of *in situ* radiogenic argon (Buikin et al., 2018). The question is why most of other samples follow the same trend despite the fact that they do not contain high enough potassium concentrations (if at all) to contribute severely to argon budget? A possible explanation for Guli rocks is that the

source composition (SCLM) lies somewhere on the trend. Indeed, SCLM is characterized by higher ^{40}Ar contribution than MORB-type mantle, and its $N_2/^{40}Ar$ ratios must be lower. Samples from Sang Valley most probably reflect contribution from nitrogen of non-molecular form (not N_2), likely from inorganic nitrogen that exists as NH_4^+, which fails to completely homogenize with the other components from the source (Basu, Murty, 2015). On the $^{40}Ar/^{36}Ar$ - $N_2/^{36}Ar$ plot all the carbonatites follow the trend from air-like compositions to E-MORB type mantle, while Guli ultramafic rocks form their own trend – to lower nitrogen-argon ratios.

Thus, the studied Guli ultramafic rocks clearly differ from carbonatites by their nitrogen-argon systematics, which can point to different fluid sources and/or different evolution of their fluid phases.

This work was supported by the RFBR grant №19-05-00681.

References

Allen M.B., Anderson L., Searle R.C., Buslov M. Oblique rift geometry of the West Siberian Basin: Tectonic setting for the Siberian flood basalts // Journal of the Geological Society. 2006. Vol. 163(6). P. 901-904

Basu S., Murty S.V.S. Nitrogen and argon in Sung Valley and Ambadongar carbonatite complexes: Evidence of incomplete homogenization of mantle and recycled components // Journal of Asian Earth Sciences. 2015. Vol. 107. P. 53-61.

Buikin A.I., Verchovsky A.B., Sorokhtina N.V., Kogarko L.N. Composition and Sources of Volatiles and Noble Gases in Fluid Inclusions in Pyroxenites and Carbonatites of the Seblyavr Massif, Kola Peninsula // Petrology. 2014. Vol. 22(5). P. 507-520.

Buikin A.I., Verchovsky A.B., Kogarko L.N., Grinenko V.A., Kuznetsova O.V. The Fluid Phase Evolution during the Formation of Carbonatite of the Guli Massif: Evidence from the Isotope (C, N, Ar) Data // Dokl. Earth Sci. 2016. Vol. 466(2). P. 135–137.

Buikin A.I., Kogarko L.N., Hopp J., Trieloff M. Light Noble Gas Data in Guli Massif Carbonatites Reveal the Subcontinental Lithospheric Mantle as Primary Fluid Source. // Geochemistry International. 2017. Vol. 55(5). P. 457–464.

Buikin A.I., Kamaleeva A.I., Sorokhtina N.V. On the Separation Efficiency of Entrapped and in Situ Formed Noble Gas Components at Sample Crushing in Vacuum. // Geochemistry International. 2018. Vol. 56(6). P. 601-607.

Egorov L.S. Ijolite–Carbonatite Plutonism: Maimecha–Kotui Complex of the Polar Siberia. Nedra, 1991. Leningrad. [in Russian].

Fischer T.P., Burnard P., Marty B., Hilton D.R., Furi E., Palhol F., Sharp Z.D., Mangasini F. Upper-mantle volatile chemistry at Oldoinyo Lengai volcano and the origin of carbonatites // Nature. 2009. Vol. 459. P. 77-80.

Verchovsky A.B., Sephton M.A., Wright I.P., Pillinger C.T. Separation of planetary noble gas carrier from bulk carbon in enstatite chondrites during stepped combustion // Earth and Planetary Science Letters. 2002. Vol. 199. P. 243–255.

LOW-TITANIUM LAMPROITES OF ALDAN SCHIELD: POSSIBLE IMPLICATIONS FOR GOLD, PGE AND REE DEPOSITS

Chayka I.F.[1,2], Izokh A.E.[1,2], Vasyukova Ye.A.[1,2], Lobastov B.M.[3]

[1]V.S.Sobolev Institute of Geology and Mineralogy SB RAS, Novosibirsk, Russia, ivanlab211@gmail.com

[2]Novosibirsk State University, Russia

[3]Siberian State University, Krasnoyarsk, Russia

Introduction and geological setting. Petrology and ore potential of lamproites, kimberlites and other high-potassic igneous rocks is a widely discussed topic. Lamproite magmatism is expressed within different tectonic settings from active-margin to intraplate, as well as kimberlite magmatism providing information about deep mantle processes. Meanwhile, lamproite rocks are in numerous cases are spatially affiliated with trace-element deposits and some lamproites are diamond-bearing (Hoa et al. 2016; Vladykin 2008).

In the Central Aldan high-potassic province (Aldan shield, Russia) there are many synchronous mesozoic (125-134 Ma) (Shatov, et al. 2012; Mues-Schumacher et al. 1995) subvolcanic bodies of lamproites and lamproite-like rocks, spatially and temporally connected with Au-bearing (Ryabinoviy, Yukhtinskiy), PGE-bearing (Inagli) massifs and carbonatites (Murun massif). These occurrences were previously studied by a number of authors (Bilibin 1952; Vladykin 2008; Rokosova and Panina 2013; Mues-Schumacher et al. 1995). Although lamproites and lamprophyres are found all around Central Aldan and are united by some researchers into Tobuk complex (Shatov et al. 2012), within Ryabinovoye gold deposit (Ryabinoviy massif) a wide range of high-potassic dyke rocks outcrops on a very small area, being a unique case of differentiation of lamproite magma from Ol-Di-Phl-lamproites to microsyenites, most varietes of which are found within the other massifs of Central Aldan province (Bilibin, 1952). Taking into account their low degree of alteration and weathering, this complex can be considered as a "model example" for Aldan shield Mesozoic lamproites.

We studied in details mineralogical and chemical evolution of these lamproite-series rocks and compared some of their features with ones of Inagli dunites (Chayka and Izokh 2018) and with potassic rocks being responsible for Ryabinovoye Au-porphyry deposit. REE-apatite-carbonate-fluorite assemblages, occurring as gangues and segregations within the lamprophyre dykes were studied in details as well. In this paper we summarize all these results and briefly discuss ore potential of such lamproite magmas.

The Ryabinoviy massif is located in the central part of Central Aldan high-potassic province in the Northern-Western part of Elkon horst. Its emplacement is controlled by the intersection of Yakokutskiy and Yukhukhtinskiy faults, having area (with apophysis) about 50 km^2. Host rocks are granites and gneisses of Aldan shield and Vend-Cambrian sedimentary layers (Maksimov et al. 2010). Lamproite-series rocks occur there within a small area of Muskovitoviy location of Ryabinovoye gold deposit. The complex includes a diatreme-like body, comprised by Ol-Di-Phl- and Di-Phl- lamproites and a sequence NE-striking dykes having composition from Ol-Di-lamproites to minettes and microsyenites. It is noteworthy that the dykes cross-cut diatreme and each other in homodrome sequence.

Results. Petrographical study shows that rocks of these dykes form a continuous series from Ol-Di-Phl-lamproites through Di-Phl-lamproites and minettes to microsyenites. Ol-Di-Phl-lamproites consist of major olivine (in phenocrysts), diopside, poikilitic phlogopite, K-feldspar (in groundmass); minor minerals are Cr-spinel (from Mg-chromite to Cr-magnetite), apatite, pseudo-leucite. Di-Phl lamproites contain euhedral phenocrysts of diopside, zoned phlogopite, rare olivine replaced by carbonate and talk, groundmass anhedral and poikilitic K-feldspar; minor minerals are magnetite and apatite. Minettes consist of euhedral zoned biotite and groundmass subhedral K-feldspar with minor magnetite, aegirine-augite, apatite and carbonate. Microsyenites are similar to minettes, but contain less biotite, while K-feldspar is generally euhedral. Generalized sequence of crystallization is: (Cr-spinel+olivine+leucite) – (Cr-spinel+diopside+apatite) – (diopside+phlogopite (#Mg>70) +magnetite) – (aegirine-augite+biotite (#Mg<70)) – K-feldspar – carbonate.

Although of major minerals was studied in details, here we show only the essential chemical features of minerals:

1. Olivine cores have an extremely high #Mg up to 95 and high NiO content (up to 0,45 wt.%), rims' #Mg is about 75-88 (Chayka et al, 2018).
2. Cr-spinel composition varies from Mg-chromite (big euhedral grains, inclusions in olivine cores) to chromite (inclusions in olivine rims and diopside grains) Cr-magnetite (groundmass grains);
3. Mica (annite-phlogopite series) phenocrysts are distinctly zoned: cores (#Mg=80-85) contain higher amounts of F (0,7-1,2 wt.%), than rims (#Mg=55-70, F – 0,5-0,9 wt.%), although other incompatible elements (Ba, Ti) are regularly higher in rims.
4. Apatite grains are inversely zoned in F content, as well as micas. Apatites from lamproites (less fractionated rocks) are about 5 to 15 times enriched in LREE, Y, U and Th in comparison with those from minettes and syenite-porphyries.

Major element composition was determined using XRF-analysis, also we used data published by V.V.Sharygin (Sharygin 1993). Geochemistry of major elements shows regular trends for MgO, SiO_2 and alkali content in studied rocks. Studied series is subalkaline to alkaline, high-potassic. Significant feature of studied series is dispersion of CaO content in minettes: CaO content varies in them from 4 to 12 wt.%, strongly deviating from the main CaO-MgO trend.

Very intriguing is REE-apatite-fluorite-carbonate mineralization within the studied rocks. During field-works and further studies four different spatially-divided associations, containing these minerals, were distinguished:

1. Silicate-carbonate and carbonate micro-globules in silicate matrix in minettes and syenite-porphyries. They are round and oval-shaped, 0,05 to 2 mm in diameter and surrounded by laths of mica. Their composition varies from dolomite+calcite+phlogopite to calcite+K-feldspar.
2. Big carbonate globules are found in some minette dykes. They are 1-3 cm in diameter and have zoned structure (Fig. 1A).
3. Calcite-apatite-fluorite gangue was found in dyke of microsyenites. It consists of major deep-purple fluorite, apatite and minor calcite, barite, celestine and various REE-minerals, including quite abundant squaly bastnasite, burbankite, included in fluorite and others (Fig. 1B-D).
4. Carbonate in inclusions (up to 30 vol. %), hosted by olivine phenocrysts and mantle olivine xenocrysts.

Based on chemical features of the minerals, structural relations and also considering results of previous researches (Rokosova 2013), we colncluded, that these associations can be united into a single phosphate-fluoride-carbonate mineralization, which can be suggested as result silicate-carbonate immiscibility and subsequent carbonate-salt separation (Chayka and Izokh 2017), although hydrothermal origin of some of these (e.g. big carbonate globules and gangues) should not be ruled out.

We studied as well distribution of trace elements in this mineralization and compared their concentrations with those in silicate portion. This problem was solved in two ways: by comparison trace-element composition of studied minerals (calcite, dolomite, fluorite and apatite) with bulk trace-element composition of minettes and by comparison of trace-element composition of apatites from silicate rocks with gangue apatite. The results show that apatite-fluorite gangue is enriched in LREE, U, Th, Sr and Ba, while carbonate globules are depleted in most of trace-elements.

Relationship of the studied rocks with some ore-bearing complexes.

Based on structural relations, Aldanskiy potassic intrusive complex, which is responsible for Ryabinovoye Au-Cu-Mo- deposit, is considered as an earlier phase than the studied dyke complex. But according to the previous researches (Shatov et al. 2012), there is no significant time-lapse between emplacement of these complexes. Moreover, there is a great similarity in their mineral compositions and major-element features. This background makes reasonable discussing a hypothesis that these complexes were produced from several magmatic pulses of similar parental melt. Comparison of their geochemistry as well as chemistry of micas and pyroxenes from these rocks reveals close similarity between rocks of lamproite-series complex and Aldanskiy ore-bearing complex (Chayka and

Vasyukova, 2017). Thus we can conclude that parental melt for Au-bearing Aldanskiy intrusive complex could have composition of low-titanium lamproite melt. We have not appropriate data to state full identity between parental melts, but it is very likely that they were identical at least in major-elements composition and very similar in trace-element composition.

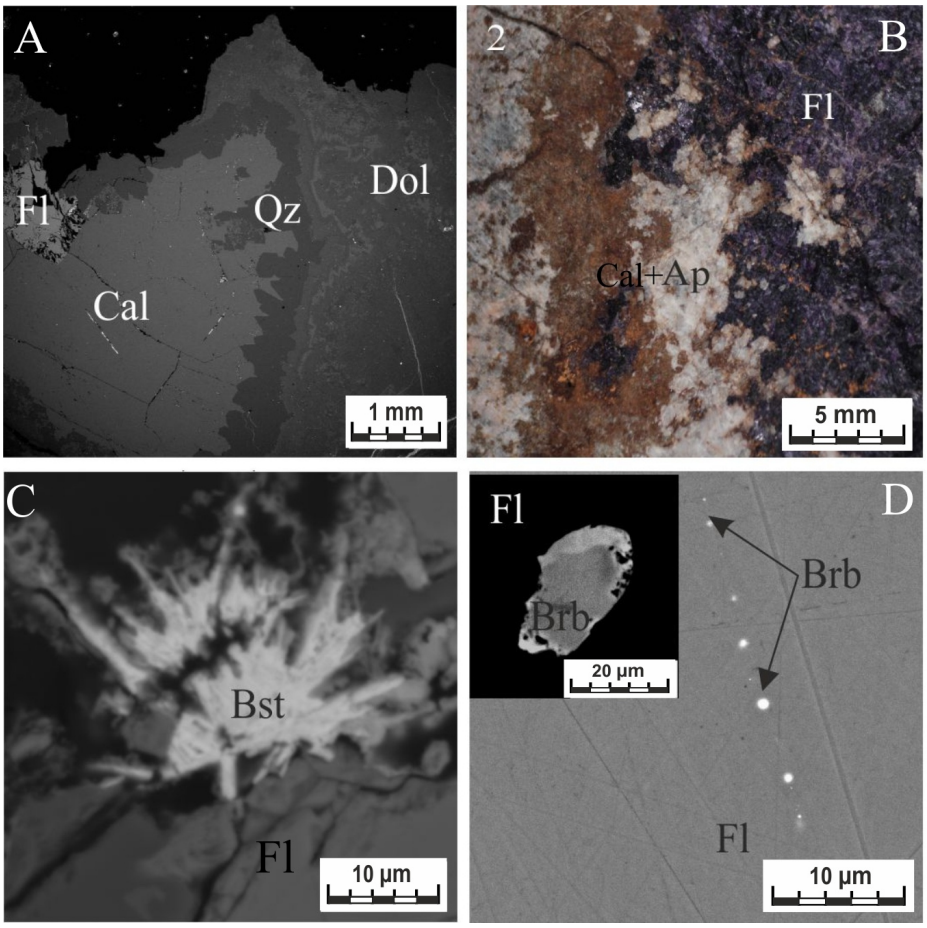

Figure 1. REE-apatite-fluorite-carbonate assemblages within the studied rocks: A) Fluorite-carbonate globule (BSE-photo), B) REE-carbonate-apatite-fluorite gangue (fragment), C, D) – rare-earth mineralization within REE-carbonate-apatite-fluorite gangue (BSE photos).

Although elevated concentrations of PGEs were reported for numerous Mesozoic complexes of Central Aldan province, currently explored PGE-placers are located within and outside of the Inagli ultramafic massif, which is a circular intrusion with dunite core and clinopyroxenite-shonkinite rim, situated at the Western part of Central Aldan potassic province. High degree of secondary (hydrothermal and weathering) alternations makes it difficult to determine parameters of parental melt for this massif. Some researchers (Mues-Schumacher et al. 1995) suppose that the parental melt was very magnesian (MgO ~ 25%) and add that it can be close to lamproites of Central Aldan. In order to test this hypothesis we studied in details chemical composition of Cr-spinel from both lamproites of Ryabinoviy massif and ultramafic rocks from the core of Inagli massif. The study was especially focused on composition of Cr-spinel hosted silicate inclusions (Chayka and Izokh 2018). The results show similar compositions and evolution of Cr-spinel (considered Cr, Fe, Al, Mg, Ti). Accessory magnesian chromites from dunites (Inagli massif) and magnesian-chromite grains from Ol-Di-Phl-lamproites (Ryabinoviy massif) are most similar. Study of silicate inclusions in Cr-spinel from lamproites from Ryabinoviy massif and dunites from Inagli massif show, that their phase compositions are very close: they contain diopside and phlogopite as major minerals and minor apatite and sulphides such as pentlandite and chalcopyrite. Chemical features of phlogopite, diopside and apatite are close as well. We considered Na, Ti and Ba contents in phlogopite, Na and Al - in diopside, F and Sr content in apatite. These elements were chosen because they are relatively minor elements in Cr-spinel and do

are not significantly affected by silicate-spinel equilibrium. On the other hand their content in studied minerals is sensitive to their activity in melts. Obtained results show that dunites from the core of PGE-bearing Inagli massif could represent metamorphosed cumulates of olivine and Cr-spinel, crystallized from low-titanium high-potassic, high-F parental melt, which is close to parental melt for lamproite series rocks of Ryabinoviy massif. This conclusion is also confirmed by previous researches (Mues-Schumacher et al. 1995; Okrugin 2004).

Relationship of the studied rocks with rare metal deposits is somehow more complicated. However, in Northern Vietnam there are Cenozoic REE-U-F-Ba- deposits, located in Nam Xe area and genetically related with lamproite and lamprophyre rocks of Fansipan uplift (Hoa et al. 2016). These rocks and the studied ones possess very similar major-element compositions and evolutionary trends, as well as features of olivine compositions, especially – Ca, Ni contents and Mg# value, implying hence that chemical compositions of their sources and melting conditions were very close to each other.

As mentioned before, we studied apatite-fluorite-carbonate mineralization in dykes of Ryabinoviy massif and supposed that it was a result of silicate-carbonate and carbonate-salt immiscibility (Chayka and Izokh 2017). At the stage of clinopyroxene and phlogopite crystallization in magmatic chamber, silicate-carbonate-salt immiscibility occurs. A hybrid carbonate-salt melt contains different amounts of P, F, Cl and SO_4, and then (probably with tectonically-caused decompression) it can separate into carbonatite and salt fractions (Rokosova and Panina 2013). Study of trace-element distribution between parts of apatite-fluorite-carbonate mineralization shows that Th, U, LREE, Sr and Ba migrate into immiscible carbonate-salt part and then – into salt fraction, forming apatite-fluorite gangues with minor calcite, barite, celestine and REE-mineralization. This model suggests a genetic mechanism of trace-element deposits, related to high-potassic basic rocks and fluorite carbonatites, such as those at Fansipan uplift (Nothern Vietnam).

Summing-up all the results, several conclusions can be made: firstly, the studied complex provides useful data on evolution of low-titanium lamproite magma and hence on Mesozoic lamproite magmatism all over Central Aldan. Concerning ore potential, obtained results indicate that evolution of low-titanium lamproite melts in certain conditions probably can lead to formation of Au, PGE and U-Ba-REE deposits. In addition similarity of Central Aldan and Fansipan lamproite-series rocks signs on possible presence of Th-U-Ba-REE deposits, like Nam Xe, within the Central Aldan province.

We thank Nikiforov A.V. (IGEM RAS, Moscow) for rock samples, Saprykin A.I. and Medvedev N.S. (NIIC SB RAS) for LA-ICP-MS analysis, Simakin S.G., (YB IPT RAS, Yaroslavl) for SIMS-analysis, Veksler I.V. (Potsdam Univercity, Germany), for useful and interesting discussion.

The study is done on state assignment of IGM SB RAS and is supported by grants Russian Scientific Foundation (projects №15-17-20036 and № 19-17-00019).

References

Bilibin Yu. A. Selected works. Publishing of Academy of Sciences USSR, USSR (in Russian), 1952.

Chayka I.F, Izokh A.E. Phosphate-fluoride-carbonate mineralization in lamproite rocks of the Ryabinoviy pluton (Central Aldan): mineralogical and geochemical features and origin // Mineralogiya, 2017, № 3, p. 39-51 (in Russian).

Chayka I.F, Izokh A.E., Dunites of the Inagli massif (Central Aldan), cumulates of lamproitic magma. Russian Geology and Geophysics // 2018, Vol. 59, p. 1450-1460.

Chayka I.F., Izokh A.E., Sobolev A.V., Batanova V.G., Low-titanium lamproites of the Ryabinoviy Massif (Aldan Shield): crystallization conditions and lithospheric source. Doklady Earth Sciences, 2018, Vol. 481, p. 1008-1012.

Chayka I.F., Vasyukova Ye.A., Mineralogy, geochemistry and isotope chemistry of lamproite rocks of Tobuk complex and their relation to Au-ore Ryabinoviy massif (Central Aldan) // Metallogeniya Drevnikh I Sovremennykh Okeanov, №1, p. 232-237 (in Russian).

Maksimov E.P., Uyutov V.I., Nikitin V.M., The Central Aldan gold-uranium ore magmatogenic system, Aldan-Stanovoy shield, Russia // Russian Journal of Pacific Geology Vol. 4, p. 95-115.

Mues-Schumacher U, Keller J, Konova V, Suddaby P. Petrology and age determinations of the ultramafic (lamproitic) rocks from the Yakokut complex, Aldan shield, Eastern Siberia // Mineralogical Magazine, 1995, Vol. 59, p. 409-428.

Okrugin A.V. Crystallization-immiscibility model of PGE-chromitite ores origin in mafic-ultramafic complexes // Tikhookeanskaya Geologiya, 2004, Vol. 23, p. 63-75 (in Russian).

Rokosova E.Yu., Panina L.I. Shonkinites and minettes of the Ryabinovyi massif (Central Aldan): composition and crystallization conditions // Russian Geology and Geophysics, 2013, Vol. 54, p. 613-626.

Sharygin V.V. Potassic picrites of Ryabinoviy massif // Russian Geology and Geophysics, 1993, Vol. 4, p. 60-70.

Shatov V.V., Molchanov A.V. et al., Petrography, geochemistry and isotopic (U-Pb and Rb-Sr) dating of alkali magmatic rocks of Ryabinoviy massif (Southern Yakutia, Russia) // Regional Geology and Metallogeny, 2012, Vol. 51, p. 62-78 (in Russian).

Trong-Hoa Tran, Polyakov G.V. et al. Intraplate Magmatism and Metallogeny of North Vietnam. Springer, Switherland, 2016.

Vladykin N.V. Potassium alkaline lamproite-carbonatite complexes: petrology, genesis, and ore reserves // Russian Geology and Geophysics, Vol. 50, p. 1119–1128.

PETROLOGICAL CONUNDRUMS OF CHROMITE-PGE-ENRICHED ROCKS OF NORILSK-1 INTRUSION: EVIDENCE FROM Cr-SPINEL HOSTED INCLUSIONS

Chayka I.F.[1,2,3], Kamenetskiy V.S.[3,4], Izokh A.E.[1,2], Zhitova L.M.[1,2], Tolstykh N.D.[1], Yakich T.Yu.[5], Lobastov B.M.[6]

[1]V.S.Sobolev Institute of Geology and Mineralogy SB RAS, Novosibirsk, Russia, ivanlab211@gmail.com

[2]Novosibirsk State University, Russia

[3]Institute of Experimental Mineralogy RAS, Chernogolovka, Russia

[4]University of Tasmania, Hobart, TAS, Australia

[5]Tomsk State University, Russia

[3]Siberian State University, Krasnoyarsk, Russia

Chromite-PGM-enriched, sulfide-poor reefs are known in layered complexes (e.g. Bushveld and Stillwater) being important resources of PGEs, for which, however, mechanisms of PGM concentration in the absence of sulfides and their relationships with chromite are unclear. In case of Norilsk-type intrusions PGEs are mined from sulfide-rich ores of the lower zones of the intrusions, while in the upper zones, there are layers and lenses, characterized by dense Cr-spinel dissemination and extremely high PGE concentrations (up to 70 ppm), called "low-sulfide ores" (Sluzhenikin et al., 2016). Cr-spinel in these rocks hosts plenty of inclusions, and since inclusions can provide a powerful tool for petrological investigations of chromite-PGE assemblages (Li et al., 2005; Spandler et al., 2005), in this research we consider composition of inclusions, hosted by Cr-spinel from "low sulfide" PGE ores of the Norilsk-1 intrusion upper contact zone.

Four samples (MR-14, MR-20, MR-30 and MR-31), collected from Medvezhy Ruchey mine, were studied. The rocks are characterized by inhomogeneous texture, consisting mainly of altered plagioclase, clinopyroxene and olivine with fine-grained (10-100 μm) Cr-spinel, scattered in most of the silicates (Fig. 1). Cr-spinel composition varies in wide ranges, evolving from high-Al chromite with Mg# value reaching 50 mole % towards Ti-Cr-magnetite and high-Cr ulvospinel depending on Fe^{3+} content, which is distinct for each sample. Compositional variations are so broad that the observed ranges, overlapping with LIP, OIB fields on the discrimination plot (Kamenetsky et al., 2001), do not distinctly correspond to any known igneous Cr-spinel. Less magnesian Cr-spinel occurs within extensively altered silicates and tend to form sintered aggregates within chlorite or saussurite (Fig. 1), probably implying metasomatic process, which led to alteration of silicates and recrystallization of Cr-spinel with increasing of Fe and Ti contents.

Cr-spinel-hosted inclusions are commonly represented by relatively large size inclusions, located in the grain center, by groups of small inclusions and by single small inclusions, not related to the grain center. The following compositional types of the inclusions are distinguished: silicate chlorite-poor, chlorite-rich, sulfide-dominated and ilmenite-dominated ones. The first two types dominate, while sulfide and ilmenite inclusions are rare. Mainly chlorite-poor inclusions were studied since variety of silicates, enclosed in them, provides useful genetical information. Their composition, including major orthopyroxene, alkaline feldspar, Na-phlogopite, amphibole, clinopyroxene and chlorite, is different from rock-forming assemblage, but reveals similarity with Cr-spinel hosted inclusions from many other PGE-bearing localities (Bushveld complex, ophiolites and zoned complexes) for some of which non-magmatic origin of Cr-spinel is proposed (Li et al., 2005; Borisova et al., 2012; Pushkarev et al., 2007). Among the minor phases (Cl-apatite, sulfides, baddeleyite, ilmenite, epidote, calcite, cordierite, native gold) more than a half are hardly affiliated with high temperatures of magmatic Cr-spinel crystallization, originating generally in metamorphic/metasomatic or hydrothermal settings. Heated at 1250°C and chilled inclusions consist of glass, olivine, rare orthopyroxene, sulfide and Cr-spinel. Glass compositions, having low CaO (<8 wt. %), extremely high ZrO_2 (0.01-1 wt. %) contents and broad compositional ranges, neither reveal any trends of magmatic evolution, nor correspond to any igneous rocks of Norilsk region (Ryabov et al., 2014). Instead, their few compositional trends may be controlled by relative amounts of mineral phases. These facts imply heterogeneous entrapment of solid phases into the inclusions and question "pure magmatic" origin of

their assemblages. Concerning this, we note that the assemblage, dominated by orthopyroxene and alkaline feldspar, being unusual in magmatic rocks, is typical for high-T metamorphites. In their turn, orthopyroxene-bearing hornfels-like rocks are developed in the contact zones of Norilsk-type intrusions (Turovtsev, 2002), while scattered Cr-spinel is characteristic for skarns in contacts of Talnakh intrusion (Ryabov et al., 1996).

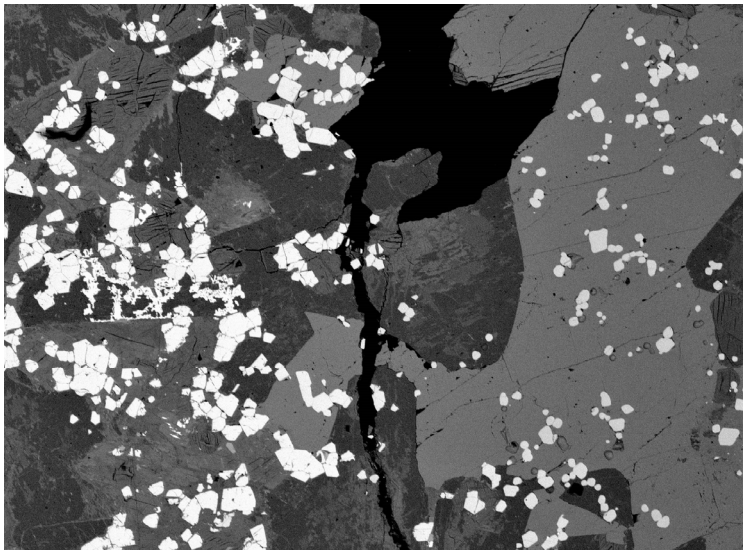

Figure 1. Cr-spinel scattering within sample MR-31. Note textural differences within unaltered (at the right sight) and altered silicates (at the left side).

This way obtained data on Cr-spinel with enclosed silicate inclusions from PGE-rich rocks of the upper zone of Norilsk-1 intrusion may challenge "pure-magmatic" nature of these rocks, probably implying significant contribution of contact-metamorphic or metasomatic processes.

The study is done on state assignment of IGM SB RAS and is supported by grant of Russian Scientific Foundation №19-17-13013.

References

Borisova A. Y., Ceuleneer G., Kamenetsky V.S. et al., A new view on the petrogenesis of the Oman ophiolite chromitites from Microanalyses of chromite-hosted inclusions // Journal of Petrology, 2012, Vol.53, p.2411-2440.

Kamenetsky V.S., Crawford A.J. and Meffre S., Factors controlling chemistry of magmatic spinel: an empirical study of associated olivine, Cr-spinel and melt inclusions from primitive rocks // Journal of Petrology, v.42, p.655-671.

Li C., Ripley E.M., Sarkar A., Shin D., Maier W.D., Origin of phlogopite-orthopyroxene inclusions in chromites from the Merensky Reef of the Bushveld Complex (South Africa) // Contributions to Mineralogy and Petrology, 2005, Vol.150, p.119-130.

Pushkarev E.V., Kamenetsky V.S., Morozova A.V., Khiller V.V., Glavatskykh S.P. and Rodemann T., Ontogeny of ore Cr-spinel and composition of inclusions as indicators of the pneumatolytic-hydrothermal origin of PGM-bearing chromitites from Kondyor massif, the Aldan shield // Geology of Ore deposits, 2015, Vol.57, p.352-380.

Ryabov V.V., Shevko A.Ya., Simonov O.N., Anoshin G.N., Composition of PGM-bearing high-chromian skarns of Talnakh intrusion (Norilsk region) // Geologiya I Geophysica, 1996, Vol.37, p.60-75 (in Russian).

Ryabov V.V. Shevko A.Ya., Gora M.P., Trap magmatism and ore formation in the Siberian Noril'sk region, Springer, 2014, 627 p.

Sluzhenikin S.F., Distler V.V., Grigor'eva A.V., Low-sulfide ores of Norilsk region – perspective resources of precious metals // Arctic: ecology and economics, Vol. 24, p. 32-45.

Turovtsev D.M., Contact metamorphism of Noril'sk intrusions: Moscow: Scientific World, 2002 (in Russian).

PARTITIONING OF TRACE ELEMENTS BETWEEN CALCITE, FLUORITE AND CARBONATITIC MELT IN THE SYSTEM $CaCO_3$+CaF_2+Na_2CO_3±$Ca_3(PO_4)_2$ AT 100 MPa AND 650-900°C

Chebotarev D.A.[1,2], Veksler I.V.[1,2,3], Wohlgemuth-Ueberwasser C.[2], Doroshkevich A.G.[1,4], Koch-Müller M.[2]

[1]V.S. Sobolev Institute of Geology and Mineralogy, Siberian Branch of Russian Academy of Sciences, pr. Akad Koptyuga, 3, Novosibirsk, 630090, Russia

[2]German Research Centre for Geosciences, GFZ, Telegrafenberg, 14473 Potsdam, Germany

[3]Institute of Earth and Environmental Science, Potsdam University, 14476 Potsdam-Golm, Germany

[4]Geological Institute SB RAS, Ulan-Ude, Sakhyanovoy Str., 6a, 670047, Russia

Low degree partial melting of a carbonated mantle source, which is presumed in the origin of primary carbonatitic magma, appears to be insufficient for the formation of carbonatitic rare metal ore deposits (Sweeney 1994; Foley et al. 2009) and further enrichment is required either by liquid-liquid or solid-liquid fractionation at shallower depths. The distribution of elements between immiscible carbonate and silicate liquids has been well constrained by experimental studies (Martin et al. 2012, 2013; Veksler et al. 1998, 2012). Experimental constraints for the solid-liquid element partitioning in carbonatitic magmas at crustal conditions are currently insufficient: experimental estimates of the partition coefficients for REE have been obtained for peridotite and eclogite mineral assemblages at upper mantle P-T conditions (Prowatke and Klemme 2006; Blundy and Dalton 2000; Dasgupta et al. 2009; Ryabchikov et al. 1993; Girnis et al. 2013; Sweeney et al. 1995; Hammouda et al. 2009, 2010 and others). Herewith, the estimates of the partition coefficients of trace elements for apatite are controversial and there is a lack of partition coefficients for calcite, dolomite and fluorite. Investigations of partition coefficients at lower pressures and temperatures for ore-bearing carbonatites, formed by fractional crystallization, are practically missing in the published literature.

The solubility of HFSE in carbonatitic melts is another important constraint on rare metal enrichment for which experimental data are insufficient and contradictory. According to Jago and Gittins (1993), the solubility of Nb in a $CaCO_3$-$Ca(OH)_2$ melt at 100 MPa and 600-900°C was estimated at around 5-7.5 wt.% Nb_2O_5. The authors found that introduction of alkalis into the system in form of Na_2CO_3 lowered Nb solubility approximately 10 times to below 0.75 wt.%, whereas addition of F in amounts of 1 wt.% and more stabilized pyrochlore instead of lueshite as the liquidus Nb-phase. Low solubility of Nb in Na-bearing carbonatitic melts was not confirmed, however, in a study of the system $CaCO_3$-$Ca(OH)_2$-$NaNbO_3$ (Mitchell 1997; Mitchell and Kjarsgaard 2002). In this study the cotectic crystallization of lueshite and calcite was observed and concentration of Nb_2O_5 in the melt was around of 48 wt.% at 100 MPa and 650°C. Later the same authors reported high Nb solubility, at about 14 wt.% Nb_2O_5, in the system $CaCO_3$-CaF_2-$NaNbO_3$ with pyrochlore instead of lueshite as the stable liquidus phase (Mitchell and Kjarsgaard 2004). Such a high Nb solubility is at odds not only with the results published by Jago and Gittins (1993) but also with petrographic observations implying relatively early pyrochlore crystallization in calciocarbonatite parental magmas.

This study aims at filling some of the above-mentioned gaps in our knowledge. We have studied the distribution of REE, Sr and a broad number of HFSE between a synthetic carbonatitic melt, calcite and fluorite in the system Na_2O-CaO-CO_2-P_2O_5-F at 650-900°C and 100 MPa. The study of HFSE distribution was hampered by unexpectedly low solubility of the elements in our carbonatitic melts, which lead to concentrations in calcite and fluorite that were below the detection limit of our analytical instruments. In the discussion, we apply our results to natural carbonatitic minerals and consider possible causes for the low HFSE solubility in our experiments.

Starting materials were mixtures of reagent-grade $CaCO_3$, Na_2CO_3, $Ca_3(PO_4)_2$ and CaF_2 doped with 10% of trace element mixture, composed of oxides of Zr, Hf, Nb, Ta, Ti, W, Mo, all REE (including Y) and CeF2, Li_2CO_3 and $SrCO_3$ in equal weight proportions (table 1). Six additional mixtures were prepared by adding 20 wt.% of $Ca_3(PO_4)_2$ to the mixtures. This was done in expectation to obtain liquidus apatite but, as discussed below, apatite never crystallized as a liquidus phase in our runs. Starting materials were put in gold capsules. Experiments performed at the pressure of 100 MPa

and over the temperature interval of 650-900 °C in rapid-quench cold-seal pressure vessels at the German Research Centre for Geosciences (GFZ Potsdam). Run times varied from 18 to 26 hours. Oxygen fugacity was not controlled, but is believed to have been close to that of the Ni–NiO equilibrium, buffered by oxidation reactions of the water used as pressure medium and the Ni–Cr alloy of the autoclave. Quenching performed by dropping the gold capsule into cold zone inside the autoclave, resulting in isobaric quenching in less than a second. The temperature was measured using an external Ni-CrNi thermocouple, which is calibrated against the melting temperature of gold. Temperature measurements are precisely corrected for a temperature gradient inside the autoclave.

The samples after experiments were composed of translucent glass-like material of quenched melt with inclusions of gas bubbles and crystals of fluorite, calcite, Hf-bearing baddeleyite, perovskite-lueshite solid solution and suspension of fine needle-like quench apatite in case of samples with addition of phosphate. We interpret the gas bubbles as a result of quench "boiling" of the vapor phase, originated during experiment and dominated by CO_2. Our charges were nominally dry but some water inside the sealed containers cannot be ruled out because of possible hydrogen diffusion from the surrounding H_2O vapor used as the pressure media.

We believe that clusters of small (few micrometers) Hf-bearing baddeleyite crystals and perovskite-lueshite solid solution were produced by reaction of carbonatitic melt with fine powders of pure Ti, Nb, Zr and Hf oxides in the reactant mixtures, which are dissolved poorly in designed carbonatitic melts. The solubilities of these four elements appear to decrease with temperature and tend to be higher in P-bearing melts. The solubilities of Ti, Mo and W are approximately two orders of magnitude higher, than Nb, Ta, Hf and Zr. This is an interesting side result of this study which deserves a more detailed study in the future.

The distribution coefficients were calculated according to the Nernst formula as mass ratios of element concentrations in a crystalline phase to their concentrations in the melt: $D_t^{Crystal/Melt} = C_t^{Crystal} / C_t^{Melt}$

All the studied trace elements are moderately or strongly incompatible with calcite and fluorite. The highest D values, from 0.48 to 0.80, were found for Sr in calcite (fig. 1 a). The other D values are far below 1 and rarely exceed 0.3. REE tend to be slightly more compatible with fluorite rather than calcite with the maximal D^{Fl}/Melt measured for Y at 0.18-0.3. There is a general increase of the DREE values with the atomic number for both minerals; it is more pronounced for fluorite and appears to go through a maximum or flattening at Ho-Er. Overall, we did not detect any systematic dependence of the D values on temperature and/or melt composition.

Partition coefficients are often used in igneous petrology for inversion calculations, that is, estimations of trace element abundances in a parental melt based on measured concentrations in a daughter mineral for which the D values are known. Such calculations are especially useful for carbonatitic magmas that are unquenchable, dynamic, chemically very reactive and often strongly affected by magmatic and post-magmatic metasomatic processes. Because of that, whole-rock concentrations in carbonatites, especially in plutonic ones, may poorly correspond to the trace element characteristics of the parental magma.

The distribution coefficients for calcite and fluorite, obtained in our work, can be useful tool for estimating of content of trace elements in parental carbonatitic melts. Calcite is probably the most common early-crystallizing carbonatitic mineral and it contains measurable amounts of Sr and REE, for which the D values were obtained in this study.

Some results of the inversion for natural calcite from a plutonic carbonatite Belaya Zima in Russia and subvolcanic carbonatite of the Kerimasi volcano in east Africa are presented at figure 1 b. Notably, whole-rock REE concentrations are only slightly higher than those in calcite and more than an order of magnitude lower than the expected concentrations in parental melt calculated by the inversion. If our D^{REE} values are correct and the REE concentrations in calcite are primary magmatic, mass balance relationships illustrated by the figure would mean that calciocarbonatites at both locations are calcite cumulates that retained only a small fraction of REE originally present in the parental magmas. The rest should be gone elsewhere with residual melts or fluids.

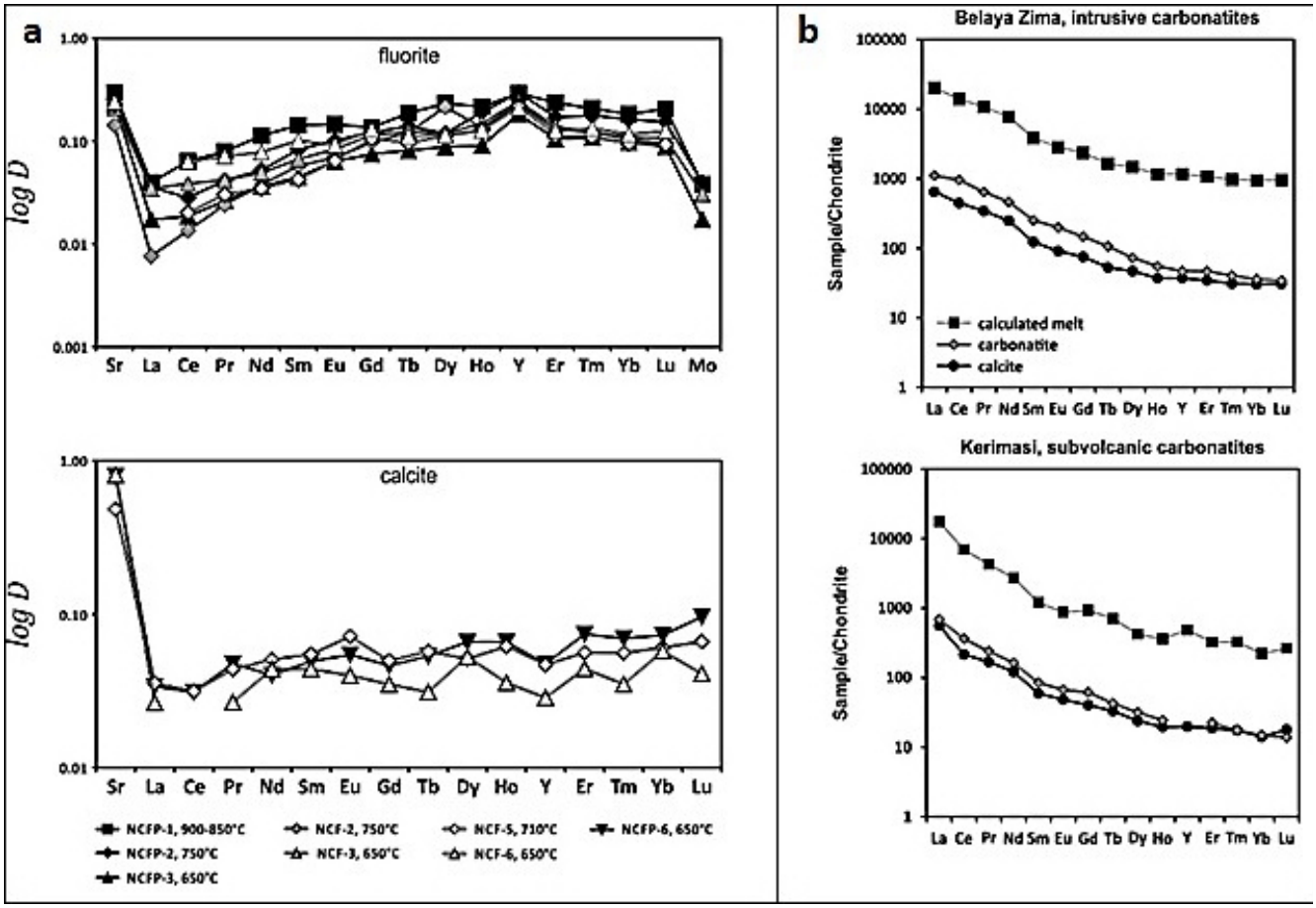

Figure 1. a - Plots of experimentally determined distribution coefficients for calcite and fluorite; b - Plots of the average contents of REE in carbonatitic calcites, carbonatites and in parental melt, calculated on the basis of the obtained distribution coefficients, for calcitic carbonatites from Belaya Zima and Kerimasi, normalized to chondritic concentration (Sun and McDonough 1989).

Extensive experimental work has been done on Nb solubility in carbonatitic melts (Jago and Gittins 1993; Mitchel and Kjarsgaard 2002, 2004) but, as briefly outlined in the introduction, the results are incomplete and contradictory. This study adds to the confusion because the Nb concentrations in our synthetic melts are much lower than any values that had been published before. Likewise, the concentrations of Ta, Zr and Hf are also very low, at the level of tens mg/kg or even lower. Furthermore, despite very high concentrations of F in our synthetic melts, pyrochlore was not observed in the run products but Nb concentrated instead in a Nb-rich perovskite phase, presumably $(Na,Ca)(Nb,Ti)O_3$. The presence of significant amounts of Ti in our starting mixtures (in contrast with the previously studied simplified synthetic systems) and stabilization of the Nb-Ti perovskite solid solution in our runs may be the main reason for the low Nb and Ta solubilities that we observe in this study. $CaTiO_3$ is a very refractory phase and its early liquidus crystallization in our charges is quite possible.

This project has been supported by Russian state assignment project № 0330-2016-0002.

References

Blundy J, Dalton J (2000) Experimental comparison of trace element partitioning between clinopyroxene and melt in carbonate and silicate systems, and implications for mantle metasomatism. Contrib to Mineral and Petrol 139: 356−371.

Dasgupta R, Hirschmann MM, McDonough WF, Spiegelman M, Withers AC (2009) Trace element partitioning between garnet lherzolite and carbonatite at 6.6 and 8.6 GPa with applications to the geochemistry of the mantle and of mantle-derived melts. Chem Geol 262:57–77.

Doroshkevich AG, Veksler I, Klemd R, Khromova EA, Izbrodin IA (2017) Trace-element composition of minerals and rocks in the Belaya Zima carbonatite complex (Russia): Implications for the mechanisms of magma evolution and carbonatite formation. Lithos 284-285:91-108.

Foley SF, Yaxley GM, Rosenthal A, Buhre S, Kiseeva ES, Rapp RP, Jacob DE (2009) The composition of near-solidus melts of peridotite in the presence of CO2 and H2O between 40 and 60 kbar. Lithos 112:274–283.

Girnis AV, Bulatov VK, Brey GP, Gerdes A, Höfer HE (2013) Trace element partitioning between mantle minerals and silico-carbonate melts at 6–12 GPa and applications to mantle metasomatism and kimberlite genesis. Lithos 160–161:183–200.

Hammouda T, Moine BN, Devidal JL, Vincent C (2009) Trace element partitioning during partial melting of carbonated eclogites. Physics of the Earth and Planetary Interiors 174:60–69.

Hammouda T, Chantel J, Devidal JL (2010) Apatite solubility in carbonatitic liquids and trace element partitioning between apatite and carbonatite at high pressure. Geochimica et Cosmochimica Acta 74:7220-7235.

Jago BC, Gittins J (1993) Pyrochlore crystallization in carbonatites: the role of fluorine. S Afr J Geol 96:149–159.

Martin LHJ, Schmidt MW, Hannes B, Mattsson HB, Ulmer P, Hametner K, Günther D (2012) Element partitioning between immiscible carbonatite–kamafugite melts with application to the Italian ultrapotassic suite. Chem Geol 320-321:96–112.

Martin LHJ, Schmidt MW, Mattson HB, Guenther D (2013) Element partitioning between immiscible carbonatite and silicate melts from dry and H2O-bearing systems at 1 - 3 GPa. J Petrol 54:2301 - 2338.

Mitchell RH (1997) Preliminary studies of the solubility and stability of perovskite group compounds in the synthetic carbonatite system calcite–portlandite. J Afr Earth Sci 25:147–158.

Mitchell RH, Kjarsgaard BA (2002) Solubility of niobium in the system CaCO3–Ca(OH)2–NaNbO3 at 0.1 GPa pressure. Contrib Mineral Petrol 144:93–97. DOI 10.1007/s00410-002-0384-3.

Mitchell RH, Kjarsgaard BA (2004) Solubility of niobium in the system CaCO3–CaF2–NaNbO3 at 0.1 GPa pressure: implications for the crystallization of pyrochlore from carbonatite magma. Contrib Mineral Petrol 148:281-287. https://doi.org/10.1007/s00410-004-0603-1.

Mitchell R.H. (2005) Carbonatites and carbonatites and carbonatites. Can. Mineral. 43:2049–2068.

Prowatke S, Klemme S, (2006) Rare earth element partitioning between titanite and silicate melts: Henry's law revisited. Geochim Cosmochim Acta 70:4997–5012.

Ryabchikov ID, Orlova GP, Senin VG, Trubkin NV (1993) Partitioning of rare earth elements between phosphate-rich carbonatite melts and mantle peridotites. Mineral Petrol 49:1-12.

Sweeney RJ (1994) Carbonatite melt compositions in the Earth's mantle. Earth Planet Sci Lett 128:259–270.

Sweeney RJ, Prozesky V, Przybylowicz W (1995) Selected trace and minor element partitioning between peridotite minerals and carbonatite melts at 18 – 46 kbar pressure. Geochim Cosmochim Acta 59:3671–3683.

Tomkute V, Solheim A, Sakirzanovas S, Oye B, Olsent E (2014) Phase equilibria evaluation for CO2 capture: CaO–CaF2–NaF, CaCO3–NaF–CaF2, and Na2CO3–CaF2–NaF. J Chem Engineering Data 59:1257–1263.

Veksler IV, Petibon C, Jenner G, Dorfman AM, Dingwell DB (1998) Trace element partitioning in immiscible silicate and carbonate liquid systems: an initial experimental study using a centrifuge autoclave. J Petrol 39:2095-2104.

Veksler IV, Dorfman AM, Dulski P, Kamenetsky VS, Danyushevsky LV, Jeffries T, Dingwell DB (2012) Partitioning of elements between silicate melt and immiscible fluoride, chloride, carbonate, phosphate and sulfate melts with implications to the origin of natrocarbonatite. Geochim Cosmochim Acta 79:20-40.

EARLY CAMBRIAN SHOSHONITIC MAGMATISM AT THE NORTHEAST OF THE SIBERIAN CRATON, RUSSIA

Demonterova E.I., Lomyga V.P., Ivanov A.V.

Institute of the Earth's Crust SB RAS, Irkutsk, Russia, dem@crust.irk.ru

Early Cambrian magmatic events mark one of the most intriguing periods of Earth history. For example, at this time, the hyperactivity of magnetic field was recorded (Pavlov et al., 2018) and marine invertebrates explosively diversified (Bowring et al., 1993). The factual basis for the investigation of the Early Cambrian events is the sedimentary and igneous formations of the north-eastern Siberia, where Verkhoyansky orogenic belt joins the Siberian Craton units (Bowring et al., 1993; Khudoley et al., 2013; Prokopiev et al., 2016; Pavlov et al., 2018). This region is remote and difficult for access and due to this it may keep some unique information, which cost to be revealed. Here we report new data on chemical and isotopic compositions of mafic dykes and sills of the Chekurovka anticline, which was not recorded by previous studies (Khudoley et al., 2013; Prokopiev et al., 2016).

The studied mafic rocks were collected during 2017 field campaign along Neleger (right tributary of Lena). Dykes and sills are located within Neoproterozoic sediments of the Neleger and Kharayutekh Formations and Early Cambrian Tyuser Formation (Oleinikov, 1983). At the base of the Tyuser Formation conglomerates are located whose pebbles have rhyolitic composition. Zircons from these pebbles were dated by U-Pb method using SHRIMP independently by (Bowring et al., 1993) and (Prokopiev et al., 2016) and the resulting age estimations 534.6 ± 0.4 Ma and 532.6 ± 3.1 Ma, respectively, were taken as the age of the Pre-Cambrian – Cambrian boundary. In previous studies (Khudoley et al., 2013; Prokopiev et al., 2016), mafic igneous rocks were analyzed mainly from Neoproterozic part of the section. Only few Early Cambrian samples were also analyzed. In our study, we analyzed only Early Cambrian rocks, extending the available information into a younger period.

Analytical work was done using equipment belonging to the Centre for Geodynamics and Geochronology, Institute of the Earth's Crust SB RAS (Irkutsk, Russia). Major and trace element concentrations of the samples have been determined by XRF and ICP-MS, respectively, using lithium tetraborate and metaborate fusion for sample preparation (Pashkova et al., 2019). The $^{87}Sr/^{86}Sr$, $^{143}Nd/^{144}Nd$, $^{87}Rb/^{86}Sr$, and $^{147}Sm/^{144}Nd$ isotopic ratios were obtained by isotope dilution TIMS using a Finnigan MAT 262 mass-spectrometer according a procedure described in (Ivanov et al., 2018).

In TAS diagram (Le Bas, Streckeisen, 1991), mafic rocks of the Chekurovka anticline fall into the fields of basalt, trachybasalt, tephrite and picritic basalts. SiO_2 concentrations vary from 41 to 51 wt.% at Na_2O+K_2O between 3 and 5.9 wt.%. All rocks belong to high-Ti rock series with TiO_2 between 2.4 and 6.5 wt. %. Unlike to the previous studies (Khudoley et al., 2013; Prokopiev et al., 2016), some of our samples are high in K_2O and classified as absarokites, thus mafic end-member of the shoshonitic series rocks (Fig. 1). K_2O/Na_2O ratio in these rocks varies between 4.4 and 18. It is interesting, that rhyolites from conglomerate pebbles are also characterized by potassic affinity and can be classified as comendites-pantellerites (Prokopiev et al., 2016). Our study shows, that there was also mafic volcanism of the shoshonitic series in the region.

In primitive mantle-normalized diagrams, most common basaltic rocks are characterized by enriched spectra, typical for intraplate tectonic settings. This was taken as evidence for their origin because of rifting between South-Taimyr and West-Verkhoyan passive continental margins (Khudoley et al., 2013; Prokopiev et al., 2016). Absarokites are characterized by more differentiated trace-element spectra with several peaks and troughs in primitive mantle-normalized diagrams. Irrespective basaltic or shoshonitic type rocks, they show positive εNd_t values (+3 – +9). εSr_t values vary from -8 to + 67, with absarokites shifted towards the higher values. Considering that the same absarokites are characterized by high Sr concentrations (650-2100 ppm), the Sr isotopic values for them were likely not modified by secondary processes.

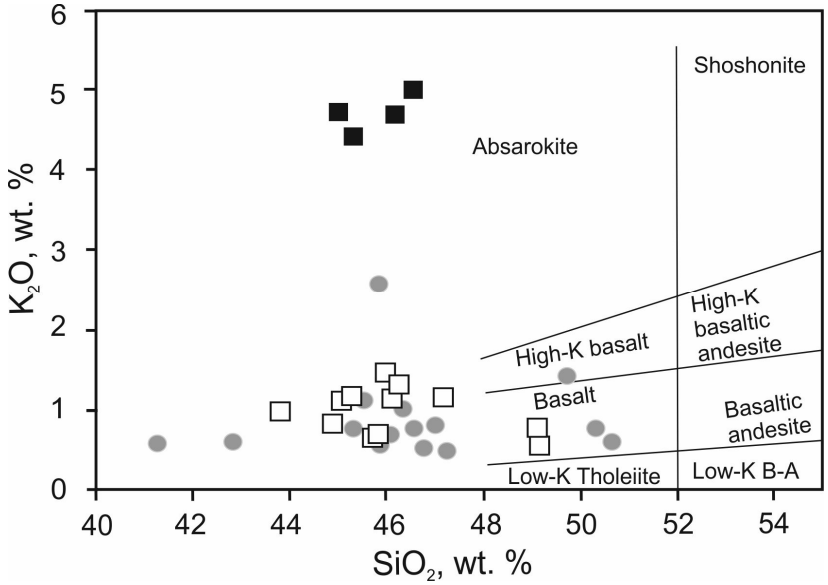

Figure 1. SiO_2-K_2O diagram for Neoproterozoic – Early Cambrian mafic rocks of the northeastern Siberia. Grey circles are from (Prokopiev et al., 2016). White and black squares are new authors' data.

Shoshonite origin is debated, though majority considers this rock type as originated in orogenic setting. If so, the appearance of comendites and pantellerites at the Pre-Cambrian – Cambrian boundary and absarokites further in time in Early Cambrian marks gradual change of the tectonic setting from rifting to compression. The significance of the recorded change in the igneous rock compositions awaits its understanding in terms of tectonic reconstructions.

This work was supported by the Russian Science Foundation (project no. 16-17-10068).

References

Bowring S.A., Grotzinger J.P., Isachsen C.E., Knoll A.H., Pelechaty Sh.M., Kolosov P. Calibrating rates of Early Cambrian evolution. Science. 1993. Vol. 261. p. 1293-1298.

Ivanov A.V., Demonterova E.I., Savatenkov V.M., Perepelov A.B., Ryabov V.V., Shevko A.Y. Late Triassic (Carnian) lamproites from Noril'sk, polar Siberia: Evidence for melting of the recycled Archean crust and the question of lamproite source for some placer diamond deposits of the Siberian Craton. Lithos. 2018. Vol. 296-299. p. 67-78.

Khudoley A.K., Prokopiev A.V., Chamberlain K.R., Ernst R.E., Jowitt S.M., Malyshev S.V., Zaitsev A.I., Kropachev A.P., Koroleva O.V. Early Paleozoic mafic magmatic events on the eastern margin of the Siberian Craton. Lithos. 2013. Vol. 174. p. 44–56.

Le Bas M.J., Streckeisen A.I. The IUGS systematics of igneous rocks. Journal of Geological Society. 1991. Vol. 148. p. 825-833.

Oleinikov B.V., Mashchak M.S., Kolodeznikov I.I., Kopylova A.G., Savinov V.T., Tomshin M.D., Tulasynov B.N. Petrology and Geochemistry of the Late Precambrian Intrusive Basites of the Siberian Platform. Nauka, Novosibirsk. 1983 (in Russian).

Prokopiev A.V., Khudoley A.K., Koroleva O.V., Kazakova G.G., Lokhov D.K., Malyshev S.V., Zaitsev A.I., Roev S.P., Sergeev S.A., Berezhnaya N.G., Vasiliev D.A. The Early Cambrian bimodal magmatism in the northeastern Siberian Craton. Russian Geology and Geophysics. 2016. Vol. 57. p. 155–175.

Pashkova G.V., Panteeva S.V., Ukhova N.N., Chubarov V.M., Finkelshtein A.L., Ivanov A.V., Asavin A.M. Major and trace elements in meimechites – rarely occurring volcanic rocks: developing optimal analytical strategy. Geochemistry: Exploration, Environment, Analysis, 2019, doi: 10.1144/geochem2017-099.

THE ZHIDOY MASSIF OF ALKALINE ROCKS AND CARBONATITES AND ITS ORE POTENCIAL (IRKUTSK REGION)

Dokuchits E.Yu., Alymova N.V., Vladykin N.V.

Institute of Geochemistry SB RAS, Irkutsk, Russia, esfor@rambler.ru; alymova@igc.irk.ru; vlad@igc.irk.ru

Abstract. In this work geological structure of the Zhidoi massif and its ore potencial has been described. The scheme of the massif magmatism has been constructed. Double correlation plots of petrogenic elements of rocks of the massif in which the unified trend of rock structures is observed, are given for verification of correctness of the scheme of magmatism. Spectra of TR and spider diagrams of concentrations of rare elements in rocks of the massif are given. Piroxenites, early rocks of the massif are ores on titanium. Titanium concentrates in three minerals: titanomagnetite, ilmenite and perovskite. The main type of titanium ores is perovskitic type, it is known only in the Zhidoi massif. Mantle sources of primary magma of the massif are concluded on the basic of geochemistry of isotopes of Sr and Nd.

Keywords: alkaline massif, carbonatites, titanium ores, perovskite, mantle sources.

Composition and location. At the present time two important objects in Eastern Sayan mountains of the Irkutsk region are preparing for mining on strategic rare elements: the Zashikhinsky massif (on Nb, Ta, Zr) (Alymova, Vladykin, 2018), and the Zhidoy massif (on Ti). Titanium is a strategic mineral, which is necessary in industry. Titanium concentrate were previously provided to Russia from gravel deposits of Ukraine, but now this element is in short supply. In Russia titanium deposits are presented by titanomagnetite, and it is difficult to extract titanium from it. In Irkutsk region titanium deposits were discovered in recent years in the Murun massif, where they are represented by quartz zones, pure TiO_2 - brukite, anatase and rutile (Vladykin, 2016; Dokuchits, Vladykin, 2018), and in the Zhidoy massif, where titanium deposits are represented by pyroxenite with perovskite, ilmenite and titanomagnetite. The Murun massif is located in inaccessible area of the Irkutsk region while the Zhidoy massif is located in 80 km from Irkutsk, close to Talyany town. Ores of the Zhidoy massif are magmatic pyroxenites of the main phase, occupying 95% of area of the massif with outcrops.

There are four types of pyroxenites with different varieties of successive Ti-ores:

1) pyroxenite with titanomagnetite (broken down to magnetite and ilmenite) without perovskite;

2) pyroxenite with titanomagnetite (broken down to magnetite and ilmenite) with separate segregations of ilmenite;

3) pyroxenite with titanomagnetite and ilmenite enriched in perovskite in 7 %;

4) pyroxenite enriched in titanite with little titanomagnetite and without perovskite (non ore-bearing).

The massif is not well researched. Beyond pyroxenites there are outcrops of veins bodies of ijolites, alkaline and nepheline syenites. Previously only two small bedrock outcrops (up to one meter) of carbonatite dykes were known. At the present time by the performed drilling operations which were made, a carbonatite body with thickness 60 m was found. In in one of its sides a rare-metal zircon-pyrochlore mineralization has occurred. It's similar with those of the Belaya Zima carbonatite province, to which the Zhidoy massif belongs. That's why carbonatites can be of industrial interest as sources of rare elements (Alymova, Vladykin, 2018). In some publications this massif called Zadoy (Rasskazov et al., 2007), which leads to confusion, because there is another Zadoy massif of ultrabasic rocks in Prisayanye area, that's why it's necessary to assign the old name Zhidoy to the massif.

The Zhidoy massif is located in 80 km from Irkutsk, in the Nephelinovy Creek when flowing into the Bolshoy Zhidoy river, in early-precambrian Sharyzhalgaisky block of the Prisayanye basement high of the Siberian platform. It cuts through biotite-hornblend gneisses. Phenites are originated in north part of the massif in exocontact part, they were explored by boreholes, drilled in contact wallrocks. The massif covers an area of 0,85 km2 and its territory is horseshoe-shaped, with the length of intrusion of 2 km and width of 600 m. According to a geophysical data rocks of the massif continue all the way to the Bolshoy Zhidoy river.

The massif of the alkaline-ultrabasic carbonatite formation contains 90% of ore pyroxenites with different compositions of titanomagnetite, ilmenite and perovskite. It is considered that the massif has four phases of intrusion: pyroxenites, ijolites, syenites and calcite carbonatites (Konev, 1917; Rasskazov et al., 2007). Last three phases form small dykes and can be recognized as dykes of additional intrusions. The massif is hypabyssal, as evidenced by fine-grained pyroxenites; also it's possible that there are ore-bearing carbonatites containing rare elements in deeper layers. In some places carbonatites have silicate-carbonate composition, including pure albite. That's why one of the main challenges is detailed research of these carbonatites on potential to rare-metal productivity. Data on isotopic research on Sr and Nd in five varieties of rocks had been received in collaborative work with geochemists from the Shinsu University and Niigara University, Japan; according to these data the age of the massif is 570-610 mln years (Morikiyo et al., 2000; Vladykin et al., 2005). It's necessary to continue the study of isotope geochemistry and clarify the age of the massif by zircons using the U-Zr method of analysis.

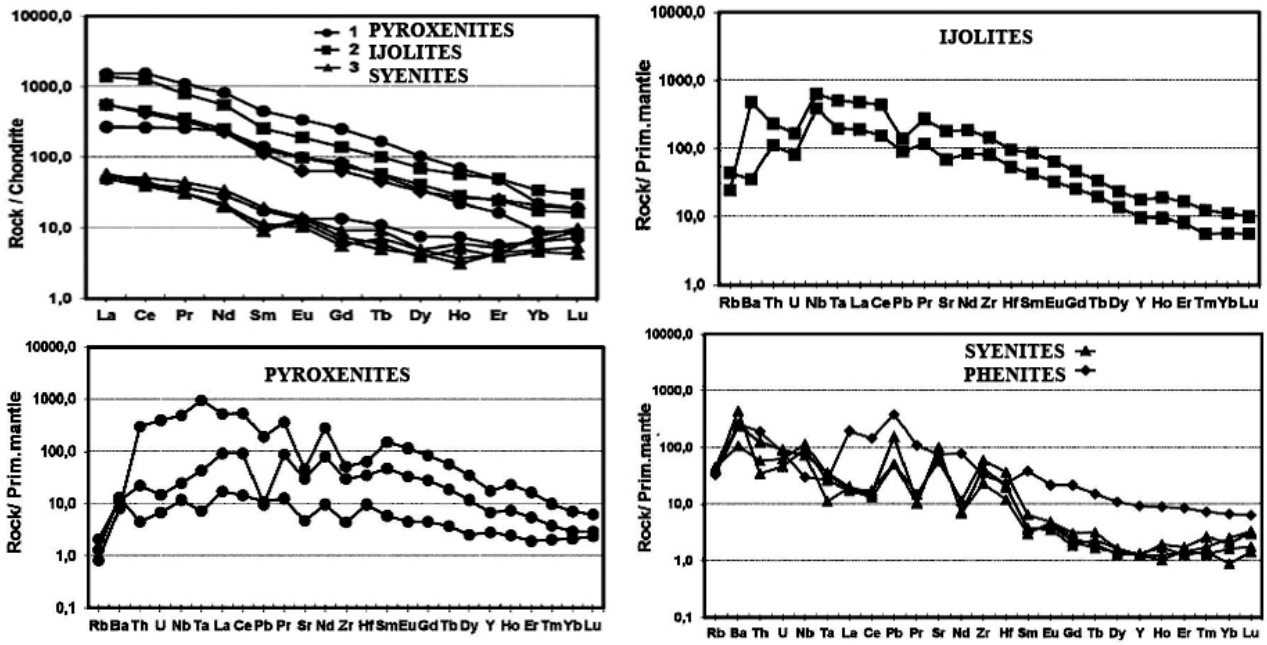

Figure. Spectra of REE and spider plots of rare elements in rocks of the Zhidoy massif.

Geochemical research. Studies of concentration of rare elements in rocks by the ICP-MS method had been made (IGC SB RAS, analyst - Mitrofanova A.Yu.). Spectra and spider plots of rare elements are shown in figure. As shown in plots, spectra of REE of rocks of the massif are idential, reflecting the genetic connection of these rocks. The highest concentrations are observed in perovskite pyroxenites and the lowest are in syenites. Increasing concentrations of high lanthanides are observed in syenites starting with Ho. Behavior of rare elements in pyroxenites is similar to those of ijolites. Negative anomalies of Pb, Sr, Zr and Hf and flat curves of REE are observed.

Different trends are observed in syenites: distinctly positive anomalies of Sr, Pb, Zr, Hf, which can be explained by differentiation processes in syenites, which are late rocks. A distribution of elements in phenites is different from those of magmatic rocks.

Conclusions:

1. Three varieties of ore-bearing pyroxenites with titamonagnetite, ilmenite and perovskite ore are given.

2. Common trends of compositions of rock-forming elements are observed in petrochemical diagrams reflecting the genetic connection of these rocks and their crystallization from primary parent magma.

3. Geochemical data are also confirm genetic connection of rocks of the Zhidoy massif.

The work was supported by the Russian Foundation for Basic Research (grant 17-45-3880045) and Integration project ISC block 2.1.

References

Alymova N.V., Vladykin N.V., Ore potencial of rare-metal granites of the Zashikhinsky massif (Irkutsk region) and minerals concentrators Ta, Nb, Th, Zr, Tr // The Bulletin of Irkutsk State University. Series: the Earth Sciences. 2018. V. 25. pp. 15-29. DOI: 10.26516/2073-3402.2018.25.15

Dokuchits E.Yu., Vladykin N.V. Composition and genesis of silicate-carbonate rocks of charoite complex // Proceeding of XXXV International conference "Magmatism of the Earth and related strategic metal deposits". 3-7 September, 2018. Moscow, Russia, p. 73-75.

Konev A.A. Zhidoysky alkaline-ultrabasic pluton. - M.: Nauka, 1970. - 84 p

Rasskazov S.V., Ilyasova A.M., Konev A.A., Yastsygina T.A., Maslovskaya M.N., Fefelov N.N., Demonterova E.I., Saranina E.V. Geochemical evolution of the Zadoy massif of Prisayanye // Geochemistry, 2007. - № 1. p. 3-18.

Morikiyo T., Takano K., Miyazaki T. et al. Sr, Nd, C and O isotopic compositions of carbona- tite and peralkaline silicate rocks from the Zhidoy complex, Russia // J. Mineralogical and Petrological Sciences. – 2000. – V. 95. – p 162–172.

Vladykin N. V., Morikiyo T., Miyazaki T. Sr and Nd isotopes geochemistry of alkaline and carbonatite complexes of Siberia and Mongolia and some geodynamic consequences // Problems of sources of deep magmatism and plumes. – Irkutsk, 2005. –V. 1. – p. 19–37.

Vladykin N.V. Genesis and crystallization of ultramafic alkaline carbonatite magmas of Siberia: ore potential, mantle sources and relationship with plume activity // Geology and geophysics, V. 57, 2016, p. 698-712.

EPITAXIC AND SYNTACTIC INTERGROWTH OF STRUCTURAL RELATED SPINELS, MINERALS OF HÖGBOMITE SUPERGROUP, NEŽILOVITE AND RINMANITE FROM PELAGONIAN MASSIF, MAKEDONIA

Ermolaeva V.N.[1,2], Chukanov N.V.[3,4], Varlamov D.A.[1,4], Van K.V.[1], Jančev S.[5]

[1]Institute of Experimental Mineralogy RAS, Chernogolovka

[2]Vernadsky Institute of Geochemistry and Analytical Chemistry RAS, Moscow

[3]Faculty of Geology, Moscow State University, Vorobievy Gory, Moscow, 119991, Moscow

[4]Institute of Problems of Chemical Physics RAS, Chernogolovka

[5]Faculty of Technology and Metallurgy, Saints Cyril and Methodius University, Skopje, Macedonia

Minerals of the spinel group, högbomite supergroup (MHS), nežilovite and rinmanite were found in the Pelagonian massif, Macedonia in two types of metasomatic rocks enriched in chalcophile elements (As, Sb, Pb, Zn). The first type is represented by a predominantly oxide mineral association composed by gahnite, franklinite, hetaerolite, and zincovelesite-6*N*6*S*. Other oxides (hydroxycalcioroméite, almeidaite, Mn analogue of plumboferrite), silicates (zircon, Zn-containing talc), and As-containing fluorapatite, as well as quartz and baryte, are present as minor and accessory minerals. Single grains of zincochromite are present as relicts of an earlier association (Ermolaeva et al., 2016). This rock contains numerous hydrothermal veinlets, predominantly composed of ferricoronadite (Chukanov et al., 2016). The second type is represented by granular aggregates composed of baryte and/or tilasite as well as silicate minerals (clinopyroxene, amphibole, alkaline feldspars) and contains variable amounts of oxides (Zn spinels, zincohögbomite-2*N*6*S*, zincovelesite-6*N*6*S etc.*). Minerals of pyrochlore and epidote supergroups, zircon, hematite, almeidaite, As-containing fluorapatite are presented as accessory components. Zn-containing talk and quartz occur as relicts of an earlier association (Ermolaeva et al., 2016).

Electron microprobe analyses were carried out using a Tescan VEGA-II XMU electronic microscope (EDS mode, 20 kV, 400 pA). Data reduction was carried out by means of a modified INCA Energy 450 software package. The size of the electronic beam is 157-180 nm in the analytical mode and 60 nm in the scanning mode. The excitation zone reached 5 μm. The time of data accumulation was 100 s. The sample-to-detector distance was 25 mm. BSE imaging was carried out with magnifications from 40 to 1670x. The standards used are: MgF_2 for F, albite for Na, MgO for Mg, Al_2O_3 for Al, SiO_2 for Si, $LaPO_4$ for P, FeS_2 for S, sanidine for K, wollastonite for Ca, InAs for As, SrF_2 for Sr, BaF_2 for Ba, $LaPO_4$ for La, $CePO_4$ for Ce, $NdPO_4$ for Nd, PbTe for Pb, UO_2 for U; Ti, Cr, Mn, Fe, Zn, Y, Zr for Zr Nb, Sb for corresponding elements.

Minerals of the spinel group (gahnite, franklinite) and hetaerolite (so-called "spinellides") form isometric grains or graphic intergrowths (figs. 1a), and MHS occur as subparallel aggregates of thin plates (fig. 1b-f). Gahnite often forms partial or full pseudomorphs after franklinite and hetaerolite grains (Ermolaeva et al., 2016; fig. 1a). MHS are trigonal or hexagonal minerals whose structures are formed by different kinds of regular alternation of spinel (*S*) and nolanite (*N*) modules (Armbruster, 2002). In particular, periodically repeating unit of described by us earlier zincohögbomite-2*N*6*S* from Pelagonian massif (Chukanov et al., 2015) consists of 2 nolanite and 6 spinel modules. In the MHS nomenclature approved by the IMA CNMNC, two criteria are accepted to distinguish mineral groups within MHS: composition of the spinel module and a high-valence cation (*e.g.* Ti^{4+} or Sn^{4+}) which prevails (in atomic units) in the nolanite module. In all MHS known until recently, Al dominates in the spinel module over other 3-valent cations (Fe^{3+}, Mn^{3+}). The new MHS zincovelesite-6*N*6*S* $Zn_3(Fe^{3+},Mn^{3+},Al,Ti)_8O_{15}(OH)$ approved recently by IMA CNMNC (Chukanov et al., 2018) in an ore occurrence of the Pelagonian massif is the first Fe^{3+}-dominant member of högbomite supergroup, and, thus, the "ancestor" of a new group of these minerals. The repeat unit of this mineral consists of 6 nolanite and 6 spinel modules. Detailed research of compositional variations of MHS from non-sulphide endogeneous Pb-Zn-Sb-As associations occurring in the Pelagonian massif shows that chemical variability of these minerals is beyond that accepted in their nomenclature. In particular, Mn^{4+} or Sb^{5+} may play the role of the main charge-balancing high-valent cations (Ermolaeva et al., 2018).

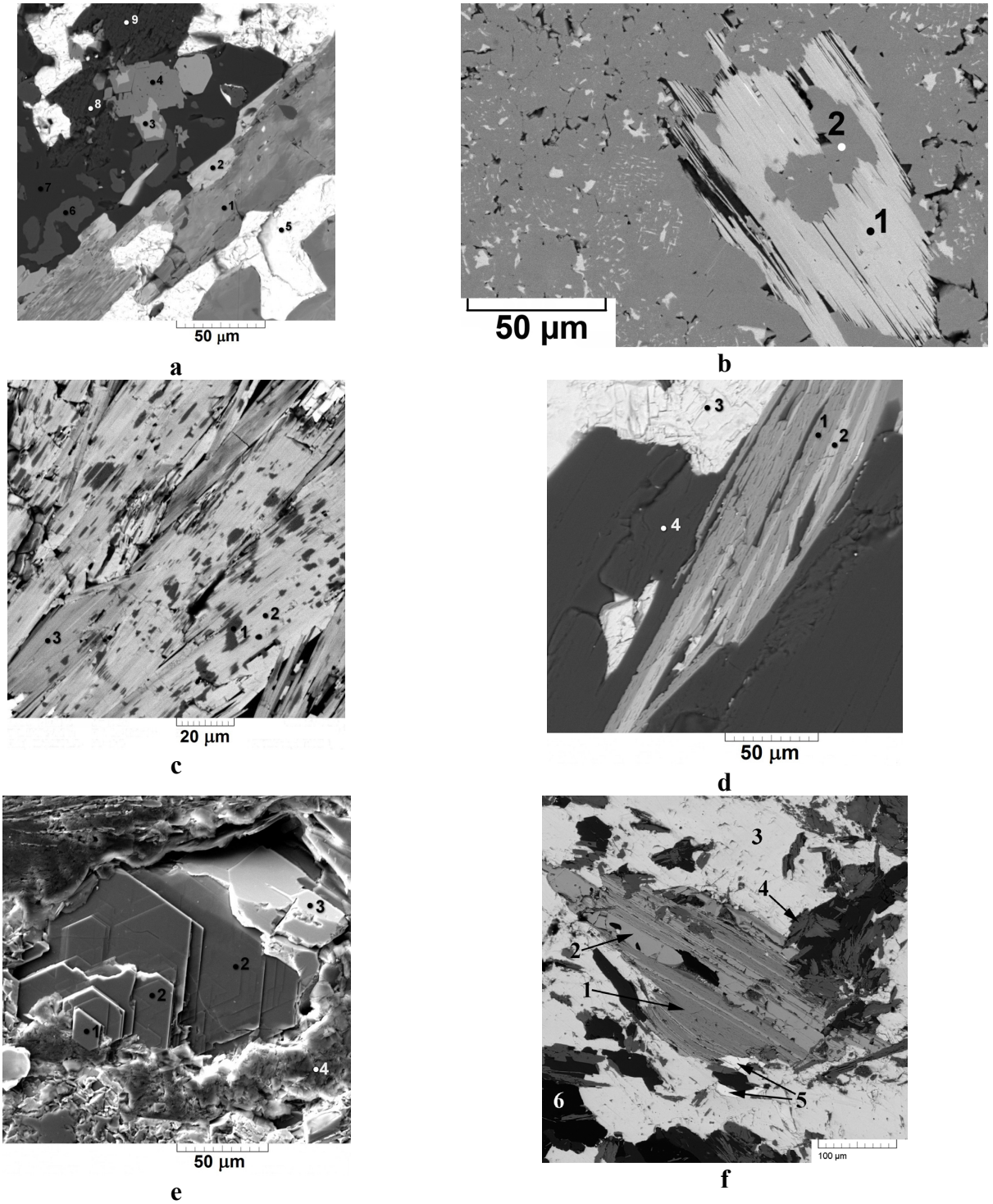

Figure 1. a. Piemontite (1), "ferripiemontite-(Pb)" (2), franklinite (3), gahnite (4), barite (5), aegirine-augite (6), albite (7), quartz (8), Zn-containing talk (9). Sample 2017-3. b. Zincovelesite-6*N*6*S* (1), gahnite (2), franklinite (3). Sample FeCor-1. c. Relicts of gahnite (1) in zonal aggregate of zincovelesite-6*N*6*S* (light zones, 2) and zincohögbomite-2*N*6*S* (dark zones, 3). Sample 2017-2. d. Syntactic intergrowth of zincovelesite-6*N*6*S* (1) with nežilovite (2) in barite (3) and Zn-containing phlogopite (4) aggregate. Sample 2017-13. e. Sb-analogue of zincohögbomite-2*N*6*S* (1), zincohögbomite-2*N*6*S* (2), barite (3), Zn-containing talk (4). Sample 2017-15. f. Epitaxic intergrowth of zincovelesite-6*N*6*S* (1) with rinmanite (2) in barite (3) in association with zincohögbomite (4), gasparite-(Ce) (5), quartz (6). Sample 2018-5. Polished sections. BSE images.

Often regular intergrowths of earlier zinc shpinels with later MHS are observed (figs. 1b, c). Obviously, the presence of spinel module in MHS structures promoted the formation of epitaxic intergrowths of MHS with gahnite and franklinite individuals.

In turn, MHS often form close epitaxic and syntactic intergrowths with nežilovite (fig. 1d). Outer zone of these parallel intergrowths of nežilovite and MHS are composed by zincohögbomite, which confirms that the latter was formed after nežilovite and other MHS. The latest mineral in intergrowths of this type is apparently Sb-analogue of zincohögbomite (point 1 in fig. 1e). The formation of parallel intergrowths of MHS with nežilovite is caused by the similarity of *a*-parameters of unit cells of these minerals (5.74 Å for zincohögbomite-2*N*6*S* (Chukanov et al., 2015), 5.90 Å for zincovelesite-6*N*6*S* (Chukanov et al., 2018), and 5.85 Å for nežilovite (Bermanec et al., 1996)), as well as commensurability of *c*-parameters of unit cells of zincovelesite-6*N*6*S* (55.87 Å) and nežilovite (22.81 Å).

Zincovelesite-6*N*6*S* also forms close intergrowths with rinmanite $Mg_2Fe_4Zn_2Sb_2O_{14}(OH)_2$ (fig. 1f), one more oxide structurally related to MHS. The formation of parallel intergrowths of these minerals is also caused by the proximity of *a*-parameters of unit cells (5.99Å for rinmanite, 5.90 Å for zincovelesite-6*N*6*S*), as well as commensurability of *c*-parameters of rinmanite (9.35Å) and zincovelesite-6*N*6*S* (55.87 Å).

The work was supported by the Russian Foundation for Basic Research (projects no. 18-05-0051_a and 17-05-00179).

References

Ermolaeva V.N., Chukanov N.V., Jančev S., Van K.V. Endogenic oxide parageneses with chalcophile elements in the orogenic zone related to the “Mixed Series” of the Pelagonian massif, Republic of Macedonia // New data on minerals. 2016. Vol. 51. P. 12-19.

Chukanov N.V., Aksenov S.M., Jančev S., Pekov I.V., Göttlicher J., Polekhovsky Yu.S., Rusakov V.S., Nelyubina Yu.V., Van K.V. A new mineral species ferricoronadite, $Pb[Mn^{4+}_6(Fe^{3+},Mn^{3+})_2]O_{16}$: mineralogical characterization, crystal chemistry and physical properties. Phys. Chem. Minerals. 2016. Vol. 43. P. 503–514.

Armbruster T. Revised nomenclature of högbomite, nigerite, and taaffeite minerals. European Journal of Mineralogy. 2002. Vol. 14. P. 389–395.

Chukanov N.V., Jančev S., Pekov I.V. The association of oxygen-bearing minerals of chalcophile elements in the orogenetic zone related to the “Mixed Series” complex near Nežilovo, Republic of Macedonia. Macedonian J. of Chemistry and Chemical Engineering. 2015. Vol. 34(1). P. 115–124.

Chukanov N.V., Krzhizhanovskaya M.G., Jančev S., Pekov I.V., Varlamov D.A., Göttlicher J., Rusakov V.S., Polekhovsky Y.S., Chervonnyi A.D., Ermolaeva V.N. Zincovelesite-6*N*6*S*, $Zn_3(Fe^{3+},Mn^{3+},Al,Ti)_8O_{15}(OH)$, a new högbomite-supergroup mineral from Jacupica mountains, Republic of Macedonia // Mineralogy and Petrology. 2018. Vol. 112. P. 733-742.

Ermolaeva V.N., Varlamov D.A., Jančev S., Chukanov N.V. Spinelids and högbomite-supergroup minerals from sulfide-free endogeneous Pb-Zn-Sb-As association in the Pelagonian massif (Macedonia) // ZRMO. 2018. Vol. 147. № 3. P. 27-43. (in Russian).

Bermanec V., Holtstam D., Sturman D., Criddle A.J., Back M.E., Scavnicar S. Nežilovite, a new member of the magnetoplumbite group, and the crystal chemistry of magnetoplumbite and hibonite. The Canadian Mineralogist. 1996. Vol. 34. P. 1287–1297.

RARE EARTH ELEMENT MOBILITY IN REGOLITH FORMED ON ALKALINE GRANITE BEDROCK OF THE SOUTHEAST UNITED STATES

Foley N.K., Ayuso R.A.

U.S. Geological Survey, Reston VA, 20192, USA, nfoley@usgs.gov

Regolith-hosted rare earth element (REE) ion-adsorption clay deposits are of global economic importance. We present results of mineralogical, REE geochemistry, and radiogenic isotope (Nd-Sr-Pb) studies of weathered regolith formed on metaluminous-to-alkaline igneous rocks of the Southeast United States. Our studies are aimed at understanding the genesis of REE-enriched regolith profiles and how that information can be used to discern whether there is significant potential for economic REE clay deposits in the United States. This class of deposits is known to occur in China and countries of Southeast Asia. REE clay deposits of China have mineable grades from ~500 to over 3000 ppm total rare earth oxide. There are two endmember types—light REE-enriched (La-Sm) regolith deposits with chondrite normalized La/Lu of ~10, and heavy REE-enriched (Eu-Lu) regoliths with chondrite normalized La/Lu of 1. South China clay deposits enriched in heavy REE currently supply virtually all heavy REE to global markets (Yang et al., 2013).

The main exploration criteria for this class of deposits include 1) the presence of large igneous suites composed of granitic rocks, 2) long periods of intense weathering with little subsequent erosion, and 3) evidence for mobility and enrichment of REE within the developing regolith profile. Source rocks for the South China deposits are described mainly as granitic rocks that range from calc-alkaline to alkaline compositions. REE mobilization processes are thought to include late-magmatic-to-deuteric alteration and deep lateritic weathering. The REE can occur as ionic REE adsorbed to clay and other mineral substrates, and as secondary soluble REE-carbonate and/or phosphate minerals. These deposits have been the focus of intense research in recent years; however, there remains considerable ambiguity regarding the origin and potential global distribution of this deposit type.

Our studies focus on two major belts of igneous rocks. One belt consists of Neoproterozoic anorogenic plutons (Tollo et al., 2004) and related rocks of the Blue Ridge and Piedmont physiographic provinces that have highly silicic compositions; high contents of Ga, F, Nb, Sn, Ta, Y, and Zr; and high total REE (ΣREE = 500~1500 ppm) (e.g., Robertson River, Suck Mountain, Stewartsville, and Striped Rock). The other belt consists of Alleghanian plutons (Sinha and Zietz, 1982) of the Piedmont physiographic province that have larger volumes of weathered rock and less enriched compositions (ΣREE = 100~300 ppm) (e.g., Petersburg, Liberty Hill, Elberton-Sparta). Since the early Triassic, granitic rocks of the Southeast United States have been subjected to periods of intense chemical weathering, comparable to those of South China. Warm temperate-to-subtropical regimes that result in formation of kaolinite and other weathering products continue to the present. The region has average current annual rainfall of ~1500 mm and average temperature of ~17ºC. Characterization of Nd-, Sr-, Pb-isotope, and trace element geochemistry of parent rocks, weathered granite, saprolite and soils, and anthropogenic inputs is providing critical data for allocating *in-situ* vs. transported REE in regolith materials. For example, Pb-isotope signatures can be used to discriminate natural versus anthropogenic Pb in soils (Ayuso et al., 2008) and, by inference, indicate local anthropogenic addition of REE to a profile from clay-based agricultural amendments. A moderate scatter in Nd-isotope ratios and Sm/Nd values in the surficial materials, compared to bedrock, is consistent with mineral weathering.

Weathered bedrock-soil profiles were collected for plutons in the Neoproterozoic belt. These include the 680 Ma Stewartsville granite (U-Pb zircon age by SHRIMP; this study), the 680 Ma Suck Mountain pegmatitic granite (Tollo et al., 2004), and the 748 Ma Striped Rock pluton (Essex, 1993). The Stewartsville pluton is a medium- to coarse-grained biotite granite containing abundant allanite and fluorite and characterized by steep chondrite-normalized patterns (light REE-enriched, 200x chondrite). REE data for profiles (~30-meter thick) through regolith of saprolite and soil over the pluton show systematic increases from 300 to 2880 ppm REE from bedrock to clay-rich soils. A negative Eu anomaly in the granite is retained in weathered alluvium; uppermost soil samples show a small negative Ce anomaly due to oxidation in the weathering profile. Normalized to the original

granite composition, clay-rich regolith shows pronounced increases in light to middle REE. Leaching of regolith samples using a weak acid-ion exchange process to extract cations adsorbed to clays, carbonate, and organics (humic and fulvic components) resulted in yields of up to 52% (ΣREE ~1460 ppm) from clay-bearing soils, compared to ΣREE from total digestion. For these Neoproterozoic sub-alkaline plutons, the presence of primary allanite and REE-enriched hydrothermal zircon (containing up to 1.8 wt. % REE) appear to be distinguishing characteristics of the parent rocks. Mobility-related selective enrichment of REE in the regolith is predominantly a result of weathering primary allanite (Figure) to vermiculite and kaolinite, with subsequent fixing of REE as hydroxide ions and in secondary and poorly crystalline oxide, niobate, carbonate, and phosphate minerals (e.g., ceria, fergusonite, bastnaesite, and monazite).

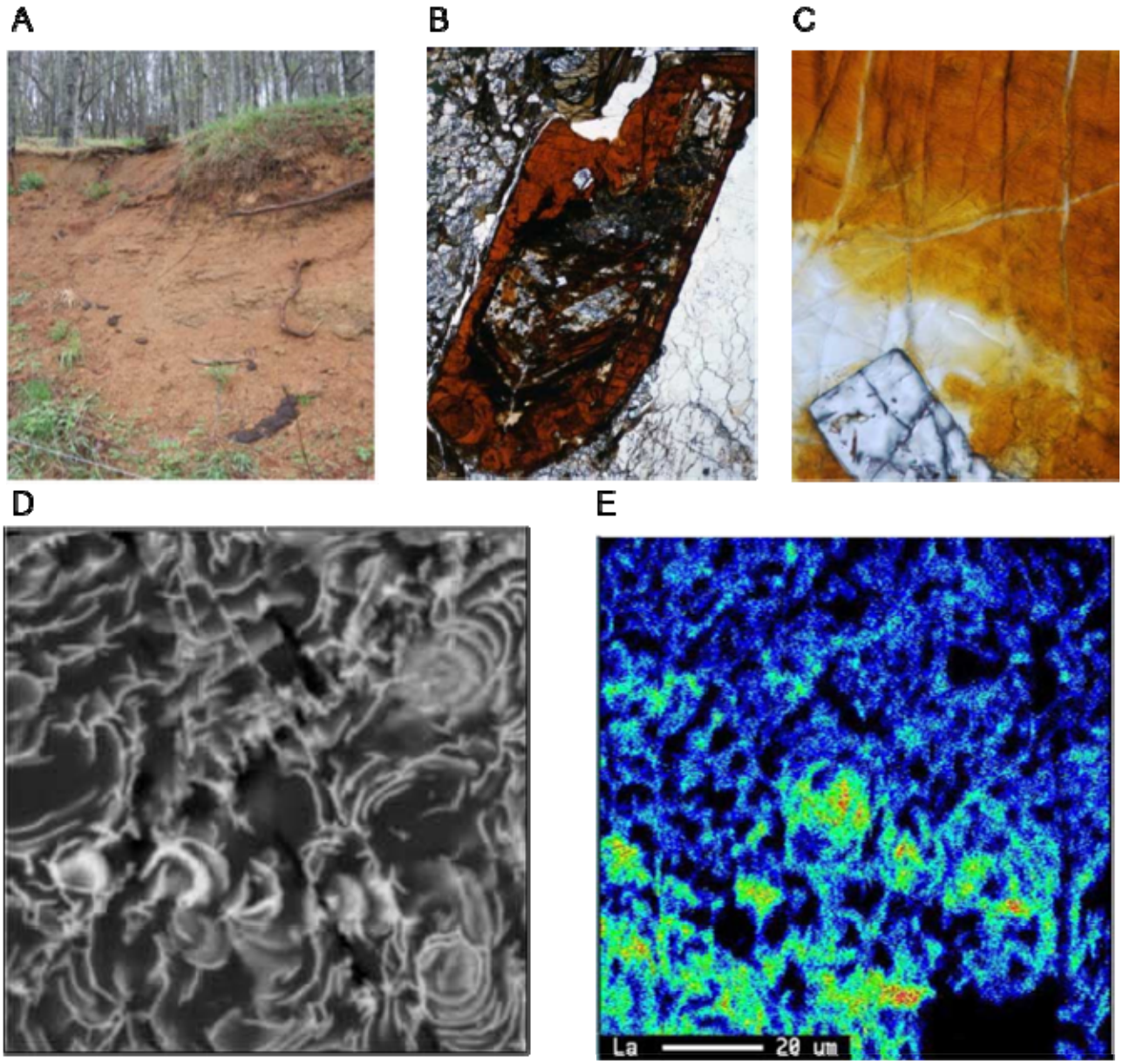

Figure. A) Typical regolith developed on granite pluton, Blue Ridge Mountains, Virginia, U.S.A. B) Weathered allanite crystal from regolith. C) Photomicrograph of altered allanite grain, with zircon. D) Back-scatter scanning electron microscope image showing rare earth elements (white) interlaying and edging kaolinite and nontronite. E) Electron microprobe map of area of Fig. D showing lanthanum (bright green to red) on clay minerals.

Large igneous suites of the Southeast United States generally match the compositional range that characterizes granitic rocks associated with some South China REE ion adsorption clay deposits. REE

clay deposits can form under a wide range of weathering environments, including warm-temperate, subtropical, and tropical climate regimes, which also result in major kaolin resources. The chemical and mineralogical processes producing REE-enriched regolith profiles in granitic rocks in the Southeast United States are analogous to those leading to the formation of REE clay deposits currently being mined in China. The distinguishing factors in REE enrichment patterns are accessory mineral composition and modal content of the weathered plutons The Stewartsville bedrock-soil profile most closely resembles REE ion adsorption clay deposits formed by weathering of the Heling pluton, an allanite and apatite-bearing biotite granite, as described by Bao and Zhao (2008). The examples given above highlight the importance of weathering allanite and apatite in generating REE-enriched regolith materials.

Our studies demonstrate a remarkable coincidence in mineralogy and inferred processes of REE transfer and accumulation occurring in both Neoproterozoic and Alleghanian granite-derived regoliths of the Southeast United States and in REE clay deposits of South China and Southeast Asia. This work is a first step in assessing whether granite-related REE resources of this type exist in the Southeast United States. The behavior of REE in regolith materials that form over igneous intrusions subjected to deep weathering is both mineralogically and geochemically complex and, in spite of substantive progress, REE-bearing ion-absorption and related clay deposits remain imperfectly understood. All weathered materials can contain some exchangeable REE; the importance of weathering of REE-enriched parent material is in the generation of high concentrations of readily extractable REE in a regolith. More detailed studies are underway to establish the full range of potential source rocks and surface processes involved in the formation of REE-bearing clay deposits in granitic rocks of the Southeast United States. It remains to be established whether regoliths containing high enough concentrations of readily extractable REE occur in large enough volumes to be considered a future resource.

This work was supported by the U.S. Geological Survey, Mineral Resources Program.

References

Ayuso, R., Foley, N., and Lipfert, G., 2008. Lead isotopes as monitors of anthropogenic and natural sources affecting the surficial environment. In: DeVivo, B., Belkin, H., and Lima, A., (Eds.), Environmental Geochemistry: Site Characterization, Data Analysis and Case Histories. Elsevier, Chapter 12, p. 291-318.

Bao, Z., and Zhao, Z., 2007. Geochemistry of mineralization with exchangeable REY in the weathering crusts of granitic rocks in south China. Ore Geology Reviews, 33: 519–535.

Essex, R.M., 1993. Age and petrogenesis of the Striped Rock pluton, Virginia: unpublished M.S. thesis. Virginia Tech., p. 1-98.

Sinha, A.K., and Zietz, Isidore, 1982. Geophysical and geochemical evidence for a Hercynian magmatic arc, Maryland to Georgia. Geology, 10: 593-596.

Tollo, R.P., Aleinikoff, J.N., Bartholomew, M.J., and Rankin, D.W., 2004. Neoproterozoic A-type granitoids of the central and southern Appalachians: intraplate magmatism associated with episodic rifting of the Rodinian supercontinent. Precambrian Research, 128: 3-38.

Yang, X. Jin, Lin, Aijun, Li, Xiao-Liang, Wu, Yiding, Zhou, Wenbin, and Chen, Zhanheng, 2013. China's ion-adsorption rare earth resources, mining consequences and preservation. Environmental Development, 8: 131-136.

STABLE ISOTOPE GEOCHEMISTRY OF CARBONATITES FROM KAMTHAI AREA, BARMER, INDIA: IMPLICATIONS FOR REE MINERALISATION

Ghosh P.[1], Vladykin N.[2], Fosu B.[1], Viladkar S.[3]

[1]Centre for Earth Sciences, Indian Institute of Science, Bangalore, India 560 012

[2]Institute of Geochemistry, Siberian Branch of Russian Academy of Sciences, Russia;

vlad@igc.irk.ru

[3]Earth and Environmental Sciences, Indian Institute of Science and Education and Research Bhopal

Stable isotopes of carbon ($\delta^{13}C$) and oxygen ($\delta^{18}O$), in combination with other geochemical systematics have been widely used to deduce the nature, source and evolution of carbonatite magmas and related fluids. Clumped isotope geochemistry (Δ_{47}), is a relatively new tool which has shown great potential for estimating formation temperatures and reconstructing past climates [1]. It is unique in the sense that it fundamentally depends on the thermodynamic ordering of C-O bonds in carbonates and does not require prior knowledge of fluids from which these carbonates precipitate. In this study, we measure the clumped isotope compositions of REE-rich carbonatites and associated minerals from the Kamthai area to constrain temperature and mineralisation conditions in such outcrops.

The Kamthai Rare Earth Deposit (KRED) forms part of the Tertiary Alkaline Complex (TAC) of Sarnu-Dandali in Rajasthan. The TAC, essentially made up of a suite of nephelinite syenites, ijiolites, phonolites and carbonatites intrude the Neoproterozoic Malani rhyolites basement and Cretaceous sandstones [2]. The Kamthai deposits are not dated but are speculated to be coeval (~65 Ma) or younger than Deccan lava flows. At the KRED, carbonatites occur as plugs and dykes which cut through ijiolite-nephelinites. Three distinct carbonatite varieties have been identified on the field.

Type-I calcite carbonatites with bastnaesite-synchysite-ancylite assemblages form dykes with intergrowth of calcite and REE minerals (a *panther skin-type* feature; Fig. 1E). REE minerals (dominantly bastnaesite) fill interstitial spaces of both calcite and Fe-rich carbonates and are commonly cut through by carbocernaite-rich veins. Other mineral phases present in these rocks incluPowders X Ray diffraction analyses of the carbonatites revealed the presence of calcite, ankerite, siderite and strontianite as constituent carbonate phases. Other detected minerals include ancylite, carbocernaite, bastnaesite and barite. Whole rock carbonate and calcite separates were digested with 104% H_3PO_4 in enclosed reaction vessels to release CO_2 for concurrent $\delta^{13}C$, $\delta^{18}O$ and D47 analyses in dual inlet mode on a Thermo MAT-253. $\delta^{13}C$ and $\delta^{18}O$ values are reported in VPDB and VSMOW respectively, while Δ_{47} is given in the absolute reference frame (ARF).de barite, cerianite, albite and microcline.

Type-II is Sr-calcite carbonatites (sovitic; Fig 1F), in which the dominant REE mineral is carbocernaite-(Ce) with abundant celestine and less frequent strontianite. Carbocernaite-(Ce) is commonly intergrown with bastnaesite-(La), bastnaesite-(Ce) and daqingshanite-(Ce). This outcrop has characteristic REE fluorocarbonate assemblage of bastnaesite, synchysite and parasite. Other identified minerals are ankerite, apatite, amphiboles and biotite.

In other parts of the complex, smaller ferrocarbonatite veins intrude ijiolites and nephelinites. REE minerals are less abundant in this sample type.

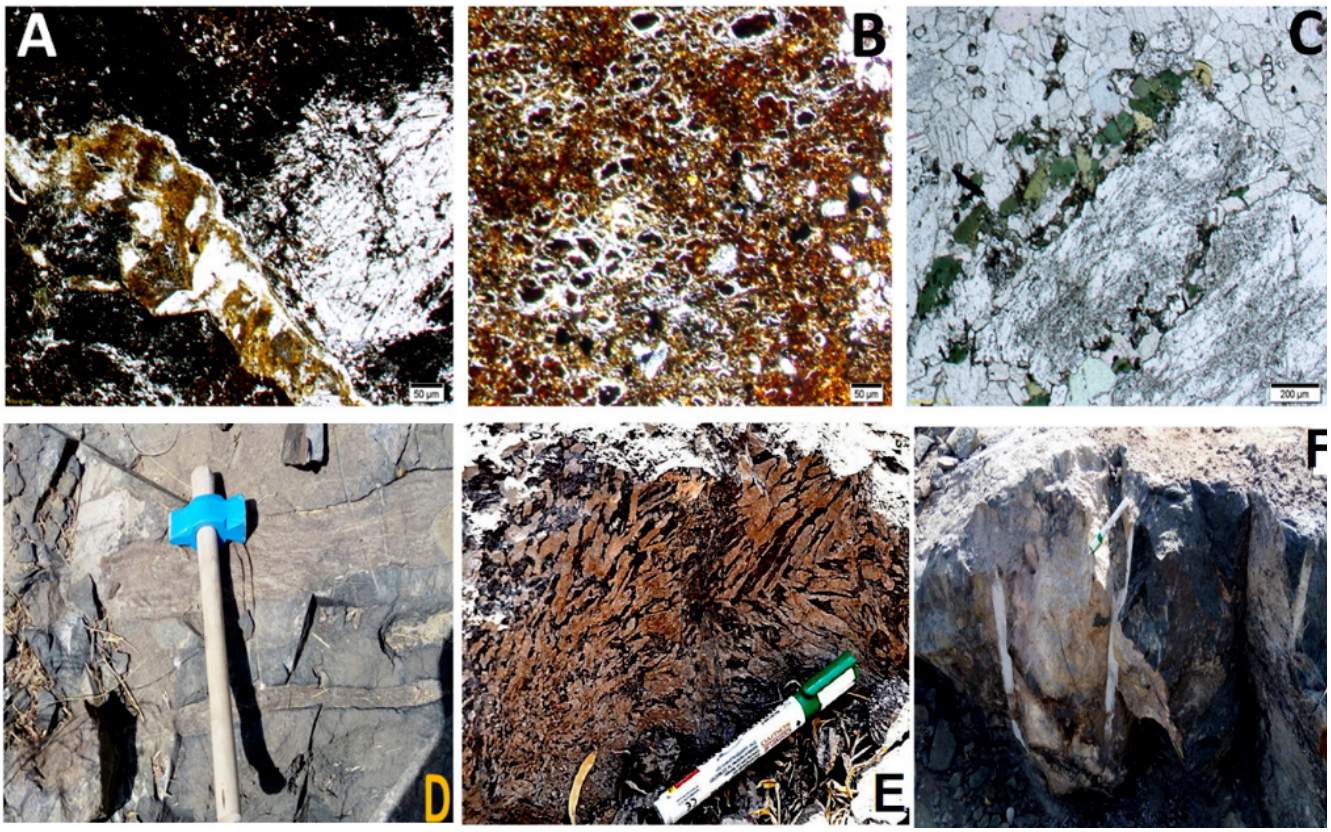

Figure 1. Different rock exposures and photomicrographs of Kamthai area REE deposits (A,B) Type-I calciocarbonatite in thin section (PPL). (B) Photomicropgraph of Type-II calciocarbonatite. (D) Multiple ferrocarbonatite veins in ijiolite. (E,F) Field exposures of Type-I and type-II calciocarbonatites.

Powders X Ray diffraction analyses of the carbonatites revealed the presence of calcite, ankerite, siderite and strontianite as constituent carbonate phases. Other detected minerals include ancylite, carbocernaite, bastnaesite and barite. Whole rock carbonate and calcite separates were digested with 104% H_3PO_4 in enclosed reaction vessels to release CO_2 for concurrent $\delta^{13}C$, $\delta^{18}O$ and D47 analyses in dual inlet mode on a Thermo MAT-253. $\delta^{13}C$ and $\delta^{18}O$ values are reported in VPDB and VSMOW respectively, while Δ_{47} is given in the absolute reference frame (ARF).Primary igneous carbonatites (PIC) have distinctive C-O isotope compositions that reflect their mantle origin (see mantle box in Fig 2A). Kamthai carbonatites are predominantly magmatic as revealed by the calcite $\delta^{13}C$ (-6.47 to -4.65 ‰) and $\delta^{18}O$ (6.11 to 13.9 ‰) values. The relatively higher $\delta^{13}C$ (-4.65 ‰) and $\delta^{18}O$ (13.90 ‰) values in some samples, likely indicate mixing between magmatic calcite and REE-carbonates (Fig 2A). Ferrocarbonatites and REE-carbonates on average, have lighter $\delta^{13}C$ values: carbocernaite (-4 ‰), ankerite (-2.2 ‰) and bastnaesite (-1.67 ‰). Similarly, $\delta^{18}O$ values are higher: carbocernaite (25 ‰), ankerite (26 ‰) and bastnaesite (27 ‰). The minimum Δ_{47} values determined for these samples are 0.360, 0.672, 0.707 and 0.727 ‰ which correspond to apparent equilibrium temperatures of 272, 32, 21 and 15 °C for calcite, ankerite, carbocernaite and bastnaesite respectively. These recorded temperatures (in calcites) are characteristically low, as thermodynamic C-O bond ordering in carbonates follow a closure temperature-like behaviour which allows Δ_{47} re-equilibration to ambient temperatures. Perhaps, the most interesting results is the very low temperatures of ankerite and REE-carbonates. This is an indication that REE mineralisation in Kamthai carbonatites, like many other carbonatite complexes worldwide is driven by low temperature processes. We speculate that the mineralising fluids are mostly of hydrothermal/meteoric origin. Our results also show that REE mineralisation is sensitive to temperature of carrier fluids and indicate the potential use of clumped isotopes in understanding the genesis of carbonate-hosted REE minerals and ore deposits.

Primary igneous carbonatites (PIC) have distinctive C-O isotope compositions that reflect their mantle origin (see mantle box in Fig 2A). Kamthai carbonatites are predominantly magmatic as

revealed by the calcite $\delta^{13}C$ (-6.47 to -4.65 ‰) and $\delta^{18}O$ (6.11 to 13.9 ‰) values. The relatively higher $\delta^{13}C$ (-4.65 ‰) and $\delta^{18}O$ (13.90 ‰) values in some samples, likely indicate mixing between magmatic calcite and REE-carbonates (Fig 2A). Ferrocarbonatites and REE-carbonates on average, have lighter $\delta^{13}C$ values: carbocernaite (-4 ‰), ankerite (-2.2 ‰) and bastnaesite (-1.67 ‰). Similarly, $\delta^{18}O$ values are higher: carbocernaite (25 ‰), ankerite (26 ‰) and bastnaesite (27 ‰). The minimum Δ_{47} values determined for these samples are 0.360, 0.672, 0.707 and 0.727 ‰ which correspond to apparent equilibrium temperatures of 272, 32, 21 and 15 °C for calcite, ankerite, carbocernaite and bastnaesite respectively. These recorded temperatures (in calcites) are characteristically low, as thermodynamic C-O bond ordering in carbonates follow a closure temperature-like behaviour which allows Δ_{47} re-equilibration to ambient temperatures. Perhaps, the most interesting results is the very low temperatures of ankerite and REE-carbonates. This is an indication that REE mineralisation in Kamthai carbonatites, like many other carbonatite complexes worldwide is driven by low temperature processes. We speculate that the mineralising fluids are mostly of hydrothermal/meteoric origin. Our results also show that REE mineralisation is sensitive to temperature of carrier fluids and indicate the potential use of clumped isotopes in understanding the genesis of carbonate-hosted REE minerals and ore deposits.

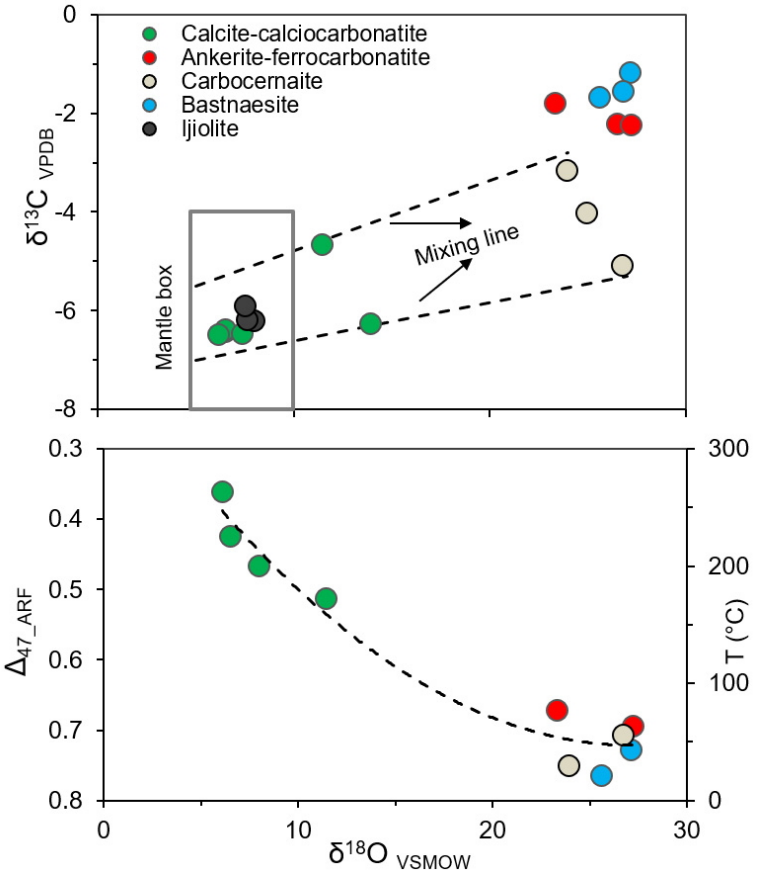

Figure 2. Stable and clumped isotope compositions of Kamthai area carbonatites.

This work was supported by the the Russian Foundation for Basic Research (grant 17-55-45028).

References

1. Ghosh P, Adkins J, Affek H, et al. 13C-18O bonds in carbonate minerals: A new kind of paleothermometer. *Geochim Cosmochim Acta*. 2006; 70(6): 1439-1456.

2. Bhushan SK. Geology of the Kamthai Rare Earth Deposit. *J Geol Soc India*. 2015; 85(5): 537-546.

LAMPROITES IN THE NORTHEASTERN TAIMYR

Goloburdina M.N., Antonov A.V.
A. P. Karpinsky Russian Geological Research Institute Saint Petersburg, Russia,
marina_goloburdina@vsegei.ru, anton_antonov@vsegei.ru

Lamproites are specific rocks, emplaced during alkalic magmatism pulses; their ultramafic varieties can be industrially diamondiferous. Middle to Late Triassic potentially diamond-bearing alkaline-ultrabasic magmatism is known in the Taimyr Peninsula: alneites and mica kimberlites (Sobolev, 1937; Moor, 1941) occur in Central Taimyr, while lamproite (Romanov, 1997) in the Western Taimyr, while injection breccias of ultrabasic composition at the Eastern Taimyr (Proskurnin, Gavrish et al., 2017). This contribution describes the lamproite of the Northeast Taimyr.

Eluvial-deluvial lamproite tali have been found in the Faddey and Goltsovaya rivers watershed among the northeast striking Late Proterozoic intrusions of amphibolized gabbro-dolerite. The host-rocks are strongly dislocated and metamorphosed volcanogenic-carbonate-clastic Late Proterozoic unit. The morphology of the lamproite bodies is not determined due to poor exposure.

The lamproite are brownish-gray in color, a fine- to medium-grained massive rock belonging to the leucite-phlogopite type. Microscopically, they are porphyric, with flow texture and microlitic structure of the ground mass. Main minerals are phlogopite (45%), altered leucite (30%), carbonatde xeno- (or pheno-) crystals of olivine and / or pyroxene (10%), pyroxene, apatite and Ti-phases (ilmenite, rutile), enclosed in potassium feldspar. Carbonates (15%, dolomite, magnesite) in the rock, replace main minerals and ground mass, while silica (few percent) fills interstices.

Phlogopite forms phenocrysts (mg# 87-93) and microliths (mg# 85), their composition demonstrates evolutionary trend towards higher contents TiO_2 and FeO_t with relatively little variation of Al_2O_3 (Figure). At this composition, Mg content decreases leading to formation of Ti-biotite in fringes (mg# 50-70). This so called wolgidite trend (Mitchell and Bergman, 1991) is typical of phlogopites from lamproite of Spain, Greenland and Russia (Aldan Shield).

The altered leucite has rounded shapes, emphasized by a thin rim of mica microliths. The leucite is replaced mainly by potassium feldspar in association with quartz, less commonly carbonate. The potassium feldspar forms anhedral prismatic crystals forming the bulk of the rock. By the composition (Na_2O 1.3-2.5; Fe_2O_3 1.1-2.6; BaO to 0.93; $K_2O/(K_2O + Na_2O)$ 0.83-0.9%) is comparable to potassium feldspar from lamproites (Mitchell and Bergman, 1991). Xeno- (pheno-) crystals have oval or angular shapes and replaced by magnesite, dolomite and ore mineral. The pyroxene, which survived alteration forms small subhedral prismatic and acicular crystals with intense pleochroism in greenish tones and corresponds in composition to aegirine and aegirine augite. Morphological features of some crystals and their interrelations with prismatic crystals replaced by carbonate indicate that they sometimes form rims over earlier clinopyroxene. Accessory minerals are apatite, ilmenite, rutile, titanium-zirconium oxides of variable composition, and anhedral zircon.

The studied rocks are ultra-potassium (K_2O / Na_2O 8.7%), ultra-alcalic (K_2O / Al_2O_3 0.76%), with moderate titanium (TiO_2 1.5%). Considering this and the "Niggli" parameter (k 0.85; 0.9; mg 0.7; 0.76) and the ratio of CaO (8.3; 9.2%) to SiO_2 (44.2; 42.5%) and Al_2O_3 (10; 9.8%) they correspond to lamproite.

Comparing microelements concentration in the studied leucite-phlogopite lamproite with phlogopite lamproites of the world (Mitchell and Bergman, 1991), it should be noted that by the content of the iron group elements (V 117; 124; Cr 496; 535; Co 31.8; 32.5; Ni , 197; 243; Cu 62; 63.5 ppm) and Sc (14.9; 13.5 ppm) they are comparable to the West Kimberley, Smoky Butte, Leucite Hills, Francis, Murcia-Almeria, Sisco, and Gaussberg lamproites, by their Ba content (1980; 2020 ppm) with lamproites of Francis, Murcia-Almeria, Sisco. Concentrations of Sr (1340; 1450 ppm) are at the level of lamproites of West Kimberley and Francis. By the Zr / Nb ratio (32; 34) and La / Yb (49.9; 54.6), the studied rocks overlap with the phlogopite lamproite compositions of Murcia-Almeria and Francis.

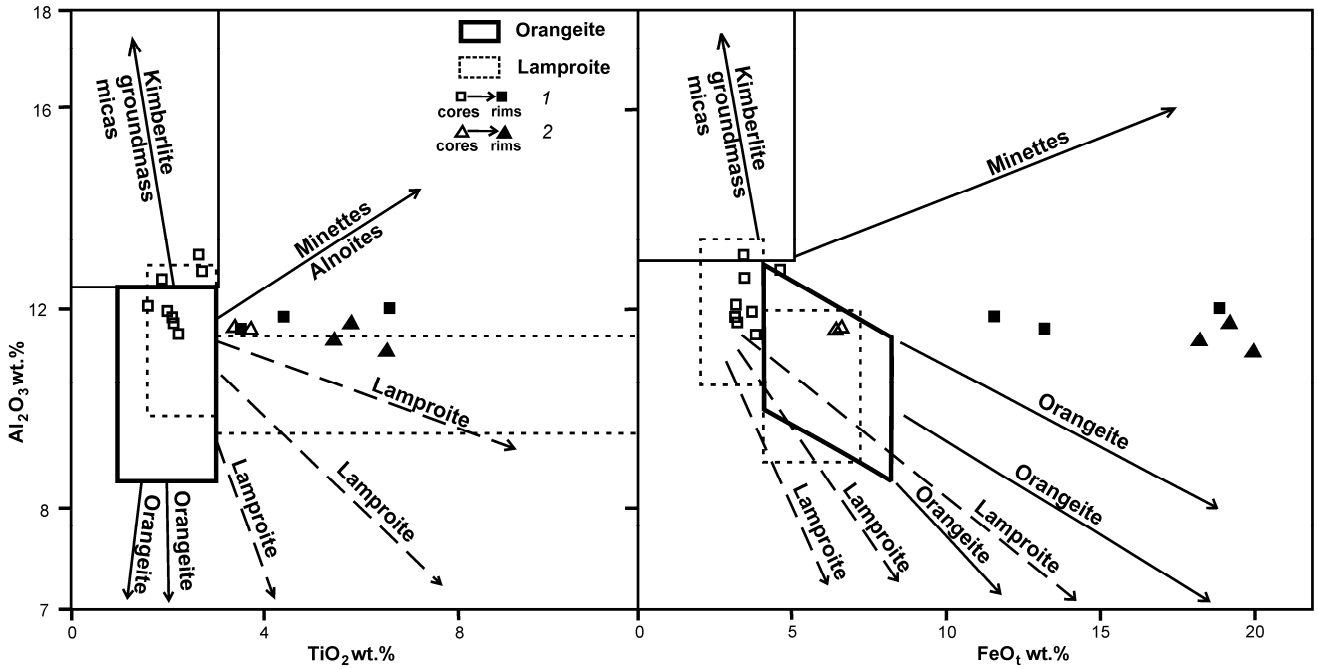

Figure. Compositional variation Al_2O_3 versus TiO_2 and FeO_t for phlogopite phenocrysts (*1*) and groundmass micas (*2*) in lamproite of the Northeastern Taimyr. Compositional fields and trends for kimberlites, lamproite, orangeite and minette micas from R.H. Mitchell (1995).

The authors thank O. L. Galankina (IGGD RAS) for microprobe analytical data.

The study was conducted using the data obtained during regional geological survey according to the state contract No. 049-00031-16 of 11.03.2016.

References

Mitchell R.H. Kimberlite, orangeites and related rocks. – New York: Plenum Press, 1995. 410 p.

Mitchell R.H., Bergman S.B. Petrology of lamproites. – New York: Plenum Press, 1991. 472 p.

Moor G.G. About mica kimberlites in the north of Central Siberia // DAN SSSR. 1941. Vol. XXXI. № 4, p. 361–363. (In Russian).

ProskurninV.F., Gavrish A.V., Petrov O.V., Galkin A.S., Vinogradova N.P., Naumov M.V., Silaev V.I., Luk`yanova L.I., Ronina E.E., Saltanov V.A. Potentially diamondiferous Early Mesozoic injection breccias at the Eastern Taimyr Peninsula // Region. geologiya and metallogeniya. 2017. № 72, pp. 78-90. (In Russian).

Romanov A.P. Prospects of diamondiferousness of the Mountain Taymyr // In Nedra Taimyr. Noril'sk: Izd-vo VSEGEI. 1997. Iss. 1, pp. 185–198. (In Russian).

Sobolev V.S. Features of magmatic manifestations and metallogeny of platforms on the example of the formation of Siberian trapps. Abstracts of the XVII IGC. 1937. Moscow; Leningrad. (In Russian).

APATITE-CLINOPYROXENE PHLOGOPITITE IN THE NORTHEASTERN TAIMYR: COMPOSITION AND AGE

Goloburdina M.N., Antonov A.V., Lepekhina E.N.

A. P. Karpinsky Russian Geological Research Institute Saint Petersburg, Russia,
marina_goloburdina@vsegei.ru, anton_antonov@vsegei.ru, elena_lepekhina@vsegei.ru

In the Northeastern Taimyr a dunite-harzburgite massif occurred in the middle reaches of the Stanovaya River is cut by a small alkali-ultrabasic (phlogopitite) body (Goloburdina, 2018). Occurrence of the both rocks within a single fault zone and their spatial closeness is rather unusual since of ultramafic and alkalic igneous rocks commonly cohabit within zoned magmatic complexes. However a growing number of publications on carbonatites occurrence in non-typical tectonic settings (Jones et al., 2013) allows for a different scenario, broadening areas potential for REE and trace element ores. This urges a thorough examination of those rocks, including their geochemistry and isotope signature.

The phlogopitite forms a flat body, probably a sill c. 0.3 m as thick, emplaced into completely serpentinized ultramafics with sharp intrusive contacts. Exocontact zone comprises a 1 cm layer of whitened serpentinite. The phlogopitite contains the serpentinite boudins.

The phlogopitite is grey-colored rock with greenish-brownish hue, fine-grained and massive. Textures are hypidiomorphic or poikilitic, main minerals are phlogopite (60%), clinopyroxene (20%) apatite (15%) and titanite (<1%) with uneven secondary carbonate (up to 10%). In the endocontacts clinopyroxene more abundant up to 40% and the rock texture transitionally passes to fine prismatic-granular due to prismatic tracht of the composing minerals, which form radial aggregates. Accessories, recovered by EDX, are REE silicates, baddeleyite, zircon, thorianite, and Mn-ilmenite (MnO=8.9-12.4%).

Phlogopite (Mg#=80, TiO_2 0.7-1.03 %) forms pseudo-hexagonal and tabular plates, unevenly chloritized up to complete substitution at the endocontact. It is variably saturated with fine inclusions (Fe-Ti-oxides).

Clinopyroxene forms subhedral elongated prismatic and sub-isometric fractured corroded zoned crystals (Fig. 1) of diopside composition (Wo 47.22-49.8; En 39.53-44.25; Fs 7.5-12.44). Zoning is formed by a variable content of iron (FeO 4.6-9.6%) and increase of Na_2O (up to 1.25%) towards the final stages of crystallization.

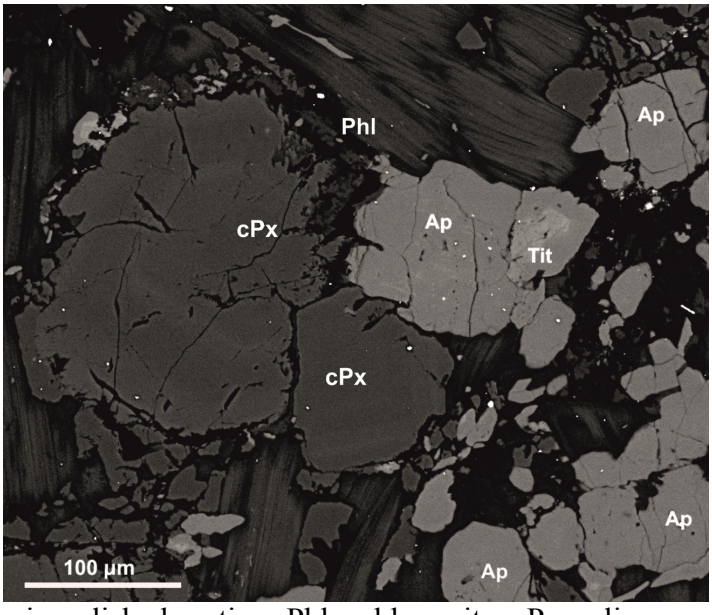

Fig. 1. Phlogopite in polished section: Phl - phlogopite, cPx - clinopyroxene, Ap – apatite, Tit – titanite.

Apatite forms anhedral interstitial crystals. Less commonly, it forms euhedral prismatic and acicular crystals, sometimes included within the clinopyroxene and contains up to 0.74% of F.

Titanite and baddeleyite are the most common accessory minerals of the rock. Titanite occurs as relatively large zoned xenomcrysts and smaller wedge-shaped grains of uniform composition; sometimes it forms lamellae in mica. The titanite zoning is caused by enrichment of central and intermediate zones with iron (FeO 0.75– 2.43%) and submicron inclusions of Zr– and Nb–bearing rare-earth phases. The lamellas of titanite have a ferruginous composition (FeO 0.95-1.88%).

Baddeleite forms subprismatic subhedral and anhedral crystals, replaced by zircon and submicron rare-earth phases that are difficult to determine. The baddeleyite-zircon aggregates, commonly contain micro inclusions of thorianite - coffinite are.

The rock contains segregations of small subhedral prismatic rare-earth silicates, with pleochroic haloes.

Ilmenite mainly occurs in the near-endocontact and endocontact parts of the body, forming subhedral elongated prismatic crystals, sometimes - symplectic intergrowths with clinopyroxene. The ilmenite is enriched with ilmenite (65-77) and pyrophanite (19-26) minals but depleted with geikielite (0-12) minal, which differs from ilmenite from carbonatites (Mitchell, 1995). It should be noted that ilmenites from carbonatite complexes by their ilmenite-pyrophanite-heykelite proportions form isolated groups. The compositions of the studied ilmenites demonstrate a compositional trend with growing geikielite minal from ilmenite of orangeite (Sover Mine) to those close to ilmenite of calcitic kimberlite (Premier mine).

Petrography and petrochemical features of the rock (SiO_2 35.5; Al_2O_3 7.62; TiO_2 1.49; Fe_2O_3 0.9; FeO 7.28; MnO 0.17; MgO 18.8; CaO 14.9; Na_2O 0.21; K_2O 1.08; LOI 7.79%) indicate its potassium ultramafic nature. The content of K_2O is lower due to replacement of the phlogopite with chlorite. Concentrations and distribution of rare-earth elements in the rock studied (□ = 613 ppm; La/Yb = 45.6) resemble those in the phoscorites of the Maymecha-Kotui province (□ = 472-4324 ppm; La/Yb = 43.2-159 according to L. N. Kogarko, in press).

The phlogopitite age was determined by U-Pb analysis of relatively large titanite crystals employing SIMS (SHRIMP-II, Center for Isotopic Research, VSEGEI, St. Petersburg) following the standard technique [Rodionov et al., 2018] and titanite standard OLT1 (1015 Ma, [Kennedy et al., 2010]).

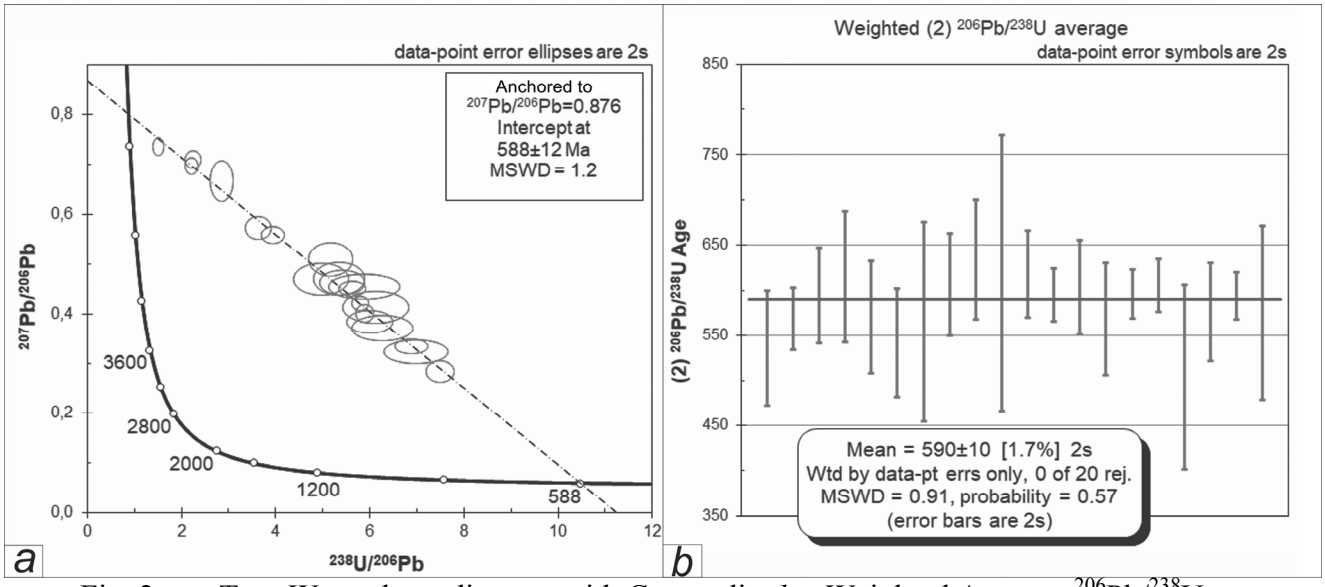

Fig. 2. *a* – Tera-Wasserburg diagram with Concordia; *b* – Weighted Average $^{206}Pb/^{238}U$ age.

The titanite U-Pb age has been calculated using common-Pb uncorrected ratios, plotted in Tera-Wasserburg Concordia diagram (Fig. 2). Assuming that the U-Pb system of titanite is concordant, a mixing line was constructed between radiogenic and common Pb. The intersection of this line with y-axis corresponds to common (initial) $^{207}Pb/^{206}Pb$ at the moment of crystallization. In our case, the

regression upper intercept has been anchored at $^{207}Pb/^{206}Pb$ = 0.876, corresponding to common Pb composition at c. 590 Ma. The lower intersection of the regression with the Concordia at 588 ± 12 Ma (Fig. 2) determines the titanite age. Weighted average $^{206}Pb/^{238}U$ age (N=20, ^{207}Pb corrected) is 590 ± 10 Ma. These results coincide within the error limits, confirming the titanite age, implying the Early Vendian emplacement of the apatite-diopside phlogopipite.

This suggest that the Early Vendian alkalic magmatic pulse in North-Eastern Taimyr is potentially fertile for ores.

The authors thank O.L. Galankin (IGGD RAS) for microprobe analytical data.

The study was conducted using the data obtained during regional geological survey according to the state contract No. 049-00031-16 of 11.03.2016.

References

Goloburdina M.N. Alkali-ultrabasic rocks in the northeast of Taimyr (Russia) // In «Magmatism of the Earth and related strategic metal deposits». Abstracts of XXXV International Conference. / Editors V.N. Ermolaeva, V.A. Zaitsev. – M.: GEOKHI RAS, 2018. P. 98-100.

Jones A.P., Genge M., Carmody L. (2013) Carbonate Melts and Carbonatites**,** Reviews in Mineralogy and Geochemistry, 75, 289-322.

Kennedy A.K., Kamo S.L., Nasdala L., Timms N.E. Grenville skarn titanite: potential reference material for SIMS U-Th-Pb analysis // Canad. Miner., 2010, v. 48 (12), p. 1423—1443.

Kogarko L. N. (in press) Potential of strategic metals in alkali rocks of Polar Siberia (rare earth and radioactive metals).

Mitchell R.H. Kimberlite, orangeites and related rocks. – New York: Plenum Press, 1995. 410 p.

Rodionov N. V., Lepekhina E. N., Antonov A. V., Kapitonov I. N., Sergeev S. A. 2018. U-Pb SHRIMP-II ages of titanite and timing constraints on apatite-nepheline mineralization in the Khibiny and Lovozero alkaline massifs (Kola Peninsula) Russian Geology and Geophysics, Vol 59, Iss 8, pp. 962-974.

ULTRAMAFIC-MAFIC INTRUSIONS AND SUPERLARGE DEPOSITS IN THE MARGINAL ZONES OF THE SIBERIAN PLATFORM

***Gongalsky B.I.*[1]*, Krivolutskaya N.A.*[2]**

[1]*Institute of Geology of Ore Deposits, Petrography, Mineralogy and Geochemistry of the Russian Academy of Sciences, Moscow, Russia, brgon@mail.ru;*

[2]*Vernadsky Institute of Geochemistry and Analytical Chemistry, RAS, Moscow, Russia, nakriv@mail.ru*

World-class vanadium, titanium, iron, chromium, platinum metals and nickel deposits are related to large ultrabasic-basic complexes of different age. Ores of these metals are represented by either oxides or sulfides and are usually separated in space. However, in some cases there is a rare combination of these ores within a single intrusion. An examples of such combination of oxide and sulfide ores are Chineysky and Dyumtaleysky massifs localized in the marginal southern and northern zones of the Siberian platform respectively: in the Kodaro-Udokan district (Polyakov et al., 2006; Gladkochub et al., 2012; Gongalsky, Krivolutskaya, 1993, 2019) and on the Taimyr Peninsula (Komarova et al., 1999; Krivolutskaya, Gongalsky, 2013; Malitch et al., 2016, 2017). Despite the difference in age and rock composition, their structure and mineralization are extremely close to one another, that are essential for our understanding of their genesis.

The southern part of the Siberian platform is characterized by occurrence of numerous basic-ultrabasic intrusions, some of them contain mineralization. The Paleoproterozoic layered intrusions of the Chineysky complex (Mylovsky, Luktursky and Chineysky massifs; Gongalsky, Krivolutskaya, 2019) located in the Kodar-Udokan area (500 km to east from the Lake Baikal) have the most important economic value. The Chineysky layered gabbro-anorthosite lopolith (square is 120 km^2, 1 880 Ma, Popov et al., 2009) comprises very rich Fe-Ti-V ores and represents the largest V deposit in Russia. At the same time this intrusion contains Cu-Ni sulfide ores enriched in PGE (Tolstykh, 2008). The Chineysky pluton consists of four rock groups: 1 - coarse-grained anorthosite and monzodiorite (that occur mostly in the eastern part of the pluton and are observed as large sheet-like blocks and xenoliths in gabbro); 2 - high-Ti gabbro rocks (the most important rock group due to economic value Fe-Ti-V mineralization) taking 60% of the pluton volume; 3 - norite, gabbronorite, and much less abundant melanonorite and leucogabbro (titanomagnetite content, as a rule, does not exeedes 5 vol %; the rocks of this group mainly occur in the lower part of the pluton under the high-Ti gabbro rocks and as thin sills in gabbro rocks of the second group); 4 - fluid-magmatic breccia with lamprophyre cement (the rocks of this group are limited in abundance, they are located in the zone between gabbro rocks of 1^{th}, 2^{d}, 3^{d} groups).

The distinctive feature of the Chineysky pluton is its layering. The high-Ti gabbro demonstrates the most distinct layering in comparing with low-Ti varieties. Due to the amount of titanomagnetite, the rocks of this group are subdivided into (a) titanomagnetite gabbro series in the lower position in the sequence and (b) leucogabbro series in the upper position. The titanomagnetite gabbro series is characterized by fine layering caused by fluctuations of contents of major minerals (mostly titanomagnetite) within separate layers (gravity layering), whereas the leucogabbro series is distinguished by rough layering made up of anorthosite and leucogabbro layers, 2–3 m thick, against the background of massive gabbronorite and gabbro. The first type of layering is rarely established in rocks exposed at the surface, but it is commonly observed in borehole cores. This series consists of various melanocratic (pyroxenite, melanorite), mesocratic (gabbro, gabbronorite), and subsidiary leucocratic gabbro rocks (leucogabbro, anorthosite) with gradual transitions between them. In the leucogabbro series, the mesocratic gabbronorite passing into leucocratic varieties becomes dominant. A great amount of anorthosite and leucocratic varieties as distinct layers and making up rough layering is a typical feature.

The composition of rocks have been studied in two sections based on outcrops and boreholes 83 and 11. The maximal diversity in rock compositions is fixed by MgO and TiO_2 distributions that reflect the mineral composition of different parts of the vertical section. The lower part of the section in borehole 83 (drilled in the central part of the intrusion) consists of norite, gabbronorite with

Table. Composition of rocks.

Sample	LP-1-1118	LP-1-1420-5	LP-1-1677-7	11-603	11-837	303
SiO2	43,25	45,22	46,89	46,00	51,85	54,18
TiO2	3,93	1,95	1,61	2,28	0,97	0,70
Al2O3	13,52	6,34	9,74	15,12	12,53	14,73
FeO	14,67	12,40	14,19	16,66	14,58	11,01
MnO	0,17	0,22	0,18	0,21	0,21	0,21
MgO	6,07	15,63	14,50	5,52	10,80	8,44
CaO	12,43	15,07	10,18	10,63	6,15	7,18
Na2O	2,54	0,85	0,45	2,51	1,82	2,41
K2O	0,34	0,08	0,38	0,35	0,57	0,70
P2O5	0,67	0,08	0,04	0,11	0,06	0,07
LOI	2,11	1,97	1,67			
Total	99,70	99,81	99,82	99,38	99,53	99,64
Rb	5,93	1,83	20,4	10,2	17,2	21,4
Ba	243	46,7	209	195	198	239
Th	1,30	0,37	0,76	0,87	2,48	3,07
U	0,40	0,13	0,43	0,35	0,64	0,88
Nb	13,1	3,50	3,11	2,16	2,35	2,66
Ta	0,93	0,26	0,23	0,16	0,16	0,21
La	27,5	5,58	6,64	8,03	11,5	10,6
Ce	65,5	15,6	13,7	16,0	22,6	21,4
Pb	3,46	0,88	11,1	6,64	5,46	4,96
Pr	8,77	2,61	1,84	2,16	2,56	2,54
Nd	40,6	14,2	9,21	9,26	9,83	10,2
Sr	804	301	428	281	208	267
Sm	9,37	4,13	2,61	1,90	1,80	2,07
Zr	142	64,1	43,2	34,7	31,4	70,8
Hf	4,02	2,27	1,57	0,99	0,90	1,62
Eu	2,64	1,35	0,91	0,74	0,55	0,62
Gd	8,53	4,47	2,85	1,99	1,68	2,05
Tb	1,19	0,65	0,41	0,29	0,25	0,31
Dy	6,29	3,64	2,32	1,39	1,69	1,95
Ho	1,07	0,64	0,43	0,40	0,34	0,41
Y	27,8	15,5	12,1	10,1	9,69	11,0
Er	2,74	1,49	1,21	1,05	1,04	1,21
Tm	0,34	0,18	0,17	0,16	0,16	0,18
Yb	2,04	1,09	1,12	1,13	1,11	1,20
Lu	0,23	0,14	0,15	0,15	0,17	0,18
Ni	116	435	521	115	159	67,2
Cu	148	23	361	639	106	85,0
Co	35	100	41,1	78	100	66,3

Note: Oxides are given in %, elements in ppm. Major components were analyzed by XRF at IGEM (analyst AI Yakushev), trace elements by LA-ICP-MS at MPI (analyst DV Kuzmin).

pyroxenite and is characterized by elevated MgO contents (up to 12 wt%) and low TiO_2 content which is an evidence of low titanomagnetite concentration in rocks. Upper part of the section contains many layers of anorthosite and is characterized by elevated Al_2O_3. The gradual elimination of melt refractory components – titanomagnetite, orthopyroxene and lower rhythms - has led to the enrichment of its SiO_2, Al_2O_3, CaO, Na_2O, K_2O, P_2O_5 with a decrease in the proportion of Ti-magnetite and orthopyroxene in the middle parts of the section. The representative analyses of rocks from the different parts of the Chineysky pluton are given in Table.

Massive titanomagnetite ores occur in the high-Ti gabbro as a layers with titanomagnetite concentration >80 vol.%. The second type of massive titanomagnetite ores is represented by lenses or irregular-shape bodies of 30-40 m. Economic sulfide mineralization is located in the endo- and exo-contact zones of the intrusion. Sulfide minerals also occur in titanomagnetite massive and disseminated ore as well (up to 15 vol. %). They are represented by chalcopyrite-pyrrhotite association with small amount pentlandite. Due to this mineralogical composition Cu/Ni ratio in ore has a range 5-100.

The Dyumtaleysky massif is a thick (600 m) and long (50 km) intrusive body located in the central part of the Taimyr Peninsula (Krivolutskaya, Gongalsky, 2013; Malitch et al., 2016). This intrusion is located within the Siberian Large Igneous Province and its age is 251Ma (Burgess, Bowring, 2015; Malitch et al., 2017). It consists of two rock groups: gabbro and olivine gabbro with elevated titanomagnetite contents (upper zone, 300 m of thick) and peridotites with titanomagnetite as well (300 m). The upper zone is characterized by thin layering which is similar to layering caused by fluctuations of titanomagnetite contents in the Chineysky massif. The lower zone is similar to low-Ti norite series of the Chineysky massif. The titamomagnetite ores occur in the upper part of massif as thin layers with 80-90 vol.% titanomagnetite, lenses and irregular bodies were not found within the Dyumtaleysky massif. The rock compositions have been studied in the core of borehole LP-2 penetrated all rocks of the Dyumtaleysky intrusion (Table). The two-members structure of the intrusion is reflected in the distribution of the MgO and TiO_2 (including other elements) in the vertical section and have many similarities with the structure of the Chineysky massif. Sulfide minerals abound in the lower part of the massif where they form economic mineralization. Disseminated ores are characterized by Cu/Ni ratio 0.5-2 in average. Veinlet-disseminated ores occur on the boundary of the gabbro and peridotite zones.

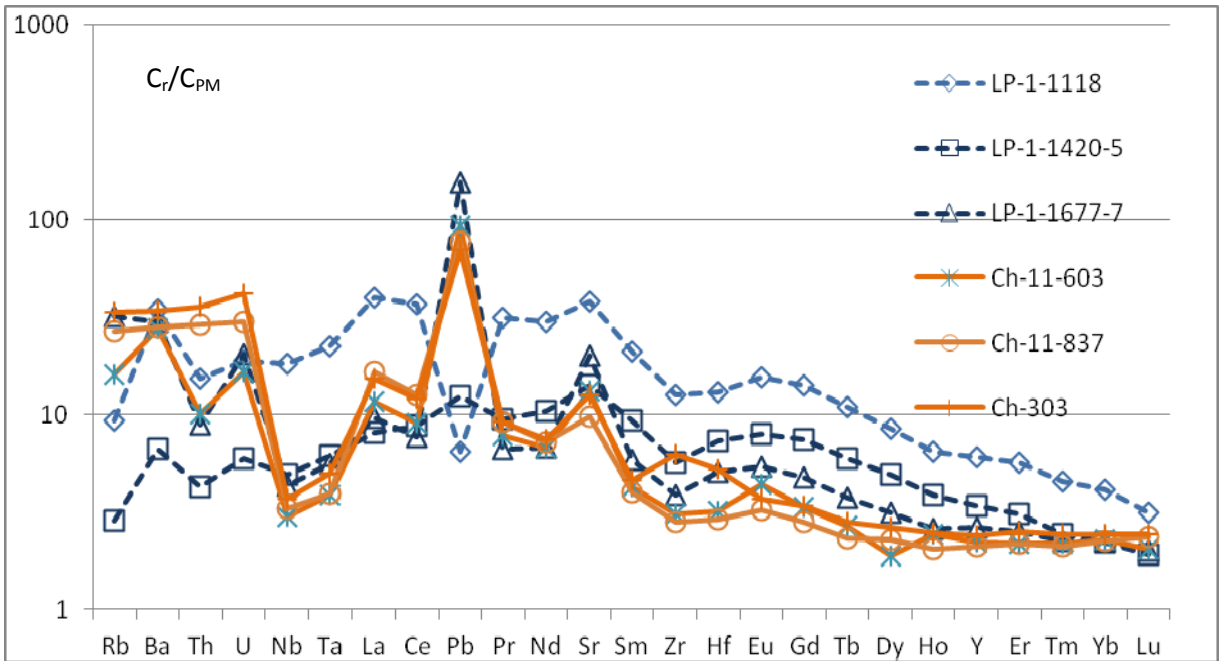

Figure. Spider-diagram for rocks of the Dyumtaleysky (blue lines) and Chineysky (red lines) intrusions (normalized after Hofmann, 1988).

Despite the similar internal structures of the Chineysky and Dyumtaleysky intrusions the rock compositions in term of rare elements distributions are absolutely different (Figure). The patterns of the Chineysky massif have negative Ta-Nb and positive Pb anomalies and low Gd/Yb ratio while patterns of the Dyumtaleysky intrusion are devoid of these anomalies and have high Gd/Yb ratio. The isotopic characteristics of the rocks (Sr, Nd, Pb) are different as well. All this geochemical data show different sources for parental magmas that formed these massifs: mantle for the Dyumtaleysky intrusion (Hofmann, 1989) and crustal (Rudnic, Gao, 2003) for the Chineysky pluton. Nevertheless, the titanomagnetite and sulfide ores of these massifs have very close composition. Main ore minerals are chalcopyrite, pentlandite, pyrrhotite; millerite, cubanite, violarite are very abundant. The lists of rare minerals are similar in the both massifs and include froodite, maichenerite, moikhukite, sperrylite.

The results of this study demonstrate the absent of a correlation between magma compositions and their mineralization. The oxide ores were formed during consequent differentiation of primary magmas (maybe at several stages) which led to concentration of Fe, Ti and V for economic contents. The origin of sulfide ores is more complexes. High volume of the sulfide melt could not appeared in the modern chamber taking into account the low sulfur solution in basaltic melts. It is suggested that sulfides were not accumulated from one magma by only crystallization differentiation but they were segregated from different portions of the magma during a long geological history of this area. Many different processes could take part in sulfide ore formation including assimilation, metamorphism and magmatism.

This study was supported by RFBR (project No 18-05-70094).

References

Burgess S.D., Bowring S. A. High-precision geochronology confirms voluminous magmatism before. during. and after Earth's most severe extinction // Science Advances 2015. No 1. e1500470.

Gladkochub D.P., Donskaya T.V., Ernst R., Mazukabzov A.M., Sklyarov E.V., Pisarevskiy S.A., Wingate M., Sederlund W. Mafic magmatism of the Siberian Craton during the Proterozoic: An overview of the main stages and their geodynamic interpretation // *Geotektonika.* 2012. No. 4. p. 28–41.

Gongalsky B.I, Krivolutskaya N.A. Chineysky layered pluton. Novosibirsk, Nauka. 1993. 187 p. (in Russian)

Gongalsky B.I, Krivolutskaya N.A. World-Class mineral deposits of Northeastern Transbaikalia, Siberia, Russia // Springer Nature Switzerland AG. 2019. 321 p.

Gongalsky B.I, Krivolutskaya N.A., Ariskin A.A., Nikolaev G.S. The Chiney gabbronorite-anorthosite layered massif (Northern Transbaikalia, Russia): its structure, Fe-Ti-V and Cu-PGE deposits, and parental magma composition // Mineral Deposita. 2016. Vol. 51. No 8. p. 113–1034.

Hofmann A.J. Chemical differentiation of the earth: relationships between mantle, continental and ocean crust // Earth Planet. Sci. Lett. 1988. Vol. 90. p. 297-314.

Komarova M.Z., Kozyrev S.M., Kokorin NI, KnaPff V.V. Petrology and ore potential of the Dyumtaleysky layered intrusion // Nedra Taimyra. 1999. No 3. p. 42-67.

Krivolutskaya N.A., Gongalsky B.I. Dyumtaleysky massif, Taimyr, Russia: a magmatic derivative from a complex mantle source // Mineral research for a high-tech world; Sweeden, Uppsala. 2013. No 3. p. 1036-1040.

Malitch K.N., Badanina I., Yu., Romanov A.P., Sluzhenikin S.F. U-Pb age and Hf-Nd-Sr-Cu-S isotope systematics of the Binyuda and Dyumtaley ore-bearing intrusions (Taimyr, Russia) // Lithosphera. 2016. No 1. p. 107- 128. (in Russian).

Malitch K.N., Belousova E.A., Griffin W.L., Badanina I.Yu., Latypov R.M., Sluzhenikin S.F. New insights on the origin of ultramafic-mafic intrusions and associated Ni-Cu-PGE sulfide deposits of the Noril'sk and Taimyr provinces, Russia: evidence from radiogenic and stable isotope data // Processes and ore deposits of ultramafic-mafic magmas through space and time. Elsevir. 2017. No.7. p. 198-237.

Polyakov G.V., Isokh A.E., Krivenko A.P. Platiniferous ultramafic–mafic formations of mobile belts of central and southeastern Asia // Russian Geol Geophys. 2006. Vol. 47. No 12. p. 1227–1241.

Popov N.V., Kotov A.B., Postnikov A.A., Sal'nikova E.B., Shaporina M.N., Larin A.M., Yakovleva S.Z., Plotkina Y.V., Fedoseenko A.M. Age and tectonic position of the Chiney layered massif, Aldan Shield // Dokl Earth Sci. 2009. Vol. 424. No 1. p. 64–67.

Rudnic R.L., Gao S. Composition of the continental crust // Treatise on geochemistry, 3; Elsivier-Pergamon: Oxford, UK. 2003. p. 1–64.

Tolstykh N.D. PGE mineralization of marginal sulfide ore of the Chinei layered intrusion // Mineral Petrology. 2008. No. 92. p. 282-306.

EXPERIMENTAL MODELING OF MANTLE-CRUST INTERACTION: THE PHASE COMPOSITION AND CRITICAL RELATIONSHIPS IN THE PERIDOTITE-BASALT-FLUID SYSTEM AT T = 1400°C, P = 4 GPa

Gorbachev N.S., Kostyuk A.V., Gorbachev P.N., Nekrasov A.N., Soultanov D.M.
D.S. Korzhinskii Institute of Experimental Mineralogy RAS, Chernogolovka, Russia,
gor@iem.ac.ru, nastya@iem.ac.ru

The most important mechanism for large-scale exchange of matter between the crust and the mantle is the subduction of the oceanic crust, which leads to the eclogitization of basalts and the formation of mantle-rich volatile reservoirs with protolites of the subducted crust (Taylor, Neal, 1989). Their important feature is the existence at high pressures and temperatures of critical relations between the melt and the fluid due to their high mutual solubility (Gorbachev, 2000; Keppler, Audetat, 2005; Wyllie, Ryabchikov, 2000). The phase relations in the peridotite–basalt–$(Na, K)_2CO_3$–fluid (H_2O, $H_2O + CO_2$) system, an experimental model of the mantle reservoir with protolites of the subducted oceanic crust, were studied experimentally at P = 4 GPa, T = 1400°C.

Experiments were carried out in IEM RAS on the anvil with hole (NL–40) using a multi-ampoule technique with Pt-peridotite ampoule (Gorbachev, 1990). Specially prepared peridotite ampoule was filled with a mixture of powders of tholeiite basalt, sodium and potassium carbonate, with the addition of a fluid source. The starting composition (wt.%): peridotite – 55 wt.%, basalt – 25 wt.%, sodium and potassium carbonate – 10 wt.%. The source of the fluid was distilled H_2O and oxalic acid dihydrate $H_2C_2O_4x2H_2O$. Equipped peridotite ampoule was placed in Pt ampoule, which was hermetically welded. The temperature was measured by Pt30Rh/Pt6Rh thermocouple, the pressure at high temperatures was calibrated by quartz–coesite equilibrium. The accuracy of temperature and pressure is estimated at ± 5°C and ± 1 kbar (Litvin, 1991). The duration of the experiment was 18–24 hours. The products of the experiments – polished preparations of quenching samples were studied on an electronic scanning microscope CamScan MV2300 c YAG detector of secondary and reflected electrons and energy dispersive x-ray microanalyzer with semiconductor Si(Li) detector Link INCA Energy.

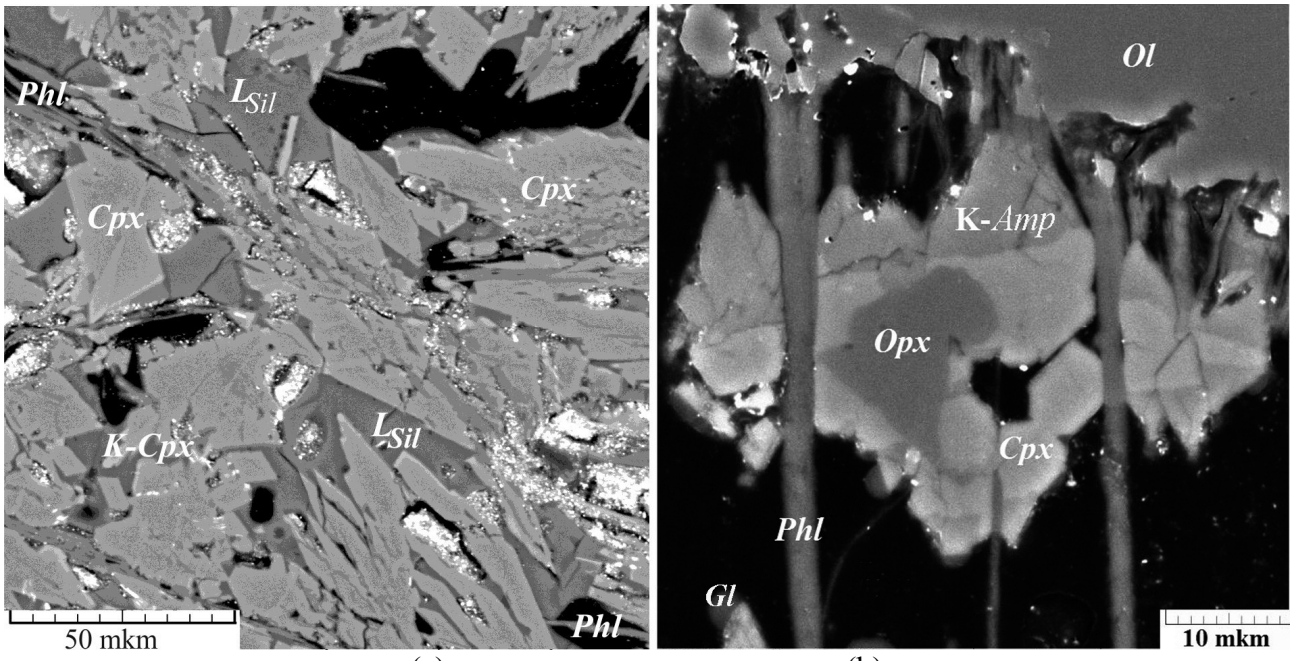

(a) (b)

Figure 1. BSE images of experimental run products. Coexisting phases in: (a) peridotite-basalt-Na_2CO_3-K_2CO_3-(H_2O+CO_2) system; (b) peridotite-basalt-Na_2CO_3-K_2CO_3-H_2O system. P = 4 GPa, T = 1400°C.

Peridotite–basalt–Na_2CO_3–K_2CO_3–(H_2O + CO_2) system. In the process peritectic melting occurred homogenization peridotite and basaltic components of the original sample with the formation of polymineral restite composition of the augite–K-clinopyroxene–orthopyroxene–phlogopite and trachyandesite melt (fig. 1a). Should pay attention to the absence of olivine among restite minerals (table 1).

Table 1. Composition of coexisting phases (in wt.%)

	SiO_2	TiO_2	Al_2O_3	FeO	MnO	MgO	CaO	Na_2O	K_2O	Cr_2O_3	SO_3	Total
peridotite–basalt–(Na, K)$_2CO_3$–(H_2O+CO_2) system												
L_{Sil}	53.00	0.14	17.94	0.56	0.00	0.23	3.92	3.38	1.51	0.00	0.00	80.68
K-Cpx	45.72	0.42	11.72	3.78	0.32	19.13	10.08	2.33	0.67	0.67	0.18	95.02
Cpx	50.95	0.47	8.84	4.83	0.17	16.05	16.51	0.84	0.00	0.47	0.00	99.12
Phl	41.35	0.36	14.44	2.94	0.20	22.29	0.06	1.33	6.76	0.38	0.82	91.2
peridotite–basalt–(Na, K)$_2CO_3$–H_2O system												
Ol	40.23	0.40	0.78	6.08	0.12	50.20	0.18	0.38	0.04	2.36	0.17	100.75
K-Amp	41.78	0.85	15.02	6.56	0.21	14.36	10.87	2.09	1.50	0.10	0.23	93.62
Cpx	49.11	0.61	8.34	4.16	0.23	16.00	19.69	1.07	0.00	0.00	0.00	99.20
Opx	54.29	0.28	4.88	3.54	0.13	33.33	1.69	0.00	0.00	1.03	0.06	99.23
Phl	40.67	0.35	14.20	2.89	0.20	21.92	0.06	1.31	6.65	0.37	0.81	89.70
Gl	53.08	0.24	18.60	0.10	0.12	0.00	0.22	6.81	2.83	0.04	0.13	82.30
L_{Cb}	6.04	0.10	2.31	1.14	0.51	3.26	40.41	0.61	0.73	0.02	0.11	55.25

The interaction of the fluid and the fluid-containing melts with peridotite was accompanied by pyroxenization and phlogopitization of peridotite:

$Mg_2SiO_4^{(Ol)} + (SiO_2)^{(LSil + Fl)} = 2MgSiO_3^{(Opx)}$

$Mg_2SiO_4^{(Ol)} + MgSiO_3^{(Opx)} + (3CaCO_3 + 4SiO_2)^{(LSil + Fl)} = 3CaMgSi_2O_6^{(Cpx)} + 3CO_2^{(Fl)}$

$3Mg_2SiO_4^{(Ol)} + (K_2O + Al_2O_3 + 3SiO_2 + 2H_2O)^{(LSil + Fl)} = 2KMg_3AlSi_3O_{10}\,(OH)_2^{(Phl)}$

Peridotite–basalt–Na_2CO_3–K_2CO_3–H_2O system. Critical relationships between the carbonated silicate melt and the fluid were achieved during the melting process. This is evidenced by the texture and phase composition of the peridotite and basalt components of the original sample. Peridotite of the ampoule is represented by isolated relics Ol + Opx + Cpx, which were replaced by newly formed Ca-clinopyroxene, K-containing amphibole, carbonate. Intergranular glass – an indicator of partial melting, was absent, which contributed to the destruction of the peridotite ampoule in the quenching sample. When quenching supercritical fluid melt, a powder mixture of small crystals (up to 5 microns) of silicates, carbonates, phlogopite, globules of aluminosilicate glass (Gl) is formed (fig. 1b).

Thus, in peritectic melting of a fluid-containing peridotite mantle with protolites of the oceanic crust at *P–T* close to the mantle adiabate, the phase relations depend on the composition of the fluid. When the alkaline-water-carbonate fluid formed alkaline melts trachyandesite composition. The composition of the restite was determined by the interaction with the fluid and the melt, which dissolved olivine, formed a restite association of the composition of orthopyroxene, Ca- and K-clinopyroxene, phlogopite.

In the water-containing system, critical relations between the fluid and the silicate melt are observed. As a result of the action of supercritical fluid-melt olivine–orthopyroxene–clinopyroxene peridotite were replaced by Ca-clinopyroxene, K-amphibole, phlogopite, carbonate. During the quenching of the supercritical fluid-melt, a microcrystalline condensate of the polymineral composition was formed. The features of the texture and phase composition of the samples under supercritical conditions allow us to conclude about the zonal structure of the reservoirs with protolites of the subducted oceanic crust: the outer zone is a metasomatically changed disintegrated restite of the harzburgite composition, which has undergone "refertilization" as a result of the formation of new minerals in it, the inner zone is isolated lenses of the supercritical fluid melt. Disintegration of the

peridotite substrate at supercritical pressures can lead to the formation of tectonically weakened zones, fluid pathways and upper mantle plumes.

This work was supported by grant RFBR 17-05-00930a.

References

Gorbachev N.S. Fluid-magma interaction in sulfide-silicate systems // International Geology Review. 1990. 32(8):749-831.

Gorbachev N.S. Supercritical State in the Hydrous Mantle: Evidence from Experimental Study of Fluid-Bearing Peridotite at P = 40 kbar and T = 1400°C // Doklady Akademii Nauk. 2000. V. 370. P. 147–150.

Keppler H., Audetat A. Fluid-mineral interaction at high pressure. Mineral behavior at extreme conditions // EMU Notes in Mineralogy. 2005. V. 7. P. 225–251.

Litvin Yu.A. Physical and chemical studies of the melting of the Earth's deep matter // Nauka, Moscow. 1991. 312 p.

Taylor L.A., Neal C.R. Eclogites with oceanic crustal and mantle signatures from the Bellsbank kimberlite, South Africa, part 1: mineralogy, petrography, and whole rock chemistry // Journal of Geology. 1989. V. 97. P. 551–567.

Wyllie P.J., Rhyabchikov I.D. Volatile components, magmas, and critical fluids in upwelling mantle // Journal of Petrology. 2000. V. 41. P. 1195–1206.

MINERALOGICAL AND GEOCHEMICAL CONSTRAINS OF THE ARAVALLI ULTRAMAFIC SEQUENCE EVOLUTION, RAJASTHAN, INDIA

Grabarczyk A.[1], Wiszniewska J.[2], Krzemińska E.[2], Ahmad T.[3]

[1]University of Warsaw, Faculty of Geology, Institute of Geochemistry, Mineralogy and Petrology, Żwirki i Wigury 93, 02-089 Warsaw, Poland, anna.grabarczyk@student.uw.edu.pl

[2]Polish Geological Institute, ul. Rakowiecka 4, 00-975 Warsaw, Poland, janina.wiszniewska@pgi.gov.pl

[3]Department of Geology, University of Delhi, Delhi-110007, India, tahmad001@yahoo.co.in

Geology. The Precambrian rocks of the Aravalli Craton, Rajasthan, NW India were separated into three lithological units (Fig.): (1) The Banded Gneiss Complex (BGC) (3.5-2.5 Ga) composed mainly of granite gneiss with pegmatite veins and numerous enclaves of amphibolites, fuchsitic quartzite and calcareous rocks; (2) the Aravalli sequence which represents the oldest supracrustal units (2.5-2.0 Ga) mainly comprise of basic metavolcanics, which subsequently are succeeded by thick units of calcereous and argillaceous sediments and (3) the Delhi Supergroup (2.0-1.7 Ga) composed predominantly of arenaceous and calcareous sediments in the lower part and calcareous sediments in the upper (Heron, 1953; Ahmad, Tarney, 1994).

Mafic metavolcanic rocks from the basal of Aravalli sequence (Fig.) are best exposed in the Nathdwara-Delwara section at the contact of basal Aravalli with BGC. Here we present petrological bulk-rock data in an attempt to constrain the petrogenesis of the volcanic sequence.

Methods. Electron microprobe analyses of mineral composition were undertaken using a CAMECA SX –100 in the Inter-Institute Analytical Complex from Minerals and Synthetic Substances, University of Warsaw. Analyses were performed with 15 kV accelerating voltage and a beam current of 10 nA. Collected natural and synthetic silicates and oxides were used for calibration. Raw data were corrected by the ZAF method. The whole-rock samples for major elements and some trace elements were analyzed in the Polish Geological Institute – Polish Research Institute (PIG-PIB) laboratory using ISP-ES method for major elements and the ISP-MS for trace elements.

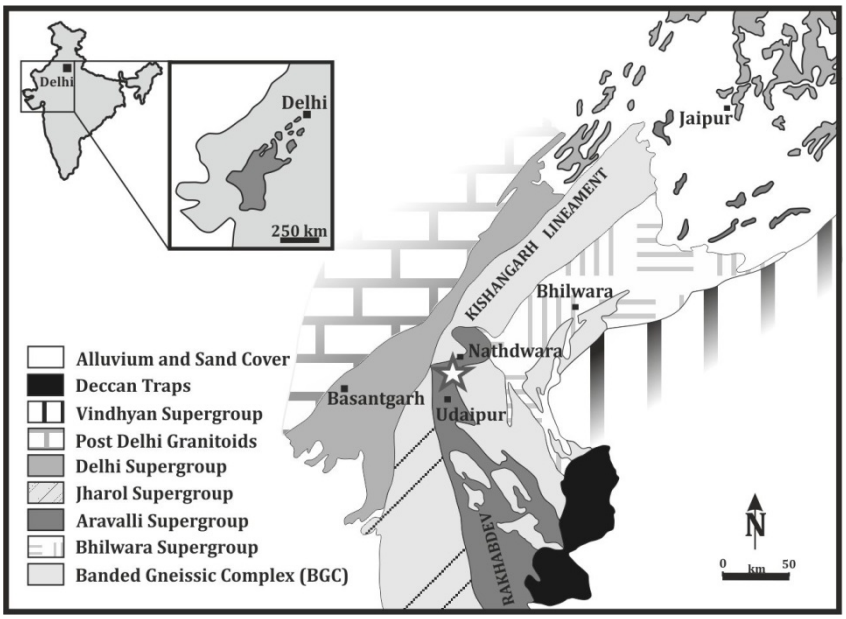

Figure. Simplified geological map of the Aravalli Craton.

Petrography. Mafic metavolcanic rocks from Aravalli sequence has been recognized in a form of pillow lavas with a coarse-grained core. A *spinifex-like* texture has been observed at the margin of the pillow, which suggests the fast quenching of high magnesium lava under water condition and existence of the komatiite-like rocks in these area (*sensu* Viljoen, Viljoen, 1969). Although *spinifex-like* texture has been indicated, the majority of the samples have schistose textures.

Aravalli rocks are composed of fine-grained plagioclase, of oligoclase and andesine composition, often with Ca-enriched rims, and of a large euhedral, elongated amphibole grains with prominent zonation. According to Hawthorne et al. (2012) classification, the Aravalli amphiboles are dominantly magnesio-(ferri-) hornblende with minor ferri-tschermakite, actinolite and cummingtonite. It is very likely that amphiboles were altered after olivine or pyroxene but no relicts of these minerals were found. The Ti and Al content in amphiboles correlates positively with temperature and pressure thus represent a relatively quantitative geothermobarometer (Ernst, Liu, 1998). Combined isoplots show that the temperature not exceeded of 550˚C with the pressure in range 1.5- 2.5 GPa, which imply that the amphiboles crystallized in medium thermal regime, typical for retrogressive changes. Retrograde minerals are epidote and chlorite of clinochlore-chamosite series with constant ripidolite composition (Fe/(Fe+Mg)) ranges from 0.364-0.399. Chlorite– bearing alterated parts of amphibolites were used for the chlorite thermometry and has defined the last stage of metamorphic evolution. The chlorite formation temperatures, calculated according to Kranidiotis and MacLean (1987) and Cathelineau and Nieva (1985) calibrations, indicate similar range from 310 to 330 □±□16°C and from 290 □to 303□±□8°C respectively.

Since these rocks have been altered in greenschist to lower amphibolite facies conditions the skeletal olivine or pyroxene crystals have been replaced by hornblende, epidote and chlorite, still preserving *pseudo-spinifex* texture.

Geochemistry. Earlier geochemical data of komatiites and tholeiites from Nathdwara region (Ahmad, Tarney, 1994) were used for comparison with new samples collected from basal Aravalli sequence.

Bulk-rock compositions indicate a wide range of Mg# from 0.24 to 0.55, with MgO content from 5.32 up to 16.85 wt. %. A Ti content is relatively low (1.08-2.48 wt. % TiO_2) and the sum of the alkalis do not exceeding 6 wt. % (usually not exceed~~ing~~ 3 wt.%). The rocks are also enriched in incompatible and LREE elements with large range for $(Ce/Yb)_N$ ratios from 2.3 to 6.9 and $(Gd/Yb)_N$ ratios from 1.4 to 2.7.

TAS classification diagram have shown on changeable composition of pillow lavas from picrobasalts and more often basalts and andesite basalts, up to trachybasalts. On the AFM plot samples have shown a typical tholeiitic iron enrichment trend.

The chemistry of the magma may potentially be changed by crustal contamination during thermal influence of mafic magma. Positive correlation between element ratio such as La/Sm, Zr/Y and Al_2O_3/TiO_2 and negative Nb anomaly (Arndt et al., 1988) may confirm such a hypothesis.

The new samples from pillow lavas represent features of tholeiites (SiO_2 vs Al_2O_3/TiO_2) and komatiite basalts and tholeiites (SiO_2 vs Fe_2O_3/MgO) in accordance to chemical classification, variation diagrams in a function of MgO, REE and multi-element~~s~~ spidergrams but also in general nomenclature used in previous papers on Aravalli Craton rocks. This results correspond to the composition of the komatiite basalts and tholeiites from Nathdwara region.

Geotectonics. Evolution of Aravalli pillow lavas sequences could be the most probably connected with magmatic events of 2.5-2.0 Ga and supracrustal Aravalli Supergroup genesis.

The application of geotectonic setting discrimination diagrams in mutual relation of incompatible trace elements, confirms a very complex problem of geotectonic magmatic setting estimation.

On La-Y-Nb diagram (Cabanis, Lecolle, 1989) a real komatiites, komatiite basalts and tholeiites from Nathdwara, and also new samples of pillow lavas from Aravalli, are projected mostly in the field of CAB – calc-alkali basalts of volcanic arcs and in continental basalts and continental rift fields. On Ti-Zr-Y triangle (Pearce, Cann, 1973), a significant number of points are included in the CAB – calc-alkali basalt field and in WPB field – within plate basalts. Discrimination (Nb-Zr-Y), with using of incompatible Nb instead of titanium (Meschede, 1986), place most of Nathdwara and Aravalli rocks in VAB and WPT (volcanic arc basalts and within plate alkali tholeiites) fields. Another points, though projected in VAB field, demonstrated also strong relation with P-MORB, that are enriched by influence of mantle plume. Two most alkalic samples from Aravalli are expanded additionally on WPA field – within plate alkaline basalts.

We believe, that in mature continental regions with thicker subcontinental lithosphere, the opportunity for interaction of the superhot komatiite diapir with the lithospheric rock region is greater. The crustal contamination would yield a higher proportion of basalts/tholeiites relative to komatiites. Lavas of the Aravalli rocks was rather less Mg-rich than the komatiites from many other Archaean greenstone belts and basalts seem to be more iron-rich in composition. These data and assumption are coherent with earlier paper by Ahmad and Tarney (1994).

References

Ahmad T., Tarney J. (1994) Geochemistry and petrogenesis of Late Archaean Aravalli Volcanics, basement enclaves and granitoids, Rajasthan // Precambrian Research. 1994. Vol. 65. p. 1-23.

Arndt N.T., Teixeira N.A., White W.M. Bizarre geochemistry of komatiites from the Crixas greenstone belt, Brazil // Contributions to Mineralogy and Petrology. 1989. Vol. 101(2). p. 187-197.

Cabanis B., Lecolle M. (1989) Le diagramme La/10 –Y/15 –Nb/8: un outil pour la discrimination des series vocaniques et mise en evidence des processus de mélange et /ou de contamination crustale. C.R.Acad. Sci. Ser.II. 1989. Vol. 309 p. 2023-2029.

Cathelineau M., Nieva D. A chlorite solid solution geothermometer the Los Azufres (Mexico) geothermal system // Contributions to Mineralogy and Petrology. 1989. Vol. 91(3). p. 235-244.

Ernst W.G., Liu J. Experimental phase-equilibrium study of Al- and Ti-contents of calcic amphibole in MORB-A semiquantitative thermobarometer // American Mineralogist. 1998. Vol. 83. p. 952–969.

Hawthorne F.C., Oberti, R., Harlow, G.E., Maresch, W.V., Martin, R.F., Schumacher, J.C., Welch, M.D. Nomenclature of the amphibole supergroup. American Mineralogist. 2012. Vol. 97(11-12). p. 2031-2048.

Heron A.M. Geology of Central Rajputana // Geol. Surv. India. Mem. 1953. Vol. 79. p. 389.

Meschede M. (1986) A method of discriminating between different types of mid-ocean ridge basalts and continental tholeiites with the Nb-Zr-Y diagram. Chem. Geol. 1986. Vol. 56. p. 207-218.

Pearce J.A., Cann J. R. Tectonic setting of basic volcanic rocks determined using trace element analysis. Earth Planet. Sci. Lett. 1973. Vol. 19. p. 290 - 300.

Kranidiotis P., Maclean W.H. Systematics of chlorite alteration at thehelbsDodge massive sulfide deposits, Matagani, Quebec. Econ. Geology. 1987. Vol. 82. p. 1898 -1811.

Viljoen M. J., Viljoen R. The geology and geochemistry of the lower ultramafic unit of the Onverwacht Group and a proposed new class of igneous rocks. Geological Society of South Africa Special Publication. 1969. Vol. 2. p. 55-86.

RARE METALS AND RARE EARTH ELEMENTS IN MINERALS FROM DEVONIAN ULTRABASIC ALKALINE ROCKS, DEEP CRUSTAL STRUCTURES (BELARUS)

Ignatkevich E.S.[1], Varlamov D.A.[2], Mikhajlov N.D.[3]

[1]Belarusian scientific research and designed institute of oil, Gomel, Belarus, eihnatkevich@gmail.com

[2]Institute of Experimental Mineralogy RAS, Chernogolovka, Rassia, dima@iem.ac.ru

[3]State Enterprise "Research and Productoin Center for geology", Minsk, Belarus

Upper Devonian igneous rocks of the Pripyat Paleorift are the most interesting object which is promising for identifying carbonatites and (or) primary sources of diamonds (kimberlite-like rocks, lamproites, etc.). The Pripyat Paleorift consists of the Pripyat Paleograben and Braginsky and Loevsky Saddle, the North Pripyat Shoulder and Zhlobin Saddle.

The detailed analysis of Devonian igneous and volcanogenic clastic rocks of the Pripyat Paleograben was carried out mainly in the 60-70s of the last century when there were absent modern instrumental capabilities for the analysis of minerals. So it did not allow characterizing mineral phases and assemblages fully. At the same time mineralogical criteria are very important while determining mineragenic type of rocks and making overall assessment of metallogeny of specific alkaline provinces because average petrochemical indicators may not be sufficient for the formation differentiation of ultrabasic alkali rocks due to their extreme convergence. The consistent patterns of the distribution of minerals of rare metals (Nb, Sr, Ba, etc.) and rare earth elements (REE) which are a direct reflection of the results of geochemical processes are very essential (Хомяков, 1990).

The work on identifying the structure and typomorphism of accessory minerals for the Devonian igneous complex of Belarus was carried out for the first time. The structures of the minerals were studied on a Tescan VEGA-II XMU electron scanning microscope with an INCA Energy 450 energy dispersive spectrometer of the Institute of Experimental Mineralogy (Chernogolovka, Russia). Ti-magnetite, copper sulphides, sphene, apatite as well as barite are the most common accessory minerals in ultrabasic alkaline rocks. The microprobe analysis showed that apatite and barite have a significant strontium admixture which indicates the alkaline nature of magmatism. As a result of the detailed microprobe studies of nephelinite from Yastrebovskaya 3 drill-hole core (depth 958–977 m), alkaline picrite from Vasiliyevskaya 1 drill-hole core (1785–1788 m depth) and nephelinite from Tsentrolit 2 drill-hole core (420 m) we managed to reveal minerals of rare and rare-earth elements: fluorcaphite (Ignatkevich, Varlamov, 2014), monazite, thorite and chabazite-Sr which were previously unknown for Devonian magmatic formation of Belarus. We also obtained information about their relationship with the rock-forming components and identified the characteristics of their chemical structure.

The results of the study of the characteristics of the morphology and chemical structure (Table 1) of the monazite which was first discovered in the rocks of the Devonian igneous complex of Belarus were given in this work. Monazite is an important rare-earth indicator of mineralization and rock-forming conditions (Ковальчук, 2011). This mineral together with neodymium-ceric area of specialization forms small (about 5 microns) grains in chlorite-phlogopite glass in alkaline picrite from Vasiliyevskaya 1 drill-hole core. It is often formed in the immediate vicinity of apatite (Figure). It should be noted that the obtained analyzes are not suitable for carrying out calculations due to the small size of the detected grains and they are given in the work to diagnose the mineral species.

As it is known (Пеков, 2001), monazite is a product of late hydrothermal activity in strongly alkaline (agpaite) complexes in contrast to less alkaline complexes where this mineral is a part of the high-temperature early coexisting. According to the structural relationship with accessory apatite (Figure) monazite was formed in situ due to the phosphorus released by dissolving this phosphate.

Thorite is a typomorphic mineral of ultra-alkaline igneous complexes. It forms small (4-5 microns) crystals in the rutile congeries in nephelinite from Yastrebovskaya 3 drill-hole core. Thorite is isomorphic with zircon and rutile. The device sensitivity didn't allow separating the phases. The content of thorium dioxide is up to 28.1 % wt. and 32.5 % wt., of zirconium – 22.7 % wt. and 29.6 % wt. and titanium – 0.1 % wt. and 10.1 % wt. which correspond to a solid solution of thorite with zircon as well as to a solid solution of a mixed structure (zircon-thorite-rutile). As a rule similar compounds

are formed due to intergrowth inside and / or at the primary accessory phase outer circle. Their formation is determined by the modification of previous minerals due to the effect of fluids (Пеков, 2001).

Table 1. Composition of monazite.

Crystal	1	2
P_2O_5	30,9	30,1
CaO	24,2	20,3
Ce_2O_3	9,2	11,8
La_2O_3	5,1	6,5
Pr_2O_3	0,8	0,7
Nd_2O_3	2,5	3,3
ThO_2	*0,3*	0,6
SmO	*0,2*	*0,2*
Gd_2O_3	0,6	0,6
EuO	*0,0*	*0,3*
Ga_2O_3	*0,0*	*0,2*
V_2O_5	*0,0*	*0,2*
MgO	6,4	6,0
Fe_2O_3	1,6	1,4
TiO_2	0,5	0,5
Al_2O_3	2,7	2,3
SiO_2	6,0	6,2
Total	84,9	85,1

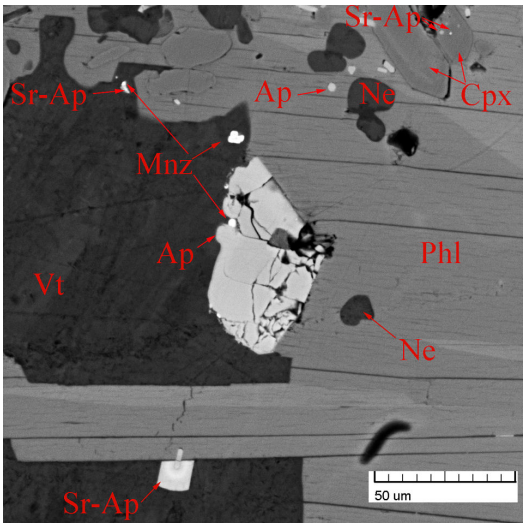

Figure. Minerals from alkaline picrite from Vasilyevskaya 1 drill-hole core.

Chabazite-Sr is the mineral found exclusively in hydrothermalites of ultragpaitic rocks (Пеков, 2001). Such Sr-zeolites are widely developed in the late differentials of the Khibino-Lovozero alkaline complex on the Kola Peninsula. The representatives of chabazite, thomsonite and heulandite series are the main concentrators of strontium in hydrothermalites of many types. Strontium is dispersed in asperolite, aspidelite and other minerals at the igneous stage of development of alkali complexes. Strontium is bound to calcium at hydrothermal stages, compounds with zeolite cavities in the structure become its haven. It has been experimentally proven that strontium enters chabazite in appreciable amounts only in solution, where its concentration is up to 7%. The content of strontium oxide in chabazite does not exceed 0.9 % wt. at strontium lower concentrations in the washing solutions (Ловская, 2005).

We found strontium zeolite in the nephelinite from Tsentrolit 2 drill-hole core. Seeing that the crystals (microns) are of the small size and their percentage in the rock (single grains) is small, only a preliminary diagnosis of the mineral species has been carried out by studying the chemical composition of the mineral by electron microsounding. Mineral was preliminary classified to chabazite-Sr. It was established SrO % wt. was 22.9 in chabazite-Sr (?) which implies the replacement of calcium with strontium in the structure of chabazite and probably it is associated with exposure to high-strontium solutions with a concentration of at least 7%. Besides strontium zeiolites there were revealed fluorite and celestine in the same nephelinite sample by microprobe studies. Their presence may be an indicator of hydrothermal exposure.

Thus, the minerals fluorcaphite, monazite, thorite, chabazite-Sr (?) previously unknown for Upper Devonian igneous complex were found in the ultrabasic alkaline rocks of Pripyat Paleograben and Braginsky and Loevsky Saddle. The presence of such rare and rare-earth minerals in the rocks of this complex indicates the highly alkaline conditions of their crystallization, magma differentiation,

possible association with rare metal carbonatites and, as a consequence, the potential prospects of Pripyat Paleograben and conjugate structures for industrially valuable phosphorus ores, rare and rare earth metals.

This research was carried out with financial support from the Belarusian Republican Foundation of Fundamental Investigations (grant № X14M-088).

References

Ковальчук Н.С., Шумилова Т.Г., Козырева И.В. Морфология и особенности химического состава монацита в карбонатитах Косьюкского массива (Средний Тиман) // Известия Коми научного центра УрО РАН. 2011. Вып.1(5). С. 48-52.

Ловская, Е.В. Катионный обмен как важнейший фактор, влияющий на химический состав шабазита в щелочных массивах // Геохимия магматических пород: труды Всероссийского семинара с участием стран СНГ, Москва, 2005, с. 41-42.

Пеков И.В. Ловозерский массив: история исследования, пегматиты, минералы. Москва, 2001, 432 с.

Хомяков А.П. Минералогия ультраагпаитовых щелочных пород. Москва, 1990, 196 с.

Ignatkevich, E.S., Varlamov D.A. Typochemism of the apatite supergroup minerals from Devonian ultrabasic alkaline rocks found in the Braginsky and Loevsky saddle (Belarus) // Ore potential of alkaline, kimberlite and carbonatite magmatism: abstracts of XXX International conference, Antalya, 2014, p. 77–78.

PHASES OF THE Ca–Al–O SYSTEM AT P-T PARAMETERS OF THE TRANSITION ZONE AND LOWER MANTLE: SYNTHESIS, FEATURES OF CRYSTAL STRUCTURES, ISOMORPHISM, EQUATION OF STATE

Iskrina A.V.[1], Spivak A.V.[2], Bobrov A.V.[1,2,3], Dubrovinsky L.S.[4], Eremin N.N.[1], Marchenko E.I.[1]

[1]Lomonosov Moscow State University, Department of Geology, Moscow, Russia, grigoryeva_av888@mail.ru

[2]Institute of Experimental Mineralogy RAS, Chernogolovka, Russia

[3]V.I.Vernadsky Institute of Geochemistry and Analytical Chemistry RAS, Moscow, Russia

[4]Bayerisches Geoinstitut, University of Bayreuth, Bayreuth, Germany

Aluminum takes the first place among metals and the third place among the elements after oxygen and silicon by the prevalence in the Earth's crust. The concentration of aluminum in the Earth's crust, according to various researchers, reaches 16.4 wt. % (Green et al. 1979). Aluminates may be the hosts of aluminum under the conditions of the transition zone and lower mantle of the Earth (Ringwood, 1976; Irifune and Tsuchiya, 2007). There are Ca-aluminates, which may include various cations, such as Fe, Mg, Na, influencing the phase relations in the $CaO–Al_2O_3$ system. To date, several intermediate compounds are known in the $CaO\text{-}Al_2O_3$ system ($CaAl_2O_4$; $CaA_{l4}O_7$; $CaAl_{12}O_{19}$; $Ca_3Al_2O_6$; $Ca_2Al_2O_5$; $Ca_{12}Al_{14}O_{33}$) (Ito et al, 1980; Lazic et al, 2006; Janakova, Salavcova, Renaudin et al, 2007; Jerebtsov and Mikhailov, 2001; Filonenko and Lavrov, 1949; Ivanova et al, 2002; Ma, Kampf et al, 2011; Mikouchi, Zolensky et al, 2009). They are stable over a wide range of pressures and temperatures.

Table 1. Crystal data for $CaAl_2O_4$ and $Ca_2Al_6O_{11}$.

	$Ca_2Al_6O_{11}$ (tetragonal)	$CaAl_2O_4$ (orthorhombic)
Formula	$Ca_2Al_6O_{11}$	$CaAl_2O_4$
Space group	$P4_2/mnm$(#136)	*Pnma*(#62)
	Cell parameters	
a	11.1675(4)	8.8569(10)
b	11.1675(4)	2.8561(4)
c	2.83180(10)	10.2521(11)
α	90°	90°
β	90°	90°
γ	90°	90°
V	353.16(2)	259.34(5)
Z	2	8
ρ (g/cm^3)	3.93	4.08

Experiment on synthesis of the phases in the Ca-Al-O (±Fe) system were carried out using a high pressure - high temperature 1000-t multi-anvil Sumitomo press and 1200-t multi-anvil Haymag press at Bayerisches Geoinstitute (BGI). The phases of $CaAl_2O_4$, $Ca_2Al_6O_{11}$ and $Ca(Al,Fe)_2O_4$ were synthesized at 1600°C and 15, 24 GPa, respectively. Compounds of these phases were studied by different methods including optical microscopy, SEM and microprobe analysis. The method of single-crystal X-Ray diffraction allowed us to refine the structures (Table 1) and to determine the crystal chemical formulae of the phases. All studied phases with the stoichiometry AB_2O_4 have the $CaFe_2O_4$-type structure. The structures of the synthesized phases were refined by the method of single-crystal X-Ray diffraction using synchrotron radiation. The compressibility of the $Ca(Al,Fe)_2O_4$ phase was studied up to ~60 GPa. In this pressure range, no phase transformations were detected, but the spin transition for iron was registered. As one of the results of this study, it was possible to obtain the equation of state for the $Ca(Al,Fe)_2O_4$ phase (Fig. 1).

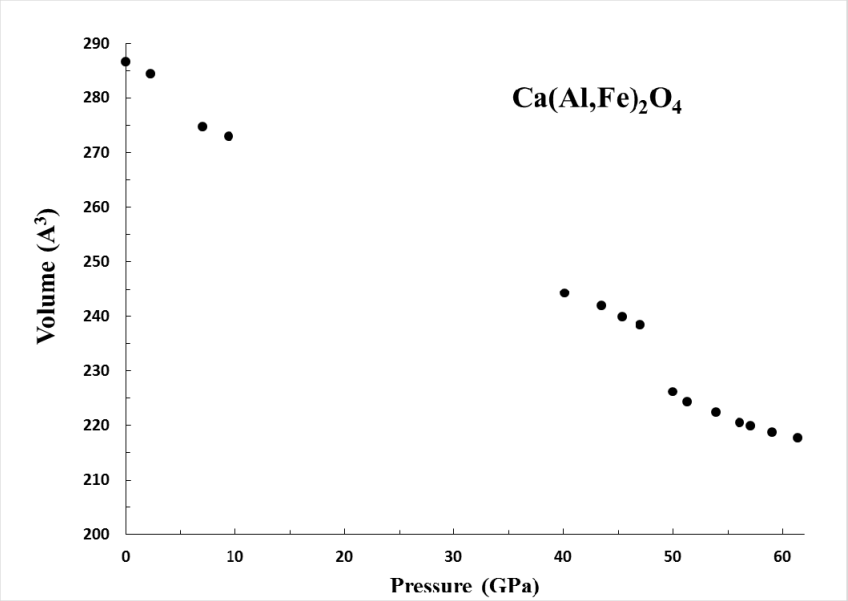

Figure 1. The diagram of the dependency for volume of the cell from the pressure for $Ca(Al,Fe)_2O_4$ phase.

The data obtained may be applied to construction of a P–T phase diagram in the $CaO\text{-}Al_2O_3$ system (the current diagrams are limited to a pressure of 16 GPa).

The studied phases are stable in the transition zone and lower mantle of the Earth and can be considered as potential aluminum concentrators in the Earth's deep geospheres.

This work was supported by the Russian Science Foundation, project no. 17-17-01169.

References

Filonenko N.E., Lavrov I.V. Critical evaluation and optimization of the thermodynamic properties of the $CaO\text{-}Al_2O_3$, Dokl. Akad.Nauk S.S.S.R., 1949, Vol.66., p. 673 – 676.

Green D.H., Hibberson W.O., Jaques A.L. Petrogenesis of mid-ocean ridge basalts. In: The Earth: its origin, structure and evolution (ed. M.W. McElhinney), Academic Press, London, 1979, pp. 265–299.

Irifune T., Tsuchiya T. Mineralogy of the Earth – Phase Transitions and Mineralogy of the Lower Mantle, Ehime University, Matsuyama, Japan, 2007.

Ivanova M.A., Petaev M.I., MacPherson G.J., Nazarov M.A., Taylor L.A., Wood J.A. The first known natural occurrence of calcium monoaluminate, in a calcium-aluminum-rich inclusion from the CH chondrite Northwest Africa 470, Meteoritic and Planetary Science 37, 2002, p. 1337-1344.

Ito S., Suzuki K., Inagaki M., Naka S. High pressure modifications of CaAl2O4 and CaGa2O4, Mat. Res. Bull.,Vol. 15, 1980, p. 925-932.

Janakova S., Salavcova L., Renaudin G., Filinchuk Y., Boyer D., Boutinaud P. Preparation and structural investigations of sol–gel derived Eu3+-doped CaAl2O4, Journal of Physics and Chemistry of Solids 68, 2007, P. 1147–115.

Jerebtsov D.A., Mikhailov G.G. Phase diagram of CaO±Al2O3 system, Ceramics International 27, 2001, p. 25-28.

Lazic B., Kahlenberg V., Konzett J., Kaindl R. On the polymorphism of CaAl2O4 — structural investigations of two high pressure modifications, Solid State Sciences 8, 2006, p. 589–597.

Ma C., Kampf A.R., Connolly Jr. H.C., Beckett J.R., Rossman G.R., Smith S.A.S., Schrader D.L. Krotite, CaAl2O4, a new refractory mineral from the NWA 1934 meteorite, American Mineralogist, Vol. 96, 2011, p. 709–715.

Mikouchi T., Zolensky M.,Ivanova M., Tachikawa O., Komatsu M., Le L., Gounelle M. Dmitryivanovite: A new high-pressure calcium aluminum oxide from the Northwest Africa 470 CH3 chondrite characterized using electron backscatter diffraction analysis, American Mineralogist,Vol. 94, 2009, p. 746–750.

Ringwood A.E. Composition and Petrology of the Earth's Mantle, McGraw-Hill, Dusseldorf, 1976, 618 p.

PGE AND Au IN ORE-FREE DOLERITE SILLS OF THE SIBERIAN TRAPS: ESTIMATION OF INITIAL METAL CONCENTRATIONS IN MAFIC MELTS

Ivanov A.V.[1], Demonterova E.I.[1], Marfin A.E.[1], Dudkin T.V.[1], Fiorentini M.L.[2], Kamenetsky V.S.[3,4]

[1]Institute of the Earth's Crust, Siberian Branch of the Russian Academy of Sciences, Irkutsk, Russia, aivanov@crust.irk.ru, dem@crust.irk.ru, marfin1309@gmail.com, timur-dudkin@mail.ru

[2]The University of Western Australia, Perth, Australia, marco.fiorentini@uwa.edu.au

[3]University of Tasmania, Hobart, Australia, dima.kamenetsky@utas.edu.au

[4]Institute of Experimental Mineralogy, Chernogolovka, Russia

The classic example of sulfide Cu-Ni±Pt-Pd deposits located within mafic intrusions is the Noril'sk-Talnakh group of deposits in the northwestern Siberian Platform. It is commonly assumed that sulfide ores are formed by liquation (Ryabov et al., 2014). Many sulfides of such deposits, however, are characterized by heavy sulfur isotopes (Grinenko, 1985; Li et al., 2003). This fact is interpreted in favor of contamination of mafic melts by sulfur from sulfate-rich sediments and sulfur-rich gases (Grinenko, 1985; Li et al., 2003).

The source of metals in sulfide melts is questionable. Again, it is commonly assumed that metals are derived from mantle and when they meet crustal sulfur, a sulfide melt is formed within silicate melt matrix. Heavy sulfide melt sinks to the bottom of a magmatic conduit, while remained barren silicate melt flows away. We wish to test this model for the Noril'sk-Talnakh group of deposits by the mass balance calculations in the following way; (1) estimate the metals' concentrations in initial mafic melts, (2) estimate the overall metals' abundance within the deposits, (3) calculate the volume of mafic melts required to produce the deposits by knowing the first two parameters, (4) compare the calculated melt volume with the available volume of the intrusive and extrusive phases in the region of interest. Each of these four steps is a nontrivial task. Thus, this study aims to the first step only.

What rocks should be taken for analysis to estimate concentrations of PGE and Au in initial melts? Intrusions in the Noril'sk-Talnakh area are rich in these metals, whereas barren intrusions, according to the explained model above, may be existed by the elements of interest. It was shown, that intrusions in the Angara-Taseeva syncline of the southern Siberian Traps province, on one hand, free of ore component and, on the other hand, have geochemical analogues among extrusive formations of the Noril'sk-Talnakh area (Ivanov et al., 2008). So, they were taken as the case study.

We collected 17 samples of dolerite sills with large MgO variations from surface outcrops within the Angara-Taseeva syncline. These samples were analyzes for major, trace elements, including PGE and Au, and Sr-Nd isotopes. According to chemistry and Sr-Nd isotopes, the dolerite sills of the Angara-Taseeva syncline resemble low-Ti basalts of the Noril'sk-Talnakh area and, except PGE and Au concentrations, do not differ from ore-bearing and barren intrusions of the same region.

Table 1. Estimated concentrations of PGE and Au (ppb) for mafic melts.

	High MgO	Most differentiated	Average
Au	3	12	4
Pt	5-10	33	11
Pd	9-10	40	14
Rh	n.e.	n.e.	0.6
Ru	n.e.	n.e.	0.2
Ir	n.e.	n.e.	0.06

n.e. – not estimated, because there is no significant variations among different compositions

As for PGE and Au, there are no significant variations for Ir, Ru, Rh among different by chemistry dolerite sills. On average, concentrations of these elements are at sub-ppb level (Table 1). Au correlates positively with TiO_2 and FeO_{total} (Fig. 1) and negatively with MgO and Mg#. This shows that in sulfur-undersaturated melts Au behaves as incompatible element and accumulates in course of differentiation. The difference between the most differentiated and the most primitive rock samples is

fourfold (Table 1). The difference in TiO_2 and FeO_t concentrations is ~5-fold and ~2-fold, suggesting that the major crystalizing mineral phases were olivine, plagioclase and orthopyroxene in agreement with petrographic and geochemical observations (Feoktistov, 1978; Ivanov et al., 2008).

Pt and Pd behave similarly to Au. In general, their concentrations also increase, though some sample deviate from this behavior (Fig. 1). Probably in course of differentiation, sulfur concentrations also increases and if a threshold value is reached it immediately form Pt or Pd sulfide phase.

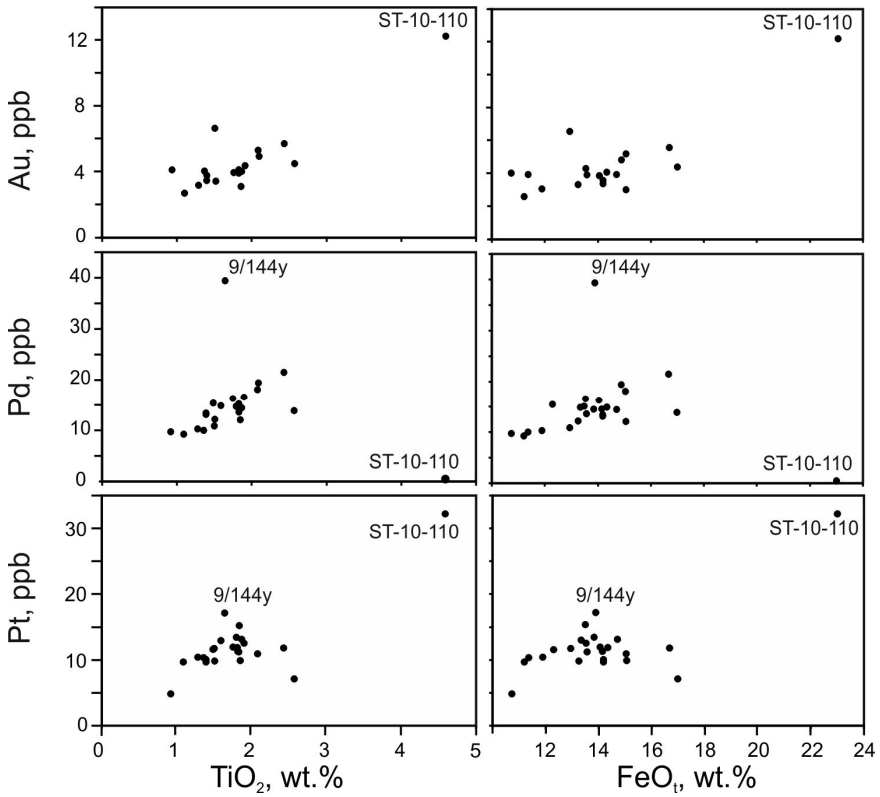

Figure 1. Variations of Pt, Pd and Au vs TiO_2 and FeO_t in dolerite sills of the Angara-Taseeva syncline, southeastern Siberian Traps province. Sample numbers of some extreme sample are shown.

Considering the trends in Fig. 1, we estimate probable concentrations of Pt, Pd and Au for the most primitive and the most differentiated rocks (Table 1). Generally speaking, the most primitive rocks are characterized by 3 ppb Au, 5-10 ppb Pt and 9-10 ppb Pd. These should be used as initial concentrations for any further consideration of ore process in the Noril'sk-Talnakh ore district in regards the testing liquation model.

This work was supported by the Russian Science Foundation (grant no 16-17-10068).

References

Feoktistov G.D. Petrology and conditions for formation of trap sills. Novosibirsk: Nauka. 1978. (In Russian).

Grinenko L.N. Hydrogen sulfide-containing gas deposits as a source of sulfur for sulfurization of magma in ore-bearing intrusives of the Noril'sk area // International Geology Review. 1985. Vol. 27, p. 290-292.

Ivanov A.V., Demonterova E.I., Rasskazov S.V., Yasnygina T.A. Low-Ti melts from the southeastern Siberian Traps Large Igneous Province: Evidence for a water-rich mantle source? Journal of Earth System Science. 2018. Vol. 117. p. 1-21.

Li C., Ripley E. M., Naldrett A. J. Compositional variations of olivine and sulfur isotopes in the Noril'sk and Talnakh intrusions, Siberia: implications for ore-forming processes in dynamic magma conduits. Economic Geology. 2003. Vol. 98, p. 69-86.

Ryabov V.V., Shevko A.Ya., Gora M.P. Trap magmatism and ore formation in Siberian Noril'sk region. Trapp Petrology. Vol. 1. Springer. 2014.

ZONATION AND GENESIS OF THE KOVDOR PHOSCORITE-CARBONATITE PIPE

Ivanyuk G.Yu., Pakhomovsky Ya.A., Kalashnikov A.O., Mikhailova Yu.A., Yakovenchuk V.N., Panikorovskii T.L., Konoplyova N.G., Bazai A.V.

Kola Science Center of the Russian Academy of Sciences, Apatity, Russia, g.ivanyuk@gmail.com

The Kovdor phoscorite-carbonatite complex occurs within the Devonian Kovdor massif of peridotite, foidolite–melilitolite, and related diopsidite, phlogopitite and skarn-like rocks. The complex forms pipe-like concentrically-zoned body, 1.5×0.7 km that, gradually tapering, goes to a depth of more than 2 km (Mikhailova et al., 2016). Petrographic zonation of the pipe has been reconstructed by means of 3D mapping using the Micromine-16 program and all drilling data obtained in 1950–2015 (Ivanyuk et al., 2016; Kalashnikov et al., 2017): there is a gradual change of marginal (apatite)-forsterite phoscorite to intermediate low-carbonate magnetite-rich phoscorite and then to calcite-rich phoscorite that transforms in calcite carbonatite when the calcite content reaches 50 modal %. Between the intermediate and axial zones of the pipe, there occurs ring-like fractal (D=2.5) stockwork of vein calcite carbonatite, and NE linear zone of dolomite carbonatite dikes and related magnetite-dolomite-serpentine rock (Mikhailova et al., 2016).

Detailed study of the pipe zonation concerning geochemistry of rocks, content, morphology, granulometry, composition, crystallochemistry, and peculiarities of subsolidus alteration of the most rock-forming and accessory minerals allowed to build a complex 3D mineralogical model of the Kovdor phoscorite-carbonatite pipe (Figure). Analysis of this model allows us to make the next conclusions:

1. Crystallization of phoscorite started from forsterite, which launched destruction of silicate-carbonate-ferriphosphate subnetworks of the melt followed by precipitation of apatite and magnetite from the pipe wall to its axis with formation of carbonatite melt in the axial zone (Mikhailova et al., 2016, 2018);

2. Geochemical evolution of the phoscorite-carbonatite complex includes consequent increase of C, S, Ca, Sr, Ba, *REE*, U, Th, Nb, Ta, Cu and Pb contents at the expense of Si, Ti, Al, Mg, Na, K, Rb, Cr and Ni amount, while Fe, P, F, Zr, Hf, V, Sc, Zn, Co and Ag concentrate in intermediate low-carbonate magnetite-rich phoscorite;

3. In marginal (apatite)-forsterite phoscorite, there occur Fe^{2+}-rich forsterite, Mn-Ti-Si-rich magnetite with exsolution inclusions of ilmenite, Fe-Mg-bearing hydroxylapatite, Mn-Fe-Si-bearing baddeleyite, Ca-F/O-dominant minerals of the pyrochlore group, and Ni-rich pyrrhotite -4*C* with exsolution inclusions of pentlandite. Intermediate low-carbonate magnetite-rich phoscorite contains Fe^{3+}-rich forsterite, Mg-Al-rich magnetite with exsolution inclusions of spinel, impurities-free hydroxylapatite and baddeleyite, Na/Ca-OH-dominant Ta-rich minerals of the pyrochlore group, and Ni-Co-rich pyrrhotite-4-5*C* with exsolution inclusions of (cobalt)pentlandite. Axial calcite-rich phoscorite (Cb=10–50 modal %) and related calcite carbonatite (Cb≥50 modal %) include Mn-Fe^{2+}-rich forsterite, Ti-V-Ca-rich magnetite with exsolution lamellae of ilmenite-geikielite, Ba-Sr-*REE*-bearing hydroxylapatite, Hf-Ta-Nb-Sc-rich baddeleyite, Na-OH-dominant Ti-rich minerals of the pyrochlore group, and Co-rich pyrrhotite-5-6*C* with exsolution lamellae of cobaltpentlandite (Ivanyuk et al., 2016, 2017, 2018a,b, 2019; Kalashnikov et al., 2016; Mikhailova et al., 2018);

4. (Multi)fractal analysis of geometry of calcite and dolomite clusters has shown that formation of carbonate stockwork in all studied scales (from 10 μm to 100 m) occurred due to percolation of carbonate-bearing melts and fluids through anisotropic fractal fracture network (D_0 = 2.5), with gradual increase of size, compactness and density of carbonate clusters from peripheral zone of phoscorite-carbonatite pipe (D = 2.1–2.7, Λ = 1.5–0.5) toward its axial zone (D = 2.7–3.0, Λ = 0.5–0.2);

5. Subsolidus evolution of through minerals includes exsolution of solid solutions, temperature of which decreases, from the pipe margins towards its axis, from 500 to 400 °C for calcite-dolomite pair, from 500 to 300 °C for magnetite-ilmenite pair, and from 250 to 150 °C for pyrrhotite-pyrite pair (Ivanyuk et al., 2017, 2018a);

6. The Fe^{3+}/Fe^{2+} ratio in pyrrhotite linearly decreases in the natural rock sequence, from host foidolite and diopsidite to phoscorite and then to carbonatites evidences gradual decrease of oxygen fugacity accompanied by decrease of agpaitic index of the rocks. According to magnetite-ilmenite oxometer, fO_2 decreases in this sequence from NNO+1 to NNO–2 (Ivanyuk et al., 2017, 2018a);

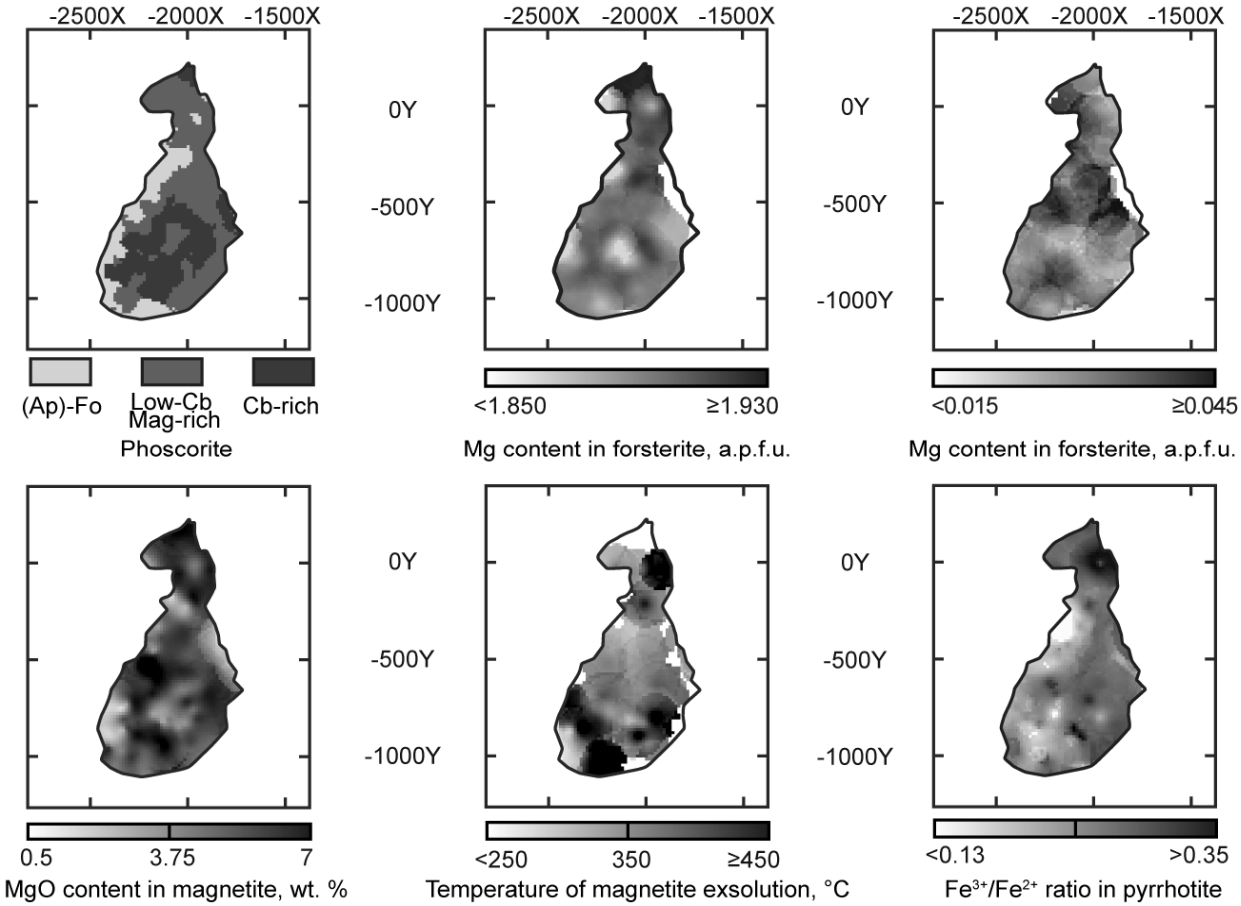

Figure. Zonation of the Kovdor phoscorite-carbonatite pipe at –110 m horizon

7. Alteration of primary rock-forming and accessory minerals by late hydrothermal F-rich solutions causes formation of numerous rare structuraly complex minerals and polytypes, in particular, hydroxynatropyrochlore, juonniite and kampelite (after Sc-Nb-rich baddeleyite), quintinite-1*M*, -3*R*, -2*H*-3*c* (after Mg-Al-rich magnetite), пирротин-6*C* and pakhomovskyite (after pyrrhotite-1-5C), the crystallization temperature of that was not exceeding 100 °C (Kalashnikov et al., 2016; Yakovenchuk et al., 2017; Zhitova et al., 2018; Ivanyuk et al., 2018a,b, 2019).

This work was supported by the Kola Science Center of RAS (0226-2019-0051) and the Russian Science Foundation (16-17-10173).

References

Ivanyuk G.Yu., Kalashnikov A.O., Pakhomovsky Ya.A., Bazai A.V., Goryainov P.M. Mikhailova J.A., Yakovenchuk V.N. Konopleva N.G. Subsolidus evolution of the magnetite-spinel-ulvöspinel solid solutions in the Kovdor phoscorite-carbonatite complex, NW Russia // Minerals. 2017. Vol. 7. P. 215.

Ivanyuk G.Yu., Kalashnikov A.O., Pakhomovsky Ya.A., Mikhailova J.A., Yakovenchuk V.N., Konopleva N.G., Sokharev V.A., Bazai A.V., Goryainov P.M. Economic minerals of the Kovdor baddeleyite-apatite-magnetite deposit, Russia: mineralogy, spatial distribution, and ore processing optimization // Ore Geology Reviews. 2016. Vol. 77. P. 279–311.

Ivanyuk G.Yu., Yakovenchuk V.N., Panikorovskii T.L., Konoplyova N.G., Pakhomovsky Ya.A., Bazai A.V., Bocharov V.N., Krivovichev S.V. Hydroxynatropyrochlore, $(Na,Ca,Ce)_2Nb_2O_6(OH)$, a

new member of the pyrochlore group from the Kovdor phoscorite-carbonatite pipe (Kola Peninsula, Russia) // Mineralogical Magazine. 2019. Vol. 83. P. 107–113

Ivanyuk, G. Y.; Pakhomovsky, Y. A.; Panikorovskii, T. L.; Mikhailova, J. A.; Kalashnikov, A. O.; Bazai, A. V.; Yakovenchuk, V. N.; Konopleva, N. G.; Goryainov, P. M. Three-D Mineralogical Mapping of the Kovdor Phoscorite-Carbonatite Complex, NW Russia: II. Sulfides // Minerals 2018a. Vol. 8. P. 292.

Ivanyuk, G.; Konopleva, N.; Yakovenchuk, V.; Pakhomovsky, Y.; Panikorovskii, T.; Kalashnikov, A.; Bocharov, V.; Bazai, A.; Mikhailova, J.; Goryainov, P. Three-D mineralogical mapping of the Kovdor phoscorite-carbonatite complex, NW Russia: III. pyrochlore supergroup minerals // Minerals, 2018b, Vol. 8. P. 277.

Kalashnikov A.O., Ivanyuk G.Yu., Mikhailova J.A., Sokharev V.A. Approach of automatic 3D geological mapping: the case of the Kovdor phoscorite-carbonatite complex, NW Russia // Scientific Reports. 2017. Vol. 7. P. 6893

Kalashnikov A.O., Yakovenchuk V.N., Pakhomovsky Ya.A., Bazai A.V., Sokharev V.A., Konopleva N.G., Mikhailova J.A., Goryainov P.M., Ivanyuk G.Yu. Scandium of the Kovdor baddeleyite–apatite–magnetite deposit (Murmansk Region, Russia): Mineralogy, spatial distribution, and potential resource // Ore Geology Reviews. 2016. Vol. 72. P. 532–537.

Mikhailova J.A., Ivanyuk G.Yu., Kalashnikov A.O., Pakhomovsky Ya.A., Bazai A.V., Panikorovskii T.L., Yakovenchuk V.N., Konopleva N.G., Goryainov P.M. Forsterite as a key indicator of phoscorite-carbonatite petrogenesis: a case of the Kovdor complex, NW Russia // Minerals. 2018. Vol. 8. P. 260–283

Mikhailova, J.A., Kalashnikov, A.O., Sokharev, V.A., Pakhomovsky, Ya.A., Konopleva, N.G., Yakovenchuk, V.N., Bazai, A.V., Goryainov, P.M., Ivanyuk, G.Yu. 3D mineralogical mapping of the Kovdor phoscorite–carbonatite complex (Russia) // Mineralium Deposita. 2016. Vol. 51. P. 131–149.

Yakovenchuk V.N., Ivanyuk G.Yu., Pakhomovsky Ya.A., Panikorovskii T.L., Britvin S.N., Krivovichev S.V., Shilovskikh V.V., Bocharov V.N. Kampelite, $Ba_3Mg_{1.5}Sc_4(PO_4)_6$ $(OH)_3 \cdot 4H_2O$, a new very complex Ba-Sc phosphate mineral from the Kovdor phoscorite-carbonatite complex (Kola Peninsula, Russia) // Mineralogy and Petrology. 2017. Vol. 112. P. 111–121.

Zhitova E.S., Krivovichev S.V., Yakovenchuk V.N., Ivanyuk G.Yu., Pakhomovsky Ya.A., Mikhailova J.A. Crystal chemistry of natural layered double hydroxides. 4. Crystal structures and evolution of structural complexity of quintinite polytypes from the Kovdor alkaline massif, Kola peninsula, Russia // Mineralogical Magazine. 2018. Vol. 82. P. 329–346.

MINERALOGY OF OGOL LAVA (CRATER HIGHLANDS, TANZANIA)

Ivashchenkova O.V.
Department of Mineralogy, St. Petersburg State University, lelia1991@yandex.ru

Several thick rift structures are known within the African continent, the formation of which occurred at different geological times. One of these structures, the East African Rift system, contains two distinct tectonic zones - the Eastern Rift that includes the Ethiopian and Kenyan Rift (also known as Gregory Rift) and the Western Rift, or the Western Branch (e.g. Belousov et. al., 1974).

The Gregory Rift extends approximately 900-1000 km, between Turkana Lake in Kenya to the lakes of Manyara and Balangida in northern Tanzania. Geological activity within the Gregory Rift began approx. 35-30 Ma within the northern part, and continues currently within the southern part (carbonatite-nephelinite-phonolitic Oldoinyo Lengai active volcano). The geological time frames of volcanism development in the area of the modern Gregory Rift is examined in various publications and many geological, geochemical and mineralogical studies of various volcanic rocks have been described (e.g. Dawson, 2008).

The Crater Highlands area is located within the northern part of the Gregory Rift. This area is formed by large volcanoes and separate lava flows, the formation of which had taken place between 4.5 and 0.8 Ma (Mollel and Swisher, 2012). The volcanoes are distinguished into two types by the chemical composition of eruptive rocks. The first type - volcanoes of mainly basaltic and trachytic composition (Ngorongoro, Lemagrut and Oldeani), and the second type – volcanoes with predominately nephelinitic rocks (Sadiman and possibly Embakai). Separate lava fields that are spatially not connected with large volcanoes are located in the South-Western part of the upland. These lavas are known as Ogol lavas, which are the subject of research.

Table 1. Major elements composition of the Ogol lava

Rock name	Ogol Lava, basalts	
Type	**I**	
Variety	a	b
	High Cr and Ni	Low Cr and Ni
Samples	A16_06	A16_29
wt.%		
SiO_2	45.16	46.53
TiO_2	3.54	3.11
Al_2O_3	8.45	11.37
Fe_2O_3	15.45	15.01
MnO	0.19	0.22
MgO	10.97	6.98
CaO	11.23	9.41
Na_2O	1.90	2.45
K_2O	1.00	2.33
P_2O_5	0.41	0.55
LOI	1.36	1.67
Total	99.66	99.63
Total Alkalis	2.90	4.78
Mg#	0.87	0.72

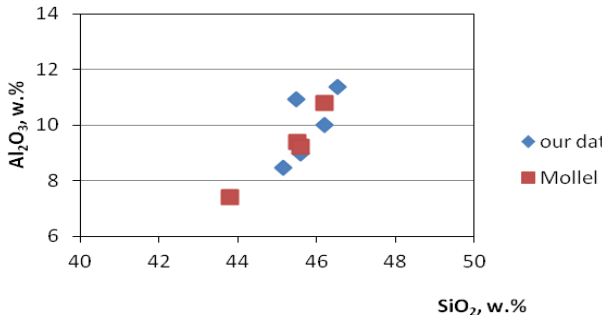

Fig. 1. Al_2O_3 versus silica, Harker diagram.

The Ogol lava flows erupted from small separate channels (craters) or cones. These channels and cones stretch in a west to easterly direction for approx. 25 km, and are 0.5 to 1.5 km in diameter and from 50 to 150 m in height (Hay, 1987). The Ogol lavas are basaltoid porphyritic rock with olivine, augite, biotite, alkali feldspar phenocrysts, as well as with plagioclase and nepheline microphenocrysts. By chemical composition the Ogol lavas are high-magnesian rocks (Mg# = 56-59) with high chromium content (514-863 ppm). In comparison to other volcanic rocks, known in the Crater Highlands, these are the most primitive (poorly differentiated) volcanic rocks.

Two mineral assemblages were observed in basalts: primary (magmatic) (forsterite, plagioclase, diopside, magnetite, apatite, amphibole, chromite) and secondary (hydrothermal) (baryte, calcite).

Among the studied specimens at the very least two basalt varieties can be distinguished: a) olivine-pyroxene basalts and b) pyroxene-olivine basalts are present as phenocrystals forsterite (66.6-89.5 wt. %, NiO = 0-0.30 wt.%) and diopside (Cr_2O_3 content to 1.1 wt.%). Apatite, chromite, magnetite, which is enriched in chromite (up to 2.4 wt.% TiO2) and pyrrhotite are present as minor minerals.

The geochemical data obtained for the samples show that, by composition, the Ogol basalts are distinguished into two types, the first is rocks with relatively high magnesia (Mg # = 0.48–0.58) and high chromium (323-542 g / t) and nickel (154-197 g / t), and the second type is basalts contents with approximately the same magnesia (Mg # = 0/48), but low chromium (57 g / t) and nickel (74 g / t) . The magnesia indicators in the Ogol lavas, as well as the concentration of chromium, are the highest compared to other lavas of volcanoes that are located in the Crater Highlands (Lemagrut, Olduani).

Harker diagrams show a continuous decrease in TiO_2, FeO, MgO, CaO and P_2O_5, and increase in Al_2O_3, Na_2O and K_2O with increasing silica content (Fig. 1).

The Ogol lava may be genetically related to nearby Lemagrut volcanism and may be distal flows that flows erupted from small separate channels (craters) or cones.

The new data acquired from the Ogol lavas basalt mineralogy will help to improve the understanding of the volcanism history of the Crater Highlands, and together with the future geochemical (including radigenic isotopes) data permits answering the question of whether the genetic relationship between the Ogol lavas and large volcanoes exist.

This research is supported by the Russian Foundation for Basic Research (grant №18-05-00835) and Alexander von Humboldt-Stiftung.

References

Dawson J.B. The Gregory Rift Valley and Neogene-Recent volcanoes of northern Tanzania Geological Society Memoirs. Vol. 33. 2008. 102 p.

Hay R.L. Geology of the Laetoli area. In Laetoli: a Pliocene Site in Northern Tanzania. Oxford: Oxford University Press. 1987. pp. 23-47

Mollel G.F. Petrochemistry and Geochronology of Ngorongoro Volcanic Highland Complex (NVHC) and its relationship to Laetoli and Olduvai Gorge, Tanzania. PhD thesis, Rutgers University, 2007. 254 p.

Mollel G.F., Swisher III C.C. The Ngorongoro Volcanic Highland its relationships to volcanic deposits at Olduvai Gorge and East Africa Rift volcanism // Journal of Human Evolution. 2012. Vol. 63. pp. 274-283.

CLINOPYROXENE IN KIMBERLITE AND AILLIKITE: IMPLICATIONS WITH RESPECT TO ITS ORIGIN AND THE KIMBERLITE–AILLIKITE RELATIONS

Kargin A.V.[1], Nosova A.A.[1], Sazonova L.V.[2], Lebedeva N.M.[1]

[1]Institute of Geology of Ore Deposits, Petrography, Mineralogy, and Geochemistry, Russian Academy of Sciences (IGEM RAS), Moscow, Russia, kargin@igem.ru

[2]Lomonosov Moscow State University, Moscow, Russia

Herein, we suggest the evolution of kimberlite magma, including megacryst formation, and mantle metasomatism during the generation of the mantle melt conduit based on our study of the compositions of the main types of clinopyroxene from the peridotitic xenoliths and megacrysts in the Grib kimberlite pipe (Arkhangelsk province, Russia). Additionally, we verified the existing relations among kimberlite and ultramafic lamprophyric magmas based on the composition of the aillikitic clinopyroxene from the Chadobets area (the Siberian Craton, Russia).

Introduction. Kimberlite (Group 1 kimberlite from South Africa) exhibits a complex composition comprising a (i) juvenile magmatic material and (ii) mantle and crustal xenoliths as well as xenocrysts. The same xenocrystic minerals could exhibit different origins, including (i) disintegrated fragments of the mantle and crust rock, (ii) antecrysts crystallised from proto and/or evolved kimberlite melts stalled in the mantle depths (such as olivine, orthopyroxene, phlogopite and ilmenite), and (iii) megacrysts (commonly garnet, clinopyroxene, phlogopite, olivine and ilmenite; less commonly, orthopyroxene) that may be genetically related to the protokimberlite melt during its reaction with the lithospheric mantle.

In contrast to other alkaline ultramafic rocks, majority of the kimberlites do not contain phenocrystic clinopyroxene (e.g. Mitchell, 1995) in the groundmass. However, clinopyroxene may be the main mineral in peridotite xenoliths, and clinopyroxene xenocrysts are common in kimberlites. The garnet peridotite xenoliths generally display evidence of mantle metasomatism based on fluids and melts having variable compositions (O'Reilly, Griffin, 2013). D.G. Pearson suggested the metasomatic addition of clinopyroxene to several cratonic peridotites (Pearson et al., 2002). Petrological investigations of the mantle xenoliths and megacrysts from kimberlite have denoted that the clinopyroxene composition is useful for investigating the origin of peridotite xenoliths and of the stages and the pressure and temperature (P–T) conditions of mantle metasomatism. Clinopyroxene and phlogopite play a key role during the progressive metasomatism of garnet peridotite (harzburgite) to garnet phlogopite-peridotite and phlogopite-peridotite (garnet-free lherzolite) to phlogopite wehrlite (e.g. O'Reilly, Griffin, 2013; Kargin et al., 2017b, 2019).

Based on the analysis of published studies on kimberlite and mantle xenoliths and xenocrysts, we distinguished between two opposite approaches of petrologic data interpretation. The first approach indicates that a significant proportion of the studied xenoliths, xenocrysts and megacrysts represent the lithospheric mantle section that was formed before the generation of kimberlite magma. Using this approach, multiple metasomatic events affected the mantle lithosphere and that the kimberlite magma transports xenoliths and their disintegrated fragments from the mantle to the surface (for instance, this approach has been used for the Grib kimberlite xenoliths and garnet xenocrysts (Shchukina et al., 2015)). The second approach suggests that the generation and ascent of the kimberlite magma is a multistage process, with the protokimberlite melts being stalled in the mantle (Giuliani et al., 2016). Using this approach, successive pulses of ascending kimberlite magma are observed to progressively metasomatise the conduit along which the later kimberlite pulses ascend, progressively producing a decreasing interaction with the surrounding mantle rock (Giuliani et al., 2016). Further, the ascent of kimberlite magma through the lithospheric mantle involves the process of percolative fractional crystallisation (e.g. Harte, 1983), which ensures the crystallisation of the high-Cr megacryst suite and the introduction of lherzolitic clinopyroxene and garnet into the surrounding mantle (e.g. Bussweiler et al., 2018). In this case, several xenoliths sampled from the kimberlite are obtained from the kimberlite magma's wall rock and, hence, may not represent the entire lithospheric mantle (Bussweiler et al., 2018). The same mechanism has been proposed for peridotite xenoliths and clinopyroxene megacrysts in the Grib kimberlite (Kargin et al., 2016, 2017a, 2017b).

The carbonate-rich ultramafic lamprophyres (UMLs), including aillikites and damtjernites, are closely related to the kimberlites in terms of the texture as well as the mineral and chemical compositions. However, the origins of all these UMLs (lamprophyres and kimberlites) are still debated. Further, the central points of contention are the genetic relations between aillikites and kimberlites, including the consideration of the aillikites as protokimberlite melts (see review in Nosova et al., 2018).

Results. Clinopyroxene obtained from the Grib kimberlite. The geology and petrography of the Grib kimberlite (the Arkhangelsk province) have been previously described (Larionova et al., 2016 and references therein). We have distinguished between two main groups of clinopyroxene in the Grib kimberlite and its included xenoliths (Table 1). Those in *Group 1* were observed to form before host-kimberlite magma capturing, whereas those in *Group 2* were observed to form during transportation by the host kimberlite melt.

Group 1 minerals can be separated into the following three main subgroups:

(1a) High-Mg# and low-Ti clinopyroxene with extensively variable Cr_2O_3 content. In the garnet peridotite xenoliths, high-Mg# and low-Ti clinopyroxene commonly occurs as grains with an elongated curved shape and sharp contacts with olivine, which exhibits a non-equilibrium texture. At times, this clinopyroxene has been observed to have formed relict central zones in zoned grains. According to prior peridotite xenolith study, this clinopyroxene could be in geochemical equilibrium with lherzolitic garnet (Kargin et al., 2016). Further, this clinopyroxene denotes a relatively high level of geochemical heterogeneity based on the wide variation in the rare earth element (REE) concentrations, indicative of the REE fractionation (Fig. 1). The increase in the La/Sm ratio suggests the generation of this clinopyroxene during the percolation of the kimberlite melt through the lithosphere (Kargin et al., 2016).

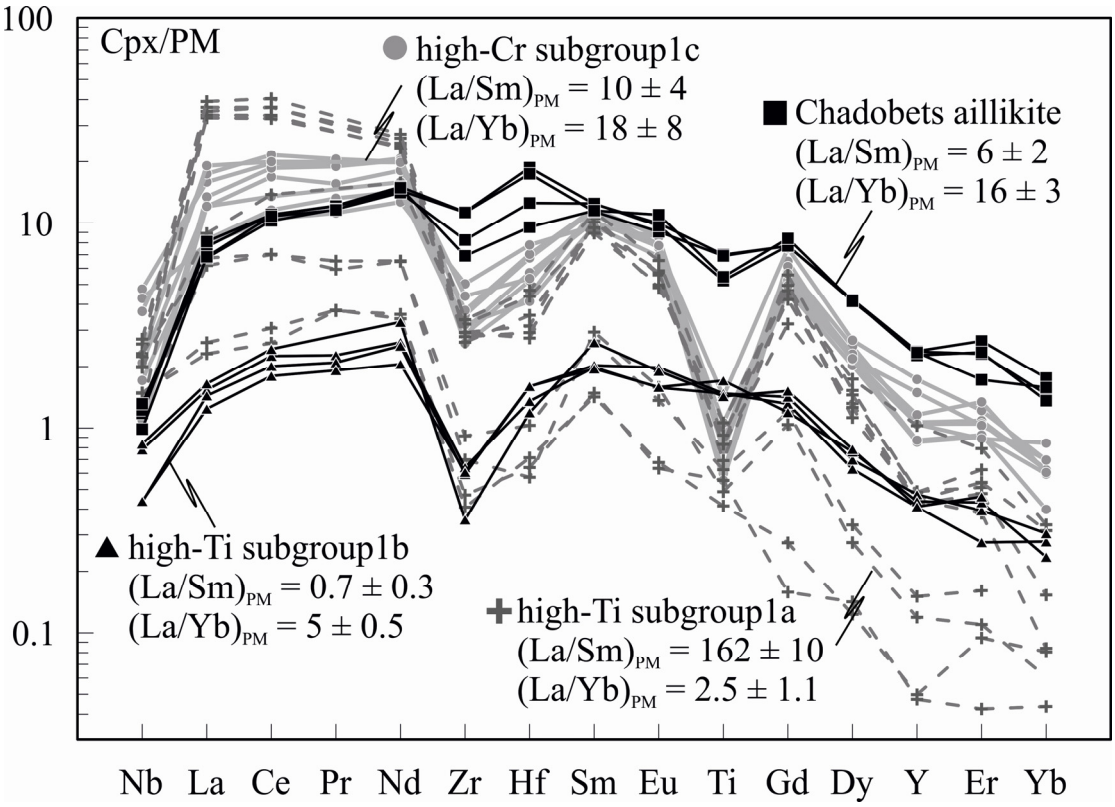

Figure 1. PM-normalized HFSE patterns (McDonough, Sun, 1995) studied clinopyroxene.

(1b) Low-Mg#, high-Ti and low-Cr clinopyroxene occurring in association with high-Ti garnet having a composition similar to that of the megacryst in sheared peridotite xenoliths whereas clinopyroxene replacing orthopyroxene and olivine or as inclusions in low-Cr and high-Ti garnet megacrysts. Clinopyroxene exhibits low levels of high-field-strength elements as well as a low degree

of REE fractionation (Fig. 1). The non-equilibrium textures of the sheared peridotite (Kargin et al., 2017b) indicate that this clinopyroxene was formed shortly before being captured by the host kimberlite melt.

(1c) High-Cr clinopyroxene with intermediate Mg# and Ti contents between the *subgroups 1a* and *1b*. This clinopyroxene has a composition close to that of the worldwide high-Cr megacrysts (Kargin et al., 2017a) even though it differs in terms of petrography and in occurrence or association. Clinopyroxene has been found as (i) grains in the garnet peridotite xenoliths, (ii) rims on high-Mg# and low-Ti clinopyroxene (*subgroup 1a*) in the peridotite xenoliths, (iii) grains associated with large veinlets or dissolution channels in olivines within the garnet peridotite xenoliths, (iv) grains associated with low-Ti and low-Cr phlogopite within the clinopyroxene phlogopite xenoliths and (v) large (>1-cm) discrete high-Cr megacrysts in the kimberlitic groundmass. The clinopyroxenes are enriched in light REEs exhibiting a high level of REE fractionation and strong Ti negative anomalies (Fig. 1). This may indicates their possible equilibrium with the kimberlite melts (Kargin et al., 2017a).

Group 2 clinopyroxenes exhibit petrographic and compositional characteristics, suggesting a host-kimberlite-related origin. They commonly form sharply bounded late rims on *Group 1* clinopyroxenes, exhibit a spongy texture and are associated with the late kimberlite-related veinlets in xenoliths. When compared with the central zone compositions, these clinopyroxenes commonly exhibit higher Ti concentrations, lower Mg# values and comparable Cr contents, although they may also have high-Na compositions.

Clinopyroxene from aillikite (Chadobets area, Siberia, Russia). We have studied clinopyroxene and phlogopite in aillikites from the Chadobets area in the southwestern part of the Siberian Craton, Russia, and reviewed prior published detailed geological and petrographic data of these rocks (Nosova et al., 2018). The aillikitic rocks usually contain phenocrysts of clinopyroxene and phlogopite (e.g. Mitchell, 1995). The composition of these minerals primarily differ from that of the kimberlitic ones by the higher concentrations of TiO_2 and FeO as well as their lack of Cr_2O_3 (Table 1). Further, the REE patterns of the aillikitic clinopyroxene indicate a low degree of REE fractionation that is comparable to that of the *Group 2* clinopyroxene from the Grib kimberlite but exhibits higher REE abundances.

Discussion. In most of the cases, the petrographic analysis of *Group 1* clinopyroxene indicates non-equilibrium with the peridotite minerals, and the texture is also consistent with that obtained by the metasomatic addition of clinopyroxene to several cratonic peridotites (Pearson et al., 2002). This indicates that the *Group 1* clinopyroxene could have been formed shortly before being captured by the host kimberlite melt during the generation of the kimberlite magma mantle conduit (Giuliani et al., 2016; Bussweiler et al., 2018). Detailed geochemical investigations of the clinopyroxene composition suggest that (i) clinopyroxene and phlogopite belonging to the *subgroup 1c* were in geochemical equilibrium with the kimberlitic-like magmas (Kargin et al., 2017a, 2019), (ii) clinopyroxene and associated garnet belonging to the *subgroup 1a* may have been formed during the percolation of kimberlitic-like melts through the lithospheric mantle (Kargin et al., 2016) and (iii) the *subgroup 1b* was in geochemical equilibrium with the carbonate-bearing alkaline ultramafic melt (Kargin et al., 2017b). Thus, on the one hand, these events could be explained by the different magmatic episodes within the Arkhangelsk province (Shchukina et al., 2015). On the other hand, the formation of *Group 1* minerals may reflect the evolution of the stalled protokimberlite during the generation of the kimberlite mantle conduit, as has been proposed for the Lac de Gras kimberlites (Bussweiler et al., 2018).

The *Group 1* clinopyroxenes denote extensive variation in the Cr_2O_3 and TiO_2 concentrations as well as the Mg# values in different subgroups (Table 1). Simultaneously, they exhibit common evolutionary trends on binary diagrams, which could indicate their generation during the geochemical evolution of a single system. The variation of the Cr_2O_3 concentration in the clinopyroxene of *subgroups 1a* and *1c* could be associated with the interaction of parental or equilibrium melt with the surrounding lithospheric mantle during its percolation through the lithospheric mantle (e.g. Harte, 1983; Kargin et al., 2016; Bussweiler et al., 2018). This process has been inferred for clinopyroxene belonging to the *subgroup 1c* on the basis of the dissolution channels in olivines within the garnet peridotite xenoliths that could have resulted from the percolation of the kimberlite melts through the

lithospheric peridotite. In addition, the percolation of the kimberlite melt may have been accompanied by the fractionation of the Fe- and Ti-bearing phases (garnet and ilmenite, which are minerals associated with clinopyroxene belonging to the *subgroup 1b*) as megacrysts. Our P–T estimates for the clinopyroxenes of different subgroups denote that the high-Ti clinopyroxene belonging to the *subgroup 1b* was formed under pressures ranging from 7–8 (similar to that at the base of the lithospheric mantle) to 5 GPa, whereas the clinopyroxenes belonging to the *subgroups 1a* and *1c* were formed under pressures of 3–5 GPa.

Table 1. The composition of clinopyroxene from various groups.

Clinopyroxene type	**TiO_2 wt %**	**Cr_2O_3 wt %**	**Mg#**	**P GPa***	**T ^oC***
kimberlite xenoliths and xenocrysts					
Group 1a - high-Mg# peridotite clinopyroxene	0.19 ± 0.13 n=48	2.32 ± 0.83 n=48	0.94 ± 0.01 n=48	3.0 ± 0.5 n=34	730 ± 90 n=34
Group 1b - high-Ti peridotite clinopyroxene	0.34 ± 0.02 n=65	0.87 ± 0.16 n=65	0.89 ± 0.01 n=65	7.5 ± 1.4 n=13	1170 ± 80 n=13
Group 1b - high-Ti inclusion in garnet megacrysts	0.32 ± 0.03 n=9	1.34 ± 0.73 n=9	0.91 ± 0.01 n=9	5.0 ± 0.7 n=9	1080 ± 80 n=9
Group 1c - High-Cr megacrysts	0.19 ± 0.05 n=147	2.25 ± 0.82 n=147	0.92 ± 0.01 n=147	4.1 ± 0.7 n=74	860 ± 50 n=74
Group 2 – secondary clinopyroxene	0.45 ± 0.21 n=26	1.68 ± 0.63 n=26	0.91 ± 0.02 n=26	4.2 ± 8 n=0.6	790 ± 100 n=6
Group 2 - secondary high-Na clinopyroxene	0.23 ± 0.04 n=27	3.31 ± 0.49 n=27	0.91 ± 0.01 n=27	3.6 ± 0.1 n=3	810 ± 15 n=3
aillikite					
Chadobets groundmass clinopyroxene	1.86 ± 1.18 n=80	0.09 ± 0.16 n=80	0.82 ± 0.01 n=21		

* P-T conditions were calculated using the enstatite-in-clinopyroxene thermometer and Cr-in-Cpx barometer by (Nimis, Taylor, 2000).

According to our proposed model, megacrysts were formed along the channel walls during the intrusion of the kimberlite magma from its interaction with the mantle rock and resulted in large crystal sizes at high melt/rock ratios (Bussweiler et al., 2018). The surrounding mantle at some distance from the kimberlite intrusion, where the melt flow was percolative and the melt/rock ratios were low, experienced metasomatism with the generation of newly formed clinopyroxene, phlogopite and, probably, garnet. The numerous kimberlite infiltration events provided multiple generations of the *Group 1* minerals.

Thus, the minerals belonging to the *subgroup 1b* may have been in equilibrium with the carbonate-bearing alkaline ultramafic melt enriched in Fe and Ti (Kargin et al., 2017b). This melt may have been aillikitic in composition because such melts are enriched in Fe, Ti and carbonate. The aillikitic clinopyroxenes indicate trace-element patterns close to those exhibited by the *subgroup 1b* but exhibit higher levels of REEs, TiO_2 and FeO even though they lack Cr_2O_3. In binary diagrams, aillikitic clinopyroxene is observed to extend the compositional trends from the high-Mg# clinopyroxene belonging to the *subgroup 1a* to the high-Ti clinopyroxene belonging to the *subgroup 1b*. However, aillikitic clinopyroxene was directly crystallised from the alkaline ultramafic melt, whereas clinopyroxene belonging to the *subgroup 1b* was a metasomatic product of the interaction of alkaline ultramafic melt with the surrounding lithospheric mantle. Further, we cannot rule out the possibility that the percolation of the aillikitic melt through the lithospheric mantle and the fractionation of the high-Ti low-Cr megacrysts result in decreasing Fe and Ti contents and increasing Mg and Cr contents in the melt as well as the further evolution of the aillikite to kimberlite magmas.

The study of clinopyroxene from the Grib kimberlite (Arkhangelsk province) was by supported the Russian Science Foundation (project no. 19-17-00024). The study of clinopyroxene from the

Chadobec aillikite (Yakutian province) was supported by the Russian Foundation for Basic Research, Project Nos. 18-05-00644 A.

References

Giuliani A., Phillips D., Kamenetsky V.S., et al. Constraints on kimberlite ascent mechanisms revealed by phlogopite compositions in kimberlites and mantle xenoliths // Lithos, 2016, vol. 240–243. pp. 189–201.

Bussweiler Y., Pearson D.G., Stachel T., et al. Cr-rich megacrysts of clinopyroxene and garnet from Lac de Gras kimberlites, Slave Craton, Canada – implications for the origin of clinopyroxene and garnet in cratonic lherzolites // Mineral. Petrol., 2018, vol. 112, no. S2. pp. 583–596.

Harte B. Mantle peridotites and processes - the kimberlite sample // Continental basalt and mantle xenoliths red. C. Hawkesworth, M. Norry. Nantwich: 1983. pp. 46–91.

Kargin A. V., Sazonova L. V., Nosova A.A., et al. Phlogopite in mantle xenoliths and kimberlite from the Grib pipe, Arkhangelsk province, Russia: Evidence for multi-stage mantle metasomatism and origin of phlogopite in kimberlite // Geosci. Front., 2019, in press DOI 10.1016/j.gsf.2018.12.006.

Kargin A.V., Sazonova L.V., Nosova A.A., et al. Composition of garnet and clinopyroxene in peridotite xenoliths from the Grib kimberlite pipe, Arkhangelsk diamond province, Russia: Evidence for mantle metasomatism associated with kimberlite melts // Lithos, 2016, vol. 262. pp. 442–455.

Kargin A.V., Sazonova L.V., Nosova A.A., et al. Cr-rich clinopyroxene megacrysts from the Grib kimberlite, Arkhangelsk province, Russia: Relation to clinopyroxene–phlogopite xenoliths and evidence for mantle metasomatism by kimberlite melts // Lithos, 2017a, vol. 292–293. pp. 34–48.

Kargin A.V., Sazonova L.V., Nosova A.A., et al. Sheared peridotite xenolith from the V. Grib kimberlite pipe, Arkhangelsk Diamond Province, Russia: Texture, composition, and origin // Geosci. Front., 2017b, vol. 8, no. 4. pp. 653–669.

Larionova Y.O., Sazonova L.V., Lebedeva N.M., et al. Kimberlite Age in the Arkhangelsk Province, Russia: Isotopic Geochronologic Rb-Sr and 40Ar/39Ar and Mineralogical Data on Phlogopite // Petrology, 2016, vol. 24, no. 6. pp. 562–593.

Mitchell R.H. Kimberlites, Orangeites, and Related Rocks // Boston, MA: Springer US, 1995. 410 p.

Nimis P., Taylor W.R. Single clinopyroxene thermobarometry for garnet peridotites. Part I. Calibration and testing of a Cr-in-Cpx barometer and an enstatite-in-Cpx thermometer // Contrib. to Mineral. Petrol., 2000, vol. 139, no. 5. pp. 541–554.

Nosova A.A., Sazonova L.V., Kargin A.V., et al. Olivine in ultramafic lamprophyres: chemistry, crystallisation, and melt sources of Siberian Pre- and post-trap aillikites // Contrib. to Mineral. Petrol., 2018, vol. 173, no. 7. pp. 55.

O'Reilly S.Y., Griffin W.L. Mantle Metasomatism // Metasomatism and the Chemical Transformation of Rock SE - 8 red. D.E. Harlov, A. Håkon. : Springer Berlin Heidelberg, 2013. pp. 471–533.

Pearson D.G., Irvine G.J., Carlson R.W., et al. The development of lithospheric keels beneath the earliest continents: time constraints using PGE and Re-Os isotope systematics // Geol. Soc. London, Spec. Publ., 2002, vol. 199, no. 1. pp. 65–90.

Shchukina E.V., Agashev A.M., Kostrovitskii S.I., et al. Metasomatic processes in the lithospheric mantle beneath the V. Grib kimberlite pipe (Arkhangelsk diamondiferous province, Russia) // Russ. Geol. Geophys., 2015, vol. 56. pp. 1663–1678.

FIND OF A KAOLINITE LINEAR ZONE AT MT. VUDYAVCHORR (KHIBINY)

Karpov S.M., Lyalina L.M., Zhirov D.V., Semenov V.L., Telezhkin A.A.
Geological Institute of the Kola Science Centre RAS, Apatity, Russia, zhirov@geoksc.apatity.ru

The Fennoscandian Shield hosts a number of area and linear kaolinite weathering rinds with an estimated age of the upper Triassic to the beginning of the lower Jurassic period (Yevzerov, Kol'ka, Nazarenko, 1993; Yevzerov, 2014). Redeposited kaolinites accumulated at slopes of the Fennoscandian Shield (e.g. Southern Sweden) in the lower to middle Jurassic (Afanasyev, 1980b). These kaolinites were produced by erosion of these weathering rinds by water in inner parts of the areas, which the central part of the Kola region referred to. Nowadays, the root zone of these kaolinite rinds is confined to a sublatitudinal belt stretching and expanding from the Keivy mountains to Lapland in Finland through the Middle Ridge (Yevzerov, 2014). No relics of such kaolinite weathering rinds had been formerly found in the Devonian Khibiny and Lovozero alkaline plutons, which suggested a deep-seated bedding of these intrusions in the upper Triassic-lower Jurassic.

In July, 2018, a work group of the Geological Institute KSC RAS (Semenov V.L., Karpov S.M. and Ushko A.V.) discovered a linear zone of kaolinites with a thickness of up to 15-20 m and a length of at least 1 km at the southern slope of Mt. Vudyavchorr (Skalistoye Gorge) in the Khibiny Massif. This linear zone is composed of intensively ferruginated and silicified vesicular rocks of the kaolinite composition mainly, contrasting with a background of host trachitoid khibinites (nepheline syenites). Small relics of the Mesozoic kaolinite weathering rind of the area (up to 10 m thick) and linear types had been formerly registered in metamorphic rocks of the Imandra-Varzuga complex and in the northern foothills of the Lovozero Tundra, as well as along fenites to the south of the Khibiny and Kovdor Massifs (Afanasyev,1980a, b). The genesis of area and linear kaolinite weathering rinds is associated with an evolution of peneplanation in a humid tropical climate of the lower Mesozoic (upper Triassic) (Afanasyev, 1980a, b; Yevzerov, 2014). The origin of clayey gruss (hydromica) weathering rinds of the linear type, which are widespread both in the Khibiny and in the Lovozero Massifs, is explained by the Miocene-Pliocene planation in a humid climate (Afanasyev, 1980a, b; Dorfman, 1962; Dudkin, 2002). These weathering rinds have been repeatedly studied (Dorfman, 1958, 1962, Mineralogy..., 1978, Kozyreva, 1983 et al.), but kaolinite has been registered there as a secondary mineral only. Silicification has been defined in tectonic zones near the Svintsovy Stream and Mt. Yuksporr. It has been explained by the impact of adjacent xenoliths of corneous rocks (Dorfman, 1962). The discovered kaolinite zone is the first find of the Mesozoic kaolinite weathering rind of the linear type in the largest Khibiny and Lovozero alkaline plutons. At the same time, there are linear zones of sungulite weathering rinds that are similar to kaolinite rinds in their conditions for genesis in the Kovdor, Vuoriyarvi and Afrikanda Massifs (Yevzerov, 2014).

The linear weathering rind at the southern slope of Mt. Vudyavchorr has an azimuth strike of 65-75º, dipping north-westwards under angles of 50-70º (Fig. 1). There is a zoning across and, presumably, along the strike. An up to 3-4 m thick zone of brecciation, silicification and vesicular rocks occurs nearby the footwall contact (see No. 4 in Fig. 1). Here, the hypergenesis was preceeded by the tectonic alteration of primary rocks, which further transformation was accompanied by intensive leaching and silicification. The rock has totally transformed with no preserved relics of primary minerals in the silicification area and adjacent territories (towards the footfal contact). Kaolinite develops towards the hanging wall, preserving the initial texture of the rocks (see No. 2 in Fig. 1). The share of kaolinite subgroup minerals, including crystalline dickite and nacrite, is about 60% in average. The intensity of kaolinitization drops steeply towards the footwall, as the rocks gently convert to unaltered khibinites. Noteworthy, the linear structure had only minor tectonic changes. Original textures were preserved after kaolinitazion, except for a relatively narrow cataclase and brecciation zone (ca. 1/3 of the total thickness). The kaolinite zone is traced for ca. 1 km at the slope of Mt. Vudyavchorr. Its flank is likely to appear in range of the strike in rischorrites of the Gorodskaya Shchel' Gorge at the slope of Mt. Aykuayvenchorr (~3.5 km to the east – north-east), where secondary alterations of rocks are observed. Results of the structural research (Zhirov et al., 2016) suggest that the block with the kaolinite zone displaced along the fault for 70-100m down, while the slope of Mt.

Aykuayvenchorr with constructions of the Kirovsk town slipped along the right-hand fault for 100-150m (see lines 1 and 2 in Fig. 1A).

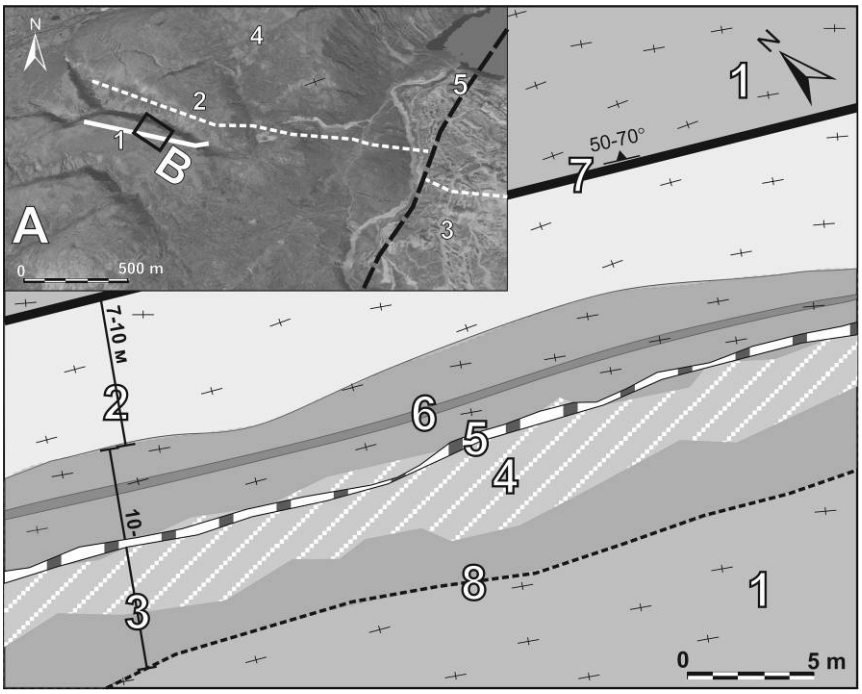

Fig. 1. Geological scheme of the linear kaolinite weathering rind at the southern slope of Mt. Vudyavchorr. Section A – fragment of an airial photograph with the locattion of the zone: 1 – traced boundaries and contour of the geological plan, 2 – suggested boundaries, 3 – constructions of the Kirovsk town, 4 – southern slope of Mt. Vudyavchorr, 5 – suggested radial fault displacing the kaolinite zone. Section B – geological plan: 1 – unaltered coarse-grained trachidoid khibinites (nepheline syenites), 2 – zone of "bleached" kaolinites; 3 – zone of red-bed kaolinites, 4 – zone of intensive leaching and silicification: quartz, hematite, goethite, kaolinite, rutile (Leucoxene pseudomorps), goyazite, fluorite, bastnaesite-(Ce), phosphates, etc., 5 – zone of altered, presumably, secondary microclines with hematite and goethite, 6 – rutile-rich zone of grey (to black) kaolinites: rutile, dickite, nacrite, hematite, goethite, zircon, etc., 7 – tectonized contact of the hanging wall of host khibinites, 8 – suggested boundary of kaolinitization area (footwall of host khibinites).

Table 1. Mineral composition of the linear kaolinite weathering rind.

Class	Mineral species
Silicates and alumosilicates	**Kaolinite, dickite, nacrite,** montmorillonite, nontronite, zeolite gr., zircon, stilpnomelane
Oxides, hydroxides and oxyhydrides	**Quartz**, **hematite**, ilmenite, anathase, **rutile**, manganosite, tantite, **goethite**, kleberite
Halogenides	Fluorite
Phosphates	Goyazite, apatite gr.
Carbonates	Bastnaesite-(Ce)
Not diagnosed	Oxides and hydroxides of manganese, Ce-Mn-Pb-phase, Ce-Mn-Sr-phase

Note. The most common mineral species are marked in bold.

The conducted research has revealed the diversity of mineral species in weathering rind and limelighted specific features of its geochemistry. According to the obtained data, the rocks contain minerals of different classes (Table 1). The provisional analysis has indicated some of the mineral species to be rare (kleberite, manganosite) and defined in rocks of the Kola Peninsula for the first time. A number of minerals (quartz, rutile, zircon) are suggested to have a polygenerative origin. We are

certainly at the very beginning of studying this peculiar geological object. Therefore, the list of mineral species is far from being complete. The metallogenic/geochemical specialization of the area is characterized by increased contents of Ti, Zr, Nb, Y, Ce and Mn as compared to original rocks.

Not only mineralogy, but also the genesis and age are relevant to the study of the kaolinite zone. At the current stage of the research, the priority concept suggests this zone to be relics of a thick lower Mesozoic kaolinite weathering rind, which is spatially confined to a pre-Mesozoic fault in an alkaline pluton. However, a low-temperature hydrothermal or heterogenic origin of the zone is also possible (spreading of the rind along previously hydrothermally altered rocks).

Mineralogical studies of a zircon sampling from kaolinites have been provided before isotope dating. It allowed us to define their morphological types and characterize features of their internal structure.

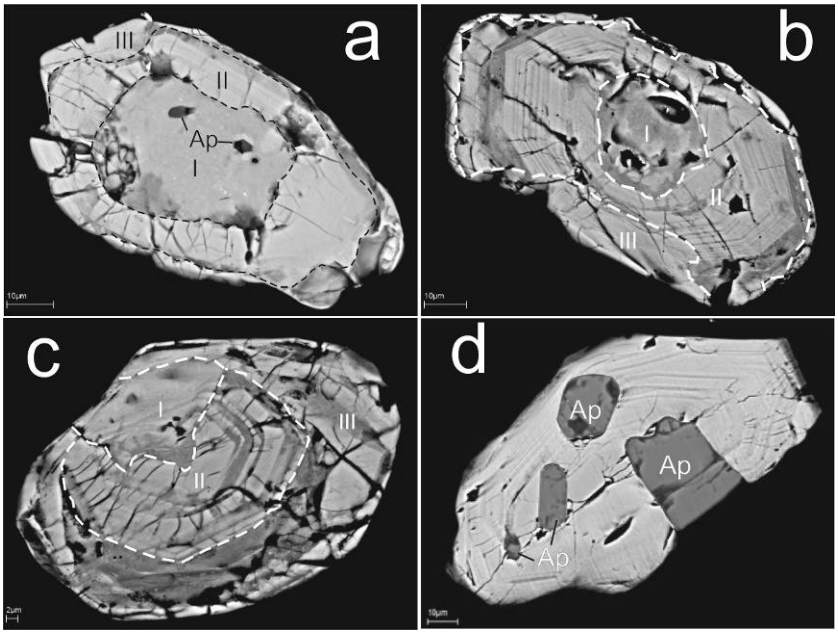

Fig. 2. Internal textures of the 1 morphological type of zircon. SEM, BSE images. I – core, II – mantle, III – rim zones in zircon crystals. Ap – inclusions of apatite group minerals.

Type 1 is represented by hypidiomorphic and idiomorphic short-prismatic and prismatic crystals, lengthening up to 0.16 mm, Ky≈2. Zircon is transparent, colorless or slighly yellowish, brownish. The lustre is glossy and rarely diamond. The crystals differ in their internal structure. The most common are the crystals with an intraphase heterogeneity of two orders (type 1-1) and one order (type 1-2). The crystals of type 1-1 have distinct inner (I – «core»), intermediate (II – «mantle») and outer (III – «rim») zones that can be referred to the first-order heterogeneity (Fig. 2 a-c). The inner zone has only a phase heterogeneity, which is represented by inclusions of the apatite group and, presumably, potassic feldspar (Fig. 2a). A twisted boundary between the inner and intermediate zones indicates dissolution of zircon, which preceeded the growth of zone II («mantle»). The intermediate zone can overgow in a markedly assymmetric way (Fig. 2c). The intermediate zone has a fine-rhythmic zoning (intraphase heterogeneity of the second order) with idiomorphic boundaries of the zones (Fig. 2) and altered zircon along some zones. No inclusions are detected. In the intermediate zone, zircon is commonly cut by feather joints going from the boundary with the «core» (Fig. 2a, c). The presence of such a jointing is explained by processes of matamictization of zircon and an increased volume of the inner zone matter and respective fracturing of the outer zone (Zircon. Reviews…, 2003). The outer zone («rim») occurs not everywhere. It has a strongly varying thickness and an uneven, bay-shaped in places, boundary with the intermediate zone. In some areas, the upper zone «cuts» the picture of a rhythmic zoning of the second order in the intermediate zone. Jointly with a bay-shaped pattern of the boundary, it indicates the dissolution of zircon before the growth of the outer zone. The outer zone is dissected by vari-oriented rough cracks (some of them are feather cracks). Cracks and defects emphasize the

boundary between the intermediate and outer zones. The rhythmic-zonal intraphase heterogeneity of the second order is expressed in crystals of the type 1-2 (Fig. 2d). The boundaries of the zones are straight and idiomorphic; the thickness varies. The phase heterogeneity is represented by inclusions of the apatite (Fig. 2d) and mica groups. Intensive alterations of zircon are expressed along certain zones. Crystals with no distinct or a weak intraphase heterogeneity are the least-spread in the first morphological type (type 1-3).

Type 2 is far more rare and occurs as prismatic to elongated prismatic crystals lengthening up to 0.22 mm, Ky ≈ 2.5-3. Zircon is transparent, colorless or brownish with a glossy to greasy lustre. Structurally, there are crystals with an intraphase heterogeneity of two orders (similar to type 1-1) and crystals with no distinct intraphase heterogeneity («homogenous», similar to type 1-3).

Along with faceted individuals, the rock contains a lot of zircons in the form of xenomorph segregations (aggregates) (**type 3**) in quartz. In some areas, angular fragments of zircon are cemented by quartz. Thus, crystals of zircon of a prismatic habitus only, which is typical of zircon from acid rocks, have been detected in the kaolinite weathering rind on khibinites. The internal structure suggests at least three stages of the mineral crystallization. Xenomorphic segregations of quartz-cemented zircon can indicate manifistations of the inter-mineralization tectonics (Grigoriev, 1961).

Investigations of the object are carried out in the framework of the planned scientific research contracts NoNo. 0226-2019-0051 (mineralogy) and 0226-2019-0053 (metallogeny).

References

Afanasyev A.P. Formation patterns of weathering rinds and associated minerals at the Phanerozoic stage of the Baltic Shield evolution. / Autoabstract of Dr. Sci. (Geol.-mineral.) Thesis. - M.: IGEM USSR AS, 1980a. 59 p.

Afanasyev A.P. Formation history of weathering rinds and hypergenic minerals on the Kola Peninsula in Meso-Cenozoic. // In book: Geology and minerals of Meso-Cenozoic formations of the Kola Peninsula. - Apatity: KB USSR AS, 1980b. p. 5-36.

Grigoriev D.P. Ontogeny of minerals. 1961. Publ. by Lvov Univ. 284 p.

Dorfman M.D. ГеохимичGeochemical features of weathering processes in nepheline syenites of the Khibiny. - Geochemistry, 1958, No. 5, P. 424- 434.

Dorfman M.D. Mineralogy of pegmatites and weathering zones in ijolite-urtites of Mt. Yukspor of the Khibiny Massif. - M.-L., Publ. by USSR AS, 1962. P. 168.

Dudkin O.B. Phanerozoic weathering rinds in alkaline massifs of the Kola region. // Murmansky Vestnik, Volume 5, N 1, 2002. P. 3-8.

Yevzerov V.Ya. Minerageny of a loose cover in the north-eastern part of the Baltic Shield. Murmansk: MSTU, 2014. 255 p.

Yevzerov V.Ya., Kol'ka V.V., Nazarenko V.O. New finds of kaoline on the Kola Peninsula and an estimated age of kaoline deposits in the Fennoscandian Shield // A complex estimation of deposits of non-metallic mineral raw materials. – Saint Petersburg, 1993. P. 129-132.

Zhirov D.V., Sim L.A., Marinin A.V. Recostructed paleo-stress conditions in the southern part of the Khibiny pluton (eastern Fennoscandian Shield) / Proceedings of the All-Russian Scientific Conference «Topical issues of the dynamic geology in the study of platform areas» Moscow, Geological Faculty of M.V. Lomonosov's MSU on 24-26 May, 2016. - M: "Pero" Publ. House, 2016. P. 39-44.

Kozyreva L.V. On joint areas of weathering on the territory of the Khibiny Massif. // In book.: Weathering rinds and hypergenic minerals of the eastern Baltic Shield. - Apatity: KB USSR AS, 1983. P. 80-84.

Mineralogy of the Khibiny Massif, V. 1. Ed. Chukhrov F.V. Authors: Kostyleva-Labuntsova E.E., Borutsky B.E., Sokolova M.N., Shlyukova Z.V., Dorfman M.D., Dudkin O.B., Kozyreva L.V., Ikorsky S.V. - M.: "Nauka", 1978. 230 p.

Zircon. Reviews in Mineralogy & Geochemistry. 2003. Vol. 53. J.M. Hanchar and P.W.O. Hoskin, eds.

NEW DATA ON THE GEOLOGICAL STRUCTURE OF KALYUMNOYE (RUSSIA, TRANSBAIKALIA, SYNNYR RIDGE) SYNNYRITE DEPOSIT AND COMPLEXITY OF ITS ALKALI ROCK DIAGNOSTICS

Kayukov A.E.[1,2], Shatova N.V.[2]

[1]LLC"BAYKAL NEDRA GEO", Nizhneangarsk, Buryatia, ak@bngeo.com

[2]Saint-Petersburg State University, Saint-Petersburg, Russia, narlin.ros@mail.ru

The unique synnyrites (ultrapotassic kalsilite syenites) are viewed as a possible source of raw materials for potassic chlorine-free fertilizers and alumina. The largest resources of these ores are found within Synnyr alkaline intrusion, the place where from the end of 70-s to mid 80-s prospect evaluation survey was held allowing to outline the world's largest possible synnyrite deposit – subsurface site Kalyumnoye.

Since the beginning of 2018 LLC "Baykal Nedra Geo" has been carrying out geological prospecting work on the subsurface site Kalyumnoye. Following the results of the first surveying season a vast mass of factual material and geological information was obtained by means of various prospecting exploration methods which allowed to drastically change the view of the geological structure of this object. At that working stage the team of LLC "Baykal Nedra Geo" has either confirmed and specified the predecessors' data or falsified them. Some geological findings are presented for the first time ever.

The rocks of stratified intrusive series (including synnyrites) within the area have different ribbon-like modes of occurrence varying from a rather flat (10-20 degrees) to a considerably steep (50-70 degrees) ones, but with a regular general north-west dip. This is to a large extent inconsistent with the predecessors' understanding of the steep, almost subvertical mode of synnyrite occurrence (Zhidkov, Ushakov 1987).

Multiple fault zones of different order and orientation, having led to the occurrence of sometime immensely thick disintegrated rock areas, are also observed on the area. The faultings of the second and third order appear more intensively than was suspected earlier. Fault system and strongly marked neotectonic depositional series in two directions can be noticed on the area. And various faultings altogether form separate large-sized blocks.

Gradual, multiple stage autometasomatism of intrusive rock reconstitution proveniances as well as their intensity are directly confined to the thickest fault zones, which causes the changes of orebody limits. Note that the term autometasomatism needs closer and wider definition valid for the given geological setting.

In the north part of the area under study a minimal power lamprophyric dyke-like bodies evolution field (first dozens cm) has been uncovered, although locally the total number of these rocks up to 10-20% of the whole amount of alkali complexes can be observed. According to the try-outs, which need to be specified, the age of lamprophyres is estimated as Lower Jurassic, whereas the groundmass of Synnyr intrusion formed between 290 and 310 million years ago.

The interpretation of aeromagnetic measurements data carried out on the limited part of the object (about 20% of subsurface site under study) together with the magnetic susceptibility of the rocks of the deposit analysis suggest the occurrence of vast bodies of biotite-pyroxen content shonkinites on the substantial depth of subsurface.

Two generations of melanocratic biotite-pyroxen rocks (shonkinites) have been accurately identified. The first one is conformable with the laminated depositional sequence of alkali and feldspathoid syenites the other is in crosscutting relations with them.

Ultrapotassium feldspathoid syenite groundmass is marked by cryptocrystalline structure with the occurrence of highly pelitic textures (dactylotype or micrographic ones). The complexity of the diagnostics of protogenic leucite separation into potassium feldspar and kalsilite or possibly into kalsilite and nephelite should be emphasized.

Autometasomatic processes being exposed locally but greatly influencing the dilution of synnyrite deposites are expectedly accompanied by substantial potassium subtraction and evident silica input up to the appearance of quartzy (5-7%) rocks, which is observed for the first time ever.

During the examination of the site and the gathering of insights the formation phases could not be completely unraveled and proved so far, but it is obvious that on the final stages of laminated rocks series genesis the bodies of scapolite, almost monomineralic rocks are formed, minor crosscutting carbonatite runs high in phosphorus and thorium (conceivably carbonatites) appear, which may indicate substancial calcum enrichment of melting residual solutions.

Indistinctly formed bodies of low-temperature buildups containing large-nested concentrations of talcum peach, scolecite, hematite and sulphide shot have been first encountered.

Disputable secondary processes represented by mixed zeolitization are difficult to diagnose, for instance microcline pelitization could be taken for zeolitization, decaying rock and cancrinitization, especially in circumstances where these processes occur either collectively or individually and having varying intensity.

The geological setting of Kalyumnoye subsurface site as well as of the whole Synnyr mass has turned out to be more complex than it was earlier estimated. Alkali depositional sequence formation lasted for longer periods of time, however, physicochemical characteristics of rock formation were highly unstable, variable and tectonic activity was of long-term and gross nature.

Zeolitization manifests itself in finely flaked and cryptocrystalline aggregates developing at potassic fieldspar that is microcline and nepheline. Zeolites are represented by thomsonite, chabazite, heulandite, boehmite, natrolite, rarely by georgecharoit and a hydrous zeolite analcime. Despite the variety of zeolites, the process is developed locally and is 6-7% at maximum, and the size of the crystals does not reach first microns on the average.

Fenitization. The manifestation of fenitization as euhedral aggregates of irregular structure and veinlet new formations of aegirite-augite garnetiferous structure in coarse-crystalline potassic feldspar leucocratic augitic syenites and synnynites. Fenitization is well-developed, local, confined to near-border areas, and reaches up to 5%. This process is typical of other alkali solids as well.

The main secondary process may be considered to be the formation of liebnerite and muscovite, which causes the emergence of greatly altered rocks – liebnerite-microcline metasomatites, where secondary minerals are 50-60%. In alkali feldspar syenites there is sodalitization, cancrinitization and the emergence of analcite.

Supposedly these processes have taken place in shallow facies starting at a temperature of 200°C (the beginning of analcite metasomatite formation) and pH7, and up to 700°C (fenitization) and pH9 (Bardina, Popov, 1991). The mechanism of the secondary processes, as well as their incidence need thorough study and further investigation.

Reference

Bardina N., Popov V. Classification of metasomatic rocks and facies of shallowness metasomatism // Soviet geology. – 1991.

PETROMAGNETIC METHODS OF THE TUNGUS SYNECLISE BASIT CLASSIFICATION

Kirguev A.A.[1], Konstantinov K.M.[1,2], Vasilyeva A.E.[3]

[1]Geo-Scientific Research Enterprise ALROSA (PJSC), Mirny, Russia, KirguevAlA@alrosa.ru

[2]Institute of the Earth's Crust, Irkutsk, Russia, KonstantinovKM@alrosa.ru

[3]Diamond and Precious Metal Geology Institute, Yakutsk, lexy_v@rambler.ru

Nowadays, the main prospects for searching of primary diamond sources are associated with the Tungus syneclise eastern board territory, where trappean formations are developed in the upper part of section (4 and 5 geotypes), characterized by significant variations in the values of physical parameters (density and magnetic). Basits can create false anomalies-barriers, therefore, probability of missing for the magnetic anomalies from kimberlite pipes under basits is high enough. In this situation, application of the gravity-magnetic exploration, as basic search method of kimberlite bodies, will be ineffective. Many researchers fairly consider that the problem can be solved with help of a basit petromagnetic legend (PML), in which for each version of its varieties there are specific quantitative magnetic condition (Konstantinov et al, 2006). However, the decision of this problem is complex enough, as magnetization of basits depends on variety of forms of occurrence (dikes, sills, etc.), significant variations of mineralogical, chemical and petrographic structures, etc. factors. As a result, petromagnetic characteristics of the Permo-Triassic traps are strongly differentiated both on sizes, and in directions. Therefore, to describe as much as possible signs of traps magnetization, many researchers based their legends on petromagnetic groups (PMG) (Cox, Bell, 1982). Their essence reduced to an establishment of the general communications between geological (petrographic, mineralogical, geochemical structures, etc.) and petrophysical (volumetric density, magnetic susceptibility æ and vectors of natural residual magnetization (NRM, In) etc.) the parameters, described, as a rule, statistically homogeneous (unimodular) samples. However, attempts to explain all variety of magnetic properties of traps by means of generated thus PMG have not led to expected results. The problem consist that among PMG of trapps still there was wide enough number of objects for which anyhow it was not possible to establish law of distribution of magnetic parameters on the basis of the elementary statistical analysis. This, in turn, generated a necessity of an increase of quantity of PMG and, as consequence, difficulty for interpreters to perception of petromagnetic legends and diagrams. Thus, there was a necessity in development of a modern PML, reflecting actual geological-geophysical conditions.

In modern scheme of basit magmatism, which constructed on features of petrographic and geochemical compositions, as well as facies appurtenances, three phases are distinguished: 1-Intrusive γßP2, 2 - vulcan-subvolcanic β0-γβP2-T1 and 3 - Intrusive γβT1 (Tomshin et al, 2001). According to the Verkhnevilyuysky sheets series of Russian State geological scale map 1:200000 the listed above phases correspond to the Olenek-velingninsky, Katangsky, and Kuzmovsky intrusive complexes (Salikhov et al, 2005). As a result of complex interactions of phases among themselves and enclosing rocks, the magnetization space of basits with homogeneous chemical, petrographic, etc. parameters, we recommend not to call PMG, and call petromagnetic taxa (PMT). PMT are the main elements in the PML terminology (Konstantinov, 2014). In contrast to previously proposed methods, which based on extensive experience of the authors research works, it is necessary and enough to use the measurement results of modular values of parameters such as volume density (σ), magnetic susceptibility (□), residual magnetization (In) and Koenigsberger coefficient (Q factor). The problem becomes simpler, if samples will be oriented (for a core enough on a vertical).

In contrast to previously known classifications, taxa of traps, whose magnetic characteristics vary in space, should be called petromagnetic groups (PMG). The number of PMGs can be numerous (but not infinite). Allocation of PMG as a unitary taxa of PML is explained by the fact that the magnetization of Permo-Triassic basits was affected by the following physical and geographical factors, namely:

1. Siberian platform paleogeographic high-latitude and current position.

2. Earth's magnetic field inversion during basite intrusion. First and second early basit phases were magnetized in a straight N polarity (according to modern field), and third late in reverse R polarity (Kravchinsky et al, 2002).

Such combination of factors determined 250 million years ago in the Tungus syneclise traps characteristic abrupt positive and negative primary NRM vectors directions. Influence of a modern magnetic field and a variety of basit phases mutual intersections in space; have much more complicated a problem in PML development of the Tungus syneclise eastern board. As a result, the PMT remained, which did not submit to signs of PMG. Such taxa are accept to define, as petromagnetic heterogeneities (PMH) - is PMT of traps, which magnetic characteristics vary in time. Nowadays, in Permo-Triassic basits the four genetic types of PMHs are established: 1-st type was generated due to magnetic reversal by a geomagnetic field; 2-nd type is due to roasting of early basit introduction phase by late intrusive phase; 3-rd type - as a result of titanomagnetite self-revers effect ; 4-th type - as a result of lightning strikes.

PMHs are characterized by complex distribution of a spectrum of magnetic parameters and have an amorphous structure: their borders conditional (washed away) also cannot coincide with morphology of bodies and geological (rock dense) borders! Ignoring of PMHs as structural elements of the physical-geological model can negatively affect to solution of scientific and applied geological problems. PMHs completely and is easier explain availability in one or another basit magmatism phase NRM vectors with opposite sign than previously put forward hypotheses for the Tungus syneclise eastern board.

Experience of works on PML development has shown that its classification into PMT needs a comprehensive approach to solving this problem. First of all, the reliability of PML depends on the quality of field works on the selection of oriented samples from different phases of basite magmatism. At the beginning, it is necessary to solve correctly the «forward problem» - getting petrophysical characteristics according to reference objects. For this purpose, 11 sites were selected on the territory of Daldyn-Alakitsky diamondiferous region, within which the presence of three main phases of basit magmatism was established: Alakit, Bystry, Vodorazdelny, Vysotny, Microdoleritovy, Morkoka, Sohsolooh-Marhinsky, Sytykan, Trassa, Chorny and Chukuka. The outcrops of multiphase basits near-contact zones were studied especially scrupulously. Oriented samples from which were then taken.

Laboratory petrophysical, magnetic-mineralogical and paleomagnetic researches were carried out in the laboratories on modern instrumentation and equipment.

By the results of statistical processing and complex interpretation of all received materials, for each subfacies of basit magmatism (doleritic, microdoleritic, near-contact, tuffaceous, etc.) received their petrophysical description — average values of σ, æ, In and Q factor. There are still a little more than 30 out of about 150 of these PMT. After that, depending on the phase (intrusive complex) and the facies affiliation, a specific «symbol» was assigned to each PMT. For example, KA2RZ number means that PMT refers to the Katangsky intrusive complex 2 subphases and represents the roasting zone (PMH 2 type). The figurative points taken out on the In-æ-Q graph have formed quite separate domains of distribution of these parameters (Fig. 1), which it is expedient to use to identify PMT of basits (Kirguev, Konstantinov, 2018).

Developed PML allows to classify the basits into phases and facies of intrusion with a high degree of probability for the Tungus syneclise eastern board. It is not so bulky, the most readable and understandable for geologists and geophysicists, than the legends proposed earlier. By means of basit PMT, it is possible to form physical-geological models of primary diamond deposits in 4-5 geotypes areas more correctly, which has a positive effect on their search by geophysical methods. The proposed PML table also predicts the existence of other PMT that may be found during geological surveys.

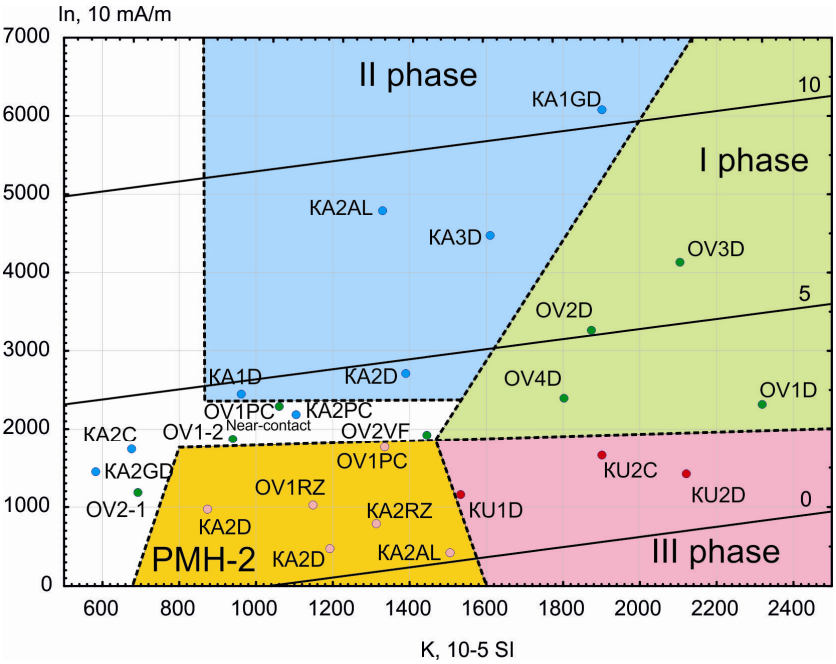

Figure. 1. Scheme dolerite facies of the PMT (Tungus syneclise eastern board).

References

Konstantinov K.M. et al. Development of the petromagnetic legend of the trap formations of the Yakutsk diamondiferous province / Volcanism and geodynamics: materials of the 3rd All-Russian Symposium on Volcanology and Paleovolcanology. Ulan-Ude. BSC SB RAS publishing house, 2006. T. 1. – P. 33-36. (in Russian).

Cox C.G., Bell J.D., Pankhurst R.J. Interpretation of igneous rocks. M .: Nedra, 1982. p. 414

Tomshin M.D. et al. The development scheme of the trap magmatism of the eastern side of the Tungus syneclise / Domestic geology № 5, 2001. P. 19-24. (in Russian).

Salikhov R.F., Salikhova V.V., Ivanushin N.V., Ohlopkov V.I. State geological map of the Russian Federation scale 1: 200 000, Verkhnevilyuyskaya series (second edition). Sheet Q-49-XXI, XXII (Aikhal). Explanatory note. S.-Pb.: 2005. p. 284. (in Russian).

Konstantinov K.M., 2014. Magnetism of Kimberlites and Trappes in the Junction Zone of the Vilyui and Tunguska Synclines in the Siberian Platform. PhD Thesis (Geology and Mineralogy). Irkutsk State University, Irkutsk, 34 p. (in Russian). (in Russian).

Kravchinsky V.A. et al. Paleomagnetism of East Siberian traps and kimberlites: two new poles and paleogeographic reconstructions at about 360 and 250 Ma / Geophys. J. Int. (2002) № 48. p. 1-33.

Kirguev, A.A., Konstantinov, K.M. Petromagnetic taxa as a reflection of the evolution of basic magmatism (using the example of the eastern side of the Tunguska syneclise) / Geological exploration for diamonds: predictive-resource, methodological, innovative and technological ways to increase it. - Mirny, 2018. p. 276-280. (in Russian).

MAFIC-ULTRAMAFIC CONCENTRICALLY-ZONED MARINKIN MASSIF (MIDDLE VITIM HIGHLAND): PETROLOGY AND ORE FORMATION

***Kislov E.V.*[1,2], *Kamenetsky V.S.*[3,4], *Malyshev A.V.*[1], *Vanteev V.V.*[1,2]**

[1]*Geological institute, Siberian Branch, Russian Science Academy, Ulan-Ude, Russia, evg-kislov@ya.ru*

[2]*Buryat State University, Ulan-Ude, Russia*

[3]*University of Tasmania, Hobart, Australia, dima.kamenetsky@utas.edu.au*

[4]*Institute of Experimental Mineralogy, Russian Science Academy, Chernogolovka, Russia*

Marinkin dunite-troctolite-gabbro massif is located around of the Marinkin creek on the right bank of Tuldun river (left inflow of Vitim). The massif was mapped by G.A. Kibanov in 1961-1963. V.S. Kosinov noted a disseminated sulfides and chromitite at 1964 during geological mapping 1:50,000. E.L. Prudovsky studied the intrusion in detail, including the copper-nickel mineralization zones and asbestos, at 1968. He named the massif after his daughter. The pluton's petrology was subsequently studied and reported in review monographs (Balykin et al., 1986; Konnikov, 1986; Tsygankov, 2005) and conference proceedings (Kislov, et al., 2009a, 2009b, 2018).

Pluton is traced for 5.5 km along a long axis in the northwest direction (320-330°). The maximum width in a northwest part of 4 km, in average – 2 km; the area – 11 km^2. The Marinkin creek cuts the massif down on 700 m up amphibolites after effusives near the intrusion bottom.

The age of intrusion is 825±12 million years by the Sm-Nd method (Izokh et al., 1998). The host granites are similar to plagiogranites of Krivoy creek with the age of 815 million years (Rytsk et al., 2001), related to Muya gabbro-diorite-plagiogranite complex earlier.

The massif is concentrically zoned. Dunites and plagioclase dunites compose a ellipse-like core with area of 2 km^2. Serpentinites and serpentine-actinolite rocks were developed after dunites. Gabbros and troctolites are replaced by zoisite, zoisite-saussurite-actinolite rocks almost everywhere. The ultramafic and mafic rocks are connected by mutual transitions and are considered as intra chamber differentiates.

Minerals are constant on composition rather. Olivine is chrysolite (f = 9–16.3%), plagioclase is bytownite, anorthite less often ($An_{70–94}$), clinopyroxene is subcalcic low-aluminous high-magnesian augite (f = 13–23%), orthopyroxene is alumobronzite (f = 16.2%), amphibole is low-titanous horn blende (f = 19%), Cr_2O_3 in chrome-spinel is 19-32% (Balykin et al., 1986).

Marinkin massif belongs to an island arc association (Tsygankov, 2005). REE profiles of the Marinkin are similar to those of other island arc massifs' (Akkermanovsky, Kirpichninsky, Galmoenansky, Lukindinsky, Munilkansky, Nuralinsky, the Ural platinum-bearing belt). The massif was formed at the Neoproterozoic stage of mafic-ultramafic magmatism at South-East folded frame of the Siberian platform. Intrusion is related to formation of the Baykal-Muya oceanic basin of the Paleoasian Ocean and the Kelyana island arc system.

Nickel-copper sulfide mineralization is localized in the ultramafic core. Both areal disseminated sulfides, and linear zones of nested and veinlet mineralization are observed. The disseminated mineralization is mainly presented. It is typical for all rocks. The amount of sulfides usually does not exceed 0.5–1% of the rock. Fine grains of pentlandite and troilite are characteristic of such mineralization. Monomineral grains are rare. Small drop-like inclusions of sulfides are observed in olivine.

Two zones of nested and veinlet mineralization size 100×500, 100×750 m and strike to North-West were opened (Prudovsky, Grudinin, 1972). Maximum contents are: Ni - up to 0.6%, Co - 0.08%, Cu – 0.15%. The content of sulfides exceeds up 10% in breccia rocks. Branchy veinlets up to 10-15 cm long and 0.1-0.2 cm wide are observed. Lenses of sulfides up to 1.0-1.5 cm long and grains of sulfides up 0.5-2.0 mm, rarely 2–4 mm in size are observed. Pyrrhotite and pentlandite prevail, chalcopyrite is found less often. Chrome-spinel and magnetite are frequent, chalcocite and violarite are minor minerals.

We analyzed the sulfur isotope composition of pyrite from the bottom amphibolite sampled on Marinkin creek bank in the central part of the intrusion and pentlandite and troilite from dunite in the central part of ultramafic core (table 1).

Table 1. Sulfur isotope composition of sulfides from the intrusive and country rocks of Marinkin massif.

No. of the sample	Mineral	Rock	$\delta^{34}S$, ‰ (CDT)
M-13/1-08	Pyrite	Amphibolite	2.2
M-13/2-08	Pyrite	Amphibolite	1.4
M-8/1-08, M-8/2-08	Pentlandite, troilite	Dunite	1.6

Note. The analyses were conducted at the Laboratory of stable isotopes of Analytical center FEB DVB RAS (Vladivostok) on an isotope mass spectrometer of Finnigan MAT 253 using system of double focusing. Analyst T.A. Velivetskaya.

The sulfur isotope relations in sulfides of intrusive and host rocks change in very narrow limits which demonstrates the sulfur source uniformity. The relations are insignificantly heavier than the meteoric standard which corresponds to its mantle origin. Sulfur could be introduced to the host rocks from magma. It is also impossible to exclude the assimilation of sulfur by magma from the host rocks but amphibolite effusive origin contradicts to this version.

The Marinkin massif ultramafic rocks contain grains of accessory chrome-spinel from 2 to 10% everywhere. Chrome-spinel is disseminated in dunite irregularly and forms isometric grains and octahedrons from 0.0n to 0.6 mm in size. Small crystals form inclusions in olivine. Larger crystals, being located closely, localize in joints of olivine grains. Chrome-spinel contains inclusions. The chrome-spinel in the troktolites form small (up to 0.5 mm) evenly scattered octahedrons, with frequent inclusions, which are found both in the interstices, and in plagioclase, and more rarely - in olivine. The Cr_2O_3 concentration in dunites reaches 1.5%.

Massive and nested chromitites at dunite core were described by V.S. Kosinov and E.L. Prudovsky (Prudovsky, Grudinin, 1972). Chromitites compose a linear zone about 300 m long and about 1 m thick, traced by fragments and blocks in deluvial talus. Chromitite fragments are also noted at other places of dunite core. The chromitites represent medium-grained black color rocks with brown olivine roundish grains. The olivine concentration increases up to 30-50% in ore zone contact parts, the chromitite gains have spotty shape.

Chrome-spinel forms crystals with the prevailing octahedron form and xenomorphic grains up to 3-4 mm in size. Their contents are up to 90% in massive chromitites. The chrome-spinel often contains mineral inclusions. Chromitites contain olivine grains and clusters of crystals. These olivine peripheral parts contain up to 20-30% of small chrome-spinel inclusions on the border with chrome-spinel. The central part of olivine grains is free from them. Chrome-spinel is sometimes surrounded by magnetite borders on the periphery or contains magnetite plates. The olivines, carbonates and pentlandites are observed in the interstices. Pentlandite forms the worm-shaped grains in chrome-spinel in contact with olivine. Cr_2O_3 concentration in chromitites reaches 18.87%.

We studied dunites with high concentration of disseminated chrome-spinel. Isometric forms and weathered crust's black color are characteristic of them at the outcrop. These are massive panidiomorfic rocks. Olivine forms grains size from 0.n up 10 mm. The size of olivine grains is extremely irregular. The olivine fine grains sometimes form inclusions in large grains. Some olivine grains have keyboard blackout and distinguishable lamellas. Inclusions of magnetite (sometimes as lamellas), chlorite, dolomite, halite, brucite are observed in olivine. Chlorite and dolomite form aggregates in joints of olivine grains. Fanlike aggregates of crystals are characteristic of chlorite. Chlorite crystals sometimes intrude into edges of olivine grains' edges because of the olivine grains' borders having jagged outlines. Olivine grains are crossed by cracks filled with dolomite, and sometimes – with films of iron hydroxides.

Chrome-spinel is represented in the form of euhedral grains up to 1.5 mm in size, evenly distributed in the rock. Octahedrons of smaller size form inclusions in olivine. Chrome-spinel single

grain can content different composition parts up to pure chromite. Chrome-spinel replacement by ferrochromite is observed on the periphery and in cracks in some grains. The inclusions of olivine, chlorite, halite, dolomite, amphibole, phlogopite, chlorapatite, pentlandite, brucite, magnetite, dyopside, perhaps chlorides of calcium, magnesium, potassium are observed in the majority of chrome-spinel grains (fig. 1). A galena-pentlandite stringers are observed in cracks of chrome-spinel grains. Chrome-spinel is often surrounded by chlorite and dolomite aggregates, more rarely it is corroded and replaced by them. The chlorite, dolomite, brucite, chalcopyrite, pentlandite and phlogopite are also observed around chrome-spinel grains. Brucite and dolomite contain iron often.

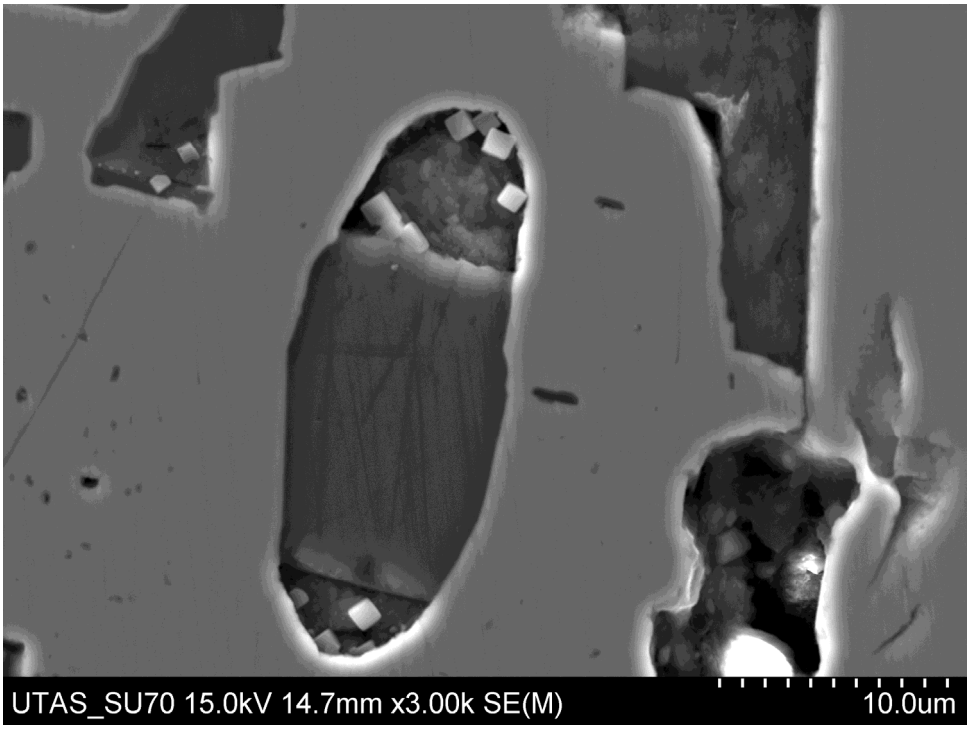

Figure. Inclusions in chrome-spinel in sample 27-15: dolomite (in the center with high relief), chlorite (top and bottom parts of inclusion in the center, an inclusion at the left above), halite (small light cubes).

Spinel is observed in the form of single euhedral grains in interstices of olivine grains. In addition, the spinel forms inclusions in olivine grains. It is colorless without polarizer. Sulfides are rare, up to 0.5 mm in size, distributed unevenly. Combined grains are noted: pyrrhotite + chalcopyrite + magnetite, pentlandite + chrome-spinel + pyrrhotite, magnetite + pyrrhotite + pentlandite, chalcopyrite grain with exsolution pentlandite and dolomite inclusions. Magnetite forms both euhedral grains in sulfides, and stringers on cracks, independent fine isometric grains among olivine and dolomite. Magnetite is chemically pure. The greenockite grain with isomorphic iron, copper and zinc is noted in magnetite.

Features of Marinkin massif composition, petrology and mineralogy demonstrate considerable influence of late granites. The ultramafic rocks were regenerated, and as a result the mafic rocks were changed. The disseminated sulfides of liquid origin form a veinlet mineralization as a result of dunite regeneration. Chromite mineralization also occurred during regeneration of dunites. Lack of serpentine, composition of non-magmatic inclusions in chrome-spinels, olivines and sulfides, inhomogeneity of chrome-spinel grains, lamellas of olivine, euhedral chlorite grains, isometric magnetite grains of pure composition without titanium indicate that phenomenon.

The reported study was executed within the Geological Institute state task on the IX.130.3.3. project, No. state registration AAAA-A17-117011650012-7 and funded by RFBR according to the research project № 19-05-00337.

References

Balykin P.A., Polyakov G.V., Bognibov V.I., Petrova T.E. Proterozoic ultrabazite-bazite formations of the Baikal-Stanovoy area. Novosibirsk: Science, 1986. 200 p. (In Russian).

Grudinin M.I. Bazite-giperbazite magmatism of the Baikal mountain region. Novosibirsk: Science, 1979. 156 p. (In Russian).

Izokh A.E., Gibsher A.S., Zhuravlev D.Z., Balykin P.A. Sm-Nd age of ultrabasite-basite massifs from Eastern part of the Baikal-Muya ophiolite belt // Doklady Akademii nauk. 1998. Vol. 360, № 1. p. 88–92 (In Russian).

Kislov E.V., Malyshev A.V., Orsoev D.A. Marinkin massif – platinum metals-nickel-copper locality at the Middle Vitim mountain region, East Siberia // Northwestern Geology. 2009. Vol. 42. p. 185–188.

Kislov E.V., Malyshev A.V., Orsoyev D.A., Balykin P.A. Marinkin massif – platinum group elements-copper-nickel ore occurrence in the Middle Vitim highland // In: Ultrabazite-bazite complexes of folded areas and the related deposits. Yekaterinburg: IGG UrB RAS, 2009. T. 1. p. 222-225. (In Russian).

Kislov E.V., Malyshev A.V., Vanteev V.V. Marinkin ultramafite-mafite massif, Middle Vitim highland – geodynamics and ore-forming complex composition // In: Questions of geology and complex exploitation of natural resources of East Asia: Fifth All-Russian Scientific conference with international participation. Blagoveshchensk: IGIP FEB RAS, 2018. T. 1. p. 33-36. (In Russian).

Konnikov E.G. The differentiated giperbazite-bazite complexes of the Precambrian of Transbaikalia (petrology and ore formation). Novosibirsk: Science, 1986. 127 p. (In Russian).

Prudovsky E.L., Grudinin M.I. Features of geological structure and material composition of Marinkin dunite-troktolite massif (Middle Vitim highland) // Geological formations of the Baikal region and Transbaikalia. Chita, 1972. p. 13-14. (In Russian).

Rytsk E.Y., Amelin Y.V., Rizvanova N.G., Krimsky R.S., Mitrofanov G.L., Mitrofanova N.N., Perelyaev V.I., Shalaev V.S. Age of rocks in the Baikal-Muya foldbelt // Stratigraphy and Geological Correlation. 2001. Vol. 9, N 4. p. 315-326.

Tsygankov A.A. Magmatic evolution of the Baikal-Muya volcano-plutonic belt in the late Precambrian. Novosibirsk: SB RAS, 2005. 306 p. (In Russian).

COMPOSITION OF APATITE AND GENETIC PROBLEMS OF THE KHIBINY APATITE DEPOSITS

Kogarko L.N.
Vernadsky Institute of Geochemistry Moscow, Russia, kogarko@geokhi.ru

Khibiny, one of the largest of the world's peralkaline intrusions, hosts gigantic apatite deposits. The formation of apatite deposits within KACP has been addressed in a large number of studies (Borutzky, 2010). The, two leading models include separation of primary iiolite-urtite magma into two immiscible melts (phosphate and aluminosilicate) and the second hypothesis relates to the formation of apatite ores with processes of crystallization differentiation.

This paper is focused on the trace element composition of apatite from several Khibiny apatitenepheline deposits. The trace elements, particularly Sr and REE, are used as effective monitors of the magmatic evolution leading to ore formation in Khibiny complex.

The geology of the Khibiny alkaline complex has been described in a large number of publications (Borutzky, 2010, Zak et al., 1972), and we do not give a description here.

Composition of Khibiny Apatite

Over 900 apatite grains from several Khibiny apatite deposits have been analyzed. The specimens were collected from drill holes of four Khibiny apaite deposits (Table 1). Rusvumchorr drill hole sampled a complete stratigraphic section through deposit. Samples of apatite of Kukisvumchorr and Nuorkpakhk deposits were obtained from surface outcrops Table1 Khibiny apatite contains exeptionaly high levels of SrO (4.5 wt % on average), which varies markedly within 0.16–9.8 wt % in different ore deposits. The concentration of Sr in apatite is much higher compared to the host magma (0.2 wt % (Kogarko, 1977). We investigated the composition of apatite in the vertical section (up to 600 m depth) of the Rasvumchorr deposit. Despite significant variations in the concentrations of Sr in apatites at the same level, an increase in the content of Sr upwards is observed along the borehole crossection.

Apatite and titanite are the main minerals that host REE in the Khibiny deposits. The total REE content in apatite ranges from hundredths of percent to over 1.5% with an average of 8891 ppm. Such concentration of rare earth in millions of tons of apatite ores defined Khibiny deposit as world-class (Zaitsev et al., 2014) Chondrite-normalized REE plots of Khibiny apatites demonstrated significant enrichment of the light rare earths over heavy REE, Ce/Yb is very high with an average of 682. It is worth noting that all chondrite-normalized REE plots of apatite lack negative Eu anomaly. This confirms our conclusion that the oxygen fugacities of apatite-bearing intrusion of the Khibiny complex were close to the QFM buffer system and apatite contained Eu^{+3}.

The Eu anomaly and levels of Sr are also controlled by the plagioclase which concentrate Eu^{2+} from the melt (KdEu in plagioclase—3.8–7.9, KdSr—2.7–10).

In the process of crystallization differentiation of KACP primary magma of olivine nephelinites composition plagioclase did not crystallize plagioclase. Main minerals of this process, such as olivine, melilite and clinopyroxene do not typically concentrate Eu and Sr, because of the very low distribution coefficients of Eu and Sr in these minerals.

According to new nomenclature (Pazero et al., 2010), most of the studied apatites correspond to fluorapatites Fluorine contentvaries from 4.73 to 3.33 wt %. The chlorine concentration is very low-hundredths of a percent.

To establish the geochemical signature of Khibiny apatites, we used previously published data (Belousova et al., 2002) and several discrimination plots, including Sr versus Y, Sr versus Mn, and Ce/Yb versus REE (According to our data, apatite from that the Khibiny complex is characterized by the highest levels of Sr among all rock varieties. It should be noted that apatite from the Khibiny complex shows characteristically low levels of Y and heavy REEs, especially in comparison with the Si rich granitoids. Mn value is close to that of apatite from carbonatites and much lower relative to granitoids, granitic pegmatites, jacupirangites, and dolirites (Belousova et al., 2002).

The obtained geochemical signature of Khibiny apatite suggests a residual character of the Khibiny alkaline magma and it indicates that the differentiation of the primary magma developed

without fractionation of mineral-concentrators of Sr and Eu (such as plagioclase). Our data confirm previous findings regarding the olivine-nephelinitic nature of the primary magma of Khibiny apatite intrusion (Arzamastsev et al., 2001, Kogarko, 1977).

Table 1. Examples of the distribution of elements in the apatites of various fields of Khibiny massif. (1200 * analyses).

	Rasvumchorr (38 samples)	Oleniy ruchey (43 samples)	Koashva (62 samples)	Uksporr (12 samples)	Khibiny massif
Element	**Average**	**Average**	**Average**	**Average**	**Average**
Ce/Yb (ppm)	441	705	940	416	682
ΣREE (ppm)	7 451	7 379	12 979	7 218	8 891
Ce	3 334	3 283	6 086	3 202	4 040
La	2 294	2 247	4 293	2 152	2 799
Pr	314	308	521	309	367
Nd	1 085	1 101	1 637	1 111	1 243
Sm	150	157	182	156	162
Eu	41	44	45	45	44
Gd	113	120	117	122	118
Tb	13	14	12	14	13
Dy	62	64	52	64	60
Ho	10	10	8,3	10	9,8
Er	21	21	16	21	20
Tm	2,2	2,0	1,5	2,0	1,9
Yb	10	10	7,0	9,3	8,9
Lu	1,0	1,0	0,7	1,0	0,9
Si	1 123	-	-	-	1 123
Na	1 100	-	1200	-	1 150
Sr	30 149	30 543	64 771	18 947	38 520
Hf	0,02	-	0,1	0,1	0,1
Ta	0,003	-	0,1	0,1	0,0
Pb	1,4	-	1,0	1,4	1,2
Th	19	-	23	25	22
U	2,0	-	1,3	2,5	1,8
Mg	-	4 181	22	58	2 225
Sc	0,04	3	0,6	1,2	1,6
Mn	150	157	114	136	142
Fe	88	313	89	99	182
Y	283	265	171	277	245
Zr	2,3	8	7,2	7,1	6,6
Nb	0,1	1	0,6	0,1	0,4
Ba	331	418	318	326	363
Zn	0,4	-	-	-	0,4

* - The average is obtained from all apatite analyses.

Apatite is a common accessory mineral and it has been extensively used to obtain significant genetic information (Chakhmouradian, 2002, Borutzky, 2010). This mineral is found in virtually all igneous rocks due to expanded crystallization fields. Experimental studies of the apatite solubility in the wide variety of silicate melt compositions have shown strong dependence of apatite saturation level upon silica activity and to a lesser extent concentration of Al, Fe, alkalis and oxygen fugacity (Watson,

1980). Apatite is soluble in basic melts as compared to leucocratic magmas and its solubility in magmas decreases markedly with the increasing silica content and falling temperature (Watson, 1980, Kogarko, 1986). Our experimental studies demonstrated the extremely high solubility of apatite in olivine melilite nephelinitic melts (Kogarko et al., 1986). At a temperature of 1250 _C, basaltic melt, containing 50% SiO_2 dissolves 3–4 wt % P_2O_5, (Watson, 1980) and olivine melilite nephelinite, containing 41% SiO_2 under the same conditions of 8–9% P_2O_5. Previous detailed studies of Kola Alkaline Carbonatite Province (KACP) (Arzamastsev et al., 2001, Downesa et al., 2005) have established that the composition of primary magma corresponded to a sodic melilitite or olivine melanephelinite (24.5–26.7% SiO_2) (Arzamastsev et al., 2001, Kogarko, 1977). The mantle is generally P-depleted (86 ppm and it only ultra-alkaline silica-undersaturated magmas produced at very low degrees of partial melting of metasomatised P-enriched mantle could then be saturated in apatite at near liquidus conditions. Highly undersaturated character of Kola primary magmas suggests the significant potential of P_2O_5 in alkaline rocks and carbonatites. Giant apatite deposits are associated with Khibiny peralkaline nepheline syenites.

The age of apatite ores Khibiny massif-370 Ma (Kogarko et al., 2010, Kramm & Kogarko, 1994). The initial Hf, Sr, Nd isotope ratios are similar to the isotopic signatures of OIB indicating depleted mantle as a source (Kramm & Kogarko, 1994). This leads to the suggestion that the origin of this gigantic alkaline intrusion and super large apatite deposits is connected to a deep seated mantle source and metasomatic interaction between mantle material and fluid-melts transporting phosphorus and rare elements into magma-generation zones (Kogarko, 2010).

2. Genetic Problems of the Khibiny Apatite Deposits

The phase equilibria of the apatite-bearing ijolite-urtite rocks of Khibiny can be approximated in the system $NaAlSiO_4$-$CaMgSi_2O_6$-$Ca_5(PO_4)_3F$ (Kogarko, 1977). Composition represents a weighted average of the bulk composition of the apatite-bearing complex under consideration. From melt of such a composition nepheline would crystallize first. Apatite and nepheline would be the next to crystallize as the temperature falls. Apatite, nepheline, and pyroxene begin to precipitate as the temperature is lowered further. This crystallization sequence is in agreement with petrographic observations of the rocks. Thus, from the viewpoint of experimental phase equilibria, an alumina-silicate melt with 2.4 wt % P_2O_5 could have been the parental magma of the ore apatite complex. Such a magma would crystallize about 10–15% of nepheline before reaching the nepheline apatite-pyroxene cotectic and all these minerals would crystallize simultaneously. The close to eutectic character of apatite-bearing intrusion and the coincidence of the order of crystallization of apatite ores with the regularities of crystallization of experimentally studied phosphate-silicate systems indicate that the main process in the formation of apatite deposits was crystallization differentiation. It should be pointed out that field of existence of two liquids-phosphate and aluminosilicate is separated from the average composition of apatite intrusion by the temperature barrier, which means that the "immiscibility" model is not realistic. In addition, the temperature of melting of monomineral apatite ore should be higher than 1500 °C.

As it has been demonstrated by a number of authors, a convective regime must exist in magmatic reservoirs with thickness exceeding 10 m. However, the style of the convection withcrystallization is likely steady-state conditions (Spera et al., 1995).

One outstanding problem that is presented by the apatite-ore bodies concerns the manner in which accumulation of nepheline, apatite and pyroxene occurs in terms of steady-state convection.

The consideration of the values of the velocity of sedimentation calculated according to Stokes law and viscosity, temperature difference, densities, and heat-conductivity gives (Bartlett, 1969):

$$ln\frac{Np_1}{Np_2} = -0.66\Delta\rho\rho^{\frac{2}{3}}\eta^{-2}k^{-\frac{2}{3}}\alpha^{-\frac{1}{3}}\Delta T^{-\frac{1}{3}}C_p^{-\frac{1}{3}}\mathbf{g}^{\frac{1}{3}}\mathbf{a}^2$$

where:

$\Delta\rho = \rho_s - \rho_l$ the difference between densities of melt and crystals (g cm−3);

η viscosity (poise);

k coefficient of heat-conductivity (cal cm^{-1} s^{-1} k^{-1});

α thermal expansion coefficient (k^{-1});
ΔT temperature difference between roof and foot-wall;
C_p heat-capacity ($cal.g^{-1}\ k^{-1}$);
g gravity acceleration (980 cm s^{-2}); and,
a dimensions of crystals (cm).
N_{P1}/N_{P2}—mineral particle number ratio near the roof and the floor of the magma chamber.

This equation shows that the strongest influence on the distribution of particles is that of their size; with particles above a certain size-nepheline (up to 3–5 mm across), the stirring effect of the convection ceases to act and the particles are settled to the bottom of the magma chamber, forming a lower cumulus layer (massive urtite), while smaller particles-apatite (up to several tenths of mm) are stirred more efficiently and enrich the later (upper) cumulative layers (rich apatite ore).

Very important is the presence of sorting of minerals (Kalashnikov et al., 2016) which suggests that the mechanism of accumulation of minerals and formation of apatite ores was the gravitational differentiation of the close to eutectic apatite- intrusion in conditions of convective motion. Sorting coefficients of apatite, nepheline, and pyroxene are close to unit. Such values of sorting coefficients are characteristic of well-sorted sedimentary deposits, for instance, sands. According to the calculations, pyroxenes should accumulate in the middle part of apatite deposits, which corresponds to the distribution of this mineral in the vertical section of deposits. In the formation of massive urtites, very small apatite crystals were suspended and captured by the interstitial melt, demonstrating a significant difference in the sizes of these minerals in the early stages of crystallization (Figure 1). Thus crystals of apatite remained in suspension until the settling velocity is small as compared with the velocity of convective currents.

Figure 1. Thin section of massif urtite. Small crystals of apatite in interstitial between large crystals of nepheline.

At cooling of intrusion convection falls and even the small crystals of apatite forms accumulations and ores. This model is supported by the composition of Khibiny apatite. Very homogeneous character of Khibiny apatite and weakly expressed zoning suggest crystallization of apatite in a large volume of magmatic chamber, in which inevitably there is strong convection leading to active mixing.

References

Arzamastsev A.A.; Bea F.; Glaznev V.N.; Arzamastseva L.V.; Montero P. Kola alkaline province in the Paleozoic: Evaluation of primary mantle magma composition and magma generation conditions. Russ. J. Earth Sci. 2001.

Bartlett R.W. Magma convection, temperature distribution and differentiation. Am. J. Sci. 1969, 267, 1067–1082.

Belousova E.A.; Griffin, W.L.; O'Reilly, S.Y.; Fisher, N.I. Apatites as an indicator mineral for mineral exploration: Trace-element compositions and their relationship to host rock type. J. Geochem. Explor. 2002, 76, 45–69.

Borutzky B.E. Modern Understanding of the Nature and Geological History of the Formation of Rocks of the Khibiny Alkaline Massif. (Critical Comparison of the Proposed Hypotheses and Comments to Them). In Proceedings of the Materials of the All-Russian (with International Participation) Field Conference Dedicated to the 80th Anniversary of the Kola Science Centre RAS, Apatity, Russia, 20–23 June 2010; Geological Institute KSC RAS, Kola Branch of Russian Mineralogical Society: Apatity, Russia, 2010.

Downesa H.; Balaganskaya E.; Beard A.; Liferovich R.; Demaiffe D. Petrogenetic processes in the ultramafic, alkaline and carbonatitic magmatism in the Kola Alkaline Province: A review. Lithos 2005, 85, 48–75.

Dunworth E., Bell K. The Turiy Massif, Kola Peninsula, Russia: Isotopic and Geochemical Evidence for Multi-source Evolution. J. Pet. 2001, 42, 377–405.

Kalashnikov A.O.; Konopleva N.G.; Pakhomovsky Y.A.; Ivanyuk G.Y. Rare Earth Deposits of the Murmansk Region, Russia—A Review. Soc. Econ. Geol. Inc. Econ. Geol. 2016, 111, 1529–1559.

Kogarko L.N. Genetic Problems of Agpaitic Magmas; Nauka: Moscow, Russia, 1977; 294p. (In Russian).

Kogarko L.N., Krigman L.D.; Krot T.V.; Ignatenko K.I. Influence of chemical composition of magmatic melt on the solubility of P_2O_5. Geochem. Int. 1986, 10, 138.

Kogarko L.N.; Lahaye Y.; Brey G.P. Plume-related mantle source of super-large rare metal deposits from the Lovozero and Khibiny massifs on the Kola Peninsula, Eastern part of Baltic Shield: Sr, Nd and Hf isotope systematics. Miner. Pet. 2010, 98, 197–208.

Kramm U.; Kogarko L. Nd and Sr isotope signatures of the Khibiny and Lovozero agpaitic centres, Kola Alkaline Province, Russia. Lithos 1994, 32, 225–242.

Spera F.J.; Oldenburg C.M.; Christensen C.; Todesco M. Simulations of convection with crystallization in the system $KAlSi_2O_6$-$CaMgSi_2O_6$: Implications for compositionally zoned magma bodies. Am. Miner. 1995, 80, 1188–1207.

Watson E.B. Apatite and phosphorus in mantle source regions: An experimental study of Apatite/melt equilibria at pressures to 25 kbar. Earth Planet. Sci. Lett. 1980, 51, 322–335.

Zaitsev A.; Williams T.; Jeffries T.; Strekopytov S.; Moutte J.; Ivashchenkova, O.; Spratt, J.; Petrov, S.; Wall, F.; Seltmann, R.; et al. Rare earth elements in phoscorites and carbonatites of the Devonian Kola Alkaline Province, Russia: Examples from Kovdor, Khibiny, Vuoriyarvi and Turiy Mys complexes. Ore Geol. Rev. 2014, 61, 204–225.

Zak S.L.; Kamenev E.A.; Minakov P.V.; Armand A.L.; Mikheichev A.S.; Petersilie J.A. The Khibiny Alkaline Massif; Nedra Publishers: Leningrad, Russia, 1972. (In Russian).

NEW APPROACH TO MINERAL PROCESSING OF HIGH-CARBONATE ORES FROM KOVDOR MASSIF

Kondratyuk V.A.[1], Borozdin A.P.[1], Petrov S.V.[1,2], Shelukhina Y.S.[1,2], Kolusheva O.S.[1]
[1]LLC "LIMS", Saint-Petersburg, Russia, kondratyuk@lims-lab.com
[2]Saint-Petersburg State University, Saint-Petersburg, Russia

Annotation. The laboratory testing of beneficiation processes of apatite-carbonate ores from Kovdor deposit and the flowsheet of thermal dissociation of ore are presented in the paper. Three products were obtained as a result of processing of the ore: magnetite concentrate, apatite concentrate and chemically precipitated chalk.

Introduction. The content of useful components in ores of the deposits that were discovered in the last century and have been mined for decades decrease from year to year. Additional exploration of flanks of the deposit and deep exploration do not provide an increase in the contents of useful components. At the beginning of its exploration the ores of Kovdor deposit contained 7 wt.% of P_2O_5 (Afanasev, 2011) and now the average contend has decreased to 3-5 wt.%.

Additional problem for the ore beneficiation, apart from the low P_2O_5 content, is the high content of calcium in ores, which can be up to 80 wt.%. Most of the floatation reagents used in floatation flowsheets do not let to extract the pure apatite, a significant amount of calcite contaminates the concentrate.

The study of apatite-calcite and carbonate ores from Kovdor deposit has been carried out since 1983, but due to beneficiation and economic difficulties, this type of ores was never taken for processing (Petric et. al., 2012).

Company LIMS conducted the processing tests on this ore and as a result the enrichment flowsheet was designed that allow to obtain not only the conditioned magnetite and apatite concentrate, but also a new product – chemically precipitated chalk. This flowsheet allows to double the cost of useful components contained in one ton of ore compared with the option of using a calcite product for cement industry (Kudinova, 2004). The total potential value of the ore depends primary on the carbonate products obtained, as due to the high content, calcite accounts for about 80-90%.

Ore composition. Two samples of apatite-carbonate ores with P_2O_5 content of 4.4 wt.% and 1.8 wt.% were studied. Both samples due to high calcite content are characterized by high carbonate index: ratio CO_2/P_2O_5 in first sample is 7.6, in second is 20.3. Apart from this ratio, the chemical composition of both samples is almost identical.

The main mineral for both samples is calcite, with the content of 77.8% and 82.8% respectively. Apatite content is 10.5% in first sample and 4.2% in second. Minor minerals are phlogopite (3.9% and 5%), magnetite (2.9%), dolomite (1.3%) and olivine (1%). All other minerals present in the amount of less than 1%.

Results of beneficiation tests of ore by physical and mechanical methods. Series of tests were conducted on the samples of apatite-carbonate ores to separate by density properties. The test results show that the gravity separation do not occur at any grain size. Apatite is spread among all gravity products and it is not possible to get good quality products. Thus, the gravity methods of beneficiation could not be used in pre-enrichment of this ore type.

On the material of the first sample, experiments were carried out on the stage reduction crushing of ore with the gravitational enrichment of the depleted product. As a result, the value of carbonate index in the enriched product was reduced from 7.6 to 3.8% and the recovery of phosphorus pentoxide increased to 67%. However, significant losses of phosphorus pentoxide are associated with the slurry material. Subsequent flotation carried out on the material of the enriched product did not allow to achieve acceptable indicators for the extraction of phosphorus and the quality of the concentrates. The negative influence of calcite, that has the similar floatation properties as apatite, does not allow to reach good separation of apatite and calcite. Tests were performed both with the floatation reagents used at the processing plant and with the additional reagents and additional operations (preheating to 300-400 ° C, steaming with liquid glass, etc.). The selective reagents mentioned in (Tikhonov, etc.,

1983) – IM-50, IMR-25, Flotol-7,9 – that allow to separate these minerals, are not currently manufactured industrially.

Carbonate products obtained by enrichment under the scheme with stage reduction crushing and gravity enrichment have low quality with a whiteness of not more than 81% and can only be used to produce lime.

Results of beneficiation tests of ore by thermochemical methods. The flowsheet based on the difference of the mineral behavior during firing was designed (fig. 1). According to the flowsheet the apatite-calcite ore is crushed up to -10+0 mm and then fed to dry magnetic separation in magnetic fields with the intensity of up to 3000 oersted.

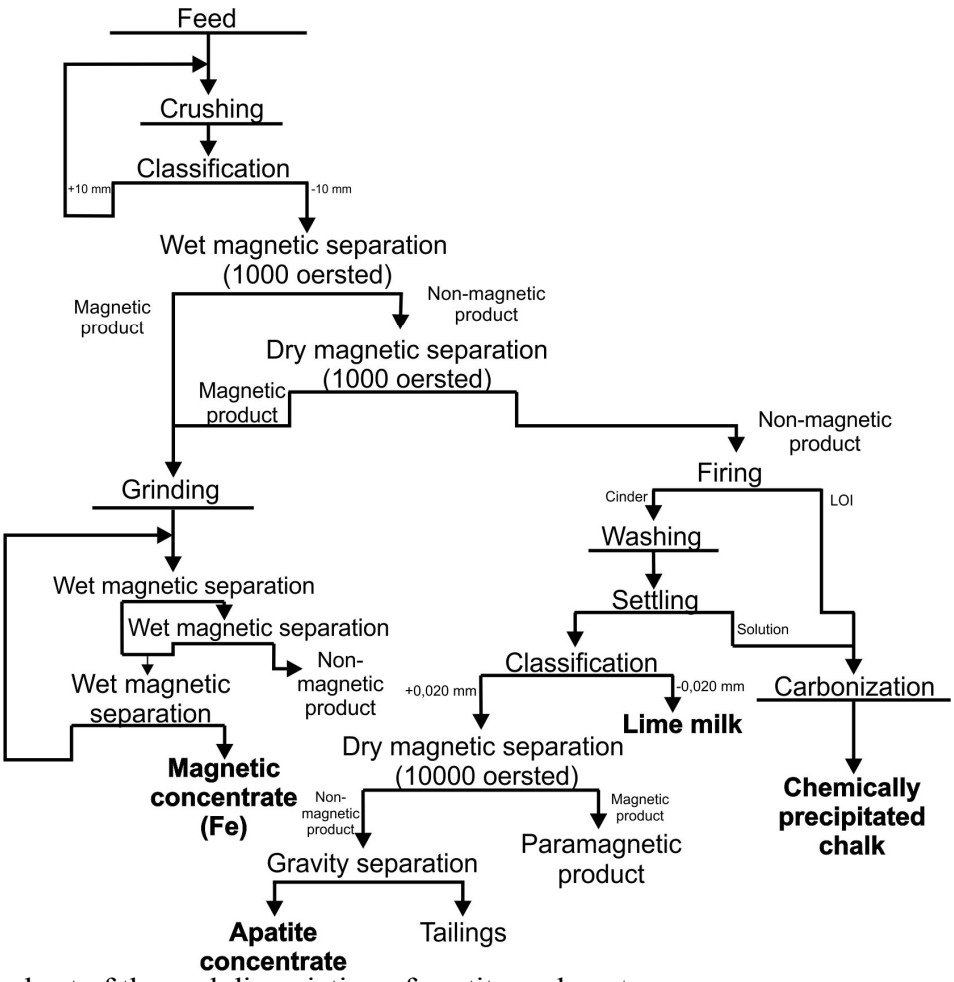

Figure 1. Flowsheet of thermal dissociation of apatite-carbonate ore.

The magnetic product with the yield of 13% is sent for grinding in the ball mill with subsequent enrichment using wet magnetic separation to produce a magnetic concentrate with the yield of 3% from initial ore and grade of 69% of total Fe. The recovery of P_2O_5 in non-magnetic product (yield 10% from ore) is 5.6%.

Non-magnetic product of dry magnetic separation with the grain size -10+0 mm (yield 87% from ore) is the feed product for thermal decomposition. Thermal decomposition is carried out in tubular furnace at the temperature of 1000°C. Exhaust gases are subject to partial utilization during the subsequent carbonization of lime products. In the firing process, 29.4% of the feed mass is lost, due to the decomposition of calcite carbonatites ($CaCO_3 \rightarrow CaO + CO_2 \uparrow$), sulfur from sulfides burn out, mica flakes swell, and other minerals, including apatite, do not change.

After unloading the cinder, consisting of quicklime (CaO) mixed with primary ore minerals, it is slaked with water to produce calcium hydroxide ($CaO + H_2O = Ca(OH)_2$).

After the lime is slaked, the lime paste is diluted with water to a solid to liquid ratio 1:50. As a result of this operation, a calcium hydroxide solution is obtained. The resulting pulp is classified on a

cone classificator by the size of 0.02 mm, the drain is sent to settle in a thickener to obtain a clear solution of calcium hydroxide and lime milk.

As a result, three products are obtained:

1. The calcium hydroxide solution (with a yield of 9% on a solid), which, after clarification (filtration), is subjected to carbonization by carbon dioxide, which is utilized from the exhaust gases of a rotary kiln to burn the feed product. As a result, a solution of pure dispersed calcium carbonate (chemically precipitated chalk) precipitates in the solution: $Ca(OH)_2 + CO_2 = CaCO_3 + H_2O$. The residuum settles, thickens, and before drying, a modifier is added to it to create a hydrophobic surface of the material particles (sodium stearate solution). The resulting hydrophobic calcium carbonate slurry is filtered and dried to a fine powder. The content of stearic acid in the finished product - 2%.

2. Lime milk pulp (with a yield of 29% on a solid) can be used to prepare chemically precipitated calcium carbonate. Chemically precipitated chalk from lime milk pulp is obtained according to the same principle as from a solution of calcium hydroxide. Calcium carbonate is precipitated, which is separated by hydro-cyclone, and then the product is filtered and dried.

3. Sands of classification (fraction +0.02 mm with a yield of 19.5%) are subjected to gravity beneficiation at concentration tables with the production of an enriched apatite product in the heavy fraction, which is subjected to thickening, filtration and drying. The dry material is subjected to high-intensity magnetic separation with the recovery of the paramagnetic fraction, which is sent to the feed of the gravity beneficiation unit. The non-magnetic fraction of high-intensity magnetic separation is a standardized apatite concentrate with a yield of 11%, the concentrate contains 39.5% of P_2O_5, and the recovery of phosphorus pentoxide is 88.3% of the ore.

Conclusion. The flowsheet with thermal decomposition of ore allow to recover around 88% of phosphorus pentoxide with the production of apatite concentrate with a grade of about 39.5 wt.% P2O5. Within this flowsheet calcite is thermally decomposed and quicklime is obtained. After quenching with water and carbonatization with carbon dioxide, it is converted into chemically precipitated chalk, which has a high whiteness (> 97%) and, depending on the content of impurities, is divided into two varieties.

Chemically precipitated chalk is used as a filler in various industries: in the production of paper, polymeric materials, in rubber, paint and varnish, food and chemical industries. The wholesale prices of chemically precipitated chalk can vary from 100 to 500 euros per 1 ton, depending on the morphology of the particles and the purpose of the material.

There are at least two reasons for producing precipitated calcium carbonate. Firstly, in the process of obtaining the chemically precipitated chalk there are several points in the beneficiation process in which it is possible to organize the purification of the initial or intermediate materials.

Secondly, the process of obtaining the chemically precipitated chalk allows growing crystals of various sizes and different shapes: needles, cubes, prisms, rhombohedrons, which have different physical properties, such as powder density, surface area and oil absorption. In addition, the precipitation process also allows to grow very small particles, up to nanometers or hundredths of microns, i.e. much finer than one could get by simply grinding limestone. These ultra-thin nano-particles of chemically precipitated chalk have special applications and extremely high price.

References

Afanasev B.V. Mineral resources of alkaline-ultramafic massifs of Kola peninsula // SPb, ed. «Roza vetrov», 2011, 224 p.

Kudinova I.N. Microcalcite: production, import, export, price // Snabzhenetz, 2004, №4.

Petric A.I., Bykhovetz A.N., Sokharev V.A., Perein V.N., Serdyukov A.L. Modernization of the mineral resource base in the long-term development strategy of the Kovdorsky GOK // Gorniy Zhurnal, 2012, №10

Tikhonov S.A., Eremenko G.K., Popova R.M., Lyutnya L.M. Composition and beneficiation of low-grade apatite-carbonate complex ores. Moscow, 1983, 38 p.

EARLY PERMIAN ALKALINE INTRUSIONS OF WESTERN TIEN SHAN: A TERMINATION OF HERCYNIAN POST-COLLISIONAL MAGMATISM?

Konopelko D.L. [1,2]

[1]*St. Petersburg State University, 7/9 University Embankment, St. Petersburg, 199034, Russia, d.konopelko@spbu.ru*

[2]*Novosibirsk State University, 1 Pirogova St., Novosibirsk, 630090, Russia*

The Tien Shan orogen formed during the late Paleozoic (Hercynian) collision between the Precambrian microcontinents of Karakum and Tarim in the south and the early Paleozoic Kazakhstan continent in the north (Zonenshain et al., 1990; Şengör et al., 1993). The western Tien Shan is composed of three major tectonic units or terranes: (1) the Northern Tien Shan, the deformed margin of the Paleo-Kazakhstan continent; (2) the Middle Tien Shan, a Late Paleozoic volcano-plutonic arc; and (3) the Southern Tien Shan, an intensely deformed fold and thrust belt formed during the final closure of the Paleo-Turkestan Ocean. These east-west trending linear terranes are cut by the NW trending Talas-Fergana Fault with a total dextral offset of about 200 km (Fig. 1). Voluminous late Paleozoic granitoid series of western Tien Shan formed during two episodes of subduction in Silurian – early Devonian and middle – late Carboniferous. Subduction-related magmatism was followed by the early Permian post-collisional magmatic pulse (Konopelko et al., 2017). Subduction-related magmatic series are spatially bound to the Middle Tien Shan terrane, which developed as a northern active margin of the Turkestan Ocean, while the post-collisional magmatism affected the whole western Tien Shan across terrane boundaries. In the Middle Tien Shan the post-collisional magmatic pulse followed the supra-subduction magmatism successively without interruption in time, while in the Southern Tien Shan, which developed during the late Paleozoic as a southern passive margin of the Turkestan Ocean, the post-collisional magmatic pulse was preceded and followed by more than 50 Ma long amagmatic periods (Fig. 2).

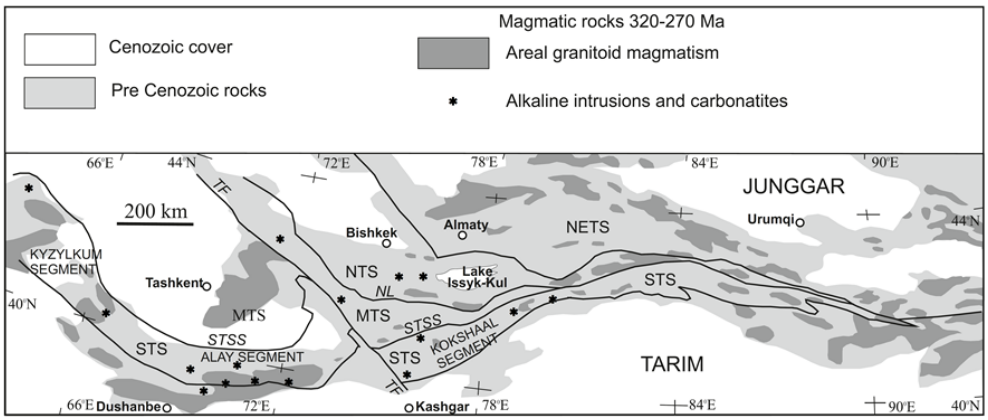

Figure 1. Principal terranes of the Tien Shan belt and distribution of late Paleozoic granitoids and alkaline intrusions. Abbreviations: NTS — Northern Tien Shan, NETS — North-Eastern Tien Shan, MTS — Middle Tien Shan, STS Southern Tien Shan, NL—Nikolaev Line, STSS—Southern Tien Shan Suture, TF—Talas - Fergana strike–slip fault.

Intrusions of alkaline rocks and carbonatites form a regionally developed suite in the Middle and South Tien Shan terranes where they associate with post-collisional granitoids and minor mafic rocks (Fig. 1). Several alkaline and carbonatitic intrusions of the area, such as Dara-i-Pioz, Akkulen, Chagatai and Karashoho intrusions, are known for their peculiar rock types and rare mineral assemblages (Fig. 3), which made them a focus of numerous mineralogical and petrographic studies (e.g. Shinkarev, 1966; Faiziev et al., 2010). However emplacement ages of the alkaline rocks and carbonatites remain poorly studied and their tectonic setting is still debated (e.g. Vrublevskii et al., 2018). In this work we review published single grain zircon ages of four alkaline intrusions and discuss them in combination with ages of associated granitoids in order to constrain the timing of the

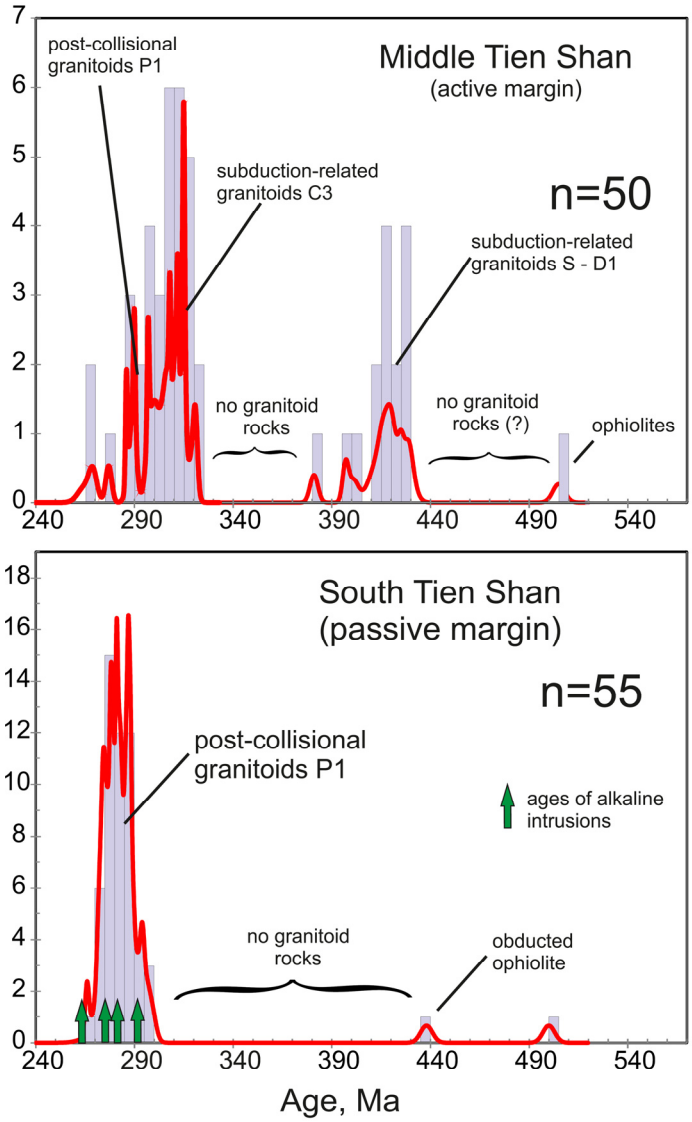

Figure 2. Histograms showing distribution of ages of late Paleozoic subduction-related and post-collisional granitoid intrusions at former active and passive margins of the Turkestan Ocean. Ages of alkaline intrusions are shown for comparison. Compiled from Seltmann et al. (2011), Dolgopolova et al. (2017), Konopelko et al. (2007, 2017, 2018).

alkaline magmatism within the frame of Hercynian collisional events in the western Tien Shan orogenic belt.

The geochronologically investigated alkaline rocks include alkaline syenites from the Akkulen (Fig. 3) and Surteke intrusions, located to the east of the Talas-Fergana Fault, nepheline syenite from the Dara-i-Pioz intrusion, representing the alkaline rocks of the Alai range, and the granite vein crosscutting diamondiferous mafic alkaline rocks of the Karashoho pipe in Kyzylkum desert. Alkaline syenites of the Akkulen massif were emplaced in the Middle Tien Shan while three other intrusions represent alkaline suites of the South Tien Shan terrane. Zircon grains from the Akkulen, Surteke and Karashoho rocks were dated by SHRIMP-II in VSEGEI and yielded ages 292 + 1 Ma, 284 + 1 Ma and 276 + 4 Ma, respectively. Zircon grains from the Dara-i-Pioz syenite were dated at 267 + 2 Ma utilizing LA-ICP-MS in the Natural History Museum, London, UK. These ages were published separately by Seltmann et al. (2011), Dolgopolova et al. (2017) and Konopelko et al. (2017) and are discussed here collectively for first time. The obtained ages of four alkaline intrusions are presented on histograms showing distribution of ages of late Paleozoic subduction-related and post-collisional granitoids at former active and passive margins of the Turkestan Ocean (Fig. 2). As seen in Fig. 2, the ages of alkaline intrusions generally correspond to the early Permian and match well the ages of post-collisional intrusions elsewhere in Tien Shan. Thus, emplacement of alkaline magmas was

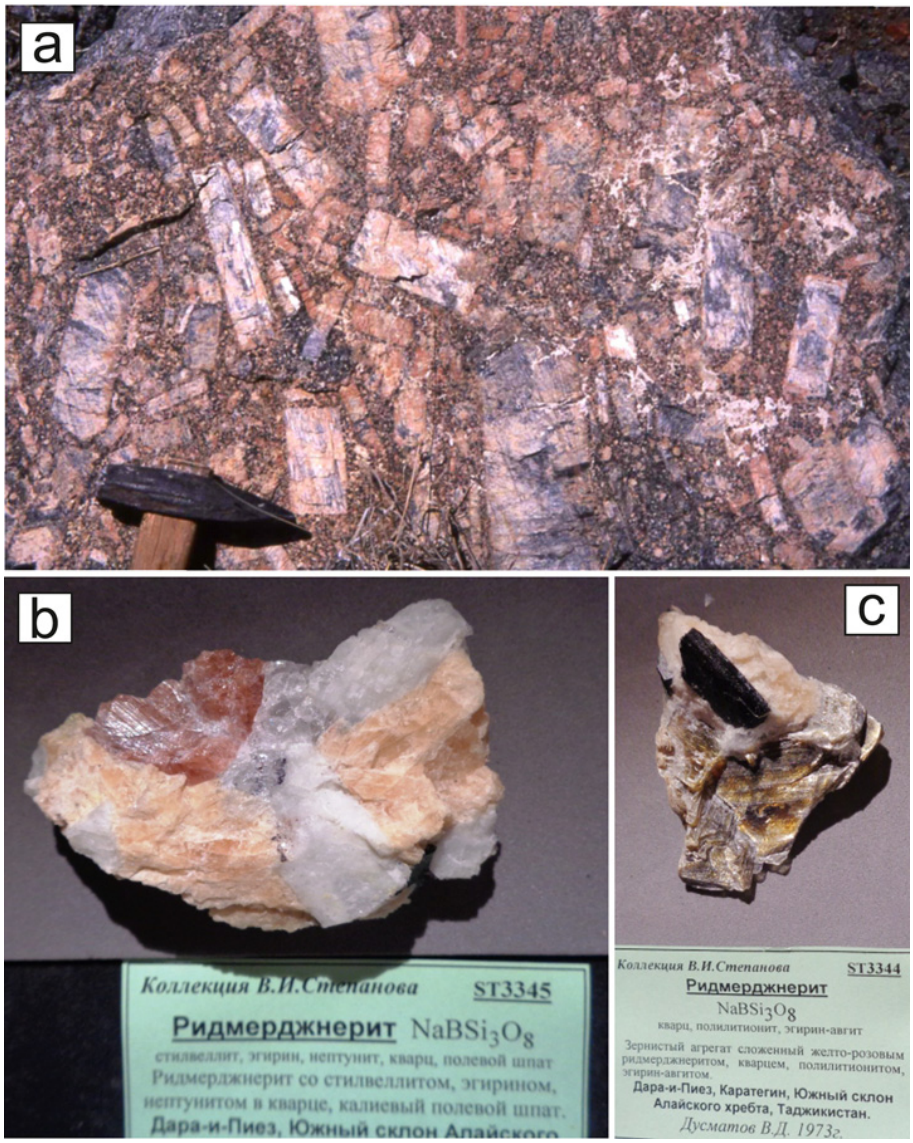

Figure 3. Specific rock types and rare mineral assemblages characteristic for alkaline intrusions of western Tien Shan: a – Kfs-megacrystic syenite with interstitial nepheline from the Akkulen intrusion; b and c – reedmergnerite $NaBSi_3O_8$ (yellowish cream-colored aggregates) from the Dara-i-Pioz intrusion. Photographs b and c represent samples from Fersman Mineralogical Museum, Moscow (http://geo.web.ru/druza/l-Dara-i-Pioz.htm).

probably triggered by the post-collisional processes and was unrelated to Permo-Triassic intraplate extension, as it was suggested by some authors (e.g. Vrublevskii et al., 2018).

To explain the geodynamic setting of Hercynian post-collisional intrusions Konopelko et al. (2007) proposed a model of post-collisional plate-scale displacements based on the model for the San Andreas fault in California (Teyssier and Tikoff, 1998). According to this model, after the late Carboniferous collision, the Tien Shan was affected by trans-crustal strike–slip motions that created a number of regional faults including the Talas-Fergana fault, which was active since early Permian (Fig. 1). It is suggested that transfer of displacement from the mantle to the upper crust was accommodated in the lower-middle crust by flat-lying detachment zones. This transpressional system provided suitable conduits for ascending asthenospheric material and influx of heat into the crust. Mantle-derived melts triggered melting of various crustal protoliths and emplacement of compositionally diverse post-collisional granites. In this scenario coeval alkaline magmas originated as a result of interaction between ascending asthenospheric material and lithospheric keels of accreted continental blocks with Precambrian basements.

This work was supported by the Ministry of Education and Science of the Russian Federation (project No 14.Y26.31.0018).

References

Dolgopolova A., Seltmann R., Konopelko D., Biske Yu.S., Shatov V., Armstrong R., Belousova E., Pankhurst R., Koneev R., Divaev F. Geodynamic evolution of the western Tien Shan, Uzbekistan: insights from U-Pb SHRIMP geochronology and Sr-Nd-Pb-Hf isotope mapping of granitoids // Gondwana Research. 2017. Vol. 47. P. 76–109.

Faiziev A.R., Gafurov F.G., Sharipov B.N. Carbonatites of the Dara-i-Pioz alkaline massif, Central Tajikistan, and their compositional features // Geochemistry International. 2010. Vol. 48 (11). P. 1084–1096.

Konopelko D., Biske G., Seltmann R., Eklund O., Belyatsky B. Post-collisional granites of the Kokshaal Range, Southern Tien Shan, Kyrgyzstan: age, petrogenesis and regional tectonic implications // Lithos. 2007. Vol. 97. P. 140–160.

Konopelko D., Seltmann R., Mamadjanov Y., Romer R.L., Rojas-Agramonte Y., Jeffries T., Fidaev D., Niyozov A. A geotraverse across two paleo-subduction zones in Tien Shan, Tajikistan // Gondwana Research. 2017. Vol. 47. P. 110–130.

Konopelko D., Wilde S.A., Seltmann R., Romer R.L., Biske Yu.S. Early Permian intrusions of the Alai range: Understanding tectonic settings of Hercynian post-collisional magmatism in the South Tien Shan, Kyrgyzstan // Lithos. 2018. Vol. 302–303. P. 405–420.

Seltmann R., Konopelko D., Biske G., Divaev F., Sergeev, S. Hercynian postcollisional magmatism in the context of Paleozoic magmatic evolution of the Tien Shan orogenic belt // Journal of Asian Earth Sciences. 2011. Vol. 42. P. 821–838.

Şengör A.M.C., Natal'in B.A., Burtman V.S. Evolution of the Altaid tectonic collage and Paleozoic crust growth in Eurasia // Nature. 1993. Vol. 364. P. 299–307.

Shinkarev, N.F. Late Paleozoic Magmatism of Turkestan-Alai. Leningrad University Publ. House, Leningrad. 1966. 150 pp. (In Russian).

Teyssier C., Tikoff B., Strike–slip partitioned transpression of the San Andreas fault system: a lithospheric-scale approach // Holdsworth R.E., Strachan R.A., Dewey J.F. (Eds.), Continental Transpressional and Transtensional Tectonics. Special Publications. Vol. 135. Geological Society, London. 1998. P. 143–158.

Vrublevskii V.V., Morova A.A., Bukharova O.V., Konovalenko S.I. Mineralogy and geochemistry of Triassic carbonatites in the Matcha alkaline intrusive complex (Turkestan-Alai Ridge, Kyrgyz Southern Tien Shan), SW Central Asian Orogenic Belt // Journal of Asian Earth Sciences. 2018. Vol. 153. P. 252–281.

Zonenshain L.P., Kuzmin M.I., Natapov L.M. Geology of the USSR: A Platetectonic Synthesis // AGU Geodynamics Series 21. American Geophysical Union, Washington, DC. 1990. 242 pp.

ZONATION OF THE KHIBINY MASSIF RELATIVE TO COMPOSITION OF ROCK-FORMING AND ACCESSORY MINERALS

Konopleva N.G.[1], Ivanyuk G.Yu.[1,2], PakhomovskyYa.A.[1,2], Yakovenchuk V.N.[1,2], Mikhailova Yu.A.[1,2], Kalashnikov A.O.[1,2], Bazai A.V.[1,2]

[1]Nanomaterials Research Centre KSC RAS, Apatity, konoplyova55@mail.ru

[2]Geological Institute of the KSC RAS, Apatity

The Khibiny pluton, composed by 70 vol % of monotonous nepheline syenite (foyaite), is divided into roughly equal parts by Main conical fault zone, 28 km in diameter and 0.5-2.0 km in width at the surface. This fault zone is filled with melteigite-urtite and apatite-nepheline rock, while overlying foyaite has been transformed into leucite-normative poikilitic kalsilite-nepheline syenite (rischorrite) and transitional inequigranular nepheline syenite (lyavochorrite) as a result of kalsilite-orthoclase poikiloblastesis (Ivanyuk et al., 2012). Most of the listed rocks composed of nepheline, alkali feldspars, clinopyroxenes and amphiboles, which are distinguished by pronounced typochemistry. Minerals composition has been studied from rock specimens taken along profile A-B-C-D-E-F across all rock complexes of the pluton from its western margin (point *A*) via the Minor Arc (*B*) and Main Ring (*C*) to the center (*D*) and further via the Koashva deposit (*E*) to southern contact (point *F*) (fig. 1).

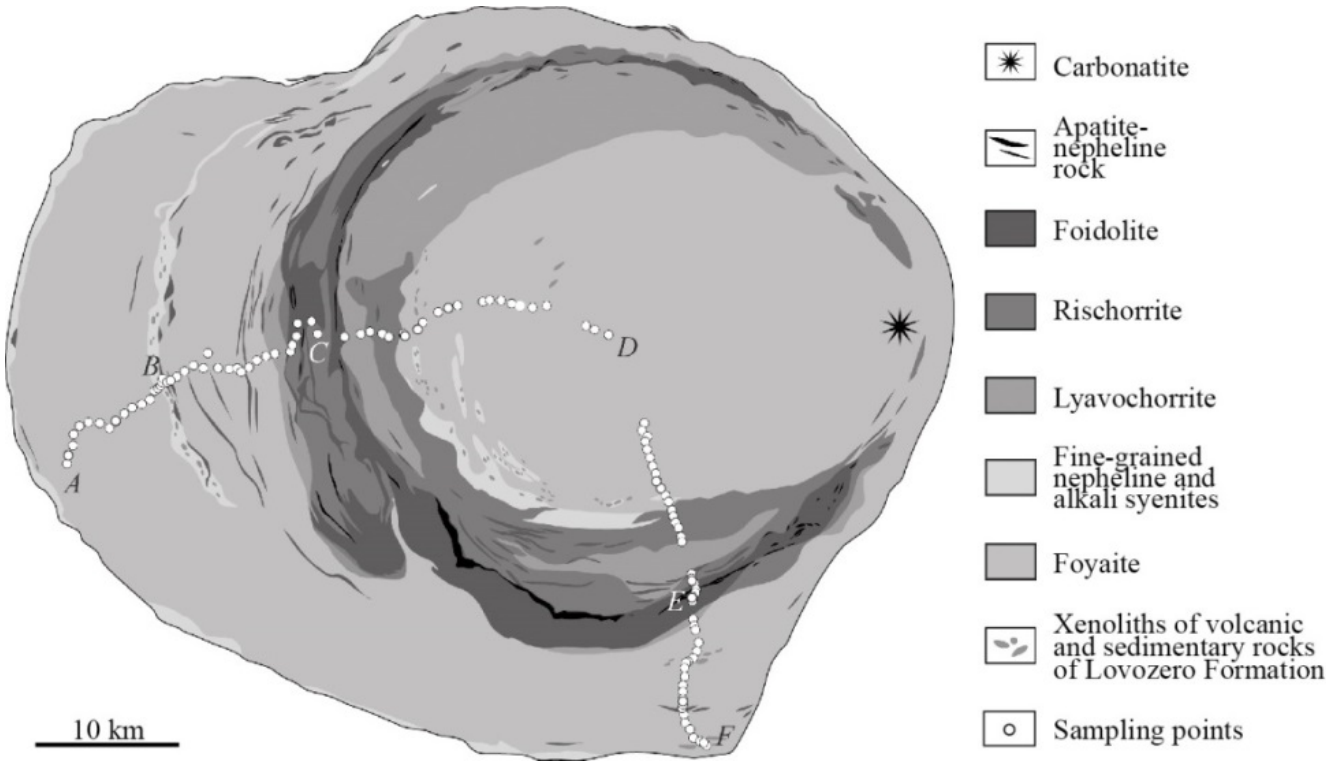

Fig. 1. Simplified geology map of the Khibiny massif (after Snyatkova et al., 1983). *A-B-C-D-E-F* – profile with sampling points.

<u>*Nepheline*</u> is a rock-forming mineral of foidolites, nepheline and alkaline syenites, fenite and pegmatite-hydrothermal veins where its content varies from the first per cent up to 90 vol. %/ Silica content in nepheline changes according temperature of rock forming (Yakovenchuk et al., 2010): 4.3 apfu in hornfels and foyaite (about 900 ^{o}C), 4.2 apfu in foidolite (about 500 °C), 4.1 a.p.f.u in rischorrite and apatite-nepheline rock (about 400 °C), and 4.0 a.p.f.u in pegmatite-hydrothermal veins (about 200 °C).

The chemical composition of nepheline in foyaite samples picked along the *A–B–C–D–E–F* profile (see Fig. 1) shows a regular change at moving from the outer and central parts of the massif towards the Main Ring. Thus, the change in nepheline composition from the outer and central parts of the massif towards the Main Ring can generally be expressed by the formula: $\square_B + (Si^{4+} + Fe^{3+})_T \leftrightarrow$

K^{+}_{B} + $2Al^{3+}_{T}$. Near the Main Ring, the substitution of Si for Al in nepheline from foyaite is accompanied by increasing of Na content in it (on the average, up to 3.2 atoms per molecule), whereas in nepheline from foidolites the preferred substitution of Si for trivalent Fe is compensated by K and Ba:

$$\square_A + K_B + Si_T \leftrightarrow Na_A + \square_B + Al_T \text{ – foyaite,}$$
$$Na_A + \square_B + Si_T \leftrightarrow \square_A + K_B + Fe^{3+}_{T} \text{ – foidolites.}$$

As a result, the high-potassium and iron-rich nepheline of foidolites is essentially different in composition from the high-sodium and iron-poor nepheline of the adjacent foyaite and, partly, rischorrite. Besides, the initially potassium-rich ijolite-urtite melt seems to have caused not only the subsequent wide development of orthoclasizing and kalsilitizing processes within foidolites (including apatite-nepheline rocks), but the alteration of ambient nepheline syenites as well.

Microcline and *orthoclase* are major minerals of alkaline and nepheline syenites, feldspar-bearing ijolite-urtite, fenite, hornfels of volcanogenic-sedimentary rocks, phonolits, alkali-feldspar trachytes and pegmatite-hydrothermal veins. Orthoclase essentially dominates in rischorrite, foidolites, fine-grained nepheline syenites and hornfels (in hornfels, together with anorthoclase); microcline is more common in pegmatite veins, while foyaite contains both the modifications, although in different proportions. Orthoclase-bearing foyaite is generally concentrated within the 5-km outer zone of the massif, and also on the periphery of the Main Ring where its gradational transformation to lyavochorrite and rischorrite is observed (Ivanyuk et al., 2010). The "purest" orthoclase is concentrated in outer parts of the foyaite complex, whereas in the center of the massif and in the Main Ring area the feldspar is represented by a variety transitive to anorthoclase. Feldspars in the central part of the pluton (point *D*) and the area of the Main Ring (points *C* anf *F*) are enriched in Al at the expense of Si. The replacement is compensated by the following schemes:

$$\text{(1) (K, Na) + Si} \leftrightarrow \text{(Ba, Ca) + (Al, } Fe^{3+}\text{) and (2) } \square + Si \leftrightarrow \text{(Na, K) + Al,}$$

which control the principial difference in the composition of the minerals studied in the central Khibiny massif and its Main foidolite ring. Thus, the potassium feldspar from foyaite from the central part of pluton is characterized by a chemical substitution corresponding to scheme (2) and this from nepheline syenite of the Main Ring corresponds to scheme (1) with participation of Ba. Feldspars from the ore (point *E*, Koashva deposit) and mineralized rock (point *C*) of the Main Ring primarily differ in the Na/K ratio. Orthoclase from large operating deposits is depleted in Na. Orthoclase of rischorrite, compared to that of foyaite, is essentially enriched with ferri-orthoclase and celsian constituents. The role of Ba and Fe increased at the final stages of orthoclase poikiloblasts formation owing to which the marginal zones of such poikiloblasts, both in rischorrite and in ijolite-urtite, are quite often represented by iron-rich hyalophane.

Taking into account the data on foyaite complex textural zonation, it becomes obvious that this complex initially had monotonous zonation with an orthoclase-dominant outer zone and microcline-dominant central part, and that the orthoclase-bearing rocks near the Main Ring were formed due to warming-up and metasomatic alteration of ambient foyaite by fluidized foidolite melts filling the ring fault.

The clinopyroxenes of the Khibiny massif, predominating in the majority of rocks, are represented by diopside, hedenbergite, augite, aegirine-augite and aegirine (Yakovenchuk et al., 2008). Diopside is a rock-forming mineral of alkali-ultrabasic rocks, alkali-feldspar trachytes, melteigite-urtite, metamorphosed to hornfels volcanogenic-sedimentary rocks of basalt composition and their host foyaite. Hedenbergite is observed in fenitized hornfels (after tuffite) where it together with aegirine forms parallel-columnar coronas around fayalite inclusions in albite.

Aegirine-augite is the main mineral of all types of nepheline syenites (5–50 vol. %), foidolites (up to 90 vol. %), apatite-nepheline rocks, fenitized rocks of the massif frame and xenoliths of volcanogenic-sedimentary rocks in foyaite. In foyaite of the outer and central parts of the massif, it predominates among the other iron-magnesium-bearing silicates and quite often occupies a position subordinated in relation to aegirine, alkaline amphiboles, and annite in foyaite, lyavochorrite and rischorrite of the Main Ring zone. Aegirine is a ubiquitous primary and/or secondary mineral forming

marginal zones around diopside-aegirine-augite crystals or separate needle-like crystals obviously formed later than the other clinopyroxenes.

Diagrams of a change in clinopyroxene composition along the *A–B–C–D–E–F* profile shows, above all, a different degree of rock differentiation in the Main Ring in its rich (the Koashva deposit, the *E* point) and poor ore (Mt. Marchenko Peak, the *C* point) parts. As the Main Ring is approached in the area at Mt. Marchenko Peak, the clinopyroxenes of foyaite feature increasing contents of Ca, Mg and Fe^{2+} at the expense of Na and Fe^{3+}, which proceeds on transition to rischorrite attaining the maximum in ijolite-urtite. Quite opposite is the situation in the area of the Koashva deposit, where the clinopyroxene of foyaite is represented by aegirine with traces of Ca, Mg and Fe^{2+}. However, the concentrations of these elements increase on transition to rischorrite and foidolites, with ijolite-urtite also containing clinopyroxenes of the diopside-hedenbergite series.

Diagram of the change of the Mg and Fe^{2+} ratio in clinopyroxene composition demonstrates consecutive increasing of the hedenbergite constituent from the border of the massif to the Main Ring, where all rocks contain clinopyroxene with a maximal content of Fe^{2+}, followed by an abrupt decrease in Fe^{2+}concentration to the center of the massif. The Mn content in the clinopyroxene composition decreases from the border to the Main Ring, suddenly rising in the massif's central part. The local maxima of Ti and V contents in clinopyroxenes are confined to the rock complexes of the Main Ring, whereas the increased content of Zr shows the position of the albitization ring at the contact between rischorrite and foyaite in the central part of the massif. Moreover, clinopyroxene in all types of rocks found on the Main Ring area are deficient in silicon compensated by aluminium and/or iron.

Amphiboles of the Khibiny massif are rather variegated (Konopleva et al., 2008): the total number of members in this group, scattered within the massif according to its general zonation, was found to be 25. Foyaite contains richterite, ferrorichterite, ferroeckermannite, arfvedsonite, magnesioarfvedsonite, katophorite, ferrikatophorite, magnesioferrikatophorite, ferrinyboite, and ferric-ferronyboite. Rischorrite is mostly characterized by the presence of potassicarfvedsonite, foidolites – of potassicrichterite. Dykes of alkali-ultrabasic rocks and alkali-feldspar trachytes contain pargasite, ferropargasite, hastingsite, magnesiohastingsite, and kaersutite; pegmatite-hydrothermal veins include potassicrichterite, potassicarfvedsonite, arfvedsonite, and magnesioarfvedsonite; in xenoliths of metamorphized volcanogenic-sedimentary rocks are present edenite, fluoredenite, magnesioferrikatophorite, arfvedsonite and ferric-ferronyboite.

The contents of almost all elements in amphiboles varies symmetrically relative to the Main Ring (point C), except for Si, whose content decreases from the margin of the Khibiny pluton to its center, and Zn, which appears in amphiboles only in the central part of pluton. Thus, amphiboles from foyaite adjoining the rischorrite–foidolite rocks of the Main Ring (0–2.5 km from the contact) correspond largely to richterite, ferrorichterite, and ferroeckermannite in composition. Amphiboles of the intermediate zone (2.5–10 km from the contact) include arfvedsonite and magnesioarfvedsonite in the outer, relative to the Main Ring, part of the Khibiny pluton. In the inner part, ferrinyboite, ferriferronyboite, magnesiokatophorite, and magnesioferrikatophorite are the most abundant. In foyaite of the marginal zone of the Khibiny pluton, amphiboles are identified as richterite, while in the central part, as katophorite, ferrikatophorite, and ferrorichterite.

Titanite is a through accessory (in places, rock-forming) mineral of all the rocks in the Khibiny massif (Ivanyuk et al., 2016). Its greatest concentration is observed in foidolites (up to 90 vol. % in apatite- and nepheline-titanite rocks) and nepheline syenites contacting with foidolites, especially those overlying the latter (up to 30 vol. %). Quite often, fenitized hornfels in xenoliths of volcanogenic-sedimentary rocks are enriched with titanite, up to the formation of orthoclase-ilmenite-titanite rocks containing 30–70 vol. % of this mineral. The composition of accessory titanite in foyaite varies along the *A–B–C–D–E–F* profile symmetrically to the massif's centre. In foyaite contacting with the rocks of the Main Ring, as well as in these rocks, titanite is appreciably enriched with Sr and Ti in comparison with titanite from the marginal zone and the central part of the foyaite complex:

$$(Ca, Mn)^{2+}Zr^{4+} \leftrightarrow Sr^{2+}Ti^{4+};\ Ce^{3+}(Fe, Al)^{3+} \leftrightarrow Sr^{2+}Ti^{4+}.$$

Here again, the composition of titanite, on transition from foyaite to rischorrite and, further, to foidolites, is observed to have increasing Ca contents (at the expense of *REE*, Na and Mn), Zr and Fe

(at the expense of Ti), and also Al (at the expense of Si), though this is not so pronounced as in foyaite from the parts far removed from the Main Ring.

Fluorapatite is a through accessory mineral of all the Khibiny massif rocks, becoming a rock-forming mineral in apatite-nepheline rocks. The content of fluorapatite is 0.2–1.0 vol. % in nepheline syenites, 1–7 vol. % in melteigite-urtite, achieving up to 98 vol. % in apatite-nepheline rocks (Konopleva et al., 2014). An examination of fluorapatite composition along the mentioned profile has shown that fluorapatite is released from Na, *REE*, and Si impurities in favour of Ca, Sr and P, as the foidolite ring is approached from the outer and central parts of the massif:

$$REE^{3+} + Si^{4+} \leftrightarrow (Ca, Sr)^{2+} + P^{5+} \text{ and } Na^{+} + REE^{3+} \leftrightarrow 2(Ca, Sr)^{2+}.$$

The behaviour of Ca and Sr is different in the ore and barren parts of the Main Ring: the larger deposit the lower Sr content. It is important that similar behaviour of these elements was also observed within the apatite deposits: the higher the ore grade (high content of P_2O_5) in fluorapatite, the smaller the quantity of Sr in its composition.

The above cited data on the features of rock-forming and accessory minerals composition within the Khibiny massif indicate that the majority of "through" minerals change the composition as the Main Ring is approached. The extreme contents of some of the elements in mineral compositions, which are related to the Main Ring, are usually superimposed on original monotonous zonation of the foyaite complex, manifesting itself in gradational change of the contents of these elements from the border to the center of the massif. During the formation of substantial zonation of the Khibiny massif, there occurred both plain concentration of elements in the composition of suitable phases and their redistribution between coexisting minerals parallel with their "auto-purification" from impurities. In the course of this process, the first to be formed are transitive metastable phases. At the next stage, numerous rare minerals are crystallized in situ, both in interstices of rock-forming minerals of the same rocks and in various types of pegmatite-hydrothermal veins. The zone of maximal differentiation in the mineral chemical composition is confined to the Main Ring, as is the zone of maximal differentiation of rocks.

This research was funded by the Kola Science Centre of RAS (Project 0226-2019-0051) and Presidium of the Russian Academy of Sciences (Program No 48).

References

Ivanyuk G.Yu., Konopleva N.G., Pakhmovsky Ya.A., Yakovenchuk V.N., Mikhailova Yu.A., Bazai A.V. Titanite of Khibiny Alkaline Massif (Kola Peninsula): New Data // ZRMO. 2016. No 3. P. 36–55 (in Russian).

Ivanyuk G.Yu., Pakhmovsky Ya.A., Konopleva N.G., Kalashnikov A.O., Korchak Yu.A., Selivanova E.A., Yakovenchuk V.N. Rock-Forming Feldspars of the Khibiny Alkaline Pluton, Kola Peninsula, Russia // Geology of Ore Deposits. 2010. Vol. 52. No 8. P. 806–817.

Ivanyuk G., Yakovenchuk V., Pakhomovsky Ya., Konoplyova N., Kalashnikov A., Mikhailova J., Goryainov P. Self-organization of the Khibiny alkaline massif (Kola Peninsula, Russia) // Earth Sciences (Ed. Imran Ahmad Dar). INTECH, 2012. P.131-156.

Konopleva, N., Ivanyuk, G., Pakhomovsky,Ya., Yakovenchuk, V., Men'shikov, Yu., Korchak,Yu. Amphiboles of the Khibiny alkaline pluton, Kola Peninsula, Russia // Geology of Ore Deposits. 2008. Vol. 50. No. 8. P. 720–731.

Konopleva N.G., Ivanyuk G.Yu., Pakhomovsky Ya.A., Yakovenchuk V.N., Mikhailova Yu.A. Typomorphism of Fluorapatite in the Khibiny Alkaline Pluton, Kola Peninsula // Geology of Ore Deposits. 2014. Vol. 56. No 7. P. 576-588.

Yakovenchuk, V., Ivanyuk, G., Konopleva N.G., Korchak Yu.A., Pakhomovsky Ya.A. Nepheline of the Khibiny alkaline pluton (Kola Peninsula) // ZRMO. 2010. No 2. P. 80–91 (in Russian).

Yakovenchuk, V., Ivanyuk, G., Pakhomovsky,Ya., Men'shikov, Yu., Konopleva, N., Korchak,Yu. Pyroxenes of the Khibiny alkaline pluton, Kola Peninsula // Geology of Ore Deposits. 2008. Vol. 50. No. 8. P. 732–745.

PROTEROSOIC QUARTZ-PORHYRY ASSOCIATED WITH RAPAKIVI GRANITES (SALMI BATOLITH)

Konyshev A.A.[1,2], Rusak.AA.[1,3], Anosova M.O.[1], Alekseev I.A.[4]

[1]Vernadsky Institute of Geochemistry and Analytical Chemistry, Moscow, Russia

[2]Institute of Experimental Mineralogy RAS, Chernogolovka, Russia

[3]Moscow State University, Moscow, Russia

[4]Saint-Petersburg State University, Saint-Petersburg, Russia,: icelopa@gmail.com

This work contains new data about quartz-porphyry associated with the Salmi batholith, which belongs to anorthosite-rapakivigranitic complexes (ARGC) of rocks. We have identified: the absolute age of the rocks by the zircon U-Pb method; the composition of the captured melt silicate inclusions, including their trace element composition; temperature of rock formation by various mineral thermometers; the presence of sulfide melt in the formation of rocks.

Introduction. At the end of the paleoproterozoic – the beginning of the mesoproterozoic (1.8-1.5 Ga), wide effused intraplate felsic magmatism of increased alkalinity took place on Earth. These events occurred on the site of stabilized early paleoproterozoic orogens. Large non-metamorphosed intrusions of anorthosite-rapakivigranite complexes (ARGC) are associated with the belts of this magmatism. Biotite-hornblende granites (rapakivi) are the earliest felsic rocks included in the ARGC. These rocks are rich in K, Fe, F, and oxygen fugacity during their formation was below the FMQ buffer. These granites have the largest area of distribution among the acid rocks of the ARGC. Effusive formations associated with rapakivi granite are known, but rare, often strongly altered, some of them are described in (Belyaev, 2013; Ehrlich et.al, 2013; Vorma, 1975; Kisvarsanyi, 1972). Effusive and sub-effusive formations, due to the more rapid formation compared to intrusions, can be a source of information about events that can be obscured or destroyed as a result of prolonged crystallization. Such information may be the mode of volatile components, the presence of such phase concentrators of the ore substance as sulphide or other non-silicate melt. Also, an extremely urgent task is to establish the relative temporal relationships of the rocks belonging to the ARGC, since often their absolute ages overlap within the limits of analytical errors. This work will discuss sub-effusive formations - igneous breccias with cement represented by quartz-porphyry.

Geological essay. The batholith is a member of the ARGC (Sharkov, 2005), located in South Karelia on the eastern shore the Ladoga lake at the junction of the Svekofen crust and the Karelian craton (Larin, 2011), formed in the range of 1549-1537 Ma (Amelin et al., 1994; Neymark et al., 1997). In the southwestern extremity of the Lupikko gneiss-granite dome (AR_2-PR_1), some researchers noted quartz-porphyry and magmatic breccia outcrops (Trustedt, 1907; Sviridenko, 1968; Sviridenko, 1984; Belyaev, 1985).

Quartz-porphyry are the series of backstage-like dikes located in the south-eastern tip of the Lupikko gneiss-granite dome (Sviridenko, 1968). Unfortunately, at the moment, quartz-porphyry outcrops noted earlier in the literature, are not available for observation, since are located at the bottom of a quarry flooded with water. Not altered quartz-porphyry were found in dumps along the quarry walls, and altered (potassic alteration) were found in the outcrop in the immediate vicinity of the dumps. The investigating sample of breccia consisting from cement represented by quartz-porphyry and fragments of host rocks. Xenoliths: gneisses of domes (AR_2-PR_1), amphibolites and mica schists (PR_1), and earlier granite phases: biotite-amphibole rapakivi granites with a texture of “rapakivi” (wiborgites), biotite fine-grained granites (their confinedness with the granites of the Salmi batholith is not currently defined), as well as altered xenoliths with clinopyroxene relics (magnesian skarn?).

Petrography. Quartz porphyry is a gray rock with a porphyritic structure due to the presence of resorbed quartz phenocrysts up to 6–8 mm in cross-section (1st Q generation) and iridescent potassium feldspar (Kfs) crystals up to 4 mm. Quartz and Kfs phenocrystals are unevenly distributed throughout the rock. The ground mass is represented by a fine-crystalline aggregate of, Kfs, albite and idiomorphic quartz crystals 100-300 μm in cross-section (2nd Q generation). Dark-colored silicates are represented by amphibole and biotite. Accessory mineralization: zircon, apatite, ilmenite, rutile,

pyrrhotite, chalcopyrite, sphalerite, galena. Quartz, Kfs, zircon - contain numerous silicate melt inclusions, also, inclusions of sulfide melts were found in quartz and zircon.

Research methods. Quartz-porphyry cement, for further study was cutted out from samples of breccia using a diamond circular saw. Petrochemistry of quartz-porphyry has been studied by XRF and ICP-MS. Transparently polished slide and polished slide were made from the obtained material for studying by optical microscopy and X-ray microanalysis (RSMA).

For isotope studies, zircons were separated from the rock. For the composition study of melt inclusions in minerals, zircons and two generations of quartz were separated from rock. Zircons from the rock were separated by dissolving the rock in HF and subsequently separation in heavy liquids. Due to the longer dissolution of quartz in HF compared to feldspars, idiomorphic quartz crystals 100–300 μm in diameter were also separated along with zircon. The larger resorbed quartz phenocrysts were cutted from sample by a thin (0.1 mm) diamond saw.

Quartz crystals with melt inclusions were heated with visual control on a «Linkam 1500» thermal cell at atmospheric pressure, but all inclusions were opened. After that, a series of experiments were carried out at the "gas-bomb" (UVGD-10000) in platinum ampoules with added or absence deuterium water. The pressure in the experiment was taken with a "margin", since the modern erosion section of the granitoid rocks of the Salmi batholith corresponds to depths with pressures up to 200 MPa (Rub et al., 1986; Poutiainen, Scherbakova, 1998). The experiments were carried out at temperatures: 850-875-900-950-1000 ^{o}C. Exposure from 3 to 20 hours, followed by rapid quenching, was made by dropping the ampoule into the cold zone. The products of the experiments were studied by RSMA, SIMS. Isotopic and geochemical zircon studies were carried out using LA-ICP-MS.

Estimation of the temperatures of mineral formation and capture of melt inclusions was carried out by evaluating the occurrence of Ti in quartz and zircon (Wark et al., 2008; Watson et al., 2006), as well as by evaluating the solubility of Zr in the melt (Watson, Harrison, 1983).

The resulting data. The age of the U-Pb method for zircons was determined (31 analyzes, concordia, LA-ICP-MS): 1541 +/- 9.4 Ma (MSWD 1.7). This data is close to the age of the "third magmatic impulse" (Larin, 2011), with the formation of rapakivi granites -1540-1538 Ma (Amelin et al., 1994, Neymark et.al., 1997).

The geochemistry and the distribution of REEs spectra of studied quartz-porphyry to be close to rapakivi granites of the Salmi batholith. The age of rapakivi granites falls within the limits of the analytical error of a certain age, but judging by the presence of their xenoliths with the characteristic rapakivi texture in quartz-porphyry cement - they were formed somewhat before the formation of quartz-porphyry.

Even at 20 hours of exposure at 1000 °C 300 MPa not all inclusions became homogeneous, it does not correlate with the dimensions of inclusions. Practically all inclusions from small idiomorphic quartz crystals did not achieve homogeneity up to the maximum parameters for the exposure time and T-P, have significant amount of Kfs (heterogeneous capture?). In all quartz crystals, a grid of cracks is present, probably originating from the α-β transition, in large resorbed phenocrystals this is more pronounced than in small idiomorphic crystals.

According to SIMS data, it was revealed that all analyzed heated melt inclusions from 1st Q generation (5 analyzes) contain from 0.124 to 0.004% by weight of deuterium water with a total content of protium water from 4.36% to 0.935% by weight (last data with 0.004% deuterium). Melt inclusions from 2nd Q generation (5 analyzes) contain from 0.269 to 0.088% by weight of water (deuterium not added). Silicate melt inclusions in zircon are too small to be studied using SIMS, less than 30 microns.

Quartz-porhyry has a composition that corresponds to rhyolite, close to the boundary of trachyrhyolite. The compositions of melt silicate inclusions have a trend from phonolite (in 2nd Q generation) to low-alkaline rhyolite (1st Q generation). The compositions of melt inclusions of two generations of quartz intersect in the zone of trachyte/trachydacite/pantellerite/trachyriodacite. In this zone there is also the main swarm of compositions of melt inclusion in zircons. Also several compositions of melt inclusion in zircon is located in the field of phonothephrite/trachyandesite.

The content of trace elements in silicate melt inclusions. Melts during the formation of quartz porphyry are characterized by elevated concentrations of zinc, an average of 160-200 ppm, which is close to the content in the rock (194ppm). Cu and Ni contents averaged 5,8 and 2,9 ppm, which is almost by half an order of magnitude less than the content in the rock (38 and 16 ppm respectively). The content of Ta and Nb in general correlate with each other, but Ta is somewhat larger in glass (on average, 2.9 ppm Ta relative to 3,5 in rock and 37 ppm Nb relative to 48,2 in rock). This is probably due to the occurrence of Nb in ilmenite, where content of Nb according to RSMA is up to 0.4 – 0.5 wt.%. In melt inclusions from 2nd Q generation Rb is distributed higher than 2-3 times for the rock, which probably indicates a heterophase capture of a Kfs with the melt. The spectrum of Kfs was been determined by RAMAN spectroscopy in not completely homogeneous melt inclusions in 2nd Q generation.

Estimates of mineral formation temperatures. The method of incorporating Ti into zircon (Watson et al., 2006) provides estimates of the mineral formation temperatures of 700–870 °C with a distribution peak at 780–840 °C. A single grain gave an estimate of the temperature of 950 °C. The determinations were carried out using RSMA (14 measurements) and LA-ICP-MS (14 measurements).

The method of incorporating Ti into quartz (Wark et al., 2006) provides temperature estimates for quartz phenocrysts of 725-790 °C (1st Q generation, 13 measurements) and for idiomorphic quartz crystals 620-830 ° C (2nd Q generation, 7 measurements). All Ti values in quartz are determined using RSMA. In the calculations, it was assumed that $\alpha Ti = 1$.

Estimates of the capture temperature of inclusions. The Zr melt saturation method (Watson et al., 1983) showed a temperature range from 720 to 870 °C with a peak of 820-840 °C. All Zr values in melt inclusions were determined using SIMS, 6 analyzes for each inclusion in quartz (1 and 2 generations). The same method for a rough estimate of the rock formation temperature (by Zr in Rock) it gives an estimate of the temperature 914 °C.

Sulfide inclusions. Inclusions of sulphide melts were found in zircons and single inclusions in 2nd Q generation. Sulphide melt inclusions have rounded shapes, sometimes non-isometric, up to 20-25 microns in cross-section. Melt inclusions of heterophase capture of sulphide-silicate composition were also detected. Inclusions of sulphide melts are closer in composition to pyrrhotite, from the mineral phases inside such an inclusion - chalcopyrite was found. In sulphide inclusions, textures of the solid solution splitting are observed. According to RSMA, elevated concentrations of some chalcophile elements are observed: Cu, Co, Ni, Zn up to 0.2, 1, 0.25, 0.6 wt% respectively. There are references in the literature about inclusions of sulphide melts in zircons of phanerozoic quartz porphyry (Simpson, 2014).

In the study on elements-pollutants in bottom sediments of Ladoga Lake, a correlation of Cd are related to Zr and Hf was found (Ivanter et al., 2016; Slukovsky, 2013), it was concluded that the elevated concentrations of Cd is connected to zircons. Cd is cannot isomorphically icorporated in zircon due to a different valence and ionic radius. Although Cd in sulphide melt inclusions was not detected by us using RSMA, its presence is theoretically possible due to its chalcophilicity. Probably, zircon in bottom sediments of Ladoga lake contains sulphide melt inclusions or phases of sulphides. The Wyborg batholith has known preserved cover of quartz-porphyry (Belyaev, 2013; Ehrlich et al., 2012). Probably, the Salmi batholith also had effusives of quartz-porphyry in the past, destroyed by erosion with the formation of sedimentary rocks around Ladoga lake - source of zircon with Cd in modern sediments.

Conclusion. The quartz-porphyry of the Salmi batholith is 1541 +/- 9.4 Ma, their formation occurred after the formation of rapakivi granites. Their formation occurred in the range from 870 to 700-725 °C. Resorbed grains of quartz and Kfs can be associated with melting as a result of an adiabatic uplift of magma, with which droplets of sulphide melt of unknown origin were captured. The formation of these rocks occurred at fO_2 below the FMQ buffer.

Acknowledgments. *Simakin S.G., Kovalchuk E.V., Shcherbakov V.D., Terekhin A.A., and Kuznetsov N.I. For assistance in conducting analytical and experimental work. This work is supported by RFBR grant 18-05-01101.*

References

Amelin Yu., V., Larin A. M., Tucker R. D. Chronology of the Salmi Rapakivi granite-anorthosite complex, Baltic Shield: Implications for Magmatic Evolution // Mineral. Petrol. 1997. V. 127. p. 353-368.

Belyaev A.M. Patterns of distribution of ore elements in pegmatites, pegmatoid granites and granite gneisses of the Northern Ladoga area // In the book. “Regularities of concentration of ore elements in granitoid formations of the Karelian-Kola region”, Apatity, 1985, p. 89-96 (in Russian).

Belyaev A.M. Petrology of volcanic rocks of the rapakivi formation (Gogland Island) // Regional geology and metallogeny, No 55, 2013 (in Russian).

Ehrlich K., Ver. E., Kirs J., Soesoo A. Using a titanium-in-quartz geothermometer for crystallization temperature estimation of the Palaeoproterozoic Suursaari quartz porphyry // Estonian Journal of Earth Sciences, 2012, 61, 4, 195.204.

Ivanter E.V., Slukovsky Z.I., Dudakova DS, Medvedev A.S. Svetov S.A. Evidence of the zircon nature of the cadmium anomalies in the bottom sediments of the northern part of Lake Ladoga // Reports of the Academy of Sciences, 2016, vol. 468, No 5, p. 562–565 (in Russian).

Kisvarsanyi E.B. Petrochemistry of Precambrian igneous province, St. Petersburg Francois Mountains, Missouri // Report of Investigations. N 51. Rolla, Missouri, USA, 1972. - 97 p.

Larin A.M. Rapakivi granites and associated rocks // Ed. "The science" . St. Petersburg. 2011. 402 p. (in Russian).

Neymark L. A., Amelin Yu. V., Larin A.M. Pb-Nd-Sr isotopic and geochemical constraints of the 1.54-1.56 Ga Salmi rapakivi granite-anorthosite batholith (Karelia, Russia) // Mineral. Petrol. 1994. V. 50. p. 173–193.

Poutiainen M, Scherbakova, T. F. Fluid and melt inclusions evidence for the origin of idiomorphyc quartz crystal in topaz-bearing granites from the Salmi batholith, Karelia, Russia // Lithos, 1998, V. 44. P. 141—151.

Rub M.G., Khetchikov L.N., Kotelnikova Z.A., Rub A.K. Inclusions of mineral-forming environments in the minerals of Precambrian tin-bearing granites of the Northern Ladoga area // Proceedings of the Academy of Sciences of the USSR, geological series, 1986, No. 1, p. 30-36. (in Russian).

Sharkov E.V. The Proterozoic anortosite-rapakivigranite complexes of the East European Craton are a technique for intraplate magmatism under conditions of anomalously powerful sialic crust // Lithosphere, 2005, № 4, p. 3-21.

Simpson, R., Sulfide inclusions in zircon and their significance to understanding the evolution of copper porphyries in the Macquarie Arc, New South Wales, Bachelor of Science (Hons.), School of Earth and environmental Sciences, University of Wollongong, 2014, 197p.

Slukovsky Z.I. The origin of cadmium in the bottom sediments of the rivers of the city of Petrozavodsk: technogenesis or nature? // Geology and minerals of Karelia. - 2013. - Vol. 16. - pp. 132–136.

Sviridenko L.P. Petrology of the Salmi granite-rapakivi massive (Karelia) // Petrozavodsk: Karelia Publishing House, 1968. 116 p. (in Russian).

Sviridenko L.P., Svetov A.P., Golubev A.I., Pavlov G.M. Topaz-containing tuffisites of the southern margin of the Baltic Shield // Reports of the Academy of Sciences, vol. 276, No. 6, 1984, pp. 1449-1452. (in Russian).

Trüstedt, O., 1907. Die Erzlagerstätten von Pitkäranta amLadoga-See // Bulletin de la Commission Geologique de Finlande no 19. Frenckellska Tryckeri-Aktiebolaget, Helsingfors.

Vorma A. On two roof pendants in the Wiborg rapakivi massif, Southeastern Finland // Geological Survey of Finland Bull. 272, Geologinen tutkimuslaitos Espoo, 1975. - P. 2–46.

Wark, D.A., Watson, E.B. TitaniQ: a titanium-in quartz geothermometer // Mineral. Petrol., 2008, 152, 743.754.

Watson E.B., Harrison M.T. Zircon saturation revisited: temperature and composition effects in a variety of crustal magma types // Earth and Planetary Science Letters, 1983, 64 295-304.

Watson E.B., Wark D.A., Thomas J.B. Crystallization thermometers for zircon and rutile // Contrib Mineral Petrol, 2006, 151: 413–433.

PATHWAYS AND LIMITATIONS OF CATION DIFFUSION IN ION-EXCHANGED SINGLE CRYSTALS OF THE MICROPOROUS TITANOSILICATE ETS-4

Kostov-Kytin V.V., Nikolova P.N.

Bulgarian Academy of Sciences, Institute of Mineralogy and Crystallography "Acad. Ivan Kostov", 1113 Sofia, Bulgaria, vkytin@abv.bg

The synthetic zeolite-like titanosilicate ETS-4 (Engelhard Titanium Silicate-4), was patented by Kuzniki et al. in 1989. Since then the interest of the scientific community towards preparation of microporous and layered titanosilicates with potential application in various areas of technology such as catalysis, gas separation, energy storage, optoelectronics, radioactive waste management, etc. has steadily increased. ETS-4 has as a natural analogue the mineral zorite. Sandomirskii and Belov recognized the order-disorder character of zorite structure and solved its superposition (family) structure in the space group Cmmm (1979). The averaged structure model of these authors is also applicable to ETS-4 materials (as-synthesized and ion-exchanged forms). It can be described as consisting of chains of TiO6 octahedra (Ti1) parallel to the [010] direction laterally linked by a chain of four SiO4 tetrahedra along [100] direction. These SiO4 groups are linked in [010] direction by a chain-bridging unit including the Ti2 site disordered over two sites that are symmetrically equivalent relative to the (001) mirror plane (Fig. 1). Detailed discussion on the crystal chemical peculiarities of zorite and Na-ETS-4 and their behavior upon heating is presented by M. Sacerdoti and G. Cruciani in 2012 and in the references, therein. The ion-exchange forms of zorite and ETS-4 have also been intensively studied: (Spiridonova et al. 2012 and references therein; Nikolova et al. 2013; Tsvetanova et al. 2015, 2018).

In the present study single crystal and polycrystalline synthetic samples of ETS-4 prepared hydrothermally (Kostov-Kytin et al. 2007) have been subjected to identical ion-exchange procedures thus expanding the existing knowledge for this material. Initial samples have been treated with 1M chloride solutions of the chosen exchangeable cations at 60 °C for three days. Certain trends and consistencies have been revealed between the ionic radii, charge, and degree of sites occupancy of the exchangeable cations and the thermal stability of their host-compound. These relations have been considered from a crystal chemical point of view. Ionic radii of the exchangeable cations and distances measured for certain inter-structural directions predetermining pathways and limitations for the extra-framework cation diffusion have been involved. Appropriate data for such approach have been taken from (Shanon, 1976) and the effective distances have been obtained by subtracting twice the oxygen radius (1.35 Å) from the distances between the centers of the atoms.

Table 1 provides data for the type of the extra-framework cations and the degree of the achieved ion-exchange upon the applied experimental conditions. For certain cases the results are remarkable in terms of the theoretical capacity calculated for the ideal formula of the studied compound (Young, 2011) and reveal ETS-4 affinity for large divalent cations (e.g. Ba, Sr, Mn and Zn) and large monovalent ones (e.g. Cs and Ag). The data obtained for the smaller divalent cations (e.g. Mg, Cu, and Ni) are somewhat ambiguous and rather imply the idea for leaching of the extra-framework (Na, K) cations from the as-synthesized samples upon the experimental procedures. Figure 1 illustrates the extra-framework cations diffusion pathways and limitations in terms of the 6- and 8-memebered rings constructing the channels running along [010] and the 7-membered apertures [001] including the Ti2-bridging units which plug transitions along the 12-membered rings forming channels along the *c*-direction. The extra-framework cation sites distinguished into three groups by Spiridonova et al. (2012) and denoted as AI, AII, AIII have also been shown. Cs is the only cation registered in AIII position and its residence there has obviously been due to the size of its cations (Nikolova et al., 2013). Smaller cations continue their drift from the 8MR gates within the 12MR cages towards the 6MR channels. A preference is given to the divalent cations obviously due to the stronger bonds they form with the framework cations. The initially residing in the 6MR channels Na cations (AI position) are readily replaced by Ag, Zn, Mn, however the bigger Sr and Ba cannot penetrate and the smaller ones like Cu and Ni cannot hold, therein. Data for Mg are contradictory as seen from comparison of the chemical compositions from single crystal and polycrystalline samples. Sr, Ba as well as the rest of the

Table 1. Chemical composition of ETS-4 and its ion-exchanged forms obtained by EPMA and single crystal X-ray diffraction and related physico-chemical data.

Extra-framework cations	(R.D. Shannon, Acta Cryst., A32. 1976)		EPMA – poly-crystalline samples*	EPMA – single crystal samples*	Stoichiometric formula from single crystal X-ray analyses (this study)	Thermal stability upper limit (°C)** (this study)
	Coord. Number	Ionic radii (Å)				
1	2	3	4	5	6	7
Na^+	4-8 (Na^+)	1.13-1.18	-	-	**$Na_9Si_{12}Ti_5O_{38}(OH)\bullet 12H_2O$** Ideal formula (Young, D.N., 2011)	-
K^+	4-8 (K^+)	1.37-1.51	$Na_{8\text{-}9}$ $K_{1\text{-}1.5}$	$Na_{8.8}$ $K_{1.1}$	**$H_{2.36}Na_{5.92}K_{0.72}Si_{12}Ti_5O_{38}(OH)\bullet 11.3H_2O$** (As-synthesized single crystals)	240
Cs^+	6-8	1.67-1.74	$Cs_{4.21}$ $Na_{2.41}$	$Cs_{3.28}$ $Na_{3.06}$	**$H_{3.79}Cs_{4.01}Na_{1.2}Si_{12}Ti_5O_{38}(OH)\bullet 8.12H_2O$**	500
Ba^{2+}	6-8	1.35-1.42	$Ba_{1.68}$	$Ba_{3.84}$	**$H_{0.38}Ba_{4.31}Si_{12}Ti_5O_{38}(OH)\bullet 4.52H_2O$**	380-400
Ag^+	4-8	1.02-1.28	$Ag_{7\text{-}9}$	$Ag_{8.29}$	**$H_{3.17}Ag_{5.83}Si_{12}Ti_5O_{38}(OH)\bullet 9.9H_2O$**	300
Sr^{2+}	6-8	1.18-1.26	-	$Sr_{3.95}$ $Na_{0.65}$	**$Na_{0.64}Sr_{3.86}Si_{12}Ti_5O_{38}(OH)\bullet 11.5H_2O$****	330-350
Mn^{2+}	4-8	0.66-0.96	$Mn_{3.8}$ $Na_{0.3}$ $K_{0.4}$	$Mn_{2.13}$ $Na_{1.48}$ $K_{0.89}$	**$H_{0.08}Mn_{4.46}Si_{12}Ti_5O_{38}(OH)\bullet 8.73H_2O$**	360-380
Zn^{2+}	4-8	0.6-0.9	$Zn_{4.34}$	$Zn_{3.52}$ $Na_{0.20}$ $K_{0.13}$	**$H_{0.14}Zn_{4.43}Si_{12}Ti_5O_{38}(OH)\bullet 9.84H_2O$**	350
Mg^{2+}	4-8	0.57-0.89	$Mg_{0.88}$ $Na_{2.3}$ $K_{0.78}$	$Mg_{2.95}$ $Na_{0.90}$ $K_{0.74}$	**$H_{1.70}Mg_{3.10}K_{1.10}Si_{12}Ti_5O_{38}(OH)\bullet 8.8H_2O$**	170
Cu^{2+}	4-8	0.57-0.73	-	$Cu_{2.16}$	**$H_{3.66}Cu_{2.67}Si_{12}Ti_5O_{38}(OH)\bullet 7.40H_2O$**	-
Ni^{2+}	4-8	0.55-0.69	$Ni_{0.5—2.0}$	$Ni_{0.51}$ $Na_{0.60}$ $K_{0.61}$	**$H_{5.08}K_{0.001}Ni_{1.96}Si_{12}Ti_5O_{38}(OH)\bullet 6.44H_2O$**	-

* Electron probe microanalyses. Only calculated exchangeable atoms per formula unit are presented.

** Data taken from thermogravimetric and differential thermal analysis (TG/DTA) of powdered samples and in situ time resolved powder X-ray diffraction experiments except for Sr-exchanged samples for which data are taken from (Nair et al., 2001).

Ag, Zn, Mn entering the structure appear to be trapped in the AII position nearby the 7MRs. Suchlike arrangement of the extra-framework cations is predetermined as by their charge as well as by their size and of course the degree of site occupancies which on its side depends also on the applied experimental procedure conditions. Previous investigations on heat-treated Sr-exchanged and as-synthesized ETS-4 samples have pointed to the fact that the (SiO4) 8MRs exhibits amazing flexibility expressed in its expanding and contraction upon the dehydration process at certain directions (Nair et al., 2001; Sacerdoti and Cruciani, 2012). Recently, Kostov et al. (2018) have reported that after the dehydration is complete and upon further heating this basic fragment in the structure of Zn-exchanged ETS-4 is affected by new expansion that occurs on the account of the adjacent 6MR channels contraction and distortions of the Ti1-O-Ti1…chains where subsequently the structural collapse starts from.

Our study suggests that the extra-framework cations type and disposition especially within the 6MR channels play a key-role over the structural stability of the exchanged forms upon heating. The big cations residing within the 8MR channels (position AIII in Figure 1) can restrict from inside their thermal expansion because of their bonds with the framework oxygens. Table 1 provides data for the

Cs-form stability up to 450-500 °C. On the other hand, the cation species from the 6MR channels withstand such expansion from outside the 8MR. The bigger their sizes, the stronger their bonds with the framework oxygens, and the greater the degree of site occupancies, the slower the enlargement of the 8MRs and the contraction of the 6MRs (AII position in Fig 1) and the subsequent structural collapse. The same suggestions refer to the impact of the cations positioned in AI. In this respect the exchange processes concerning the smaller cations (Mg, Cu, and Ni) can be considered as a leaching procedure for the treated material affecting its bulk composition and depriving it from the supporting its structural stability upon heating extra-framework cations (Table 1, thermal data for Mg).

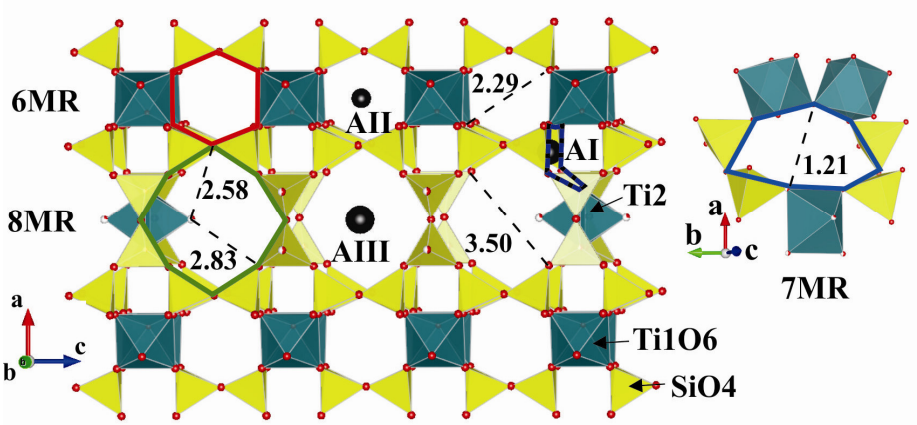

Fig. 1. Framework of the as-synthesized Na-K-ETS-4; AI, AII, and AIII – groups of extra-framework cation sites (Spiridonova et al., 2012); the numbers are the smallest effective distances (see text) measured in Å within the 6-, 7-, and 8-membered rings, designated as 6MR (red contour), 7MR (blue one), and 8MR (green one), correspondingly.

This work was financially supported by the National Science Fund of Bulgaria under contract No. DNTS/Russia 02/8 from 15.06.2018.

References

Kostov-Kytin V., Nikolova R., Avdeev G. XRD study on the structural evolution of Zn-exchanged titanosilicate ETS-4 during thermal treatment // Bulgarian Chemical Communications, Volume 50**,** Special Issue F. 2018. p. 62–72.

Kostov-Kytin V., Ferdov S., Kalvachev Yu., Mihailova B., Petrov O. Hydrothermal synthesis of microporous titanosilicates // Microporous Mesoporous Materials., 2007, **105**, 232-238.

Kuzniki S.M. Large-pored crystalline titanium molecular sieve zeolites // US Patent, 1989, 4:853–202.

Nair S., Jeong H.K., Chandrasekaran A., Braunbarth C., Tsapatis M., Kuznicki. Synthesis and structure determination of ETS-4 single crystals // Chem Mater. 2001 13: p. 4247–4254.

Nikolova R., Shivachev B., and Ferdov S. Crystal structures of Mg 2+, Ba 2+ and Cs+ exchanged K–Na–ETS-4 // Microporous and Mesoporous Materials. 2013. 165: p. 121-126.

Sacerdoti M., and Cruciani G. Comparison of Structural Changes upon Heating of Zorite and Na-ETS-4 by In Situ Synchrotron Powder Diffraction // In: S.V. Krivovichev (ed.) Minerals as Advanced Materials II., Springer, 2011, p. 187-197.

Sandomirskii P.A., Belov N.V., The OD structure of zorite // Sov. Phys. Crystallogr. 1979, 24:686–693, Kristallographiya 24: p. 1198–1210.

Shannon R.D. Revised Effective Ionic Radii and Systematic Studies of Interatomic Distances in Halides and Chalcogenides // Acta Cryst. 1976. A32, p. 751-767.

Spiridonova D.V., Krivovichev S.V., Britvin S.N., and Yakovenchuk V.N. Crystal Chemistry of Ion-Exchanged Forms of Zorite, a Natural Analogue of the ETS-4 Titanosilicate Material // in In: S.V. Krivovichev (ed) Minerals as Advanced Materials II., Springer, 2012, p. 199-204.

Tsvetanova L., Petrova N., Ferdov S., Kostov-Kytin V., Nikolova R., Crystal structure of Ag+ exchanged ETS-4 at room temperature and 150 K // Bulgarian Chemical Communications, Volume 47, Number 1. 2015. pp. 201–207.

Tsvetanova L., Kostov-Kytin V., Ferdov S., Nikolova R. Elastic behavior of the titanosilicate framework in Mn-ETS-4 // Bulgarian Chemical Communications, Volume **50**, Special Issue F. 2018. pp. 80-85.

Young D.N. Cation exchange properties of highly charged swelling micas and titanosilicates // A Dissertation in Soil Science, 2011, pp. 1-138.

EXPERIMENTAL STUDY OF POSTMAGMATIC PROCESSES IN GABBROIDES OF TIKSHEOSERSKY MASSIF (NORTH KARELIA)

Kovalskaya T.N., Varlamov D.A., Shapovalov Yu.B., Kotelnikov A.R., Kalinin G.M.
D.S. Korzhinskii Institute of Experimental Mineralogy of Russian Academy of Sciences, Chernogolovka, Russia, tatiana76@iem.ac.ru

Tikshozersky massif refers to the formation of ultrabasic alkaline massifs with carbonatites. In contrast to the well-known alkaline massifs with the Caledonian-Hercynian carbonatites the Tikshozersky massif belongs to the earliest Proterozoic sub-platform complex on the territory of the Fennoscandinavian shield. The Tiksheozersky massif is represented by a round-elliptical body with a diameter of about 20 km, and is composed of olivinites, gabbros, pyroxenites (sometimes with nepheline), ijolites, carbonatites, amphibole-calcite-cancrinite rocks. The carbonatites of the massif compose the rod-shaped bodies with the size of tens of meters, eruptive formations of breccia-like texture, veins and veinlets (Safronova, 1990). The largest body of carbonatites of the Tikshozersky massif is traced by drilling to a depth of 450 m. Apatite-calcite ores of a complex type are found in the carbonatites of the massif (Metallogenia ..., 2001). All rocks of the Tikshozersky massif are highly modified, but if the changes observed in olivinites and pyroxenites are typical of ultrabasic rocks, then changes in gabbroids have a pronounced "alkaline" character. The rims of alkaline amphiboles of the pargasit-cataphoritic-rhyterite series appear around the clinopyroxenes of the diopside-hedenbergite series. Mineral associations of the Tikshozero massif are described in more detail in Kovalskaya et al., 2018.

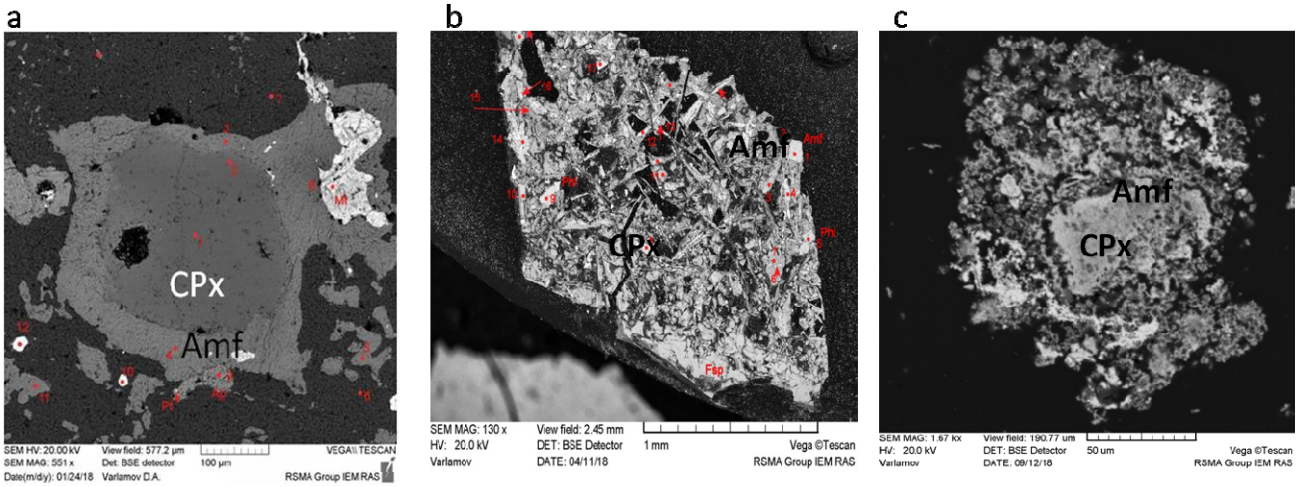

Figure 1. Clinopyroxenes with amphibole rim from Tiksheozersky massif (a) and experiments (b, c).

With the aim of recreating the conditions of post-magmatic changes formation in gabbro, experiments were carried out in modeling of gabbro amphibolization, as there were detected amphibole rims around clinopyroxene in the samples of gabbro from the Tiksheozersky massif. The experiments were carried out in platinum ampoules of Ø 4-5 mm. The duration of experiment was from 10 to 14 days. As a starting mixture, finely ground gabbro from the Lukkulaisvaara massif (Karelia) was used, since these rocks are practically not subject to secondary changes, and their mineral composition is close to the Tiksheozero gabbro massif. Solutions with a concentration of 0.5 M, 1 M, and 2 M, respectively, were used as the fluid. The experiments were carried out with chlorine-containing and fluorine-containing fluids, co-cracking and fluorine and chlorine were accumulated in the ant groups of sodalite, apatite, and biotite. The sample to fluid ratio was 10: 1. First, for three hours, the reaction mixture was maintained at a temperature of 1100 and a pressure of 3 kbar, then isobaric cooling occurred to 850. The products of the experiments were greenish crystalline formations. during the study with Tescan Vega II XMU (Tescan, Czech Republic) equipped with an INCA Energy 450 X-ray microanalysis system with energy dispersive (INCA Xsight) and crystal

diffraction (INCA wave 700) X-ray spectrometers (Oxford Instruments, England) and the software platform INCA Energy +. A scanning electron microscope obtained the following results. In the products of the experiment, where 0.5 M solution of potassium fluoride and potassium chloride were used as fluids, alkaline amphiboles were not detected, single fluorite grains and biotite were diagnosed. Amphiboles obtained in experiments with a 1 M solution of KF are similar in composition to the natural alkaline amphiboles, but they contain less calcium. One of the reasons for this phenomenon may be the late carbonatization of rocks that occurred. The closest in composition to natural amphiboles were diagnosed in experiments with 1 M KCl (fig. 1, tabl. 1). Probably, this is the most probable mechanism for the formation of alkaline amphibole rims around clinopyroxenes in the gabbroids of the Tikshozersky massif. The latter assumption is confirmed by the presence of coexisting chlorine - sodalite and amphibole in parageneses at lower temperatures. The formation of alkaline amphibole-sodalite paragenesis requires further experimental study.

Table 1. Composition (in wt.%) of amphiboles from Tiksheozersky massif and experiments.

component	Natural samples						Experimental samples	
	T176-140	T7	t158-203	t158-210	t158-213	t158-203	Synthetic amphibole (1M KF)	Synthetic amphibole (1M KCl)
SiO_2	44.08	41.33	43.27	49.10	40.21	51.91	47.18	46.12
TiO_2	0.48	0.06	1.41	0.91	1.07	0.94	1.32	0.86
Al_2O_3	11.20	17.28	10.91	6.53	14.30	4.06	12.78	10.42
FeO^*	16.43	20.44	18.57	13.23	19.38	13.75	14.94	15.91
MnO	0.00	0.13	0.05	0.00	0.19	0.09	0.25	0.03
MgO	11.81	6.36	10.81	15.60	9.06	14.70	12.32	13.81
CaO	13.47	11.96	9.00	8.68	10.93	7.30	6.14	8.01
Na_2O	1.29	1.85	5.16	5.43	3.57	6.66	2.24	3.71
K_2O	1.24	0.58	0.81	0.52	1.30	0.59	1.83	1,13
Total	100.00	100.00	100.00	100.00	100.00	100.00	100.00	100.00

All iron in microprobe analyzes is presented as total FeO.

In experiments with 2 M solutions, clinopyroxns relicts were not observed, all of them were replaced by newly formed amphibole. Kalsilite -like phases were also diagnosed. In these experiments, the appearance of noticeable amounts of magnetite was also observated, which was not the case in experiments with lower concentrations of salts (KCl and KF) in the fluid. It may be necessary to introduce sodium into the system, since in natural samples an increase in the sodium content of late amphiboles is described.

References

Kovalskaya T.N., Varlamov D.A., Kotelnikov A.R., and Kalinin G.M. Tikshozero Massif Mineral Associations (North Karelia, Russia), in the IX International Symposium "Mineral Diversity — Research and Conservation" . October 16-18, 2017. Reports. Sofia, Bulgaria, pp. 183–190, National Museum of Land and People Sofia, Bulgaria, 2018.

Metallogeny of magmatic complexes of intraplate geodynamic settings. M .: GEOS, 2001, 640 p. In russian.

Safronova G.P. Rock-forming carbonates and apatite of the Tikshozero massif // New in mineralogy of the Karelian-Kola region Petrozavodsk, 1990. P. 25–39. In russian.

MECHANISM OF ENRICHMENT OF LATE CARBONATITES BY HEAVY RARE-EARTH ELEMENTS: CASE STUDY OF THE PETYAYAN-VARA FIELD (VUORIYARVI MASSIF, NW RUSSIA)

Kozlov E.N., Fomina E.N.

Geological Institute, Kola Science Centre, RAS, Apatity, Russia, kozlov_e.n@mail.ru

Carbonatites are known as a source of light rare earth elements (LREE). However, heavy rare earths (HREE) are of greater interest for modern industry. Occasionally, early (magmatic) carbonatites are enriched with HREE (Xu et al., 2007). Late carbonatites with HREE mineralization associated with late-stage hydrothermal phenomena are more widespread [e.g., Tundulu, Malawi (Ngwenya, 1994); Songwe-Hill, Malawi (Broom-Fendley et al., 2017); Bear Lodge, U.S. (Moore et al., 2017); Lesser Qinling, China (Smith et al., 2018)]. The researchers emphasize several hypotheses on the reasons for the HREE enrichment of late carbonatites. Among the possible versions are the HREE enrichment of the primary source, the passive enrichment of minerals due to the selective removal of LREE, and the REE transfer agency of fluids rich in sulfur, phosphorus, chlorine and/or fluorine. Probably, several mechanisms are responsible for the enrichment of late carbonatites with heavy rare earths. As a result of these mechanisms, xenotime-(Y) (Wall et al., 2008; Andersen et al., 2016; Smith et al., 2018), brockite-(Y) (Andersen et al., 2016), mckelveyite-(Y), ewaldite, donnayite-(Y) (Zaitsev et al., 1998) and other HREE mineral phases were formed in these rocks. However, Y-rich fluorapatite is the main concentrator of HREE in late carbonatites. For several complexes, it is associated with economic potential. In carbonatites of the Petyayan-Vara field (Vuoriyarvi massif), this mineral is also the principal HREE carrier.

In the Petyayan-Vara, apatite mineralization (hereafter, “apatitization”) is associated with Ti-rich rodbergites. The principal minerals of these rocks are Ca-Mg-Fe carbonates, sodium- and barium-free microcline, and titanium and iron oxides (mainly brookite and hematite, respectively). Quartz, calcite, Ti-rich phlogopite, apatite, Ti-rich aegirine, and albite are occasionally the rock-forming phases as well. However, the mineral composition of Ti-rich rodbergites varies, and generally, these minerals are either scarce or absent. Sulfides, magnetite, zircon, pyrochlore, strontianite, baryte, ancylite-(Ce), and monazite were found as accessory phases.

Apatite providing up to 7.5 wt% P_2O_5 for the Ti-rich rodbergites, but usually no more than 0.5 wt% P_2O_5. In an assemblage with calcite and sometimes with aegirine, apatite constitutes a vein network intersecting the groundmass, which indicates its later formation. Apatite is also contained in mineralized veinlets from magnesiocarbonatites surrounding Ti-rich rodbergites. This also suggests an overprinted character of apatite mineralization. Apatite is exclusively fluoride. It rims different minerals (e.g., sulfides), forms clusters of anhedral grains or radial aggregates of small euhedral crystals (Figure). Anhedral grains are the earliest apatite phases and mainly occur in the rock tissue as apatite-rich spots, while the rims and idiomorphic crystals of apatite are distributed along the fissures. Anhedral grains are almost free of impurities. In contrast, the composition of both the rims and idiomorphic crystals is highly variable even within a single grain. On the BSE images, this compositional variability is expressed as the fine oscillatory zonation (Figure). In the described apatite crystals, sulfur content varies in the range of 0.2–0.8 wt%, Sr concentration reaches 2.5 wt%, Na – 2.2 wt%, and Th – 0.8 wt%. Total REE amount is 7.5 wt%, with predominant enrichment by medium and heavy REE (Gd is up to 0.5 wt% and Y – 1.5 wt%). The concentrations of Na, REE, and Th are inversely correlated with Sr content. The concentration of Si in most analyzes does not exceed 0.2 wt%, indicating the predominance of the $REE^{3+} + Na^{+} = 2Ca^{2+}$ isomorphism scheme over the $REE^{3+} + Si^{4+} = Ca^{2+} + P^{5+}$ scheme.

In rocks with apatite mineralization, HREE content is about 300-500 ppm, while in other carbonatites (including ancylite ores) of the Petyayan-Vara field it is decreased to 20-50 ppm. The correlation coefficients between P and HREE are 0.87…0.93, and between P and LREE they are -0.12…-0.01 (0.13 for Eu). In this regard, apatitization and the identified separation of light and heavy rare earth elements are related. This kind of separation of HREE and LREE is not an endemic feature of the Petyayan-Vara carbonatites. In the Montviel Carbonatite Complex (Abitibi, Canada), the Ba-Sr

metasomatic zone with LREE mineralization is separated from the P-F metasomatic zone with HREE minerals (Nadeau et al., 2015). However, in our case, it is not obvious, whether the HREE enrichment and the apatitization were synchronous.

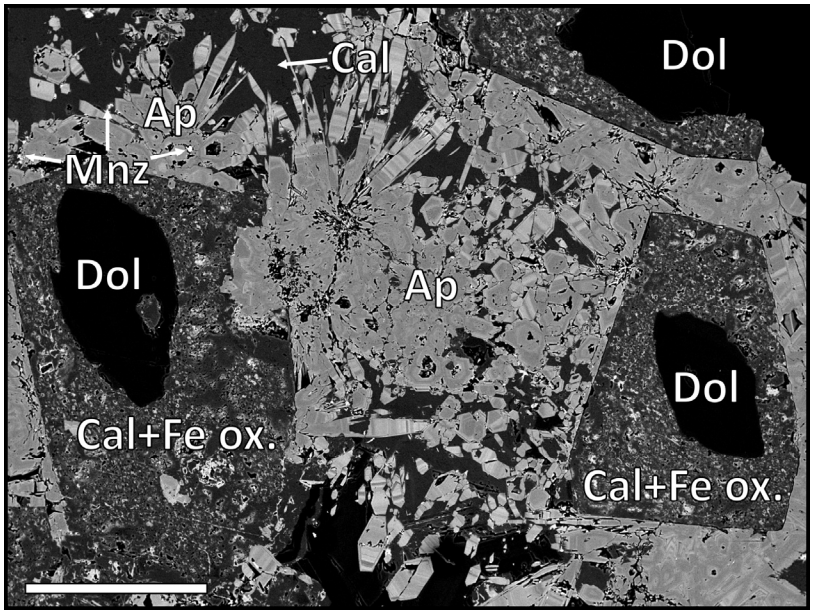

Figure. Late-generation idiomorphic apatite crystals in the vein that crosscuts Ti-rich rodbergite. The scale bar is 200 μm.

In the studied rocks, apatite undoubtedly was derived from a fluid. This is evidenced by the structural characteristics of rocks composed of anhedral early apatite, which is free of impurities. Also, fluids controlled the growth of late HREE-rich apatite in cavities and cracks. Its morphology is typical of hydrothermal apatite (Chakhmouradian et al., 2017). HREE enrichment is also common for hydrothermal apatite from similar objects (e.g., Broom-Fendley et al., 2016). However, the solubility of REE in phosphate solutions is low (Migdisov and Williams-Jones, 2014; Migdisov et al., 2016, and references therein). According to experimental data, *«…the main REE transporting ligands are chloride and sulfate, whereas fluoride, carbonate, and phosphate likely play an important role as depositional ligands*»(Migdisov et al., 2016). This suggests a low probability of phosphate fluid to be responsible for the concentration of (H)REE.

This discrepancy is conditioned by the features of late apatite responsible for the enrichment of carbonatites of the Petyayan-Vara with HREE. First, late apatite is localized in cracks and cavities near the areas saturated with early apatite. Coupled with the anatomy and morphology of late apatite, this permits us to infer, that, most likely, it was formed by dissolution of early apatite and reprecipitation of the released substance in situ in a fluid environment. Second, the chemical composition of late apatite (admixtures of Sr, REE) relates it to the mineral assemblages of Ba-Sr-REE carbonatites. The high sulfur content in late apatite indicates a high S activity in the medium of mineral formation (Nikolenko et al., 2018, and references therein). Third, the fluids controlling the formation of late apatite influenced the dolomite of protolith in the same way as the fluids, that caused ancylite formation. In both cases, dolomite was pseudomorphically substituted by calcite, and the newly formed calcite hosts a lot of inclusions of Fe oxides. Consequently, this fluid (a) was non-equilibrium with rocks exposed to its influence (both primary magmatic magnesian and Ti-rich rodbergites) and (b) had high calcium activity.

Based on the above observations, we propose the following model of HREE enrichment of the studied rocks. At the first stage, dense fine-grained Ti-rich rodbergites were formed. Then, lengthwise the weakened (brittle) fluid-permeable zones of these rocks, an REE-free phosphate substance was injected. Afterwards, the same weakened zones became a channel for the sulfate REE-fluid, that induced the generation of ancylite ores in the Petyayan-Vara. This fluid caused another act of carbothermal-metasomatic processing. As a result, dolomite was locally replaced with calcite, the

original apatite was partially dissolved and reprecipitated in situ, and Ba-Sr-REE minerals were deposited from a supersaturated solution into cracks and cavities. Most of Ba, Sr, and LREE were removed through the cracks, whereas HREE were absorbed by the growing apatite of the second generation. Hence, we suppose the trigger for HREE accumulation was the interaction of orthomagmatic carbonatite fluid with phosphate-bearing rocks. This is in a good agreement with the model proposed in (Louvel et al., 2015).

The experimental investigations (Gysi et al., 2015; Louvel et al., 2015; Migdisov et al., 2016) demonstrated that the REE fractionation can potentially be caused by a change in the fluid's pH due to buffering of fluids by surrounding rocks. In natural examples of hydrothermal REE-containing systems, LREE are preferably mobilized to greater distances from their magmatic source than HREE, which are restricted to the "high-temperature input zone" (Williams-Jones et al., 2012). This suggests that the source of the REE fluid was relatively close to the rocks of the Petyayan-Vara field.

The investigation of xenotime mineralization from Lofdal, Namibia (Wall et al., 2008; Gysi et al., 2015) have shown that the high HREE content is associated not only with the primary enrichment of the parent carbonatite melt with REE but also with the high HREE/LREE ratio in it. Within the Petyayan-Vara, the HREE/LREE ratio in parental melts was not as high as that in Lofdal. This is the possible reason for the lower HREE content in the apatite-bearing rocks of Petyayan-Vara compared with HREE deposits.

Apparently, the rarity of industrially significant HREE carbonatite-hosted deposits is determined by the rarity of the necessary combination of several factors, favourable for HREE accumulation. These are the presence of phosphorus either in the primary magma-derived minerals or in the products of superimposed processes; reprocessing of P-rich rocks by REE-rich fluids; the proximity of the fluid source to the rocks; and a high content of HREE in the fluid phase.

This work was carried out in the Geological Institute KSC RAS under the state order No. 0226-2019-0053.

References

Andersen, A.K., Clark, J.G., Larson. P.B., and Neill, O.K. Mineral chemistry and petrogenesis of a HFSE(+HREE) occurrence, peripheral to carbonatites of the Bear Lodge alkaline complex, Wyoming // American Mineralogist. 2016. Vol. 101. P. 1604–1623, doi: 10.2138/am-2016-5532.

Broom-Fendley, S., Brady, A.E., Horstwood, M.S.A., Woolley, A.R., Mtegha, J., Wall, F., Dawes, W., and Gunn, G. Geology, geochemistry and geochronology of the Songwe Hill carbonatite, Malawi // Journal of African Earth Sciences. 2017. Vol. 134. P. 10–23, doi: 10.1016/j.jafrearsci.2017.05.020.

Broom-Fendley, S., Styles, M.T., Appleton, J.D., Gunn, G., and Wall, F. Evidence for dissolution-reprecipitation of apatite and preferential LREE mobility in carbonatite-derived late-stage hydrothermal processes // American Mineralogist. 2016. Vol. 101. P. 596–611, doi: 10.2138/am-2016-5502CCBY.

Chakhmouradian, A.R., Reguir, E.P., Zaitsev, A.N., Couëslan, C., Xu, C., Kynický, J., Mumin, A.H., and Yang. P. Apatite in carbonatitic rocks: Compositional variation, zoning, element partitioning and petrogenetic significance // Lithos. 2017. Vol. 274–275. P. 188–213, doi: 10.1016/j.lithos.2016.12.037.

Gysi, A.P., Williams-Jones, A.E., and Harlov, D. The solubility of xenotime-(Y) and other HREE phosphates ($DyPO_4$, $ErPO_4$ and $YbPO_4$) in aqueous solutions from 100 to 250 °C and p sat // Chemical Geology. 2015. Vol. 401. P. 83–95, doi: 10.1016/j.chemgeo.2015.02.023.

Louvel, M., Bordage, A., Testemale, D., Zhou, L., and Mavrogenes, J. Hydrothermal controls on the genesis of REE deposits: Insights from an in situ XAS study of Yb solubility and speciation in high temperature fluids (T<400°C) // Chemical Geology. Vol. 417. P. 228–237, doi: 10.1016/j.chemgeo.2015.10.011.

Migdisov, A.A., and Williams-Jones, A.E. Hydrothermal transport and deposition of the rare earth elements by fluorine-bearing aqueous liquids // Mineralium Deposita. 2014. Vol. 49. P. 987–997, doi: 10.1007/s00126-014-0554-z.

Migdisov, A., Williams-Jones, A.E., Brugger, J., and Caporuscio, F.A. Hydrothermal transport, deposition, and fractionation of the REE: Experimental data and thermodynamic calculations // Chemical Geology. 2016. Vol. 439. P. 13–42, doi: 10.1016/j.chemgeo.2016.06.005.

Nadeau, O., Cayer, A., Pelletier, M., Stevenson, R., and Jébrak, M. The Paleoproterozoic Montviel carbonatite-hosted REE–Nb deposit, Abitibi, Canada: Geology, mineralogy, geochemistry and genesis // Ore Geology Reviews. 2015. Vol. 67. P. 314–335, doi: 10.1016/j.oregeorev.2014.12.017.

Ngwenya, B.T. Hydrothermal rare earth mineralisation in carbonatites of the Tundulu complex, Malawi: Processes at the fluid/rock interface // Geochimica et Cosmochimica Acta. 1994. Vol. 58. P. 2061–2072, doi: 10.1016/0016-7037(94)90285-2.

Nikolenko, A.M., Redina, A.A., Doroshkevich, A.G., Prokopyev, I.R., Ragozin, A.L., and Vladykin, N. V. The origin of magnetite-apatite rocks of Mushgai-Khudag Complex, South Mongolia: mineral chemistry and studies of melt and fluid inclusions // Lithos. 2018. Vol. 320–321. P. 567–582, doi: 10.1016/j.lithos.2018.08.030.

Smith, M., Kynicky, J., Xu, C., Song, W., Spratt, J., Jeffries, T., Brtnicky, M., Kopriva, A., and Cangelosi, D. The origin of secondary heavy rare earth element enrichment in carbonatites: Constraints from the evolution of the Huanglongpu district, China // Lithos. 2018. Vol. 308–309. P. 65–82, doi: 10.1016/j.lithos.2018.02.027.

Wall, F., Niku-Paavola. Vol.N., Storey, C., Muller, A., and Jeffries, T. Xenotime-(Y) from carbonatite dykes at Lofdal, Namibia: Unusually low LREE:HREE ratio in carbonatite, and the first dating of xenotime overgrowths on zircon // The Canadian Mineralogist. 2008. Vol. 46. P. 861–877, doi: 10.3749/canmin.46.4.861.

Williams-Jones, A.E., Migdisov, A.A., and Samson, I.M. Hydrothermal Mobilisation of the Rare Earth Elements - a Tale of ‘Ceria’ and ‘Yttria’ // Elements. 2012. Vol. 8. P. 355–360, doi: 10.2113/gselements.8.5.355.

Xu, C., Campbell, I.H., Allen, C.M., Huang, Z., Qi, L., Zhang, H., and Zhang, G. Flat rare earth element patterns as an indicator of cumulate processes in the Lesser Qinling carbonatites, China // Lithos. Vol. 95. P. 267–278, doi: 10.1016/j.lithos.2006.07.016.

Zaitsev, A.N., Wall, F., and Bas, M.J. Le REE-Sr-Ba minerals from the Khibina carbonatites, Kola Peninsula, Russia: their mineralogy, paragenesis and evolution // Mineralogical Magazine. 2007. Vol. 62. P. 225–250, doi: 10.1180/002646198547594.

GEOCHEMISTRY AND MINERALIZATION OF BASIC INTRUSIONS IN NW SIBERIAN TRAP PROVINCE (KULYUMBER RIVER VALLEY)

Krivolutskaya N.[1], Gongalsky B.[2], Belyatsky B.[3], Svirskaya N.[1],Gareev B.[4], Beskova E.[5], Dragulesky E.[1]

[1]*Vernadsky Institute of Geochemistry and Analytical Chemistry RAS, Moscow, Russia, nakrivv@mail.ru*

[2]*Instituteof Geology of Ore deposits, Petrography, Mineralogy and Geochemistry RAS, Moscow, Russia, brgon@mail.ru*

[3]*A.P.Karpinsky Russian Geological Research Institute, St.-Petersburg, Russia,* bbelyatsky@mail.ru

[4]*Kazan University, Kazan, Russia,* bulat@gareev.net

[5]*LomonosovMoscow State University, Moscow, Russia, belizaveta556@gmail.com*

The presence of unique PGE-Cu-Ni deposits in the North-West Siberian platform raises the question of a possibility of discovering similar rich ores in other parts of the Siberian trap province (Dodin, 2002). In this respect special attention of geologists is attracted by areas with geological structure resembling the Norilsk area (Zolotukhin et al., 1986; Eastern Siberia, 2002; Pavlenkova, Pavlenkova, 2014; Krivolutskaya et al., 2019). The greatest interest is the Kulyumber river valley (right tributary of the Yenisey river), where sulfide mineralization was discovered in the late 1990's. A distinctive feature of this territory is its location within two different tectonic structures, in the southern part of the Norilsk-Igarka paleorift zone (Malich et al., 1978), in which the Norilsk deposits are localized too, and in the western part of the Tunguska syncline (Figure). Magmatism of each structure has specific characteristics. They simultaneously occur in the Kulyumber river valley.

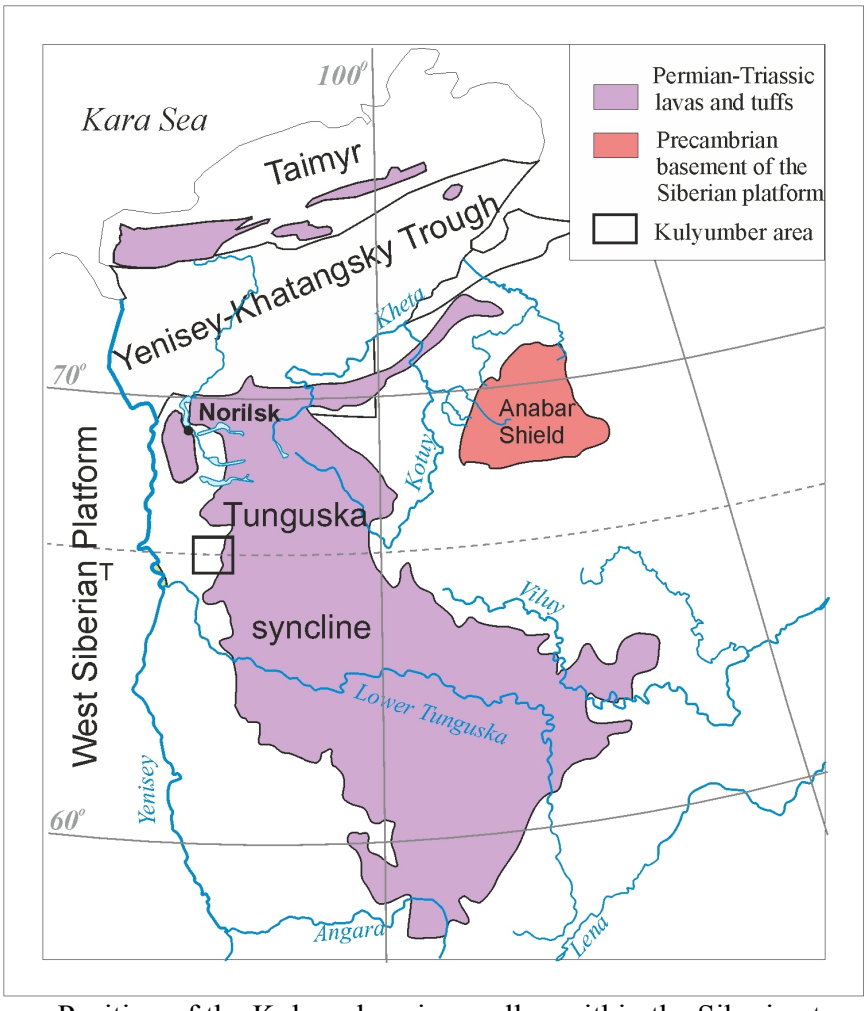

Figure. Position of the Kulyumber river valley within the Siberian trap province

The considered area is located within west zone of the Nirungrinsky Trough composed of the Cambrian–Carboniferous sedimentary rocks and volcanites of the Syverninsky, Hakanchansy, Tuklonsky and Nadezhdinsky Permian-Triassic Formations (Geological map..., 2002). Intrusive rocks are represented by massive gabbro-dolerite sills (often with olivine). Their length is 10-20 km and thickness is 5-50 m. Sills are situated in sedimentary-terrigenous rocks. Based on geological mapping of this area intrusive rocks were subdivided into six complexes: Katangsky, Kurejsky, Norilsk (Norilsk and Kruglogorsky subcompelxes), Daldykansky, Ergalakhsky, Kuzmovsky (Zolotukhin et al., 1986; Geological map..., 2002). About 90 % of all intrusions belong to the first two mentioned complexes. The sills consist of (volume %): clinopyroxene (40-60, Mg#=40-61), orthopyroxene (0-10, Mg#=38-59), plagioclase (30-70, An_{48-66}), Ol (0-10, Fo_{57-61}).

Table 1. Representative compositions (wt%) of the intrusive rocks in the Kulyumber river valley.

	1	2	3	4
SiO_2	51.06	47.58	46.93	46.36
TiO_2	2.42	1.46	1.56	1.32
Al_2O_3	13.88	14.71	12.83	14.81
Fe_2O_3	13.68	12.77	14.07	13.52
MnO	0.135	0.214	0.215	0.194
MgO	3.1	7.58	7.25	9.21
CaO	6.73	8.07	10.93	10.26
Na_2O	3.2	3.96	3.15	2.44
K_2O	2.05	0.78	0.89	0.48
P_2O_5	0.78	0.17	0.22	0.17
Cr_2O_3		0.03		0.02
LOI	2.82	2.55	1.86	1.1

Note. 1-4 Intrusive complexes: 1- Ergalakhsky, 2-Katangsky, 3-Kurejsky, 4-Kruglogorsky.
Empty cell – analysis was not carried out.

However, this classification was not confirmed by sufficient geochemical data. For the first time we have studied 17 massifs of this area using modern geochemical methods (XRF, ICP-MS, Sr and Nd isotopes). In most cases, samples were collected from the central part of each intrusive body. The compositions of some sills were studied along a strike. 87 samples have been analyzed, including 5 carbonate-terrigenous rocks and 9 basalts. The obtained data confirmed that they belong to mentioned early volcanic formations.

Analysis of intrusive rocks leads us to the conclusion that Ergalakh complex differs from other ones the most. It is represented by subalkaline rocks (Na_2O+K_2O=5.5 wt%, TiO_2= 2.4 wt%), while the other sills are composed of rocks of normal alkalinity. The last ones are characterized by compositions corresponding to typical tholeiitic basalt (SiO_2=47-50 wt%, MgO 6-7.5 wt%) with TiO_2 contents of 1.31-1.56 wt% . Only two massifs have elevated MgO content reaching up to 8.5 wt%. One intrusive body was earlier referred to the Kruglogorsky subcomplex of the Norisk complex, where MgO concentration ranges from 7.9 to 9.2 wt%, reflecting magma differentiation from the top to the basement of the body. Typically, the concentration of Al_2O_3 changes in the rocks from 12 to 14 w%. Only one intrusive body with a predominance of leucogabbro in its structure, attributed to the Kruglogorsky subcompex of the Norilsk intrusive complex, contains up to 18.5 wt% Al_2O_3. A distinctive feature of the considered intrusions is a stable TiO_2 content varying from 1.3 to 1.55 wt%.

Based on rare elements distributions in rocks, three types of intrusions can be recognized. The Ergalakh complex has Gd/Yb ratio =1.5 and $\varepsilon_{Nd}(T)$=-6.5. The patterns of the main group intrusions are characterized by a moderate accumulation of rare elements with clearly manifested negative Ta-Nb and positive Pb and Sr anomalies. These features are similar to the spectra of volcanic rocks of the

main stage of trap magmatism within the Siberian platform (the Morongovsky-Samoedsky lavas, $\varepsilon_{Nd}(T)$=-0.5-+0.5). Thus, this group of intrusions can be attributed to the Katangsky intrusive complex. Kurejsky intrusive complex in this territory is represented by the Khalilsky intrusion, which has more leucocratic composition in comparison with the other massifs of this area. However, its chemical composition is similar to the intrusion compositions of the Katangsky complex.

There is a single intrusion in the Kulyumber river valley which has a very specific composition. It is located on the Kulyumber river board, near the mouth of the Khalil Creek. Its thickness is 20. The content of major components and its isotopic characteristics (Sr, Nd) are similar to the intrusions of the Katangsky complex. But it is characterized by slightly elevated concentrations of alkali metals (Na_2O+K_2O=5 wt%), high Gd/Yb ratio (of 1.9) and small Ta-Nb anomaly. Taking into account these features this massif must be attributed to a new intrusive complex.

Sulfide mineralization was found in some sills belonging to different intrusive complexes. The richest one is related to the Kruglogorsky intrusive subcomplex. It is represented by disseminated sulfides in leucogabbro. The main ore minerals are chalcopyrite, pyrrhotite, pentlandite; cubanite and violarite were recognized. Oxides are represented by titanomagnetite and ilmenite. Chalcopyrite dominates in another mineralized sill of the Katangsky intrusive complex. Currently, Ltd. Norilskgeologia carried out geological work and drilling in this area.

Conclusion: this study did not reveal a difference between the intrusions of the Katangsky and Kurejsky complexes. Massifs attributed to them have similar composition of the rocks and sulfide mineralization.

This study was supported by Russian Foundation for Basic Research (project No 18-05-70094).

References

Geological Map of Russian Federation, scale 1:1 000 000 (R-(45)47). Eds. Yu.G. Staritsky, E.V. Kovrigina. St.-Petersbourg, VSEGEI, 2000, 240 p.

Dodin D.A. Metallogeny of the Taimyr-Noril'sk area (north of the Central Siberia). St.-Petersburg, Nauka, 2002,822 p.

Eastern Siberia. (Eds. V.P. Orlov, N.S. Malitch). St-Petersburg, VSEGEI, 2002, 396 p.

Krivolutskaya N., Latyshev A., Dolgal A., Gongalsky B., Makareva E., Makarev A., Svirskaya N., Bychkova Ya., Yakushev A., Asavin A. Unique PGE–Cu–Ni Noril'sk Deposits, Siberian Trap Province: Magmatic and Tectonic Factors in Their Origin // Minerals 2019. 9(1). 66.

Malitch, N.S., Grinson, A.S., Tuganova, E.V., Chernyshev, N.M., 1988, Rifting of the Siberian platform: 28th session of International Geological Congress// In Tectonic processes, Moscow, Nauka Press, p.184-193.

Pavlenkova N.L, Pavlenkova G.A.Structure of the Crust and Upper Mantle of the Northern Eurasia based on data of seismic profiles with nuclear explosion. Moscow, GEOS, 2014, 192 p.

Zolotukhin, V. V., Vilensky, A. M., Dyuzhikov, O. A., 1986, Basalts of the Siberian Platform. Novosibirsk, Nauka, 289 p. (in Russian).

RARE-EARTH AND TRACE ELEMENT MINERALOGY IN KARELIA'S DIFFERENTIATED ALKALINE AND MODERATELY ALKALINE COMPLEXES

Kuleshevich L.V., Dmitrieva A.V.
IG KarRC RAS, Petrozavodsk Russia, kuleshev@krc.karelia.ru

Some of Karelia's ore occurrences contain high Ti, P, Ba, Sr, REE, Zr, Nb and other trace element concentrations. In NW Russia, Karelia is undoubtedly a promising region for some types of REE-RE raw materials. Therefore, their study, analysis and evaluation are essential. Most of known rare-earth-rare-metal (REE-RE) ore bodies are complex; they are confined to alkaline and moderately alkaline rocks of various ages. The goal of our study was to evaluate Karelia's REE potential. Our major tasks were to estimate the concentrations and mineral assemblages of rare-earth and associated trace elements in highly alkaline rocks, particularly in differentiated complexes, ultramafic rocks, carbonatites and ores. Elevated REE concentrations were revealed in the following major rock types of differentiated massifs: 1 – ultramafic alkaline rocks and carbonatites of the Tiksheozero-Yeletozero complex; 2 – ultramafic-mafic alkaline rocks and titanite-apatite ores of the Elisenvaara complex; 3 – lamproites of the Kostomuksha Structure; 4 – moderately alkaline massifs of the Syargozero complex (Kuleshevich & Dmitrieva, 2019).

Tiksheozero massif (2.0 Ga). The rare-earth (REE) and rare-metal (RE) mineralization is confined to apatite-bearing carbonatites and alkaline metasomatic rock zones and occurs in the aureole of cross-cutting syenite dykes. The average P_2O_5 concentration in the apatite ore of the carbonatites is 2.94-4.18 % (up to 16.2 %) and its total predicted resources are up to 51000 thousand tonnes (Mineral…, 2006). Associated with apatite ore are the highest REE (970-1250 ppm) and Sr (0.45 %) concentrations. REE are concentrated in phosphates and carbonates such as apatite, monazite, rhabdophanite, bastnesite, synchisite, ancylite and carbocernaite. Earlier minerals, such as monazite and orthite, are intergrown with apatite; TR-carbonates (bastnesite) occur in microfractures that cut carbonatites, schistosity zonules and interstices between calcite grains. Sr concentration (1317-4163 ppm) is correlated with the amount of apatite; the central portions of its grains contain up to 1.52 % Sr. Besides, Sr is part of Sr-carbonates (ancylite and carbocernaite), Sr-bearing calcite (0.26 at. %), strontianite, Ce-Na-strontianite and strontiobarite (up to 8.6 % Sr). Barite contains 1.16-6 % Sr. Ancylite (Ca-Sr-Ce-Nd-carbonate) forms inclusions in Sr-barite and is intergrown with chlorite.

Zr, Hf, Nb and Ta concentrations in the carbonatites are non-uniform (Zr 337-1000 ppm, Hf 12.6-20, Nb up to 930 ppm, Ta 35.5 (Nb/Ta=30÷9), Y 15-48, Th 3-30 and U 0.3-1.7 ppm. The main phases of Zr are baddeleyite and zircon. Baddeleyite occasionally forms fine acicular crystals in apatite, carbonate and the perovskite of metasomatic rocks and is replaced by zircon. Higher U concentrations (up to 255 ppm) are due to the presence of U-betafite and hatchettolite. Pyrochlore and betafite carry up to 0.8-5.92 % Ce. Niobates occur as the isomorphic series "pyrochlore–Ti-betafite–microlith"; U-microlith (hatchettolite?) with 13-16 % U and up to 10 % Th is occasionally encountered. Pyrochlore occurs as prismatic crystals in apatite and is also intergrown with calcite, phlogopite and sulphides.

The Elisenvaara complex (~1.78 Ga) is represented by the Kaivomäki and Raivomäki massifs located in the NW Ladoga area. The massifs are differentiated from ultramafic and mafic to intermediate rocks. The highest REE concentrations are associated with ladogites (local name coined for the major differentiates of the complex, after R.A. Khazov), toensbergite and Ba-Sr-P-Ti ores in them. The typomorphic minerals of these rocks are clinopyroxene, amphibole, K-feldspar (up to 20-80 %), titanite, apatite, accessory REE and RE-minerals. P_2O_5 concentrations in the mafic and ultramafic rocks are 0.43-10.5 % (average concentration 2.5-5 %), SrO 0.45-2.2 %, BaO 0.23-2.0 % and F 0.12-1.5 %. Ba and Sr are mainly part of K-feldspar. The rocks of the complex contain ΣREE 1586-10380, Y 62-171, Nb 10-128, Ta 0.4-9, Th 10-77, Zr 120-940, Hf 2-14.7 and Ga up to 302 ppm. ∑REE concentration in the rocks is 0.22-0.4 %, Zr 220-940 ppm; ∑REE is 1-1.7 % in titanium concentrates and 0.45-1.36 % in apatite. REE-concentrating minerals are represented by monazite, TR-apatite, titanite, allanite, TR-epidote, TR-carbonates and more recent lanthanite, bastnesite and Ca-Sr-Ce-carbonates. Zircon and baddeleyite prevail in syenites with perthitic Ba-Sr-feldspar.

Kostomuksha Structure lamproites (1.23 Ga) form several clusters (Taloveis, Kostomuksha and Korpanga) consisting of about 50 dykes. The lamproites contain elevated trace element concentrations (ppm): ΣREE 1300, Nb 223, Ta 10, Zr 933, Y 25, Sr 2950 and Ba 2346. However, as the dykes are thin and short, they are not promising.

Central Karelia's **Neoarchean moderately alkaline intrusions** occur as 2.74 Ga Sharavalampi, Syargozero, Panozero, Zapadno-Khizhyarvi and Elmus differentiated massifs of gabbro-pyroxenite-monzonite-syenite composition. Elevated REE and Sr concentrations are characteristic of an early gabbro-pyroxenite phase with apatite-titanite mineralization. ΣREE in the Syargozero complex (Syargozero and Sharavalampi massifs) is up to 1458 ppm. Ore mineralization is represented by titanite, magnetite and apatite; REE are concentrated in apatite, titanite, allanite, epidote and late TR-F-carbonates. The felsic differentiates of the complex typically display high Ba (up to 4300 pmm) and Sr (up to 1700–4000 ppm) concentrations that are part of K-feldspar and more recent minerals such as barite and celestine.

To sum up, the results obtained suggest that rare-earth mineralization in Karelia is most likely to be associated with alkaline and moderately alkaline massifs with apatite or apatite-titanite ores in them. Preliminary appraisal of the complex raw materials and REE-mineralization of the Elisenvaara complex has shown that the total REE oxide resources in the ladogalites are 15 M t, of which apatite concentrate makes up 5 M t and titanite concentrate 3 M t (average TR_2O_3 concentration is 1.0 and 1.5 %) after R.A. Khazov. Associated with Tiksheozero carbonatites are complex apatite-carbonatites that contain Sr, Zr, Nb-Ta and light REE. The resources have not been evaluated for REE. Other massifs and dyke bodies are too small to be of interest.

References

Kuleshevich L.V. & Dmitrieva A.V. Rare-earth mineralization in Karelia's alkaline and moderately alkaline complexes and associated metasomatic rocks and ores // Gorny zhurnal. 2019. No. 3. P. 45-50.

The mineral raw materials base of the Republic of Karelia / Edited by V.P. Mikhailov and V.N.Aminov. Petrozavodsk: Karelia Publishers. 2006. Vol. 2. P. 356.

SILICATE INCLUSIONS IN ISOFERROPLATINUM: CONSTRAINTS ON ORIGIN OF PLATINUM MINERALIZATION IN URAL-ALASKAN COMPLEXES

Kutyrev A.V.[1,2], Sidorov E.G.[1], Kamenetsky V.S.[2,3], Chubarov V.M[1]

[1]Institute of Volcanology and Seismology FEB RAS, Petropavlovsk-Kamchatsky, Russia, anton.v.kutyrev@gmail.com

[2]Institute of Experimental Mineralogy RAS, Chernogolovka, Russia

[3]University of Tasmania, Hobart, Australia

INTRODUCTION. Platinum-group elements (PGE) are among the rarest and irregularly distributed elements in the Earth mantle and crust with concentrations barely reaching first ppb and in rare cases climbing to ppm levels. It is widely believed that the most efficient mechanism of PGE transport and accumulation is with sulfide liquids for which these elements have very strong affinity. The efficient scavenging of PGE from silicate magmas into immiscible sulfide melts has been championed in genetic models for several orthomagmatic deposits such as Norilsk, Bushweld etc. (Naldrett, 2004). The same process may be responsible for the formation of micron-scale platinum group minerals (PGM) in ophiolites, where PGE are mostly stored in sulfides – laurite RuS_2 and erlichmanite OsS_2, as well as Ru-Os-Ir alloys and isoferroplatinum that possibly result from desulfurization of PGE-bearing sulfides (Peregoedova et al., 2004). The role of sulfide liquids in PGE accumulation has been recently de-emphasized by several discoveries of PGE alloys in high-temperature volcanic rocks (e.g., Kamenetsky et al., 2015). Furthermore, sulfur-poor environments are typical of chromitites in the Ural-Alaskan mafic complexes and associated placer deposits that are a significant source of PGE. For example, platinum aggregates up to 150 g were reported in lode deposits related with Ural-Alaskan complexes (Betekhtin, 1954) and nuggets up to 9 kg were found in the associated placers (Orlov, 2010).

Formation and high abundance of PGM in the chromitites of the Ural-Alaskan complexes, especially in the absence of PGE-bearing sulfide melts, remain unresolved. Secondly, inhomogeneous distribution of PGM in largely dunitic rocks and their intimate affiliation with disseminated lenses and schlieren of Cr-spinel further challenges the reigning orthomagmatic model. Furthermore, the mineral assemblage in multiphase inclusions (e.g., albite, feldspar, mica) within platinum nuggets from the alluvial deposits (Dmitrenko & Mochalov, 1989; Nixon et al., 1990; Johan, 2006, Sidorov et al., 2019) is in stark contrast to liquidus association in mafic magmas. The studies of mineral inclusions in PGM nuggets have made only hypothetical links between alluvial PGM nuggets and nearby dunites, thus making genetic constraints unreliable. In this paper, we present the first study of multiphase inclusions in Pt-Fe alloys intergrown with Cr-spinel in dunite from the Ural-Alaskan-type mafic-ultramafic complex in Far East Russia.

PLATINUM MINERALIZATION IN THE MATYSKEN MASSIF. Matysken massif is located at the northernmost part of the Koryak-Kamchatka Platinum Belt. It shares all typical features of the Ural-Alaskan type massifs, such as zonal structure, absence of orthopyroxene-dominant rocks and the predominance of Pt over all other PGE. Most of platinum mineralization belongs to chromite veins in the olivine-rich lithologies (dunites). These veins may wedge out, bifurcate and/or disperse into disseminated Cr-spinel grains intergrown with high-magnesian olivine (Fo_{95}) and sometimes with rare diopside. Morphologically they resemble podiform chromitites of alpine-type complexes, however, the Matysken chromitite accumulations do not exceed first meters in length and lack nodular texture.

Platinum group minerals were found in heavy mineral concentrates of crushed chromitites (Fig. 1a) and in polished sections (Fig. 1b). The main PGE mineral phase is isoferroplatinum, which forms close intergrowths with Fe-rich chromite. Another common mineral is native osmium, which forms euhedral inclusions in both platinum and chromite.

COMPOSITION OF MULTIPHASE INCLUSIONS. Inclusions were found in associated Cr-spinel and isoferroplatinum in the dunites that are characteristically unaltered, i.e. < 0.5 vol. % of serpentine and 0.5 wt. % of OH^-. Both isoferroplatinum- and chromite hosted inclusions are usually of polygonal shape which reflects the negative crystallography (Fig. 1c-f). A total 45 in isoferroplatinum

and much more that 100 in chromite were studied by the moment of publication. Their distribution is extremely uneven: most grains lack the inclusions while some may contain tens of them (Fig. 1e).

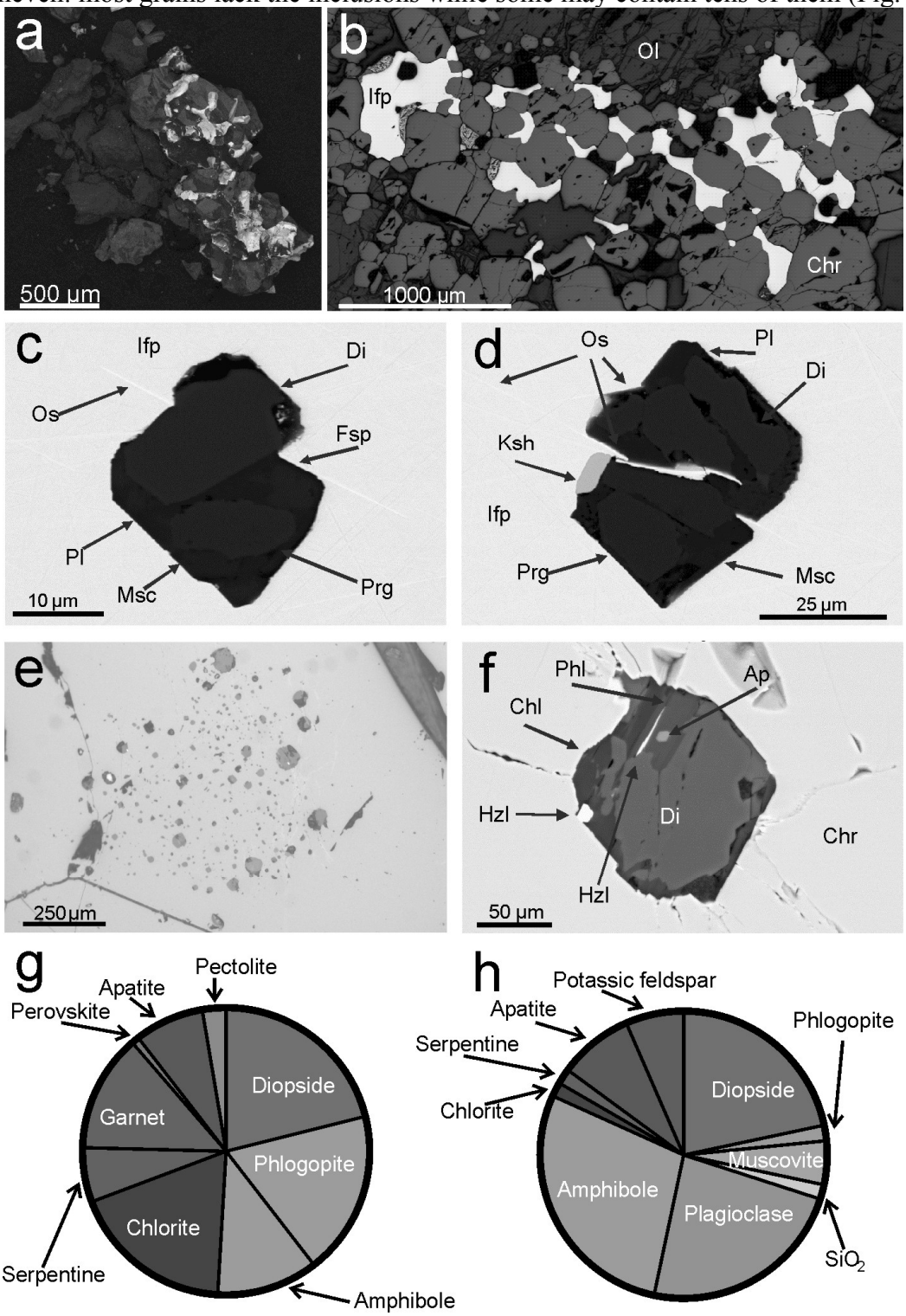

Fig. 1. (a) – chromite intergrowthing with isoferroplatinum, (b) – posidhed sample of chromite (Chr) shlier in dunite (Ol for olivine) and huge isoferroplatinum (Ifp) aggregate, (c) – multimineral inclusion in isoferroplatinum composed of diopside (Di), pargasite (Prg), plagioclase (Pl), muscovite (Msc) and potassic feldspar (Fsp);the border of the inclusion is subordinate to the native osmium (Os) crystal, (d) – inclusion of pargasite, diopside, muscovite, and plagioclase in isoferroplatinum; note euhedral kashinite (Ksh) and native osmium (Os), (e) – multiple inclusions in chromite, (f) – inclusion of diopside, chlorite (Chl) and apatite (Ap) in chromite, (g) – abundances of minerals in the inclusions in chromite and in isoferroplatinum (h). Images "a", "c", "d", "f" are in BSE, images "b" and "e" are in reflected light.

Inclusions hosted by isoferroplatinum are composed of several mineral phases (Fig. 1c, d, h). Most abundant minerals are diopside and pargasite – at least one of them occurs in every inclusion and is dominant in size. The third most abundant mineral is plagioclase which is interstitial to diopside and pargasite. K-feldspar, muscovite, phlogopite, silica and apatite are also sporadically present. Their relations point on the in-situ crystallization. Euhedral crystals of Rh sulfides and laurite are recorded in ~50% of inclusions.

Multiphase inclusions in Cr-spinel are common in all samples studied, including the sample with inclusions hosted in isoferroplatinum. Similarly to inclusions described above, diopside, pargasite, apatite and phlogopite are common, but plagioclase, feldspar and silica were not observed (Fig. 1). Another difference between phase composition of inclusions in Pt and Cr-spinel is abundance of garnet (andradite and/or uvarovite), chlorite, perovskite, serpentine and base metal sulfides (BMS) in the latter.

DISCUSSION. Despite the tight association of isoferroplatinum and chromite, the composition of multiphase inclusions in these supposedly related minerals is dramatically different. The inclusions in both associated minerals have one thing in common: their phase composition is completely alien to that of dunite. This observation is consistent with other published accounts of multiphase inclusions in Pt-Fe alloys, for example those sampled in placers around the Ural-Alaskan Tulameen massif (Nixon et al., 1990). Unlike rare records of isoferroplatinum-hosted inclusions, multiphase silicate inclusions in chromite received much more attention in the literature. The similarities in their shape, presence of both type of the inclusions in one sample and close spatial and temporal relationships between isoferroplatinum and chromite imply that popular models of chromite-hosted inclusions formation are also applicable to isoferroplatinum. The following models for Cr-spinel accumulations are considered by igneous petrologists:

1) Chromite as an early magmatic phase, which entraps the melt. This model generally refers to layered intrusions; however, it is not particularly relevant to podiform chromitites in ophiolites and Ural-Alaskan complexes as they are hosted in largely metamorphic dunite;

2) Entrapment of random minerals during recrystallization and enlargement of chromite grains was proposed for Bushveld chromitites (e.g., Hulbert and von Gruenewaldt, 1985). This model is generally applicable to all post-magmatic environments, where the phase compositions of the inclusions reflect those in the parental media/ environment;

3) Late-magmatic crystallization due to reactions between a boninitic melt that filtrates through ultramafic solid rocks, followed by leaching Cr and subsequent formation of chromitites (Arai, 1997). This model provides insights into textural features of chromitite occurrences in dunites. It is also somewhat echoed by the Nixon et al. (1990) model of isoferroplatinum-hosted inclusions formation;

4) Simultaneous entrapment of the silicate melt, fluid phase and/or solid particles, as proposed Pushkarev et al. (2007) for the origin of multiphase inclusions in Cr-spinel in dunites.

Based on the morphological and compositional similarities between chromite- and isoferroplatinum-hosted inclusions we attempted to fit the above models with the results in our study. However, all scenarios, where some kind of melt is involved, suffer from contradicting empirical and experimental data. For example,

a) The problem of low PGE solubility in any silicate melt. Figure 1 shows parts of chromite veins where isoferroplatinum represents about 10% of the segregation (see supplementary page 1 for whole sample photo). As it has been previously shown in the studies dedicated to chromite-hosted PGM inclusions in volcanic rocks (e.g., Kamenetsky et al., 2015), the amount of platinum forming mineral inclusions in chromite is about 8 orders of magnitude less than the volume of the host chromite. This is also supported by micron-sized PGE alloy inclusions in the Ural-Alaskan chromitites. This casts strong doubts on the direct crystallization of isoferroplatinum from an intercumulus silicate melt;

b) The problem of direct PGM precipitation can be bypassed if platinum is extracted together with chromium from the ultramafic country rocks during melt/rock interaction However, the

mechanism of magmatic PGE extraction from ultramafic rocks and further transportation remains unconstrained;

c) Significant differences in mineral assemblages recorded for multiphase inclusions in coexisting isoferroplatinum and Cr-spinel chromite-hosted inclusions are hardly accountable by any orthomagmatic hypothesis.

CONCLUSIONS. The data obtained in our study allow to disregard popular orthomagmatic models in the origin of multiphase silicate inclusions hosted by coexisting Cr-spinel and isoferroplatinum. The systematic difference in the composition of chromite- and isoferroplatinum-hosted inclusions is also a matter of future debate that may fall outside the realm of melts and magma-derived fluids. Importantly, low solubility of PGE in silicate melts is the strongest argument against magmatic accumulation of PGE in the sulfide-free system. However, if we consider the role of low-temperature PGE extraction, transport and accumulation, constraints on the exact mechanisms may require novel experimental evidence and thermodynamic modelling.

This work was supported by the Russian Science Foundation, project No 16-17-10145.

References

Arai, S. Origin of podiform chromitites // Journal of Asian Earth Sciences. 1997. V. 15. p. 303-310.

Betekhtin, A.G., 1954. Primary platinum deposits in the Urals // In: Mineralogy of the Urals. Izd. AN SSSR, Moscow, pp. 25–57. (in Russian).

Dmitrenko, G.G. and Mochalov, A.G. Origin of hydrous silicate inclusions in PGM and Cr-spinels from ultramafic rocks // Dokl. Akad. Nauk SSSR, 1989. V. 307. pp. 1207–1211.

Johan, Z. Platinum-group minerals from placers related to the Nizhni Tagil (Middle Urals, Russia) Uralian-Alaskan-type ultramafic complex: ore-mineralogy and study of silicate inclusions in (Pt, Fe) alloys // Mineralogy and Petrology. 2006. V. 87. p. 1–30.

Kamenesky, V.S., Park, J.-W., Mungall, J.E., Pushkarev, E.V., Ivanov, A.I., Kamenetsky, M.B. and Yaxley, G.M. Crysallization of platinum-group minerals from the silicate melts: Evidence from spinel-hosted inclusions in volcanic rocks // Geology. 2015. Vol. 43. p. 903-906.

Naldrett, A.J. Magmatic sulfide deposits. 2004. Springer-Verlag. 727 P.

Nixon, G.T., Cabri, L.J., Laflame, G.J. Platinum-group-element mineralization in lode and placer depositds associated with the Tulameen Alaskan-type comples, British Columbia // The Canadian Mineralogist. 1990. V. 28. p. 503-535.

Orlov, V.N. Platinum nuggets from the Diamond Fund of the Russian Federation: witnesses of history // Mineralogical Almanac. 2010. Vol. 15. p. 4-27.

Peregoedova, A., Barnes, S.-J., Baker, D.R. The formation of Pt-Ir alloys and Cu-Pd-rich sulfide melts by partial desulfurization of Fe-Ni-Cu sulfides: Results of experiments and implications for natural systems // Chemucal Geology. 2004. Vol. 208. p. 247-264.

Pushkarev, E. V., Anikina, E. V., Garuti, G. & Zakkarini, F. Chrome-platinum deposit of Nizhnetagilsky type on Ural: Structure and compositional characteristics and petrogenetic problem // Lithosphere. V. 3. p. 28-65. (in Russian).

Sidorov E.G., Kutyrev A.V., Zhitova E.S., Chubarov V.M., Khanin D.A. Origin of platinum-group mineral assemblages from placers in rivers draining from the Ural-Alaskan type Itchayvayamsky ultramafics, Far East Russia // The Canadian Mineralogist, 2019, vol. 57, №1, pp. 91-104.

A PRELIMINARY MODEL FOR THE MIGRATION OF SULFIDE DROPLETS IN A MAGMATIC CONDUIT AND THE SIGNIFICANCE OF VOLATILES

Li Y.[1], Yao Z.[1,2], Mungall J.E.[1], Qin K.[2]

[1]Dept of Earth Sciences, Carleton University, Ottawa, Canada

[2]Key Laboratory of Mineral Resources, Institute of Geology and Geophysics, Chinese Academy of Sciences, Beijing, China

Many major Ni-Cu-PGE sulfide deposits have been known to share a close relationship with magmatic conduit systems, such as the world-class Noril'sk-Talnakh deposit in Russia (Czamanske et al., 1995, Li et al., 2009). However, the present understanding of sulfide transport mechanism during magma ascent is mainly based on empirical studies and has not been extensively tested by numerical modelling. Thus, we propose a preliminary quantitative model to address the dynamics and feasibility of upward transport mechanisms of sulfide droplets by examining limiting parameters such as size, transport velocity and the magma's maximum carrying capacity as a function of these parameters.

To simplify the complex dynamic environment in feeder dikes, we focus solely on the magma flow within the thinner dike tail that is essentially controlled by the balance between magma buoyancy and viscous resistance (Lister & Kerr, 1991, Menand & Tait, 2002). In the Confort 15 model, we assume a cylindrical conduit of fixed diameter and an adiabatic magma cooling path without heat loss to the wall rock. 200 and 25 MPa are considered to represent the initial pressure at the bottom and top of the conduit respectively, based on the estimated pressure conditions for some large-scale layered mafic intrusions that approximate to magma chambers (Cawthorn & Davies, 1983, Sharpe & Hulbert, 1985, Mastin, 2002). Given that most physical properties of Etna and Stromboli basalts have been well categorized, they were adopted as the initial melt in order to obtain a detailed quantitative simulation.

Transport velocity of sulfide droplet in ascending magma is determined by the vertical component of magma velocity and the settling velocity of sulfide droplets. The magma velocity away from the staging chamber is proposed to fall between 0.001-0.02 m/s, while the relative settling velocity of sulfide droplet follows the Hadamard-Rybczynski equation which relates velocity most strongly to drop sizes. Possible perturbation of droplet size can be driven by coalescence and growth/dissolution during magma ascent, but their influences are considered negligible. With these simplifying assumptions, our model shows that mm-scale sulfide droplets in ascending magma undergoes upward transport at rates similar to the flow rate of the enclosing melt with minimal dissolution and no break-up in the most plausible circumstances. Additions of crystal phases and/or sulfide droplets significantly increase magma viscosity and diminish magma buoyancy, which limits the maximum carrying capacity of magma due to the balance between buoyancy-driven pressure and viscous resistance in dyke propagation. Hydrous magmas have a larger carrying capacity for sulfide droplets because the addition of volatiles strongly reduces the magma density and viscosity when they are dissolved in melt. As vesiculation occurs at shallower depth due to decompression, the sulfide entrainment in magma is further facilitated by reducing bulk magma density.

In addition, with the appearance of a magmatic volatile phase, compound drops (attachment of sulfide droplets to vapor bubbles) are able to form due to surface tension effects, which are evident both by experimental observation and empirical study (Mungall *et al.*, 2015, Iacono-Marziano *et al.* , 2017, Le Vaillant *et al.*, 2017). Although the density of compound drops is highly variable in terms of the whole decompression process due to rapidly increasing bubble volumes during decompression, and the volume ratio between vapor bubble and sulfide droplet is unconstrained, the model is capable of showing that the formation of buoyant compound drops comprising vapor and sulfide liquid greatly enhances the carrying capacity of magma for a wide range of parameter choices. As they continue to grow during pressure decrease, the compound drops may break down when their capillary numbers exceed a critical threshold, allowing the sulfide liquids to be collected in traps in the conduit system (Figure 1; Yao et al., 2019).

The conduit geometry, in addition to factors mentioned above, may also play an important role in controlling vapor-sulfide bubble transport and sulfide deposition. Many experimental studies of two-phase flow have observed a sharp increase of bubble fraction just downstream of a sudden expansion

of conduit diameter, confirming that the bubble phase may be partially separated from the flow and occupy most of the recirculation zone. Application of this concept to transport of immiscible sulfide droplets suggests that there will be significant concentration of sulfide droplets in widened parts of vertical magma conduits. Furthermore, a strong expansion of the conduit may reduce the outlet flow velocity to values below the relative settling velocity, which may cause sulfide droplets to rain down and accumulate at the widened part of the conduit. This model provides a simple physical explanation to the occurrence of massive ore bodies within the funnel-like openings of magmatic conduit.

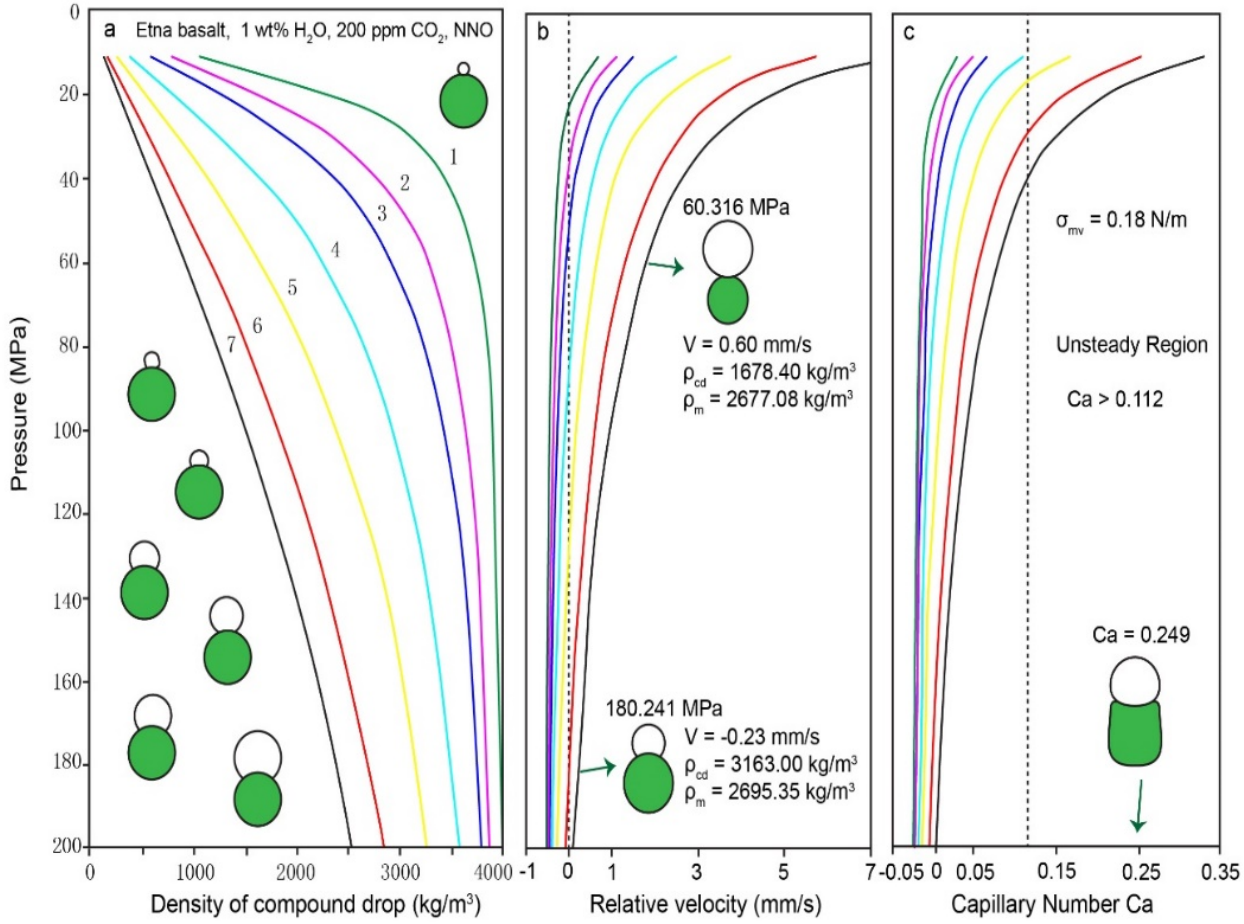

Figure 1. (**a**) Density, (**b**) relative velocity and (**c**) capillary number of compound vapour-sulfide drop variations during ascent of Etna basalt (Yao et al., 2019). Different initial volume ratios between vapour bubble and sulfide droplet *VV*/*VS* (case 1, 0.003; case 2, 0.03; case 3, 0.061; case 4, 0.151; case 5, 0.302; case 6, 0.603; case 7, 0.905) are modeled and shown in (**a**). The variation of relative velocity from negative to positive and the associated variations of density and morphology for compound drop (case 5) are shown in (**b**). Evolution of the ascending compound drop enters an unsteady region (the grey area in **c**) at Ca > 0.112, when the dense sulfide is easily separated from vapour phase.

This work has significant implications to many magmatic sulfide deposits, especially the Noril'sk-Talnakh deposit. We demonstrate the feasibility of transporting dense sulfide droplets from a deep hypothetical staging chamber where high R factor could be attained in a flow-through system up into sills sit in the shallow crustal level where the orebodies are now situated. Our model reconciles the problems of high R factor found in the deposits, which are hosted by small blind intrusions having low silicate/sulfide mass ratios, and can account for discrepancies in S isotope between the Siberian flood basalts and the mineralized Ni-Cu-PGE deposits beneath them.

This work was supported by the National Key Research & Development Program of China (2017YFC0601204), the TGI V program of NRCan, the NSFC project (41830430) and a visiting grant provided by the Chinese Scholarship Council.

References

Cawthorn, R. & Davies, G. (1983). Experimental data at 3 kbars pressure on parental magma to the Bushveld Complex. Contributions to Mineralogy and Petrology 83, 128-135.

Czamanske, G. K., Zen'ko, K. E., Fedorenko, V., Calk, L. C., Budahn, J. R., Bullock, J. H., Fries, T. L., King, B. S. & Siems, D. F. (1995). Petrographic and geochemical characterization of ore-bearing intrusions of the Noril'sk Type, Siberia, with discussion of their origin. Resource Geology (Special Issue) 18, 1-48.

Iacono-Marziano, G., Ferraina, C., Gaillard, F., Di Carlo, I. & Arndt, N. T. (2017). Assimilation of sulfate and carbonaceous rocks: experimental study, thermodynamic modeling and application to the Noril'sk-Talnakh region (Russia). Ore Geology Reviews 90, 399-413.

Le Vaillant, M., Barnes, S. J., Mungall, J. E. & Mungall, E. L. (2017). Role of degassing of the Noril'sk nickel deposits in the Permian–Triassic mass extinction event. Proceedings of the National Academy of Sciences 114, 2485-2490.

Li, C., Ripley, E. M. & Naldrett, A. J. (2009). A new genetic model for the giant Ni-Cu-PGE sulfide deposits associated with the Siberian flood basalts. Economic Geology 104, 291-301.

Lister, J. R. & Kerr, R. C. (1991). Fluid□mechanical models of crack propagation and their application to magma transport in dykes. Journal of Geophysical Research: Solid Earth 96, 10049-10077.

Mastin, L. G. (2002). Insights into volcanic conduit flow from an open□source numerical model. Geochemistry, Geophysics, Geosystems 3, 1-18.

Menand, T. & Tait, S. R. (2002). The propagation of a buoyant liquid□filled fissure from a source under constant pressure: An experimental approach. Journal of Geophysical Research: Solid Earth 107, ECV 16-11-ECV 16-14.

Mungall, J. E., Brenan, J. M., Godel, B., Barnes, S. J. & Gaillard, F. (2015). Transport of metals and sulphur in magmas by flotation of sulphide melt on vapour bubbles. Nature Geoscience 8, 216.

Sharpe, M. R. & Hulbert, L. (1985). Ultramafic sills beneath the eastern Bushveld Complex; mobilized suspensions of early lower zone cumulates in a parental magma with boninitic affinities. Economic Geology 80, 849-871.

Yao, Z., Mungall, J.E., Qin, K. (2019). A preliminary model for the migration of sulfide droplets in a magmatic conduit and the significance of volatiles, with application to the emplacement of sulfide-rich magmatic suspensions at Noril'sk. Journal of Petrology. In review.

GENESIS OF DIAMOND-BEARING ROCKS FROM THE UPPER MANTLE XENOLITHIC ASSOCIATIONS IN KIMBERLITES (BY MINERALOGIC AND EXPERIMENTAL EVIDENCE)

Litvin Yu.A., Kuzyura A.V.

D.S. Korjinsky Institute of Experimental Mineralogy, Russian Ac. Sci.

Diamond-bearing peridotites, pyroxenites, eclogites and grospydites, being well-stirred with similar diamond-free bedrocks, have been revealed among the upper-mantle xenoliths in kimberlites. Nevertheless, the unaltered rock-forming minerals in the diamond-bearing and diamond-free xenoliths exhibit dissimilar compositions. On the contrary, the major minerals of the diamond-bearing rocks are of identical composition over the analogous phases included into their diamonds what is illustrated in the Table. The compositional identity for the mineral phases of diamond-hosted inclusions and rock-forming minerals of diamond-bearing xenoliths may be evaluated as the key evidence of the fact that diamonds, mineral inclusions therein, and rock-forming minerals of diamond-bearing rocks represent products of the unitary diamond-producing processes within the chamber-reservoirs of their common parental melts. The genetic scenario is in excellent agreement with the requirements of the experimentally justified syngenesis criterion regarding the compositions and physicochemical properties of the natural parental media for diamonds and their minerals included (Litvin, 2007). The syngenesis criterion provides the basis for the mantle-carbonatite theory of genesis of diamonds and associated phases (Litvin et al., 2016; Litvin, 2017). A distinguishing feature of this theory is the concordance of mineralogical analytical data and experimental physicochemical results for the multicomponent systems with nature-like boundary compositions.

The mantle-carbonatite theory substantiates that diamond-bearing ultrabasic peridotite-pyroxenite and basic eclogite-grospydite rocks have principally originated in a common parental media together with individual diamonds and their primary inclusions. The parental media represent completely miscible multicomponent silicate-(±oxide)-carbonate melts with dissolved carbon. On evidence derived from the mineralogical data (Sobolev, 1977), the natural silicate-carbonate parental melts of diamonds and their primary inclusions as well as of diamond-bearing rocks are changeable within the ultrabasic-basic compositions. By petrological information (Marakushev, 1984) and ^{13}C-isotope geochemical data (Galimov, 1991), the effect of compositional changeableness is also a characteristic feature of the upper mantle silicate magmas and diamond-free rocks. The physicochemically agreed processes of crystallization of natural diamonds and diamond-hosted mineral inclusions as well as rock-forming minerals of diamond-bearing rocks proceeded simultaneously within the upper-mantle chamber-reservoirs of the diamond-producing silicate-carbonate-carbon melts. The diamond-free bedrocks of the differentiated mantle material are the enclosing upper mantle rocks for the chambers. Hence the physicochemical conditions of petrogenesis of the diamond-bearing and diamond-free rocks with similar rock-forming minerals are different. Their combination within the upper mantle xenoliths in kimberlites has been in progress due to their transportation by kimberlitic magmas from the mantle to the Earth‘s crust depths.

Experimental study at 6 GPa of melting relations on the olivine (Ol) – diopside (Di) – jadeite (Jd) – garnet (Grt) system has revealed the peritectic reaction of olivine and jadeite-enriched melt with formation of garnet. The reaction position is schematically demonstrated as point P in the boundary Ol – Di – Jd join of the development of the Ol-Di-Jd-Grt system at the Fig. It is possible to see that the univariant curves Ol+Grt+L and Ol+Cpx+L can join together with temperature lowering in the quasi peritectic point P at 1380-1420^{o}C. During reaction in the peritectic association Ol+(Cpx/Omph)+Grt+L the Ol phase has to be disappeared and the univariant curve Omph+Grt+L, controlling formation of the basic eclogites, is formed. In the regime of fractional crystallization, these processes provide a transition from the olivine-normative compositions of the residual melts to the silica-normative ones and, correspondingly, from formation of the ultrabasic materials of the upper mantle garnet-peridotitic facies to the basic materials.

Table. Examples of the identity of mineral compositions for the diamond-hosted inclusions and diamond-bearing eclogites.

	Mir, Yakutia (Sobolev et. al., 1972)				Udachnaya, Yakutia (Shatsky et al., 2008)			
	Grt		Omph		Grt		Omph	
Oxide	Inclus	Rock	Inclus	Rock	Inclus	Rock	Inclus	Rock
SiO_2	40.00	39.70	54.80	55.50	42.35	42.40	56.27	56.40
TiO_2	0.46	0.43	0.48	0.56	0.08	0.12	0.33	0.19
Al_2O_3	22.00	21.50	9.79	9.39	23.20	23.30	4.84	4.91
Cr_2O_3	0.04	0.07	0.05	0.06	0.09	0.10	0.07	0.11
MgO	9.02	9.79	8.97	8.96	19.72	20.50	15.30	14.60
FeO	20.90	18.20	4.94	4.48	9.76	10.20	3.17	2.64
MnO	0.52	0.39	0.07	0.04	0.16	0.53	0.11	0.13
CaO	8.18	8.53	13.10	12.70	4.01	3.18	16.42	17.60
Na_2O	0.17	0.17	6.70	6.82	0.02	0.10	2.61	2.68
K_2O	-	-	0.30	0.08	-	-	0.54	0.60
Total	101.29	99.28	99.20	98.59	99.40	100.43	99.65	99.86

Comment. Inclus. – inclusion in diamond, Rock – diamond-bearing rock, Grt – garnet, Omph – omphacite.

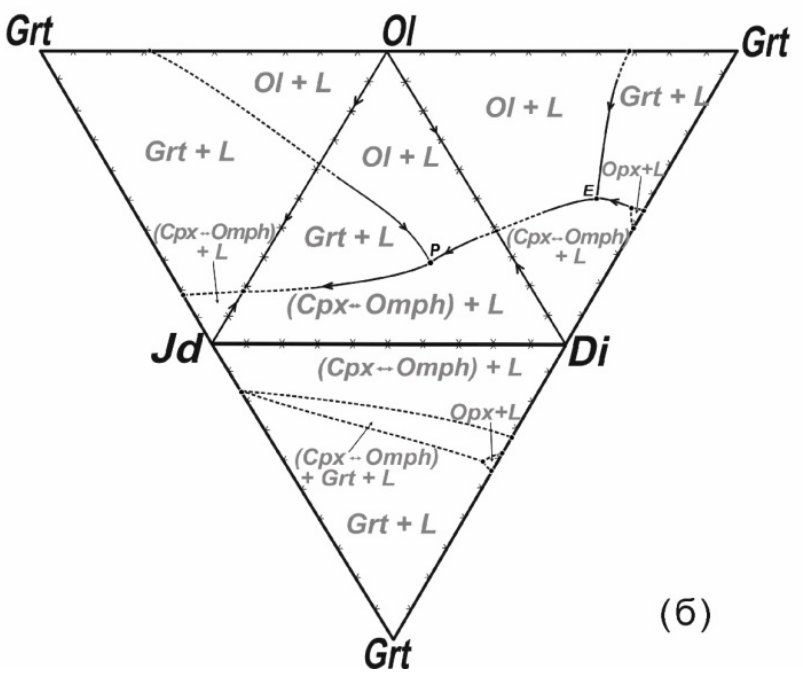

Fig. Melting relation for the boundary joins of the Ol-Di-Jd-Grt system by the relevant experimental data.

Genesis of the continuous ultrabasic-basic series of the diamond-bearing peridotite-pyroxenite-eclogite rocks contemporaneously with the diamond-hosted inclusions of peridotitic and eclogitic paragenesises has to be under control of fractional crystallization of their parental melts. The ultrabasic-basic evolution of the diamond-producing melts occurrs with elimination of olivine and orthopyroxene as the result of their peritectic reactions with melts that is revealed in physicochemical experiments. The peritectic reaction of orthopyroxene and melt is resulted in formation of clinopyroxene (Litvin, 1991). The major product of the peritectic reaction between olivine and jadeite-enriched melt is garnet. It should be pointed out that this process is well correlating with reactionary formation of pyrope in the forsterite-jadeite system above 4.5 GPa (Gasparik, Litvin, 1997).

The mechanical stirring of the diamond-bearing peridotites, pyroxenites, eclogites and grospydites with similar diamond-free bedrocks has been in progress within the streams of kimberlitic magma and locked in the crust cumulative cameras during the process of kimberlite magma solidification in them. Under this scenario, the ascending streams of kimberlite magma has destroyed the parental chambers and, inside of them, captured individual diamond crystals with primary inclusions, as well as diamond-bearing rocks, separate minerals and their intergrowths. Therewith, the kimberlite magmas have also captured the upper mantle diamond-free enclosing rocks at the magmas destructive entrance into and egress from the parental chambers. The chamber-extracted and enclosing upper mantle materials, being permanently intermixing, were transferred by kimberlitic magma to the crust cumulative cameras where the mix of genetically different diamond-bearing and diamond-free rocks were locked due to hardening of the kimberlite magma. Under the hardening processes within the cumulative cameras, the kimberlitic magmas liberate a strongly compressed fluid phase. At critical high pressure the fluid stream must force its way up through the cumulative camera roof for formation of explosive kimberlitic pipes. In the process the mechanically stirred diamond-bearing and diamond-free xenolith together with containing them kimberlite were transferred into the pipes.

Support: Program of the Presidium of Russian Academy of Sciences 1.08.P.

References

Galimov E.M. (1991). Isotope fractionation related to kimberlite magmatism and diamond formation. Geochim, Cosmochim. Acta 55, 197-1708.

Gasparik T., Litvin Yu.A. (1997). Stability of Na2Mg2Si2O7 and melting relations in the forsterite-jadeite join at pressures up to 22 GPa. Eur. J. Mineral. 9, 311-326.

Litvin Yu.A. (1991). Physicochemical Studies of Melting in the Earth's Interior. Moscow: Nauka, 312 p. (in Russian).

Litvin Yu.A. (2007). High-pressure mineralogy of diamond genesis. In: Advances in High-Pressure Mineralogy (edited by Eiji Ohtani). Geological Society of America Spesial Paper 121, p. 83-103.

Litvin Yu.A. (2017). Genesis of Diamonds and Associated Phases. Springer, 137 p.

Litvin Yu.A., Spivak A.V., Kuzyura A.V. (2016). Fundamentals of mantle carbonatite concept of diamond genesis. Geochem. Int.. 54(10), 839-857.

Marakushev A.A. (1984). Nodules of peridotites in kimberlites as indicator of the deep-seated structure of lithosphere. In: Lectures of Soviet Geologists at the XXYII Session of the International Geological Congress. Petrology. Moscow: Nauka, p. 153-160 (in Russian).

Shatsky S., Ragozin A., Zedgenizov D., Mityukhin S. (2008). Evidence for multistage evolution of diamond-bearing eclogite from the Udachnaya kimberlite pipe. Lithos 105, 289-300.

Sobolev N.V. (1977). The Deep-Seated Inclusions in Kimberlites and the Problem of the Composition of the Upper Mantle. Washington: AGU. 304 p.

Sobolev V.S., Sobolev N.V., Lavrentiev Yu.G. (1972). Inclusions in diamond from diamondiferous eclogite. DAN SSSR 207(1), 164-167 (in Russian).

PARENTAL MELT COMPOSITION FOR JACUPIRANGITE-MELTEIGITE SERIES OF GULI PLUTON

Makhatadze G.V.[1], Asavin A.M.[1], Serova L.D.[1,2], Buikin A.I.[1]

[1]Vernadksy Institute of Geochemistry and Analytical Chemistry RAS, Moscow, Russia, makhatadzeg36@gmail.com

[2]Lomonosov Moscow State University, Moscow, Russia, serova-larisa@mail.ru

Introduction. Jacupirangite-Melteigite Phase of polyphase Guli Pluton formed as third phase right after larnite-normative Foidite-Melilitolite Phase. There are multiple estimations of parental magma composition for melilitolitic series (Brey, Green, 1977; Kjarsgaard, 1989; Krigman et al., 1995; Rass, Plechov, 2000; Medard et al., 2004) which formed the whole variety of rocks there are in this series: kugdite, turjaite, uncompahgrite, melilitolite, okaite. However, low-Ca alkaline melts are studied much less thoroughly. Therefore, this would be of great interest to obtain new data on these magmas' composition.

Table 1. Compositions of mineral-hosted melt inclusions (wt%).

No.	SiO_2	TiO_2	Al_2O_3	FeO	MnO	MgO	CaO	K_2O	Na_2O
Inclusions in spinel from nepheline picrite 9769									
18	48.20	3.36	5.99	2.31	0.14	17.00	17.88	1.09	1.64
22	46.09	4.06	8.10	0.07	0.07	17.72	16.85	1.17	2.50
21	45.49	6.19	8.97	0.00	0.00	19.38	13.13	2.60	2.52
20	44.25	4.04	11.39	0.00	0.00	21.39	10.35	2.46	3.54
19	42.14	7.49	10.97	0.00	0.00	22.52	8.31	2.93	3.43
17	56.97	0.43	1.10	0.09	0.09	22.31	7.03	1.94	5.86
15	57.64	0.33	0.72	0.07	0.07	22.88	6.96	2.00	5.87
16	57.07	0.43	1.05	0.00	0.00	22.62	7.00	1.83	5.98
Inclusions in melilite from melilitolite GX3									
39	27.60	4.33	19.25	5.91	0.08	0.40	42.42	0.00	0.04
21	36.05	0.01		12.12	0.34	18.06	33.36	0.01	8.62
40	54.40	0.23	0.82	0.23	0.10	0.10	35.47	0.04	6.45
Inclusion in titanite from jacupirangite 9774									
11	56.87	0.31	1.53	1.94	0.00	24.98	7.20	0.72	7.53
1	55.43	1.21	2.15	7.47	0.15	22.22	3.78	0.06	0.00

We studied primary igneous minerals in samples of jacupirangite (9774) and nepheline picrite (9769) – pyroxene and early spinel respectively. We detected melt inclusions, most of them devitrificated though, however their bulk composition is measurable with EPMA using defocused electron beam. Assuming those inclusions contain melt which was present at the time of these rocks formation, obtained compositions (table 1, melt inclusions in pyroxene from melilitolite GX3 are also shown) can be interpreted as its composition after some corrections are made. The corrections in question are (1) for possible host-mineral addition into analysis (which was subtracted using Cr for spinel, Ti for titanite and K & Ti for melilitolite) and (2) normalization for 100%. As it could be seen in the table 1, composition are different even for inclusions from the same host grain. This is either due to rapid melt evolution or due to analysis imperfections.

The bulk rock samples and also hand-picked minerals from some of them were analyzed for trace elements using ICP-MS. Results are presented in table 2. For diagrams concentration values were normalized on CI chondrite according to Tompson (1982) or on concentrations in minerals (respective explanation is below).

Melt inclusions. Melt inclusions in pyroxene from ijolites (Isakova et al., 2015) are low-magnesium (<10 wt% MgO) and are closest in composition to melteigites and olivine-melteigites. The inclusions in pyroxene of jacupirangite (this study) are high-magnesium (<22 wt% MgO) and low-

calcium. Melt inclusions in spinel from picrite vary in wide range of compositions in between jacupirangite and ijolite. They form a linear trend in coordinates MgO-different main components and have a range of MgO content of 17-22 wt%. On one end of this trend the glass is practically identical to bulk composition of jacupirangite. Jacupirangites studied by different researchers (Egorov, 1991; Bogatikov et al., 1983) contain less magnesium. These points thus occupy the area between melteigites and jacupirangites on diagram MgO-CaO (Fig. 1a). Also, it is important to note that jacupirangites have similar compositions to melt inclusions from ijolites.

Table 2. Trace elements concentrations in bulk rocks and minerals (ppm); WR – for whole rock, Px – for pyroxene, Mel – for melilite, Mag – for magnetite.

	9769 WR	9774 WR	9774 Px	GX3 WR	GX3 Mel	GX3 Mag
Rb	29.37	8.39	2.61	1.31	0.39	0.31
Sr	820.30	157.60	123.82	870.27	923.89	56.89
Y	21.40	3.56	2.65	5.60	1.74	3.78
Ba	412.69	42.12	11.12	37.07	21.51	7.75
La	52.21	4.50	3.20	63.30	16.61	46.56
Ce	114.14	11.95	8.67	120.20	30.89	86.87
Pr	13.96	1.79	1.34	12.80	3.42	9.20
Nd	64.89	9.48	7.28	51.79	14.23	36.42
Sm	11.80	2.06	1.57	7.57	1.98	5.62
Eu	3.26	0.60	0.46	1.90	0.52	1.40
Gd	10.51	1.93	1.48	8.21	2.34	6.12
Tb	1.36	0.24	0.19	0.79	0.21	0.59
Dy	6.78	1.17	0.88	3.54	0.88	2.44
Ho	0.87	0.16	0.12	0.32	0.09	0.22
Er	2.43	0.41	0.31	0.97	0.28	0.68
Tm	0.23	0.05	0.04	0.06	0.03	0.04
Yb	1.42	0.27	0.21	0.32	0.11	0.21
Lu	0.18	0.04	0.04	0.04	0.02	0.03
Hf	7.80	1.36	1.04	0.54	0.11	1.55
Pb	3.38	1.76	0.74	0.76	0.82	0.26
Th	4.40	0.25	0.19	4.88	0.76	3.36
U	1.12	0.14	0.06	0.86	0.13	0.53
Cr	1110.69	636.66	2170.91	26.00	197.53	984.05
Zn	80.53	13.78	10.80	37.17	42.29	53.73
Zr	368.31	37.91	26.78	17.69	4.06	60.24
Nb	67.15	3.94	1.99	48.82	9.28	38.95
Mo	5.69	1.59	2.93	0.14	19.35	2.09
Cs	0.24	0.09	0.03	0.02	0.01	0.01
Ta	4.34	0.22	0.10	4.56	0.81	3.13

To summarize our observations there are 3 groups of melts detected in inclusions:

1) high in Mg, Si, K & Na and low in Ca – from jacupirangites;

2) low-magnesium (<10 wt% MgO) and high-alkali, close in its composition to the most differentiated melteigites – from ijolites;

3) very high-calcium (up to 42 wt% CaO) and almost without magnesium – from melilitolites.

On petrochemical diagrams with main components (Fig. 1a) these three local groups are connected by compositions of melt inclusions from nepheline picrite and bulk compositions of jacupirangites and melteigites.

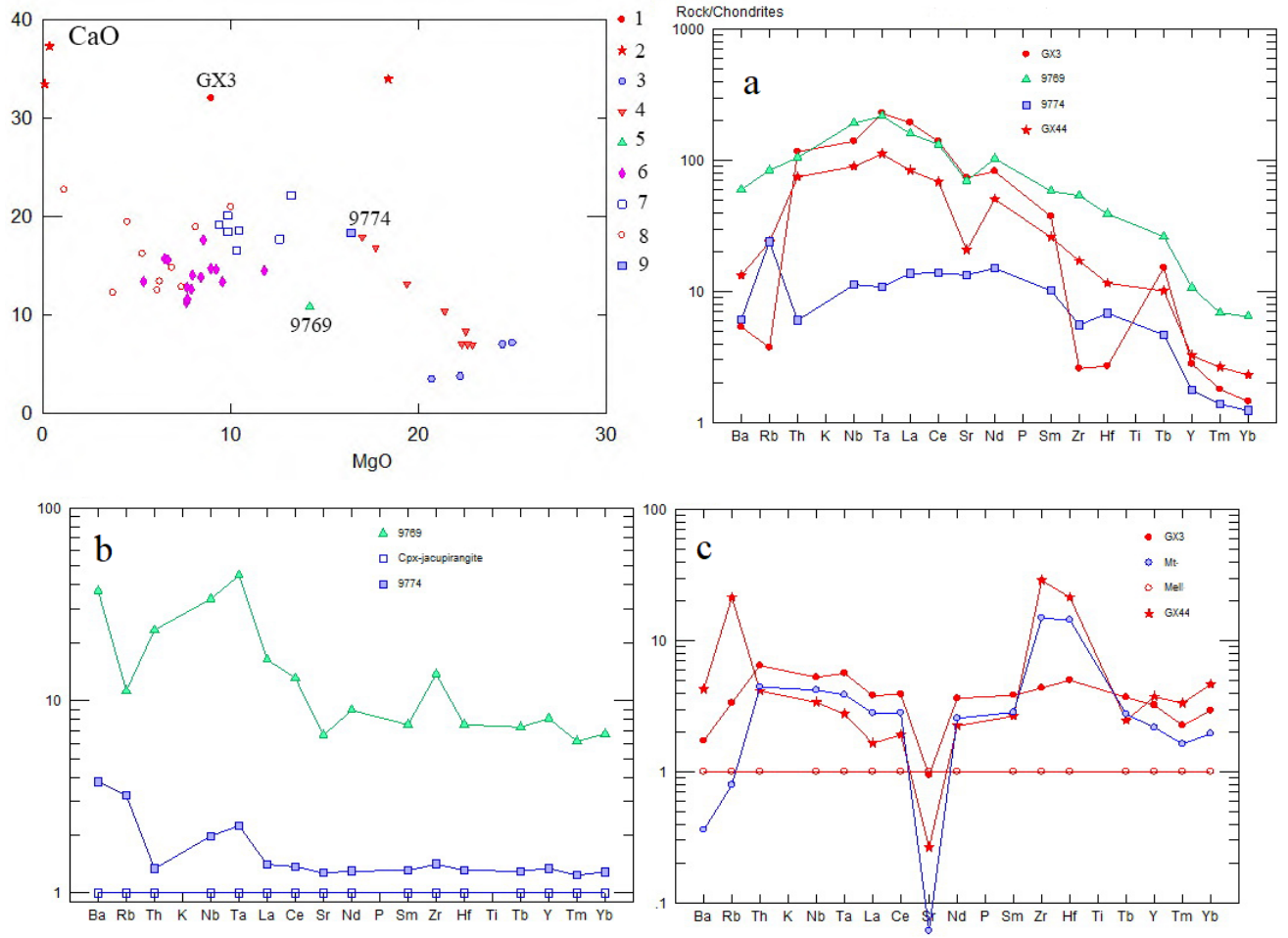

Figure 1. a) MgO-CaO diagram for melt inclusions and bulk rocks; 1 – GX3 WR, 2 – MIs (melt inclusions) in melilitolite; 3 – MIs in jacupirangite, 4 – MIs in spinel from picrite, 5 – 9769 WR, 6 – melteigite WR (Bogatikov et al., 1983; Egorov, 1991), 7 – jacupirangite WR (literature), 8 – MIs in ijolite (Isakova, 2015), 9 – 9774 WR; b-c-d) trace elements concentrations in bulk rocks and minerals; a – chondrite-normalized; b – Px from jacupirangite 9774-normalized; c – Mel from melilitolite GX3-normalized.

It is difficult to interpret these data in terms of petrogenesis right now. However, we can make preliminary conclusions. The 1st group is unlikely to represent jacupirangite parental magma due to its low-Ca and high-Mg for it to be placed in the field on monomineralic crystallization of pyroxene. The melt inclusions from picrite are on contrary very likely to represent the parental magma for 2 reasons. (1) They show a clear differentiation trend which points to jacupirangites composition. (2) Nepheline picrite and jacupirangite share their mineral association.

The 2nd group might be considered as the final product of differentiation of magmas which formed the jacupirangite-melteigite-ijolite series. It is also possible that they represent early interstitial melts in magma chamber.

The 3rd group has no connection to the series under the study. Its composition points out the independency of evolution of melilitolite and nepheline-pyroxene phases. Probably, these inclusions represent the parental magma for carbonatitic rocks.

Trace elements. The spider-diagrams are shown on figure 1. Trace elements concentrations in nepheline picrite are unexpectedly high (Fig. 1b). They are close to or even higher than (for Zr, Hf, Ba, Rb & Sr) concentrations in 2nd melilitolitic phase. This means that parental melts of jacupirangite-melteigite series were initially enriched in trace elements and that they have high ore potential in terms of HFSE, LILE and REE.

Trace elements concentrations in melilitolite are higher than those in uncompahgrite (apart from Zr, Hf, Ba). Melilitolite is considered as late subphase in the foidite series and these enrichments are thus expected. However, strong depletion in Zr & Hf is difficult to explain since there are no Zr-minerals reported for early stages of differentiation.

On figures 1c and 1d trace elements distributions normalized to main rock-forming mineral are shown (pyroxene for jacupirangite and melilite for melilitolite). This way of data presentation is used to show the effect of minerals crystallization on elements fractionation on residual melt.

Pyroxene from jacupirangite has low concentrations of trace elements which is in line with pyroxene-melt partition coefficients being much lower than 1 (Kuehner et al., 1989; Gaetani, Grove, 1995; Huang et al., 2006; Lofgren et al., 2006; Asavin, 2017). Jacupirangite consists mostly of the only pyroxene and this explains very close match of two spectra. Bulk rock contains more Nb, Ta, Ba & Rb than pyroxene which is apparently due to mica and titanite presence. If we consider jacupirangite as a cumulus from crystallization of model melt with composition of nepheline picrite 9769, we will expect them to have similar trace elements distributions which is the case (Fig. 1c). They have similar positive anomalies in Nb, Ta, Ba and negative one in Th. However, zirconium behavior is different: it shows positive anomaly. Concentrations differ at the level of one order of magnitude which implies long differentiation history. Residue melts ought to be even more enriched up to concentrations typical for ores. This is evidential of pyroxene-nepheline magmas having high potential in REE and Nb ore-forming.

The similar situation exists for melilitolitic subphase rocks. Zr, Hf & Rb are positively anomalous and Sr is negatively anomalous in uncompahgrite. This is very spectacular and means that melilite fractionated during the evolution of larnite-normative magmas. High (>1) partition coefficient of Sr for melilite-melt is reported (Kogarko et al., 1978). Its fractionation will thus explain the depletion of melt in Sr.

Conclusion. This study is a part of bigger research project which aims to determine the origin of the early phases of Guli Pluton. In order to do this one must answer several questions. Here are presented preliminary results on one of them – parental magma composition for Jakupirangite-Melteigite Phase which is absent in the literature.

This work was supported by RFBR grant No.19-05-00681.

References

Asavin A.M. Partition coefficients in the system melt-olivine-Ca-pyroxene and rare elements fractionation in alkaline melts based upon experimental and natural data. 2017. PhD Thesis. Irkutsk. Inst Earth Crust SB RAS. [in Russian].

Bogatikov O.A. (Chief Ed.) Magmatic rocks. M.: Nauka. 1983. 365 pp.

Brey G., Green D.H. Systematic Study of Liquidus Phase Relations in Olivine Melilitite + H2O + CO2 at High Pressures and Petrogenesis of an Olivine Melilitite Magma. Contrib Mineral Petrol. 1977. Vol. 61. P. 141-162

Egorov L.S. Ijolite–Carbonatite Plutonism: Maimecha–Kotui Complex of the Polar Siberia. Nedra, 1991. Leningrad. [in Russian].

Gaetani G.A., Grove T.L. Partitioning of rare earth elements between clinopyroxene and silicate melt Crystal-chemical controls. 1995. Geochim Cosmochim Acta. Vol. 59(10). P. 1951-1962.

Huang F., Lundstrom C.C., McDonough W.F. Effect of melt structure on trace-element partitioning between clinopyroxene and silicic, alkaline, aluminous melts. 2006. Amer Mineral. Vol. 91(8-9). P. 1385-1400.

Isakova A.T., Panina L.I., Rokosova, E.Yu. Carbonatite melts and genesis of apatite mineralization in the Guli pluton (Northern East Siberia). // Russian Geology and Geophysics. 2015. Vol. 56(3). P. 466-475.

Kjarsgaard B.A. Phase relations of a carbonated high-CaO nephelinite at 0.2 and 0.5 GPa. Geochim Cosmochim Acta. 1989. Vol. 53. Iss. 12. P. 3115-3131.

Kogarko L.N., Petrova E.N., Krigman L.D. Strontium fractionation during crystallization of apatite-bearing ijolite-urtite magmas. 1978. Doklady AN SSSR. Vol. 242. Iss. 6. P. 1403-1406. [in Russian].

Krigman L.D., Kogarko L.N., Veksler I.V. Melilite-melt equlibria and melilite role in evolution of ultra-alkaline magmas. 1995. Geokhimiya. Vol. 1. P. 3-15. [in Russian].

Kuehner S.M., Laughlin J.R., Grossman L., Johnson M.L., Burnett D.S. Determination of trace element mineral/liquid partition coefficients in melilite and diopside by ion and electron microprobe techniques. 1989. Geochim Cosmochim Acta. Vol. 53. Iss. 12. P. 3115-3131.

Lofgren G.E., Huss G.R., Wasserburg G.J. An experimental study of trace-element partitioning between Ti-Al-clinopyroxene melt: Equilibrium and kinetic effects including sector zoning. 2006. Amer Mineral. Vol. 91(10). P. 1596-1606.

Medard E., Schmidt M.W., Pierre S. Liquidus surfaces of ultracalcic primitive melts formation conditions and sources. Contrib Mineral Petrol. 2004. Vol. 148. N. 2. P. 201-215.

Rass I.T., Plechov P.Yu. Melt inclusions in olivine of olivine-melilite rock from Guli Massif, North-West Siberian Platform. 2000. Doklady RAN. Vol. 375. Iss. 3. [in Russian].

LA-ICPMS ANALYSIS OF THE PREDOMINANT ORE MINERALS FROM VARIOUS TYPES OF ORES WITHIN THE OKTYABRSKOE DEPOSIT (TALNAKH-NORIL'SK ORE DISTRICT)

Marfin A.E.[1], Abramova V.D.[2], Yakich T.Y.[3], Bestemianova K.V.[4], Ivanov A.V.[1], Kamenetsky V.S.[5,6]

[1]Institute of the Earth's Crust, Siberian Branch of the Russian Academy of Sciences, Irkutsk, Russia

[2]Institute of Geology of Ore Deposits, Petrography, Mineralogy, and Geochemistry, Russian Academy of Sciences, Moscow, Russia

[3]National Research Tomsk Polytechnic University, Tomsk, Russia

[4]National Research Tomsk State University, Tomsk, Russia

[5]School of Natural Sciences, University of Tasmania, Hobart, Australia

[6]Institute of Experimental Mineralogy, Russian Academy of Sciences, Chernogolovka Russia

There are unique Cu-Ni-Pt-Pd deposits associated with trap magmatism arising at the P-T boundary in the north-eastern part of the Siberian Platform (Ryabov et al., 2014). The main feature of these deposits is the predominance of Pd over Pt, which leads to 75% of world production of Pd. One of the largest deposits in this region is the Oktyabrskoe deposit. It is located and genetically related to the Kharaelakh intrusion. The host rocks for the deposit are terrigenous aluminosilicate and carbonate-sulfate sediments of Devonian (Zolotukhin et al., 1975).

The predominant sulfides within the Oktyabrskoe deposit are the minerals of the pyrrhotite group, chalcopyrite, and pentlandite, and also in significant amounts are noted such minerals as cubanite, talnakhite, mooihoekite, millerite, bornite, valleriite, covellite, heazlewoodite and others. Sulfide minerals are part of the industrial types of ores, which are subtracted by their structural and mineralogical characteristics. The major industrial types are massive (rich), disseminated and lenticular-disseminated (sometimes called «brecciated» or «copper-bearing»).

In massive ores, the sulfide mineralization reaches to 85-95%, they are usually concentrated in the intrusion base, on contact with host rocks, sometimes forming fissile veins over the host sedimentary rocks. Lenticular-disseminated ores contain from 30 to 50% sulfides. They are concentrated on the front face and in the roofing parts of the intrusion. Disseminated ores are located in the intrusion body, in the picritic and taxitic gabbro-dolerites horizon. The content of sulfide minerals varies from the first percent to 15-20%.

According to classical concepts, the formation of the massive sulfide ores is associated with the processes of liquation between sulfide and aluminosilicate melts. When the sulfide liquid was separated from the aluminosilicate part by the gravitational forces, the sulfide liquid sank out to the bottom of the magmatic chamber, forming a horizon of massive sulfide ores. At the same time, some drops that did not have time to sink out to the bottom of the chamber crystallized in the intrusion body, forming a zone of disseminated ores. Lenticular-disseminated ores are associated with contact-metamorphic and metasomatic mineral associations.

We have studied 3 main sulfide minerals (pyrrhotite, chalcopyrite, pentlandite) from three samples of various industrial types of ore. These specimens were studied under scanning electron microscope (SEM) TESCAN VEGA 3 SBU and energy-dispersive adapter OXFORD X-Max 50 with 20 kV accelerating voltage, sample current 10-50 nA (TPU, Tomsk). An example of SEM visualization and analyzes is shown in Fig. 1a,b. The composition of trace element was determined by inductively coupled plasma mass spectrometry with laser ablation (LA-ICPMS) (IGEM, Moscow). The instrument was Thermo Xseries 2 quadrupole mass spectrometer with ESI NWR 213 laser. The beam size was 20-30 μm (Fig. 1a). Three sulfide reference materials were used to control the quality of analytical results: MASS-1 (US Geological Survey) - certified Synthetic Polymetallic Sulfide ZnCuFeS as pressed pellets; in-house standard po-stc, containing 20 ppm Au, Ag and PGE in a pyrrhotite matrix, manufactured according to a method described in (Wohlgemuth-Ueberwasser et al., 2007); UQAC-FeS1 (UQAC, Chicoutimi, Canada) pressed natural sulfide doped with trace elements. Iron isotope-57 was used as an internal standard.

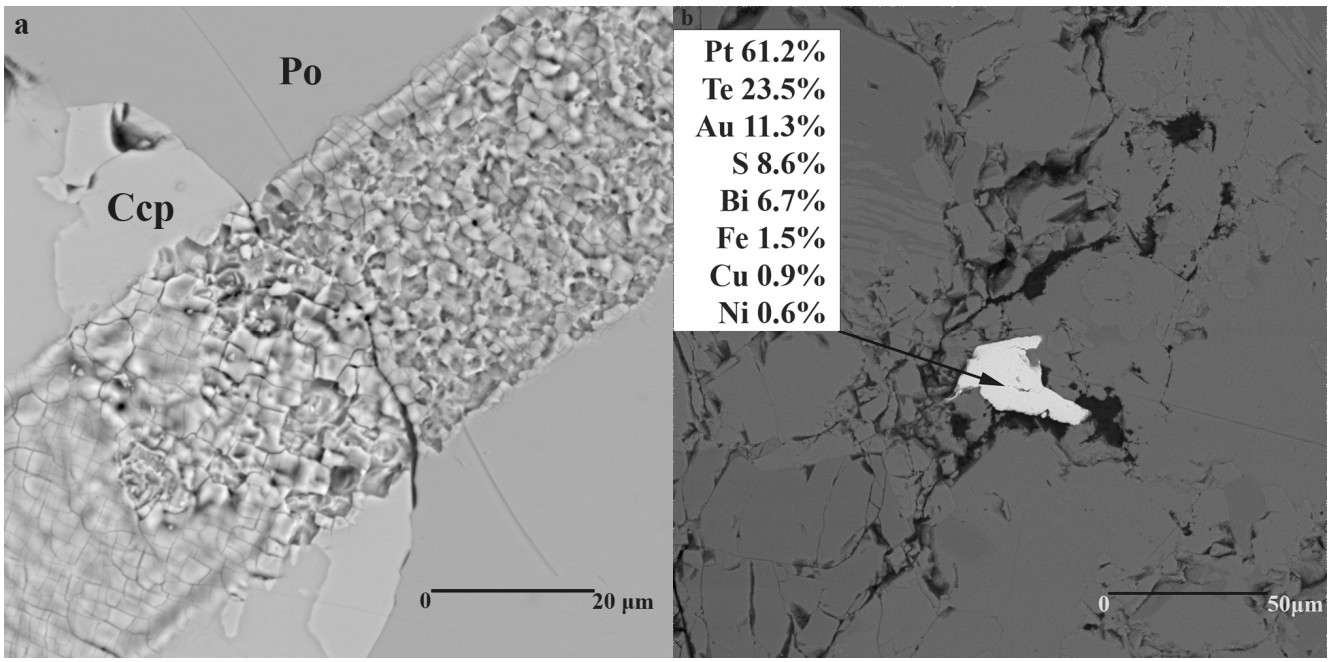

Fig. 1. An example of SEM visualization. In Fig.1a a laser ablation track is evident across chalcopyrite (Ccp) and pirrhotite (Po) boundary. In Fig. 1b non-identified mineral (Pd-Au-rich cooperite?) is shown.

Sample AM59 is a massive ore of chalcopyrite-pyrrhotite, containing a few insets of such minerals as anhydrite, calcite, and chlorite. Ore mineralization is represented by pyrrhotite, chalcopyrite, pentlandite, and Co-rich pentlandite. Cooperite, Pd-Au-Pt sulfide (Pd-Au-rich cooperite? (Fig. 1.b)) and native gold with an admixture of silver are also present. PGE minerals of 25-50 μm in size are usually confined to the boundaries of sulfide phases.

Sample AM51 represents lenticular-disseminated ore. Sulfide mineralization is represented by pyrrhotite, chalcopyrite, pentlandite, Ag-, Co-containing pentlandite. The silicate part is represented by the hedenbergite-diopside pyroxene, the composition of pyroxene varies, from virtually pure diopside to pure hedenbergite. According to the results of LA-ICPMS, pyrrhotite is characterized by traces of Co (90 ppm), Ni (0.2%), Pb (14 ppm), chalcopyrite - Co (4-10 ppm), Ag (1-10 ppm), Cd (30-600 ppm), In (2-5 ppm), Te (10-35 ppm), Pb (5-40 ppm), pentlandite - Co (0.8-1.2%), Pd (470-850 ppm), Ag (0.2-2.5 ppm).

Sample AM68 represents disseminated ore. Sulfide mineralization is represented by unevenly distributed sulfide, amoebae drops. The composition of the drops is pyrrhotite, chalcopyrite, pentlandite, Co-rich pentlandite. According to the results of LA-ICPMS analysis, pyrrhotite contains Ni (1-1.5%), Co (200-770 ppm), Cd (46-63 ppm), In (0.3 ppm), Pb (0.7-20 ppm), Bi (0.2- 5 ppm), chalcopyrite - Co (0.8-45 ppm), Ni (50-75 ppm), Ag (3-30 ppm), Cd (35-100 ppm), Sn (16-25 ppm), Pb (2.3- 10 ppm) Bi (0.6-2 ppm). Pentlandite is rare and was not sampled by the laser ablation tracks.

The most characteristic trace elements in sulfide minerals are shown in Table 1. It can be seen that Ni, Co, Pb are permanent element in pyrrhotite. Pt was found only in pyrrhotite from massive ore, while pyrrhotite of disseminated ore is characterized by the presence of Cd, In, Bi, and pyrrhotine from lenticular-disseminated ore is the poorest in trace elements.

Table 1. The most common trace elements in major sulfide minerals are industrial types of ores.

Minerals / Ore types	pyrrhotite	chalcopyrite	pentlandite
Massive	Ni, Co, Pb, Pt	Ag, Cd, Pt, Pb, Bi	Co, Pd, Au
Lenticular-disseminated	Ni, Co, Pb	Co, Ag, Cd, Pb, In, Te,	Co, Pd, Ag
Disseminated	Ni, Co, Pb, Cd, In, Bi	Ni, Co, Ag, Cd, Pb, Bi, Sn	Not analysed

Ag, Cd and Pb impurities are characteristic of chalcopyrite from all types of ores. Perhaps this is due to the inclusion of galena. Pt was found only in chalcopyrite from massive ore. The analyzed pentlandite is characterized by a constant admixture of Co and Pd, while Au and Ag are found in varying amounts.

Abnormally high concentrations of Pd are found only in pentlandite. The analysis was performed at surface areas with no visible inclusions of other minerals. However, it is possible that tiny inclusions of the Pd minerals were located below the surface and were captured during the analysis. While for Ag and Au, it is possible to assume their isomorphic entry into the lattice of sulfide minerals.

Thus, there are some patterns in the distribution of trace elements in the main sulfides of the three types of ores:

1. Pt is a characteristic of pyrrhotite and chalcopyrite of massive ores only.
2. Chalcopyrite and pyrrhotite of disseminated ores are characterized by the greatest variety of trace elements.
3. Explicit fractionation of Pt and Pd is detected. Pd is concentrated in pentlandite only.

The work is supported by the Russian Science Foundation (grant no 16-17-10068).

References

Ryabov, V., Shevko, A.Y., Gora, M.. Trap Magmatism and Ore Formation in the Siberian Noril'sk Region: Volume 1. Trap Petrology. Springer Science & Business Media., 2014, pp 390.

Wohlgemuth-Ueberwasser C.C., Ballhaus C., Berndt J., Stotter née Paliulionyte V., Meisel T. Synthesis of PGE sulfide standards for laser ablation inductively coupled plasma mass spectrometry (LA-ICP-MS) // Contributions to Mineralogy and Petrology. – 2007. – Vol. 154. – №. 5. – p. 607-617.

Zolotukhin, V., Ryabov, V., Vasil’ev, Y.R., Shatkov, V. Petrology of the Talnakh ore-bearing differentiated trap intrusion. Nauka Press, Novosibirsk, 1975, pp. 432.

SODIUM- AND TITANIUM-RICH PHASES IN THE EARTH'S MANTLE (EVIDENCE FROM EXPERIMENTS IN THE Na_2O-MgO-SiO_2-TiO_2 SYSTEM AT 7–24 GPa)

Matrosova E.A.[1], Bobrov A.V.[1,2], Bindi L.[3], Irifune T.[4]

[1]Vernadsky institute of Geochemistry and Analitycal Chemistry RAS, Moscow, Russia
ekaterina.a.sirotkina@gmail.com
[2]Geological Faculty, Moscow State University, Moscow, Russia
[3]Dipartimento di Scienze della Terra, Università di Firenze, Via La Pira 4, 50121 Florence, Italy
[4]Geodynamics Research Center, Ehime University, Matsuyama 7908577, Japan

Despite significant interest of experimentalists to the study of geophysically important phase equilibria in the Earth's mantle, incorporation of minor elements in mantle phases was mostly studied on a qualitative level. The influence of such elements on structural peculiarities of high-pressure phases is poorly investigated, although even small concentrations of these elements may significantly influence the physical properties of mantle phases (Panero et al., 2006; Andrault, 2007). According to the existing models (Ringwood, 1966), titanium and sodium are characterized by the low bulk concentrations in the Earth's mantle (0.2 wt % TiO_2, 0.57 wt % Na_2O). However, Ti- and Na-rich lithologies may occur in the mantle as a result of oceanic crust subduction. Our experiments aimed on the study of phase relations, synthesis of Ti- and Na-bearing phases in the Na_2O-MgO-SiO_2-TiO_2 system at 7–24 GPa and 1000–1700°C.

The Na–Ti-bearing pyroxene was synthesized at 7 GPa and 1700 °C. Synthesis experiments were performed at the Vernadsky Institute of Geochemistry and Analytical Chemistry RAS, using the high-pressure toroidal 'anvil-with-hole' apparatus, which is a modifcation of the Bridgeman-type anvil assembly. Solid-state cells of 30-mm outer diameter were manufactured from pressed mixture of MgO and BN in equal parts. They contained an ultrapure graphite heater, into which experimental starting materials were loaded. The temperature measurement accuracy was ±10°C. Run pressure was controlled to ±0.5 GPa. Details of experimental techniques were described by Bobrov and Litvin (2009).

Experiments with Na-Ti-pyroxene ($Na(Mg_{0.5}Ti_{0.5})Si_2O_6$) starting material were carried out at the Ehime University (Matsuyama, Japan) at 10–24 GPa and 1000–1300°C using a 2000-t Kawai-type multi-anvil high-pressure apparatus. Samples were compressed by eight cubic tungsten carbide anvils with 4- and 3- mm truncation edges. High temperature was achieved using a cylindrical $LaCrO_3$ heater. The sample was loaded into a platinum capsule and was isolated from the heater by a MgO insulator (Sirotkina et al., 2015). Sample pressure was calibrated at room temperature using the semiconductor–metal transitions of Bi, ZnS and GaAs (Irifune et al., 2004). The e□ect of temperature on pressure was further corrected using the α–β and β–γ phase transitions of olivine (Katsura, Ito, 1989). The starting material was prepared by mixing MgO, SiO_2, TiO_2 and Na_2SiO_3 in stoichiometric proportions for the garnet-like $Na_2MgTi_2Si_3O_{12}$ and pyroxene-like $Na(Mg_{0.5}Ti_{0.5})Si_2O_6$ composition. The quenched samples were examined on a single-crystal X-ray diffractometer, and the composition of phases was analyzed using SEM-EDS.

Depending on the PT-parameters the main phases obtained in experiments were Na-Ti-pyroxene (at 10 GPa) with rutile and clinoenstatite (at 7 GPa), association of Na-Px, stishovite and $Na(Ti_{1.5}Mg_{0.5})O_4$ with calcium ferrite-type structure (at 16 GPa) and $MgSiO_3$-bridgmanite (at 24 GPa). The content of these phases in the run products is higher than 90 vol %. An association of Na-Ti-pyroxene, rutile and pyroxene is stable at a pressure 7 GPa and 1700°C. The texture of the experimental sample is formed by an aggregate of euhedral Na–Ti-pyroxene crystals with a size of >50 μm in the quenched groundmass of elongate rutile and pyroxene crystals with length up to 100 μm. Increase of pressure up to 10 GPa and decrease of temperature up to 1000–1300°C result in the formation of a single-phase field of Na-Ti-pyroxene. This mineral forms massive aggregates with a size of individual grains up to 25 μm. A paragenesis of Na-majorite and phase $Na(Ti_{1.5}Mg_{0.5})O_4$ with the calcium ferrite (Cf) structure-type appears at 16 GPa. The sample texture is formed by relatively small euhedral Na-majorite crystals with size up to 10 μm, small subhedral Cf grains and stishovite with size up to 20 μm. The stability field of $MgSiO_3$ bridgmanite opens up at pressures of >24 GPa.

Bridgmanite forms large euhedral crystals with a grain size of up to 100 μm in the fine-grained groundmass of elongate Cf crystals with length up to 10 μm and smaler Na-majorite crystals.

Na-Ti-pyroxene synthesized in the Na_2O-MgO-SiO_2-TiO_2 system shows wide compositional variations. Based on six oxygen atoms, the formula of Na–Ti-pyroxene synthesized at 7 GPa is $Na_{0.86}Mg_{0.71}Ti_{0.43}Si_{2.00}O_6$. This means that studied Na-Ti-pyroxene is a solid solution between enstatite ($Mg_2Si_2O_6$) and $Na(Mg_{0.5}Ti_{0.5})Si_2O_6$ with the following substitution mechanism: $Na^{+}+(Ti^{4+}\square)/2+(Mg^{2+})/2=2Mg^{2+}$. Na-Ti-pyroxene synthesized at 10 GPa characterized by the following composition (wt %: SiO_2 57.23, MgO 9.52, Na_2O 14.39, TiO_2 17.41, total 98.55) is basically identical to that of pure Na-Ti-Px with formula $Na_{0,99}(Mg_{0,51}Ti_{0,47})Si_{2,03}O_6$. It was established that increase of temperature resulted in a slight decrease of the titanium content in Na-Ti-pyroxene.

Na-majorite was registered in association with *$Na(Ti_{1.5}Mg_{0.5})O_4$ with calcium ferrite-type structure* and stishovite at 16 GPa. Na-Maj is characterized by small admixture of Ti (up to 4.5 wt % TiO_2, 0.23 Ti pfu). Cf is characterized by a small silicon admixture (up to 2 wt % SiO_2, 0.060 Si pfu). $MgSiO_3$ *bridgmanite* demonstrates the higher titanium solubility. The content of TiO_2 in Brd reaches 12.9 wt % which is corresponds to 17 mol % $MgTiO_3$. It is important to note that the sodium content in this phase reaches 3.8 wt % Na_2O.

It was established that incorporation of Ti into low-Ca (Opx), high-Ca (Cpx), and Ti-rich Aeg pyroxenes proceeds through the different substitution mechanisms. In particular, $Na(Mg_{0.5}Ti_{0.5})Si_2O_6$ component described in this study plays the major role in low-Ca Px, whereas Ti-rich Aeg (Curtis, Gittins, 1979), is most likely characterized by the presence of Ca-Ti end-members, such as Ca-Ti analogues of Tschermak molecule ($CaTi^{4+}Al_2O_6$ and $CaTi^{3+}AlSiO_6$), as well as the component $Ca(Mg_{0.5}Ti^{4+}_{0.5})AlSiO_6$. Joint incorporation of sodium and titanium in the composition of pyroxenes may be explained by two completely different mechanisms. The first type of substitution suggests incorporation of sodium in pyroxene together with trivalent cations as components like $NaM^{3+}Si_2O_6$. This type of substitution is preferable for high-Ca monoclinic pyroxene. The second type of substitution occurs as a result of involving the Na-Ti component $Na(M^{2+}_{0.5}Ti^{4+}_{0.5})Si_2O_6$. Examples of substitution of the second type are low-Ca pyroxenes from inclusions in diamonds and mantle xenoliths, with the TiO_2 and Na_2O concentrations <0.25 and 0.35 wt %, respectively (Bishop et al. 1978; Ionov et al. 2010).

Acknowledgments: This study was supported by the Russian Science Foundation (project no. 17-17-01169).

References

Andrault D. Properties of lower-mantle Al-(Mg,Fe)SiO_3 perovskite. // Geological Society of America. Special Papers. 2007. Vol. 421. P.15–36.

Bishop F.C., Smith J.V., Dawson J.B. Na, K, P and Ti in garnet, pyroxene and olivine from peridotite and eclogite xenoliths from African kimberlites. // Lithos. 1978. Vol. 11:155–173.

Bobrov A.V., Litvin Y.A. Peridotite–eclogite–carbonatite systems at 7.0–8.5 GPa: concentration barrier of diamond nucleation and syngenesis of its silicate and carbonate inclusions. // Russian Geology and Geophysics. 2009. Vol. 50:1221-1233.

Curtis L.W., Gittins J. Aluminous and titaniferous clinopyroxenes from regionally metamorphosed agpaitic rocks in central Labrador. // J Petrol. 1979. Vol. 20: 165-186.

Ionov D.A., Doucet L.S., Ashchepkov I.V. Composition of the Lithospheric Mantle in the Siberian Craton: New Constraints from Fresh Peridotites in the Udachnaya-East Kimberlite. // J Petrol. 2010. Vol. 51:2177–2210.

Irifune T., Kurio A., Sakamoto S., Inoue T., Sumiya H., Funakoshi K. Formation of pure polycrystalline diamond by direct conversion of graphite at high pressure and high temperature. // Phys. Earth Planet. Inter. 2004. Vol. 143. P. 593–600.

Katsura T., Ito E. The system Mg_2SiO_4–Fe_2SiO_4 at high pressure and temperatures: precise determination of stabilities of olivine, modified spinel and spinel. // J. Geophys. Res. 1989. Vol. 94. P. 15663–15670.

Panero W.R., Akber-Knutson S., Stixrude L. Al_2O_3 incorporation in $MgSiO_3$ perovskite and ilmenite. // Earth Planet. Sci. Lett. 2006. Vol. 252. P. 152–161.

Ringwood, A.E. The chemical composition and origin of the Earth. // In: Advances in Earth science. Hurley, P.M. (Editors), M.I.T. Press, Cambridge. 1966. P. 287–356.

Sirotkina E.A., Bobrov A.V., Bindi L., Irifune T. Phase relations and formation of chromium-rich phases in the system $Mg_4Si_4O_{12}$–$Mg_3Cr_2Si_3O_{12}$ at 10–24 GPa and 1,600 °C // Contrib Mineral Petrol. 2015. V. 169:2. DOI: 10.1007/s00410-014-1097-0.

EUDIALYTE COMPLEX OF THE LOVOZERO ALKALINE MASSIF (KOLA PENINSULA, RUSSIA): MINERAL CHEMISTRY AND FORMATION

Mikhailova Yu.A., Pakhomovskiy Ya.A., Kalashnikov A.O., Yakovenchuk V.N., Bazai A.V., Ivanyuk G.Yu.

Geological Institute KSC RAS, Apatity, Russia, ylya_korchak@mail.ru

The Lovozero alkaline layered intrusion consists of two large complexes: Eudialyte (18 vol. %) and Layered (77 vol. %). The Eudialyte complex lies at the top of the massif and has no layering. This complex is composed by foid syenite and foidolite enriched in eudialyte-group minerals (eudialyte lujavrite). Within the Layered Complex, there is well-defined layering, the elementary unit of that is the "rhythm" (from the bottom up) of urtite-foyaite-lujavrite. In this sequence, there occurs a gradual transition from almost monomineral nepheline foidolite (urtite) to leucocratic foid syenite (foyaite), and then to meso- and melanocratic foid syenite (lujavrite). The structure of rocks changes from massive (in urtite) to trachytic (in lujavrite) due to the gradual ordering of tabular feldspar crystals. The sequence "urtite-foyaite-lujavrite" is repeated regularly (Vlasov et al., 1959; Gerasimovskii et al., 1966; Bussen, Sakharov, 1972). Other rocks (poikilitic foid syenites, pegmatites and hydrothermal veins) form sub-horizontal sheet-like bodies and lenses within the Eudialyte and Layered complexes (Semenov, 1972; Pekov, 2001). Xenoliths of volcano-sedimentary rocks are ubiquitous (Korchak et al., 2011).

We investigated the rocks of the Eudialyte complex within the area of Mts Alluiave and Kedykvyrpakh. Brief petrographic description of rocks is as follows. Among the studied samples, medium- or coarse-grained malignite (Le Maitre, 2005) as well as ijolite and shonkinite (meso- and melanocratic rocks) are predominated, with gradual transitions between them. The rock-forming minerals include microcline-perthite, nepheline, sodalite, natrolite, aegirine-(augite), (magnesio)arfedsonite and eudialyte-group minerals (EGM).

Euhedral plates of microcline-perthite are elongated on (001) up to 3 cm, with dominant pinacoidal faces (010), and the side ratio is 10:6:1. Often the microcline-perthite crystals are curved and cracked. They have complex perthitic structure where albite marks fractures in microcline and forms braid perthites. Perthitic albite occupies about 17 vol. % of the crystal, being intensively replaced by secondary natrolite. Foid grains are located between the microcline-perthite plates. The most common of foid, nepheline, forms grains of two morphological types. Nepheline-I occurs as euhedral crystals with numerous small inclusions of aegirine and microcline. Nepheline-II is represented by lense-like anhedral grains with small inclusions of aegirine-(augite) in marginal zone. Sodalite and natrolite, except for pseudomorphs on nepheline and albite, form primary grains, similar in morphology with crystals of nepheline-II and coexisting with them. Inside the grains of primary sodalite, there are natrolite and/or natrolite-sodalite aggregates. The feldspar, foid and natrolite grains are surrounded by "streams" of subparallel prismatic crystals of mafic minerals. The marginal parts of the "streams" are composed by long-prismatic aegirine-(augite) crystals, and the axial zones consist of larger anhedral amphibole and EGM grains. The edge parts of the amphibole grains usually contain clinopyroxene inclusions oriented along to the general direction of the "stream".

The space between the mafic minerals of the "streams" is filled by natrolite. If the proportion of natrolite is large, the clinopyroxenes and amphiboles occur as euhedral short-prismatic crystals. For EGM, round or lenticular forms are usual, while their euhedral crystals are rare. The marginal parts of EGM grains are enriched in inclusions of aegirine-(augite) and amphiboles. These inclusions are also oriented according to the general direction of the "stream". The total length of boundaries between grains of EGM and clinopyroxene+amphibole exceeds that between EGM and leucocratic minerals as 9:1. The accessory minerals of meso- and melanocratic rocks are located in the interstices of pyroxene-amphibole aggregate. The most common of them (above 50% of studied samples) are loparite, lueshite, stronadelphite, pyrochlore-group minerals, lamprophyllite, baritolamprophillite, chlorbartonite, sulfides (sphalerite, pyrrhotite, chalcopyrite), thorite and thorianite.

The colour index M′ (Le Maitre, 2005) increases in malignite → shonkinite and ijolite → melteigite series due to growth of EGM content, while the total amount of other mafic minerals does not exceed 38 mod. % (in average 30 mod. %).

Among the meso- and melanocratic rocks, there are irregularly located sub-horizontal layers and lenses (0.01 to 70 m thick) of subsolvus leucocratic rocks namely foyaite and urtite. The transition between (meso-)melanocratic and leucocratic rocks is gradual, but the interval of this transition is very narrow. Orientation of grains of rock-forming minerals (such as feldspar and clinopyroxene) in melanocratic and leucocratic rocks is the same near the contact. Set of rock-forming minerals in foyaite and urtite coincides with that in malignite, shonkinite and ijolite, but they contain two primary feldspar: microcline and albite. Nepheline forms euhedral crystals with both inclusions of microcline+aegirine, and without inclusions. Natrolite not only replaces nepheline, but also forms primary grains in association with unchanged nepheline. Primary sodalite is present. Mafic minerals in the leucocratic rocks do not form "streams": fine-grained aggregates of prismatic aegirine-(augite) and rounded EGM grains fill interstices between microcline-perthite (with axial ratio 1:2:5), albite and nepheline grains, while amphiboles form poikilitic crystals. When the color index M′ decreases, poikilitic crystals, in addition to amphiboles, begin to form first pyroxenes, and then EGM.

For leucocratic rocks, the lovozerite-group minerals are characteristic, which can sometimes be rock-forming. Typomorph accessory phosphorus-bearing minerals include stronadelphite, fluorapatite, lomonosovite, vuonnemite, bornemanite, monazite-(Ce), xenotime-(Y), nastrophite and nabaphite.

Sometimes the foyaite has a fine-grained or porphyry structure. Fine-grained rock consists of euhedral albite (in average 30 vol. % of rock), anhedral grains of microcline (without perthite) and nepheline. Prismatic crystals of aegirine(-augite) and rounded EGM grains are either uniformly dispersed in the rock or form small lenses in the mass of leucocratic minerals. Microcline-perthite and nepheline form phenocrysts in fine-grained mass. Elongation of albite plates and aegirine(-augite) prisms is almost parallel to the phenocryst faces. The content of phenocrysts varies from single grains to 40 modal %. With increase in the content of microcline-perthite and/or nepheline phenocrysts, fine-grained foyaite transforms into medium- to coarse-grained ones.

Features of chemical composition of rock-forming minerals are as follows. Microcline-perthite in meso-and melanocratic rocks consists of pure Ab_{100} and microcline $Mi_{94-99}Ab_{1-6}$ with permanent impurities of Fe_2O_3 (up to 0.64 wt.%) and BaO (up to 0.20 wt.%). In leucocratic rocks, the average composition of microcline-perthite phenocrysts is $Mi_{91-98}Ab_{2-9}$, and perthites are represented by pure albite. Microcline from the fine-grained foyaite has composition of $Mi_{80-92}Ab_{6-17}$, with relatively high content of Fe_2O_3 (up to 0.91 wt.%) and BaO (up to 0.31 wt.%). In leucocratic rocks, the composition of primary albite is $Ab_{94-99}Or_{1-6}$, with permanent impurity of Fe_2O_3 (up to 0.30 wt.%).

Morphological types of nepheline from meso- and melanocratic rocks are clearly separated by the content of Qtz minal. The composition of nepheline-I is $Nph_{67-78}Ks_{15-23}Qtz_{1-12}$, while anhedral grains of nepheline-II contain more Qtz-component: $Nph_{61-74}Ks_{13-21}Qtz_{9-23}$. The composition of nepheline from leucocratic rocks is $Nph_{62-75}Ks_{15-22}Qtz_{3-20}$. Iron (up to 2.13 wt.% Fe_2O_3) is a permanent impurity in nepheline, and rare impurities found in only 1% of samples are Ca (up to 0.62 wt.% CaO) and Ba (up to 0.10 wt.% BaO). The iron content is positively correlated with Si and negatively with Al and K, according to the scheme: $\square_B + (Si^{4+} + Fe^{3+})_T \leftrightarrow K^+_B + 2Al^{3+}_T$ (if the composition of nepheline is expressed by the formula $A_3BT_8O_{16}$). In meso- and melanocratic rocks, contents of Si, Fe^{3+}, Al and K in nepheline-I correlate with amount of Fe^{3+} in coexisting microcline-perthite. There is no significant correlation between the compositions of nepheline-II and coexisting alkali feldspar in these rocks. The compositions of coexisting nepheline and microcline from fine-grained foyaite are completely correlated.

Chemical composition of clinopyroxenes in rocks of the Eudialyte complex varies widely, but does not depend on the type of rock. In all types of rocks, clinopyroxenes are represented by aegirine (96 % of samples) and aegirine-augite with high content of titanium (up to 5.55 wt.% TiO_2), zirconium (up to 2.35 wt.% ZrO_2) and aluminum (up to 1.20 wt.% Al_2O_3). Their composition is determined by two isomorphic schemes:

$$Na^+ + Ti^{4+} + Al^{3+} \leftrightarrow Ca^{2+} + Mg^{2+} + Zr^{4+} \text{ and}$$

$$(Al,Fe)^{3+} + Fe^{3+} \leftrightarrow Si^{4+} + Fe^{2+}.$$

The zirconium content increases with growth of Ca and Mg amounts reaching maximal values in aegirine-augite. High concentrations of titanium, on the contrary, are characteristics of aegirine. It is important to note presence of constant admixture of manganese (up to 1.09 wt.% MnO) in clinopyroxenes.

Amphiboles of the Eudialyte complex are represented by magnesioarfvedsonite, while the edge parts of some zonal crystals are composed of arfvedsonite. The compositional zonation is especially characteristics of poikilitic amphibole crystals from fine-grained foyaite. Characteristic impurities in amphiboles of the Eudialyte complex include Li (up to 1.00 wt.% LiO_2), Ti (up to 2.40 wt.% TiO_2), Mn (up to 3.87 wt% MnO), while Zr (up to 0.25 wt.% ZrO_2) and Zn (up to 0.54 wt. % ZnO) are comparatively rare. The dominant substitution mechanism seems to be the coupled substitutions:

$$Ca^{2+} + Mg^{2+} + Al^{3+} \leftrightarrow (Na, K)^{+} + (Fe, Mn)^{2+} + Si^{4+} \text{ and}$$

$$Fe^{2+} + Fe^{2+} \leftrightarrow Fe^{3+} + Li^{+}.$$

In leucocratic rocks amphiboles are enriched in Na, Mn and Si. In meso- and melanocratic rock, cations of the same name in the compositions of coexisting pyroxenes and amphiboles have positive correlations. In leucocratic rocks, no significant correlations between compositions of pyroxenes and amphiboles were found.

The composition of eudialyte-group minerals from the rocks of the Eudialyte complex varies widely. In meso- and melanocratic rocks, EGM contain significantly more Zr and Fe and slightly less Sr, REE, Si than in leucocratic rocks. The contents of Na, Ca, Nb, Ti, Al and Cl are the same for EGM from all lithologies. Excess zirconium (above 3 apfu) replaces silicon and niobium in position M(3) (Johnsen et al., 2003), up to the predominance of zirconium in this position (Zr-rich eudialyte$_{ss}$). In general, the following substitutions occur in EGM:

$$(Fe, Mg)^{2+} + Zr^{4+} + 2Na^{+} \text{ (eudialyte}_{ss}) \leftrightarrow$$

$$Si^{4+} + Mn^{2+} + \textit{REE}^{3+} + Nb^{5+} + (Ca, Sr)^{2+} \text{ (kentbrooksite)}$$

High content of the kentbrooksite end-member is characteristics of EGM from leucocratic rocks. In meso-and melanocratic rocks, there occur zonal EGM grains: Zr-rich eudialyte$_{ss}$ (core) → eudialyte$_{ss}$ (periphery) and/or eudialyte$_{ss}$ (core) → kentbrooksite (periphery). In leucocratic rocks, EGM do not form zonal grains. A correlation between the compositions of coexisting pyroxenes and EGM (central parts of the grains) is found in meso- and melanocratic rocks. Calcium and magnesium contents in pyroxenes have positive correlations with calcium amount in EGM and negative correlations with Zr content in EGM.

Thus, the Eudialyte complex is composed of two groups of rocks. The first is the hypersolvus meso- and melanocratic rocks with rock-forming EGM and the ratio $(Na_2O + K_2O)/Al_2O_3$ from 0.83 to 1.28. The second group includes more evolved rocks (foyaite, fine-grained foyaite, urtite) with primary albite and microcline-(perthite), rock-forming minerals of the lovozerite group, a large variety of accessory phosphates and silico-phosphates and the ratio $(Na_2O + K_2O)/Al_2O_3$ from 0.68 to 0.95. In the variation diagrams, leucocratic rocks are enriched in Si, Al, K, and P, while melanocratic rocks contain more Zr, Ti, Fe, Mg, Mn, and Ca.

We assume that the leucocratic rocks (foyaite, fine-grained foyaite, urtite) are the product of the crystallization of residual melt formed during the crystallization of melanocratic rocks. Crystallization of salic minerals from the melt that formed the Eudialyte complex can be considered using the "residua system" $NaAlSiO_4 – KAlSiO_4 – SiO_2 – (H_2O)$ {see Figure (Bowen, 1937; Schairer, 1950). Alkali feldspar crystallized first at a temperature of 700^0C (Elkins and Grove, 1990). The morphology and orientation of its crystals indicate crystallization in free flow of magma (Higgins, 1991). Fractionation of feldspar quickly changed the composition of the melt towards nepheline composition, and joint crystallization of nepheline-I and alkali feldspar began. As a result, euhedral nepheline-I crystals with small inclusions of feldspar were formed. According to Hamilton (1961), nepheline-I crystallized at a temperature of 700–775° C. As the magma crystallizes, calcium accumulates in residual melt. An insignificant increase of the calcium content in the melt was the trigger to the beginning of the aegirine crystallization (Nolan, 1966). The clinopyroxene composition indicates their rapid crystallization (Mollo et al., 2013) and absence of the zirconium minerals at that time (Jones, Peckett, 1980).

Nepheline-II crystallized together with aegirine, it is substantially enriched with iron and therefore there is a lot of Qtz-component in its composition. If the water activity increase, natrolite is formed instead of nepheline. The binding of water in the composition of natrolite causes a decrease of chlorine solubility and, consequently, the formation of sodalite. As the melanocratic "streams" crystallize from their edges to axes, the water content increases, and the clinopyroxenes become replaced by amphiboles (on this reason, the compositions of these minerals are significantly correlated). EGM are ones of the latest rock-forming minerals.

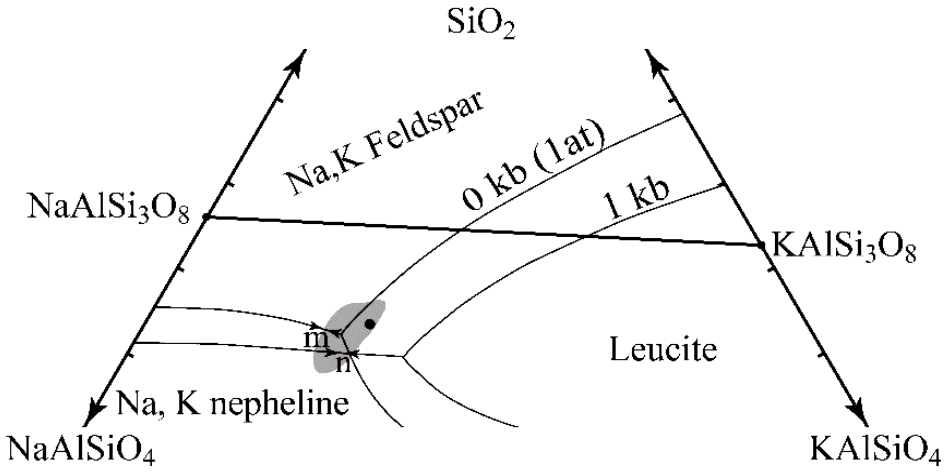

Phase equilibrium diagram of the system $NaAlSiO_4$ – $KAlSiO_4$ – SiO_2 – H_2O for P = 1 atm and PH_2O = 1 Kbar (Schairer, 1950). Plot of the salic normative compositions of the melanocratic (gray), leucocratic (dark gray) rocks, average composition of Eudialyte complex {black point (Gerasimovsky et al., 1966)}; m and n are minimums on the feldspar-nepheline field boundary ("phonolite" minimum) for 1 atm and PH_2O = 1 Kbar, respectively.

The residual melt that formed the leucocratic rocks was probably separated at the stage of clinopyroxene crystallization. Composition of this melt was very close to the phonolitic minimum (point n). The crystallization rate determines which rocks (coarse, fine-grained or porphyritic) will be formed. The residual low-temperature liquid was crystallized *in situ* forming lenses and layers among the melanocratic rocks. The residual nature of leucocratic rocks is also confirmed by zirconosilicate compositions. In particular, lovozerite-group minerals as more agpaitic than EGM (Khomyakov, 1990) are characteristics of rocks with a low $(Na_2O + K_2O)/Al_2O_3$ ratio.

This work was supported by the Kola Science Center of RAS (team 0226-2019-0051) and the Presidium of RAS (program I-48).

References

Bussen I. V., Sakharov A. S. Petrology of the Lovozero alkaline massif // Nedra, Leningrad. 1972. 296 p.

Gerasimovskii V. I., Volkov V. P., Kogarko L. N., Polyakov A. I., Saprykina T. V., Balashov Yu. A., Geochemistry of the Lovozero Alkaline Massif // Nauka, Moscow. 1966. 395 p.

Elkins L. T., Grove T. L. Ternary feldspar experiments and thermodynamic models // American Mineralogist. 1990. V. 75. №. 5-6. p. 544–559.

Hamilton D. L. Nephelines as crystallization temperature indicators //The Journal of Geology.1961. V. 69. №. 3. p. 321–329.

Higgins, M. D. The origin of laminated and massive anorthosite, Sept Iles intrusion, Quebec, Canada // Contributions to Mineralogy and Petrology. 1991. V. 106. № 3. p. 340–354.

Johnsen O., Ferrarris G., Gault R.A., Grice J.D., Kampf A.R.; Pekov I.V. The nomenclature of eudialyte-group minerals // The Canadian Mineralogist. 2003. V. 41. p. 785–794.

Jones A. P., Peckett A. Zirconium-bearing aegirines from Motzfeldt, south Greenland // Contributions to Mineralogy and Petrology. 1981. T. 75. №. 3. p. 251–255.

Khomyakov A. P. Mineralogy of hyperagpaitic alkaline rocks // Nauka, Moscow. 1990. 200 p.

Korchak Y. A. Men'shikov, Y. P., Pakhomovskii, Y. A., Yakovenchuk, V. N., Ivanyuk, G. Y. Trap formation of the Kola Peninsula // Petrology. 2011. V. 19. №. 1. p. 87–101.

Le Maitre R. W. et al. (ed.). Igneous rocks: a classification and glossary of terms: recommendations of the International Union of Geological Sciences Subcommission on the Systematics of Igneous Rocks. Cambridge University Press, 2005. 254 p.

Mollo S., Blundy J. D., Iezzi G., Scarlato P., Langone A. The partitioning of trace elements between clinopyroxene and trachybasaltic melt during rapid cooling and crystal growth // Contributions to Mineralogy and Petrology. 2013. V. 166. p. 1633–1654.

Nolan J. Melting-relations in the system $NaAlSi_3O_8$–$NaAlSiO_4$–$NaFeSi_2O_6$–$CaMgSi_2O_6$–H_2O, and their bearing on the genesis of alkaline undersaturated rocks // Quarterly Journal of the Geological Society. 1966. V. 122. №. 1–4. p. 119–155.

Pekov I. V. Lovozero massif: history, pegmatites, minerals // Ocean Pictures Ltd. 2001. 464 p.

Schairer J. F. The alkali-feldspar join in the system $NaAlSiO_4$-$KAlSiO_4$-SiO_2 // The Journal of Geology. 1950. T. 58. № 5. p. 512–517.

Semenov E. I. Mineralogy of the Lovozero alkaline massif //Acad. Nauk SSSR, Moscow. 1972. 307 p.

Vlasov K. A., Kuzmenko M. V., Yeskova E. M. Lovozero alkalic massif // Akad. Nauk SSSR, Moscow. 1959. 623 p.

PERIOD AND SEQUENCE OF FORMATION OF PLACER-FORMING TYPES OF THE PLATINUM GROUP MINERALS OF THE ALKALINE ULTRAMAFIC MASSIF KONDYOR

***Mochalov A.G.*[1], *Yakubovich O.V.*[1,2]**

[1]*Institute of Precambrian geology and geochronology RAS, Saint-Petersburg, Russia, mag1950@mail.ru*

[2]*Saint-Petersburg State University, Saint-Petersburg, Russia, olya.v.yakubovich@gmail.com*

The Kondyor massif is located within the Batomgsky geoblock of the Aldan Shield. The rocks of the massif include the ultramafic series (dunites, werhlites and pyroxenites), monzonite series (koswite, gabbro, diorites, etc.), alkaline series (alkaline and feldspar syenites and their pegmatites) and subalkaline granites. All igneous rocks break through the crystalline formations of the Archean and terrigenous rocks of the Proterozoic age and form a single dome-ring structure with a central "dunite core". Under the influence of ultramafic, mafic, alkaline and granite intrusions, polycyclic cumulative dunites are repeatedly synmagmatically recrystallized and metasomatically converted. This is manifested in the widespread distribution of facies varieties of dunites and metasomatites. The alkaline-ultramafic Kondyor massif is the main source of the unique alluvial deposit of the Kondyor-Uorgalan (more than 100 tons of platinum) discovered in the middle of the 20th century (Mochalov and Khoroshilova, 1998).

Despite previous good geological, petrological, mineralogical and geochemical studies, the concept of the age of earlier ultramafic rocks of the Kondyor massif is contradictory (Proterozoic/Mesozoic). The age of alkaline rocks is established as early Cretaceous. In this regard, the concept of the sequence of ore formation of platinum group minerals (PGM) was mainly oriented to the ontogeny of the aggregates of PGM with silicates, oxides and sulphides. Ontogeny is evidence in favor of late-magmatic and, mainly, superimposed fluid-metamorphic and metasomatic processes in the formation of PGM in the primarily magmatogenous ultramafic matrix. The principal possibility of direct determination of the age of PGM was demonstrated by Yu. A. Shukolyukov and colleagues at the IPGG RAS by the ^{190}Pt-^{4}He method (Shukolyukov et al., 2012). In view of the established, high retention of radiogenic helium in native minerals of platinum, it became possible to approach the solution of the fundamental problem, to estimate the time of the onset of the formation of PGM and its stages during the petrogenesis of the silicate matrix.

Studies of PGM in dunites made it possible to distinguish several mineralogical-geochemical and genetic types: 1) the platinum type (Pt) is magmatogenic in fine-grained dunites and magmatogenic-fluid-metasomatic in coarse-grained dunites with "black olivine" (black color due to micro-inclusions of chromian spinel, magnetite and clinopyroxene); 2) magmatogenic-fluid-metasomatic osmium-platinum in schlieren and lenticular veins of clinopyroxenite in dunites (Pt> Os-Cpx); 3) fluid-metamorphogenic iridium-platinum (Pt> Ir) in light medium-, coarse-grained dunites (Pt> Ir-Ol) and chromite (Pt> Ir-Spl); 4) magmatogenic-fluid-metasomatic palladium-platinum Pt> Pd in dunite metasomatites: apatite-titanomagnetite-biotite-clinopyroxene, amphibolite and zeolite with copper sulphides and oxides. These metasomatites in dunites generate magmatic veins of koswites (magnetite clinopyroxenite), hornblendites, alkaline pegmatites, alkaline syenites and subalkaline granites, in which Pt, Pd, Au, Ag, Cu, Pb, Sn, Bi, Zn, Te, Sb, As and S are distributed.

Numerous nuggets of Pt minerals are common in placer deposits of the Kondyor-Uorgalan rivers. Nuggets (fraction more than 1 cm) make up 1.5% by weight of the schlich PGM in a Kondyor river placer. The average weight of nuggets lighter than 100 g is 14.5 g, and heavier than 100 grams - 242.5 grams, the largest of which is 3.5 and 2.2 kg. Nuggets have much in common with the nuggets from Urals and Koryak highland. However, the Kondyor massif also have unique crystalline examples of isoferroplatinum (whose weight reaches 20 g). These crystalline examples are common among the Pt> Pd type (Mochalov and Khoroshilova, 1998).

In the placer and bedrock of Kondyor, 91 PGM and about 200 of their varieties are established. Despite the mineral and type diversity, the main mineral of all types is isoferroplatinum - Pt_3Fe and cryptoaggregates Pt_3Fe + tetraferroplatinum - PtFe (Mochalov et al., 1988). They also make up the dominant part of the nuggets. For ^{190}Pt-^{4}He dating, well-studied homogeneous Pt_3Fe individuals

weighing 1-10 mg, without inclusions or a small number of PGM inclusions were selected: Individuals and aggregates of Pt_3Fe of 1) Pt> Ir-Ol type, from schlieren and vein chromitites; 2) Pt> Ir-Spl type, from the schlieren of clinopyroxenite; 3) Pt> Os-Cpx type; and 4) from apatite-titanomagnetite-biotite-clinopyroxene metasomatites on contacts with alkaline syenites and pegmatites of Pt> Pd type. The grains of aggregates of isoferroplatinum of Pt> Ir and Pt> Os types were isolated from fragments of dunites, chromites and pyroxenites with visible PGM. Crystalline individuals of the isoferroplatinum Pt> Pd type were derived from large samples of eluvium of metasomatites (about 10 m^3) enriched on hydrocradle during exploration. For samples of Pt_3Fe of Pt type ^{190}Pt-^4He age was not determined because of their micron size (less than 100 μm) in dunites.

Table 1. Concentrations of ^{190}Pt and ^4He in studied samples.

№	Sample №	Rock type	Weight, mg	Pt, wt. %	$^{190}Pt,\times10^{15}$at	σ	$^4He,\times10^9$at	σ
1	B5	Pt>Ir-Ol, dunite	2.67	85.7	0.90	0.01	57	3
2	K210p		1.01	85.7	0.34	0.00	56	2
3	K210p		3.98	85.3	1.33	0.01	61	4
4	**1 Ol_N**		**3.71**	**89.5**	**1.30**	**0.01**	**71**	**4**
5	**2 Ol_N**		**5.35**	**85.0**	**1.79**	**0.02**	**59**	**4**
6	**3 Ol_N**		**2.347**	**83.5**	**0.77**	**0.01**	**59**	**3**
7	B4.3/79.1	Pt>Ir-Spl, Shlieren and veins of chromitites in dunite	1.70	84.4	0.56	0.01	57	2
8	B4.3/79.2		1.13	84.4	0.37	0.01	56	2
9	B4.3/79.3		1.37	84.4	0.45	0.01	57	2
10	B4.3/79.4		1.60	84.4	0.53	0.01	60	2
11	B4.3/79.5		1.06	84.4	0.35	0.00	58	2
12	K214p.2b		3.99	85.1	1.33	0.01	67	4
13	K214p.2c		10.26	85.1	3.43	0.03	62	6
14	T5p.3		14.7	67.5	3.90	0.04	51	7
15	Ap.50p.1		8.01	47.5	1.49	0.01	31	4
16	**1 Spl_N**		**3.17**	**84.3**	**1.05**	**0.01**	**59**	**3**
17	**2 Spl_N.1**		0.96	85.5	0.32	0.01	55	2
18	**2 Spl_N.2**		**1.95**	**85.5**	**0.65**	**0.01**	**64**	**3**
19	**2 Spl_N.3**		1.38	85.5	0.46	0.00	58	2
20	**2 Spl_N.4**		2.35	85.5	0.79	0.01	54	3
21	**2 Spl_N.5**		1.50	85.5	0.50	0.01	63	2
22	Ap100 l.1	Pt>Os-Prx	4.19	85.6	1.41	0.01	62	4
23	**1Cpx_N**		**3.72**	**85.5**	**1.25**	**0.01**	**63**	**4**
24	A250.1	Pt-Pd, metasomatite after dunite	2.94	89.7	1.04	0.01	73	4
25	A250.3		3.08	87.0	1.05	0.01	61	3
26	A250.4		2.59	90.6	0.92	0.01	60	3
27	P200.4		11.58	89.7	4.08	0.04	67	7
28	P200.5		7.69	89.7	2.71	0.03	69	6
29	P200.2		14.19	89.7	5.00	0.05	66	8
30	**1 C_N**		**2.62**	**86.1**	**0.89**	**0.01**	**59**	**3**

Bold is for nuggets;

Letter in a sample name indicates the following location: B for stream Begun; K – r. Kondyor; Ap – str. Appendix; A – str. Anomalniy; P – str. Pryamoy.

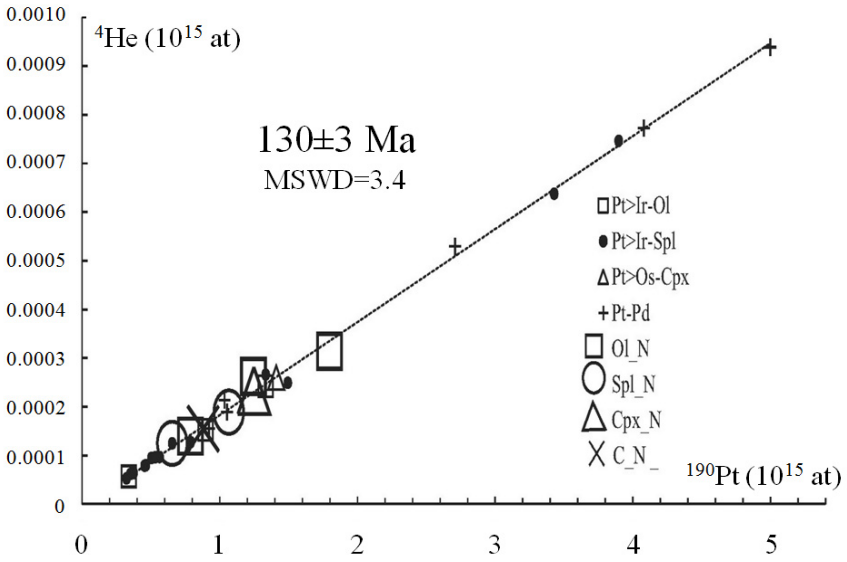

Figure. ^{190}Pt-^{4}He "isochron" constructed on data (Table 1) obtained for isoferroplatinum grains of Pt> Ir–Ol, Pt> Ir–Spl, Pt> Os–Prx and Pt–Pd-mineralogical-geochemical types and nuggets of the PGM: Ol_N, Spl_N, Cpx_N and Pt-Pd_N of the Kondyor massif.

^{190}Pt-^{4}He age of Pt_3Fe of the studied 24 samples of various mineral-geochemical types of the Kondyor massif is 129 ± 6 Ma. This indicated: 1) the ore formation of mineralogical-geochemical types of PGE of the alkaline-ultramafic Kondyor massif took place in a fairly narrow range of geological time, between the end of the Jurassic period and the early Cretaceous (J_{3tt} - K_{1g}); 2) Platinum-ore formation of magmatogenic, fluid-metamorphogenic, metasomatic genesis was carried out in a synchronous-sequential evolution, first of the picritic and then monzonitic and alkaline melts of the Mesozoic tectonic magmatic activation of the Aldan Shield (Mochalov et al., 2016).

Nuggets that corresponds to Pt_3Fe, Pt> Ir-Ol, Pt> Ir-Spl, Pt> Os-Cpx and Pt> Pd mineral-geochemical types were selected. From these nuggets fragments with a weight ranging from 5-10 mg were separated and divided into several groups with weights 2-3 mg to measure the concentrations of Pt and ^{4}He. The obtained data on the content of ^{190}Pt and ^{4}He in 7 nuggets were plotted on the chart with "isochron|" of previously studied 24 samples of Pt_3Fe from various mineral-geochemical types. The age obtained from the tangent of the "isochron" slope, plotted for all points including the nuggets, is 130 ± 3 Ma (MSWD = 3.4; calculated in Isoplot). If we consider the "isochron" constructed for all studied Pt_3Fe and nuggets separately, then their ^{4}He/^{190}Pt ratio are practically inseparable, which unambiguously attests to their common age and genesis. Thus, it can be assumed that platinum nuggets were formed in exceptional clusters of PGE during magmatic, fluid-metamorphogenic or metasomatic platinum-metallic ore formation.

This work was supported by Russian Foundation for Basic Research, project 18-05-00718.

References

Mochalov A.G., Khoroshilova T.S. The Konder alluvial placer of platinum metals // International platinum. Athens: Theophrastus publications, 1998, pp. 206–220.

Shukolyukov Yu.A., Yakubovich O.V., Mochalov A.G., Kotov A.B., Salnikova E.B., Yakovleva S.Z., Korneev S.I., Gorokhovskiy B.M. New geochronometer for the direct isotopic dating of native platinum minerals (^{190}Pt-^{4}He method) // Petrology. 2012. Vol. 20:6. p. 491-505.

Mochalov A.G., Zernovskiy I.V., Dmitrenko G.G. Composition and abundance of native minerals of platinum and iron in ultramafic rocks // Geology of ore deposits. 1998. Vol. 5. p. 47-58, in Russian.

Mochalov A.G., Yakubovich O.V., Bortnikov N.S. ^{190}Pt–^{4}He age of PGE ores in the alkaline–ultramafic Kondyor massif (Khabarovsk district. Russia) // Doklady Earth Sciences. 2016. Vol. 469:5. p. 602-606.

EVOLUTION OF PYROCHLORE-GROUP MINERALS FROM THE ILMENO-VISHNEVOGORSKY MIASKITE-CARBONATITE COMPLEX (SOUTH URALS): INSIGHTS FROM TRACE ELEMENT AND U-Pb-ISOTOPE DATA

Nedosekova I.L [1], Belyatsky B.V.[2], Sharygin V.V.[3], Lepekhina E.N.[2], Antonov A.V.[2]

[1]A.N.Zavaritsky IGG UB RAS, Ekaterinburg, Russia, vladi49@yandex.ru

[2]IR VSEGEI, St.Petersburg, Russia bbelyatsky@mail.ru elena.lepekhina@gmail.com anton_antonov@vsegei.ru

[3]V.S.Sobolev IGM SB RAS, Novosibirsk, Russia sharygin@igm.nsc.ru

The Ilmeno-Vishnevogorsky miaskite-carbonatite complex (IVAC) is located in the Ural Fold Belt. It consists of two intrusive miaskite plutons, Vishnevogorsky and Ilmenogorsky (20–25 × 6 km), connected by the Central Alkaline Belt with a length of 150 km from north to south at a width of 4–6 km, composed of fenites, feldspar metasomatic rocks, small bodies of miaskites, syenites, silicocarbonatites, and carbonatites containing Nb-Zr mineralization (U-(Ta)-pyrochlore, pyrochlore, zircon). From the north and west, the complex is surrounded by small massifs of ultramafic rocks containing carbonate veins with Nb-REE mineralization (pyrochlore, columbite, aeschynite, monazite) related to carbonatite as well. Numerous deposits and ore occurrences of pyrochlore-bearing carbonatite are observed in the Vishnevogorsky miaskitic massif, Central Alkaline Belt and in the ultrabasic massifs (Buldym, Spirikhinsky, Haldihinsky). Among the largest are the Vishnevogorskoe, Potanino, and Buldymskoe Nb deposits (Levin et al., 1997; Nedosekova et al, 2013).

Pyrochlore, the major rock-forming mineral of Nb deposits within the IVAC, occurs in many rocks: miaskite, syenite, especially their pegmatoid varieties, miaskitic pegmatite (biotite-nepheline-microcline), syenitic pegmatite (biotite-microcline and aegirine-augite-microcline), and silicocarbonatite. The highest contents of pyrochlore are common of carbonatites of the early and late stages of the carbonatite formation (sovites I, II, and III) and associated metasomatic rocks (fenite, albitite, and other rocks).

The IVAC pyrochlore-group minerals represented by fluorcalciopyrochlore, oxycalciopyrochlore and hydroxycalciopyroclore (including U-(Ta)-, Ta-, REE-Sr-rich varieties) according to nomenclature (Atencio et al, 2010).

U-(Ta)-rich hydroxy- and oxycalciopyrochlore (UO_2: 15-24, Ta_2O_5: 1-14 wt.%) are found in the early high-temperature silicocarbonatites and are formed on the late-magmatic stage of crystallization, earlier than other types of pyrochlores.

Fluorcalciopyrochlore with the highest Nb_2O_5 (65-69 wt.%) and low trace-element contents (<0.5 wt.%) commonly occurs in the pegmatoid miaskites and associated carbonatites (sövites I). Ta-containing fluorcalciopyrochlore (Ta_2O_5: 1.5-5 wt.%) is found in the miaskite-pegmatites.

Sr-REE-rich fluorcalciopyrochlore ($LREE_2O_3$: 3-6, SrO: 1.5-7 wt.%) is common in late carbonatites (sövites II) and fenite-hosted syenitic pegmatite and clinopyroxene-calcite veins. It is heterogeneous in composition and contains relics of the earlier pyrochlore. Probably, its formation is related to the final stages of the IVAC.

Despite numerous studies on the IVAC pyrochlore-group minerals, the questions on the genesis and the duration of the ore formation stages at the Zr-Nb deposits remain relevant.

The pyrochlore-group minerals have been selected from miaskite-pegmatites, different types of carbonatites (sövites I-III), and syenite-pegmatite. 12 samples and 200 grains of pyrochlore from the main types of the IVAC rocks were investigated by optical microscopy, electron microprobe and ion microprobe analysis (IMS-4f and CamScan-2500). U-Pb dating of the pyrochlore-group minerals from the IVAC Zr-Nb deposits has been carried out. The age of individual pyrochlore crystals was determined at the CIR VSEGEI (St. Petersburg) by local U-Pb isotope methods: secondary-ion mass spectrometry (SHRIMP-II); laser ablation and ICP-MS (in the case of high-U pyrochlores with $UO_2 \geq$ 2.5 wt.%).

The compositions of the IVAC pyrochlore-group minerals are shown in the binary diagram Nb-F, which is illustrating the sequence of their formation and the geochemical evolution (Fig. 1).

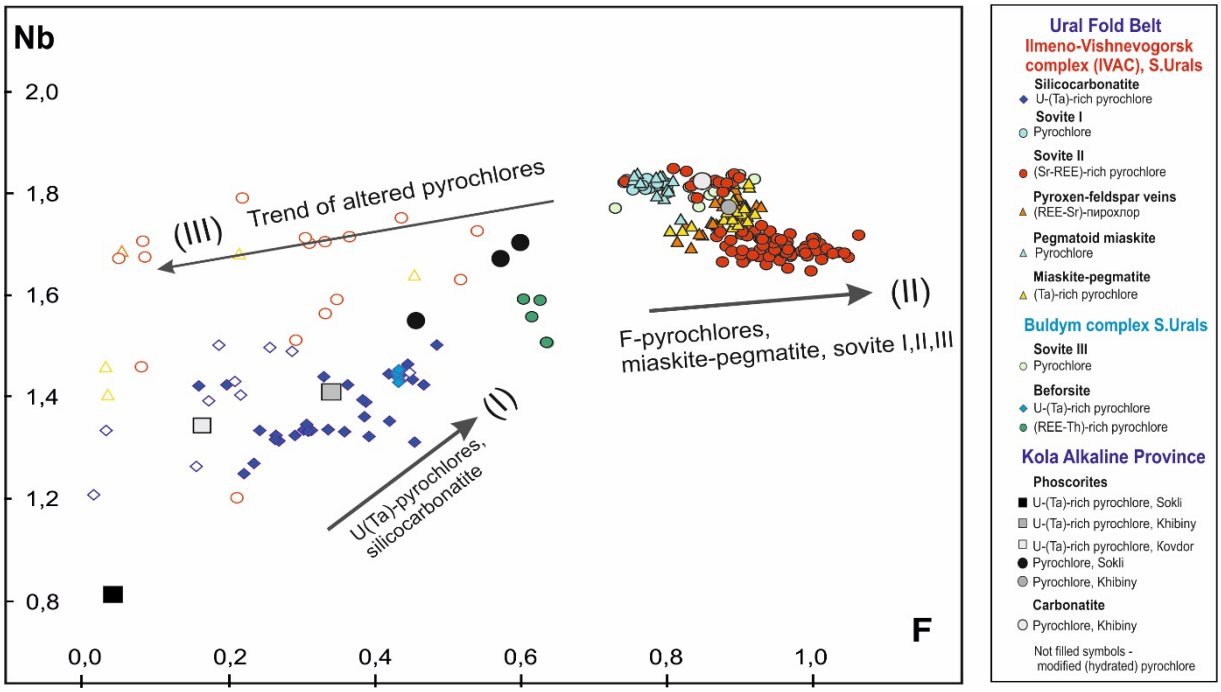

Fig. 1. The Nb–F binary compositional diagram for pyrochlore-group minerals from the IVAC.

The arrows indicate the direction of evolution of the composition of the IVAC pyrochlores:

I – the silicocarbonatitic trend, II – the miaskite-pegmatite and late carbonatitic trend, III – the trend of alteration (hydratation) with the formation of keno-, hydroxy-, and hydropyrochlores.

Trend I corresponds to the crystallization of the IVAC uranopyrochlores (Potanino deposit).

Trend II – crystallization of the IVAC fluorocalciopyrochlores (Vishnevogorsky, Buldym, Potanino deposits).

For comparison, the composition of pyrochlore from the rocks of Kola ultrabasic alkaline-carbonatite complexes are given (Chakhmouradian, Williams, 2004; Zaitsev et al, 2011).

Trend I (early carbonatite trend) illustrates continuous change in the composition of U-(Ta)-rich oxycalciopyrochlores (or uranopyrochlore according to Hogart (1977)) with increasing F and Nb, which is followed by a sharp change of composition of the crystallizing pyrochlore. Fluorcalciopyrochlore begins to crystallize, forming *trend II (miaskite-pegmatite and late carbonatite trend)*. This trend shows a pronounced change of the conditions and chemistry of the mineral-forming environment. Trend III reflects the secondary alterations in pyrochlores associated with exposure to aqueous fluid, which results in the extraction of Na, Ca and F from the structure of pyrochlores, the appearance of vacancies in the A-position, which are then partially filled with Si, Fe, Ta, Ti, Th, REE and Sr. Thus, hydroxyl-, keno- and hydropyrochlores are being formed.

It should be noted that the compositions of IVAC uranopyrochlores from silicocarbonatites are similar to the earliest generations of uranopyrochlore from late magmatic phoscorites of the Kola carbonatite complexes (Chakhmouradian et al, 2004; Zaitzev et al, 2011). These data, as well as geological and petrographic observations, confirm that the IVAC U-(Ta)-rich pyrochlores were formed at the late-magmatic stage of crystallization of alkali-carbonatite melts. The compositions of the IVAC fluorcalciopyrochlores differ from the early (primary) pyrochlores from the Kola phoscorites and carbonatites. This difference might be due to other formation conditions of the IVAC fluorcalciopyrochlores at the post-collisional development stage of the Ural folded region.

U-Pb systems of the studied pyrochlore samples indicate a multi-stage formation of the Nb-mineralization at the IVAC (Nedosekova et al., 2018). The earliest stage of ore formation (378 ± 4.9 Ma) is recorded by U-(Ta)-pyrochlore from silicocarbonatites and seems to be associated with the primary crystallization in the alkaline-carbonatite magmatic system (Krasnobaev et al., 2010; Nedosekova et al., 2014).

The following ore stages are recorded by U-Pb isotope systems of fluorocalciopyrochlore from sövites I (255±2.5 Ma) of the Vishnevogorsk deposit, and Sr-REE-rich fluorocalciopyrochlores from

sövites II of Vishnevogorsk (230±1.5 Ma) and Potanino (217±1.9 Ma) deposits. So, the U-Pb isotope system of the IVAC fluorcalciopyrochlores fixes the late ore-forming stages: for the spatially close Vishnevogorsky massif, the final stage of the mineralization was almost synchronous ~ 230-250 m.y. ago. As in the Potanino deposit, located in the Central Alkaline Zone, ore formation was cessation later – 216-218 Ma ago.

A similar age of 245±8 Ma was previously obtained by the Rb-Sr mineral isochron for the IVAC miaskites and it is correlated with the late collision metamorphism (Kramm et al., 1983; Puchkov, 2010). The slightly older U-Pb ages were obtained for the IVAC zircons from miaskites (279±10 Ma), miaskite-pegmatites (251±6 Ma), and carbonatites (280±8 Ma) (Krasnobaev et al., 2010, 2016; Nedosekova et al., 2014, 2016). All these data confirm the late stages of rare-metal ore formation in the IVAC on the late collision and post-collision stages of the Urals Fold system.

Conclusions. The difference in the age of 120-160 Ma between U-(Ta)-pyrochlores and fluorcalciopyrochlores of the IVAC indicates two stages of ore genesis. The first stage is associated with the final process of magmatic crystallization of alkaline rocks and carbonatites (~ 380 Ma). The second, rather long stage of ore formation (interval - 255-217 Ma), is probably associated with later partial melting and/or metasomatic events on the post-collision stages of the Urals Fold Belt.

This work was supported by the RFBR grant No. 17–05–00154.

References

Atencio D., Andrade M.B., Christy A.G., Giere R., Kartashov P.M. The pyrochlore supergroup of minerals: nomenclature // Canadian Mineralogist, 2010. Vol. 48. P. 673-698.

Chakhmouradian A.R. Williams C.T. Mineralogy of high field strength elements (Ti, Nb, Zr, Ta, Hf) in phoscorite and carbonatitic rocks of the Kola Peninsula, Russia // In Phoscorites and Carbonatites from Mantle to Mine: the Key Example of the Kola Alkaline Province, edited by F. Wall and A.N. Zaitsev. Mineralogical Society, Series, 10. London, 2004, pp. 293-340.

Hogarth, D.D. Classification and nomenclature of the pyrochlore group //American Mineralogist, 1977. Vol. 62. P. 403-410.

Krasnobaev A.A., Rusin A.I., Valizer P.M., Busharina S.V. Zirconology of calcite carbonatites of the Vishnevogorsky Massif (S. Urals) // Doklady Earth Sciences, 2010. T. 431. No. 3. P. 1-4.

Krasnobaev A.A., Valizer P.M., Busharina S.V., Medvedeva E.V. The zirconology of the miaskites of the Ilmeny mountains (S. Urals) // Geochemistry International, 2016. No. 9. P. 797-813.

Levin V.Ya., Ronenson B.M., Samkov V.S. Alkaline carbonatite complexes of the Urals. Ekaterinburg: Uralgeolkom, 1997. 274 p.

Nedosekova I.L., Belousova E.A., Sharygin V.V., Belyatsky B.V., Baynova T.B. Origin and evolution of the Il'meny-Vishnevogorsky carbonatites (Urals, Russia): insights from trace-elements compositions, Rb-Sr, Sm-Nd, U-Pb and Lu-Hf isotope data // Mineralogy and Petrology, 2013. V. 107. Issue 1. P. 101-123.

Nedosekova I.L., Belyatsky B.V and Belousova E.A. Trace elements and Hf isotope composition as indicators of zircon genesis in the evolution of the alkaline-carbonatite magmatic system (Ilmeno-Vishnevogorsky complex, Urals, Russia) // Russian Geology and Geophysics, 2016. V.57. Pp. 891-906.

Nedosekova I.L., Belousova E.A., Belyatsky B.V. U-Pb-age and Lu-Hf isotopic systems of zircons of the Ilmeno-Vishnevogorsky alkaline-carbonatite complex, S. Urals // Litosfera, 2014. N. 5. P. 19-32.

Nedosekova I.L., Koroteev V.A., Belyatsky B.V., Sharygin V.V., Lepekhina E.N., Pribavkin S.V. U-Pb-dating of ore niobium minerals of the pyrochlore group (Ilmen-Vishnevogorsky carbonatite-miaskite complex, South Urals) // Litosfera, 2018. T.18. №5. Pp. 758-773.

Puchkov V.N. Geology of the Urals and Urals (current issues of stratigraphy, tectonics, geodynamics and metallogeny). Ufa: Design Poligraph Service, 2010. 280 p.

Zaitsev A.N., Williams C.T., Wall F., Zolotarev A.A. Evolution of the chemical composition of the pyrochlore-group minerals from phoscorites and carbonatites of the Khibiny alkaline massif // Notes of the Russian Min. Society, 2011. V.XXXX. № 3. P. 40-55.

MINERALOGICAL AND GEOCHEMICAL FEATURES AND GENESIS OF MIASKITES OF THE ILMENOGORSKY COMPLEX, SOUTH URALS, RUSSIA

Nemov A.B., Medvedeva E.V.

Ilmeny State Reserve FRC MG UB RAS, Miass, Russia, mev_62@inbox.ru

The Ilmenigorsky complex includes biotite, amphibole, pyroxene–amphibole, and garnet–amphibole miaskites and plagiomiaskites. Textures, structures, mineral composition, and rare earth and trace element pattern of miaskites indicate their multistage transformation. The rocks were formed as a result of mantle fluid melt release during the formation of a long-living deep fault, which led to partial melting of alkaline rocks and metamorphic series. Processes of metasomatic mantle replacement occurred in the lower crust under viscous plastic deformations of rocks favorable for the formation of syntectonic miaskites.

The Ilmeny miaskite complex (IMC) is located in the southern part of the Ilmeny-Vishnevogorsky polymetamorphic complex (IVPC) and is mainly composed of nepheline syenites (miaskites). The complex of the IVPC alkaline rocks includes Ilmeny (in the south) and Vishnevogorsky (in the north) miaskitic blocks linked by a Central Alkaline Band (CAB) of intensely dislocated syenitic rocks including bodies of carbonatites and metasomatites and blocks (boudines) of metamorphic and igneous rocks.

Several hypotheses are known on the formation of the IVPC nepheline syenites: anatectic under influence of mantle fluids (Ronenson, 1966; Levin et al., 1997; Rass et al., 2006), riftogenic magmatic (Bazhenov, 2006), and disintegrated alkaline-ultramafic central-type intrusion (Rusin et al., 2006; Nedosekova, 2009).

Structural and textural features of rocks were studied on an Olympus BX 51 optical microscope. The contents of major elements are analyzed using atomic absorption (analysts L.B. Lapshina, N. V. Sharshueva), the contents of rare earth and trace elements are determined using ICP-MS (analysts K. A. Filippova, M. S. Svirenko). The minerals are also studied on a Tescan Vega3 sbu SEM equipped with an Oxford Instruments X-act EDS (analyst I.A. Blinov) and a REMMA 202M SEM equipped with a LZ-5 Link EDS and a Si–Li detector (analyst V.A. Kotlyarov) at an accelerating voltage of 20–30 kV.

The drop-like IMC 18×4.5 km in size has heterogeneous structure with two saddle-shape miaskite bodies: western, composed mainly of amphibole miaskites (AMs) and eastern, composed mainly of biotite miaskites (BMs). The IMC central part consists of intercalated bodies of miaskites and fenitized rocks [Levin et al., 1974, 1997]. The IMC miaskites host bodies 0.1 m–0.5 × 0.5–10 m in size of pyroxene–amphibole (sandyites) and garnet–amphibole (firsites) miaskites and veins of albitized miaskites (plagiomiaskites). The boundaries between the rock types are gradual, locally, with sharp contacts between pyroxene–amphibole and albitized miaskites and their country amphibole miaskites. The pyroxene–amphibole and garnet–amphibole miaskites have latitudinal strike. The bodies of albitized miaskites are often concordant with foliation of country rocks and are found in both IMC and CAB. It isaccepted to ascribe the pyroxene–amphibole and garnet–amphibole miaskites to skialiths (Levin, 1997). The CAB biotite miaskites form linear longitudinal bodies.

All miaskites are characterized by heterogranoblastic, nematoblastic, granolepidoblastic, and porphyroblastic textures; the porphyroclastic texture is characteristic of protomylonites and mylonites. The texture within individual bodies often varies from heterogranoblastic to mylonitic. All IVPC rocks underwent mylonitization of various degrees (protomylonites in the IMC and ultramylonites in the CAB). The mylonitization products reflect brittle–plastic nature of deformations (Trouw et all., 2010).

Feldspar and nepheline are major leucocratic rock-forming minerals of miaskites. The composition of K-feldspars varies from microcline to orthoclase with abundant flame perthites. The K-feldspar contains BaO (up to, wt. %): 6.14 (marginal part of microcline) in firsite, 2 in pyroxene–amphibole miaskite, and 1 in BMs. Secondary albite forms interstitial small-grained aggregate and myrmekites at the boundary with microcline.

Biotite (f 58–100) is most abundant dark-colored rock-forming mineral. It exhibits widely variable composition. The TiO_2 content (wt. %) of biotite is 2.59–6.02 in BMs (IMC) and 2.85–5.45

(CAB), 0.59–3.55 in AMs, and 1.77–3.55 in sandytes and firsites. The Al_2O_3 content (wt. %) is 13.4–16.7 in BMs (IMC) and 14.65–23.22 (CAB), 13.8–18.1 in AMs and 12.1–16.36 in sandytes and firsites. The biotite individuals are mostly homogeneous, locally, exhibiting zonality with decreasing TiO_2 and increasing Al_2O_3 contents from center to rim, e.g.: $K_{0.95}(Fe_{2.18}Mg_{0.43}Mn_{0.07}Ti_{0.32})_{3.0}[Ti_{0.06}Al_{1.31}Si_{2.63}O_4](OH)_2 \rightarrow$ $K_{0.95}(Fe_{2.24}Mg_{0.47}Mn_{0.06}Ti_{0.23})_{3.0}[Ti_{0.03}Al_{1.34}Si_{2.63}O_4](OH)_2$ in BMs (IMC) and $K_{0.95}(Fe_{1.98}Mg_{0.6}Mn_{0.02}Ti_{0.32}Al_{0.09})_{3.01}[Al_{1.37}Si_{2.63}O]_4(OH)_2 \rightarrow$ $K_{0.95}(Fe_{1.9}Mg_{0.6}Mn_{0.03}Ti_{0.23}Al_{0.24})_{3.0}[Al_{1.31}Si_{2.69}O_4](OH)_2$ (CAB) and $K_{0.95}(Fe_{1.91}Mg_{0.57}Mn_{0.13}Ti_{0.22}Al_{0.17})_{3.0}[Al_{1.28}Si_{2.72}O]_4(OH)_2 \rightarrow$ $K_{0.89}(Fe_{2.08}Mg_{0.48}Mn_{0.13}Al_{0.27}Ti_{0.05})_{3.01}[Al_{1.31}Si_{2.69}O_4]$ $(OH)_2$ in AMs. The general trend reflects the decrease in the TiO_2 content and increase in the Al_2O_3 content from biotite of the IMC BMs to CAB BMs and AMs. Biotite of AMs is characterized by significantly higher MnO content.

Amphibole mainly includes taramite with homogeneous composition. In AMs, its composition is characterized by following parameters: $Al^{IV}/^{VI}$ ratio of 1.99–2.09/0.76–1.09, 0.11–0.12 f.u. Ti, 1.22–1.39 f.u. Ca $^{(B)}$, 0.95–1.36 f.u. Na, and 0.41–0.45 f.u. K. Taramite of sandytes exhibits the $Al^{IV}/^{VI}$ ratio of 1.73–2.30/0.76–1.32, 0.08–0.16 f.u. Ti, 1.19–1.53 f.u. Ca $^{(B)}$, 0.92–1.64 f.u. Na and 0.37–0.50 f.u. K. Firsites contain taramite with $Al^{IV}/^{VI}$ ratio of 2.17–2.21/0.13–0.18, 0.10 f.u. Ti, 1.36–1.40 f.u. Ca $^{(B)}$, 0.98–1.13 f.u. Na, and 0.45–0.49 f.u. K and hastingsite with $Al^{IV}/^{VI}$ ratio of 2.35–2.39/0.51–0.59, 0.07–0.08 f.u. Ti, 1.69–1.72 f.u. Ca $^{(B)}$, 0.64–0.76 f.u. Na, and 0.48–0.50 f.u. K.

Pyroxene is aegirine–diopside ($Jd_{5\text{-}13}\,Di_{47\text{-}50}\,Ae_{40\text{-}45}$) with high FeO (19.6–20.8 wt. %) and CaO (12.3–13.0 wt. %) and low Al (0.01–0.03 f.u.) and Ti (0.16–0.23 f.u.) contents and slightly variable Na_2O content (5.6–7.0 wt. %). Garnet includes grossulare–andradite $Py_{0–1}Scho_{4–5}Sps_{8–13}Grs_{9–17}Adr_{70–73}$ and andradite–grossulare $Py_{0–2}Scho_{1–2}Sps_{3–5}Alm_{4–9}Adr_{27–34}Grs_{54–60}$.

Accessory minerals are titanite, apatite, zircon, allanite-(Ce), pyrochlore-(Ce), ilmenite, magnetite, and carbonates with bastnesite-(Ce) and britolite- (Ce). Sandyites typically host minerals of the banalsite–stronalsite group (Medvedeva et all., 2016).

Titanite of these rocks is homogenous with variable Al_2O_3 contents in different grains and the presence of Nb_2O_5, Y_2O_3 and CeO (wt. %): 1.76–3.98 (BMs), 3.98–5.48 (AMs) and 2.5–6.1 (sandyites) Al_2O_3 and up to 0.92 (BMs), 1.11 (AMs), and 0.36–0.86, up to 1.11 (sandyites) Nb_2O_5. Titanite of AMs also contains up to 0.7 wt. % Y_2O_3. Titanite of firsites exhibits highly variable Al_2O_3 (up to 10 wt. %) and Nb_2O_5 (up to 2 wt. %) contents; it also contains F (up to 3 wt. %).

Ilmenite in all miaskite types occurs as two generations. Ilmenite 1 composes euhedral grains, often cataclastic, with low MnO content and the presence of Nb_2O_5 (wt. %): 4.74–8.51 MnO, 0.10–0.92 Nb_2O_5 (IMC) and 3.53–8.82 MnO, 0.41–1.79 Nb_2O_5 (CAB). Ilmenite 2 forms small anhedral aggregates and lamellas along cleavage in magnetite and exhibits high MnO contents without Nb_2O_5 (wt. %): 12.7–13.5 MnO (*ИМС*), 9.57–28.6 MnO (CAB).

The replacement processes are widely developed in rocks. Biotite and titanite replace amphibole along the periphery, as well titanite and pyroxene. Gradual replacement of amphibole by biotite is observed during transition from AMs to BMs. Orthoclase is replaced by microcline, which can be overgrown by albite in the margin; the Ba content increases with albitization.

Most miaskite types belong to nepheline syenites of K/Na series (K/Na ratio of 0.66–1.86). The IMC miaskites represent moderately and peralkaline species. The CAB miaskites are characterized by higher Al# value and moderate alkalinity. Sandyites are dominated by rocks with SiO_2 content of 36–49 wt. % and K/Na ratio of 0.32–1.72, corresponding to the ijolite group. The latters are characterized by high MgO, CaO, TiO_2, and Fe_{total} and relatively low Al_2O_3 contents (al' = 0.8–1.5).

In all miaskite types, LREEs are dominant over HREEs (Fig. 1, table 1). The total REE content increases from the CAB BMs to AMs and IMC BMs, reaching maximum contents in the IMC sandyites. The high Ba and Sr content of these rocks are related to their presence in feldspar and carbonates. The CAB mylonites also contain barite. The HFSE (Zr, Hf, Ta, Nb) contents decrease in a range from firsites and sandiytes to the IMC AMs and BMs, CAB BMs and plagiomiaskites. The contents of transitional siderophile elements (V, Ni, Co, Cr) in miaskites are higher than the Clarke

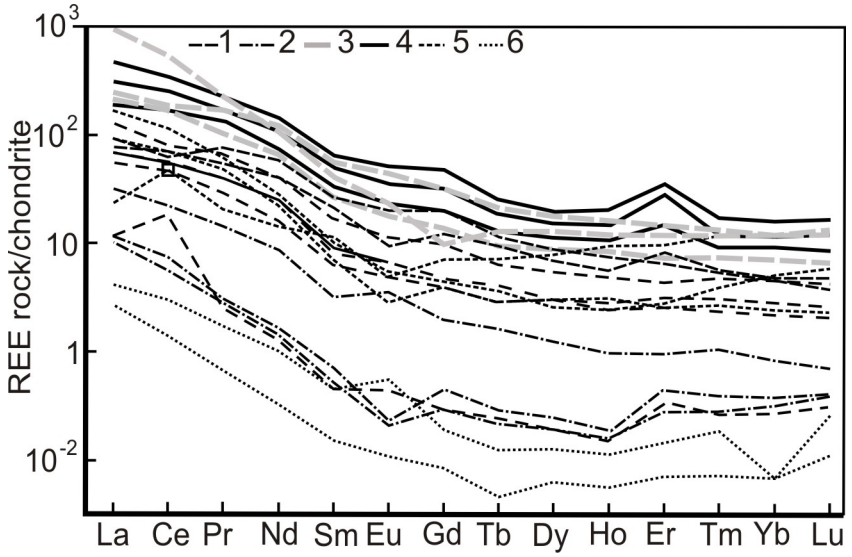

Figure. 1. REE-distribution in miaskites of Ilmenogorsky complex. 1 amphibole miaskite; 2 biotite miaskite IMC; 3 biotite miaskite CAB; 4 pyroxene–amphibole miaskite (sandyite), 5 garnet–amphibole miaskite (firsite); 6 plagiomiaskite.

Table 1. Chemical analyses REE and TE in miaskites of Ilmenogorsky complex (ppm).

Comp.	1	2	3	4	5	6	7	8	9
Rb	132,72	171,00	80,13	148,81	55,30	1800,00	1771,00	106	234,72
Sr	905,30	907,00	1630,58	64,06	5,97	215,00	126,00	1244	2,32
Ba	1716,79	70,50	1977,56	76,40	29,30	5272,00	2171,00	1254	114,65
La	92,04	86,70	42,03	48,48	7,95	457,00	238,00	54,6	4,23
Ce	171,08	153,0	83,94	103,44	0,57	48,10	21,80	69,6	0,36
Pr	24,15	12,40	8,62	9,59	1,51	162,00	70,20	5,12	1,10
Nd	83,69	32,10	29,78	24,67	0,17	24,40	9,90	13,4	0,15
Sm	12,29	2,87	4,03	2,51	0,03	7,02	2,55	1,84	0,07
Eu	3,24	0,74	1,28	0,37	0,13	21,60	9,30	0,56	0,09
Gd	9,23	1,98	3,12	1,75	0,02	2,21	0,95	2,00	0,01
Tb	1,16	0,32	0,37	0,25	0,11	11,70	5,17	0,22	0,07
Dy	6,69	1,46	2,32	1,66	0,02	2,51	1,02	1,29	0,01
Ho	1,29	0,29	0,44	0,36	0,10	12,60	2,71	0,27	0,05
Er	3,43	1,02	1,20	0,95	0,01	0,90	0,39	0,78	0,01
Tm	0,51	0,20	0,17	0,14	0,11	5,60	2,66	0,126	0,02
Yb	3,35	1,85	1,10	0,89	0,02	0,81	0,38	0,72	0,01
Lu	0.49	0.34	0,15	0,13	6.89	15.3	5.93	0.1	4.6
Th	27,20	11,20	5,42	2,40	0,88	36,10	19,50	8,55	1,25
U	8,12	1,05	0,93	0,56	0,37	2,09	1,79	2,63	9,88

Notes: 1, 2 amphibole miaskite; 3,4 biotite miaskite IMC; 5 biotite miaskite CAB; 6, 7 pyroxene–amphibole miaskite (sandyite), 8 garnet–amphibole miaskite (firsite); 9 plagiomiaskite.

values of felsic and intermediate rocks (Vinogradov, 1962). The contents of these elements in rocks increase in the same range similarly to total REE contents.

The Th/U ratio is extremely inconsistent in both individual rock groups and the entire samples of miaskites of the Ilmenogosky complex: 0.55–7.4 for IMC BMs, 3.3–10.6 for IMC AMs, 0.6–7.1 for CAB BMs, 6.1–17.3 for sandyites, 3.2–10.6 for firsites, and 0.1–0.2 for plagiomiaskites. The mean Th/U ratio of igneous miaskites is 1.8 (Smyslov, 1974). The Th/U ratio of rocks of the Guli alkaline-ultramafic complex is 2.3–4.12 (3.8, mean value) for nepheline syenites reaching up to 32 in late differentiates (carbonatites II) [Kogarko, 2012]. The Th/U ratio indicates influence of transformation processes on miaskites of the Ilmenogorsky complex and lack of magmatic tracers in them.

The U/Pb (SHRIMP) age of zircons from miaskites indicates two stages of their formation: 420–440 Ma (Middle Ordovician) and 280–220 Ma (Permian–Triassic). Geochemistry of zircons shows metasomatic characteristics of both age clusters (Krasnobaev et al., 2016). The Rb/Sr and Ar/Ar ages of feldspar, biotite and amphibole from miaskites correspond to a range of 240–250 Ma. The Ar/Ar age of amphibole (290.0 ± 3.2 Ma) and biotite (285.3 ± 3.1 Ma) of sandyites (previously considered to be the relics of the substrate for miaskites) correspond to the beginning of the regional shear processes during the final stages of collision, accompanied by active rock alteration by the fluid.

Textural and structural features of rocks of the Ilmenogorsky complex indicate intense influence of shear tectonics. The features of mineral composition, zonation of biotite, and abundant replacement processes are evident of multistage transformations of rocks. The composition of biotite from miaskites plotted on a diagram of activity of H_2O (crystallization temperature) vs. K (alkalinity) in crystallizing melts by Fe# and Al# values of biotite (Ivanov, 1970) shows high water activity (crystallization temperature) and low alkalinity for plagiomiaskites and extremely low crystallization temperature and high alkalinity for sandyites. The maximum alkalinity values and elevated temperatures are registered for mylonites and ultramylonites after IMC and CAB BMs. In the IVPK miaskites, the increase in alkalinity and enrichment in mantle (Nb, Ta, Zr, Hf, U, REE, F, Cl, etc.) and crustal (Cs, Rb, K, Ba, Sr, Th, Sn) elements is observed in a range from plagiomiaskites and CAB BMs to IMC AMs and sandyites.

Broadly variable composition of rock-forming and accessory minerals and mineralogical-petrochemical and geochemical ratios indicate metasomatic genesis of miaskites, which were formed after metaterrigenous alkaline gneisses and heterogeneous metamorphic rocks (amphibolites, marbles, shists, etc.). The age of rocks and minerals indirectly confirm the remobilization origin of miaskites. The release of the mantle fluid melt as a result of the origination of a long-living deep fault and further collapse of the orogen is most likely scenario of the formation of the IVPK rocks. These processes led to anatectic melting of early alkaline rocks and metamorphic sequences. The processes of mantle (metasomatic) replacement occurred in the lower crust under viscous plastic deformation of rocks leading to the formation of syntectonic miaskites. They consumed redistributed transitional elements from heterogeneous metamorphic substrate (Sc, Ti, V, Cr, Mn, Fe, Co, Ni, Cu, Zn) and newly gained crustal and mantle elements (K, Na, Rb, Ba, Sr, Th, U, Nb, Ta, Zr, Hf, REE, F, Cl). The high intensity of fluid reworking along with alkaline metasomatosis led to metasomatic migmatization probably followed by partial anatectic melting. The final products of this process probably include plagiomiaskites and sandyites. The further exhumation of the complex during strike-slip–normal fault movements resulted in retrograde dynamometamorphic processes and explosive decompression of the fluid, when miaskites were transformed under brittle-plastic deformations accompanied by redistribution of elements along the local tectonic zones (faults, system of transpression and transtension faults) and the formation of mylonites-ultramylonite bodies, syntectonic metasomatites and pegmatites enriched in LILEs, HFSEs and REEs.

This work was supported by State Contract of the Ilmeny State Reserve FRC MG UB RAS.

References

Bazhenov A. G. The question of the Genesis of miaskites. Geochemistry, Petrology, Mineralogy and Genesis of alkaline rocks. Geochemistry, petrology, mineralogy and genesis of alkaline rocks. Collection of Abstracts of the All-Russian Meeting. Miass: UB RAS, 2006. P. 21—25.

Ivanov.V. S. On the influence of temperature and chemical activity of potassium on the composition of biotite in granitoids. Izv. AS USSR Geol. ser. 1970. №. 7. P. 20–30.

Krasnobaev A.A., Valizer P.M., Busharina S.V., Medvedeva E.V Zirconology of miaskites of the Ilmeny Mountains (Southern Urals). Geochemistry International. 2016. № 9. P. 797-813.

Kogarko L. N. Geochemistry of radioactive elements in the rocks of the Gulinsky massif (Polar Siberia). Geochemistry. 2012. No. 9. P. 803-803.

Levin V.Ya., Ronenson B.M., Samkov V.S., Levina I.A., Sergeev N.S., Kiselev A.P. Alkaline carbonatite complexes of the Urals. Ekaterinburg, Uralgeolkom Publ., 1997. 274 p.

Medvedeva E/V/, Nemov A.B., Kotlyapov V.A. Banalsite–stronalsite from sandyites of the Ilmenogorsky miaskite massif (South Ural)//Mineralogy. 2016. №1. P/ 3-8.

Nedosekova I. L., Vladykin N. V., Pribavkin S. V., Bayanova T. B. Ilmeno-Vishnevogorsk miaskite-carbonatite complex: origin, ore content, sources of matter (Ural, Russia)). Geology of ore deposits, 2009. V. 51 №. 2. P. 157—181.

Rass I. T., Abramov S. S., et al. Role of fluids in the genesis of carbonatites and alkaline rocks: geochemical indicators. Geochemistry. 2006. №. 7. P. 692-711.

Ronenson B. M. The origin of miaskites and the connection with them of rare metal mineralization. Moscow: Nedra, 1966. 173 pp.

Rusin A.I., Krasnobaev A.A., Rusin I.A., Valizer P.M., Medvedeva E.V. Alkaline-ultrabasic association of Ilmeny-Vishnevye Mountains. Geochemistry, Petrology, Mineralogy and genesis alkaline rocks. Proc. All-Russian Conf. Miass, IMin UrO RAN, 2006. P. 222-227.

Smyslov A. A. Uranium and thorium in the earth's crust. Nedra: Leningrad. 1974. 231 pp.

Trouw R.A.J., Passchier C.W., Wiersma D.J. Atlas mylonites and related microstructures. Berlin: Springer, 2010. 322p.

Vinogradov A. P. The average content of chemical elements in the main types of igneous rocks of the earth's crust // Geochemistry. 1962.№. 7. P. 555-571.

GEOCHEMICAL AND ISOTOPIC DATA OF MUSHGAI-KHUDAG COMPLEX (SOUTH MONGOLIA)

Nikolenko A.M.[1], Doroshkevich A.G.[1,2], Redina A.A.[1], Prokopyev I.R.[1,3], Chebotarev D.A.[1]

[1]VS Sobolev Institute of Geology and Mineralogy Siberian Branch Russian Academy of Sciences (SB RAS), pr. Ak. Koptyuga 3, 630090, Novosibirsk, Russia

[2]The Geological Institute of SB RAS, st. Sakhyanova 6a, 670047, Ulan-Ude, Russia

[3]Novosibirsk State University, Pirogova Str., 2, 630090, Novosibirsk, Russia

The Mushgai-Khudag carbonatite-alkaline complex is located in the southern part of Mongolia. It is composed of wide series of silicate volcanic and plutonic rocks such as nephelinites, alkali feldspar trachytes, which are crosscut by stocks and dykes of shonkinites, alkaline syenites, and non-silicate ore-forming rocks: stocks and dykes of magnetite-apatite rocks, and dykes of carbonatites (Samoilov and Kovalenko, 1983; Andreeva, 2000, Baatar et al., 2013, Vladykin, 2013, Nikolenko et al., 2018). The latest fluorite mineralization occurs as disseminations in host rocks and forms the nets of microveinlets as well as veins up to firsts meters wide. Many zones of fluorite mineralization are brecciated and carry out fragments of host rock. Host rocks are represented by Paleozoic sedimentary-volcanogenic rocks (limestones, sandstones, argillaceous shales and basic effusive rocks) and Carboniferous granitoids.

Silicate rocks can be subdivided into three groups. The first group includes melanocratic ultrabasic effusive rocks (nephelinites), the second group includes effusive and intrusive rocks of basic and intermediate composition (alkaline syenites, trachytes, theralites, shonkinites), and the third group includes felsic effusives (rhyolites).

Nephelinites form small extrusive sheets up to 50 m in thickness. They are dark porphyritic (up to 20% phenocrysts) rocks with predominant phenocrysts of Ba-phlogopite (2-5 mm), clinopyroxene (1-2 mm) and minor apatite (up to 0.5 mm). The fine-grained groundmass is mainly composed of phlogopite, clinopyroxene, nepheline, K-feldspar; minor and accessory minerals are apatite, garnet, celestite, magnetite and titanite. Carbonatite globules (1-2 cm) are also observed in nephelinites. Clinopyroxene corresponds to diopside. Fluorapatite forms idiomorphic grains and contains SrO up to 8.0 wt.%, REE up to 1.6 wt.%, SO_3 up to 0.9 wt.%.

Alkali feldspar trachytes are represented in numerous lava flows or paleovolcanos up to 10-350 m in thickness. They have aphiric rarely porphyritic texture with the predominant phenocrysts of K-feldspar, phlogopite, clinopyroxene and apatite. The groundmass consist of K-feldspar and albite. The minor and accessory minerals are magnetite, titanite, calcite, rutile. Secondary minerals are scapolite and goethite.

Shonkinites occur as vein bodies up to 150 m in length. They are dark porphyritic rocks containing up to 30-40% phenocrysts. The phenocrysts are represented predominantly by K-feldspar, clinopyroxene, phlogopite, apatite and magnetite. The minor and accessory minerals are titanite, calcite, fluorite, garnet. The groundmass is consist of phlogopite and albite-K-feldspar aggregate. Apatite is characterized by the presence of Ce_2O_3 up to 0.8 wt.%, SO_3 up to 1.1 wt.%, Cl up to 0.2 wt.%, F up to 3.4 wt.%.

Alkaline syenites form dykes, stocks and small massifs from a few meters to 1 km wide. They are composed of varying amounts of K-feldspar (80-95%), phlogopite (5-7%), clinopyroxene (up to 5%), apatite (up to 3%). The accessory minerals are rutile, zircon, magnetite, titanite, armalcolite. Clinopyroxene corresponds to diopside. Fluorapatite is characterized by the presence of REE up to 3.0 wt.%, SrO up to 1.6 wt.%, SO_3 up to 2.2 wt.%. There is no BaO in phlogopite. The alkaline syenites are characterized by the presence of apatite-magnetite shlieren. Shlieren are consist of magnetite, fluorapatite and phlogopite. Magnetite forms crystals up to 3 cm in length immersed into apatite groundmass. Fluorapatite contains LREE up to 7.3 wt.% and SO_3 up to 2.1 wt.% (Nikolenko et al., 2018).

Felsic volcanics (rhyolites) are porphyric fine-grained pinkish-gray rocks. The phenocrysts (up to 30%) are represented predominantly by quartz. The groundmass is consist of by K-feldspar, quartz and goethite.

Magnetite-apatite rocks are exposed in two stocks 30 by 70 and 10 by 30 m in size or in numerous dykes within alkaline syenite field. They are brown, greenish-gray, dark gray with massive or trachytoidal texture. The main minerals of the magmatic association are apatite, magnetite, ilmenite and phlogopite, the accessory are goethite, phosphosiderite, monazite-Ce, celestite, rutile, quartz, fluellite, fluorite, barite, gypsum and pyrite. Modal proportions of apatite and magnetite, which constitute together about 90 % of the rock, vary considerably.

Carbonatites compose veins and dykes from a few cm to 10 m wide. The main minerals of carbonatites are calcite, dolomite, fluorite and sulfates (barite and celestite). The minor and accessory minerals are apatite, monazite-Ce, REE fluorcarbonates (bastnaesite, parisite). Carbonatites are ubiquitously associated with fluorite mineralization. Fluorite veins and stock-like bodies are occurred widespread. They are fluorite-calcite, fluorite-barite, fluorite-quartz, fluorite-celestite composition.

The geochemistry of the volcanic and plutonic silicate rocks of Mushgai-Khudag complex were published previously (Samoilov and Kovalenko, 1983; Baatar et al., 2013; Vladykin, 2013, Nikiforov and Yarmolyuk, 2019). The volcanic and plutonic silicate rocks span a large SiO_2 range from 41.5 wt.% to 73.5 wt.%. All silicate rocks show shoshonitic characteristics with high K_2O contents (generally K_2O>3.5%). Nephelinites plot in the fields of basanite and nephelinite in the TAS diagram. Basic and intermediate volcanic rocks of the complex (phonolites, trachytes) plot in the fields from phonothephrites to trachytes, intrusive varieties of these rocks (shonkinites, alkaline syenites) – from foid monzosyenites to quartz syenites. Felsic volcanic rocks plot in the field of rhyolites. According to Harker diagrams the negative correlation is observed between SiO_2 and MgO, Fe_2O_3, BaO, CaO, P_2O5, TiO_2, V, Ni, K_2O, but Al2O3, Rb, Nb, Zr generally increase following the increase in SiO_2

In the chondrite-normalized REE diagram nephelinites possesses the highest REE contents (∑REE= 1208-1566 ppm) and rhyolites the lowest (∑REE= 153-509 ppm). The chondrite-normalized REE patterns for nephelinites, alkaline syenites and trachytes are steep, relatively smooth and exhibit LREE enrichment with similar LREE fractionation (La/Sm_{CN} = 3-6). The highest LREE enrichment observe for rhyolites (La/Sm_{CN} up to 32).

Nephelinites and basic/intermediate rocks display slightly negative Eu anomalies (Eu^*/Eu = 0.71-0.93) whereas rhyolites has significantly negative Eu anomalies (Eu^*/Eu = 0.47-0.56). In the primitive mantle (PM)-normalized spidergrams, nephelinites and alkaline syenites/trachytes display a similar distribution of LILE, LREE and HFSE. Spidergrams show that these rocks are characterized by positive peaks in Ba, Sr, and Pb, and troughs in high field strength elements (HFSE: e.g., Nb, Ta and Ti) as well as Rb, while the rhyolites have more pronounced negative anomalies of Ti, and weak negative anomalies of Nb and Ta.

Magnetite-apatite rocks and carbonatites are characterized by the strong enrichments in LREE with La/Yb ratio is 110-280 and 130-340, respectively. The chondrite-normalized REE patterns for magnetite-apatite rocks and carbonatites are steep and smooth, and show a slightly negative Eu anomaly with Eu^*/Eu from 0.62 to 0.95 and from 0.61 to 0.70, respectively.

The primitive mantle (PM)-normalized spidergrams for magnetite-apatite rocks and carbonatites show strong HFSE and slight Sr negative anomalies compared to neighboring elements and enrichment in LREE, U and Ba. In comparison with magnetite-apatite rocks the primitive mantle (PM)-normalized spidergrams of carbonatites show a strongly enriched pattern in Ba and Pb and depleted in Th.

The Sr and Nd isotopic data for the rocks of Mushgai-Khudag complex have significant variations of $(^{87}Sr/^{86}Sr)_i$ ratios between 0.70532 and 0.70762 and show a narrow □Nd(t) value range from -1.23 to 1.25. The Sr–Nd isotopic range is similar to those for Early Cretaceous Bayan-Khoshu carbonatites in South Mongolia ($^{87}Sr/^{86}Sr_i$=0.70600–0.70691, $□Nd_{(t)}$= -1.9 - 0.2 (Vladykin, 2005), the Early Cretaceous volcanics from the Zaza and Uda complexes of West Transbaikalia Rift Zone (Komaritsyna et al., 2018), and Late Jurassic volcanics of Akatui massif (Sasim et al., 2016). In comparison with the Mushgai-Khudag rocks, the Late Mesozoic carbonatites and syenites from the West Transbaikalia complexes (Oshurkovo, Arshan, Khalyuta, Yuzhnoe) (Vladykin, 2005; Doroshkevich, 2013; Nikiforov and Yarmolyuk, 2019) have lower $□Nd_{(t)}$ values and similar initial $^{87}Sr/^{86}Sr$ ratios but carbonatites of Tuva complexes (Salnikova et al., 2010; Nikiforov et al., 2002;

2019) have higher □Nd(t) values and lower initial $^{87}Sr/^{86}Sr$ ratios. The Late Mesozoic carbonatites and alkaline syenites of North China massifs (Nikiforov and Yarmolyuk, 2019) are characterized by significant lower $□Nd_{(t)}$ values with a similar range of εSr in comparison with the Mushgai-Khudag rocks.

The silicate rocks have very similar Pb isotopic compositions. The samples have $(^{206}Pb/^{204}Pb)_i$=18.35–18.55, $(^{207}Pb/^{204}Pb)_i$=15.57–15.59 and $(^{208}Pb/^{204}Pb)_i$=38.23–38.38. The values of radiogenic Pb in carbonatites, fluorite rocks of Mushgai-Khudag and host limestones are similar to Pb values in silicate rocks. The magnetite-apatite rocks are characterized by higher values of initial $^{207}Pb/^{204}Pb$ and $^{208}Pb/^{204}Pb$ ratios: $(^{206}Pb/^{204}Pb)_i$=19.61, $(^{207}Pb/^{204}Pb)_i$=15.64, and $(^{208}Pb/^{204}Pb)_i$=41.38. In the $(^{206}Pb/^{204}Pb)_i$ versus $(^{207}Pb/^{204}Pb)_i$ and $(^{208}Pb/^{204}Pb)_i$ diagrams all samples are plotted to the right side of the north hemisphere reference line (NHRL; Hart, 1984), suggesting more radiogenic ^{206}Pb than ^{207}Pb and ^{208}Pb.

Decreasing of MgO, Fe_2O_3, BaO, CaO, P_2O5, TiO_2, V, Ni, K_2O and increasing of Al_2O_3, Rb, Nb, Zr from ultrabasic to felsic rocks is confirmed that silicate rocks of Mushgai-Khudag complex were formed as a result of fractional crystallization of parental melt of nephelinite composition. This melt was enriched with sulfur and fluorine, which is reflected in the elevated concentrations of these elements in the minerals (apatite, phlogopite) of nephelinites, shonkinites and syenites. The presence of magnetite-apatite shlieren in alkaline syenites allow to suggest that ore-bearing magnetite-apatite rocks were formed as a result of the processes of liquid immiscibility between the silicate and phosphate melts (Nikolenko et al., 2017).

Late Mesozoic alkaline volcanism in the Southern Mongolia exhibits geochemical and Sr-Nd-Pb isotopic characteristics similar to those of alkaline magmatism in western Transbaikalia and North China. These characteristics indicate that the rocks of the complex were formed from an enriched lithospheric mantle involving of subducted material.

Mineralogical investigations were carried out on state assignment of IGM SB RAS, No 0330-2016-0002. Geochemical and isotopic studies were supported by the Russian Science Foundation, grants No. 19-17-00013 and No 19-17-00019.

References

Andreeva I.A., 2000. Extended Abstract of Candidate's Dissertation in Geology and Mineralogy (IGEM, Moscow) (in Russian).

Baatar M., Ochir, G., Kynicky, J., Iizumi, S., Comin-Chiaramonti, P., 2013. Some Notes on the Lugiin Gol, Mushgai Khudag and Bayan Khoshuu Alkaline Complexes, Southern Mongolia. International Journal of Geosciences, 4, 1200.

Doroshkevich A.G. (2013). Petrology of Carbonatite and Carbonate-Containing Alkaline Rock Complexes in Western Transbaikalia. ScD Thesis (in Russian).

Hart, S.R. (1984). A large-scale isotope anomaly in the Southern Hemisphere mantle. Nature, 309(5971), 753.

Komaritsyna T.Y., Yarmolyuk V.V., Vorontsov A.A., 2018. Crustal Contamination of Early Cretaceous Magmatic Rocks of the Western Transbaikal Rifting Zone. In Doklady Earth Sciences, 481 (1), pp. 948-952.

Nikiforov A.V., Yarmolyuk V.V. (2019). Late Mesozoic carbonatite provinces in Central Asia: Their compositions, sources and genetic settings. Gondwana Research.

Nikolenko A., Redina A., Doroshkevich A., Prokopyev I., Ragozin A., Vladykin N. (2018) The origin of magnetite-apatite rocks of Mushgai-Khudag Complex, South Mongolia: mineral chemistry and studies of melt and fluid inclusions. Lithos 320-321, 567-582.

Samoilov V.S., Kovalenko V.I., 1983. Complexes of Alkaline Rocks and Carbonatites in South Mongolia (in Russian).

Samoilov V.S., Kovalenko V.I., Naumov V.B., 1988. The immiscibility of silicate and salt melts during the formation of the Mushugai-Khuduk alkaline complex (South Mongolia). Geochemistry, 10, 1447-1460 (in Russian).

Sasim S.A., Dril S.I., Travin A.V., Vladimirova T.A., Gerasimov N.S., Noskova Y.V., 2016. Shoshonite-latite series of the Eastern Transbaikalia: $^{40}Ar/^{39}Ar$ age, geochemistry, and Sr-Nd isotope composition of rocks from the Akatui volcano-plutonic association of the Aleksandrovskii Zavod depression. Russian Geology and Geophysics, 57(5), 756-772.

Vladykin N.V., 2013 Petrology and composition of rare-metal alkaline rocks in the South Gobi Desert (Mongolia). Russian Geology and Geophysics, 54 (4), 545-568.

ALKALINE MAGMATISM OF THE DEVONIAN RIFT SYSTEMS OF THE EAST EUROPEAN PLATFORM: AGE, GEOCHEMISTRY, TECTONIC SETTING OF THE DNIEPER-DONETS-PRIPYAT-RIFT AND THE ARKHANGELSK-KOLA PROVINCE COMPARISON

Nosova A.A.[1], Kuz'menkova O.F.[2], Kargin A.V.[1], Yutkina E.V.[1], Sazonova L.V.[1,3], Laptsevich A.G.[2]

[1]Institute of Geology of Ore Deposits, Petrography, Mineralogy, and Geochemistry, Russian Academy of Sciences (IGEM RAS), Moscow, Russia, nosova@igem.ru

[2]Institute of Geology, Republican Unitary Enterprise "Scientific-Production Center for Geology", Minsk, Belarus

[3]Lomonosov Moscow State University, Moscow, Russia, sazonova@mail.ru

In the geological evolution of the East European Platform (EEP), Devonian time was marked by alkaline-ultramafic, mafic, and alkaline magmatism, which was occurred at both the marginal and central portions of the platform. Magmatism manifested mainly in the reactivated preexisting Mesoproterozoic rift zones (e.g. Belomorian rift system) and in newly formed rift structures (Pripyat graben).

Along with the Kola alkaline and conjugate Arkhangelsk kimberlite province, another largest Devonian magmatic area in EEP is the rift system of the Dnieper–Donets-Prypiat trough (DDPT) in the southern part of the platform.

There are numerous petrological studies aimed at investigated of sources and conditions of diverse rift-related magmatism in specific rift system. However, there is a few works in which the comparison of magmatism from several rifts was made. The article with authorship of Wilson and Lyashkevich (1996) is the best example of comparative study of the Devonian rift-related magmatism of the EEP.

Over the past two decades, a lot of new data on the Devonian magmatism of the EEP has been obtained. In our presentation we will try to analyze the published and our new geochronological, petrological data for the Kola alkaline province, conjugate Arkhangelsk kimberlite province and the Dnieper–Donets-Prypiat rift system in the context of an age, composition and tectonic setting of an alkaline magmatism comparison. Special attention will be paid to the position of kimberlite (table 1).

Age of alkaline magmatism. Recently we have obtained geochronological data for kimberlites of the Arkhangelsk Diamondiferous Province (ADP) (Larionova et al., 2016). The kimberlite was dated by the Rb–Sr technique on phlogopite. Our isochron data yield the emplacement age of the kimberlite as 376 ± 3 Ma for the Grib Pipe, 380 ± 2 Ma for the Karpinsky-1 pipe, 375 ± 2 Ma for the Karpinsky-2 Pipe, and 377 ± 0.4 Ma for the Ermakovskaya-7 Pipe. Therefore, kimberlite ranging in age from 380 ± 2 to 375 ± 2 Ma.

According to the latest review of the Kola alkaline province geochronologic data (Arzamastsev and Wu, 2014), a magmatism have continued within a time span of approximately 30 Ma. The earliest magmatic events were tholeiitic and subalkaline magmatism at about 390 Ma, and the youngest dikes and diatremes were emplaced at approximately 360 Ma. The alkaline-ultramafic magmatism took place starting at 387 ± 7 Ma in the Khibina and Lovozero calderas, continued until 379 ± 7 Ma, and produced complexes with carbonatite (Kovdor, Afrikanda, etc.).

Comparison between the Arkhangelsk province kimberlite emplacement ages and the ages of Kola alkaline province magmatism obtained by (Arzamastsev and Wu, 2014), shows that the kimberlite was emplaced roughly simultaneously with the alkaline-ultramafic intrusions.

Based on adjacent spatial position of the two provinces, the synchronous ages of magmatism and magmatism diversity common for both provinces one can considered the Arkhangelsk and Kola provinces as a single larger province named the Arkhangelsk – Kola province (AKP).

Unlike the AKP, which provided by isotopic ages, the DDPT magmatism ages are derived mainly from stratigraphic relationship (e.g. Wilson and Lyashkevich, 1996; McCann et al., 2003 and references therein). An initial magmatic activity occurs as basaltic extrusions within the Donbas area and Priazov massif at Eifelian-Early Givetian (McCann et al., 2003). Two distinct phase of volcanic

activity: Late Frasnian and Late Famennian have been recognized on the base of volcanic and volcanic-sedimentary sequences analyses (Wilson and Lyashkevich, 1996 and references therein).

Widescale basalt eruptions within the Voronez anteclise are corresponded with Late Frasnian volcanic activity within the DDPT.

Table 1. Characteristics of alkaline and kimberlite magmatism of the Dnieper-Donets-Pripyat-Rift and the Arkhangelsk-Kola Province.

Characteristic	The AKP	The DDPT
Age of alkaline magmatism	from 387 ± 7 Ma to 379 ± 7 Ma	from 381±2 Ma to 387± 6 Ma
Age of kimberlite magmatism	from 380 ± 2 to 375 ± 2 Ma	from 383±4 to 385±4 Ma
Magmatism diversity	kimberlite, olivine melilitite, alkaline picrite, carbonatite, aillikite, basalts pipes, alkaline ultramafic massifs with carbonatites, agpaitic nepheline syenite massifs and basalt dyke swarms	alkaline ultramafic and nepheline syenite massifs, alkaline picrite and basalt lava floods, lamprophyre dykes and kimberlite pipes, orangeite, aillikite, carbonatite diatremes, nephelinite and alkaline basalt lavas and tuffs, phonolite and trachyte lavas and syenite sills and nephelinite lavas, basalt and dacite lavas
Kimberlite position	Kimberlite is located within Paleoproterozoic orogenic belt. Kimberlites have zonal distribution in the SE portion of the province There is lateral transition from kimberlite to alkaline ultramafic massifs with carbonatites	Kimberlite is located within Paleoproterozoic orogenic belt. There is no preferred location of kimberlite occurrences Kimberlites/orangeites, and carbonatites or alkaline ultramafic massifs are in conjunction

References see in the text.

There are a few isotopic ages of the DDPT magmatic activity. A synthesis of the old K-Ar ages of igneous rocks of the south of rift (the Donbas area) indicates volcanic activity with age 388 ± 12 Ma (Shatalov, 1986 and references therein). According to Rb-Sr phlogopite dating (Yutkina et al., 2004), kimberlites of the Priazov massif were emplacement at 383±4 Ma (Novolapsinskay Pipe) and 385±4 Ma (Yuznaya Pipe). Rb-Sr phlogopite ages for kimberlites obtained by (Tsymbal et al., 2007) are similar and range between 380 to 391 Ma. U-Pb dating of zircon from kimberlite yielded two peaks of ages: around 385 Ma that well corresponding with Rb-Sr data and older, close to 410 Ma. The first peak has been interpreted as an age of kimberlite emplacement event and the second peak probably indicate an early magmatic pulse (Shumlyanskyy et al., 2010).

Until recently, only one isotopic age for the Pripyat segment of DDPT exist: hornblendite xenolith genetically linked with Pripyat lamprophyre $^{40}Ar/^{39}Ar$ dating yielded a plateau age of 381±2 Ma (Markwick et al., 2001). We have obtained new $^{40}Ar/^{39}Ar$ dating of ultramafic lamprophyres from the Zlobin Saddle, North Pripyat area. Two phlogopite separates from aillikite and orangeite yielded plateau ages at 387± 6 Ma and 394 ± 5 Ma that corresponds to Givetian – Early Fransnian.

Presence of Middle Frasnian (Semiluki Horizon) limestone xenoliths within the lamprophyre from Zlobin pipes evidences that they were emplaced not early than Middle Frasnian. The majority of isotopic ages of the Zlobin lamprophyres (Markwick et al., 2001 and our aillikite sample) are corresponded with age derived from their stratigraphic position. However, a discrepancy between the older isotopic age of phlogopite from orangeite and the younger age of phlogopite from lamprophyre pipes emplacement is evident. It is likely that a cause of the age disconformity is xenocrysts presence

in the studied phlogopite fraction. These phlogopite xenocrysts could be formed by mantle metasomatism preceding the lamprophyre emplacement.

Geochronological data for the AKP and the DDPT, including our new data, indicate that both provinces have been formed roughly simultaneously from the end of Middle Devonian to Late Devonian.

Magmatism diversity and kimberlite position. The southeastern portion of AKP contains several kimberlite fields including the Lomonosov and Grib Pipe economic diamond deposits. Related rocks are olivine melilitite, alkaline picrite, carbonatite, aillikite, basalts. Kimberlite and other alkaline ultramafic rocks as well as basalts form numerous pipes and rare sills. The northwestern portion of AKP (the Kola Province) contains alkaline ultramafic massifs with carbonatites, agpaitic nepheline syenite massifs and basalt dyke swarms. Aillikite, olivine melilitite, carbonatite dykes and pipes are dominated within transition zone (The Tersky Coast) between two portions of the AKP.

The DDPT system hosts various magmatic associations. Within the Dnieper segment basalt and mid-alkaline and alkaline intermediate-acid lavas (Bragin–Chernigov block), alkaline ultramafic lavas (Belotserkovsky block) and dolerite dyke swarms are occurred. The Donbas segment and Priazov massif contain alkaline ultramafic and nepheline syenite massifs, alkaline picrite and basalt lava floods, lamprophyre dykes and kimberlite pipes. The Pripyat segment is characterized by orangeite, aillikite, alkaline picrite, melilitite, ultramafic foidite, carbonatite diatremes (Zlobin Saddle), alkaline ultramafic, mafic, intermediate dykes (and syenite sills), lavas and tuffs (Pripyat Trough). Abundant basalt effusions manifested in the eastern portion of the rift system (the Voronezh Anteclise).

The Middle –Late Devonian magmatism of both areas (the AKP and the DDPT) ranging in composition from carbonatite to syenite and generally is remarkably similar. The latest dacite and rhyo-dacite lava eruptions in the DDPT and lack of felsic magmatism in the AKP are marked differences. It is important that apparent volume of the deepest alkaline ultramafic magmatism in the AKP is significantly exceeded that of the DDPT.

Trace element characteristics of most igneous rocks of both AKP and DDPT suggest they were derived from a heterogeneously enriched mantle sources including a plume and metasomatized subcontinental lithosphere (Kramm and Kogarko, 1994). Isotopic data show significant variations: e.g. $\varepsilon Nd(T)$ values for whole rock samples and perovskite from kimberlite and ultramafic rocks ranging from -9 to +5.7 for the AKP (Kononova et al., 2007) and from -6 to +9 for the whole rock samples from lamprophyres and mafic rocks of the DDPT (Wilson and Lyashkevich, 1996 and our new unpublished data). The Sr isotopic data have analogous distribution. It is likely that process of crustal contamination has controlled the isotopic variations. Elemental data (elevated Pb/Ce ratio and others) also indicate that contribution of continental crustal material to the mantle melts is needed.

Kimberlites occupy significant part of the AKP territory. Their numerous occurrences are localized in southeastern portion of the province and concentrated within the zone striking NW. In this linear NW-SE zone, kimberlite pipes of the SE are replaced with some overlap by aillikites and further to the NW are changing into alkaline ultramfic massifs with carbonatites of the Kola part of AKP.

This linear NW-SE zone inherits the position of the Paleoproterozoic Lapland – Kola orogen reactivated by rift processes in the Devonian (e.g. Tectonics …, 2012).

There are only two occurrences of kimberlite and orangeite in the DDP rift system. Four kimberlite pipes and two dykes were found in the Priazov massif in close proximity with an alkaline ultramafic massif and picrite and basalt lava sequences (e.g. Yutkina et al., 2004; Shumlyanskyy et al., 2010). Kimberlite pipes cut Paleoproterozoic granites and Middle Devonian sedimentary rocks. Geological position and isotopic ages suggest that the kimberlite was formed in temporal and spatial association with other Middle-Late Devonian ultramafic and mafic rocks.

An orangeite in association with aillikite, alkaline picrite, melilites and ultramafic foidites occurs as pipes in the Zlobin Saddle at the Pripyat segment of DDPT. The Zlobin field located within the Osnitsk-Mikashevichy Belt comprises the Paleoproterozoic volcanic and plutonic complexes with juvenile supersubduction nature (Aksamentova, 2002; Shumlyanskyy, 2010).

There is an affinity between geological positions of the kimberlite within both AKP and DDPT. Firstly, they are characterized by location in Paleoproterozoic orogenic belts, not in ancient Archean

cratonic areas. Secondly, they are accompanied by related rocks: alkaline picrites, aillikites, nephelinites/mililitites and even carbonatites. However, differences should also be noted. Kimberlites of the AKP have zonal distribution in the SE portion of the province, unlike the DDPT, where there is no preferred location of kimberlite occurrences. In general terms, gradual spatial conversion from kimberlite to alkaline ultramafic massifs with carbonatites by magmatic bodies of transitional composition (e.g. aillikites) exist in the AKP. In the DDPT kimberlites/orangeites, and carbonatites or alkaline ultramafic massifs could manifest in temporal and spatial conjunction.

Tectonic setting. Geodynamic content of the Devonian magmatism as a whole in EEP is still disputable. Nowadays a dominant role is attached to plume models (e.g. Wilson and Lyashkevich, 1996; Kogarko and Veselovsky, 2019). Some plume models relate magmatism with a number of plumes: an individual plume for each of the magmatic areas is assumed (Wilson and Lyashkevich, 1996; and others). Others models suggest passage of the EEP over a stationary African superplume or their position onto the central or peripheral parts of the large low shear-wave velocity provinces (LLSVPs) in the lowermost mantle in the Devonian (e.g. Kogarko, Veselovsky, 2019).

However, many researchers (e.g. Wilson and Lyashkevich, 1996) note that Devonian rifts were formed in the EEP contemporaneously with the development of a major back-arc rift system in the Western and Central Europe (e.g. Lyngsie et al., 2007).

Contemporaneity of the Devonian rifting of the EEP and beginning of the arc-continent collision in the Uralian orogen at the Late Devonian (Puchkov, 2010) suggest correlation of these two tectonic events. Tectonic context evidences that Devonian magmatism in EEP was coeval with subduction and collisional processes in mobile belts surrounding the platform. It is support an assumption that plate motions and the rotation of EEP itself, when melts were derived from lithospheric mantle metasomatized by asthenospheric material is the cause of rifting and related magmatism (e.g. Chalot-Prat et al., 2007).

This study was supported by the Russian Foundation for Basic Research (project nos. 18-55-00006 and 17-05-00534), the Russian Science Foundation (project no. 19-17-00024) and by the Belarusian Foundation for Basic Research (project no. X18P-109).

References

Aksamentova, N.V. Magmatism and paleogeodynamics of the Early Proterozoic Osnitsk-Mikashevichy Volcanoplutonic Belt. – Minsk, 2002. – 175 p. (in Russian).

Arzamastsev, A.A. and Wu, F.Ya., U–Pb geochronology and Sr–Nd isotopic systematics of minerals from the ultrabasic–alkaline massifs of the Kola Province, Petrology, 2014, vol. 22, no. 5, pp. 462–479

Chalot-Prat, F., Tikhomirov, P., Saintot, A. Late Devonian and Triassic basalts from the southern continental margin of the East European Platform, tracers of a single heterogeneous lithospheric mantle source. Journal of Earth System Science, Volume 116, Issue 6, pp.469-495

Kramm, U. and Kogarko, L.N., Nd and Sr isotope signatures of the Khibina and Lovozero agpaitic centres, Kola alkaline province, Russia, Lithos, 1994, vol. 32, pp. 225–242.

Kogarko L.N., Veselovsky R.V. Geodynamic Regimes of Carbonatite Formation According to the Paleo-Reconstruction Method. Dokl. Earth Sc. (2019) 484: 25. https://doi.org/10.1134

Kononova, V.A., Golubeva, Yu.Yu., Bogatikov, O.A., and Kargin, A.V., Diamond resource potential of kimberlites from the Zimny Bereg Field, Arkhangel'sk Oblast, Geol. Ore Deposits, 2007, vol. 49, no. 6, pp. 421–441.

Larionova Y.O., Sazonova L.V., Lebedeva N.M., Nosova A.A., Tretyachenko V.V., Kargin A.V. (2016) Kimberlite Age in the Arkhangelsk Province, Russia: Isotopic Geochronologic RbSr and 40Ar/39Ar and Mineralogical Data on Phlogopite. Petrology. 24:562–593.

Lyngsie S.B., Thybo H., and Lang R. Rifting and lower crustal reflectivity: A case study of the intracratonic Dniepr-Donets rift zone, Ukraine, J. Geophys. Res., 2007, vol. 112, no. 12, pp. 124-142.

Markwick A. J. W., Downes H., and Veretennikov N., The Lower Crust of S.E. Belarus: Petrological, Geophysical and Geochemical Constraints from Xenoliths,"Tectonophysics. 339. 215–237 (2001).

McCann T, Saintot A, Chalot-Prat F, Kitchka A, Fokin P, Alekseev A and EUROPROBE-INTAS RESEARCH TEAM 2003 Evolution of the southern margin of the Donbass (Ukraine) from Devonian to Early Carboniferous times; In: Tracing Tectonic Deformation Using the Sedimentary Record (eds) McCann T and Saintot A, Geol. Soc. London Spec. Publ. 208.117–135.

Puchkov, V.N., 2010. Geology of the Urals and Cis-Urals (actual problems of stratigraphy, tectonics, geodinamics and metallogeny). Ufa, 280p (in Russian).

Shatalov N.N. Dykes of Priazov'e. Kiev. Naukova Dumka. 1986. 192 p. (in Russian).

Shumlyanskyy L.V., Billström K., Tsymbal S.N., Bogdanova S.V. On the nature of the kimberlites of the Eastern Azov area, Ukraine: Isotopic (U-Pb, Hf zircon and Sr, Nd, Pb rock data) evidence for a depleted mantle origin and subsequent crustal contamination. XXVII international conference Geochemistry of Alkaline rocks. 2010.

Shumlyanskyy L.V. Geochemistry of the Osnitsk–Mikashevichy Volcanoplutonic Complex of the Ukrainian Shield. Geochemistry International, 2014, Vol. 52, No. 11, P. 912–92

Tectonics of the White Sea and adjacent areas (The explanatory notes to "the Tectonic Map of the White Sea and Adjacent Areas", at a Scale of 1:1500 000) / A.S. Baluev, V.A. Zhuravlev, E.N. Terekhov, E.S. Prahiyalgovsky. Editor-in-Chief - M.G. Leonov. M.: GEOS, 2012. 104 p.

Wilson, M. and Lyashkevich, Z.M., Magmatism and the geodynamics of rifting of the Pripyat–Dnieper–Donets rift, East European platform, Tectonophysics,1996, vol. 268, № 1–4, P. 65–81.

Yutkina E.V., Kononov V.A., Bogatikov O.A,, Kniazkov A.P., Kozar N.A., Ovchinnikova G.V., Levski L.K. (2004) Kimberlites of the Eastern Azov (Ukraine) and geochemical characteristics of their sources. Petrology, v. 12, No 2, pp. 159-175.

MINERALOGICAL FEATURES OF EUDIALYTE-CONTAINIG ALKALINE ROCKS FROM KONDER MASSIF, KHABAROVSKY KRAI

Osipov A.S., Antonov A.A.

Saint-Petersburg State University, Saint-Petersburg, Russia, osipov.anst@yandex.ru

Konder massif is located in the Eastern part of the Aldan shield of the Siberian platform, in the basin of the river Maya, in the area between its left tributaries - Omnia and Maymakan. It is an alkaline-ultrabasic zonal intrusive with a diameter of 7.5 km, composed of platinum-bearing dunites, clinopyroxenites, cosvites, which are split by later dikes and vein bodies of alkaline rocks.

The samples studied in the work were selected during the expedition of a group of students and researchers of St. Petersburg state University to the Konder deposit in August 2013. In the bedding occurrence the pegmatites of nepheline syenites, pegmatites of syenites; veins of aegirine-albite composition and bodies composed mainly of minerals of the cancrinite group were met. In addition, large boulders of nepheline-aegirine pegmatites were noted among the clastic rocks. The composition and features of the aegirine-albite veins, a series of which is exposed in the North-Eastern part of the massif were studied thoroughly. The veins width reaches the first meters with a visible length of up to 10 meters. The main minerals composing rocks are albite (45-55 vol.%) and aegirine (35-45 vol%).

During the research of the aegirine-albite rocks, 27 mineral species were found. 14 of them - for the first time for the deposit (tab. 1). For the convenience of description, it has been divided into main, secondary and accessory.

Table 1. The mineral composition of aegirine-albite rocks from Konder massif.

Main		1	Aegirine	$NaFe^{3+}(Si_2O_6)$
		2	Albite	$Na(AlSi_3O_8)$
Secondary		3	Lamprophyllite	$Na_2Sr_2Ti_3(Si_2O_7)_2O_2(OH)_2$
		4	Barytolamprophyllite	$KNa_3Ba_2Ti_3(Si_2O_7)_2O_4$
		5	Microcline	$K(AlSi_3O_8)$
		6	Titanite	$CaTi(SiO_4)O$
		7	Eudialyte	$Na_{12}Ca_6Fe_3Zr_3(SI_3O_9)_2(Si_9O_{24}(OH)_3)_2$
Accessory	Silicates	8	*Calciocatapleiite*	$CaZr(Si_3O_9)\cdot H_2O$
		9	*Elpidite*	$Na_2Zr(Si_6O_{15})\cdot 3H_2O$
		10	*Bobtraillite*	$Na_{13}Sr_{11}(Zr_{13}Y)(B_6Si_{42}O_{132})(OH)_{12}\cdot 12H_2O$
		11	*Stillwellite-(Ce)*	$CeB(SiO_4)O$
		12	*Datolite*	$Ca(BSiO_4)(OH)$
		13	*Kainosite-(Y)*	$Ca_2Y_2(Si_4O_{12})(CO_3)\cdot H_2O$
		14	*Percleveite-(Ce)*	$Ce_2(Si_2O_7)$
		15	Muscovite	$KAl_2(AlSi_3O_{10})(OH)_2$
		16	Analcime	$Na(AlSi_2O_6)\cdot H_2O$
		17	Sepiolite	$Mg_4(Si_6O_{15})(OH)_2\cdot 6H_2O$
		18	Nchwaningite	$Mn_2(SiO_3)(OH)_2\cdot 3H_2O$
	Phosphates	19	Fluorapatite	$Ca_5(PO_4)_3(F)$
		20	*Stronadelphite*	$Sr_5(PO_4)_3F$
		21	*Fluorcaphite*	$CaSrCa_3(PO_4)_3F$
		22	*Xenotime-(Y)*	$Y(PO_4)$
		23	*Monazite-(Ce)*	$Ce(PO_4)$
		24	*Monazite-(Nd)*	$Nd(PO_4)$
	Other	25	Calcite	$Ca(CO_3)$
		26	*Pyrophanite*	$MnTiO_3$
		27	*Galgenbergite-(Ce)*	$Ca(Ce,La,Nd)_2(CO_3)_4\cdot H_2O$

*First time described minerals in the massif are italicized.

Among the secondary phases, the presence of pegmatoid crystals of eudialyte in the rock were most interesting. It forms as isolated grains or groups of grains in the host rock. The crystals are subidiomorphic, crimson and burgundy colors of different shades, up to 5 centimeters in diameter. In the thin sections there is a bright pleochroism from crimson to pale pink. The mineral is optically positive, grains are often bear traces of alteration.

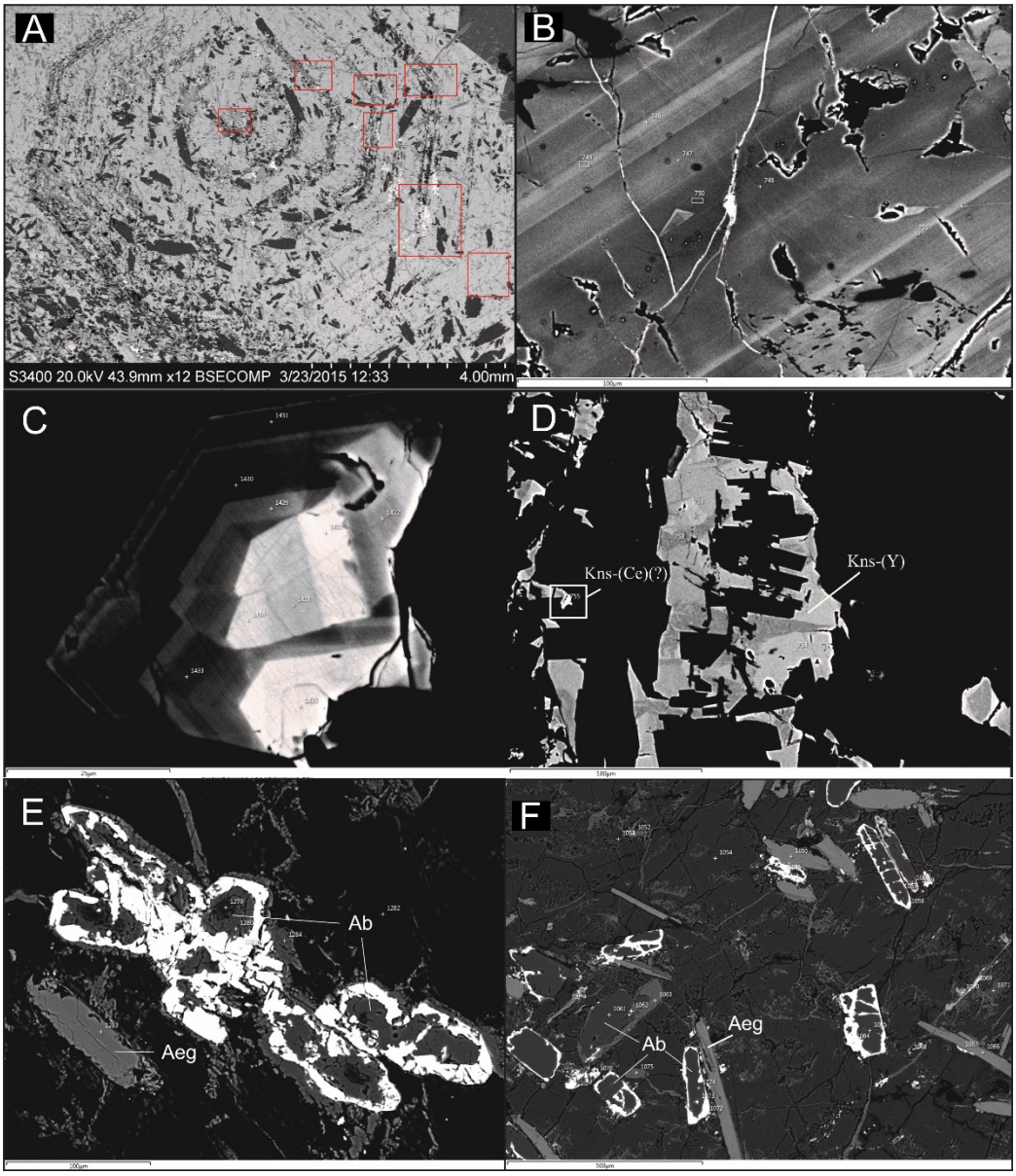

Figure 1. BSE – images of aegirine-albite rocks.
Figure 1A. The macroscopically zoning of eudialyte grain. Figure 1B. The microscopically zoning of eudialyte. Figure 1C. Fluorcaphite grain. Central zones (bright) are central zones are folded with fluorcaphite, the edge zones (Dark) are folded with Sr-reach apatite. Figure 1D. The block structure of kainosite-(Y) (Kns-(Y)) segregation and Ce-dominating zones (Kns-(Ce)?). Figure 1E,F. Galgenbergite-(Ce) crusts (bright) around the albite (Ab) grains. Aeg – aegirine crystals.

The most part of the eudialyte grains has the macroscopically visible zoning, which has the form of an irregular hexagon. As it turned out, this zoning is due to the accumulation of mineral inclusions confined to the growth zones of the crystal and it is not associated with the chemical composition of eudialyte (Fig. 1A). This inclusion formed by albite, calciocatapleite and other REE- and Sr-containing minerals.

Another type of zoning is shown at the micro level. It is represented by alternating zones, which are different in BSE-contrast (Fig. 1B). EDX-analysis and IR-spectroscopy showed the dependence of this type of zoning due to the oscillations of Ti, Ce, Pb, Sr and, apparently, H_3O^+, OH^-, CO_3^{2-} in the mineral composition.

The structure of the eudialyte was decrypted at the department of crystallography, St. Petersburg state University. The studied mineral has a typical eudialyte structure and belongs to the 12-layered eudialyte with R3(-)m symmetry. It has a unit cell parameter a=14,243(3) and C=30,371(6) A.

The chemical composition of eudialyte was studied by WDX-analysis, followed by conversion to formula coefficients taking into account structural data. As a result, there was a sharp deficit of Na and K, which seems to be compensated by the input of H_3O^+, as well as a deficit of Fe and Cl, which can be explained by the high degree of hydratation of eudialyte. The high contents of Y, Sr, Mn and Pb (up to 1.5 wt.% PbO), which is not typical for eudialyte, were marked.

By the set of the collected data, the mineral can be described as a hydrated CO_3-bearing analog of manganoeudialyte. It is the intermediate phase in the manganoeudialyte - ilyukhinite series and can not be assigned to any of this species.

In contrast to secondary minerals, accessory mineralization of aegirine-albite rocks is quite diverse. According to our observations, it has an imposed character and is confined to the leaching areas, cracks and caverns in the rock. Grains are microscopically small, rarely exceeding 150 microns. Diagnosis was carried out on the basis of EDX- and WDX-analysis. The most interesting of these minerals are presented below.

Stronadelphite. It is the rather rare mineral with theoretical formula - $Sr_5(PO_4)_3F$. The grain has an approximately 300x100 microns size. The chemical formula calculated to 3 phosphorous atoms can be written as - $(Sr_{4,13}Ca_{0,57}Ba_{0,04}Fe_{0,04})_{4,78}(P_{1,00}O_{4,13})_3F_{1,00.}$

Fluorcaphite - $CaSrCa_3(PO_4)_3F$ – the similar to apatite mineral [Khomyakov et al., 1997] belonging to the belovite group. The chemical formula calculated to 3,00 phosphorous atoms can be written as - $(Sr_{0,94}Na_{0,06})_{1,00}Ca_{1,00}(Ca_{2,74}Sr_{0,25})_{2,99}(P_{1,00}O_{4,00})_3F_{0,93}$. An interesting fact is that within the limits of one grain (size about 60 microns) (Fig. 1C, sp. 1427, 1428, 1434,1435) the central zones are folded with fluorcaphite while the edge zones are folded with Sr-reach (up to 0.88 f.c.) apatite.

Stilwellite-(Ce). The theoretical mineral formula - $CeB(SiO_4)O$. Except Ce_2O_3 (25-28 wt.%), there are significant quantities of La_2O_3 (12-16 masses.%) and Nd_2O_3 (8-13 wt.%) contains in the chemical composition of researched mineral. The empirical chemical formula based on 1,00 Si atoms can be written as $(Ce_{0,45}La_{0,22}Nd_{0,21}Ca_{0,04})_{0,92}B_{1,54}Si_{1,00}O_{5,89}$. Stillwellite were revealed as inclusions in the hydrated eudialyte. Along with it the micro ingrowths of two other boron-containing minerals - datolite and bobtraillite were discovered.

It should be noticed that the used analythic method allows only to capture only the presence of boron, but not its quantitative values, which makes some error in the calculation of the chemical formula.

Kainosite-(Y). The theoretical mineral formula is $Ca_2(Y,Ce)_2(Si_4O_{12})(CO_3)\ H_2O$. It has a strongly pronounced block structure (Fig. 1D). The segregations size is up to 200 microns. The calculated formula based on 4,00 Si atoms can be written as $(Ca_{1,76}Na_{0,36})_{2,12}(Y_{1,54}Dy_{0,17}Gd_{0,06}Er_{0,06})_{1,83}(Si_{4,00}O_{12,68})(CO_3) \cdot H_2O$, but we observed at least two areas with the generally same phases, which were Ce-dominating (Fig. 1D sp. 755, 759). It allows us to assume the presence of previously unidentified Ce-species of Kainosite-(Y). The research in this direction is continues.

Galgenbergite-(Ce) – the rare carbonate with theoretical formula $CaCe_2(CO_3)_4 \cdot H_2O$. The mineral is associated with calcite. It fills up the cavities in the host rock and, in addition, forms a crusts around the albite grains (Fig. 1E,F). The last segregation form is not typical for carbonates. The calculated ratio of (REE+Y)/(Sa+Sr), allows us to classify the mineral as galgenbergite-(Ce), always close or equal to 2/1. The calculated formula is as follows: $(Ca_{0,97}Sr_{0,05})_{1,02}(Ce_{1,11}Nd_{0,47}La_{0,24}Pr_{0,11}Sm_{0,05})_{1,98}(CO_3)_{3,99} \cdot H_2O$.

Summarizing the data obtained in the study of the aegirine-albite rocks of the Konder massif, we can highlight the following mineralogical features of the rocks.

In total there are 27 mineral species were diagnosed, 20 of them – are accessory minerals, 14 - were described for the first time for the massif. Some of them are rather rare. E.g., bobtraillite and galgenbergite-(Ce) are revealed for the second time in the world and first time in Russia (according to available data).

The absence of zircon in the abundance of other minerals of zirconium such as eudialyte, calciocatapleiite, elpidite and bobtraillite is indicating a high-agpaitic rocks specialization.

Hydrated CO_3-beaing analog of manganoeudialyte in spite of typical for eudialytes morphology, chemical composition and crystal structure, shown some quite individual features are possibly typomorphic for Konder deposit. Taking into account early magmatic crystallization of eudialyte-group minerals, the researched species can be applied as an indicator of mineral-forming processes.

The boron mineralization looks rather exotic in spite of the background of "normal" alkaline rocks minerals. It represents several boron-silicates: bobtraillite, stillwellite-(Ce) and datolite. Moreover, if datolite, in general, is quite ordinary, stillwellite-(Ce) and bobtraillite – are rare minerals.

Overall, identified features indicate a multistage process of formation of the aegirine-albite rocks of the Konder massif, which causes a variety of its composing minerals.

The source of boron remains unclear – this issue requires further study. Diagnostics of the most part of accessory minerals were executed on the basis of EDX-microanalysis. Verification of the received data by other methods, for example – KR-spectroscopy is necessary.

Optical microscopy was performed at the Department of Mineralogy of St. Petersburg state University on a microscope Leica «DM2500M». The minerals were diagnosted in the SPSU RC "Geomodel" used hardware complex, including the electron microscope Hitachi S-3400N with the analytical set-top boxes: analysis of diffraction of reflected electrons EBSD - AzTec HKL Channel 5 Advanced, quantitative energy dispersive microanalysis EDX - AzTec Energy 350, quantitative wave dispersion analysis WDS - INCA 500 (analyst – Vlasenko N.S., Shilovskih V.V.) and Raman spectrometer Horiba Jobin-Yvon LabRam HR 800 (analyst Bocharov V.N.). The chemical composition of eudialyte were obtained in the Natural History Museum (London) on the hardware complex Cameca SX-100 (analyst J. Spratt, A.N. Zaitsev). X-ray diffraction microanalysis and IR-spectroscopy were carried out in the RC SPBU "x-ray Diffraction methods" on the hardware complex Bruker "D8 Discover" (analyst Zolotarev A. A. jr.) and IR-Fourier spectrometer Bruker "Vertex 70" (analyst Panikorovsky T.L.).

References

Bulakh, A.G. and Petrov, T.G., Chemical variability of eudialyte-group minerals and their sorting // Neues Jahrbuch Mineral. Abh., 2004, vol. 3, pp. 127–144.

Bulakh, A.G., Zolotarev, A.A., and Krivovichev, V.G., Struktura, izomorfism, formuly, klassifikatsiya mineralov, (Structure, Isomorphism, Formulas, and Classification of Minerals // St. Petersburg: St. Petersburg State University Press, 2014.

Chukanov, N.V., Rastsvetaeva, N.K., Rozenberg, K.A., Aksenov, S.M., Pekov, I.V., Belakovsky, D.I., Kristiansen, R., and Van, K.V., Ilyukhinite $(H_3O,Na)_{14}Ca_6Mn_2Zr_3Si_{26}O_{72}(OH)_2 \cdot 3H_2O$ - a new eudialyte-group mineral // Zap. Mineral. O-va, 2016, no. 2, pp. 44–57.

Grice, J.D., The crystal chemistry of the eudialyte group // Can. Mineral., 1999, vol. 37, pp. 865–891.

Gurovich, V.G., Emelyanenko, E.P., Zemlyanukhin, V.N., Karetnikov, A.S., Kvasov, A.I., Lazarenkov, V.G., Malich, K.N., Mochalov, A.G., Prikhodko, V.S., and Stepashko, A.A., Geologiya, petrologiya i rudonosnost Konderskogo massiva (Geology, Petrology and Ore MineralResources of the Konder Massif) // Moscow: Nauka, 1994.

Johnsen, O., Ferraris, G., Gault, R.A., Grice, J.D., Kampf, A.R., and Pekov, I.V., The nomenclature of eudialyte-group minerals // Can. Mineral., 2003, vol. 41, pp. 785–794.

Khomyakov A.P., Kulikova I. M., Rastsvetaeva R. K.. Fluorcaphite $Ca(Sr,Na,Ca)(Ca,Sr,Ce)_3(P0_4)_3F$ – a new mineral with the apatite structural motif // Zap. Mineral. O-va, 1997, no. 3, pp. 87–97.

Khomyakov, A.P., Nechelyustov, G.N., and Rastsvetaeva, R.K., Aqualite, $(H_3O)_8(Na,K,Sr)_5Ca_6Zr_3Si_{26}O_{66}(OH)_9Cl$—a new eudialyte-group mineral from the Inagli alkaline massif, Sakha–Yakutia, Russia, and problems of oxonium in hydrated eudialyte // Zap. Mineral. O-va, 2007, no. 2, pp. 39–55.

Krivovichev, V.G., Mineralogicheskii slovar (Glossary of Mineralogy) // St. Petersburg: St. Petersburg State University Press, 2009.

Petrov, T.G. and Krasnova, N.I., R-slovar-katalog khimicheskikh sostavov mineralov, (Dictionary–Catalogue of Chemical Compositions of Minerals) // St. Petersburg: Nauka, 2010.

Rastsvetaeva, R.K. and Chukanov, N.V., Classification of eudialyte-group minerals // Geol. Ore Deposots, 2012, vol. 54, no. 3, pp. 487–497.

Rastsvetaeva, R.K., Chukanov, N.V., and Aksenov, S.M., Mineraly gruppy evdialita: kristallokhimiya, svoistva, genesis (Eudialyte-Group Minerals: Crystal Chemistry, Properties, Genesis) // Nizhny Novgorod: Lobachevsky State University, 2012.

THE FEATURES OF PGM ALTERATION DURING THE FORMATION OF DISTAL PLACERS ASSOCIATED WITH THE URAL-ALASKAN TYPE MASSIFS ON THE EXAMPLE OF THE ISOVSKO-TURINSKAYA ALLUVIAL SYSTEM, MIDDLE URALS, RUSSIA

Palamarchuk R.S.[1], Stepanov S.Yu.[2]

[1]Saint-Petersburg Mining University, Saint-Petersburg, Russia, palamarchuk22@yandex.ru
[2]Zavaritsky Institute of Geology and Geochemistry UB RAS, Ekaterinburg, Russia

Platinum placers associated with the Ural-Alaskan type massifs had been studied for a long time (Zaitsev, 1898). Nevertheless, it seems strange that the PGMs from the Ural platinum-bearing placers, such as Isovsko-Tyrinskaya and Nizhnetagilskaya, which don't have analogues in the world in terms of the extracted PGM amounts, are far from being fully studied. This paper is devoted to the peculiarities of PGM transformation during the transport processes from a primary source to a distant alluvial placer.

The object of investigation is the world's biggest Isovsko-Tyrinskaya placer system. Its formation is due to the destruction of Svetloborsky (Stepanov et al., 2017; Tolstykh et al., 2011) and, to a lesser degree, Veresovoborsky clinopyroxenite-dunite (or Ural-Alaskan type) massifs (Vysotsky, 1923), located on the Middle Urals. During investigation the lode chromitites of Svetloborsky massif were sampled as well as several placers belonging to the same drainage system and located at different distances from the lode source.

The section of modern sediments of the Vershinniy exploration site overlapping the allocated chromite-platinum zone (Stepanov et al., 2017) is given as an example of eluvial placer (Palamarchuk et al., 2017). The Travyanistyi ravine is taken as an example of a ravine, proximal or alluvial placer with a small transport distance (slightly more 1 km) of the detrital material. The sampling site of the alluvial placer with a transport distance of more than 30 km (distal placer) is represented by the Glubokinskoe site.

The concentrates and heavy concentrates consist mainly of chromite and PGM grains. Pt-Fe intermetallic compounds absolutely dominate among the PGMs, in which Os-Ir-Ru mineral inclusions are observed (Stepanov et al., 2019), as well as the PGE sulfides of the laurite – erlichmanite and kashinite – bowieite isomorphic series and the rare minerals of various composition (for example, thiospinel group minerals).

The PGM were extracted from the obtained concentrates using the "blow-off" method. The extracted PGM grains were examined using a binocular microscope, followed by their mounting on carbon conductive adhesive tape, and studied by scanning electron microscopy using a CamScan MX2500 (analyst A.V. Antonov, VSEGEI, Saint-Petersburg, Russia). After this, the grains were placed in artificial polished sections made of epoxy resin. PGM morphological features, as well as their internal structure and composition, were examined using a CamScan MV2300 SEM microscope with an INCA Energy 350 detector (analyst D.A. Varlamov, IEM RAS, Chernogolovka, Russia). The PGM chemical composition was determined using a Camebax SX50 X-ray microanalyzer with WDS detectors (analyst D.A. Khanin, MSU, Moscow, Russia).

Figure 1 shows a regular change in the mineral grain surface from the lode source-placer system. It is established that a change in the morphological features of the platinum-group minerals during the formation of placers is reduced to a gradual loss of primary morphological features. In eluvial and proximal placers, the degree of PGM mechanical transformation is insignificant. The most primary morphological features (plane-faced surfaces, growth striations) are preserved. The PGM in the distal placer are characterized by the predominance of smoothed surfaces, rarely having single grooves on the surface. Besides, the rare rims of tetraferroplatinum, being primary to Pt-Fe alloys, are completely destroyed in the distal placer. In addition, the size of the nuggets decreases with an increasing transport distance from lode mineralization in distal placer.

All studied placers are characterized by similar PGM assemblages. Most of them is isoferroplatinum. The ferroan platinum is found in subordinate amounts. Pinacoidal osmium crystals and rare iridium exolutions are found in significant amounts in Pt-Fe grains. Rarely Pt-Fe alloys

include laurite, erlichmanite, kashinite, bowieite, and very rarely tioshpinels. According to the calculated average content of impurity elements, the isoferroplatinum from some of the studied placers differs from the rest. Such differences, as a whole, do not go beyond the limits of calculation errors, and the compositions of isoferroplatinum from the placers and lode chromite-platinum ore zones are similar.

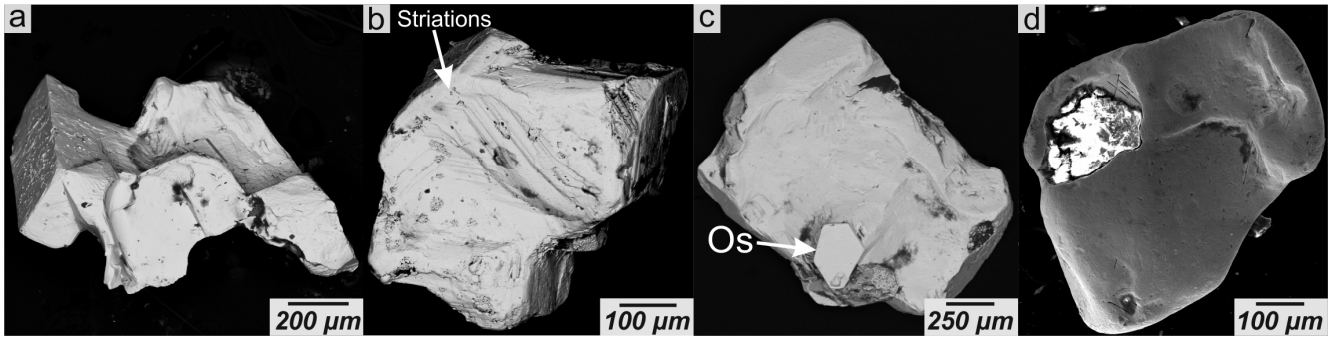

Figure 1. The main morphological features of PGM from: a – lode sourse, b – eluvial placer, c – proximal placer (transport distance slightly more 1 km), d – distal placer (transport distance more 30 km).SEM-photo in BSE mode and SE (d) mode.

Thus, the main PGM transformation in placers is reduced to a regular change in the morphological features during their transport from a lode source to a placer. At a distance of more than 10 km, the degree of PGM mechanical alteration becomes significant, and the morphological features characteristic of lode platinum are practically not preserved. In addition, the rims of the tetraferroplatinum group minerals are completely destroyed in the placers with a significant transport distance.

The results obtained indicate that the platinum bulk has entered the Isovsko-Turinskaya placer system as a result of the destruction of the chromite-platinum ore zones of the Svetloborsky massif. This proves that the chromite-platinum type of mineralization is the most important for the formation of the large placer systems associated with the Ural-Alaskan type massifs.

The coincidence of the compositional features of the PGM assemblages from the studied placers having different transport distances from the lode source may be the evidence of the absence of vertical zonality in the lode platinum mineralization within the destroyed part of the Svetloborsky massif.

This research was funded by Russian Foundation for Basic Research, grant number 18-35-00151|18. We are grateful to Anton Antonov, Dmitry Khanin, Dmitry Varlamov and Anton Kutyrev for analytical works.

References

Zaitsev, A.M. Platinum deposits in the Urals; Tomsk, Russia, 1898; 74 p. (In Russian).

Vysotsky, N.K. Platinum and its mining areas; Proceedings of KEPS, Petrograd, Russia, 1923; 343 p. (In Russian)

Palamarchuk, R.S., Stepanov, S.Yu., Khanin, D.A., Antonov, A.V., Zolotarev, A.A. Jr. Comparative characteristics of platinum group minerals from the eluvial-deluvial placer and chromitites of the Svetloborsky clinopyroxenite-dunite massif (Middle Urals). Mineralogy, 2017, № 4, p. 37–50. (In Russian)

Stepanov, S.Yu., Kozlov, A.V., Malitch, K.N., Badanina, I.Y., Antonov, A.V. Platinum group element mineralization of the Svetly bor and Veresovy bor clinopyroxenite-dunite massifs, Middle Urals, Russia // Geology of ore deposits, 2017, Vol. 59 (3), p. 244–255.

Stepanov S.Yu., Palamarchuk R.S., Kozlov A.V., Khanin D.A., Varlamov D.A., Kiseleva D.V. Platinum-group minerals of Pt-placer deposits associated with the Svetloborsky Ural-Alaskan type massif, Middle Urals, Russia // Minerals, 2019, Vol. 9 (77).

Stepanov, S.Yu., Pilyugin, A.G., Zolotarev, A.A. Jr. Comparison of the compositions of the platinum group minerals of the chromitites and placers of the Nizhny Tagil massif, Middle Urals // Journal of Mining Institute, 2015, Vol. 211 (1), p. 22–28. (In Russian)

Tolstykh, N.D., Telegin, Yu.M., Kozlov, A.P. Platinum mineralization of the Svetloborsky and Kamenushinsky massifs (Urals Platinum Belt) // Russian Geology and Geophysics, 2011, Vol. 52, p. 603–619.

CRYSTAL CHEMISTRY OF THE EUDIALYTE GROUP MINERALS FROM THE LOVOZERO EUDIALYTE COMPLEX, KOLA PENINSULA, RUSSIA

Panikorovskii T.L.[1,2], Mikhailova Yu.A.[1], Pakhomovsky Ya.A.[1], Ivanyuk G.Yu.[1]

[1]Kola Science Centre RAS, Apatity, Russia, taras.panikorovsky@spbu.ru

[2]Saint-Petersburg State University, Saint-Petersburg, Russia

The Lovozero alkiline massif (29×24 km) is composed by rhythmically interlayered trachitoid nepheline syenite of the foyaite–malignite series (lujavrite) and ijolite–urtite. The set of these layers is subdivided into two complexes (Gerasimovsky et al., 1996; Bussen and Sakharov, 1972; Kalinkin, 1974): the lower differentiated complex and the upper complex of eudialyte lujavrite. The eudialyte complex (100–800 m thick) contains numerous xenoliths of fenitized olivine basalts and their tuffs, is relatively poorly differentiated and significantly enriched with eudialyte (Kalashnikov et al., 2016).

Minerals of the eudialyte group (EGM) are secondary to the main rock-forming minerals of the eudialytic complex (up to 10 modal % in foyaites, 15 modal % in foidolites, 40 modal % in malignite–shonkinite and ijolite– melteigite, and 80 modal % in eudialytite). The interest to the Lovozero's EGM as a source of Zr and *REE* caused by giant reserves of these minerals, comparatively easy ore processing and byproduct recovery (Ivanyuk et al., 2015).

In this work, we investigated chemical composition and crystal structure of five Zr-rich EGM crystals (up to 15.24 wt.% ZrO_2 or 3.60 *apfu* Zr) extracted from drill cores LV-154/0, LV-117/76, LV-117/111, LV-153/1 and LV-157/178 situated at Mt. Kedykvyrpakhk The composition of EGM was determined with a Cameca MS-46 microprobe operated in WDS mode at 20 kV and 20–30 nA. The EGM crystal structures were studied using a Rigaku/Oxford Diffraction «XtaLAB Supernova» diffractometer at room temperature. More than a hemisphere of diffraction patterns were collected using CuKα-radiation and scanning along ω with a step of 1° and exposure time of 10 s. Empirical absorption correction was applied in the CrysAlisPro (Agilent Technologies 2014) program complex using spherical harmonics, implemented in the SCALE3 ABSPACK scaling algorithm. The unit cells were refined by the least squares method. The structure was refined in the SHELX program (Sheldrick, 2015).

The calculation of EGM formula has been performed according recommendations by Johnsen and Grice (1999). The general EGM formula can be written as:

$$N(1)_3N(2)_3N(3)_3N(4)_3N(5)_3M(2)_{3\text{-}6}M(3)M(4)[M(1)_6Z_3(Si_{24}O_{72})]O'_{4\text{-}6}X_2,$$

where $N(1–5)$ = Na, H_3O^+, K, Sr, Ln, Y, Ba, Mn and Ca; $M(1)$ = Ca, Mn, Ln, Na, Sr and Fe; $M(2)$ = Fe, Mn, Na, Zr, Ta, Ti, K, Ba and H_3O^+; $M(3)$ and $M(4)$ = Si, Nb, Ti, W and Na; Z = Zr, Ti, Nb; O' = O, (OH) and H_2O; X = Cl, F, H_2O, OH, CO_3 and SO_4.

According our chemical data, the Zr content linearly decreases with growth of amounts of Nb and Ca+*REE*+Sr+Mn: (Ca+*REE*+Sr+Mn) = 17.38 □ 3.36 × (Zr *apfu*) and Nb = 1.09 □ 0.29 × (Zr *apfu*). In other words, the minimal Zr content 3.1 *apfu* corresponds to maximal Nb content 0.2 *apfu* and vice versa. Similar dependence occurs for Ca+*REE*+Sr+Mn / Zr ratio.

The crystal structures of studied samples have been refined at the $R\bar{3}m$ space group. Refinement at the $R3m$ space group does not lead to reduction of R_1-value. The refinement was based on the model of a 12-layered eudialyte ($c \sim 30$ Å) with $R\bar{3}m$ symmetry (Johnsen and Grice, 1999) supplied with low-occupied H_2O, Cl and OH sites. The site names provided following the recommendations of the current EGM nomenclature (Johnsen et al., 2003).

Like most minerals of the eudialyte group, studied EGMs consists of Si_9O_{27} and Si_3O_9 tetrahedral rings (Figure) that form *T* layers combined by common apices with $Z(1)$ polyhedra (*Z* layers) and $M(1B)$, and $M(2A,B)$ octahedra (*M* layers) into a heteropolyhedral 3*D* framework, where nine-membered rings are centered by $M(4)$ tetrahedra with occupancy $(Si)_{0.25}$. These layers alternate along the *c* axis forming …*ZTMT*... sequence of the 12-layered structure. The cavities and channels of the framework host extra-framework cations and various anion groupings (Osipov et al. 2018). The Cl atoms are located in cavities of the M layer (Fig. 1b), which is composed of six-member rings formed

by M(1B) octahedra centered by Ca and Sr cations. They are combined by common ribs with M(2A)-centered octahedra and occupied by Fe and M(2B)-centered octahedra probabely occupied by Zr. The N(1) sites are split into N(1A) and N(1B); their refined occupancy is $(Na)_{0.75}$ and $(Na)_{0.25}$, respectively.

Table. Refined scattering factors and occupancies for Zr-rich EGM from eudialyte complex.

Site name	Refined scattering factor (e^-)				
Sample	LV-154-0	LV-117-76	LV-117-111	LV-153-1	LV-157-178
M1B	24.67	24.29	23.80	24.56	23.34
M2A	18.88	18.90	18.09	15.60	17.11
M2B	2.40	1.20	1.72	2.40	1.36
M4A	10.75	12.02	10.48	12.78	13.37
M4B	4.90	4.96	5.48	2.59	3.78
N1A	8.25	8.25	8.25	8.25	8.25
N1B	2.75	2.75	2.75	2.75	2.75
N4	13.05	11.67	12.89	12.36	13.48
N5	5.50	5.50	5.50	5.50	7.81
Site name	Refined occupancy				
M1B	$Ca_{0.88}REE_{0.12}$	$Ca_{0.89}REE_{0.11}$	$Ca_{0.90}REE_{0.10}$	$Ca_{0.88}REE_{0.12}$	$Ca_{0.91}REE_{0.09}$
M2A	$Fe_{0.73}$	$Fe_{0.73}$	$Fe_{0.70}$	$Fe_{0.60}$	$Fe_{0.66}$
M2B	$Zr_{0.06}$	$Zr_{0.03}$	$Zr_{0.04}$	$Zr_{0.06}$	$Zr_{0.03}$
M4A	$Nb_{0.20}Ti_{0.12}$	$Nb_{0.26}Ti_{0.06}$	$Nb_{0.18}Ti_{0.14}$	$Nb_{0.30}Ti_{0.02}$	$Nb_{0.33}$
M4B	$Si_{0.35}$	$Si_{0.35}$	$Si_{0.39}$	$Si_{0.19}$	$Si_{0.27}$
N1A	$Na_{0.75}$	$Na_{0.75}$	$Na_{0.75}$	$Na_{0.75}$	$Na_{0.75}$
N1B	$Na_{0.25}$	$Na_{0.25}$	$Na_{0.25}$	$Na_{0.25}$	$Na_{0.25}$
N4	$Na_{0.92}Sr_{0.08}$	$Na_{0.93}Sr_{0.07}$	$Na_{0.95}Sr_{0.05}$	$Na_{0.95}Sr_{0.05}$	$Na_{0.91}Sr_{0.09}$
N5	$Na_{0.50}$	$Na_{0.50}$	$Na_{0.50}$	$Na_{0.50}$	$Na_{0.71}$

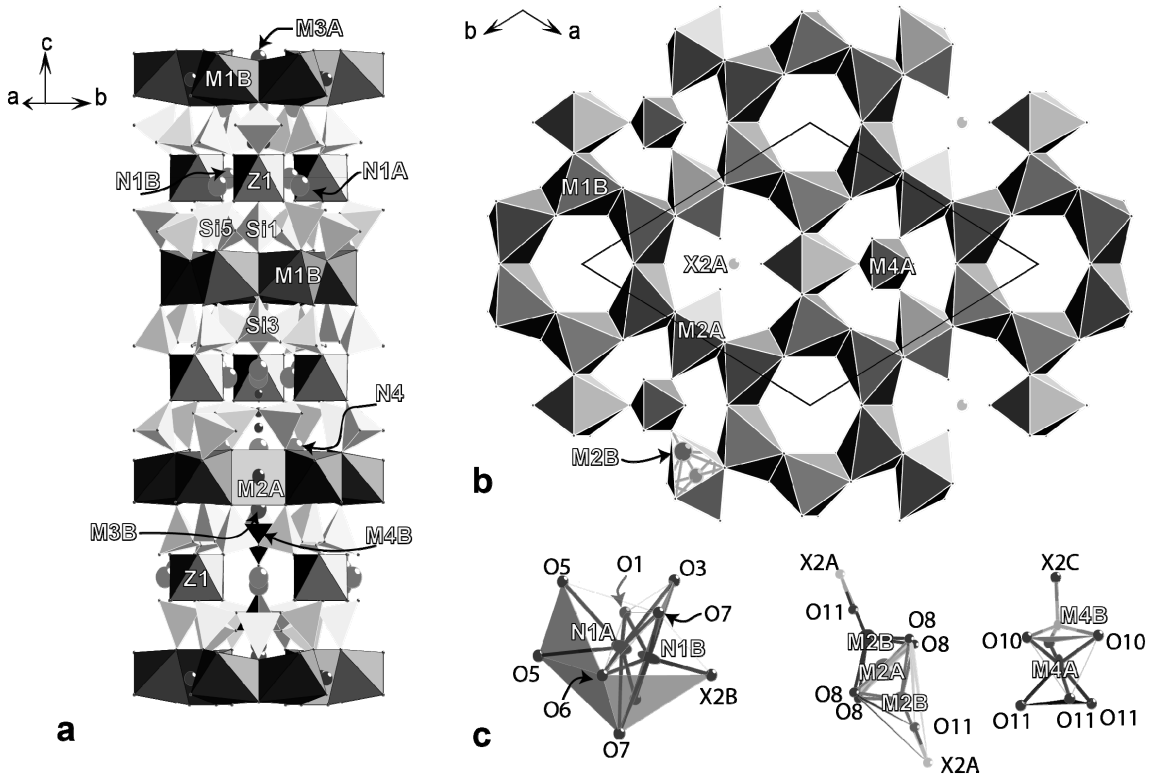

Figure 1. Crystal structure of 154-0 EGM. (a) Fragment of structure along 3-fold axis (positions *X* not shown for simplification); (b) fragment of structure in projection on plane (001); (c) coordination of splitted *M*2A,B; *N*1A,B and *M*4A,B sites.

Three *apfu* of Zr occur in fully populated *Z* sites, whill the location of excess Zr is still unidentified. According to refinement data (Table), scattering factors for *M*1*B* octahedral site remain unchanged with decrease of Ca content and increase of *REE* content, which can be caused by Zr incorporation in namely this site.

The research is supported by the Kola Science Center of Russian Academy of Sciences (0226-2019-0009) and the Russian Foundation for Basic Research (18-29-12039). Experimental studies were carried out using resources of the X-ray Diffraction Centre of Saint-Petersburg State University.

References

Agilent Technologies CrysAlis CCD and CrysAlis RED. Oxford Diffraction Ltd, Yarnton, Oxfordshire, UK, 2014.

Bussen, I.V. and Sakharov, A.S., Petrology of the Lovozero Alkaline Massif, Leningrad: Nauka, 1972, pp. 1-296. (In Russian).

Gerasimovsky, V.I., Volkov, V.P., Kogarko, L.N., Polyakov, A.I., Saprygina, T.V., and Balashov, Yu.A., Geochemistry of Lovozero Alkaline Massif, Leningrad: Nauka, 1966. (In Russian).

Ivanyuk G.Yu., Pakhomovsky Ya.A., Yakovenchuk V.N. Eudialyte-group minerals in rocks of Lovozero layered complex at Mt. Karnasurt and Mt. Kedykvyrpakhk // Geology of Ore Deposits. 2015. V. 57. No. 7. P. 600-613.

Johnsen O, Grice J. D. The crystal chemistry of the eudialyte group. // Canad Miner. 1999. Vol. 37. p. 865□891.

Johnsen O., Ferraris G., Gault R.A., Grice J.D., Kampf A.R., Pekov I.V. The nomenclature of eudialyte-group minerals. // Canad. Mineral. 2003**.** Vol. 41. p. 785□794.

Kalashnikov A.O., Konopleva N.G., Pakhomovsky Ya.A., Ivanyuk G.Yu. Rare Earth Deposits of the Murmansk Region, Russia–A Review // Economic Geology, 2016. V. 111. P. 1529-1559.

Kalinkin, M.M., New data on deep structure and tectonics of the Lovozero alkaline pluton. // In Regional Geology, Metallogeny, and Geophysics, Apatity: Kola Branch, USSR Acad. Sci., 1974, p. 58–66.

Osipov A.A., Antonov A.A., Panikorovskii T.L., Zolotarev A.A. Hydrated CO_3-Bearing Analog of Manganoeudialyte from Alkali Pegmatites of the Konder Pluton, Khabarovsk Krai // Geology of Ore Deposits, 2018, Vol. 60, No. 8, pp. 1–10.

Sheldrick G.M. Crystal structure refinement with SHELXL. Acta Crystallogr C, 2015, Vol. 71 p. 3□8.

MINERAL CRYSTAL CHEMISTRY OF TITANIUM: NEW DATA

Pekov I.V.[1,2], Chukanov N.V.[3], Zubkova N.V.[1], Agakhanov A.A.[4], Sandalov F.D.[1], Britvin S.N.[5], Siidra O.I.[5], Yapaskurt V.O.[1], Varlamov D.A.[6], Turchkova A.G.[1]

[1]Moscow State University, Moscow, Russia, igorpekov@mail.ru

[2]Vernadsky Institute of Geochemistry and Analytical Chemistry of Russian Academy of Sciences, Moscow, Russia

[3]Institute of Problems of Chemical Physics of Russian Academy of Sciences, Chernogolovka, Russia

[4]Fersman Mineralogical Museum of Russian Academy of Sciences, Moscow, Russia

[5]Saint-Petersburg State University, Saint-Petersburg, Russia

[6]Institute of Experimental Mineralogy of Russian Academy of Sciences, Chernogolovka, Russia

Titanium belongs to the most geochemically and petrologically significant elements. It is a species-defining or important admixed component of many accessory and some rock-forming minerals in different magmatic, metamorphic and metasomatic rocks. The mineralogy of titanium is diverse: three hundred valid minerals with species-defining Ti^{4+} are now known. They demonstrate strongly uneven distribution between chemical classes: the overwhelming majority belongs to silicates (*ca*. 190 mineral species) and oxides and hydroxides (*ca*. 90). The crystal chemistry of titanium has been mainly developed for these minerals while only fragmentary data are reported for natural representatives of other chemical classes.

For last several years, we have obtained not too few new data on the mineralogy and mineral crystal chemistry of titanium. The studied minerals belong not only to "traditional" for this chemical element classes of silicates and oxides but also to arsenates and sulfates. In the present paper we give an overview of these data with focus on uncommon crystal chemical features of titanium in these minerals, including such aspects as isomorphous substitutions and cation ordering with participation of this element, character of coordination polyhedra or polyhedral motifs of Ti^{4+}, and the dependence of these characteristics on physical and chemical conditions of formation, in the frame of the elaboration on the genetic aspect of crystal chemistry of titanium.

Alkaline rocks demonstrate the widest diversity of Ti minerals among all geological formations. The family of titanosilicate minerals mainly occurring in agpaitic rocks, their derivatives and related metasomatic rocks is especially interesting in this aspect.

A new zeolite-like titanosilicate kamenevite $K_2TiSi_3O_9 \bullet H_2O$ isostructural with the zirconosilicate umbite $K_2ZrSi_3O_9 \bullet H_2O$ was found in two peralkaline pegmatites in the Khibiny alkaline complex, Kola peninsula, Russia. Kamenevite demonstrates a structural feature quite rare for minerals: it is a titanosilicate with a heteropolyhedral Ti-Si-O framework containing isolated from each other octahedra TiO_6. This structural feature is very common for ZrO_6 octahedra in microporous zirconosilicates with heteropolyhedral Zr-Si-O frameworks, unlike titano- or niobosilicates in which TiO_6 or NbO_6 octahedra usually form condensed motifs, typically chains with shared oxygen vertices, *i.e*., Ti/Nb–O–Ti/Nb bridges (Pyatenko et al., 1999). This explains, *e.g*., the rarity of titanium minerals belonging to the eudialyte, lovozerite, benitoite and hilairite groups in comparison with zirconium members of these groups, in spite of significant prevailing of Ti over Zr in alkaline rocks and in Earth's crust in general. The pair umbite – kamenevite is in a good agreement with this empirical regularity: umbite is a common late-stage mineral in Khibiny whereas kamenevite has been found only in minor amount. Umbite and kamenevite are associated with one another and no solid-solution series between these minerals was found: the highest content of TiO_2 in umbite is 4.9 wt.% that corresponds to 0.24 *apfu* Ti whereas kamenevite contains up to 2.2 wt.% ZrO_2 = 0.07 *apfu* Zr (Pekov et al., 2019b).

A large mica group contains only two minerals with species-defining titanium. They were found in specific peralkaline, silica-oversaturated and lithium enriched rocks of the Darai-Pioz alkaline complex in Tadjikistan. Both these micas, orlovite $KLi_2Ti[Si_4O_{10}]OF$ and gorbunovite $CsLi_2(Ti,Fe)[Si_4O_{10}](F,OH,O)_2$ (Agakhanov et al., 2011, 2017), are trioctahedral and contain in the octahedral layer two univalent cations Li^+ per formula unit that makes possible the incorporation of a highly-valent cation Ti^{4+} in the third octahedron.

An unusual alkali pyroxene strongly enriched by titanium (7.0–7.5 wt.% TiO_2) has been identified by us in cavities within a xenolith of a Si-rich rock embedded in alkaline basalt of the Bellerberg paleovolcano, Eifel region, Germany. Initially it was probably polymictic sandstone which was thermally and chemically metamorphosed by host basalt to the rock mainly consisting of sanidine and tridymite. Average composition of the Ti-rich pyroxene corresponds to the empirical formula $Na_{1.03}(Fe^{3+}_{0.41}Mg_{0.22}Ti_{0.21}Mn_{0.06}Al_{0.06})_{\sum 0.96}Si_{2.04}O_6$. Thus, this is a variety of aegirine containing the $Na(Mg_{0.5}Ti^{4+}_{0.5})Si_2O_6$ component in the amount of *ca*. 42 mol.%.

The series of zirconolite-family minerals was studied by us on samples from alkaline volcanic rocks of the Laacher See paleovolcano in the same Eifel region. Due to very young (Pleistocene) geological age of Eifel volcanic rocks, we have a unique chance to study crystal structures of these minerals which are metamict in the majority of other known localities. The problem of isomorphism and ordering of crystallochemicaly close Ti, Zr, Nb and Fe in complex oxides of this family was studied for three new mineral species, laachite $(Ca,Mn)_2Zr_2Nb_2TiFeO_{14}$, nöggerathite-(Ce) $(Ce,Ca)_2Zr_2(Nb,Ti)(Ti,Nb)_2Fe^{2+}O_{14}$, and stefanweissite $(Ca,REE)_2Zr_2(Nb,Ti)(Ti,Nb)_2Fe^{2+}O_{14}$ (Chukanov et al., 2014, 2018b, 2019) and zirconolite-3*T* (Zubkova et al., 2018). Zirconolite-family minerals are characterized by close packing of cation-centred polyhedra. The cationic isomorphism and cation ordering in the studied minerals, even in sites with mixed occupancies, strongly depend on volume and configuration of a polyhedron. Moreover, there are no isomorphous substitutions between Zr and Ti. The crystal chemical formulae (coordination numbers of cations are indicated with Roman numerals) of the new minerals are:

laachite –
$^{VIII}(Ca_{0.28}Mn_{0.26}Ln_{0.26}Th_{0.14}Y_{0.06})^{VIII}(Ca_{0.32}Mn_{0.28}Ln_{0.24}Th_{0.14}Y_{0.02})^{VII}(Zr_{1.56}Mn_{0.44})^{VI}(Nb_{0.44}Ti_{0.40}Al_{0.16})^{VI}(Nb_{0.82}Ti_{0.18})^{VI}(Ti_{0.72}Nb_{0.28})^{IV}(Fe_{0.68}Mn_{0.20}Y_{0.12})O_{14}$;

nöggerathite-(Ce) –
$^{VIII}(REE_{0.88}Ca_{0.80}Mn_{0.24}Th_{0.08})^{VII}(Zr_{1.88}Mn_{0.12})^{VI}(Nb_{1.22}Ti_{0.78})^{VI}(Ti_{1.48}Nb_{0.48}Al_{0.04})^{IV}(Fe_{0.48}Mn_{0.08})^{V}(Fe_{0.40}Mn_{0.04})_2O_{14}$;

stefanweissite –
$^{VIII}(Ca_{0.544}REE_{0.316}Th_{0.08}Mn_{0.06})_2{}^{VII}(Zr_{0.96}Hf_{0.02}Mn_{0.02})_2{}^{VI}(Nb_{0.73}Ti_{0.27})^{VI}(Ti_{0.78}Nb_{0.21}Al_{0.01})_2{}^{IV}(Fe_{0.22}Mn_{0.03})_2{}^{V}(Fe_{0.21}Mn_{0.04})_2O_{14}$.

For zirconolite-3*T*, the cation distribution is as follows:
$^{VIII}(Ca_{0.70}Ce_{0.30})^{VIII}(Ca_{0.58}Ce_{0.32}Th_{0.10})^{VII}(Zr_{0.88}Th_{0.04}Hf_{0.02}\square_{0.06})_2{}^{VII}(\square_{0.94}Zr_{0.06})_2{}^{VI}(Ti_{0.72}Nb_{0.26}Zr_{0.02})^{VI}(Ti_{0.50}Nb_{0.47}Zr_{0.03})_2{}^{IV}(Fe_{0.355}Mn_{0.145})_2O_{14}$. We found strict ordering of major cations between sites with different coordination numbers: Fe and Mn – 4 or 5, Ti and Nb – 6, Zr – 7 and large cations Ca and *REE* – 8.

New data on minerals containing titanium together with chalcophile elements were obtained. Firstly, there are data concerning oxides in which Ti^{4+} and Sb^{5+} are in isomorphous relationship. They can be formed in different geological environments with the only common feature, high oxygen fugacity and, thus, strong deficiency of S^{2-}.

The specific "ore" metamorphic/metasomatic rocks within the Pelagonian massif near Nežilovo in Republic of Northern Macedonia contain unusually wide diversity of Sb^{5+}-bearing complex oxides with species-defining Ti^{4+}. They belong to the högbomite, crichtonite, and magnetoplumbite groups and the pyrochlore supergroup. Representatives of the pyrochlore structure type demonstrate here the widest variation of the Ti:Sb-ratio and form a continuous solid-solution series including both Ti^{4+}- and Sb^{5+}-dominant minerals (Chukanov et al., 2015, 2018a; Varlamov et al., 2018).

In the rocks of the Pelagonian massif, intermediate members of the rutile – tripuhyite $Fe^{3+}Sb^{5+}O_4$ isomorphous series were also found (Varlamov et al., 2018). The same series extending from almost end-member rutile to tripuhyite with the composition $(Fe_{0.741}Sb_{0.714}Ti_{0.460}Sn_{0.064}Al_{0.017}Cr_{0.004})_{\sum 2.000}O_{3.976}$ was reported from exhalations of active fumaroles of the Tolbachik volcano (Kamchatka, Russia). Besides Sb and Fe, Tolbachik sublimate rutile formed at the temperature above 400°C and atmospheric pressure contains some other chalcophile elements, namely copper, zinc and tin: up to 1.9 wt.% CuO, up to 0.4 wt.% ZnO and up to 11.8 wt.% SnO_2. The major substitution scheme in this solid-solution system is $Sb^{5+} + Fe^{3+} \rightarrow 2Ti^{4+}$ while other schemes

involving chalcophile elements are $Sn^{4+} \rightarrow Ti^{4+}$ and $2Sb^{5+} + M^{2+} \rightarrow 3Ti^{4+}$ (M^{2+} = Cu and Zn) (Sandalov et al., 2018). Sublimate cassiterite from the same fumarole contains up to 6.0 wt.% TiO_2.

However, the main "titanium surprise" became a discovery in Tolbachik fumaroles of a series of high-temperature H-free arsenates with Ti^{4+} including three new minerals in which it is a species-defining component. Such minerals were unknown in nature before. Katiarsite $KTiO(AsO_4)$ (Pekov et al., 2016) is the only natural representative of the KTP [$KTiO(PO_4)$] structure type well-known for numerous synthetic oxysalts including very important materials with non-linear optical properties. Arsenatrotitanite, ideally $NaTiO(AsO_4)$, having the same type of formula as katiarsite, is quite different in terms of crystal structure being belonging to the titanite structure type (Pekov et al., 2019a). Arsenatrotitanite forms a solid-solution series with durangite $NaAlF(AsO_4)$, which contains up to 12 wt.% TiO_2 (Pekov et al., 2018a). In a complicated fluoro-chloro-arsenate lehmannite $Na_{18}Cu_{12}TiO_8(AsO_4)_8FCl_5$ from the same fumarole assemblage Ti^{4+} occurs in eight-fold coordination, in the centre of almost regular cube TiO_8. It is first case of such coordination polyhedron of titanium in minerals (Pekov et al., 2018c). Arsenates are one of two, together with oxides, major forms of titanium concentration in the oxidizing-type Tolbachik fumaroles.

In deposits of active fumaroles at the Mutnovsky volcano at Southern Kamchatka Ti is mainly concentrated in sulfate form, substituting Al in godovikovite $(NH_4)Al(SO_4)_2$ which typically contains here 3–4 wt.% TiO_2.

Supergene mineralogy of titanium is very scarce and is mainly represented by different "leucoxenes", the fine-grained aggregates of Ti oxides (typically anatase or rutile) formed as products of weathering of primary, endogenous Ti minerals and occurring as pseudomorphs after them. Supergene oxysalts of titanium are known from the only locality, Alcaparrosa mine in El Loa province, Northern Chile. There are two sulfates, namely alcaparrosaite $K_3(Ti^{4+}_{0.5}Fe^{3+}_{0.5})_2(SO_4)_4O{\cdot}2H_2O$, in which Ti^{4+} and Fe^{3+} in nearly equal amounts are disordered in an octahedrally coordinated site (Kampf et al., 2012), and calamaite $Na_2TiO(SO_4)_2{\cdot}2H_2O$ (Pekov et al., 2018b). They were formed in the oxidation zone of pyrite-quartz veins under conditions of abnormally arid climate of the Atacama desert. Mafic silicates of andesitic and dacitic host rocks destroyed by abundant sulfuric acid formed as a result of pyrite oxidation were the most probable source of Ti for these minerals. The appearance of titanium sulfates seems a very bright sign of extremely high activity of natural sulfuric acid during the oxidation of pyrite ores at Alcaparrosa where titanium, which is in nature usually almost immobile under low-temperature conditions, shows sufficient activity to form sulfates. Calamaite, demonstrating novel structure type, is the first natural sulfate with a tetravalent cation octahedrally coordinated by O^{2-} but not OH^- anions.

This work was supported by the Russian Foundation for Basic Research, grants 18-29-12007 (studies of titanosilicate and zirconolite-type oxide minerals), 18-05-00051 (studies of Ti oxides with chalcophile elements), and 17-05-00179 (studies of Ti arsenates).

References

Agakhanov A.A., Pautov L.A., Karpenko V.Yu., Bekenova G.K., Uvarova Y.A. Orlovite, $KLi_2TiSi_4O_{11}F$, a new mineral of the mica group // New Data on Minerals. 2011. Vol. 46. P. 13-19.

Agakhanov A.A., Pautov L.A., Pekov I.V., Karpenko V.Y., Siidra O.I., Sokolova E., Hawthorne F.C., Muftakhov V.A., Kasatkin, A.V. Gorbunovite, IMA 2017-040. CNMNC Newsletter No. 39, October 2017, page 1280 // Mineralogical Magazine. 2017. Vol. 81. P. 1279-1286.

Chukanov N.V., Krivovichev S.V., Pakhomova A.S., Pekov I.V., Schäfer C., Vigasina M.F., Van K.V. Laachite, $(Ca,Mn)_2Zr_2Nb_2TiFeO_{14}$, a new zirconolite-related mineral from the Eifel volcanic region, Germany // European Journal of Mineralogy. 2014. Vol. 26. P. 103-111.

Chukanov N.V., Jančev S., Pekov I.V. The association of oxygen-bearing minerals of chalcophile elements in the orogenetic zone related to the “mixed series” complex near Nežilovo, Republic of Macedonia // Macedonian Journal of Chemistry and Chemical Engineering. 2015. Vol. 34. No. 1. P. 115-124.

Chukanov N.V., Krzhizhanovskaya M.G., Jančev S., Pekov I.V., Varlamov D.A., Göttlicher J., Rusakov V.S., Polekhovsky Yu.S., Chervonnyi A.D., Ermolaeva V.N. Zincovelesite-6*N*6*S*,

$Zn_3(Fe^{3+},Mn^{3+},Al,Ti)_8O_{15}(OH)$, a new högbomite-supergroup mineral from Jacupica mountains, Republic of Macedonia // Mineralogy & Petrology. 2018a. Vol. 112. P. 733-742.

Chukanov N.V., Zubkova N.V., Britvin S.N., Pekov I.V., Vigasina M.F., Schäfer C., Ternes B., Schüller W., Polekhovsky Yu.S., Ermolaeva V.N., Pushcharovsky D.Yu. Nöggerathite-(Ce), $(Ce,Ca)_2Zr_2(Nb,Ti)(Ti,Nb)_2Fe^{2+}O_{14}$, a new zirconolite-related mineral from the Eifel volcanic region, Germany // Minerals. 2018b. Vol. 8(10), paper 449. DOI:10.3390/min8100449

Chukanov N.V., Zubkova N.V., Pekov I.V., Vigasina M.F., Polekhovsky Yu.S., Ternes B., Schüller W., Britvin S.N., Pushcharovsky D.Yu. Stefanweissite, $(Ca,REE)_2Zr_2(Nb,Ti)(Ti,Nb)_2Fe^{2+}O_{14}$, a new zirconolite-related mineral from the Eifel paleovolcanic region, Germany // Mineralogical Magazine. 2019. DOI: 10.1180/mgm.2018.171

Kampf A.R., Mills S.J., Housley R.M., Williams P.A., Dini M. Alcaparrosaite, $K_3Ti^{4+}Fe^{3+}(SO_4)_4O(H_2O)_2$, a new hydrophobic Ti^{4+} sulfate from Alcaparrosa, Chile // Mineralogical Magazine. 2012. Vol. 76. P. 851-861.

Pekov I.V., Yapaskurt V.O., Britvin S.N., Zubkova N.V., Vigasina M.F., Sidorov E.G. New arsenate minerals from the Arsenatnaya fumarole, Tolbachik volcano, Kamchatka, Russia. V. Katiarsite, $KTiO(AsO_4)$ // Mineralogical Magazine. 2016. Vol. 80. P. 639-646.

Pekov I.V., Koshlyakova N.N., Zubkova N.V., Lykova I.S., Britvin S.N., Yapaskurt V.O., Agakhanov A.A., Shchipalkina N.V., Turchkova A.G., Sidorov E.G. Fumarolic arsenates – a special type of arsenic mineralization // European Journal of Mineralogy. 2018a. Vol. 30. P. 305-322.

Pekov I.V., Siidra O.I., Chukanov N.V., Yapaskurt V.O., Belakovskiy D.I., Turchkova A.G., Möhn G. Calamaite, a new natural titanium sulfate from the Alcaparrosa mine, Calama, Antofagasta region, Chile // European Journal of Mineralogy. 2018b. Vol. 30. P. 801-809.

Pekov I.V., Britvin S.N., Koshlyakova N.N., Polekhovsky Y.S., Göttlicher J., Vigasina M.F., Turchkova A.G., Sidorov E.G. Lehmannite, IMA 2017-057a. CNMNC Newsletter No. 46, December 2018, page 1185 // European Journal of Mineralogy. 2018c. Vol. 30. P. 1181-1189.

Pekov I.V., Zubkova N.V., Agakhanov A.A., Belakovskiy D.I., Vigasina M.F., Yapaskurt V.O., Sidorov E.G., Britvin S.N., Pushcharovsky D.Y. New arsenate minerals from the Arsenatnaya fumarole, Tolbachik volcano, Kamchatka, Russia. IX. Arsenatrotitanite, $NaTiO(AsO_4)$ // Mineralogical Magazine. 2019a. DOI: 10.1180/mgm.2018.134

Pekov I.V., Zubkova N.V., Yapaskurt V.O., Belakovskiy D.I., Lykova I.S., Britvin S.N., Turchkova A.G., Pushcharovsky D.Yu. Kamenevite, $K_2TiSi_3O_9 \bullet H_2O$, a new mineral with microporous titanosilicate framework from the Khibiny alkaline complex, Kola peninsula, Russia // European Journal of Mineralogy. 2019b. DOI 10.1127/ejm/2019/0031-2825

Pyatenko Yu.A., Kurova T.A., Chernitsova N.M., Pudovkina Z.V., Blinov V.A., Maksimova N.V. (1999): Niobium, Tantalum and Zirconium in Minerals. IMGRE Publishing, Moscow. 213 pp. (in Russian)

Sandalov F.D., Pekov I.V., Koshlyakova N.N., Sidorov E.G. Rutile as a concentrator of antimony in fumarolic exhalations of the Tolbachik volcano (Kamchatka, Russia) // Proceedings of XXXV International Conference "Magmatism of the Earth and related strategic metals deposits". Moscow, GEOKHI RAS, 2018, p. 263-264.

Varlamov D.A., Ermolaeva V.N., Jančev S., Chukanov N.V. Oxides of the pyrochlore supergroup from a nonsulfide endogenic assemblage of Pb–Zn–Sb–As minerals in the Pelagonian massif, Macedonia // Geology of Ore Deposits. 2018. Vol. 60. No. 8. P. 717-725.

Zubkova N.V., Chukanov N.V., Pekov I.V., Ternes B., Schüller W., Ksenofontov D.A., Pushcharovsky D.Yu. The crystal structure of nonmetamict Nb-rich zirconolite-3*T* from the Eifel paleovolcanic region, Germany // Zeitschrift für Kristallographie. 2018. Vol. 233. P. 463-468.

ORIGIN OF HIGH-Ti MEGACRYSTS FROM KIMBERLITES: PETROLOGICAL AND GEOCHEMICAL INVESTIGATIONS OF ORTHOPYROXENE-ILMENITE-GARNET ASSOCIATION IN XENOLITHS FROM THE GRIB KIMBERLITE (ARKHANGELSK, RUSSIA)

Peresetskaya E.V.[1], Kargin A.V.[2], Sazonova L.V.[1], Nosova A.A.[2]

[1]Lomonosov Moscow State University, Moscow, Russia, ekaterina.peresetskaya@gmail.com

[2]Institute of Geology of Ore Deposits, Petrography, Mineralogy, and Geochemistry, Russian Academy of Sciences (IGEM RAS), Moscow, Russia, kargin@igem.ru

Kimberlites, unlike other alkaline ultramafic rocks (ultramafic lamprophyres, carbonatites, lamproites), contain an association of megacryst minerals, such as olivine, clinopyroxene, orthopyroxene, phlogopite, ilmenite, etc (Mitchell, 1995). Initially, the term "megacryst" means large (more than one cm) mineral crystals in kimberlites. However later the term took on the genetic meaning and pointed special genesis of these minerals without distinction of their size (e.g. Moore, Belousova, 2005). Beyond that, megacrysts may form intergrowths with each other and be present in kimberlites as mantle xenoliths (e.g. clinopyroxene-ilmenite, clinopyroxene-phlogopite, garnet-ilmenite and other assemblages).

Megacrysts may be divided into two groups depending on their composition: low- and high-Cr (e.g. Moore, Belousova, 2005). Compositions of these two megacryst groups widely vary and may be overlapped with each other. Commonly low-chromium type is characterized by low Cr_2O_3 content with high FeO and TiO_2 concentrations as opposed to mantle peridotite association. High-Cr megacrysts are characterized by high Cr_2O_3 but low FeO and TiO_2 concentrations, their composition is closed by the mineral association of mantle garnet lherzolites (e.g. Kargin et al., 2017; Bussweiler et al., 2018).

Despite over 45 years of research in kimberlite-hosted megacrysts, their origin and association with kimberlites remain controversial. There are two main models for their origin (see review in Kargin et al., 2017):

(i) Megacrysts result from fractional crystallization of a silicate asthenospheric melt in lower parts of lithospheric mantle. Megacrysts may not be genetically related with kimberlite magmas and trace pre-kimberlite stage of lithospheric mantle evolution;

(ii) Megacrysts are products of crystallisation from protokimberlite melts or products of the interaction these melts with mantle peridotite. This reaction proceeds in the lithospheric mantle at the time when kimberlite magmas generate and then percolate through it (including the generation of deformed peridotite that widely spread in kimberlites as xenoliths). Crystal sizes and degree of metasomatic modifications of the lithospheric mantle may depend on the variation of the melt/lithospheric mantle ratio.

Orthopyroxene megacrysts as distinct from clinopyroxene, garnet and other minerals are rare in kimberlites. Non-peridotitic orthopyroxene closed by megacrysts in a composition may occur within polymict breccia xenoliths formed as a crystallised portion of kimberlite melts (Giuliani et al., 2014) as well as within sheared peridotite xenoliths. In both cases orthopyroxene associates with high-Ti mineral assemblage (garnet, ilmenite, clinopyroxene) which comparable by composition with low-Cr megacrysts.

Therefore, some aspects of megacryst formation remain discussion. They include questions about (i) the megacryst formation in the course of fractional crystallization or mantle metasomatism of garnet peridotites; (ii) the wide variation of their composition; (iii) problems of interrelation with host-kimberlite and protokimberlite melts. Herein, we report the results of mineralogical investigations of high-Ti orthopyroxene-ilmenite-garnet association in mantle xenoliths from kimberlites that could propose the model of the generation of low-Cr and high-Ti megacrysts within kimberlite magmas.

Samples and geological background. The mantle xenolith and megacrysts samples investigated in this study were collected from drill cores (1/1000 and 106) from the Grib kimberlite. We have studied composition (using EPMA and SIMS methods) of orthopyroxene, garnet and ilmenite from

xenoliths of garnet peridotite, orthopyroxene-ilmenite-garnet and garnet-ilmenite intergrowths, as well as megacrysts. Table 1 summarises the petrographic and mineralogical features of the studied samples.

The Grib kimberlite (376 ± 3 Ma, Larionova et al., 2016) is located in the central part of the Arkhangelsk diamond province (Russia) within the Chernoozero kimberlite field. The petrographic and geochemical features are more similar to Group-I kimberlites as opposed to Group-II kimberlites (Kononova et al., 2007). The geological setting, petrography and geochemical characteristics of the Grib kimberlite have been described in detail elsewhere (e.g. Kononova et al., 2007; Larionova et al., 2016 and references therein).

Mineral compositions. *Garnet.* Garnets in association with ilmenite from peridotite xenoliths and orthopyroxene-ilmenite-garnet rock exhibit similar compositions with minor variations (Table 1). Garnets are dominated by pyrope (72–75 mol % pyrope) and characterised by low concentrations of Cr_2O_3 and CaO with high TiO_2 contents (0.77-1.06 wt. %). The Mg# value is 0.80–0.83. The garnets have an heavy rare earth elements (HREE) enriched plateau at 6–10 times chondrite values, with light rare earth elements (LREE) and middle rare earth elements (MREE) rising smoothly to the plateau from 0.02 to 0.1 times chondrite values at La and show strong enrichment in high field strength element relative to rare earth elements (REE) contents. Such garnet composition is typical for many Cr-poor garnet megacrysts from worldwide kimberlites including the Grib kimberlite (Kargin et al., 2017b). Garnet in association with ilmenite from the sheared peridotite xenolith exhibits close to other garnets compositions but differs in elevated concentrations of LREE (Table 1).

Orthopyroxene. Orthopyroxene from the orthopyroxene-ilmenite-garnet xenolith is characterised by lower concentrations of Cr_2O_3 (< 0.3 wt. %), Al_2O_3 (< 0.75 wt. %) and higher contents of TiO_2 (0.15-0.32 wt. %) and CaO (~0.6 wt. %) than orthopyroxene from granular peridotite xenoliths within the Grib kimberlite. This composition overlaps with the composition of Mg# neoblasts from the sheared peridotite xenolith from the Grib kimberlite (sample 106-664, Kargin et al., 2017b) and is close to the composition of orthopyroxene from sheared peridotite xenoliths from the Udachnaya kimberlite, Yakutian province, Russia (Ionov et al., 2010). In general, orthopyroxene from the orthopyroxene-ilmenite-garnet xenolith couple with one from the sheared peridotite xenolith forms a common evolution trend on the binary diagrams. This trend shows intermediate position between orthopyroxene from granular peridotite xenoliths and orthopyroxene from polymict breccias xenoliths from The Bultfontein kimberlite (Giuliani et al., 2014) that could be the product of crystallisation from stalled kimberlite magmas. In general, this evolution suggests increasing of Ti, Ca contents and decreasing of Al, Cr concentrations and Mg# values in orthopyroxene equilibrated with kimberlite magmas.

Ilmenite. All studied ilmenites have high MgO concentrations varied from 12.9 to 15.5 wt. % that characterised them as picroilmenites (Table 1). By Cr_2O_3 concentrations, ilmenites can be separated into the following two groups: (i) ilmenites from the orthopyroxene-ilmenite-garnet xenolith and garnet-ilmenite intergrowths with high Cr_2O_3 contents from 2.9 to 3.3 wt. %; (ii) ilmenites from coarse and sheared garnet peridotite xenoliths with lower Cr_2O_3 concentrations from 1.6 to 2.7 wt. %. Despite the difference in Cr contents, studied ilmenites have similar trace-element abundances. REE patterns are slightly fractionated with enrichment in LREE over HREE and fractionation of LREE that is close to megacryst ilmenite compositions from the Grib kimberlite previously studied by (Golubkova et al., 2013). Studied ilmenites have compositions that are similar to those of ilmenite megacrysts from the Grib kimberlite (Table 1).

Discussion. The compositions of garnet and ilmenite from the orthopyroxene-ilmenite-garnet and peridotite xenoliths are similar to those of garnet and ilmenite megacryst. This could mean that high-Ti and low-Cr orthopyroxene-ilmenite-garnet intergrowths, garnet-ilmenite intergrowths, as well as the garnet-ilmenite association within mantle peridotite xenoliths have a common origin. The petrography of the orthopyroxene-ilmenite-garnet xenolith indicates that these minerals crystallised from a melt. The REE composition of garnet suggested that the equilibrated melt could be kimberlite-like or alkaline ultramafic by composition. According to geobarometer of (Brey, Kohler, 1990) orthopyroxene-ilmenite-garnet association was generated or equilibrated at the pressure from 4 to 5 GPa that is close to estimates of the pressure for garnet megacrysts by (Sablukov et al., 2009).

Table 1. Petrographic and mineralogical features of the studied mantle xenoliths and megacrysts hosted the Grib kimberlite.

Xenolith type	Petrographical features	Mineralogical features
Orthopyroxene-ilmenite-garnet xenolith	The texture of the studied xenolith is heterogranular, porphyroblastic, granoblastic. Garnet occurs as large porphyroblastic grains (up to 1-3 mm in size) in the fine matrix (up to 0.2 mm) of garnet (70 vol.%), ilmenite (20 vol.%) and orthopyroxene (10 vol.%) grains.	*Opx*: Cr_2O_3 0.13-0.26 wt. %; Al_2O_3 0.52-0.63 wt. %; TiO_2 0.15-0.39 wt. %; CaO 0.61-0.68 wt. %, Mg# 0.92. *Grt*: Cr_2O_3 3.3-3.5 wt. %; CaO 4.3-5.0 wt. %; TiO_2 0.9-1.1 wt. %; Mg# 0.81-0.82. *Ilm*: MgO 13.5-15.3 wt. %, Cr_2O_3 2.9-3.6 wt. %.
Garnet-ilmenite intergrowth	The xenolith consists of garnet (70 vol.%) and ilmenite (30 vol.%). Garnet forms an aggregation of isometric grains from 0.3 to 2.5 mm in size. Ilmenite occurs as fine inclusions in garnet grains or as "layers" or "veinlet" with polygranular mosaic texture of ilmenite grains.	*Grt*: Cr_2O_3 2.9-3.4 wt. %; CaO 4.4-4.5 wt. %; TiO_2 0.8-0.9 wt. %; Mg# 0.82-0.83. *Ilm*: MgO 13.1-15.1 wt. %, Cr_2O_3 3.0-3.3 wt. %.
Ilmenite-garnet coarse peridotite	The xenoliths have typical granoblastic and fine- to medium grained textures and consist of garnet – 15-20 vol.%; ilmenite – 15 vol.%; altered by serpentine minerals – 65 vol.%. Ilmenite forms intergrowths with garnet grains as well as occurs as small rounded inclusions in serpentine.	*Grt*: Cr_2O_3 2.0-2.4 wt. %; CaO 4.5-4.7 wt. %; TiO_2 0.8-1.0 wt. %; Mg# 0.82. *Ilm*: MgO 13.1-14.7 wt. %, Cr_2O_3 1.6-2.7 wt. %.
Ilmenite-garnet sheared peridotite	The sheared peridotite shows intense ductile deformations with porphyroclastic, fine-grained mosaic, locally lenticular-banded textures and consists of olivine porphyroclasts (35 vol.%) and neoblasts (35 vol.%), orthopyroxene (10 vol.%) porphyroclasts and neoblasts, clinopyroxene (15 vol.%), garnet (5 %), and accessory (<5 vol.%) ilmenite and titanomagnetite.	*Opx (neoblasts)*: Cr_2O_3 0.10-0.27 wt. %; Al_2O_3 0.44-0.88 wt. %; TiO_2 0.10-0.22 wt. %; CaO 0.55-0.88 wt. %, Mg# 0.90-0.92. *Grt*: Cr_2O_3 2.3-3.9 wt. %; CaO 4.4-5.1 wt. %; TiO_2 0.7-0.9 wt. %; Mg# 0.80-0.82. *Ilm*: MgO 12.9-14.5 wt. %, Cr_2O_3 1.9-2.2 wt. %.
Megacryst suit	Megacrysts of garnet and ilmenite are rounded or ellipsoidal, up to 2-3 cm in size. In many cases, megacrysts show evidence of intense fragmentation and mylonitization.	*Grt*: Cr_2O_3 1.7-3.9 wt. %; CaO 4.4-5.1 wt. %; TiO_2 0.6-1.3 wt. %; Mg# 0.78-0.83. *Ilm*: MgO 13.2-15.6 wt. %, Cr_2O_3 1.3-3.3 wt. %.

Grt – garnet, Ilm – ilmenite, Opx – orthopyroxene.

On the other hand, the composition of orthopyroxene from the orthopyroxene-ilmenite-garnet xenolith overlaps the composition of orthopyroxene from sheared peridotite xenoliths from different kimberlite occurrences including the Grib kimberlite (Table 1). Additionally, the composition of ilmenite from sheared peridotite xenoliths from the Grib kimberlite is similar to that of the ilmenite megacrysts as well as the high-Ti composition of garnet is similar to that of the megacrysts. The previous study of the sheared peridotite xenolith suggests that high-Ti garnet and associated clinopyroxene could be in the geochemical equilibrium with an alkaline ultramafic melt enriched in the carbonate content and close by geochemical features to kimberlite magmas at the pressure of 7-8 GPa

(Kargin et al., 2017b). In this case, the main process of generation of the high-Ti association was the mantle metasomatism.

According to investigating of Cr-rich garnet and clinopyroxene megacrysts from the Lac de Gras kimberlites (Bussweiler et al., 2018), the megacrysts formation may be linked to extensive kimberlite magmatism and accompanying mantle metasomatism preceding the eruption of their host kimberlites whereas the generation of megacrysts may be linked to failed kimberlitic magmas. In this scheme, the Cr-rich megacrysts, as well as clinopyroxene and garnet within mantle peridotite, are formed by progressive interaction of percolating melts with the surrounding depleted mantle (originally harzburgite) (Bussweiler et al., 2018). This model can be applied for origin the studied high-Ti association of garnet, ilmenite and orthopyroxene with one addition that percolative melt was enriched in the Ti content. In this case, the high-Ti association within the sheared peridotite could be formed during the percolation of high-Ti kimberlite-like (or protokimberlite) melts through mantle peridotite at the base of the lithospheric mantle (at the pressure of 7-8 GPa). The continues ascending the kimberlite-like (or protokimberlite) melts provided the generation of garnet and ilmenite megacrysts and their intergrowths as well as the introduction of high-Ti garnet and ilmenite into mantle peridotite. At the depth corresponded with the pressure of 4-5 GPa the kimberlite-like (or protokimberlite) melts were stalled and orthopyroxene-ilmenite-garnet rock was crystallised.

Experimental investigations studying the origin of kimberlite magmas show that the kimberlite melt crystallization under mantle conditions could be accompaniment by a generation of a mineral association that is similar to megacryst association (Shatskiy et al., 2017; Stamm, Schmidt, 2017). In this case, ilmenite may be in equilibrium with orthopyroxene, garnet, olivine and clinopyroxene – i.e. with minerals of lherzolitic association. It is mean that mantle peridotite xenoliths with high-Ti garnet and ilmenite are product of crystallisation of kimberlite magmas and do not represent the original surrounding lithospheric mantle. Additionally, the studied high-Ti association of garnet, ilmenite and orthopyroxene could be formed during an interaction of a kimberlite melt (or related to alkaline ultramafic melts) with the surrounding lithosphere mantle as was shown in the experimental work on the silicate-carbonate melts and peridotite interaction (Gervasoni et al., 2017).

This study was supported by the Russian President Grant for State Support of Young Russian Scientists (project nos. MK-57.2019.5) to E.P. and A.K., and by the Russian Science Foundation (project no. 19-17-00024).

References

Giuliani A., Phillips D., Kamenetsky V.S., et al. Petrogenesis of mantle polymict breccias: Insights into mantle processes coeval with kimberlite magmatism // J. Petrol., 2014, vol. 55, no. 4. pp. 831–858.

Shatskiy A., Litasov K.D., Sharygin I.S. Composition of primary kimberlite melt in a garnet lherzolite mantle source: constraints from melting phase relations in anhydrous Udachnaya-East kimberlite with variable CO_2 content at 6.5GPa // Gondwana Res., 2017, vol. 45, no. February. pp. 208–227.

Brey G.P., Kohler T.P. Geothermobarometry in four phase lherzolites II. - New thermobarometers and practical assessment of existing thermobarometers // J. Petrol., 1990, vol. 31, no. 6. pp. 1353–1378.

Bussweiler Y., Pearson D.G., Stachel T., et al. Cr-rich megacrysts of clinopyroxene and garnet from Lac de Gras kimberlites, Slave Craton, Canada – implications for the origin of clinopyroxene and garnet in cratonic lherzolites // Mineral. Petrol., 2018, vol. 112, no. S2. pp. 583–596.

Gervasoni F., Klemme S., Rohrbach A., et al. Experimental constraints on mantle metasomatism caused by silicate and carbonate melts // Lithos, 2017, vol. 282–283. pp. 173–186.

Golubkova A.B., Nosova A.A., Larionova Y.O. Mg-ilmenite megacrysts from the Arkhangelsk kimberlites, Russia: Genesis and interaction with kimberlite melt and postkimberlite fluid // Geochemistry Int., 2013, vol. 51, no. 5. pp. 353–381.

Ionov D.A., Doucet L.S., Ashchepkov I.V. Composition of the lithospheric mantle in the siberian craton: New constraints from fresh peridotites in the Udachnaya-East Kimberlite // J. Petrol., 2010, vol. 51, no. 11. pp. 2177–2210.

Kargin A.V., Sazonova L.V., Nosova A.A., et al. Cr-rich clinopyroxene megacrysts from the Grib kimberlite, Arkhangelsk province, Russia: Relation to clinopyroxene–phlogopite xenoliths and evidence for mantle metasomatism by kimberlite melts // Lithos, 2017a, vol. 292–293. pp. 34–48.

Kargin A.V., Sazonova L.V., Nosova A.A., et al. Sheared peridotite xenolith from the V. Grib kimberlite pipe, Arkhangelsk Diamond Province, Russia: Texture, composition, and origin // Geosci. Front., 2017b, vol. 8, no. 4. pp. 653–669.

Kononova V.A., Golubeva Y.Y., Bogatikov O.A., et al. Diamond resource potential of kimberlites from the Zimny Bereg field, Arkhangel'sk oblast // Geol. Ore Depos., 2007, vol. 49, no. 6. pp. 421–441.

Larionova Y.O., Sazonova L.V., Lebedeva N.M., et al. Kimberlite Age in the Arkhangelsk Province, Russia: Isotopic Geochronologic Rb-Sr and $^{40}Ar/^{39}Ar$ and Mineralogical Data on Phlogopite // Petrology, 2016, vol. 24, no. 6. pp. 562–593.

Mitchell R.H. Kimberlites, Orangeites, and Related Rocks. Boston, MA: Springer US, 1995. 410 p.

Moore A., Belousova E. Crystallization of Cr-poor and Cr-rich megacryst suites from the host kimberlite magma: Implications for mantle structure and the generation of kimberlite magmas // Contrib. to Mineral. Petrol., 2005, vol. 149, no. 4. pp. 462–481.

Sablukov S.M., Sablukova L.I., Griffin W.L. Distribution of trace elements in deep-situated minerals from kimberlite as indication of plume processes in the North of Russian Platform (In Russian) // Deep-situated magmatizm, its source and plumes. Miass: Institute of Geography SB RAS, 2009. pp. 135–170.

Stamm N., Schmidt M.W. Asthenospheric kimberlites: Volatile contents and bulk compositions at 7 GPa // Earth Planet. Sci. Lett., 2017, vol. 474. pp. 309–321.

ZEOLITES FROM HIGHLY ALKALINE VOLCANIC ROCKS FROM THE REGION OF BOURGAS, SE BULGARIA – NEW DATA

Petrov P.M.[1], Encheva S.M.[1], Kostov V.V.[2], Nikolova R.P.[2], Chukanov N.V.[3], Pekov I.V.[4]

[1]Earth and Man National Museum, Sofia, Bulgaria, petkopet@abv.bg

[2]Institute of Mineralogy and Crystallography, Bulgarian Academy of Sciences, Bulgaria, vkytin@abv.bg

[3]Institute of Problems of Chemical Physics RAS, Chernogolovka, Russia, chukanov@icp.ac.ru

[4]Lomonosov Moscow State University; Faculty of Geology; Russia, igorpekov@mail.ru

Bourgas region belongs to the East Srednogorie tectono-structural zone built of Upper Cretaceous rocks of volcanic, sedimentary, and intrusive origin. The feldspathoid basalts, trachybasalts and trachytes from this region are the most potassium-enriched alkaline volcanic rocks in Bulgaria. Subareal volcano-intrusive structures of central type are common to the area south of Bourgas, related to witch are several deposits of the VHMS type. Many impulsive linear type subaquatic volcanoes, formed in the conditions of intraarch riftogenesis, are common to the area north of Bourgas. The pillow lavas are widespread there. The Earth crust is only 27 – 29 km deep which is the minimum for Bulgaria (Stanisheva-Vassileva, 1982).

There are a lot of zeolite localities in the area. The first data about zeolites of the Bourgas region is given by Kostov (1960, 1962) and Kostov *et al*. (1959, 1968). Eleven zeolites have been described there: analcime, natrolite, gonnardite, mesolite, scolecite, thomsonite, laumontite, heulandite, stilbite, chabazite, and levyne (?). In these publications there are no chemical data on natrolite. Such data are also missing for natrolite from other Bulgarian localities. The only chemical analysis of natrolite from the Banevo quarry, Bourgas, is given by Alberti *et al*. (1982b). Kostov (1970) considers the lack of mordenite in the Eastern part of Srednogorie as a significant difference in the zeolite mineralization of this area from that of Western and Central parts of Srednogorie.

This paper presents new data on analcime, natrolite, thomsonite, gonnardite and laumontite from the Banevo quarry and reports the first data on mordenite from the village of Izvor, Bourgas municipality.

The Banevo quarry is the locality with the most abundant natrolite mineralisation in Bulgaria. This mineral is represented by two morphological types. The first type includes zonally banded spherulites up to 1.5 – 2 cm filling cracks while the second type is represented by radiated and random aggregates of prismatic to needle shaped crystals usually formed on analcime in open cavities.

The core of a spherulite consists of a hair-like aggregate. The intermediate zone is composed of acicular crystals, while the periphery is built up with radial prismatic crystals. None of the zones is homogenous. Electron microprobe analyses (Table 1), IR spectroscopy and powder X-ray diffraction revealed a change in the composition: the core consists of natrolite with some thomsonite whereas the intermediate zone is composed of thomsonite with minor natrolite, and periphery consists of natrolite with minor thomsonite (Fig. 1 c). Zonal crystals are very common. In the central and intermediate parts of the aggregates, natrolite I crystals are epitaxially overgrown by thomsonite, while for the rim zone the core consists of thomsonite, epitaxially overgrown by natrolite II (Fig. 1 a, b).

Rare gonnardite veinlets have been found in the inner and intermediate zones.

Single-crystal X-ray diffraction (XRD) of natrolite from Banevo (prismatic crystal on analcime) reveals *Fdd2* (43) space group with a = 18.6148(7) Å, b = 18.3061(8) Å, c = 6.5864(3) Å; □=β=γ=90°, V = 2244.41(16)Å^3.

Analcime forms xenomorphic aggregates with white, yellow, pink to reddish colour building peripheral parts of the veins or amygdales. Occasionally, it forms crusts of white crystals up to 1 cm in cavities. Analcime from Banevo shows strong optical anisotropy in plane polarized light. It is quite often to have a simultaneous growth with natrolite I. The latter continues to grow after the analcime crystallization completion. Chemical composition of analcime is quite typical for this mineral (Table 1).

Table 1. Average chemical composition of zeolites (in *apfu*) from Banevo (natrolite, thomsonite, gonnardite, analcime, laumontite), and Izvor (mordenite, heulandite, and chabazite).

	Natrolite	Thomsonite	Gonnardite	Analcime	Laumontite	Mordenite	Heulandite-Ca	Chabazite-Ca
Si	2.95	5.14	5.90	2.04	3.94	10.14	14.16	8.99
Al	2.05	4.86	4.10	0.96	2.06	1.86	3.84	3.01
Ca	0.03	1.64	0.89		0.63	0.81	1.67	2.09
Mg								0.05
Na	1.96	1.04	2.07	0.94	0.15	0.14	0.13	
K					0.01	0.08	0.24	0.07

Note: Formula calculations are based on $(Si,Al)_5$ for natrolite, $(Si,Al)_{10}$ for thomsonite and gonnardite, $(Si,Al)_3$ for analcime, $(Si,Al)_6$ for laumontite, $(Si,Al)_{12}$ for mordenite, $(Si,Al)_{18}$ for heulandite and chabazite.

Powder X-ray diffraction data show that yellowish analcime is tetragonal [a = 13.672(4), c = 13.743(4) Å; V = 2569(2) Å^3] and white analcime is cubic [a = 13.7018(13) Å; V = 2577.4(4) Å^3]. Infrared spectra confirm this conclusion: distinct doublet 736+767 cm^{-1} is a specific feature of cubic analcime, whereas in low-symmetry analcimes the high-frequence component of this doublet degenerates into a shoulder (Fig. 1 d). It is remarkable that tetragonal analcime from the Lovozero alkaline massif is also yellow. One can suppose that trace amounts of $^{[4]}Fe^{3+}$ substituting $^{[4]}Al$ may be the cause of both yellow colour (compare *e.g.* tetraferriphlogopite, Fe-bearing cancrinite and reedmergnerite) and symmetry lowering.

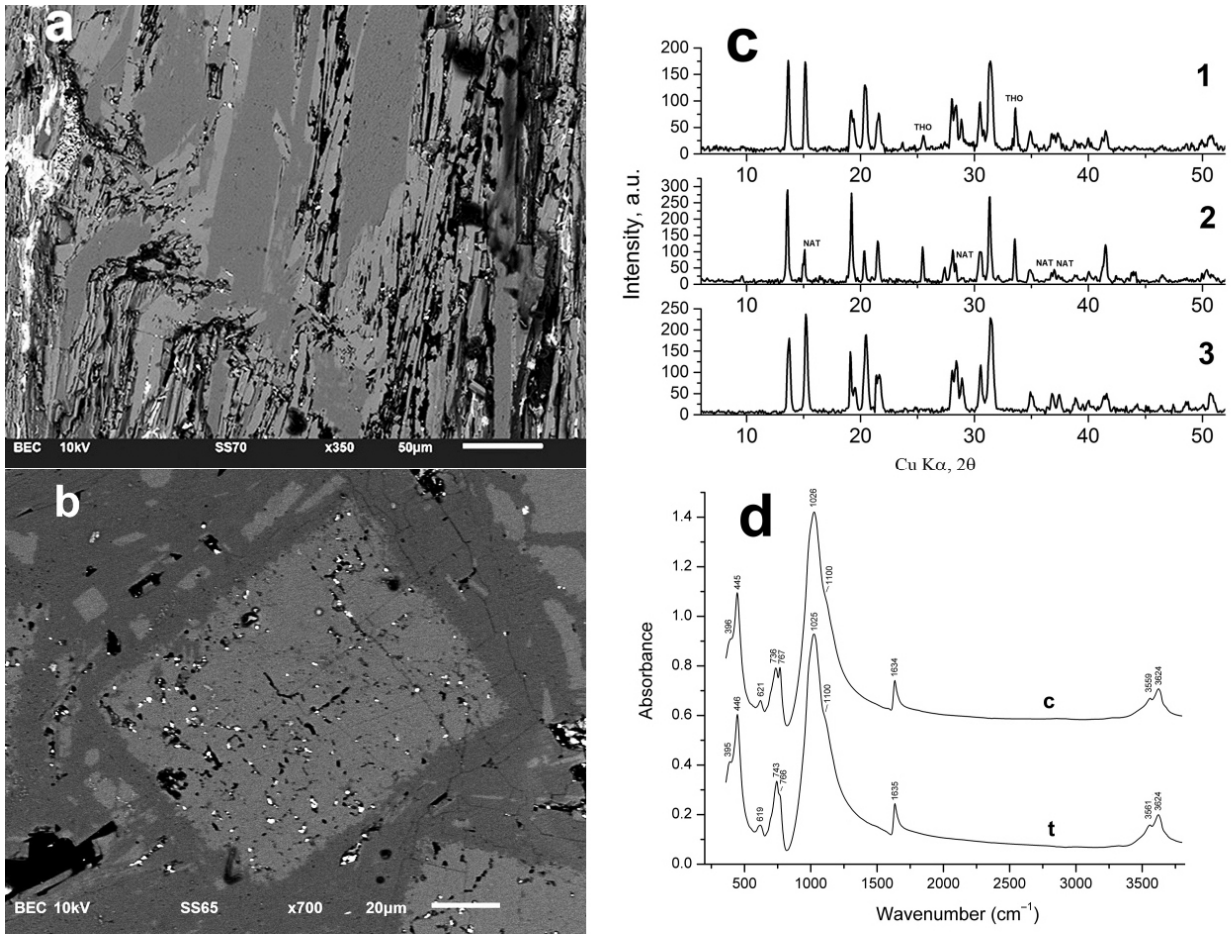

Fig. 1. SEM-BSE images: a) natrolite core and thomsonite rim in the intermediate zone of spherulites; b) thomsonite core and natrolite rim in the periphery of spherulites (view perpendicular to the elongation); dark grey – natrolite, light grey – thomsonite. c) X-Ray powder diffraction patterns of the thomsonite-natrolite aggregates – 1 core, 2 – intermediate zone and 3 periphery. d) IR spectra of cubic (c) and tetragonal (t) analcime from Banevo.

As a rule, laumontite forms monomineral veins built up with small prismatic fragile crystals. Sometimes it fills central parts of the fibrous zeolites veins. Laumontite is formed after fibrous zeolites and together or just before calcite which is the latest mineral in this paragenesis. Laumontite has a quite usual composition (Table 1). According to the single crystal XRD laumontite crystallizes in the *I*2/*m* (12) space group with a = 7.5563(3) Å, b = 13.0707(5) Å, c = 13.7974(7) Å; β = 98.497(4)°; V = 878.2(2) Å^3.

Mordenite from the village of Izvor forms coarse spherulites with a radius of 3 – 4 cm. The spherulites are well preserved due to the formation of intimate intergrowths with quartz. Mordenite is associated with earlier formed albite, epidote, pumpellyite, prehnite, native copper, and analcime. This is a calcium-rich mordenite with the maximum Na content of 0.18 apfu [for the formula with $(Si,Al)_{12}$] and typical Ca/Na ratio around 4:1. After mordenite, heulandite-Ca and chabazite-Ca (phacolith) with K dominating over Na crystallized (Table 1). The host rocks for this locality are alkaline basaltiods.

Single-crystal XRD pattern of mordenite from the Izvor locality reveals *Cmcm* (63) space group with a = 18.135(3) Å, b = 20.463(3) Å, c = 7.5225(10) Å, V = 2791.5(7) Å^3. Both the chemical analysis and the structure refinement data showed a high Ca content among the extraframework cations. Based on the structural determinations, a structural model is proposed with an extraframework site populated by Ca with the occupancy of 0.59. Careful checking in the available structural data bases has revealed that such-like pure position can be found in calcium-exchanged mordenites and in only one case of untreated natural samples – that one of diagenetic mordenite from Ponza, Italy (158009-ICSD, Passaglia et al. 1989).

General sequence of crystallization of minerals at the Banevo locality is as follows: calcite, Na => Na-Ca => Ca-Na => Na => Ca zeolites, calcite. In this direction the framework density (FD, number of framework atoms Si and Al per 1000 Å^3) decreases as follows: analcime 18.5 => natrolite I 17.8 => thomsonite 17.6 => gonnardite 17.3 => natrolite II 17,8 => laumontite 17.4 (Pekov *et al*., 2004). These regularities are also in agreement with general trends for alkaline pegmatites: maximum of Na activity at intermediate stages and increase of Ca activity right up to the latest hydrothermal stage (Khomyakov, 1995; Lovskaya *et al*., 2002; Moiseev, Chukanov, 2006).

Zeolite mineralization in Banevo was formed in a practically closed system in conditions of low P / low T metamorphic alterations of high-alkaline and low-silica volcanic rocks at gradual decrease of temperature as a general trend.

The rule for the FD decrease in the process of evolution of the mineral formation applies for zeolites from the Izvor locality too: analcime 18.5 => mordenite 17.2 => heulandite-Ca 17.1 => chabazite-Ca 14.5.

Zeolite mineralization near the village of Izvor was formed under higher temperature (prehnite-pumpellyite facies) in an open system (Si input) in an area with hydrothermal copper mineralization.

These results have been obtained in frames of the joint project DNTS/Russia № 02/8-15.06 2018 and Russian Foundation for Basic Research No. 18-55-18003 "Crystal chemistry and properties of natural zeolites and related silicates with microporous structures".

References

Alberti A, Pongiluppi D., Vezzalini, G. The cryslal chemistry of natrolite, mesolite and scolecite.//N. Jb. Miner. Abh. 1982b, 143.3, pp. 231-248.

Khomyakov A.P. Mineralogy of Hyperagpaitic Alkaline Rocks. Clarendon Press, Oxford, UK, 1995.

Kostov I. The zeolites in Bulgaria: scolecite, mesolite, natrolite, "gonnardite," and thomsonite// Ann. De L'Universite de Sofia. 1960.V 53. pp. 1-24 (in Bulgarian).

Kostov I. The zeolites in Bulgaria: analcime, chabasite, harmotome// Ann. De L'Universite de Sofia. 1962. V 55, pp. 159-174 (in Bulgarian with an English summary).

Kostov I. Tectono-magmalic significance of zeolites in the Srednogorian zone and The Rhodopes// Geochem., Mineral. and Petrol. 1970. V 19. pp. 235-241.

Kostov I., Filisova. The zeolites in Bulgaria: laumontite// Ann. De L'Universite de Sofia. 1959. V 52, pp. 159-186 (in Bulgarian).

Kostov I., Mavrudchiev B., Botev S. Zeolite mineralizations in the Eastern Srednogoriye// Geochem., Mineral. and Petrol. 1968. V 17. pp. 83-110 (in Bulgarian with a Russian and an English summary).

Lovskaya E.V., Pekov I.V., Kononkova N.N., Turchkova A.G. Mineralogy, geochemistry and genesis of high-calcium hydrothermalites of the Khibiny massif, Kola Peninsula // Zapiski Vses. Mineral. Obshch. 2002. V 131(2). pp 17-29.

Moiseev M.M., Chukanov N.V. Mineralogy of alkaline pegmatites and hydrothermalites of the Kovdor massif // New Data on Minerals. 2006. V 41. pp. 56-70.

Pekov I.V., Turchkova A.G., Lovskaya E.V., Chukanov, H.V. Zeolites of alkaline massifs. // M., Assoc. "Ecost", 2004. 168 p. (in Russian).

Stanisheva-Vassileva G. Zeolites in alkaline volcanic rocks to the north of Bourgas (villages of Banevo, Rudnik, etc.)// In: Excursion Guide 1 East Srednogorie, XIII Congress of IMA, Varna, Bulgaria. 1982. pp 32-43 (in Russian).

THE DEVELOPMENT OF PEROVSKITE MINERALISATION IN THE ULTRAMAFIC ROCKS OF THE AFRIKANDA COMPLEX: IMPLICATIONS FOR CHROMITE AND MAGNETITE MONOMINERALIC DEPOSITS

Potter N.J.[1], Kamenetsky V.S.[1,2]

[1]University of Tasmania, Tasmania, Australia, pottern@utas.edu.au

[2]Institute of Experimental Mineralogy RAS, Chernogolovka 142432, Russia

dima.kamenetsky@utas.edu.au

The Afrikanda alkaline-ultramafic complex is one of the smallest intrusions in the Devonian Kola Alkaline Province (KAP). The KAP in NW Russia and eastern Finland is one of the largest carbonatite provinces in the world and hosts more than twenty plutonic and subvolcanic bodies, including alkaline, ultramafic, carbonatite, and melilitolite suites (Kukharenko et al., 1965). Many of these complexes host ore deposits, with active mines at Kovdor (apatite-magnetite ore), Lovozero (loparite-ore) and Khibiny (nepheline-apatite ore).

The Afrikanda complex was emplaced at ~380 Ma with other alkaline-ultramafic complexes, including Kovdor, Turiy Mys, Lesnaya Varaka and Ozernaya Varaka (Arzamastsev and Wu, 2014; Potter et al., 2018). The concentric internal structure hosts texturally and modally diverse olivinites and clinopyroxenites, cross-cut by minor intrusions of carbonatitic and feldspathoidal rocks (Chakhmouradian and Zaitsev, 2004). Afrikanda is largely assumed to be a magmatic complex, with the intrusive ultramafic rocks derived by partial melting of a metasomatised lithospheric source to produce a Ca-rich melanephelinitic magma (Chakhmouradian and Zaitsev, 2004). The ultramafic rocks in the Afrikanda complex host large stock-like bodies of perovskite-titanomagnetite ores enriched in rare earth elements (Yudin and Zak, 1971). The ore contains 15-35 vol.% Ti-rich magnetite and 10-36 vol.% perovskite, with wide variations in the abundance of silicate and carbonate minerals reflecting the extreme petrographic heterogeneity of the deposit. The measured reserves, delineated to a depth of 300 m, include 34.3 Mt of ore averaging 12.5 wt.% Fe and 8.3 wt.% TiO_2 (Afanasyev, 2011).

For decades, oxide minerals, such as chromite and magnetite, have been the focus of academic studies, yet there remain many unknowns about the processes involved in their accumulation and transition into economic deposits. Deposits of oxide minerals, such as perovskite, have received little attention from the academic community due to their rarity in nature. The Afrikanda alkaline-ultramafic complex along with Powderhorn, USA and Tapira, Brazil are the only known titanium deposits where the primary titanium-bearing mineral is perovskite (Armbrustmacher, 1981; Brod et al., 2013; Yudin and Zak, 1971). All three are alkaline-carbonatite complexes hosting pyroxenites that contain perovskite-rich segregations and dikes. The rarity of perovskite ore deposits has prevented an understanding of their genesis and mineral enrichment mechanisms.

This study of perovskite and perovskite-hosted inclusions at the Afrikanda alkaline-ultramafic complex targets the understanding of mechanisms responsible for the development of massive ore textures. We identified three key perovskite textural types throughout the perovskite-rich segregations in the ultramafic olivinites and clinopyroxenites at Afrikanda. The mineralogical complexity of the perovskite-hosted inclusions and the textural transition of the perovskite grains enabled the stages of perovskite development to be determined, with the possibility of similar processes operating in other oxide deposits worldwide.

Perovskite-rich samples of olivinites and clinopyroxenites were mounted in epoxy and dry polished with 800 μm grit paper to 1 μm oil-based diamond compound and cleaned with petroleum-based solvent (shellite). All grinding and polishing was carried out using kerosene as a lubricant to avoid damage to the water-soluble contents of inclusions. Coarse-grained polishing paper was also avoided as the contrast in hardness between silicates and carbonates in the inclusions can result in the loss of the softer carbonates. All instruments used for the examination of perovskite and their hosted inclusions are located at the University of Tasmania, Australia. Samples were analysed with a Hitachi SU-70 field emission scanning electron microscope (SEM) fitted with an Oxford AZtec Xmax80 energy dispersive X-ray spectrometry (EDS) system. High-resolution backscattered electron (BSE)

images and EDS were used for element maps and semi-quantitative compositions of minerals and inclusions.

A clinopyroxenite sample that hosts perovskite grains with abundant inclusions was crushed and grains (0.3-0.5 mm) were wrapped in platinum foil (0.5 mm thick) with a piece of graphite. Three different batches of perovskite grains were heated to 800°C, 900°C and 1000°C, respectively, at 1 atmosphere for 10 minutes, then quenched in water. To reduce the risk of overheating and excessive incorporation of the perovskite host, a maximum temperature of 1000^{o}C was chosen to observe the sequence of phase transformations in inclusions (Nielsen et al., 1997). The grains were then mounted and polished with the same technique as previously stated.

The examined melilite-bearing olivinites are fine- to medium-grained, inequigranular rocks composed of forsterite, åkermanite, perovskite and magnetite cut by calcite and wollastonite veinlets. The interconnected networks and clusters of smaller euhedral perovskite grains enclose and distort the anhedral åkermanite, forsterite and magnetite grains generating intergrown, irregular and concave shapes (Fig. 1a). The examined clinopyroxenites are fine- to medium-grained, inequigranular rocks mainly composed of clinopyroxene, perovskite and magnetite with minor calcite, richterite, phlogopite, magnesiohastingsite, titanite, chlorite and various REE minerals. Perovskite revealed a range in grain sizes (0.05-2 mm), shapes (rounded to irregular) and zonation (homogeneous to complexly zoned), and varied from chains of euhedral crystals to large areas of interlocking grains.

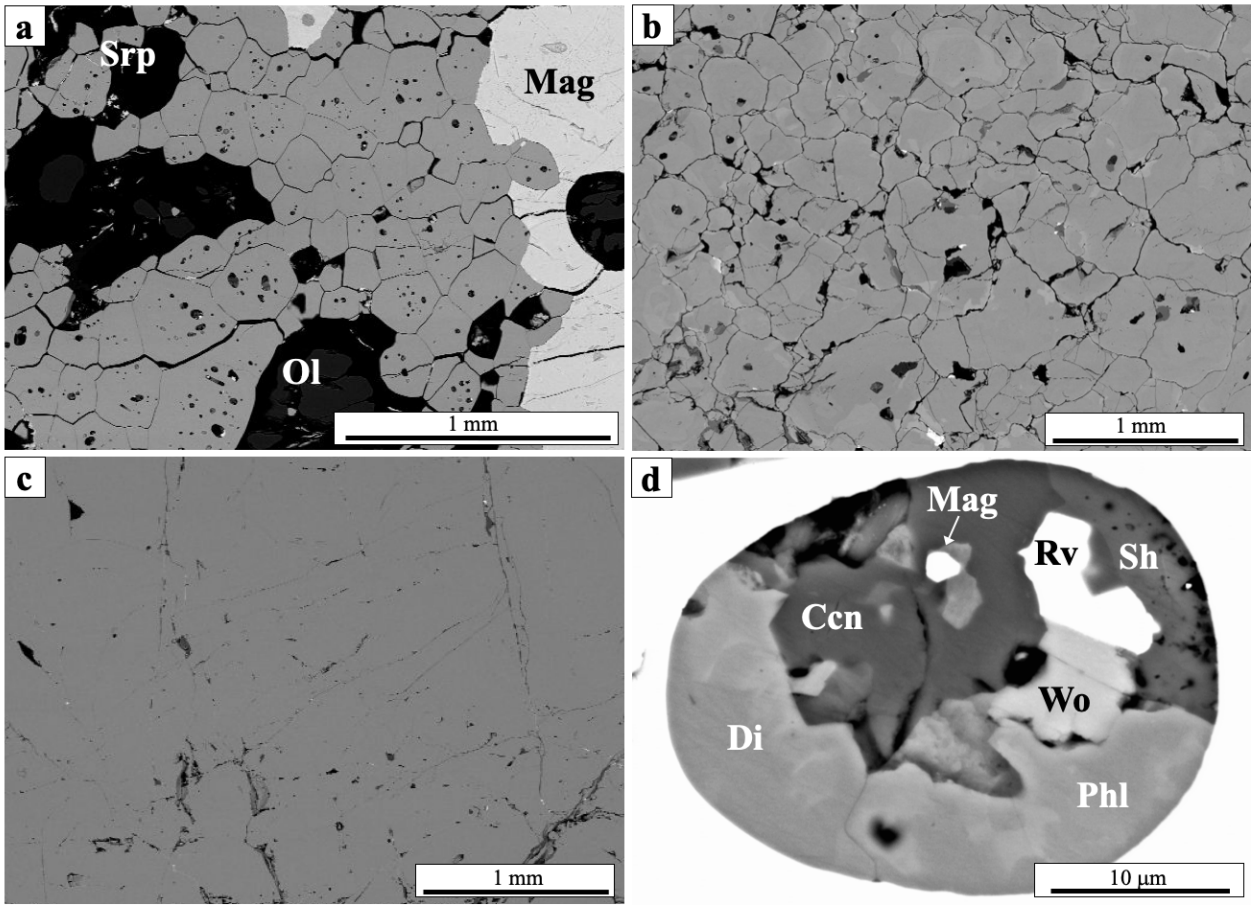

Figure 1. Representative backscattered images of perovskite textures defined by their morphology, composition, zoning patterns and abundance of inclusions, (a) type 1, (b) type 2, (c) type 3, (d) EDS X-ray compositional maps showing the texture and mineral components of a representative perovskite-hosted polymineralic inclusion. Abbreviations: Cancrinite (Ccn), Diopside (Di), Magnetite (Mag), Olivine (Ol), Phlogopite (Phl), Rasvumite (Rv), Shortite (Sh), Serpentine (Srp) and Wollastonite (Wo).

The textural examination of perovskite enabled the identification of three distinct perovskite textures in the ultramafic rocks at Afrikanda (Fig. 1a-c). These types are defined by their morphology, composition, zoning patterns and abundance of polymineralic inclusions. Textural type one (T1) perovskite is characterised by interconnected polygonal crystal clusters and networks. The euhedral pseudo-octahedral perovskite grains (50-550 μm) have straight boundaries with widespread 120° triple-junctions (Fig. 1a). Abundant randomly distributed inclusions are clustered in the cores of the perovskite with an inclusion-free rim. Type one is observed in olivinites and clinopyroxenites, while type two (T2) and type three (T3) are only identified in the clinopyroxenites. Textural type 2 is represented by an intricate mosaic of interlocking anhedral grains (0.1-1 mm), zoning is prominent in the grains and can be highly complex (Fig. 1b). Polymineralic inclusions are less abundant than in T1. Textural type three (T3) is represented by massive perovskite with patches of irregular zoning and rare polymineralic inclusions (Fig. 1c). The intensity of the zoning varies across the samples, some areas are almost homogeneous and others exhibit complex patterns due to extreme variations in Na, LREE and Nb contents.

The perovskite-hosted polymineralic inclusions have rounded, elongated and irregular shapes, and range from <5 μm to 50 μm in diameter. The inclusions are all identified as primary based on their random distribution within the grains and the lack of association with secondary features (e.g. healed fractures). The inclusions typically contain three to ten mineral phases and include anhydrous and water-bearing silicates, carbonates, oxides, sulphides and phosphates (Table 1; Fig. 1d). The mineral assemblages within these inclusions demonstrate a co-existence of minerals that are typically magmatic with those that are typically metamorphic or hydrothermal. The inclusions contain voids (up to 20% of the surface) that may have contained soluble phases, fluids or gases, that were lost when the inclusions were exposed.

We observe an overall increase in the prevalence of carbonate minerals in the inclusions from olivinites to clinopyroxenites and a transition in the chemistry of the dominant carbonate mineral with nyerereite more abundant in inclusions in olivinites and shortite and calcite more abundant in inclusions in clinopyroxenites (Table 1). This supports the transition from silicate- to carbonate-dominated and sodium- to calcium-dominated compositions.

Table 1. Abundance of dominant minerals in fifty representative perovskite-hosted polymineralic inclusions. Abbreviations: olivinites (Olvt) and clinopyroxenites (Cpxt).

Silicates	**Olvt**	**Cpxt**	**Hydrous silicates**	**Olvt**	**Cpxt**
Aegirine-augite	6	10	Cancrinite	18	38
Andradite	4	2	Clinochlore	8	10
Diopside	28	8	Cuspidine	28	14
Gittinsite	2	2	Magnesiohastingsite	10	4
Åkermanite	10	0	Pectolite	36	36
Nepheline	18	2	Phlogopite	56	54
Olivine	18	6	**Sulfides**		
Sodalite	24	16	Chalcopyrite	4	0
Titanite	4	34	Pyrrhotite	0	6
Wollastonite	18	2	Rasvumite	4	0
Carbonates			**Phosphates**		
Burbankite	4	6	Hydroxylapatite	8	4
Calcite	16	14	Fluorapatite	20	18
Nyerereite	36	14	**Oxides**		
Shortite	22	14	Magnetite	36	14

The heating of the inclusions in a clinopyroxenite sample up to 1000°C has shown that inclusions do not homogenize at this temperature. The post-heating examination of uncompromised (unfractured and unleaked) inclusions revealed the presence of bubble-free inclusions composed of a

variety of minerals. At this temperature we observed the preservation, melting and chemical alteration of all encapsulated minerals, along with the formation of new phases, with minerals such as halite, magnesioferrite and Ti-rich garnet identified in the heated inclusions, but not in the unheated inclusions. Therefore, these inclusions are composed of a mixture of co-trapped minerals and liquidus phase.

Similar textural features are observed in several chromite deposits e.g. the Oman ophiolite belt, Fiskenaesset and Bushveld. In these complexes, interconnected chains of small euhedral chromite grains with plenty of inclusions resemble networks of T1 perovskite and larger anhedral and massive oxides with few inclusions are reminiscent of T2 and T3 perovskite (Christiansen, 1985; Yudovskaya and Kinnaird, 2010). Chains of connected crystals with granoblastic-polygonal textures are also observed in disseminated magnetite ore from the Panzhihua layered mafic intrusion, China (Howarth et al., 2013). Polymineralic inclusions in chromitite complexes, such as the Oman ophiolite, Western Laouni intrusion, Bushveld and Troodos Complexes, have similar features to the perovskite-hosted inclusions in the Afrikanda complex, such as primary texture, polymineralic assemblage and compositional disparities with the surrounding matrix (Borisova et al., 2012; Lorand and Cottin, 1987; McElduff and Stumpfl, 1991; Yudovskaya and Kinnaird, 2010). The transition from inclusion-rich euhedral oxide grains to inclusion-poor anhedral oxide grains in some of these complexes has been associate with non-magmatic processes such as recrystallization, high-temperature mitigation, post-cumulus growth and contact metamorphism (Butcher and Merkle, 1987; Christiansen, 1985; Yudovskaya and Kinnaird, 2010). We suggest that a similar mechanism is responsible for the textural evolution of perovskite in the Afrikanda ultramafic rocks.

From the mineralogical and textural examination of perovskite and the hosted polymineralic inclusions, we suggest a model for the origin of the polymineralic perovskite-hosted inclusions and the development of the perovskite-rich zones in the ultramafic rocks at Afrikanda. The observed textural and mineralogical features of the polymineralic inclusions question the conventional magmatic model commonly propositioned for the formation of melt inclusions. We propose the polymineralic inclusions in perovskite formed by trapping the surrounding material between perovskite grains during an extended period of post-magmatic activity at subsolidus temperatures. This process involves small, randomly orientated magmatic grains accumulating together and developing into larger inclusion-rich aggregates. A similar process has previously been suggested for the formation of entrapment of inclusions in chromite from chromitite deposits (Hulbert and Von Gruenewaldt 1985). These inclusion-rich grains then re-orientate and form pseudo-octahedral shapes with straight boundaries that cluster together to resemble T1 perovskite (Fig. 1a). The extended period of post-magmatic activity enabled the continuation of the sintering and recrystallization, which results in the transformation of the early-formed euhedral inclusion-rich T1 crystals into coarse-grained zones of inclusion-poor T2 and T3 perovskite (Potter et al., 2018). This grain coarsening process results in the removal of physical impurities, such as inclusions, as adjacent crystals adopt similar crystallographic orientations. The trapping of the surrounding material into the perovskite grains and the subsequent transition from T1 to T3 perovskite did not necessarily occur *in situ*, and may have involved perovskite movement during the post-magmatic accumulation and development of perovskite-rich zones. The textural similarities between perovskite from ultramafic rocks at Afrikanda and monomineralic oxide layers at various igneous complexes indicates that the post-magmatic processes applied to Afrikanda, such as recrystallization, sintering and grain growth, could be applied to polymineralic inclusions in oxide minerals and may have facilitated the development of monomineralic layers in oxide ore deposits.

The authors would like acknowledge Anton Chakhmouradian, Victor Sharygin, Maya Kamenetsky and Karsten Goemann for their contribution to publications associated with this research and for their continued assistance and encouragement. We thank the Geological Institute (the Kola Science Center of the Russian Academy of Sciences) in Apatity for donating Afrikanda samples for our study. Financial support was provided by the Australian Research Council (Discovery grant DP130100257, 2013-2015), University of Tasmania (New Star Professorship, 2010-2014) and Russian Science Foundation (grant #16-17-10145) to V. Kamenetsky.

References

Afanasyev, B.V. Mineral resources of the alkaline–ultramafic massifs of the Kola Peninsula // Roza Vetrov, St. Petersburg. 2011. pp 224 (in Russian)

Armbrustmacher T. J. The Complex of Alkaline Rocks at Iron Hill, Powderhorn district, Gunnison County, Colorado // New Mexico Geological Society, 1981. p. 293-296.

Arzamastsev A., Wu F.-Y. U-Pb geochronology and Sr-Nd isotopic systematics of minerals from the ultrabasic-alkaline massifs of the Kola province // Petrology, 2014. Vol. 22. p. 462-479.

Borisova A. Y., Ceuleneer G., Kamenetsky V. S., Arai S., Béjina F., Abily B., Bindeman I. N., Polvé M., De Parseval P., Aigouy T. A new view on the petrogenesis of the Oman ophiolite chromitites from microanalyses of chromite-hosted inclusions // Journal of Petrology, 2012. Vol. 53. p. 2411-2440.

Brod J. A., Junqueira-Brod T. C., Gaspar J. C., Petrinovic I. A., de Castro Valente S., Corval A. Decoupling of paired elements, crossover REE patterns, and mirrored spider diagrams: Fingerprinting liquid immiscibility in the Tapira alkaline–carbonatite complex, SE Brazil // Journal of South American Earth Sciences, 2013. Vol. 41. p. 41-56.

Butcher A. R., Merkle R. K. Postcumulus modification of magnetite grains in the upper zone of the Bushveld Complex, South Africa // Lithos, 1987. Vol. 20. p. 247-260.

Chakhmouradian A. R., Zaitsev A. N. Afrikanda: An association of ultramafic, alkaline and alkali-silica-rich carbonatitic rocks from mantle-derived melts // Phoscorites and carbonatites from mantle to mine: the key example of the Kola Alkaline Province, Mineralogical Society (UK) Series, 2004. Vol. 10. p. 247-291.

Christiansen F. G. Deformation fabric and microstructures in ophiolitic chromitites and host ultramafics, Sultanate of Oman // Geologische Rundschau, 1985. Vol. 74. p. 61-76.

Howarth G. H., Prevec S. A., Zhou M.-F. Timing of Ti-magnetite crystallisation and silicate disequilibrium in the Panzhihua mafic layered intrusion: Implications for ore-forming processes // Lithos, 2013. Vol. 170. p. 73-89.

Hulbert, L., Von Gruenewaldt, G. Textural and compositional features of chromite in the lower and critical zones of the Bushveld Complex south of Potgietersrus // Economic Geology, 1985. Vol. 80. p. 872-895.

Kukharenko, A. A., Orlova, M. P., Bulakh, A. G., Bagdasarov, E. A., Rimskaya-Korsakova, O. M., Nefedov, E. I., Ilinskiy, G. A., Sergeev, A. S., Abakumova, N. B. The Caledonian complex of ultrabasic and alkaline rocks and carbonatites of the Kola Peninsula and Northern Karelia // Nedra, Leningrad, Russia, 1965. p. 722.

Lorand J., Cottin J. Na-Ti-Zr-H 2 O-rich mineral inclusions indicating postcumulus chrome-spinel dissolution and recrystallization in the Western Laouni mafic intrusion, Algeria // Contributions to Mineralogy and Petrology, 1987. Vol. 97. p. 251-263.

McElduff B., Stumpfl E. The chromite deposits of the Troodos complex, Cyprus - Evidence for the role of a fluid phase accompanying chromite formation // Mineralium Deposita, 1991. Vol. 26. p. 307-318.

Nielsen T. F. D., Solovova I. P., Veksler I. V. Parental melts of melilitolite and origin of alkaline carbonatite: Evidence from crystallised melt inclusions, Gardiner complex // Contributions to Mineralogy and Petrology, 1997. Vol. 126. p. 331-344.

Potter N. J., Ferguson M. R., Kamenetsky V. S., Chakhmouradian A. R., Sharygin V. V., Thompson J. M., Goemann K. Textural evolution of perovskite in the Afrikanda alkaline–ultramafic complex, Kola Peninsula, Russia // Contributions to Mineralogy and Petrology, 2018. Vol. 173, pp. 100.

Yudin B., Zak S. Titanium deposits of northwestern USSR (eastern part of Baltic Shield) // International Geology Review, 1971. Vol. 13. p. 864-872.

Yudovskaya M. A., Kinnaird J. A. Chromite in the Platreef (Bushveld Complex, South Africa): Occurrence and evolution of its chemical composition // Mineralium Deposita, 2010. Vol. 45. p. 369-391.

ORE-FORMING BRINE-MELT OF ULAN-UDE F-REE CARBONATITES (WESTERN TRANSBAIKALIA, RUSSIA)

***Prokopyev I.R.*[1,2], *Redina A.A.*[1], *Ripp, G.S.*[3]**

[1]*Sobolev Institute of geology and mineralogy SB RAS, Novosibirsk, Russia, redina@igm.nsc.ru*

[2]*Novosibirsk state university, Novosibirsk, Russia, prokop@igm.nsc.ru*

[3]*Geological Institute of SB RAS, Ulan-Ude, Russia, ripp@ginst.ru*

The F-REE carbonatites were found in Ulan-Ude town in Western Transbaikalia region of Russian Siberia a few years ago. The rocks are composed mainly of bastnaesite-(Ce) and fluorite (up to 30-55 vol.% of each). Phlogopite is a typomorphic mineral (up to 5-10 vol.%), and the minor and accessory minerals (1-3 vol.%) are K-feldspar, albite, zircon, apatite, ilmenite and Nb-rutile. Sulfates and phosphates (1-3 vol.%) are represented by glauberite, Pb-jarosite, monazite-(Ce) and corkite. The rocks are confined to the Late Mesozoic West Transbaikalia rift zone of the Central Asian carbonatite province (Yarmolyuk, Ivanov, 2000; Ripp et al., 2009).

Three types of fluid inclusions were found in the carbonatites. The first group is represented by highly concentrated saline brine-melt inclusions, which are arranged singly or in groups of 2-3 inclusions in the central parts of the bastnaesite and fluorite crystals (Fig. 1a). The shape of the vacuole of the inclusions is round, isometric, often represented as negative crystal forms. Sometimes groups of brine-melt inclusions are located in the crystal growth zones of fluorites, which confirm the primary capture o*f* the inclusions (Roedder, 1984). The brine-melt inclusions consist of mineral, liquid and gas phases. The mineral phase (80-90 vol.%) is represented by the crystal aggregate of closely touching saline grains. The gas phase (5-10 vol.%) is often deformed. The size of the brine-melt inclusions is 15-30 μm.

The second type of inclusions is represented by a similar in morphology multiphase crystal-fluid inclusions (Fig. 1b). Fluid inclusions are pseudo-secondary, since they are arranged in groups along healed cracks in the crystals of bastnaesite and fluorite. The amount of the mineral phase is 30-50 vol.% and the gas phase – 5-10 vol.%. The size of the inclusions is 15-20 μm. The third type of fluid inclusions is secondary gas-liquid water-salt inclusions, which may also contain one or two crystalline phases (up to 5-10 vol.%). Inclusions are located along cracks and planes, sometimes with traces of lacing. The shape of the vacuole of inclusions is usually elongated, less commonly isometric, irregular, and their size is 5-15 μm.

The daughter crystalline phases of the brine-melt and crystal-fluid inclusions are represented by the predominance of Na and Ca sulfates, glauberite and thenardite, as well as the presence in minor amount of silicates (with K, Cl, F) and REE-carbonates. The gas phase of the inclusions contains CO_2. Homogenization temperatures of brine-melt and crystal-fluid inclusions are in the ranges of 520-490 and 450-430°C, respectively. Secondary gas-liquid fluid inclusions have homogenization temperatures of 350-290 and 200-150°C, and contain hydrocarbonates and chlorides of Na.

Thus, the carbonatites of Ulan-Ude were formed from the alkaline (Na, K) REE-F-carbonate-sulphate melt at temperatures of about 520°C. The hydrocarbonate-chloride solutions were responsible for the late hydrothermal processes. The data obtained are consistent with the previous results of study fluid inclusions in carbonatites of the Late Mesozoic Central Asian carbonatite province (Doroshkevich et al., 2010; Prokopyev et al., 2006; Nikolenko et al., 2018).

The work was done on state assignment of the Sobolev Institute of Geology and Mineralogy SB RAS (No.0330-2016-0002) and was also partially financially supported by the grant of President of the Russian Federation MK-1113.2019.5 (microthermometry) and by the Russian Science Foundation grant No 19-17-00019 (Raman spectroscopy).

References

Doroshkevich A.G.,Ripp G.S.,Moore K.R. Genesis of the Khaluta alkaline-basic Ba-Sr carbonatite complex (West Transbaikala, Russia) // Mineralogy and Petrology, 2010, Vol. 98, p. 245-268.

Nikolenko A.M., Redina A.A., Doroshkevich A.G., Prokopyev I.R., Ragozin A.L., Vladykin N.V. The origin of magnetite-apatite rocks of Mushgai-Khudag complex, South Mongolia: Mineral chemistry and studies of melt and fluid inclusions // Lithos, 2018, Vol. 320-321, p. 567-582.

Prokopyev I.R., Borisenko A.S., Borovikov A.A., Pavlova G.G. Origin of REE-rich ferrocarbonatites in southern Siberia (Russia): implications based on melt and fluid inclusions // Mineralogy and Petrology, 2016, Vol. 110 (6), p. 845–859.

Ripp G.S., Doroshkevick A.G., Posokhov V.F. Age of carbonatite magmatism in Transbaikalia // Petrology, 2009, Vol. 17, p. 17: 73.

Roedder E. Fluid inclusions // Reviews in Mineralogy. Mineralogical Society of America. 1984, Vol. 12.

Yarmolyuk V.V. and Ivanov V.G. Late Mesozoic and Cenozoic Magmatism and Geodynamics of Western Transbaikalia // Geotectonics, 2000, Vol. 34 (2), p. 121-140.

MODEL OF MANTLE-CRUSTAL ORIGIN OF ORE-BEARING STRONTIUM-BARIUM CARBONATITE IN THE BYRRANGA MOUNTAINS: ROLE OF THE TAIMYR HOT SPOT IN ORE FORMATION

Proskurnin V.F., Petrov O.V., Saltanov V.A.

A.P. Karpinsky Russian Geological Research Institute, Saint Petersburg, Russia, Vasily_Proskurnin@vsegei.ru

The largest Fad'yukuda-Kotui gravimagnetic ring structure (Fig. 1) (Sazonov et al., 2001; Proskurnin et al., 2010; Petrov et al., 2010) and a belt of ore-bearing strontium-barium carbonatite (Pogrebitsky et al., 1965; Proskurnin et al., 2010, 2012; Petrov et al., 2010) were identified in recent years, when compiling the State Geological Map-1000/3 within the Early Cimmerides of the Taimyr Peninsula, northern part of the Siberian Platform, and the East Taymyr-Olenek folded branch of the Late Cimmerides. When considering first-order mantle convective cells and hot spots that existed before the break-up of Pangea, it was established that the ring structure occupied a definite post-trappen place in the northern Eurasian plate, corresponding to the Taimyr hot spot of the Triassic lower mantle plume (Kravchenko and Khain, 1996). Most of the ring structure is overlapped by the Jurassic-Cenozoic sediments of the Yenisei-Khatanga trough and intersected by with the Central Taimyr suture, which divides it into two parts: the semi-ring part with a diameter of 300 km south of the suture within the platform and the ring part with a diameter of 200 km within the folded Taimyr.

In the southeastern part of the hot spot at the northern termination of the Siberian Platform, there is an outcrop of the unique Guli clinopyroxenite-dunite, picrite-melanephelinite and ijolite-carbonatite volcano-pluton. L.S. Egorov (1985) described the lateral metallogenic zonality relative to the rare-metal platinum-bearing Guli massif and the group of northern intrusions. South and southeast of the Guli, at a distance of 150-250 km, the Magan, Yraas, Yessey intrusions acquire an alkaline-salic composition and end in the formation of the Kharamai kimberlite field at a distance of the center. Occurrence of Middle to Late Triassic differentiated platinum-bearing ferrogabbro-troctole-wehrlite, subalkaline-gabbro-dolerite, and plagiowehrlite-gabbro-dolerite intrusions with titanomagnetite and sulphide-copper-nickel mineralization, volcanic rocks of the trachyandesite-trachytic formation, ring intrusions of ferrogabbro-monzonite-granosyenite, nepheline-syenite formations, crustal carbonatite of various morphology, diamond-bearing alneite is a specific feature of the Byrranga Mountains.

West Taymir and East Taymir areals of small intrusions, carbonatite, fluidolite correspond to offshoots from the hot spot. West Taymir magmatism culminates in the formation of dike fields of potentially diamond-bearing lamproites and alkaline syenite diatremes (Romanov, 1994, 1997), and in East Taimyr, in carbonatite with gold-bearing polymetallic and fluorite-barite mineralization (Proskurnin et al., 2010). In Tsvetkov Cape, nonrounded chrome-bearing pyrope crystals were found in Upper Triassic deposits (Grakhanov et al., 2007), and in Early Triassic sediments, injective bodies of potentially diamond-bearing fluid-explosive breccias with nonrounded pyropes, chrome-spinellids, and picroilmenites (Proskurnin et al., 2017) were recorded. On the Olenek Channel, the diamond-bearing Angardamtassky volcanic hydro-explosive clastic complex was identified as part of the Carnian horizon (Proskurnin et al., 2012).

Areal of ore-bearing unconventional-type carbonatite bodies in the Byrranga Mountains occupies an appropriate place among Triassic magmatic formations associated with the evolution of the Taimyr hot spot. Taimyr barium-strontium carbonatite is accompanied by uranium-REE, polymetallic and fluorite-barite mineralization (Kyidinsky-Fad'yukuda, Taimyrozersky, Podkamenno-Kuldimsky potential ore districts).

Carbonatite occurs in Upper Paleozoic terrigenous rocks (C_2-P_3), which are underlain by Middle Paleozoic haloid-sulphate-carbonate sediments (D-C_2). The carbonatite forms bodies ranging in size from the first tens of metres to the first kilometres, mainly of a lenticular, dike-vein-stockwork and stock-like shapes with intersecting injection contacts. Most of them are confined to the Early Cimmerian tectonomagmatic zones of northeastern strike to form beaded chains of bodies over a distance of 50-60 km.

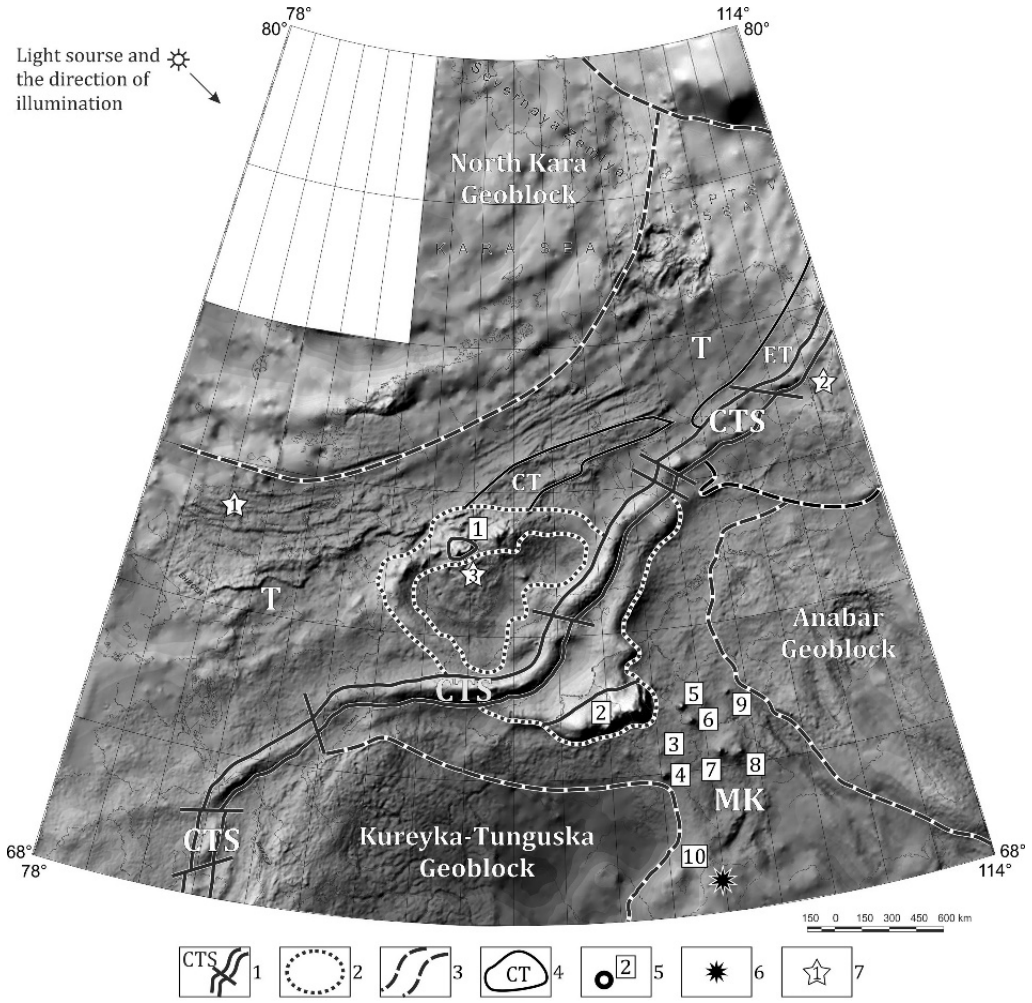

Figure 1. Location of Sr-Ba carbonatite areas in the Taimyr Peninsula and Maimecha-Kotui province intrusions relative to the Fad'yukuda-Kotui hot spot on the gravity map. Bouguer reduction, density of the intermediate layer is 2.67 g/m^3. Level is conditional (greyscale pseudorelief). Compiled in VIRG-Rudgeofizika, 2002. 1, Central Taymyr suture; 2, Fad'yukuda-Kotui hot spot; 3, boundaries of geoblocks and intergeoblock zones – carbonatite provinces: Maimecha-Kotui (MK) and Taimyr (T); 4, Taimyr carbonatite areals: ET – East Taymyr, CT – Central Taymyr; 5, the largest Early-Late Triassic intrusive massifs: Dyumtalei (1), Guli (2), Dalbykh group of intrusions (3), Bor-Uryakh and Kara Meni (4), Odikhincha (5), Kugda (6), Magan (7), Yraakh (8), Nemakit (9), Essey (10); 6, Kharamai kimberlite field; 7, predicted diamond-bearing fields related to lamproite (1), Late Triassic buried placers and fluid-explosive breccias (2); 7 – diamond-bearing alneite of the Gorbita River.

Carbonatites are spatially and temporally closely related to synkinematic moderately alkaline multiphase intrusions of ferrous and high-titanic monzonite-gabbro-dolerite, monzonite-diorite, granosyenite characterized by elevated contents of Ba, Sr, Co, Ni, Zn, Pb, Cd, Ag, Sb, Ng, etc. Age of carbonatite (238 to 219 Ma) (Proskurnin et al., 2010) and moderately alkaline ferrogabbro-dolerite, syenite (238 to 225 Ma) (Petrov et al., 2010) identified from zircons using SHRIMP-II, correspond to the Middle-Late Triassic, which is the main epoch of the Early Cimmerian Taimyr folding. Age of 241–227 Ma was obtained for ore-bearing carbonatite from Re-Os dating of sphalerite from one of ore occurrences (Koshka-East) (Saltanov, 2017).

Carbonatite is characterized by strontium-barium geochemical trend and enrichment with chalcophile group elements and low grade of rare earth and high field strength elements as compared to that of ultrabasic-alkaline rock complexes. Elevated concentrations are typical of Ag, Hg and to a lesser extent Se, Cd, Cu, Sb, As, Zn, Co.

Xenoliths and fragments of Middle Devonian – Early Carboniferous dolomite and limestone, Middle Carboniferous – Permian terrigenous rocks, Early Triassic dolerite, Middle-Late Triassic ferrogabbro-dolerite, less often syenite and granosyenite are typical of the injective carbonatite. Dolerite xenoliths are angularly rounded with distinct incrustations of contact transformations. Xenolith dimensions vary from a few to 10–15 cm, sometimes up to 20 m. Part of injective carbonate xenobreccias has features typical of fluid-explosive formations.

Morphologically, carbonatite bodies are subdivided into injective carbonatite, fluid-explosive breccias and vein-veinlet bodies characterized by multiphase and long-term formation. Following mineral types have been identified: calcitic, dolomitic, ankeritic, sideritic, fluorite-carbonate-baritic, gypsum-carbonate-anhydritic. The carbonatite hosts idiomorphic iron-free phlogopite, less often high-temperature minerals: chrome-spinellid, garnet, augite, pigeonite.

Magmatogenic-fluidogenic gypsum-anhydrite rocks identified in paragenesis with carbonatite and impregnated with grains of native metal phases, including iron-nickel intermetallics and alloys, indicate that deep-seated substances, in particular, mantle basite, participate in rock formation (Proskurnin et al., 2016). Occurrence in these rocks of Na-Ca phosphate sulphate and brannerite typical of hydrogenic uranium deposits, suggests multistage geological history of carbonatite and anhydrite, mixture of deep-seated magmatogenic and hydrogenic fluids at the intermediate crustal level.

Following accessory minerals have been identified in the carbonatite: periclase, albite, hydrodolomite, apatite, monazite, sodalite, sphene, rutile, as well as fluorite, apatite, zircon, monazite, baddeleite, xenotime, clinochlore, crystobalite, sergeevite, sassolite. The presence of fluorine- and boron-bearing carbonate rocks is noteworthy as well as occurrence of inyoite, berborite and fluorite in them. As a rule, the latter is represented by antozonite; at the final stages of its formation it is accompanied by celsian, vaterite, alstonite and paralstonite.

Hydrothermal-metasomatic carbonate rocks are composed of calcite, sometimes Sb-bearing calcite, siderite, Fe-Ca intermediate carbonate, epidote, hematite, chlorite, axinite; Sr-bearing barite was recorded in the calcite. Pyrite, pyrrhotite, magnetite, hematite, goethite, maghemite, sphalerite, galena, scheelite, chalcopyrite are common; cleiophane, arsenopyrite, gersdorffite, cinnabar, bornite, covelline, hydrozincite, minrecordite, wurtzite, stannite, sulvanite, zincite, tenorite are less widespread. Vein-disseminated pyrite locally reaches 30-40%, sometimes up to 80%.

Composition of fluids, thermobarogeochemical parameters, content and distribution of REE (Proskurnin et al., 2010) in the carbonatite indicate that it differs greatly from sedimentary carbonate rocks and that most of it formed at temperature of at least 380-410ºC during the decompression of gas-liquid carbon-dioxide-aqueous-saline fluids. On the other hand, high ratios of $^{87}Sr/^{86}Sr$ (0.7072–0.7098) in the carbonatite (Brekhov and Shergina, 2002; Petrov et al., 2010) typical of sedimentary rocks evidence high contribution of organogenic carbonate rocks during the formation of the studied carbonatite. The overwhelming prevalence of ancient, Precambrian zircons of various ages in the accessory fraction of carbonatite as in the sedimentary Devonian-Early Carboniferous sediments is indicative of possible capturing old zircons as a result of fluid-palingenic transformation of sedimentary carbonate rocks in intermediate foci.

Carbon and oxygen isotopic composition in the carbonate, which differs from the carbonate of sedimentary rocks and the mantle carbonatite, gets into the field of carbonates with exotic isotopic composition – “Taimyr carbonatite evolution trend” (Proskurnin et al., 2010; Petrov et al., 2010). As one of the options, it is assumed that it is due to the transformation of sedimentary carbonate rocks in intermediate foci at high pressures and temperatures into fluidized carbonate melt (“salt melt”), followed by the formation of fluid-explosive breccias and injective carbonatite.

Location patterns of the Taimyr ore-bearing carbonatite relative to the Taimyr hot spot, its petrographic-mineralogical, isotopic-geochronological and isotopic-geochemical features make it possible to outline a model of the mantle-crustal origin of ore-bearing carbonatite (Fig. 2).

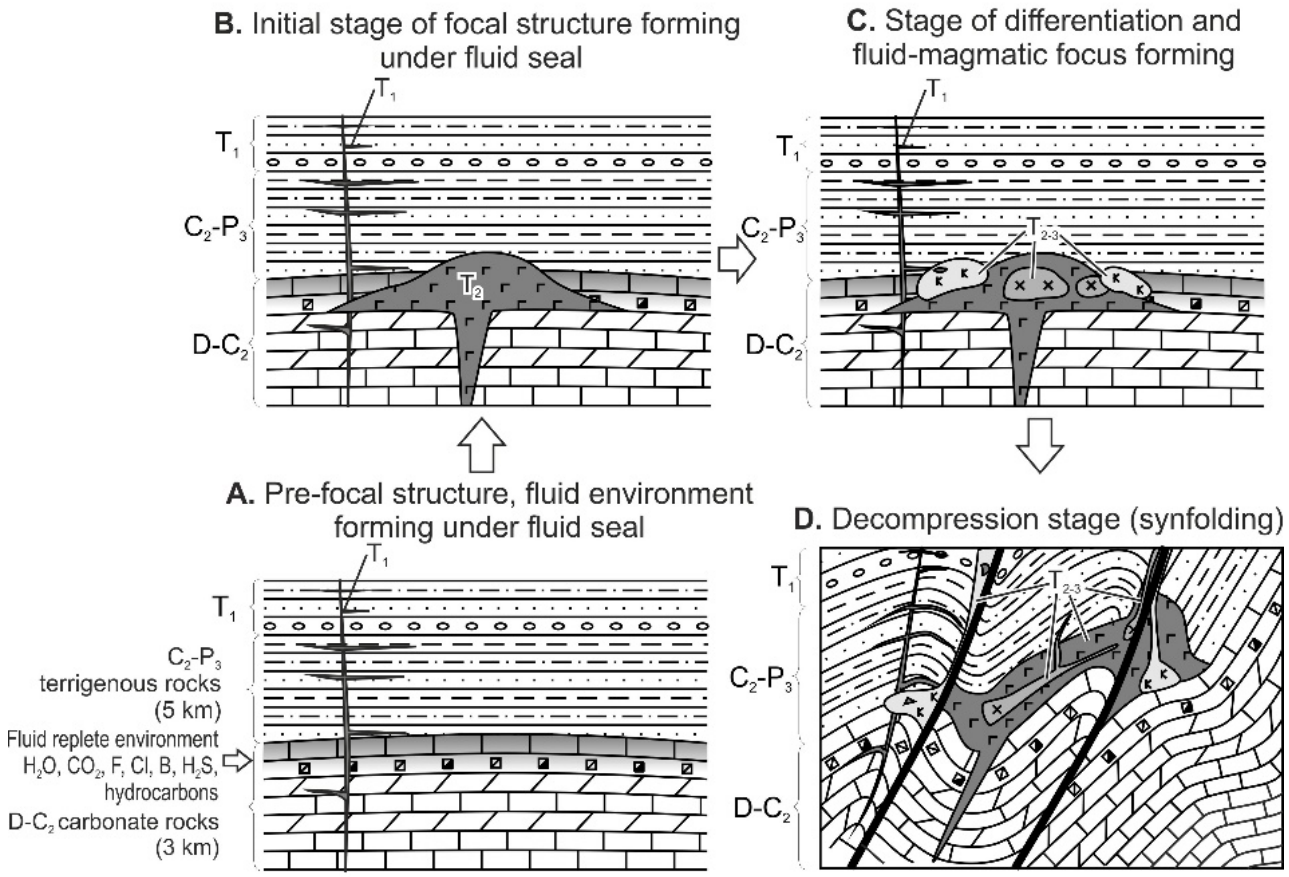

Figure 2. Geological and structural model of evolution of mantle-crustal ore-bearing carbonatite and fluidolite of the Taimyr Peninsula.

Pre-focal stage (pre-folding) on Taimyr was characterized by typical intra-plate geodynamic regime similar to the entire Siberian Platform. The general pattern for this stage was the existence (by the Triassic) of the Lower-Middle Paleozoic carbonate and Upper Paleozoic clay-terrigenous cover (Fig. 2, A). The last Middle Carboniferous-Permian structural complex was the thickest regional impermeable layer for gas-liquid stratal hydrogenic and oil-and-gas systems, mainly confined to Devonian-Middle Carboniferous deposits. The Devonian halide-phosphate-sulphate-carbonate section of the Byrranga Mountains was a significant factor for the formation of fluids' composition.

Initial stage (Fig. 2, B) in the formation of the magmatogenic-fluidogenic system was characterized by the introduction of post-trappean mantle moderately alkaline ultramafic rocks and basite related to the formation of the Taimyr hot spot; for part of them, the Late Devonian - Early Carboniferous halide-phosphate-sulfate-carbonate section with stratal fluids (mixture of hydrocarbon accumulations in water) was a kind of a trap. Further evolution of the focal structure (Fig. 2, C) consisted in the magnetogenic-fluidogenic differentiation, partial melting of the host carbonate rock to form "saline carbonate melts".

Final synfolding stage (Fig. 2, D) was characterized by regular focus unloading during the decompression (due to disjunctive-folded deformations) and introduction of successive injections into overlying Middle Carboniferous-Permian formations of moderately alkaline amphibole ferrogabbro-dolerite, monzogabbrodiorite, monzonite-diorite, granosyenite, carbonatite, anhydrite. At all stages of evolution of the magmatogenic-fluidogenic system, it was accompanied by the formation of fluid explosive breccias.

Thus, the available data indicate the mixing of juvenile and near-surface fluids as a result of the mantle-crust interaction of ultramafite-mafite magmas of the Taimyr hot spot in intermediate upper-crust foci.

This work was supported by Rosnedra under the State Contract No. 25 dated February 27, 2012.

References

Brekhov G. V., Shergina Yu. P. About the origin of the Central Taimyr «carbonatites». In: Taimyr Mineral Potential. Iss. 5. St. Petersburg, VSEGEI. 2002. P. 176—185 (in Russian).

Egorov L.S. Alkaline-ultrabasic magmatism and its minerageny // Geology of Ore Deposits. 1985. V. 4. P. 24-40. (in Russian).

Grahanov S.A., Yadrenkin A.V. Forecast of diamond content in Triassic deposits of Taimyr. Proceedings of RAS. 2007. V. 416. N 5. P. 663–656. (in Russian).

Kravchenko S.M., Hain V.E. Global structures of lithosphere and mantle convection // Proceedings of RAS. 1996. V. 347. N 3. P. 368-371. (in Russian).

Petrov O. V., Proskurnin V. F., Gavrish A. V., Mozoleva I. N., Lokhov K. I., Tolmacheva E. V., Petrushkov B. S., Bagaeva A. A. Early Mesozoic carbonatites of East Taimyr // Regional Geology and Metallogeny. 2010. N 44. P. 5-22 (in Russian).

Pogrebitsky Yu. Ye., Shanurenko N. K., Gulin S. A., Vorobiev V. A., Zakharov Yu. P. Petrogenesis and ore content of the Taimyr carbonatite association. Leningrad, NIIGA. 1965 (in Russian).

Proskurnin V.F., Petrov O.V., Gavrish A.V. et al., 2010. Early Mesozoic carbonatite belt of the Taimyr Peninsula // Lithosphere. 2010. V. 3. P. 95-102. (in Russian).

Proskurnin V.F., Vinogradova N.P., Gavrish A.V., Naumov M.V. Signs of explosive-clastic genesis of diamantiferous Carnian horizon in the Ust-Olenek region (petrographic and geochemistry data) // Geology and Geophysics. 2012. V. 6. (in Russian).

Proskurnin V. F., Saltanov V. A., Petrov O. V., Silaev V. I., Remizov D. N., Gavrish A. V. Injective carbonate xenobreccias and anhydritites in carbonatites of the Pavlovsky massif, East Taimyr // Proc. of the Russian Mineralogical Society. 2016. Pt CXLV. N 6. P. 1–19. (in Russian).

Proskurnin V. F., Gavrish A. V., Petrov O. V., Galkin A. S., Vinogradova N. P., Naumov M. V., Silaev V. I., Luk'yanova L. I., Ronina E. E., Saltanov V. A. Potentially diamond-bearing Early Mesozoic injection breccias of the Eastern Taimyr Peninsula // Regional Geology and Metallogeny. 2017. N 72. P. 78-90 (in Russian).

Romanov A. P. Taimyr lamproites and their index minerals in Mesozoic-Cenozoic collectors. In: Geology of intermediate diamond collectors. Novosibirsk: Nauka. 1994. P. 105-108. (in Russian)

Romanov A. P. Prospects of diamond potential in the Taymyr Mountain. In: Taimyr Mineral Potential. Norilsk, VSEGEI. 1997. Iss. 1. P. 185–198. (in Russian).

Saltanov V. A. Unconventional type of barite-polymetallic mineralization in crustal carbonatites of East Taimyr // Proceedings of the 5th International Conference of Young Scientists and Specialists in Memory of Academician A. P. Karpinsky. St. Petersburg, VSEGEI. 2017. P. 296-299. (in Russian).

Sazonov A. M., Zviagina E. A., Leontiev S. I. Platinum-bearing alkaline-ultrabasic intrusions of Polar Siberia. Tomsk, TsNTI. 2001. 510 p. (in Russian).

LARGE PLATINUM ORE DEPOSITS IN URAL-ALASKAN-TYPE INTRUSIONS: MYTHS AND REALITY

Pushkarev E.V.

Institute of Geology and Geochemistry, Ural Branch, Russian Academy of Sciences, Ekaterinburg, Russia, pushkarev@igg.uran.ru

The average background of platinum in dunite of Ural-Alskan-type intrusions is close to 50 ppb (Auge et al., 2005; Betekhtin, 1935; Garuti et al, 1997; Zavaritsky, 1928; Zoloev et al., 2001). It allows to calculate the amount of platinum comprising in ultramafic rocks. For example, in the well-known and classical Nizhny Tagil massif in the Ural Platinum Belt, dunite occupies area is about 30 square kilometres. So, the total amount of platinum up to the depth of 500 meters may constitute 2000-2500 tons. Such calculations were provided many times by different scientists and economic geologists since the beginning of 20th century and later (Ivanov, 1997; Kozlov et al., 2011;). The important question: “Could whole dunite represent a platinum ore or not?" -was very popular one hundred years ago. One of the first who professionally answered on this question was A.N. Zavaritsky (1928) worked at that time as a scientific supervisor of geological explorations in the Nizhny Tagil massif. He had concluded that economically profitable to develop mining only if dunite comprises chromite schlieren and segregations with high platinum concentration. Later A.G. Betekhtin (1935), a mining geologist of the "Gospodskaya Shakhta" platinum deposit confirmed the most conclusions of A.N. Zavaritsky. Taking this into account it becomes clear that the explaining of chromitite genesis and mechanisms of their PGM enrichment are the key-points for answering on the main question: "Are exist large ore platinum deposits in Ural-Alaskan-type intrusions or this is a myth?"

There are two different approaches for considering of Pt-rich chromitite genesis. In the one model chromite schlieren are considered to originate due to accumulation of liquidus chromite and PGM from the melt percolating through dunite host rocks (Auge et al., 2005). On the other hand, the magmatic origin is contradicted by textural and mineralogical data (Pushkarev et al., 2005; 2015) that demonstrate a) later formation of chromitites and their non-conformity in relation to dunites; b) lack of evidence for melt percolation in dunites in and around schlieren; c) systematic change of Cr-spinel compositions in chromitite bodies towards from the center of schlieren (Pushkarev et al., 2005); d) low temperature and highly oxidized conditions of coexisting Ol-Chr assemblages (Chashchukhin et al., 2002); e) amount of precious minerals within chromitite pods approaches 40-50%, ruling out their enrichment by magmatic processes; f) paragenetic association of chromite and PGM with low-temperature, non-magmatic minerals; g) unusually high Mg# of Cr-spinel and associated silicate minerals.

In particular, the chromite contains euhedral inclusions of extremely magnesian (Mg#>0.94) silicates – amphibole, Cr-diopside and olivine that crystallized prior to and together with their host chromite, but such mineral and compositional paragenesis excludes magmatic origin. The chromites also associate with a skarn-like assemblage of diopside, amphibole, garnet (andradite-grossular), phlogopite, glagolevite, apatite, chlorite, serpentine etc (Pushakrev et al., 2015). The PGM-bearing Cr-spinel sometimes contains numerous trails of octahedral gas and gas-liquid inclusions that are randomly disturbed and bear no evidence of magmatic crystallization of the host chromite. The chromite and PGM in the most massifs contact with phlogopite, chlorite and serpentine has “imprints” of these minerals on its surface. Pt-Fe alloys form porous aggregates and dendrites intergrown with serpentine.

All these geological, structural and compositional features of the PGM-rich chromitites allow assume their non-magmatic origin related with the re-distribution of components and mineral nano- and micro-particles within dunite at low temperature in the presence of fluid. This process could take place at the latest stage of high-temperature plastic deformations of dunite during intrusion through crustal sequence. It builds a strong limitation in volume of the ore-forming systems and in real size of ore bodies. The field observations confirm this conclusion. It is well-known that the most ore bodies approach only several meters length with thickness of few centimeters. Sometimes small ore bodies combine in longer ore zones (Gosshakhta deposit is an example), but even in this case the total

platinum resources approach only few hundred kilograms. The numerous small Pt-rich chromitites in dunite of Ural-Alaskan-type intrusions are the perfect source for big and unique platinum placers but unfortunately can't represent economically profitable target for exploiting by big mining companies.

This work was supported by State scientific program AAAA-A18-118052590029-6.

References

Auge T., Genna A., Legendre O. et al. Primary platinum mineralization in the Nizhny Tagil and Kachkanar ultramafic complexes, Urals, Russia: A genetic model for PGE concentration in chromite-rich zones // Economic Geology. 2005. Vol. 100. p. 707-732.

Betekhtin, A.G. Platinum and other minerals from platinum group. Moscow-Leningrad: AN USSR, 1935.148, pp. (in Russian).

Chashchukhin I. S., Votyakov S. L., Pushkarev E. V. et al. Oxithermobarometry of ultramafic rocks from the Ural Platinum Belt // Geochemistry International. 2002. Vol. 40. p. 762-778.

Garuti G., Fershtater G., Bea F. et al. Platinum group elements as petrological indicators in mafic-ultramafic complexes of the Central and Southern Urals: preliminary results // Tectonophysics. 1997. Vol. 276. 1-4. p. 181-194.

Ivanov O.K. Concentrically-zonal pyroxenite-dunite massifs of the Urals. Ekaterinburg: Ural State University Press, 1997. 327 pp. (in Russian).

Kozlov A. P., Chanturiya V. A., Sidorov E. G. et al. Large volume platinum ore deposits in zonal mafic–ultramafic complexes of the Ural–Alaskan-type and the outlook for their development // Geology of Ore Deposits 2011. Vol. 53, 5. p. 374–389.

Pushkarev E.V., Anikina E.V., Garuti G. et al. Postmagmatic origin of platinum deposits in the Ural-Alaskan type ultramafites: T-fO2 conditions and role of fluids // Extended abstract of the 10th International Platinum Symposium. Oulu, Finland: Geological Survey of Finland, 2005. p. 223-226.

Pushkarev E.V., Kamenetsky V.S., Morozova A.V. et al. Ontogeny of ore Cr-spinel and composition of inclusions as indicators of the pneumatolytic–hydrothermal origin of PGM-bearing chromitites from Kondyor massif, the Aldan Shield // Geology of ore deposits. 2015. Vol. 57. 5. p. 352-380.

Zavaritsky, A.N. Ore platinum deposits in the Urals. Files of General and Exploration Geology, Leningrad: Geological Committee, 1928.108. 56 pp. (in Russian).

Zoloev, K.K., Volchenko, Yu.A., Koroteev, V.A. et al. Platinum ores in different complexes of the Urals. Ekaterinburg: Ural State University Press, 2001. 199 pp. (in Russian).

POSSIBLE PARENT MAGMA FOR PHOSCORITES, KOVDOR, KOLA, RUSSIA

Rass I.T., Yakushev A.I., Kovalchuk E.V., Petrenko D.B.
Institute of geology of ore deposits, petrography, mineralogy and geochemistry (IGEM) RAS

The crustal differentiation of primary magmas that had been derived from mantle material at low-degree partial melting is known to be able produce mineral deposits of such strategically important metals as Zr, Nb, REE, and Sr (Kogarko, 1977; Kogarko et al., 1988, 2015). Alkaline ultrabasic complexes containing alkaline rocks that are derivatives of mantle magmas are genetically related to carbonatites, which are characterized by a vast ore-bearing potential.

530 massifs with carbonatites are currently known worldwide (Woolley, Kjarsgaard, 2008). Carbonatites in alkaline–ultramafic complexes are sometimes accompanied by phoscorites (Phoscorites and Carbonatites…, edited by F. Wall, A.N. Zaitsev, 2004), which are plutonic ultrabasic rocks, comprising magnetite, apatite, one of silicate minerals (forsterite, phlogopite or tetraferriphlogopite) and often carbonate – calcite or dolomite.

The Kovdor massif is a typical (and one of the most thoroughly studied) ring complexes of alkaline-ultrabasic rocks, carbonatites, and phoscorites; it hosts a unique magnetite-apatite-rare-metal deposit. The Kovdor phoscorite-carbonatite ore complex (0.8 x 1.3 km) intrudes the clinopyroxenites and the ijolites-melteigites. It forms a subvertical pipe-like body, and the carbonatites form a steep-dipping stockwork of veins (Krasnova, Kopylova, 1988). Phoscorites consist of several generations of magnetite rich apatite-carbonate ores with forsterite (or phlogopite) associated with also several generations of carbonatites (Римская-Корсакова, Краснова, 2002; Krasnova et al., 2004). Complex Ti, Nb, and Zr oxides and minerals of the perovskite, pyrochlore, and ilmenite groups are the principal trace-element concentrators (Chakhmouradian, Williams, 2004), and the contents of these accessorries in the phoscorites are higher than in the carbonatites. The highest Sr concentrations were found in the calcite carbonatite. The Zr and Nb concentrations in the phoscorites are notably higher than in the coeval carbonatites. The REE concentrations in the rocks of both types are comparable.

It was thought until lately that the uniquely high concentrations of Nb, Zr, and REE of carbonatites in alkaline-ultrabasic complexes are produced by liquid immiscibility between carbonate and silicate magmas at a high enough degree of differentiation of the primary alkaline ultramafic melts. However, recent experiments aimed at evaluating the distribution coefficients of elements between immiscible silicate magma and magmas of other composition (Veksler et al., 2012) have proved that these elements are preferably concentrated in the silicate liquid compared to the carbonate one and also that these elements can be concentrated in fluoride and phosphate (but not carbonate) melts as compared to the silicate ones.

We have analyzed 16 phoscorite and 11 carbonatite representative samples by XRF and ICP. These rocks crystallized during successive evolutionary stages of the Kovdor phoscorite-carbonatite complex that were distinguished in (Rimskaya-Korsakova, Krasnova, 2002; Krasnova et al., 2004).

The LOI values, which likely reflect mostly the CO_2 contents, and the concentrations of SiO_2 Al_2O_3 (<1% in the carbonatites and >4, up to 30 wt % SiO_2 and up to 11 wt % Al_2O_3 in the phoscorites), and CaO (37–54 wt % in the carbonatites and 1.5–31 wt % in the phoscorites) highlight the obvious differences between the rocks. Fluorine concentrations in the carbonatites slightly increase from earlier derivatives (with green phlogopite) to later ones (with tetraferriphlogopite). Concentration of this element in the phoscorites (till 0.39 wt %) is somewhat higher, and the later carbonatites contain much higher F concentrations (till 0.55 wt %), than in the agpaitic nepheline syenites: 0.14–0.20 wt % (Kogarko and Krigman, 1981).

The primitive mantle-normalized (Sun and McDonough,1989) trace-element patterns indicate that concentrations of trace elements, including REE, increase from earlier to later derivatives in both the phoscorites and the carbonatites. It is pertinent to mention that TiO_2 concentrations simultaneously and notably increase in the phoscorites and carbonatites from their earlier to later derivatives. The normalized trace-element and REE patterns of the phoscorites and carbonatites show deep negative anomalies at Eu, Pb, and Ti, and shallower anomalies at Y but no Eu anomalies and similar Nb and Ta fractionation. These features illustrate that both rock types are derivatives of deep mantle melts derived

at low degrees of melting. The gradual evolution of the composition of the phoscorites and carbonatites from their earlier to later varieties and the enrichment of the rocks in low-melting components indicates that the differentiation of all of these rocks was controlled primarily by fractional crystallization. Fluorine enrichment in the residual melt results in that fluorine concentrations increase in the successive derivatives at decreasing temperature and crystallization of apatite (and pyrochlore) from carbonate-rich magmas, similar to the silicate ones (Kogarko and Krigman, 1981). The phoscorites and carbonatites show an increase in fluorine concentrations from the cores to margins of apatite crystals, an increase in this concentration in phlogopite from the earlier carbonatites and phoscorites to later ones, and an increase in fluorine concentrations in bulk-rock samples from the earlier to later phoscorites and carbonatites. Strontium concentrations in apatite and calcite increase from the earlier to later carbonatites and phoscorites, and MgO and Al_2O_3 concentrations decrease from the cores to margins of magnetite crystals coexisting with olivine. The Fe# of micas in the carbonatites and phoscorites increases during the late crystallization of tetraferriphlogopite instead of phlogopite. In the phoscorites and carbonatites, phosphorus concentrations increases from earlier to later derivatives of the rocks.

The principal differences in the Sr, Zr, and Hf concentrations of the phoscorites and carbonatites cannot be explained without invoking additional (along with fractional crystallization) mechanisms of the evolution of the mantle magmas. Tendencies in the evolution of the petro- and geochemistry of the phoscorites and carbonatites from their earlier to later derivatives may suggest that the rocks belong to different branches or portions of the fractionating magma. For example, P shows a positive correlation with CaO and negative one with Fe_2O_3 in the phoscorites, whereas correlations between P and these elements in the carbonatites are opposite. The plots of logarithmic concentrations of pairs of incompatible elements Sr and Ce in these rocks show different evolutionary trends, none of which follows the trends in silicate alkaline-ultrabasic rocks. The plots of logarithmic concentrations of pairs of incompatible elements Nb and La, Zr and Y in these rocks also show two different evolutionary trends.

The parallel differentiation of the phoscorite and carbonatite magmas may have involved liquid immiscibility (along with fractional crystallization). The operation of these processes seems to follow from the fact that phoscorites at Sokli, Finland, and Vuorijarvi, Kola Peninsula, bear spherulitic textures made up of forsterite and magnetite, with subordinate amounts of apatite, in a calcite matrix (Lapin and Vartiainen,1983), which were also documented in phoscorites at Kovdor (Rimskaya-Korsakova and Krasnova, 2002). The hypothesis of the likely role of liquid immiscibility is also favored by other mineralogical data researches in Sokly (Lee et al., 2004). The steeply dipping layering (Krasnova, Kopylova, 1988) of the Kovdor phoscorite–carbonatite complex was described in (Yegorov, 1992) as a type related to liquid immiscibility.

A seeming immiscibility between phosphate and carbonate liquids was first detected in melt inclusions (Andreeva, Kovalenko, 2003) within the likely temperature range of $500 < T < 900^oC$. I.A. Andreeva investigated the Mushugai-Khuduk carbonatite complex in Mongolia and documented the relations in melt inclusions in apatite, which can be reasonably interpreted as the result of phosphate-carbonate liquid immiscibility.

Our data on the zoning of coexisting minerals in the phoscorites and carbonatites in the Kovdor phoscorite–carbonatite complex indicate that the partition coefficients of minor elements between coexisting phases are equal in the phoscorites and carbonatites. The SrO partition coefficients between calcite and apatite and/or the centers of their crystals in the phoscorites and carbonatites of earlier generations is 2. The MgO partition coefficients between the coexisting calcite and magnetite of the earlier generations of the phoscorites and carbonatites and/or the cores of their crystals are 4.5. This seems to indicate that the phosphorus-enriched and normal (with >32 wt % CaO) carbonatite magmas may have been in equilibrium. Evidence of this equilibrium lead us to view the phoscorite (phosphorus-enriched) and carbonatite melts as immiscible liquids.

Immiscibility between carbonate and phosphate liquids may have occurred after the segregation of the carbonatite magma enriched in phosphorus (perhaps, phosphate–iron?) at temperatures lower than those of immiscibility between silicate and carbonate magmas (as was reproduced in numerous

experiments), which were only insignificantly higher than the crystallization temperatures of carbonatites themselves.

The ilmenite-magnetite crystallization temperature, according to (Spencer, Lindsley, 1981), is 647°C at log fO_2 = -18 for the older phoscorite and 474°C for the younger one. Practically all analyzed ilmenite grains couldn't be used to determine the parameters because of their anomalously high concentrations of MgO (up to 25%) or MnO (13.6%). At the Lyulekop deposit in the Palaborwa Complex, South Africa, phoscorites started to be formed, at temperatures of 630–750°C (magnetite–ilmenite and dolomite–calcite thermometry) (Sharygin et al., 2011).

Carbonatites are derivatives of mantle alkaline ultramafic melts. Sr–Nd isotope data on Kovdor carbonatites and phoscorites (Zaitsev and Bell, 1995) provide undeniable evidence of genetic links between these rocks.

The origin of these exotic phoscorite–carbonatite complexes, as few as 21 of currently known 530 carbonatite massifs (Wall, Zaitsev, 2004; Woolley, Kjarsgaard, 2008), may be explained with some reasons that phosphorus is present in the mantle in emounts 170-210 ppm P2O5 (Wanke, 1981), comparable with those of CO2 = 100-700 ppm (Ryabchikov et al., 1989, 1991), and a first melt in the carbonated mantle may be represented by carbonate-phosphate liquids (Ryabchikov, Hamilton, 1993). High P_2O_5 concentrations of 0.55 wt % were found in melilite nephelinites, which are early derivatives of continental mantle magmas, and the solubility of this component drastically decreases in magmas at their partition (Kogarko et al., 1981).

A few experimental studies (starting with Ryabchikov et al., 1989, 1993) testify that silicate and phosphate-carbonate melts are immiscible at high pressures (20-30 kbar) and temperatures 950-1000°C, and the rare-earths and some other trace elements are concentrated in the latter. As carbonatites and phoscorites in the Kovdor complex are doubtedly magmatic rocks, they may be considered as derivatives of mantle melts. Perhaps, it is thus more appropriate to refer to carbonatite magmas that separated from silicate ones as phosphate-carbonate magmas.

The composition of the primary partial mantle melts parental for the Kola alkaline province in the Paleozoic (Arzamastsev et al., 2001) was calculated from the composition of alkaline ultramafic and phonolitic rocks of the Kola Peninsula, and the P_2O_5 concentrations in the partial melts were estimated at 0.0218 wt % (Arzamastsev and Mitrofanov, 2009). According to these calculations, the carbonatite melt that was derived in the Earth's crust, separated from alkaline silicate magma, and inherited high phosphorus concentrations, also may have had a phosphate–carbonate composition. For example, phoscorites and carbonatites in the Kovdor Massif may have been derivatives of a magma that contained, along with carbonate components, much Fe, P, and trace elements (Rass et al., 2017). Magma of such composition likely could be generated in the crust where partial mantle melts were locally (and rarely) enriched in phosphorus (along with carbon dioxide), and the alkaline ultramafic magma was highly differentiated.

This work was supported by the Institute of Geology of Ore Deposits, Petrography, Mineralogy and Geochemistry (IGEM) RAS, Moscow.

References

Andreeva I.A., Kovalenko V.I. Magma compositions and genesis of the rocks of the Mushugai-Khuduk carbonatite-bearing alkaline complex (southern Mongolia): evidence from melt inclusions // Per. Mineral 2003. Vol. 72, special issue.

Arzamastsev A.A., Mitrofanov F.P. Paleozoic plume–lithospheric processes in northeastern Fennoscandia: estimated composition of the mantle melts and parameters of magma-generating processes // Petrology, 2009. No. 3. pp. 324-336.

Arzamastsev A.A., Bea F., Glaznev V.N., Arzamastseva L.V., Montero P. Kola alkaline province: estimation of the composition of the primary mantle melts and parameters of magma-generating processes. Russian journal of Earth sciences, 2001. Vol. 3. No. 1.

Chakhmouradian A.R., Williams C.T. Mineralogy of high-field-strength elements (Ti, Nb, Zr, Ta, Hf) in phoscoritic and carbonatitic rocks of the Kola Peninsula, Russia // In Phoscorites and carbonatites from mantle to mine: the key example of the Kola alkaline province, Edited by F. Wall

and A.N. Zaitsev. Mineralogical Society Series, 10. Mineralogical Society, London, 2004, pp. 293-340.

Kogarko L.N. Genesis of agpaitic magmas. Nauka, Moscow, 1977.

Kogarko L.N., Krigman L.D. Fluorine in silicate magmas, Moscow: Nauka, 1981.

Kogarko L.N, Petrova E.N., Venturelly J.P. Phosphorus solubility in magmatic melts // Dokl. Akad. Nauk SSSR, 1981, Vol. 261, No. 6, pp. 1430-1432.

Kogarko L.N., Lazutkina L.N., Krigman L.D. Conditions of Zr concentrating in magmatic processes. Nauka, Moscow, 1988

Kogarko L.N. Geochemical models of superlarge deposits of strategical metals in alkaline rocks Eastern Fennoscandia). // Alkaline magmatism of the earth and related strategic metal deposits. Moscow: GEOKHI RAS, 2015. pp. 58-60.

Krasnova N.I., Kopylova L.N. The geological basis for mineral-technological mapping at the Kovdor ore deposit // International Geology Review, 1988. Vol. 30, pp. 307-319.

Krasnova N.I., Balaganskaya E.G., Garcia D. Kovdor – classic phoscorites and carbonatites. // In Phoscorites and Carbonatites from Mantle to Mine: the Key Example of the Kola Alkaline Province, Edited by F. Wall and A.N. Zaitsev. Mineralogical Society Series, 10. Mineralogical Society, London, 2004, pp. 99-132.

Lapin A.V., Vartiainen H. Orbicular and spherolitic carbonatites from Sokly and Vuoriyarvi. Lithos 1983 Vol. 16, pp. 53-66.

Lee M.J., Garcia D., Moutte J., Williams C.T., Wall F. Carbonatites and phoscorites from the Sokli complex, Finland. // In Phoscorites and Carbonatites from Mantle to Mine: the Key Example of the Kola Alkaline Province, Edited by F. Wall and A.N. Zaitsev. Mineralogical Society Series, 10. Mineralogical Society, London, 2004, pp. 133-162**.**

Phoscorites and Carbonatites from Mantle to Mine: the Key Example of the Kola Alkaline Province, Edited by F. Wall and A.N. Zaitsev. Mineralogical Society Series, 10. Mineralogical Society, London, 2004.

Rass I.T., Petrenko D.B., Yak ushev A.I. Problem of phoscorite-carbonatite relations in the Kovdor alkaline-ultrabasic complex // Petrology of magmatic and metamorphic complexes Tomsk, 2017. No. 9, pp. 367-370.

Rimskaya-Korsakova O.M., Krasnova N.I. Geology and mineral deposits of the Kovdor Massif, SPgU, St.-Peterburg, 2002.

Ryabchikov I.D., Baker M, Wyllie P.J. Phosphate-bearing carbonatite melts in equilibrium with mantle lherzolite at 30 kbar // Geokhimiya, 1989. No. 5, pp. 725-729.

Ryabchikov I.D**,** Edgar A.D., Wyllie P.G. Partial melting in the carbonate–phosphate–peridotite system at 30 kbar // Geokhimiya, 1991. No. 2, pp. 163-168.

Ryabchikov I.D., Hamilton D.L. Interaction of carbonate-phosphate melts with mantle peridotites at 20-35 kbar // S.Afr.J.Geol., 1993. Vol. 96, No.3, pp. 143-148.

Ryabchikov I.D., Hamilton D.L. Near-solidus melts in carbonatized mantle peridotites in the presence of apatite and uraninite // Geokhimiya, 1993. No. 8, pp. 1151-1160.

Ryabchikov I.D., Orlova G.P., Senin V.G., Trubkin N.V. Partitioning of rare earth elements between phosphate-rich carbonatite melts and mantle peridotites // Mineral. Petrol. 1993. Vol. 49, pp. 1-12.

Sharygin V.V., Zhitova L.M., Nigmatulina E.N. Fairchildite $K_2Ca(CO_3)$ in phoscorites from Phalaborwa, S. Africa: the first occurrence in alkaline carbonatite complexes. Geol Geophys. 2011. Vol. 52, pp. 261-275.

Spencer K.J., Lindsley D.H. A solution model for coexisting iron-titanium oxides // Amer. Mineral. 1981. Vol. 66, pp. 1189-1201.

Sun S.-s., McDonough W.F. Chemical and isotopic systematics of oceanic basalts: implications for mantle composition and processes. In Magmatism in the Ocean Basins, Edited by Saunders A.D., Norry M.J. Geol.Soc.Spec.Publication. 1989. Vol. 42, pp. 313-345.

Veksler I.V., Dorfman A.M., Dulski P., Kamenetsky V.S., Danyushevsky L.V. Jeffries T., Dingwell D.B. Partitioning of elements between silicate melt and immiscible fluoride, chloride, carbonate,

phosphate and sulfate melts, with implications to the origin of natrocarbonatite // Geoch Cosmoch Acta 2012. Vol. 79, pp. 20-40.

Wanke H. Constitution of terrestrial planets // Phil. Trans. Roy Soc. London, 1981. Vol. A 303, pp. 287-302.

Woolley A.R., Kjarsgaard B.A. Carbonatite occurrences of the world: map and database, Geological Survey of Canada, 2008. Open File 5796.

Yegorov L.S. Phosscorites of the Maymecha-Kotuy ijolite-carbonatite association // International Geology Review, 1993. No. 35, pp. 346-358.

Zaitsev A., Bell K. Sr and Nd isotope data of apatite, calcite and dolomite as indicators of source, and the relationships of phoscorites and carbonatites from the Kovdor massif, Kola peninsula, Russia // Contributions to Mineralogy and Petrology. 1995. Vol. 121. p. 324-335.

FORMATION CONDITIONS AND COMPOSITION FEATURES OF THE FLUORITE MINERALIZATION OF THE MUSHUGAI-KHUDUK COMPLEX (SOUTHERN MONGOLIA)

Redina A.A.[1], Nikolenko A.M.[1], Doroshkevich A.G.[1,2], Prokopyev I.R.[1,3]

[1]Sobolev Institute of Geology and Mineralogy Siberian Branch Russia Academy of Sciences, Novosibirsk, Russia, redina@igm.nsc.ru

[2]The Geological Institute Siberian Branch Russia Academy of Sciences, Ulan-Ude, Russia, doroshkevich@igm.nsc.ru

[3]Novosibirsk state university Novosibirsk, Russia, prokop@igm.nsc.ru

The formation conditions of fluorite are extremely diverse: it is fixed as a product of magmatic, greisen, pegmatite, carbonatite, skarn, hydrothermal and sedimentary processes. The process responsible for the formation of fluorite is directly related to the parameters of the mineral-forming fluid and the geochemical characteristics of the fluorite. The Mushugai-Khuduk complex belongs to the late Mesozoic alkaline province and is represented by the following plutonic and volcanic rocks: alkaline syenites, shonkinites, nephelinites, trachytes, rhyolites, carbonatites, apatite-magnetite rocks and a series of fluorite-bearing vein rocks (Samoilov, Kovaleko, 1983; Vladykin, 2013; Nikolenko et al., 2018). Fluorite is found in the majority species of rocks of the Mushugai-Khuduk complex as an accessory or main mineral. Fluorite-bearing rocks contain significant amount of fluorite from 5 up to 90%. These rocks are distributed mainly in the Eastern and South-Eastern parts of the complex. Fluorite-bearing rocks of the Mushugai Khuduk complex are represented by the following differences.

1. *Quartz-fluorite rocks.* Deep purple almost black fine-grained often massive rocks, that forms small bodies with isometric or round cross-sections.

2. *Fluorite-apatite-celestine rocks* observed as veins (up to 100 m long and 0.2-1 m wide) flooded by violet-brown or violet-yellow fine- to medium-grained rocks with a brecciform, inequigranular or porphyritic texture.

3. *Fluorite-calcite rocks*. Dark-brown, yellow, light-gray vein bodies (up to 150 long and n-30 cm wide), rock textures are massive, brecciform, inequigranular.

4. *"Early" fluorite-calcite rocks* are light-brown, yellow fine-grained and forms elongated bodies up to 20 cm wide.

A fluid inclusions study was carried out in fluorite grains from 1-3 types of fluorite-bearing rocks. Unfortunately, these studies can not be conducted for rocks of type 4, as the rocks are highly modified and there are no objects for the fluid inclusions study. Primary, pseudo-secondary and secondary (Roedder, 1984) crystal-fluid inclusions (CF), multiphase inclusions (VLS) and vapor-liquid inclusions (VL) are recognized in the doubly polished sections. Rock-forming fluid compositions and P-T parameters were found out by microthermometry and Raman-spectroscopy.

Fluorite from *quartz-fluorite rocks* contain primary CF inclusions. They have negative crystal shape and size up to 12 μm. There are ankerite, celestite, thenardite, calcite, magnetite, bastnasite and amphibole as mineral phases. Gaseous phase contains CO_2. Homogenization temperatures are in range of 500-**530**°C, salinities 59.8-**63.9** wt.% $NaCl_{equiv}$. Secondary VL inclusions are located in recrystallization rims and have irregular forms and size up to 15 μm. They are characterized by moderate homogenization temperatures (280-290°C) and salinities (6.5-13.9 wt.% $NaCl_{equiv.}$).

Fluorite-apatite-celestine rocks. Primary VLS inclusions have rounded or negative crystal shapes and size 7-15 μm. Chloride, calcite, parasite, anhydrite, celestite, strontianite, magnetite and amphibole were defined as mineral phases. Carbon dioxide is in the gaseous phase. Homogenization temperatures are 390-**470**°C. Salinities are 46.4-55.8 wt.% $NaCl_{equiv.}$ Pseudosecondary VL inclusions are rounded or elongated form up to 14 μm long. They comprise $CO_2 \pm CH_4 \pm N_2 \pm H_2$ in gaseous phase. Liquid phase are an aqueous solution, containing $FeCl_2$ and $CaCl_2$ (eutectic temperatures -48…-42°C). Homogenization temperatures of pseudosecondary VL inclusions were got in the interval 420-430°C. The values of salinity fell within the range 2.2-2.6 wt.% $NaCl_{equiv.}$ VL secondary inclusions are rounded and rather small (3-7 μm). The composition of the gaseous phase is determined as $CO_2 \pm H_2$.

This type of inclusions are described homogenization temperatures 230-250°C and salinities 2.4-3.6 wt.% $NaCl_{equiv}$.

Fluorite from the *fluorite-calcite rocks* holds primary VLS, primary and secondary VL inclusions. Primary VLS inclusions are elongated or rounded (up to 15 μm long). Multiphase inclusions from fluorite-calcite rocks are marked by chloride-siderite-phosphosiderite-calcite-amphibole-magnetite mineral phase composition. Liquid phase composition is defined as SO_4^{2-} $+CO_2+H_2O$. The dominant component of the gaseous phase is carbon dioxide. The dominant component of the gaseous phase is carbon dioxide. Homogenization temperatures are 530-550°C, salinities – 63.8-66.8 wt.% $NaCl_{equiv}$. Primary VL inclusions are rounded shape and size up to 12 μm. They contain $CO_2+H_2O\pm H_2S$ gas and Na-K-chloride solution. Primary VL inclusions are specified by homogenization temperatures (245-275°C) and salinities (5.7-6.2 wt.% $NaCl_{equiv}$.). Secondary VL inclusions are smaller (3-7 μm) and have isometric forms. These inclusions are differ in low homogenization temperatures 185-220°C and salinities 4-5 wt.% $NaCl_{equiv}$.

Chemical composition of the fluorites from different types of fluorite-bearing rocks was examined by LA-ICP MS.

The fluorites from *quartz-fluorite rocks* have the highest and variable REE concentrations (total REE=3670-144356 ppm). All analyses exhibit an enrichment in LREE to varying degrees ($(La/Yb)_{cn}$=27-961.3) and slightly negative Eu anomalies ($(Eu/Eu^*)_{cn}$=0.6-0.8).

The fluorites from *fluorite-apatite-celestine rocks* are moderate in REE (207-5854 ppm). It should be noted the steady enrichment of LREE for this fluorite type ($(La/Yb)_{cn}$=30-204). The fluorites from fluorite-apatite-celestine rocks have slightly positive Eu anomalies (Eu/Eu* = 0.9-1.3).

The REE contents in fluorites from the *calcite-fluorite veins* are the lowest ones and vary in the range of 22-197 ppm. The chondrite-normalized REE plots are rather flat ($(La/Yb)_{cn}$=0.6-59), in some cases with reverse skew.). The majority of the studied samples have a positive Eu anomaly ($(Eu/Eu^*)_{cn}$=0.9-2.3).

The results suggest that rock-forming fluids of fluorite-bearing rocks of the Mushugai-Khuduk complex are highly concentrated, mainly sulphate, and enriched in carbon dioxide. Homogenization temperatures of primary fluid inclusions are varying from 550°C for brine fluid inclusions (CF and VLS) to 250°C for aqueous ones (VL). This data suggests that the formation temperatures of fluorite-bearing rocks correspond to high-temperature hydrothermal conditions. According to the study of secondary fluid inclusions, low-temperature moderate salted fluids altered these rocks. Geochemical studies have shown that the fluorite from the Mushugai-Khuduk complex contains high levels of rare earth elements, especially LREE. Moreover, different types of rocks differ in the level of REE concentration and the presence of negative or positive europium anomaly. This suggests a complex history of the formation (participation of fluids of different genesis and changing redox environment) of different types of fluorite-bearing rocks of the Mushugai-Khuduk complex.

This work was carried out on state assignment of Sobolev Institute of Geology and Mineralogy SB RAS (No.0330-2016-0002). LA-ICP-MS analyses were supported by the Russian Science Foundation, grants No. 19-17-00013 and No 19-17-00019. Microthermometry of fluid inclusions was financially supported by the grant of President of the Russian Federation (MK-1113.2019.5).

References

Nikolenko A.M., Redina A.A., Doroshkevich A.G., Prokopyev I.R., Ragozin A.L., Vladykin N.V. The origin of magnetite-apatite rocks of Mushgai-Khudag complex, South Mongolia: Mineral chemistry and studies of melt and fluid inclusions // Lithos, 2018, Vol. 320-321, p. 567-582.

Roedder E. Fluid inclusions // Reviews in Mineralogy. Mineralogical Society of America. 1984, Vol. 12.

Samoilov V.S., Kovalenko V.I. Complexes of Alkaline Rocks and Carbonatites in South Mongolia. Nauka, Moscow, 1983 (in Russian).

Vladykin N.V. 2013. Petrology and composition of rare-metal alkaline rocks in the South Gobi Desert (Mongolia) // Russian Geology and Geophysics. 2013, Vol. 54 (4), p. 545-568.

METALLOGENY OF MEZOPROTEOZOIC SUWAŁKI ANORTHOSITE MASSIF, NE POLAND

Ruszkowski M.

Faculty of Geology, University of Warsaw Poland, ruszkowskimichal@wp.pl

The ore mineralization in the Suwałki Anorthosite Massif (SAM) is located within the rocks belonging to the AMCG suit rocks (anorthosite - mangerite - charnockite – granite rapacivi). They are associated with the tectonic structures of deep splits in the Earth's crust. The Suwalki massif covers an area of 250 km2 (Wiszniewska, 2002), and its central part is made up of massive anorthosites surrounded by a ring of norites and gabbronorites. In the area of norits and anorthites, there are located ilmenite-magnetite rocks (ferrolytes) with accompanying sulphide polymetallic mineralization (Fe-Cu-Ni-Co). These rocks were the object of research during the planning of the Suwalki Iron Ore District in the 1960s and 1970s. The result of this works was the determination of two ore fields: Krzemianka and Udryn and two prospective areas: Jeleniewo and Jezioro Okragle. These deposits have a lenticular structure and are intersected with a network of granitoid veins. The main ore levels are located at a depth of 800 to 1,200 m below ground level. The main ore minerals are titanium magnetite, ilmenite and sulphides: pyrrhotite, pyrite, chalcopyrite and pentlandite. About 1.5 billion tons of Fe-Ti-V ore have been documented in the deposits. Ores contain approx. 28% iron, 7% titanium oxides and 0.3% oxide peroxide, and 1-4% Fe-Cu-Co-Ni sulphides and other strategic elements (Wiszniewska, 2002).

The iron ores are made of ilmenite-magnetite rocks surrounded by anorthosite, norits, gabbronorites. Ores contain 25-90% by volume of ore minerals. Deposits are penetrated by veins of granitoids-pegmatite as well as numerous hydrothermal carbonate and quartz veins. The ore bodies take the form of decks, nests or lenticular forms, falling at an angle of about 45o. Presented types of ore bodies are variable and depend on the rocks that host them. A significant influence on the form of ore mineralization had two large magmatic events related to diapiric plutonium movements and injection of granitoid-pegmatite veins into the formation of tectonic fractures.

Ore mineralization has a high variability of composition and forms. The dominant ore mineral in rich ore zones is titanomagnetite. The sizes of magnetite grains vary between 1-8 mm. In the titanomagnetite grains, the dissolution of ilmenite sipes occurs in three planes, ulvöspinel and spinel with the composition of hercynite - pleonast in the form of clusters of grains, lenses and needle-like precipitates. The proper spinel is the first of the products of demixing in titanomagnetite. The changing physicochemical conditions during the evolution of the primary ore mineral alloy influenced the distribution of trace elements in magnetite and ilmenite. Under conditions of high oxygen pressure (fO2), unstable ulvöspinel containing vanadium was transformed into metastable protoilmenite and ilmenite, until the final stage of vanadium passed into the magnetite structure (Speczik et al., 1988, Wiszniewska, J. 1993). The second, most abundant ore mineral is ilmenite. It constitutes on average about 10-15% of the volume of ilmenite-magnetite rocks. The greater part of the original ilmenite crystallized simultaneously with the titanomagnetite or formed during the decomposition of a solid solution of titanomagnetite (Speczik et al., 1988). Ilmenite grains reach considerable size, even 0.5-1.0 cm, but on average they have 1-3 mm and are characterized by a higher degree of automorphism (Wiszniewska, 1993). Ilmenite is often accompanied by pleonast and hercynite spinels. The incorporation of vanadium into the ilmenite structure was associated with a drop in the system temperature and the formation of a lenticular hematite-dehiscence system in ilmenite grains.

In Suwalki Fe-Ti-V ores and rocks surrounding them in significant amounts of iron, copper, nickel and cobalt sulfides occur. The most commonly encountered sulphides are pyrite, pyrrhotite, chalcopyrite and pentlandite. They constitute from 1 to 4% of the rock volume. The ratio of oxides to sulphides is about 10: 1, and silicates up to as much as 35: 1 (Wiszniewska, 1993). The content of sulphides in the ore series and beyond is variable. In ores, the amount of sulphides is higher and it is dominated by pyrrhotite, chalcopyrite and pentlandite. There is also secondary pyrite, but its concentrations are mainly associated with cracks or hydrothermal zones. In the irregular series, pyrite, marcasite and chalcopyrite and relics of pyrrhotite are often replaced by pyrites and carbonates (Wiszniewska, 2002).

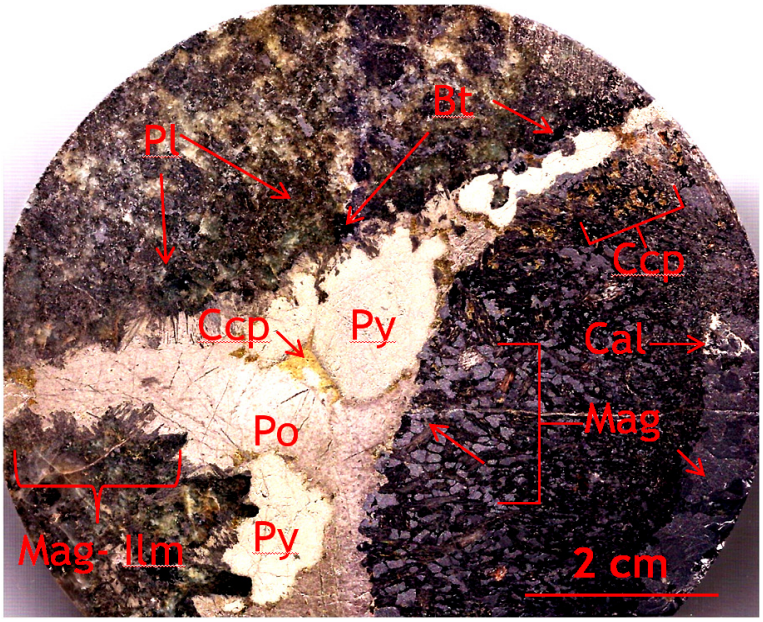

Figure. 1. Cross-section of the core of the Krzmianka 72 borehole. In cross section, a visible multi - phase vein with massive sulphides (Pl - plagioclases, Py - pyrite, Po - pyrrhotite, Ccp - chalcopyrite, Bt - biotite, Cal - calcite, Mag - magnetite, Ilm - ilmenite).

Observations and investigations carried out in the micro area showed the following percentage composition of sulphides in ores: 77% pyrrhotite, 9% pyrite, 8% chalcopyrite, 3% pentlandite and 3% inferior cubanite, bornite, sphalerite and other sulphides from the Ni-Co group. These minerals are in the form of hypautomorphic or xenomorphic crystals. The mineral composition of sulphides present in ores is slightly different than in non-ore rocks. Many of sulphide also occur as inclusions and interstitial fillings. Nanoconcentrations of REE (La, Ce, Nd), PGE, Au and zircon minerals are often present in Fe-Cu-Co-Ni sulphides as dispersed mineralisation. Their size ranges from 10-150 µm or in some cases up to 250 µm. (Ruszkowski, 2018, Ruszkowski Wiszniewska 2018).

The unique grain and nest-like accumulations of REE (La, Ce and Nd) nanoforms and precious (gold, platinum) elements were described from the SAM. The dimensions of these forms vary from 15 to 175 µm in diameter in cubanite, bornite, sphalerite, reaching 450µm in diameter in chalcopyrite. In the hydro-thermally modified ore mineralization, separate small dispersed minerals of Te are visible. Numerous small inclusions of Te-minerals (0.4–0.7 mass%) were identified in hydrothermal Fe-Cu-Co-Ni sulphides, especially in pentlandite. They are grouped in small forms that are elongated directly along with the flow of hot solutions, 2–4 mm in size of a single inclusion. New results of polymetallic and precious metal sulphides together with dispersed REE mineralization may increase the economic value of the documented Fe-Ti-V deposits within the SAM. (Ruszkowski, 2018). Geochemical studies have shown large enrichment of sulphides in mercury. The average content of mercury ranges from 85 to 150 ppm. In some cases, it exceeded even more than 1000 ppm.

Zirconium-hafnium rims were discovered and described for the first time within the Suwalki Anorthosite Massif They are observed at boundaries of Fe-Ti oxides ilmenite, hematitoilmenite and titanomagnetite with plagioclases. The most frequent forms reach 80–250 µm in length and 4–30mm in width. These are narrow rims covering even up to 70% ore mineral grains. The most spectacular forms were “blown candle flame” structures. Their average width ranges from 20 to 45µm and the length exceeds 350µm. Chemical composition analysis was carried out on the largest clusters of zircon crystals/rims which show high local enrichment in Hf (0.5–0.8% by weight). The boundaries of these crystals are cracked and blurry. This may suggest their participation in later fluids inflow processes within the rocks. The enrichment in hafnium content in zircon grains is related to a significant reduction in the amount of Th, U and Pb and increased amounts of Ti and Fe in zircon rims. A large variety of forms and variability of their chemical composition point to a complex physical chemical origin process. (Ruszkowski, Wiszniewska 2018).

Apart from the main sulphides, secondary modifications, such as sphalerite or millerite, linneite and others, are also observed. These minerals co-exist with primary sulphides and Fe-Ti oxides in the form of common aggregates and sprays inside the primary ores. In addition, they create monomineral

aggregates and fill interstitial spaces. They also act as binders of tectonic breccias, they fill impregnations and small veins (Wiszniewska, 1990, 2002). In addition to ore zones, sulphides in anorthosite, gabbronorite, norite and diorite occur in a dispersed form or small veins filling cracks. The most common are single grains or several grain aggregations of pyrrhotite, pyrite and chalcopyrite. In addition to the above-mentioned main sulphides, the sub-existence of mackinawite, linnaeite, bravoite, violarite, sphalerite, bornite and chalcocite was also found (Wiszniewska, 1993).

The described structures of oxides and sulphides are an indicator of the processes and order of formation of these minerals. On this basis, three stages of formation of ore minerals were distinguished (Speczik et al, 1988, Wiszniewska, 1993,2002):

1. Magmatic - the early and late magma phase has been distinguished.
2. Postmagmatic - divided into autometasomatosis, sulfurization.
3. Hydrothermal - a process of migration of hydrothermal fluids associated with granitoid veins intruding in the massif.

Along with the decrease of the melt temperature and the crystallization of its components, in the changing conditions of oxygen and sulfur pressure, minerals with secondary structures were formed. In the titanomagnetite ores of the Suwalki massif, the following structures have been distinguished: cloth-texture, spinel in magnetite and ilmenite, ilmenite in magnetite, magnetite in ilmenite, hematite in ilmenite, pentlandite and chalcopyrite in pyrrhotite, cubanite, mackinawite and ilmenite in chalcopyrite, millerite in ilmenite, mackinawite and chalcopyrite in pentlandite. Another group of crystalline structures formed under these conditions were crystalline structures known as replacement structures created under the influence of secondary physicochemical processes leading to the replacement of primary minerals with new minerals.

Replacement processes include the ilmenitization process in which ilmenite and spinel are formed; the process of sulphidization, which results in pyrite, marcasite, chalcopyrite, magnetite, bravoite, violarite, millerite, bornite and chalcocite, and others (Speczik et al, 1988, Wiszniewska, 2002). The term "replacement process" is understood as the reaction between sulphides and oxides, leading to the formation of magnetite, pyrite, chalcopyrite and hematite, also the process of replacing ore minerals by carbonate mineralization and partly by the graphite. The boundaries between the grains during the substitution reaction are sharp, uneven and corrosive. The most susceptible to replacement processes are cracks, grain boundaries and their cleavage zones.

The problem of metallogeny of Mezoproteozoic Suwałki Anorthosite Massif is a very complex issue and still undergoing extensive discussion among researchers. The most important metallogenic features of SAM rocks are: the conditions of formation and location of Fe-Ti-V ores in the parent rocks, petrographic-mineralogical-geochemical composition, processes of transformation, identified manifestations of ore mineralization and its relation to surrounding rocks.

This work was supported NCN project 2015/17/B/ST10/03540 and Warsaw University Foundation project 35/04/2017.

References

Ruszkowski M., 2018 – Wstępne wyniki badań mineralizacji Au-Ag-Te, REE i PGM w złożach Fe-Ti-V suwalskiego masy-wu anortozytowego (północno-wschodnia Polska). 2018 Warszawa Prz. Geol., 66, 4: 219–221.

Ruszkowski M., Wiszniewska J., 2018 − Wstępne rozpoznanie obwódek cyrkonowo-hafnowych wokół minerałów kruszcowych w złożach Fe-Ti-V w suwalskim masywie anortozytowym (północno-wschodnia Polska). 2018 Warszawa Prz. Geol., 66, 2: 107–110.

Speczik S., Wiszniewska J., Diedel R. Minerals, exsolu-tion features and geochemistry of Fe-Ti ores of the Suwałki district (North-East Poland). 1988, Mineralium Deposita, 23: 200-210.

Wiszniewska, J. Mineralizacja kruszcowa w skałach masywu suwalskiego 1993 Przewodnik LXIV zjazdu Polskiego Towarzystwa geologicznego., 29-36

Wiszniewska, J. Wiek i geneza rud Fe-Ti-V i skał towarzyszących w suwalskim masywie anortozytowym (północno-wschodnia Polska). 2002, Biuletyn Państwowego Instytutu Geologicznego. Nr 401.

INFLUENCE OF ALKALINE FLUID ON MINERAL ORE FORMATION IN ARGILLIZATION ZONE OF PRESENT-DAY PAUZHETKA HYDROTHERMAL SYSTEM (SOUTH KAMCHATKA)

Rychagov S.N.[1], Sandimirova E.I.[1], Chernov M.S.[2], Kravchenko O.V.[1]

[1]*Institute of Volcanology and Seismology FED RAS, Petropavlovsk-Kamchatsky, Russia, rychsn@kscnet.ru*

[2]*Lomonosov Moscow State University, Faculty of Geology, Moscow, Russia,* chernov@geol.msu.ru

Drilling of wells in the East-Pauzhetka thermal field and a comprehensive mineral-geochemical study of the altered rocks in the base of hydrothermal clays allowed diagnosis of alkaline-type mineralization as a reflection of the influence of deep-hole metal-bearing solutions on the discharge zone of thermal waters.

INTRODUCTION. The behaviour of rare-earth and other metals during metamorphism and in a hydrothermal environment has been in focus of many scientists (Karpov et al., 2018; Pekov, 2005; Chudaev et al., 2016; Wood, 2003; et al.). Argillized rocks and hydrothermal clays widespread in volcanic areas and having special physiochemical (including sorption), geochemical and other properties evoke a great interest in connection with study of the mechanisms of transport and concentration of metals (Eroshev-Shak, 1992; Korobov, 1994; Osipov, Sokolov, 2003; Razumova, 1977; Hemley, Jones, 1964; Reyes, 1990). Discharge of alkaline solutions in the zone of rock argillization occurs quite rarely in the modern hydrothermal systems of volcanic island arcs (Rychagov et al., 2017b) and it is probably a sequence of the influence of a reduced metalliferous fluid on the upper horizons of the earth's crust. The East-Pauzhetka thermal field serves as a model site used for study by a group of authors (Rychagov et al., 2017a; Rychagov et al., 2017, 2018), whose additional results are presented in this work.

DESCRIPTION OF EAST-PAUZHETKA THERMAL FIELD. The East-Pauzhetka thermal field belongs to the flank of the Pauzhetka hydrothermal system and is situated on the western slope of the Kambalny volcanic ridge that is characterized as a resurgent tectonic magmatic high in the Pauzhetka volcanic-tectonic depression (The Long-Lived…, 1980). The thermal field is confined to a circular upstanding block of the Quaternary age and stretched along radial tectonic faults (Structure ..., 1993). The overall dimensions of the field are ≥ 250 × 500 m, and the hottest area contoured by the 20 °C isotherm at a depth of 0.6-0.8 m is 100 × 200 m. Thermal manifestations are represented by steaming soils, steam-gas jets, mud-water boiling pots and warm ponds. The maximum temperatures of the waters that are discharged on the surface are 98 °C, the temperatures of soils are 105-107 °C, the temperatures of steam-gas jets are 108-109 °C. The thermal waters are acid sulphate and low-acid hydrocarbonate-sulphate with a broad cation composition and a general mineralization that is not higher than 0.8 g/l. Steam condensate has a similar chemical composition. The soils are hydrothermal clays that form a continuous cover and stretch far beyond the boundaries of the present-day hot area (Rychagov et al., 2017a).

LITHOLOGY OF HYDROTHERMAL CLAY MASS AND ITS BASE. The clay mass has a layered structure. The upper horizon is a typical sulphuric acid leaching zone. The clays are composed of kaolinite, hydroxides and Fe and Ti oxides, Fe-Ca-Mg-... sulphates, opal, and chalcedony. There are patches of the preserved pseudomorphic structure of block jointing of source rocks – lavas of andesites. The horizon thickness ranges from 50-80 cm in the hot area and reaches up to > 300-350 cm near boundaries. Below is a horizon with an average thickness of 150 cm composed of montmorillonite soft clays. It is characterized by a large number of lenses, films and thin streaks of opal and α-quartz dispersed in the main mass of pyrite. As described earlier (Rychagov et al., 2017b), the horizon of soft clays acts as a water-confining stratum and a thermal insulator, and it plays a crucial role in the formation of mineral ore associations within the structure of the East-Pauzhetka thermal field. Two zones were penetrated under this horizon in Rudniy (“Ore”) area (from bottom to top): silicon-carbonate-sulphide and phosphate-alumosilicate-sulphide ones. Towards the western boundary of the field, the zones converge into a single zone with a more complex composition. A horizon of “dry” sulphidized clays is also extended along the strike of the thermal field. The deposits

are smectite clays. The upper layers of the horizon are marked by transition from kaolinite to smectite with abundance of scattered coarsely crystalline pyrite (up to 2–3 mm) and semidecomposed andesite debris. Presence of fragments (up to 15–25% by volume) saturated with a siliceous substance is distinctive: they form interlayers, lenses, and "spots" in the main matrix. Most likely, the fragments were formed metasomatically through substitution of andesite debris by silica minerals, as well as smectites, etc. The deposits of the horizon near field boundaries are typical "blue clays" (saturated with sulphides), with the thickness of the horizon increasing.

The base of the clay mass is represented by metasomatic breccias and fissured andesites. This paper mainly focuses on description of hydrothermal and metasomatic alterations in these rocks. The breccias include rounded debris fragments of metasomatites over andesites; the cement is composed of hydrothermal minerals (opal-chalcedony-carbonates-zeolites-alumosilicate-sulphides-phosphates, etc.). In addition to the general alteration of the main mass, there are 3-5 to 20 cm thick zones (veins, streaks) composed of associations of secondary minerals. Fissured andesites are also intensively argillized and are broken up by quartz-carbonate-zeolite zones as well as by zones with more complex compositions. The extent of alteration, number and thickness of zones increase with depth, which is consistent with the geophysical data: rocks in this region of the section have an elevated electrical conductivity (Feofilaktov et al., 2017).

Core holes were drilled in the hot area of Vostochniy ("Eastern") and in the relatively cold western boundary (Rudniy area) of the thermal field.

MINERALIZATION OF ROCKS IN CLAY MASS OF THE VOSTOCHNIY AREA. The rocks are almost completely altered and represented by a zeolite-carbonate-chlorite-silica-alumosilicate aggregate both in the main mass (in cement and fragments of breccia "debris") and in interstices (Figure). Primary minerals include: plagioclases (An_{30-70}), titanium-containing augite, amphibole (hornblende), magnetite and titanomagnetite (TiO_2 - 1.9-17 wt. %), manganese-bearing ilmenite (MnO – 2.6-20.9 wt. %), chrome-bearing spinel (MgO – 3-6; Al_2O_3 – 8-18; Cr_2O_3 – 1-23.4 wt. %), single hypidiomorphic grains of quartz up to 1 mm in size with tiny inclusions of potassium feldspar (PFS). Ilmenite forms intergrowths with titanomagnetite, zircon and apatite. Titanium-calcium-siliceous mixtures, sphene and rutile are formed in place of primary titanium-bearing minerals, whereas zeolite is deposited in place of leached fragments. Spinelids are partially substituted by pyrite and often overgrown with pyrite rims. Probably, the extensive occurrence of Mg-Fe chlorite, PFS, quartz, calcite and zeolites can be attributed to the earliest hydrothermal-metasomatic transformations of rocks. Following minerals and mineral phases prevail among the later hydrothermal formations: calcium and sodium calcium zeolite, calcium and magnesium-carbonate, Fe-Mg chlorite, smectite, chlorite-smectite, alumosilicate formation of complex composition, siliceous alumosilicate and zeolite-chalcedony concretions as irregularly-shaped fragments. For the first time in study of the base rocks of the thermal field clays, the formation of relatively large (up to 0.1–0.2 mm) chalcopyrite precipitates and a high As content (up to 5 wt. %) in pyrite were identified. Ca hydrosilicate (possibly, okenite) – a rather rare hydrothermal mineral – was found for the first time too. It fills pores and fissures in association with quartz, calcite and zeolites. Apparently, the formation of Ca hydrosilicate reflects the most recent stage of hydrothermal alterations in the rocks of this area's section.

MINERALIZATION OF ROCKS IN CLAY MASS OF THE RUDNIY AREA. The area is located in the region of transition from the hottest part to the cooling one of the East-Pauzhetka thermal field. Here, zones with phosphate-alumosilicate-sulphide and siliceous-carbonate-sulphide mineralization were detected under the horizon of soft clays (Rychagov et al., 2017a, b). The section of the mass of hydrothermal clays is, in general, typical for this thermal field. The source rocks are represented by intensively altered and fissured andesitic lavas. Presence of hydrothermal zones (constituting more than 50 % of the thickness of the lower part of the section) completely filled with secondary minerals is distinctive. The composition of the altered rocks and hydrothermal zones is mainly the same as that of the Vostochniy area and is represented by zeolites, calcite and magnesium-bearing calcite, chlorites, opal, F-Cl-apatite. The primary ore phases have hardly remained: sphene, chlorite, pyrite and others have evolved upon them. Pyrite often contains As (up to 3-5 wt. %): arsenic is included in the composition of the bands localized along the growth zones of pyrite crystals or forms

spot areas within its structure. At the same time, the secondary mineralization of this section differs significantly. The composition of zeolites is more diversified: potassium-calcium and calcium-potassium-sodium zeolites are formed against the background of prevailing Ca-zeolites. Smectites are sparsely present among alumosilicate, and Fe-Mg chlorites prevail sometimes with a more complex composition that apparently reflects transition to chlorite-illites and hydromica. Also, this section's hydrothermal zones feature the presence of siliceous-ferruginous "concretions" as veins, lenses, crushed fragments, strip-like rims around andesite debris. The quantity of this material sharply increases towards the base of the penetrated section and makes up to 50 % of the volume of the zones of hydrothermal alterations. The siliceous-ferruginous “concretions” are formed during the first stage of hydrothermal metasomatic transformations of the base rocks of the Rudniy area clay mass. During following stages, they are crushed, fractures are filled by zeolites, carbonates, quartz, sulphides and other minerals, fragments “dissolve”, ferrous iron transforms into ferric iron, and other processes occur.

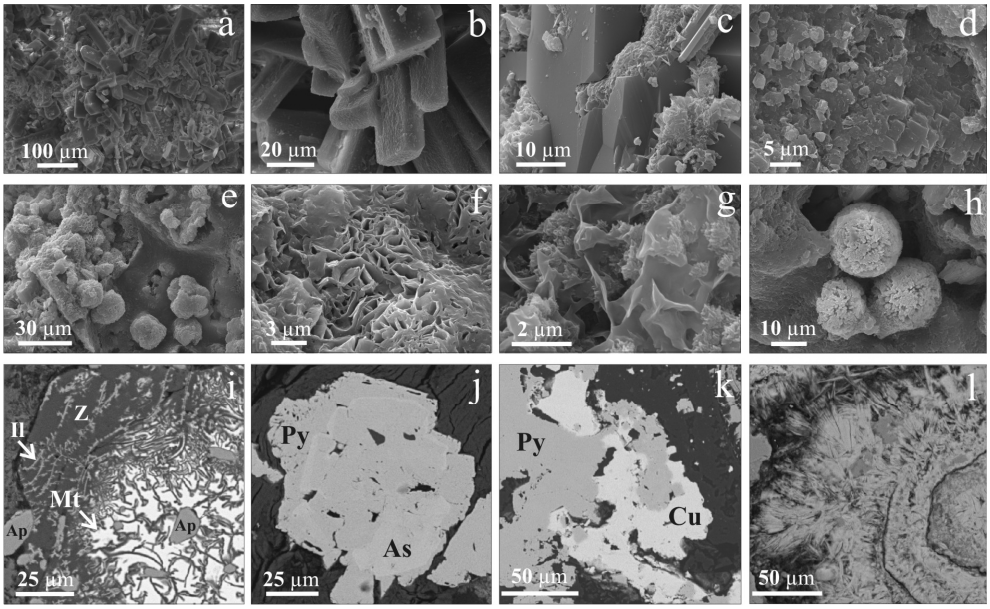

Figure. Micromorphology, alteration and formation of minerals at the base of the East-Pauzhetka thermal field clays – according to research data derived using LEO 1450VP SEM equipped with INCA EDS (a – h); and VEGA 3 SEM, equipped with X-MAX 80 EDS (i – l): a – Ca and Ca-Mg zeolites filling veinlets; b – zeolites in the “envelope” of smectite and smectite bridges cementing crystals of zeolites; c – dissolution of zeolite crystals and formation of complex alumosilicate composition aggregates; d – carbonate base of veinlet with the formation of separate grains of Ca-K-Na zeolite; e – silicon-magnesia concretions in the alumosilicate mass; f – siliceous-ferruginous cellular structures; g – the same with the formation of alumosilicate lumpy fragments at the contact of the cells; h – siliceous (opal?) balls in pores among siliceous-zeolite mass; i – altered ilmenite in accretions with F-apatite (Ap), titanomagnetite (Mt) – in the centre of the grain, dendrites of ilmenite (Il) and zeolite (Z) along the edges; j — heterogeneous As distribution in zonal pyrite; k – accretion of chalcopyrite (Cu) with pyrite (Py); l – zonal structures of calcium hydrosilicate.

CONCLUSION.The description of the mineral composition of the altered rocks and hydrothermal zones in the base of the clay mass of the East-Pauzhetka thermal field indicates a thorough transformation of the source rocks, an increase in temperature and alkalinity of the environment towards the base of the penetrated section. Mineralogical and geochemical zoning is distinguished as follows (from top to bottom): kaolinite-smectites → smectites → smectite-chlorites → zeolites-carbonates-chlorites → zeolites-illite-hydromica. The formation of the lower zones is related to the addition of alkaline and alkaline-earth elements (first of all, K and Ca) and some ore elements (As and, probably, rare-earth ones). Apparently, the formation of the zone sequence reflects the impact of an alkaline or a highly alkaline fluid on the argillization zone of the East-Pauzhetka thermal field.

This work was supported by the Russian Foundation for Basic Research (Project No. 19-05-00102) and the Far East Branch of the Russian Academy of Sciences (Project No. 18-2-003). The research was conducted by means of the equipment received in framework of implementation of M.V. Lomonosov State Moscow University Development Program.

References

Long-Lived Center of Endogenic Activity in South Kamchatka. Moscow: Nauka, 1980. 172 p.

Eroshev-Shak V.A. Hydrothermal Subsurface Lithogenesis of Kuril-Kamchatka Region. Moscow: Nauka, 1992. 131 p.

Karpov G.A., Schröder P.E., Nikolayeva.A.G. Geochemistry of rare-earth elements (La, Ce) in thermal waters of Uzon-Geyzernaya hydrothermal system (Kamchatka) // Geology and Geophysics. 2018. Vol. 59. No. 8. P. 1152-1163.

Korobov A.D. Hydrothermal Lithogenesis in Regions of Surface Volcanism. Author's abstract of Doctoral (Geol-Mineral) Dissertation. Moscow: Geological institute, 1994. 50 p.

Osipov V.I., Sokolov V.N. Clays and their Properties. Composition, Structure and Formation of Properties. Moscow: GEOS, 2013. 576 p.

Pekov I.V. Genetic Mineralogy and Crystal Chemistry of Rare Elements in Highly Alkaline Postmagmatic Systems. Author's abstract of Doctoral (Geol-Mineral) Dissertation. Moscow: MSU, 2005. 50 p.

Razumova V.N. Old Crusts of Weathering and Hydrothermal Process. Moscow: Nauka, 1977. 156 p.

Rychagov S.N., Davletbayev R.G., Kovina O.V. Hydrothermal clays and pyrite of geothermal fields: significance of modern endogenic processes (South Kamchatka) in geochemistry // Volcanology and Seismology. 2009. No. 2. P. 39-56.

Rychagov S.N., Sergeyeva A.V., Chernov M.S. Mineral Associations of the Clay Basement as Indicators of the Pauzhetka (Kamchatka) Hydrothermal System Fluid Regime // Pacific Geology. 2017. Vol. 36. No. 6. P. 90-106.

Rychagov S.N., Sergeyeva A.V., Chernov M.S. Specific Mineral Associations of Hydrothermal Shale (South Kamchatka) // Proceedings of Academy of Sciences. 2017. Vol. 477. No. 1. P. 81-86.

Structure of geothermal system. Moscow: Nauka, 1993. 298 p.

Feofilaktov S.O., Rychagov S.N., Bukatov Yu.Yu. et al. New data on the structure of the zone of discharge of fluids in the area of the Eastern Pauzhetka thermal field (South Kamchatka) // Volcanology and Seismology. 2017. No. 5. P. 36-50.

Chudayev O.V., Chelnokov G.A., Bragin I.V. et al. Geochemical Features of the Behaviour of the Main and Rare-Earth Elements in the Paratunskaya and Bolshebannaya Hydrothermal Systems of Kamchatka // Pacific Geology. 2016. Vol. 35. No. 6. P. 102-119.

Hemley J.J., Jones W.R. Chemical Aspects of Hydrothermal Alteration with Emphasis of Hydrogen Metasomatism // Econ. Geol. 1964. V. 59. No. 4. P. 238-369.

Reyes A.G. Petrology of Philippines Geothermal Systems and the Application of Alteration Mineralogy to their Assessment // Journal of Volcanology and Geothermal Research. 1990. V. 43. P. 279-309.

Rychagov S.N., Sandimirova E.I., Chernov M.S., Sergeyeva A.V. Formation of Alkaline Mineralization in Acid Leaching Zone of Pauzhetka Hydrothermal System (South Kamchatka) // Proceedings of XXXV International Conference “Magmatism of the Earth and Related Strategic Metal Deposits. Moscow, 3-7 September, 2018. Moscow: GEOKHI RAS, 2018. P. 255-259.

Rychagov S.N., Sergeyeva A.V., Chernov M.S. Mineral Ore Formation in Argillizated Rocks of Pauzhetka hydrothermal system of South Kamchatka // Proceedings of XXXIV International Conference “Magmatism of the Earth and related strategic metal deposits”. Miass, 4-9 August 2017. Moscow: GEOKHI RAS, 2017. P. 213-215.

Wood S.A. The Geochemistry of Rare Earth Elements and Yttrium in Geothermal Waters // Volcanic, geothermal and ore-forming fluids: rules and witnesses of processes within the Earth. Society of Econom. Geologists. 2003. V. 10. P. 133-158.

MANTLE PLUME ORIGIN OF THE NEOARCHEAN KEIVY ALKALINE PROVINCE: EVIDENCE FROM 2.68 Ga MAFIC DYKE SWARMS IN THE MURMANSK CRATON

Samsonov A.V.[1], Stepanova A.V.[2], Salnikova E.B.[3], Arzamastsev A.A.[3], Larionova Yu.O.[1], Egorova S.V.[2], Veselovskiy R.V.[4], Erofeeva K.G.[1], Stifeeva M.V.[3]

[1]Institute of Geology of Ore Deposits, Petrography, Mineralogy and Geochemistry, Russia, samsonovigem@mail.ru

[2]Institute of Geology Karelian Science Centre, Petrozavodsk, Russia

[3]Institute of Precambrian Geology and Geochronology, Saint-Petersburg, Russia

[4]LomonosovMoscow State University, Moscow, Russia

The Neoarchean Keivy Alkaline Province (KAP) occur in the northeastern part of the Fennoscandia and usually considered as a part of the Kola composite terraine. The dominant A-type peralkaline granites, minor alkaline gabbro and syenite bodies associated gabbro anorthosites cover the area of about 2500 km^2. All rocks exhibit similar U-Pb zircon ages of 2.65-2.68 Ga (Mitrofanov et al., 2000; Zozulya et al. 2005; Vetrin, Rodionov, 2009). OIB geochemical and isotope features of alkaline gabbro and nepheline syenite together with anorogenic-type geochemistry of granites provide evidence for the mantle plume origin of KAP (Zozulya et al. 2001; Vetrin, 2018). The primary objective of our work is to place constraints on the age and isotope geochemical features of the mantle source regions that contribute to Neoarchean mafic magmatism throughout the NE Fennoscandian Shield. In order to gain important insight into the evolution of plume-driven magmatism we investigated mafic dyke in the Murmansk craton adjacent with KAP. Two types of the Neoarchaen (ca 2680 Ma) dykes, Pl-porphyrite and ferropicrite, were recognized in the northern part of the Murmansk craton along the Barents Sea coast area.

Plagioclase-phyric dolerite dykes outcrop from Dalnie Zelentsy to Savikha Bay. The 1 - 30 m thick dykes form a large (ca 150 km) radial swarm. Orientarion of dykes vary from 315-325° in Dalnie Zelentsy area to 10-15° in Savikha Bay. The center of the radial swarm could be projected to the Keivy terrain. Most dykes have porphyritic texture with a large (up to 12 cm) plagioclase phenocrysts in a fine-grained Cpx-Pl dolerite matrix. Three U-Pb (ID-TIMS) analyses of baddeleyite from dyke in the Dalnie Zelentsy area define a Discordia with an upper intercept age of 2692 ± 10 Ma (MSWD = 1.4). The closed age of 2680 ± 5 Ma have the aphyric high-Al dolerite dyke in Tryaschina Bay area. All dykes have a tholeiitic series affinity. Low concentrations of MgO, Fe_2O_3, TiO_2, Cr и Ni, SiO_2 and Al_2O_3 enrichment, relatively flat HREE and enriched LREE, strong negative Nb anomalies and εNd_T ranging from -0.5 to +0.4 are typical for these dykes. The Pl-porphyritic dykes are similar to doleritic dykes and gabbro-anorthosite intrusions around the Keivy terrain in terms of mineral, chemical and isotopic composition.

Ferropicritic dykes form NNE-trending large (ca 70 km in width) swarm exposed between Litsky cape and Savikha Bay. The dykes within this swarm vary in thickness from 0.5 to 20 meters. In the thick (20 m) and well-preserved dyke in Litsky cape, the quenching zone is represented by olivine porphyrites, its internal part comprises medium-grained massive kersutite-bearing olivine melagabbronorites. The other dykes have similar composition, but are strongly amphibolized. U-Pb (ID-TIMS) baddeleyite concordant age of 2680 ± 2 Ma from the Litsky cape dyke define the ferropicrite dykes crystallization age. All the dykes are enriched in MgO, Fe_2O_3, TiO_2, Cr, and Ni, have low Cr/Ni ratios, highly fractionated light and heavy REE patterns and positive εNdT values varying from +0.6 to +1.5. Interestingly, the geochemical and isotope features of the Neoarchaen ferropicritic dykes are close to the “classic” Paleoproterozoic (1.98 Ga) ferropicrites of the Pechenga structure (Hanski, Smolkin, 1989, 1995).

Available data indicate the single Neoarchean geodynamic event responsible for the origin of alkaline rocks of the KAP and tholeiite and ferropicrite magmatism in the Murmansk craton. This is supported by neighboring position of these coeval complexes, similarity of chemical composition of tholeiitic dykes and gabbro-anorthosites of the KAP, as well as the geometry of a radial swarm of tholeiitic dykes with proposed focal point in the KAP area.

Formation of alkaline granite, syenite and gabbro-anorthosite complexes of the KAP can be explained in terms of delamination of lithospheric keel, leading to rapid ascent of an asthenosphere (Martin, 2012). Decompression-induced lower depth melting of the asthenosphere diapir triggered the production of parental basic melts of the gabbro-anorthosite massifs. Coeval melting the lower crust produced alkaline granite, and probably syenite massifs.

It remains unclear whether the formation of ferropicritic magmas is related to this process, because it requires high degrees of melting of Fe-Ti enriched mantle source at a depth of the garnet stability area (> 150 km) (Goldstein, Francis, 2008; Zhang et al., 2017). Therefore, our further research is aimed to answer the question whether or not the delamination of lithospheric keel could generate Fe-Ti enriched deep source and its melting could produce ferropicritic magmas? Alternatively, whether the deeply born plume, which gave birth to ferropicrites, initiated the destruction of the lithosphere and it was responsible for the formation of igneous rocks of the KAP?

This work was supported by the Russian Science Foundation (Grant 16-17-10260).

References

Goldstein S.B., Francis D. The petrogenesis and mantle source of Archaean ferropicrites from the western Superior Province, Ontario, Canada // J. Petrol. 2008. V. 49. P. 1729–1753.

Hanski E.J., Smolkin V.F. Iron- and LREE-enriched mantle source for early Proterozoic intraplate magmatism as exemplified by the Pechenga ferropicrites, Kola Peninsula, Russia // Lithos. 1995. V. 34. P. 107-125.

Hanski E.J., Smolkin V.F. Pechenga ferropicrites and other early Proterozoic picrites in the eastern part of the Baltic Shield // Precambrian Research. 1989. V. 45. P. 63-82.

Martin R.F. The petrogenesis of anorogenic felsic magmas and AMCG suites: Insights on element mobility and mutual cryptic contamination from polythermal experiments // Lithos. 2012. V. 151. P. 35–45.

Mitrofanov, F.P., Zozulya, D.R., Bayanova, T.B. & Levkovitch, N.V. The world's oldest anorogenic peralkaline granite magmatism in the Keivy structure of the Baltic shield // Doklady Earth Sciences. V. 374. P. 238–241.

Vetrin V. R., Rodionov N. V. Geology and geochronology of neoarchean anorogenic magmatism of the Keivy structure, Kola Peninsula // Petrology. 2009. V. 17. P. 537-557.

Vetrin V. R. Isotope-geochemical systematics (Sm-Nd, Lu-Hf) of Neoarchean subalkaline and alkaline rocks of the Keivy structure (Kola Peninsula): their age and genetic relations // Zapiski RMO. 2018. Pt. CXLVII. N 4. P. 1-13.

Zhang J.B., Liu Y.S., Ling W.L., et al. Pressure-dependent compatibility of iron in garnet: Insights into the origin of ferropicritic melt // Geochim.Cosmochim.Acta. 2017. V.197. P.356–377.

Zozulya D.R., Bayanova T.B., Eby N.G. Geology and age of the late Archaean Keivy alkaline province, NE Baltic Shield // The Journal of Geology. 2005. V. 113. P. 601–608.

Zozulya D.R., Eby N.G. Bayanova, T.B. Keivy alkaline magmatism in the NE Baltic Shield: evidence for the presence of an enriched reservoir in Late Archaean mantle // 4th International Archaean Symposium 2001. Volume: AGSO - Geoscience Australia, Record 2001/37.

PETROGRAPHY, MINERALOGY AND GEOCHEMISTRY OF EFFUSIVE ALKALINE ROCKS OF THE NEPHELINITIC MOSONIK VOLCANO, NORTHERN TANZANIA

Sedova A.M.

Department of Mineralogy, St. Petersburg State University, Saint-Petersburg, Russia, a.sedova@spbu.ru

The Mosonik volcano belongs to the Neogene-Resent volcanism of the Natron-Engaruka region of the East African Rift system. It is one of several stratovolcanoes located on the northeastern tip of the Gregory Rift Valley. Mosonik is attributed as having the earliest phase of eruptions in this province (Dawson, 2008) and is dated in the range 3.08 – 4.057 Ma (Isaac & Curtis, 1974; Manega, 1993; Foster et al., 1997; Muirhead et al., 2016).

In 1961, it was mapped by the Tanganyika Geological Survey (Guest et al., 1961). Then a series of works Isaac (1967), Isaacs and Curtis (1974), Foster et al. (1997) and recently Muirhead et al. (2016) were carried out to the study of relationship of volcanic Mosonik lavas with host rocks (basalt flows, basalt tuffs and depositional setting beds).

Mineralogical, geochemical and isotopic studies of volcanoes (including Mosonik) in the northern Tanzania were conducted by Paslik et al. (1995-1996). In their works concluded the mechanisms for the formation of effusives. They established the most likely mechanism is the mixing of the original magma with anhedral material from two different alkaline-basalt magmatic chambers.

According to the geological map (Guest et al., 1961), the cone of the volcano consists mainly of nephelinite-phonolitic tuffs and agglomerates, part of the lava extends east of the main cone. This part of the lava could flow out of the crater that was currently destroyed. According to Guest et al. (1961) and Dawson (2008), the composition of lava flows is represented by nephelinites and nephelinite phonolites. Dawson (2008) by some field descriptions noted that pyroclastic rocks contain fragments of nepheline- and pyroxene-porphyritic lava among which dominate is phonolites, and nephelinites are rare. In some lavas, phlogopite, titanite and melanite are accessory minerals. Blocks of pyroxenite, ijolites and syenites, xenoliths of quartzites and schists were found in the agglomerates. On the northern and western slopes of the volcano, along the traverse inside the valleys, carbonatites were found, both as in the primary outcrop and as separate blocks.

In the expeditions 2009 and 2012 A.N. Zaitsev found that the boundaries of the volcano outlined by Guest et al. (1961) are rather approximate. In addition to the previously described phonolitic and nephelinitic species of lavas, melilite nephelinites were found (Zaitsev и др., 2015). It was established that carbonatites mostly occur as boulders of various sizes within creek deposits. The carbonatite dyke was discovered in the northwestern part of the volcano, apparently reported earlier by Dawson (2008).

Analytical methods. Samples of phonolith, nephelinite lavas and xenoliths in these rocks were studied in polished thin sections and epoxi blocks. They were studied using scanning electron microscopy (SEM— Hitachi S-3400N) and energy-dispersive X-ray microanalysis (EDX—Oxford instruments X-Max 20) at St. Petersburg State University (Geomodel Resource Center). Wavelength-dispersive electron probe microanalyses (WD-EPMA) of major and minor minerals were obtained using Cameca SX-100 electron microprobe at the NHM at Tübingen University (TU). Raman spectrometer Horiba Jobin-Yvon LabRam HR 800 (St. Petersburg State University, Geomodel Resource Center) was used to refine the mineral phases. Bulk contents of major and minor elements were determined from whole rock pressed powders by X-ray fluorescence (XRF, ARL ADVANT'X, Thermo Scientific) at Karelian Research Centre RAS. Trace elements including REEs were determined after open acid digestion (HF+HNO3+HClO4) by XSeries-2 ICP-MS (Thermo Scientific, USA) at Karelian Research Centre RAS. Analytical accuracy was checked by comparison to standard rocks CHC-2 (СЭВ 2294-80) (nepheline syenite) and BHVO-2 (basalt) and was found to be within ±0.5 – 3% for all REEs and most other elements.

Petrography. Among *nephelinites* there are melilite nephelinites, nephelinites s.s., calcite-phonolite nephelinites and phonolitic nephelinites.

Melilitic nephelinites have a nephelinitic (subhedral) structure, due to the large euhedral phenocrysts of melilite (15%) and nepheline (40%); euhedral and anhedral diopside microphenocrysts,

(15-20%), euhedral apatite (7-8%), anhedral sodalite (4-5%), anhedral phlogopite (2%), euhedral titanomagnetite (5%), euhedral perovskite (3%), anhedral shorlomite (3%) and anhedral primary calcite (1-2%). Crystals of melilite, diopside (the larger ones), phlogopite are strongly resorbed up to assimilation into the bulk. Some of the smaller diopside crystals with poikilit structure retained their euhedral prismatic form.

The *nephelenites s.s.* with a nephelinitic structure is a more alkaline species. They have a similar mineral composition, but titanite appears in them. They have a different order of crystallization. The groundmass is well crystallized and composed of nepheline, aegirine-augite, amphibole, apatite, magnetite and zeolites.

In *nephelinites s.s.* with microporphy structure perovskite and garnet disappear, but sodalite and diopside-augite appear, sometimes overgrow with aegirine. The groundmass is poorly crystallized; it is represented by yellow glass, altered by zeolites and calcite.

Calcite-phonolitic nephelinites are more alkaline. They have both nephelinitic and porphyritic structure. Phenocrysts are represented by euhedral nepheline, pyroxene, titanite, subhedral apatite, euhedral crystals of primary calcite, anhedral sodalite. The groundmass is represented by nepheline, sanidine and pyroxene. Ore mineralization is show: pyrite, chalcopyrite and pyrrhotite. Perovskite, schorlomite and magnetite are noticed as inclusions in pyroxenes.

Phonolitic nephelinites are more saturated silica and alkali rocks. They have a porphyritic structure. There is sanidine in the groundmass and as anhedral phenocrysts.

The closest to nephelinites is phonolites containing poorly crystallized glass in the groundmass (*phonolites I*). *Phonolites II* include well-crystallized groundmass, which contain nepheline, sanidine and aegirine-augite needles, giving the characteristic green color to rocks. They are more enriched in silica and more saturated with alkalis.

Phonolites I include phonolites s.s. and sodalite phonolites. Actually *phonolites s.s*. with a phonolitic structure have large phenocrysts of nepheline and zonal diopside-augite, microphenocrysts of euhedral nepheline (25-30%), strongly corroded subeuhedral augite, sometimes with egirine rim (45-50%), euhedral large zonal titanite (7-10) %), large anhedral apatite (4-8%). The groundmass contains poikilitic small prismatic crystals of sanidine (10%), square euhedral nepheline, needles aegirine-augite and square-shaped magnetite. Glass is replaced by zeolites and calcite.

In *sodalite phonolite* there is an accumulation of very large phenocrysts of nepheline (up to 7.5 mm) and diopside-augite-egirine (up to 5 mm), which corresponds to the mesocumulate structure. Apparently large phenocrystals experienced additional growth of crystals. Microphenocrysts have poikilit structure characteristic of cumulates.

Phonoliths II are quite similar to each other in mineralogical composition. Variations are a different size of other phenocrysts. Phenocrysts of sanidine-anorthoclase with unusual oscillatory zonality are noted. Phenocrystals are represented by subeuhedral augite and sanidine, euhedral titanite, anhedral apatite. Mica (annit and phlogopite) are present in some rocks as nonequilibrium with the groundmass. Titanomagnetite and magnetite are surrounded by reactionary aegirine. The graundmass is composed of sanidine, nepheline (almost completely replaced by phillipsite and natrolit) and aegirine-augite needles. Abundant porous and crack space is filled with calcite and zeolites.

Mineral chemistry. The main rock-forming minerals are melilite (in melilite nephelinite), nepheline, pyroxene, feldspar, titanite, apatite, schorlomite and perovskite.

Melilite from melilite nephelinite is a regular elongated tabular phenocrysts (0.5–3 mm), significantly corroded. In terms the crystals correspond to akermanite – alumo-akermanite. A fine-grained mass of calcite-silicate aggregate develops along the rims of the crystals. The compositions of the melilites are given in table 1. Along the rim of the crystals there is a bright, more enriched Ca and Sr edge by the composition corresponding to ackermanite. The boundary between them is also significantly corroded, so we need to assume the secondary nature of them.

Nepheline is presented in all silicate rocks of the Mosonic volcanic complex, both phenocrystals and the groundmass. Its euhedral crystal form with square sections is almost always attended. Two types of nepheline are distinguished: the first are zonal, often zeolitized, sometimes even calcite altered; the second are nonzonal, often fractured.

For nepheline from melilite nephelinites zonality is slightly. They differ from the remaining nepheline with the highest content of Fe^{3+} (up to 1.81 wt.%), Ca (up to 0.95 wt.%), MgO (up to 0.06 wt.%) and low content of SiO_2 40.16 - 42.02 wt.%. In the core of crystals Fe_2O_3 detected less (1 wt.%) than in the rims (1.5 wt.%). The same low SiO_2 values are also characteristic of nephelinites from melilite nephelinites of the Kerimosi volcano (Church, 1996) and differ nephelinites from the Sadiman volcano (Zaitsev, 2012). The nepheline from the melilitic nephelinites of the Mosonic volcano noticed significantly a high content of kalsilite end member ($Ne_{66–70}$ $Ks2_{8–31}$ $Qz_{0–0.1}$). As reported by Rubie and Bas (1977), a hight kalsilite end member is an indicator of a more primary composition.

For more evolved nephelinites (II), nepheline is two zonality types. Part of the crystals (sample mos-8a) is reached Fe_2O_3 up to 1.59 wt.%. Nepheline from nephelinite II are grouped according to individual samples, it's demonstrate surprisingly clear trends in evolution of nepheline. It reflects the fractionation sequence with greater silica and lesser kalsilite end member. In the core of crystals Fe_2O_3 is less (0.7 wt.%) than in the rims (1 wt.%).

Phonolites vice versa show a narrow variation of compositions ($Ne_{72–81}$ $Ks_{6–18}$ $Qz_{2–18}$), they areas strongly overlap. Samples with zonal and nonzonal nepheline are also found. In some samples, nepheline is alteration by zeolite and calcite, in sample G12 replaced including gauin. In the core of crystals Fe_2O_3 is also less (0.6 wt.%) than in the rims (1 wt.%).

Pyroxenes are found in all silicate rocks of the volcanic complex as microphenocrysts (often phenocrysts) and microlaths in the groundmass. Pyroxenes from silicate rocks of Mosonik volcanic complex demonstrate the classic trend of evolution.

Melilite nephelinites and less evolved nephelinites contain mainly of diopside ($_{Aeg4–12}$ $Di_{53–85}$ $Hed_{10–35}$) with a complex "mix" zonality (in large crystals) and with normal and inverse zonality (in smaller crystals). It is interesting to note that in the most primitive in composition diopside presents a slight increase MnO and the minimum values of Al_2O3.

More evolved nephelinites are characterized by overgrowth of augite by diopside cores. Their compositions vary greatly in the content of Fe^{2+} and Fe^{3+}, which is possibly explain as connected with new portions of melts that are not in equilibrium with the previous melt or simultaneous crystallization of ore minerals.

In phonolites I there are two types of crystals: the first similar to the diopside from phonolites II, with a large number of inclusions, with a complex core zonality and aegirine-augite rims; the second is aegirine-augite without inclusions, with a thin concentric zonality. Both those crystals often overgrow with an aegirine rims with an impurity of Zr.

For phonolites II characteristic is similar above crystals with complex zonality. The nucleus is overgrown with a thin-zone aegirine-augite, having most corroded surface of core. In the most evolved nephelinites and phonolites, titanium-containing aegirine is present with a small zirconium impurity (TiO_2 up to 2.9 и ZrO_2 up to 0.23 wt. %).

Feldspars are represented by sanidine and anorthoclase. They are presented as microliths in evolved nephelinites and as phenocrystals and microlites in phonolites. Feldspars from phonolites differ sanidines from nephelinites in composition. The sanedines from nephelinites have a rather narrow discrete range of compositions (Or_{86-89} Ab_{16-18} An_{3-7}). As impurities contain Fe_2O_3 (up to 1 wt%) BaO (up to 0.7 wt%).

In the phonoliths the anorthoclase nucleus (Or_{21-38} Ab_{62-75} $An_{0.2-9}$) is very different from the mantle. They have a complex oscillatory zoning, in which two groups alternating composition changes occur: the first has Or_{56-70} Ab_{23-41} An_{0-13}, and the second Or_{88-98} Ab_{2-12} An_0. Often it matches with area of secondary changes, which related to form of microcline. The content Fe_2O_3 varies from 0.04 in the core to 4 wt.% in the mantle of the crystals. The content BaO and SrO in the inner part of the crystals is greater than in the outer. The content BaO varies from 0.08 to 2 wt%, SrO from 0 to 0.31 wt%.

Titanite, perovskite and garnet act as rock-forming and accessory minerals. They are represented as microphenocrysts. There is zonality in titanite and perovskite, which is not present in shorlomit.

Bulk geochemistry. The rocks contain a wide range 35.4–53.7 wt.% SiO2 and 3.6–14.1 wt.% Na2O+K2O. In the total alkali–silica (TAS) diagram, data form a broad field with points plotting in the foidite and phonolite fields (fig.).

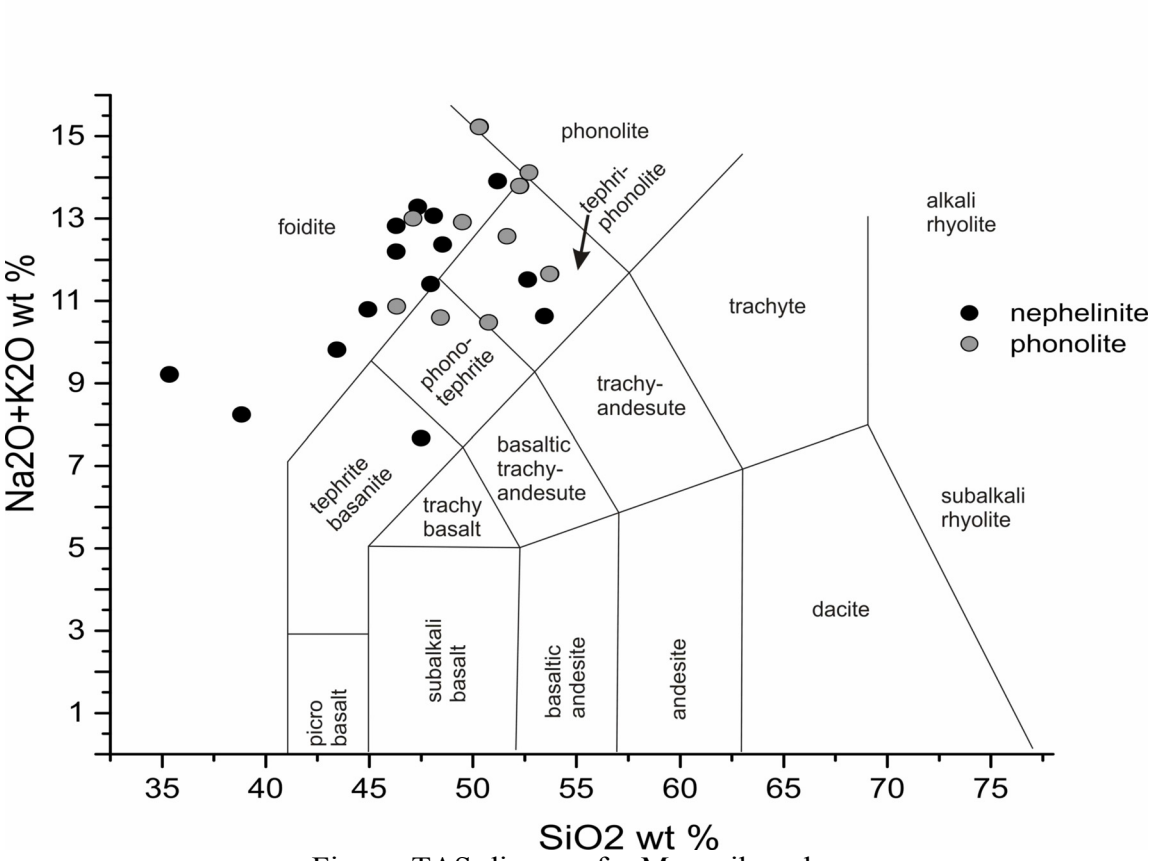

Figure. TAS-diagram for Mosonik rocks.

The work is supported by Russian Foundation of Basic Research (grant 18-05-00835) and St. Petersburg State University (Geomodel Resource Center).

References

Church A. A., The Petrology of the Kerimasi CarbonatiteVolcano and the Carbonatites of Oldoinyo Lengai with aReview of Other Occurrences of Extrusive Carbonatites. PhD Thesis (University of London, London, 1995).

Dawson J. B. The Gregory Rift Valley and Neogene-Recent Volcanoes of Northern Tanzania. London. 2008. 112 pp.

Foster, A., Ebinger, C., Mbede, E., and Rex, D., 1997, Tectonic development of the northern Tanzanian sector of the East African rift system: Journal of the Geological Society, London, v. 154, p. 689–700.

Guest N. J., James, T. C Pickering R., and Dawson J. B. Angata salei. Geol. Surv. Tanganyika. Quarter degree sheet 39. 1961.

Isaac, G. L. & Curtis, G. H. Age of the Acheulian industries from the Peninj Group, Tanzania // Nature. 1974. p.249.

Isaac, G.L., 1967, The stratigraphy of the Peninj Group - early middle Pleistocene formations west of Lake Natron, Tanzania, in Bishop, W.W., and Clark, J.D., eds., Background to evolution in Africa: Chicago, University of Chicago Press, p. 229–257.

Manega, P.C., 1993, Geochronology, geochemistry, and isotopic study of the Plio-Pleistocene hominid sites and the Ngorongoro volcanic highland in northern Tanzania: Boulder, University of Colorado, Ph.D. dissertation, 328 p.

Muirhead J.D., Kattenhorn S.A., Lee H., Mana S., Turrin B.D., Fischer T.P., Kianji G., Dindi E., Stamps D.S. Evolution of upper crustal faulting assisted by magmatic volatile release during early-stage continental rift development in the East African Rift // Geosphere (2016) 12 (6): 1670-1700.

Paslick, C., Halliday, A. N., Lange, R. A., James, D. & Dawson, J. B. Indirect crustal contamination: evidence from isotopic and chemical disequilibria in minerals from alkali basalts and nephelinites from northern Tanzania // Contributions to Mineralogy and Petrology. Vol. 125. 1996. 277–292.

Rubie D.C., Le Bas M.J. 1977. Kisingiri: The sub-volcanic alkali silicate rocks. In: Le Bas MJ, Carbonatite-nephelinite volcanism, John Wiley & Sons, New York, pp 47–79.

Zaitsev A.N., Spratt J., Sharygin V.V., Wenzel T., Zaitseva O.A., Markl G. Mineralogy of the Laetolil Footprint Tuff: A comparison with possible volcanic sources from the Crater Highlands and Gregory Rift // Journal of African Earth Sciences. Vol. 111. 2015. pp. 214–221.

Zaitsev, A.N., Marks, M.A.W., Wenzel, T., Spratt, J., Sharygin, V.V., Strekopytov, S., Markl, G., 2012. Mineralogy, geochemistry and petrology of the phonolitic to nephelinitic Sadiman volcano, Crater Highlands, Tanzania. Lithos 152, 66-83.

ORTHORHOMBIC $CaCr_2O_4$ IN PHOSPHIDE-BEARING GEHLENITE-RANKINITE PARALAVA FROM HATRURIM BASIN, ISRAEL: PRELIMINARY DATA

Sharygin V.V. [1,2]

[1] *V.S.Sobolev Institute of Geology and Mineralogy, Novosibirsk, Russia, sharygin@igm.nsc.ru*

[2] *Novosibirsk State University, Novosibirsk, Russia*

Compounds of $CaCr_2O_4$ are important components of composite materials used in metallurgy, ceramics and solid oxide fuel cells (Róg et al., 2007). These phases have good magnetic and magnetoelectric properties (Damay et al., 2010; Toth et al., 2011; Zhai et al., 2016 and references herein). The α- and β- polymorphs of $CaCr_2O_4$, corresponding to high- and low-temperature forms, are well known (Degterov, Pelton, 1996; Lee, Nassaralla, 1997). Both α-and β-$CaCr_2O_4$ are related to orthorhombic structures with space groups of *Pmmn* (No. 59) (Pausch, Müller Buschbaum, 1974; Toth et al., 2011) and *Pnma* (No. 62) (Hill et al., 1956; Hörkner, Müller Buschbaum, 1976; Damay et al., 2010), respectively. In addition to orthorhombic $CaCr_2O_4$ phases the monoclinic modifications are also known as synthetic. The β-polymorph of $CaCr_2O_4$ is isostructural with $CaFe_2O_4$ (Hill et al., 1956; Hörkner, Müller Buschbaum, 1976; Damay et al., 2010). In general, the $CaFe_2O_4$-type structure is believed as the high-pressure precursor form of many oxyspinels at the HPT conditions related to the Earth's deep mantle and may be considered as a potential geochemical reservoir for alkaline and other large cations in the mantle (Chen et al., 2003; Zhai et al., 2016 and references herein).

However, the findings of natural minerals with the $CaFe_2O_4$-type structure are not yet abundant. Xieite, a HP-polymorph of chromite $FeCr_2O_4$, was found in the shock veins of the Suizhou meteorite, China (Chen et al., 2008) and maohokite, a HP-polymorph of magnesioferrite, was reported in shocked gneiss from the Xiuyan crater in China (Chen et al., 2019). Harmunite, $CaFe_2O_4$, and wernerkrauseite, $CaFe^{3+}{}_2Mn^{4+}O_6$, have been discovered in Ca-rich pyrometamorphic rocks (Galuskina et al., 2014; Galuskin et al., 2016). The Ca-Cr oxide phase, chemically and structurally similar to synthetic β-$CaCr_2O_4$, and post-spinel $(Mg,Mn)(Cr,Fe)_2O_4$ were found in a microinclusion in a diamond from Brazil (Kaminsky et al., 2015). These phases seem to be crystallized in lower mantle conditions and might be potential hosts for Ca and Cr in the deep mantle. Here we report preliminary data for $CaCr_2O_4$ phase occasionally found in gehlenite-rankinite paralava from Hatrurim Basin, one of combustion metamorphism complexes on the territory of Israel and Jordan (Gross, 1977).

The fine-grained paralavas, containing metal-phosphide mineralization, were first found in 2011 in the Halamish wadi located in the southern part of the Hatrurim Basin, Negev Desert, Israel. These rocks are sometimes highly weathered and look like as "pseudoconglomerate", in which individual fragments are "cemented" and cross-cut by carbonate-gypsum-Ca-hydrosilicate matrix. In general the individual fragments are altered in different degree and contain vesicles now filled with Ca-hydrosilicates. The alteration degree is fixed by changing of color (from dark to white) from the centre to rim. The dark parts of some fragments are less weathered and consist of gehlenite, rankinite, larnite, flamite, cuspidine, Cr-rich pyrrhotite, fluorapatite, Si-Cr-V-rich perovskite as essential minerals. The minor and accessory phases are represented by chromite-magnesiochromite, wüstite-magnesiowüstite, wollastonite, Ti-rich cuspidine, $CaCr_2O_4$ phase, Ba-rich djerfisherite mineral, magnetite, Fe-analog of akermanite, oxysulfide 2CaO•FeO•2FeS, $(Ni,Fe)_2As$ phase, pentlandite, native iron and Fe-phosphides. The crystallization of paralava occurred into a highly reduced conditions that is fixed by chemistry of the essential minerals: Ca-silicates and perovskite are very poor in Fe, whereas sulfides (pyrrhotite, Ba-rich phase), chromite, wüstite, kamacite and phosphides are the main carriers of Fe. The metal-phosphide mineralization is mainly localized on the boundary of rock fragments with carbonate-gypsum-Ca-hydrosilicate matrix, rarely around vesicles in paralava. It forms rounded isolations varying in size (from 10 μm to 1-2 mm) and modal composition. Namely in such associations the new phosphide minerals (murashkoite, FeP; transjordanite, Ni_2P; zuktamrurite, FeP_2; negevite, NiP_2; halamishite, Ni_5P_4, polekhovskyite $MoNiP_2$) were first found at Hatrurim Basin (Britvin et al., 2015; 2017; 2019). The following metal-phosphide assemblages with Cr-V-rich pyrrhotite are most common: kamacite; steadite (Fe-P eutectics, mainly kamacite + schreibersite Fe_3P) + kamacite; barringerite Fe_2P + steadite; schreibersite + barringerite; barringerite + murashkoite;

murashkoite + transjordanite. Other phosphide phases, cohenite, graphite, copper, Mo-rich phases and daubreelite sometimes occur in such assemblages. The formation of paralava and metal-phosphide mineralization seems to be unrelated in time. Metal-phosphide paragenesises may be formed due to impact of reduced gases on solidified paralava (Britvin et al., 2015; 2017; 2019).

The $CaCr_2O_4$ phase was observed in dark unaltered part of paralava during detailed study. It forms subhedral opaque grains up to 20 μm and occurs in association with gehlenite, rankinite and pyrrhotite (Figure 1). This phase resembles in reflected light and in BSE images perovskite and chromite, which occur in the studied paralava. In general, it strongly differs from bright yellow chromatite $CaCrO_4$ in both optical characteristics and chemical composition (Table 1). Mineral relations indicate that this $CaCr_2O_4$ phase crystallized after gehlenite and rankinite, but before pyrrhotite. The EMPA-WDS data show that in chemical composition it is quite similar to ideal $CaCr_2O_4$, but rich in V and Ti, $Ca(Cr_{1.7}V_{0.2}Ti_{0.1})O_4$ (Table 1). Taking into account the reduced conditions for paralava crystallization and excess of positive charge in formula calculation, dominant three-valence state is suggested for Ti. In general, the Hatrurim mineral is very close in chemistry to $CaFe_2O_4$-type Ca-Cr oxide phase, $(Ca_{1.07}Mg_{0.02}Mn_{0.02})_{1.11}(Cr_{1.71}Fe^{3+}_{0.06}V_{0.06}Ti_{0.03}Al_{0.03})_{1.89}O_4$ (EDS data), found in association with iron carbide, orthorhombic $MgCr_2O_4$ and ferropericlase in a diamond-hosted microinclusion from Brazil (Kaminsky et al., 2015).

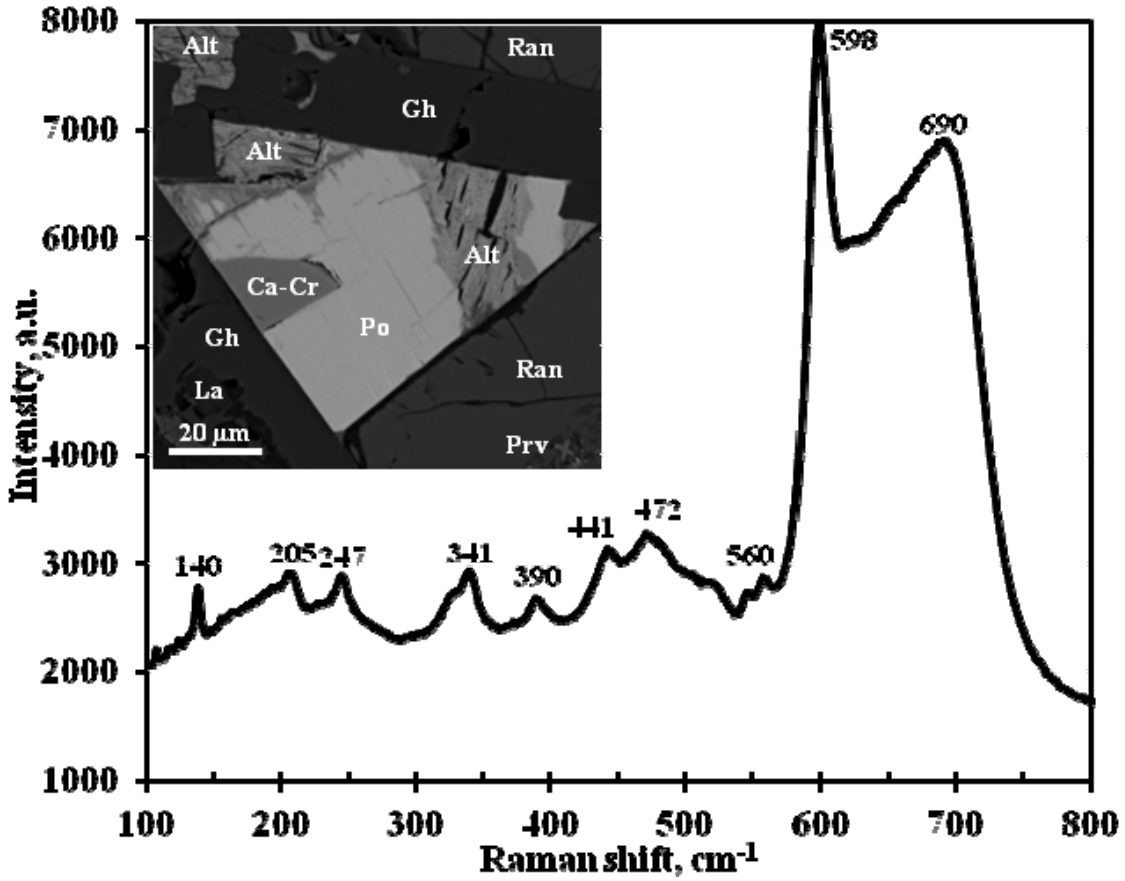

Figure 1. BSE image and Raman spectrum for orthorhombic $CaCr_2O_4$ from Hatrurim Basin, Israel. Symbols: Ca-Cr – $CaCr_2O_4$; Po – pyrrhotite; Ch – gehlenite; Ran – rankinite; La – larnite; Prv – Si-rich perovskite; Alt – alteration products after pyrrhotite.

The Raman spectrum for the Hatrurim $CaCr_2O_4$ phase shows all band set, which is common of synthetic β-$CaCr_2O_4$ (Zhai et al., 2016). However, in addition to the strong 598 cm^{-1} band, the Hatrurim phase indicates the strong and broad band at 690 cm^{-1} in respect to the synthetic compound (Figure 1). This seems to be related to crystallographic orientation of natural sample. The appearance-disappearance of some bands, their shifting and intensity change in the dependency on orientation have been shown for the Raman spectra of synthetic $CaFe_2O_4$ (Kolev et al., 2003).

Assuming the obtained chemical and Raman data we can suggest that the Hatrurim $CaCr_2O_4$ phase is β-polymorph, which is crystallized in high-temperature paralava. According to the calculated CrO-Cr_2O_3-CaO phase diagram (Degterov, Pelton, 1996), the α-β-transition for $CaCr_2O_4$ occurs at 1600°C, and below this temperature the β-$CaCr_2O_4$ is a stable phase down to room temperature. Anyway, this Hatrurim phase needs supporting by X-ray data in future. The association of gehlenite + rankinite in the studied paralavas is evidenced about liquidus temperature near 1300°C, as rankinite occupies a very narrow field at temperature >1308°C according to the phase diagram CaO-SiO_2-Al_2O_3 (Mao et al., 2006). Crystallization of pyrrhotite, one of latest phase in the paralava, seems to be near 1000°C. Melt inclusion study for schorlomite-rankinite paralava, another type of Ca-rich paralava at Hatrurim Basin, indicated rankinite crystallization at T>1160°C (Sharygin et al., 2006). Thus, at present we can assume the 1000-1300°C temperature range for the formation of the β-$CaCr_2O_4$ in the gehlenite-rankinite paralava at Hatrurim Basin.

Table 1. Chemical composition (wt.%) of orthorhombic $CaCr_2O_4$ from Hatrurim Basin in comparison with chromatite $CaCrO_4$.

	Natural $CaCr_2O_4$		Ideal $CaCr_2O_4$	Ideal $CaCrO_4$
	n=20	*sd*		
TiO_2	0.18	0.19		
Ti_2O_3	2.79	0.71		
Cr_2O_3	62.31	0.89	73.05	48.69
V_2O_3	7.29	0.43		
Al_2O_3	0.58	0.09		
FeO	0.59	0.12		
MnO	0.01	0.01		
MgO	0.01	0.01		
CaO	26.21	0.17	26.95	35.93
Na_2O	0.15	0.04		
Sum	100.11		100.00	84.62
Formula based on 3 cations and 4 oxygens				*2 cat - 4 oxy*
Ti^{4+}	0.005			
Ti^{3+}	0.080			
Cr^{3+}	1.696		2.000	
Cr^{6+}				1.000
V	0.201			
Al	0.024			
Sum	2.006		2.000	1.000
Fe	0.017			
Mn	0.000			
Mg	0.000			
Ca	0.967		1.000	1.000
Na	0.010			
Sum	0.994		1.000	1.000

EMPA-WDS data. Si, Ni, Zr, Cu, Ba and Sr are below detection limits (<0.005 wt.%). TiO_2 and Ti_2O_3 are calculated by charge balance.

This work was supported by the Russian Science Foundation (grant 17-17-01056) and the State assignment projects (IGM SB RAS 0330-2016-0005, 0330-2016-0004).

References

Britvin S.N., Murashko M.N., Vapnik Ye., Polekhovsky Y.S., Krivovichev, S.V. Earth's phosphides in Levant and insights into the source of Archean prebiotic phosphorus // Scientific

Reports. 2015. Vol. 5. Article 8355.

Britvin S.N., Murashko M.N., Vapnik E., Polekhovsky Yu.S., Krivovichev S.V. Barringerite Fe_2P from pyrometamorphic rocks of the Hatrurim Formation, Israel // Geology of Ore Deposits. 2017. Vol. 59. No. 7. P. 619-625.

Britvin S.N., Murashko M.N., Vapnik Ye., Polekhovsky Y.S., Krivovichev S.V., Vereschagin O.S., Vlasenko N.S., Shilovskikh V.V., Zaitsev A.N. Zuktamrurite, FeP_2, a new mineral, the phosphide analogue of löllingite, $FeAs_2$ // Physics and Chemistry of Minerals. 2019. Vol. 46. P. 361-369.

Britvin S.N., Murashko M.N., Vereshchagin O.S., Vapnik Y., Shilovskikh V.V., Vlasenko N.S. Polekhovskyite, IMA 2018-147. CNMNC Newsletter No. 48, April 2019, page xxx // European Journal of Mineralogy. 2019. Vol. 31.

Britvin S.N., Vapnik Y., Polekhovsky, Y.S., Krivovichev, S.V., Krzhizhanovskaya M.G., Gorelova L.A., Vereshchagin O.S., Shilovskikh V.V., Zaitsev A.N. Murashkoite, FeP, a new terrestrial phosphide from pyrometamorphic rocks of the Hatrurim Formation, South Levant // Mineralogy and Petrology. 2019. Vol. 113. P. 237-248.

Chen M., Shu J., Mao H.K., Xie X., Hemley R.J. Natural occurrence and synthesis of two new postspinel polymorphs of chromite // Proceedings of the National Academy of Science USA. 2003. Vol. 100. P. 14651-14654.

Chen M., Shu J., Mao H. Xieite, a new mineral of high pressure $FeCr_2O_4$ polymorph // Chinese Science Bulletin. 2008. Vol. 53. P. 3341-3345.

Chen M., Shu J., Xie X., Tan D. Maohokite, a post□spinel polymorph of $MgFe_2O_4$ in shocked gneiss from the Xiuyan crater in China // Meteoritics and Planetary Science. 2019. Vol. 54. P. 495-502.

Damay F., Martin C., Hardy V., Maignan A., Andre G., Knight K., Giblin S.R., Chapon L.C. Zigzag ladders with staggered magnetic chirality in the S = 3/2 compound β-$CaCr_2O_4$ // Physical Review B: Condensed Matter and Materials Physics. 2010. Vol. 81. Article 214405.

Degterov S., Pelton A.D. Critical evaluation and optimization of the thermodynamic properties and phase diagrams of the CrO-Cr_2O_3, CrO-Cr_2O_3-Al_2O_3, and CrO-Cr_2O_3-CaO systems // Journal of Phase Equilibria. 1996. Vol. 17. P. 476-487.

Galuskin E.V., Kruger B., Kruger H., Blass G., Widmer R., Galuskina I.O. Wernerkrauseite, $CaFe^{3+}{}_2Mn^{4+}O_6$: the first nonstoichiometric post-spinel mineral, from Bellerberg volcano, Eifel, Germany // European Journal of Mineralogy. 2016. Vol. 28. P. 485-493.

Galuskina I.O., Vapnik Y., Lazić B., Armbruster T., Murashko M., Galuskin E.V. Harmunite $CaFe_2O_4$: a new mineral from the Jabel Harmun, West Bank, Palestinian Autonomy, Israel // American Mineralogist. 2014. Vol. 99. P. 965-975.

Gross S. The mineralogy of the Hatrurim Formation, Israel // Bulletin of Geological Survey of Israel. 1977. Vol. 70. P. 1-80.

Hill P.M., Peiser H.S., Rait J.R. The crystal structure of calcium ferrite and β calcium chromite // Acta Crystallographica. 1956. Vol. 9. P. 981-986.

Hörkner W., Müller Buschbaum H.K. Einkristalluntersuchungen von β-$CaCr_2O_4$ // Zeitschrift für Naturforschung, Teil B: Anorganische Chemie, Organische Chemie. 1976. Vol. 31. P. 1710-1711 (in German).

Kaminsky F., Wirth R., Schreiber A. A microinclusion of lower mantle rock and other mineral and nitrogen lower-mantle inclusions in a diamond // Canadian Mineralogist. 2015. Vol. 53. P. 83-104.

Kolev N., Iliev M.N., Popov V.N., Gospodinov M. Temperature-dependent polarized Raman spectra of $CaFe_2O_4$ // Solid State Communications. 2003. Vol. 128, P. 153-155.

Lee Y.M., Nassaralla C.L. Minimization of hexavalent chromium in magnesite-chrome refractory // Metallurgical and Materials Transactions B: Process Metallurgy and Materials Processing Science. 1997. Vol. 28. P. 855-859.

Mao H., Hillert M., Selleby M., Sundman B. Thermodynamic assessment of the CaO-Al_2O_3-SiO_2 system // Journal of the American Ceramic Society. 2006. Vol. 89. P. 298-308.

Pausch H., Müller Buschbaum H.K. Die Kristallstruktur von α-$CaCr_2O_4$ // Zeitschrift für Anorganische und Allgemeine Chemie. 1974. Vol. 405. P. 113-118 (in German).

Róg G., Kozlowska-Róg A., Dudek M. The standard Gibbs free energy of formation of calcium chromium (III) oxide in the temperature range (1073 to 1273 K) // Journal of Chemical Thermodynamics. 2007. Vol. 39. P. 275-278.

Sharygin V.V., Vapnik Ye., Sokol E.V., Kamenetsky V.S., Shagam R. Melt inclusions in minerals of schorlomite-rich veins of the Hatrurim Basin, Israel: composition and homogenization temperatures // In: ACROFI I Program with Abstracts, Edited by Ni Pei and Li Zhaolin, Nanjing, China, 2006, pp. 189-192.

Toth S., Lake B., Kimber S.A.J., Pieper O., Reehuis M., Islam A.T.M.N., Zaharko O., Ritter C., Hill A.H., Ryll H., Kiefer K., Argyriou D.N., Williams A.J. 120° helical magnetic order in the distorted triangular antiferromagnet α-$CaCr_2O_4$ // Physical Review B: Condensed Matter and Materials Physics. 2011. Vol. 84. Article 054452.

Zhai S., Yin Y., Shieh S.R. Shan S., Xue W., Wang C.-P., Yang K., Higo Y. High-pressure X-ray diffraction and Raman spectroscopy of $CaFe_2O_4$-type β-$CaCr_2O_4$. // Physics and Chemistry of Minerals. 2016. Vol. 43. P. 307-314.

CAN DUNITES OF THE GULI MASSIF BE A CUMULATE OF OLIVINE-NEPHELINITE MAGMA? MELT INCLUSIONS STUDY

Sharygin V.V.[1,2], Simonov V.A.[1,2], Vasiliev Yu.R.[1], Kotlyarov A.V.[1]

[1]V.S.Sobolev Institute of Geology and Mineralogy, Novosibirsk, Russia, sharygin@igm.nsc.ru

[2]Novosibirsk State University, Novosibirsk, Russia

The genesis of large plutons of ultramafic rocks and carbonatites has been attracting a special attention of many researchers due to their mantle source. The Guli massif (Maimecha-Kotui province, Polar Siberia) is one of such huge plutons. Its square may be estimated as 2000 km^2 (geophysical data), but recent exposed surface is near 500 km^2. Other part is covered by Meso-Cenozoic and Quaternary strata of the Yenisei-Khatanga Depression. The massif is composed by diverse rocks from ultramafic to alkaline composition as well as carbonatites (Vasiliev, Zolotukhin, 1975; Egorov, 1991). The following sequence of rock formation has been established: dunites – clinopyroxenites – melilitolites – jacupirangite-urtite rock series – alkaline syenites – carbonatites. Dunites are dominant rock type (≈60 vol.% of exposed surface) of the pluton. The specific feature of the Guli massif is direct spatial contact with the Permian-Triassic alkaline volcanic rocks (olivine melanephelinites, picrites and others) and meimechites, which are crystallization products of deep mantle magma (Vasiliev, Zolotukhin, 1975; 1995; Egorov, 1991; Sobolev et al., 1991; 2009; 2011; Ryabchikov et al., 2002; 2009; Ryabchikov, 2005; Vasiliev, Gora, 2014; 2017). Owing to this specificity the Guli pluton has been studied in detail. Melt inclusion studies have been provided for the different Guli rocks and related volcanic rocks (Kostyuk, Panina, 1970; Sobolev et al., 1991; 2009; Sokolov et al., 1999; Rass, Plechov, 2000; Ryabchikov et al., 2002; 2009; Panina, Motorina, 2013; Nikolenko et al., 2018 and many other references). However, the genesis of ultramafic rocks of the Guli massif is still enigmatic and discussible. Recent data on silicate-melt inclusions in accessory Cr-spinel of the Guli dunites demonstrated the contribution of high-Mg (16-22 wt.% MgO) alkali-picritic and picrobasaltic melts to the crystallization of these ultramafic rocks (Simonov et al., 2016). During their intrachamber crystallization the composition of magmatic system evolved from picrite-meimechite to picrobasalt. In general, Cr-spinel-hosted melt inclusions from dunites are similar to inclusions in olivine phenocrysts from meimechites in the phase and chemical composition. This work is a continuation of melt inclusion study for the Guli dunites with detailed consideration of phase and chemical composition.

One of samples of clinopyroxene-containing dunite from south-west part of the Guli massif was selected for melt inclusion study. This sample (426a) was previously used for study of melt inclusions in chromite (Simonov et al., 2016). The rock is partially serpentinized and contains phenocrystal olivine (> 90 vol.%) and interstitial matrix consisting of microphenocrysts of clinopyroxene, chromite and olivine, as well as ilmenite, Ti-magnetite, fluorapatite, phlogopite, Ti-rich amphibole (kataphorite) and secondary phases (chlorite, serpentine, calcite and others). The skeletal crystals of some minerals in the matrix maybe evidenced about rapid quenching at final stage of rock crystallization. The former silicate glass was transformed into chlorite-serpentine-calcite aggregate.

In addition to chromite (Simonov et al., 2016), we found silicate-melt inclusions in olivine and clinopyroxene. Melt inclusions in chromite (5-100 μm) are primary in origin and commonly outline the individual zones in the host crystals. Their phase composition slightly varies (Fig. 1). Euhedral olivine crystal plus fine-grained matrix (± gas bubble) is most abundant type. Other inclusions do not bear olivine and are represented by "spinifex"-like matrix, which consists of clinopyroxene, fluorapatite, F-Ti-rich phlogopite, titanite, orthopyroxene, ilmenite, glass (or nepheline + K-feldspar) and sulfide blebs (pyrrhotite + pentlandite + chalcopyrite) (Fig. 1). The "spinifex" structure is an indicator of rapid crystallization and quenching. Majority of melt inclusions in olivine (5-50 μm) are secondary in origin and form trails in the host mineral (Fig. 2A). Within trails they are commonly associated with individual chromite crystallites and fluid inclusions (CO_2-rich ?). However, some large inclusions (>50 μm) are not confined to the trails and seem to be primary in origin. Most olivine-hosted inclusions are partially to completely crystallized, translucent in ordinary light and consist of trapped chromite, gas bubble and fine-grained matrix, which is similar in phase composition to that of chromite-hosted inclusions (Fig. 2). Glassy or partially crystallized inclusions with minimal amount of

daughter phases occur rarely (Fig 2B-D). Some inclusions may contain leucite or Ti-rich amphibole (kataphorite, arfvedsonite, edenite) as daughter phases (Fig. 2B); orthopyroxene was not observed. Melt inclusions in clinopyroxene (up to 10 μm) are scarce and consist of glass, Ti-magnetite, ilmenite and fluorapatite. They may be associated with crystallites of olivine and Cr-rich magnetite in the host.

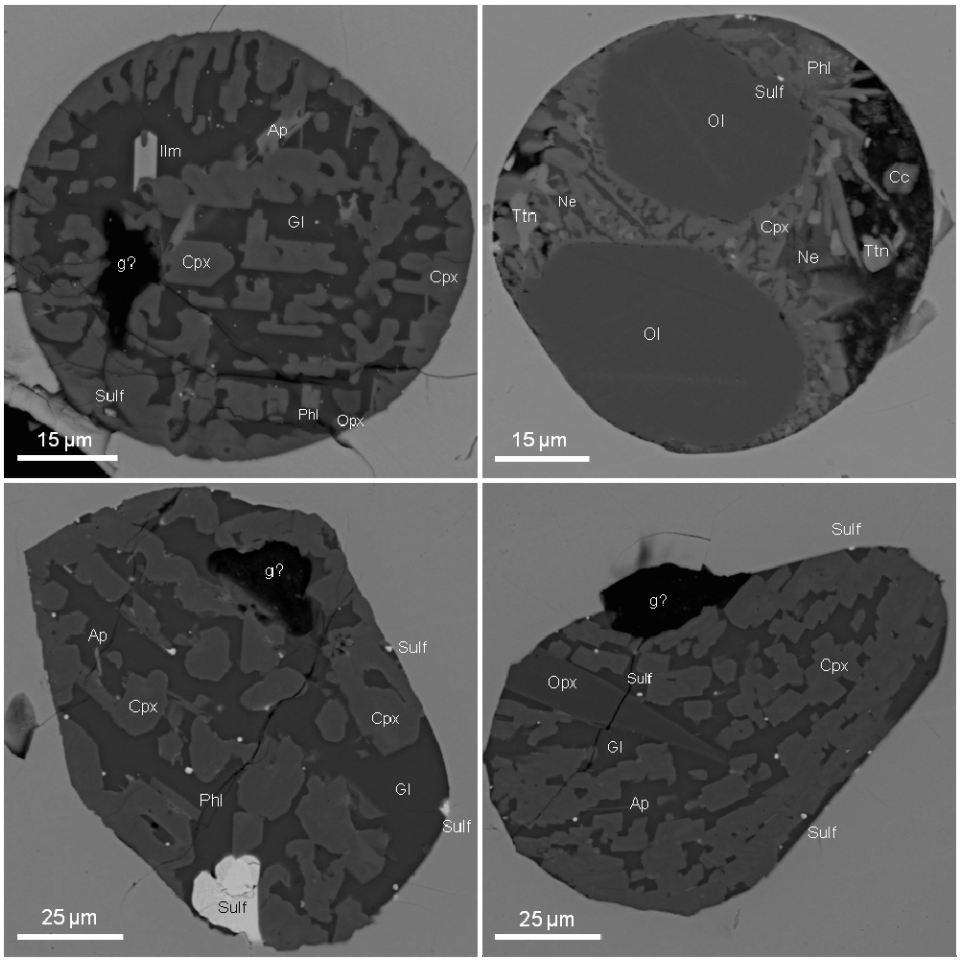

Figure 1. Primary silicate-melt inclusions in chromite from dunite of the Guli Massif (BSE images). Symbols: Gl – silicate glass; Cpx – clinopyroxene; Opx - orthopyroxene; Ol – olivine; Ap – fluorapatite; Ilm – ilmenite; Phl –phlogopite; Ne – nepheline; Ttn – titanite; Sulf – sulfide bleb (pyrrhotite + pentlandite + chalcopyrite); Cc – calcite; g? – gas bubble ?

The previous data (Simonov et al., 2016) and new chemical compositions for minerals and glasses of studied inclusions and estimation of bulk composition of fine-devitrified inclusions give a possibility to trace the evolution of initial melt during crystallization of the Guli dunites. The study of chromite-hosted inclusions heated "in blind" up to 1330°C (Simonov et al., 2016) has shown that initial magma during first stages of intrachamber crystallization gradually evolved from picrite-meimechite toward picrobasalt melt. The bulk composition of secondary fine-crystallized inclusions in olivine supports this tendency. These data are very similar to that of heated inclusion in chromite (n=4, in wt.%): SiO_2 – 46.5; TiO_2 – 7.6; Al_2O_3 – 11.9; FeO – 3.4; MgO – 4.6; CaO – 14.1; Na_2O – 4.1; K_2O – 4.7; P_2O_5 – 1.0; (Na+K)/Al – 1.0. The further abundant crystallization of mafic minerals (mainly clinopyroxene) led to alkali-rich aluminosilicate compositions depleted in femic components. It is indicated by compositions of residual glasses in partially crystallized inclusions in chromite and olivine (n=16 and n=5, respectively, in wt.%): SiO_2 – 59.8-56.4; TiO_2 – 0.7-0.6; Al_2O_3 – 19.3-18.4; FeO – 0.7-2.2; MgO – 0.6-3.95; CaO – 0.9-2.7; Na_2O – 7.0-6.2; K_2O – 7.5-8.2; P_2O_5 – 0.6-0.3; (Na+K)/Al – 1.0-1.1. However, compositions of olivine-hosted glassy inclusions (glass + gas ± Ca-Na-rich amphibole, Fig. 2D) are beyond of general tendency to be with agpaitic index higher than 2.5 (n=19, in wt.%): SiO_2 – 56.9; TiO_2 – 1.0; Al_2O_3 – 5.3; FeO – 5.6; MgO – 5.3; CaO – 4.2; Na_2O – 12.5;

K_2O – 5.8; P_2O_5 – 0.2. Such deviation may be explained by local fluctuation of melt composition during crystallization (possibly before precipitation of phlogopite, Fe-Ti-oxides and Ca-Na-rich amphibole).

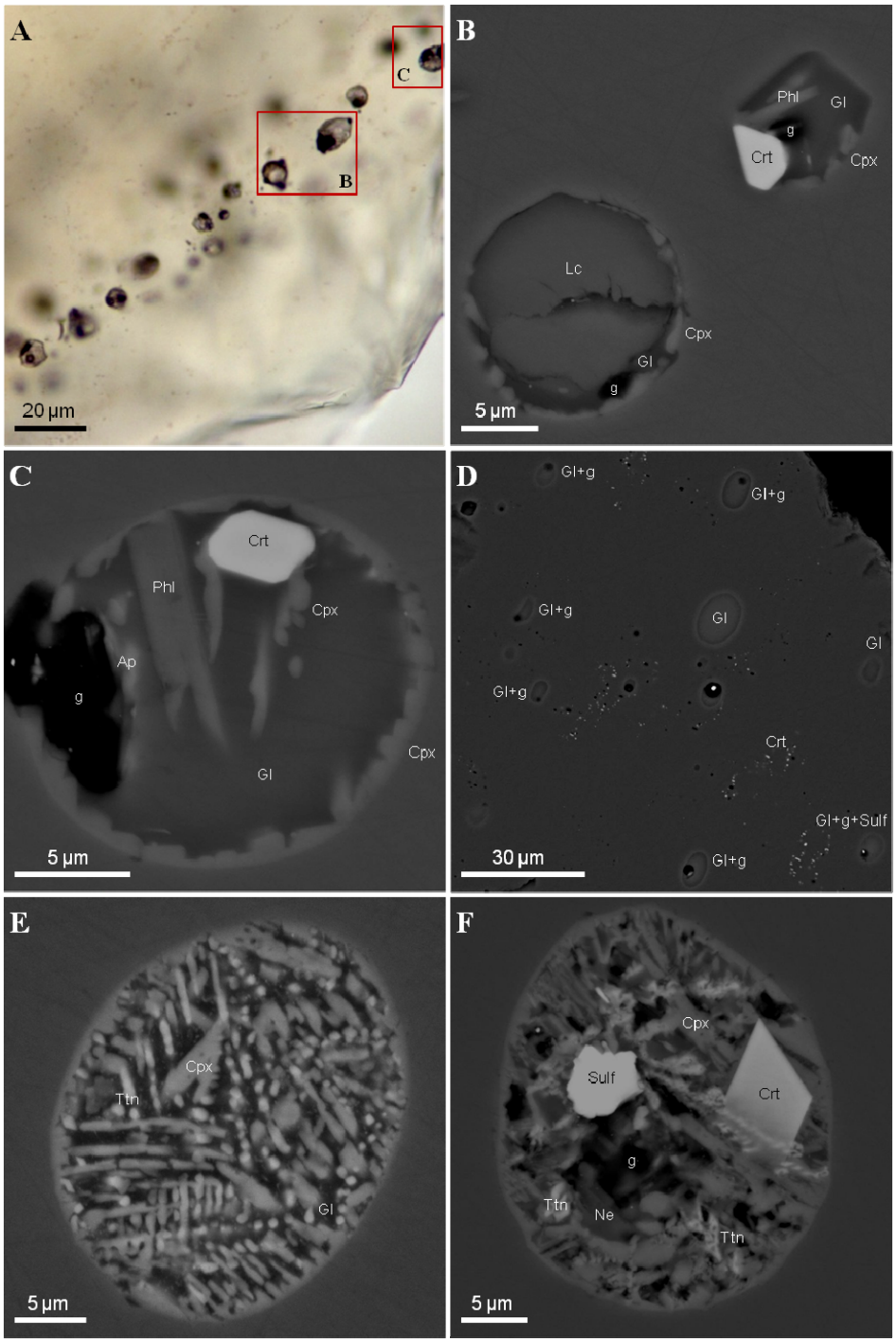

Figure 2. Secondary silicate-melt inclusions in olivine from dunite of the Guli Massif (A – transmitted light, others - BSE images). Symbols: Gl – silicate glass; Cpx – clinopyroxene; Ap – fluorapatite; Phl –phlogopite; Lc – leucite; Ne – nepheline; Ttn – titanite; Sulf – sulfide bleb (pyrrhotite + pentlandite + chalcopyrite); g – gas bubble.

New data on chemical and phase composition of silicate-melt inclusions in the Guli dunite minerals indicate that olivine-nephelinite magma maybe more favorable source for formation of the Guli pluton rather than meimechite or picrite melts. The appearance of nepheline, leucite, Ti-F-rich phlogopite and Ca-Na-Ti-rich amphiboles within mineral-hosted inclusions in the Guli dunites seems to be in support this idea. These minerals are common phases in the groundmass of neighboring

olivine melanephelinites. In addition, geochronological data are shown that olivine melanephelinites and related volcanic rocks are relatively older magmatites (251-253 Ma) than the Guli massif rocks (250 Ma) and meimechites (246 Ma) within the Maimecha-Kotui province (see review in Simonov et al., 2016).

This work was supported by the Russian Science Foundation (project 19-17-00019) and the State assignment projects (IGM SB RAS 0330-2016-0005, 0330-2016-0014).

References

Egorov L.S. Ijolite-carbonatite plutonism (exemplified by the Maimecha-Kotui complex of Polar Siberia). Nedra, Leningrad. 1991. 260 p.

Kostyuk V.P., Panina L.I. Temperature conditions of alkaline rock crystallization of the Guli intrusion // Doklady Akademii Nauk SSSR. 1970. Vol. 194. P. 919-921.

Nikolenko E.I., Logvinova A.M., Izokh A.E., Afanas'ev V.P., Oleynikov O.B., Biller A.Ya. Cr-spinel assemblage from the Upper Triassic gritstones of the northeastern Siberian Platform // Russian Geology and Geophysics. 2018. Vol. 59. P. 1345–1361.

Panina L.I., Motorina I.V. Meimechites, porphyritic alkaline picrites, and melanephelinites of Siberia: Conditions of crystallization, parental magmas, and sources // Geochemistry International. 2013. Vol. 51. P. 109-128.

Rass I.T., Plechov P.Yu. Melt inclusions in olivines from the olivine-melilite rock of the Guli Massif, northwestern Siberian Platform // Doklady Earth Sciences. 2000. Vol. 375. P. 1399-1402.

Ryabchikov I.D. Mantle magmas as a sensor of the composition of deep geospheres // Geology of Ore Deposits. 2005. Vol. 47 (6). P. 455-468.

Ryabchikov I.D., Kogarko L.N., Solovova I.P. Physicochemical conditions of magma formation at the base of the Siberian plume: Insight from the investigation of melt inclusions in the meymechites and alkali picrites of the Maimecha-Kotui province // Petrologiya. 2009. Vol. 17. P. 287-299.

Ryabchikov I.D., Solovova I.P., Kogarko L.N., Bray G.P., Ntaflos T., Simakin S.G. Thermodynamic parameters of generation of meymechites and alkaline picrites in the Maimecha-Kotui province: Evidence from melt inclusions // Geochemistry International. 2002. Vol. 40 (11). P. 1031-1041.

Simonov V.A., Vasil'ev Yu.R., Stupakov S.I., Kotlyarov A.V., Karmanov N.S. Petrogenesis of dunites of the Guli ultrabasic massif (northern Siberian Platform) // Russian Geology and Geophysics. 2016. Vol. 57. P. 1696-1715.

Sobolev A.V., Kamenetsky V.S., Kononkova N.N. New data on petrology of Siberian meymechites // Geokhimiya. 1991. Vol. 29 (8). P. 1084-1095.

Sobolev A.V., Sobolev S.V., Kuzmin D.V., Malitch K.N., Petrunin A.A. Siberian meimechites: origin and relation to flood basalts and kimberlites // Russian Geology and Geophysics. 2009. Vol. 50 (12), P. 999–1033.

Sobolev S.V., Sobolev A.V., Kuzmin D.V., Krivolutskaya N.A., Petrunin A.G., Arndt N.T., Radko V.A., Vasiliev Yu.R. Linking mantle plumes, large igneous provinces and environmental catastrophes // Nature. 2011. Vol. 477, P. 312-316.

Sokolov S.V., Veksler I.V., Senin V.G. Alkalis in carbonatite magmas: new evidence from melt inclusions // Petrologiya. 1999. Vol. 7. P. 644-652.

Vasiliev Yu.R., Gora M.P. Meimechite-picrite associations in Siberia, Primorye, and Kamchatka (comparative analysis and petrogenesis) // Russian Geology and Geophysics. 2014. Vol. 55. P. 959-970.

Vasiliev Yu.R., Gora M.P. Nature of the ultramafite-mafite complex of the Guli pluton (Polar Siberia). Doklady Earth Sciences. 2017. Vol. 476. P. 1117–1119.

Vasiliev Yu.R., Zolotukhin V.V. Petrology of ultrabasic rocks of the Northern Siberian Platform and some problems of their genesis. Nauka, Novosibirsk. 1975. 270 p.

Vasiliev Yu.R., Zolotukhin V.V. The Maimecha-Kotui alkaline-ultramafic province of the northern Siberian Platform, Russia // Episodes. 1995. Vol. 18. P. 155-164.

SILICATE MINERALIZATION FROM SUBLIMATES OF THE ARSENATNAYA FUMAROLE (TOLBACHIK VOLCANO, KAMCHATKA, RUSSIA)

Shchipalkina N.V.[1,2], Pekov I.V.[1], Koshlyakova N.N.[1], Sidorov E.G.[3]

[1]Faculty of Geology, Lomonosov Moscow State University, Moscow, Russia

[2]Shubnikov Institute of Crystallography and Photonics, RAS, Moscow, Russia

[3]Institute of Volcanology and Seismology, Far Eastern Branch of RAS, Petropavlovsk-Kamchatsky, Russia

Studies of natural samples and thermochemical modeling show that mineral assemblages formed in fumaroles include minerals (1) deposited from volcanic gas,or from volcanic gas mixed with air, (2) crystallized as a result of gas-rock interactions. If the exhalative nature of sulfates and some other oxysalts, halides, oxides, and sulfides in fumaroles in most cases is undoubted then silicates from the same assemblages typically provoke discussion for their origin. In general, silicate mineralization from volcanic fumaroles assemblages is poorly described and for majority of active volcanoes some notes on the presence of silicates in fumaroles can be found in literature. Albite, diopside, sanidine, andalusite, microcline, cordierite, anorthite were mentioned in a fumarole at the Mount St. Augustine volcano (Alaska, USA) (Getahun et al., 1996), tremolite and aegirine ("acmite") in fumaroles at Merapi (Indonesia) (Symonds et al., 1987), aegirine and andradite in fumaroles at the Kudryavy volcano (Kurily archipelago, Russia) (Tessalina et al., 2008), orthoclase and albite in fumaroles formed during Nothern Breakthrough of the Great Fissure Tolbachik Eruption 1975–1976 (NB GFTE) at the Tolbachik volcano (Kamchatka, Russia) (Vergasova, Filatov, 2016) and esseneite and melilite in a lava tube from the 2012-2013 eruption of Tolbachik (Sharygin et al., 2018). However, there are no data about their chemical composition, morphological features and occurrence in these fumaroles, except of the latter cited paper.

It was unexpected to find very rich and diverse silicate mineralization in the active fumarole Arsenatnaya located at the summit of the Second Scoria cone of the NB GFTE located 18 km SSW of the active volcano Ploskiy Tolbachik (Kamchatka, Russia). Twenty-four reliably identified mineral species belonging to silicates have been found by us there. They include representatives of all major topological types of natural silicates, namely neso-, cyclo-, ino-, phyllo-, and tectosilicates. There are forsterite, andradite, titanite, enstatite, clinoenstaite, diopside, esseneite, aegirine, potassic-fluoro-magnesio-arfvedsonite, potassic-fluoro-richterite, litidionite, fluorophlogopite, yanzhuminite, an osumilite-group member, sanidine, anorthoclase, albite, anorthite, members of celsian-anorthoclase series, leucite, kalsilite, nepheline, sodalite, and haüyne.

Several zones with different types of mineralization were distinguished by us in the Arsenatnaya fumarole (up to down): zone of gypsum and opal (I), zone of Ca, Mg and Cu sulfates (II), zone of Cu sulfates (III), polymineralic zone (IV), zone of alluaudite-group arsenates (V), and anhydrite zone (VI) (Pekov et al., 2018). Silicates occur mainly in zones IV – VI. The major mineral assemblages, including silicate and non-silicate minerals forming these zones are shown in Table.

The described silicates have several common features both in morphological and chemical aspects. All silicates from sublimates of the Arsenatnaya fumarole mostly occur as crystals which overgrow exhalative sulfates, oxides, halides and arsenates or form open-work intergrowths with them. This is a sign of crystallization in open space. These silicates are assumed to be products of direct deposition from gas. Another type of silicate mineralization (especially important for tecto-aluminosilicates) is thin crusts replacing basalt scoria. This type of mineralization is considered by us to be a result of gas-rock interactions, the process called «gaseous metasomatism» by Naboko and Glavatskikh (1983). All silicates found in the Arsenatnaya fumarole contain significant impurities (up to several wt. %) of «ore» elements such as As, Cu, Zn, Sn, Mo and W. These impurities occur not in all studied samples of silicates but for each of the above-listed minerals the varieties enriched by "ore" components were found. Arsenic in these silicates is the main admixed chalcophile element. It substitutes Si at tetrahedral sites of the crystal structure. Distinct arsenic impurity is characteristic for silicates from this locality and this chemical feature differs them from the same minerals from majority of geological formations.

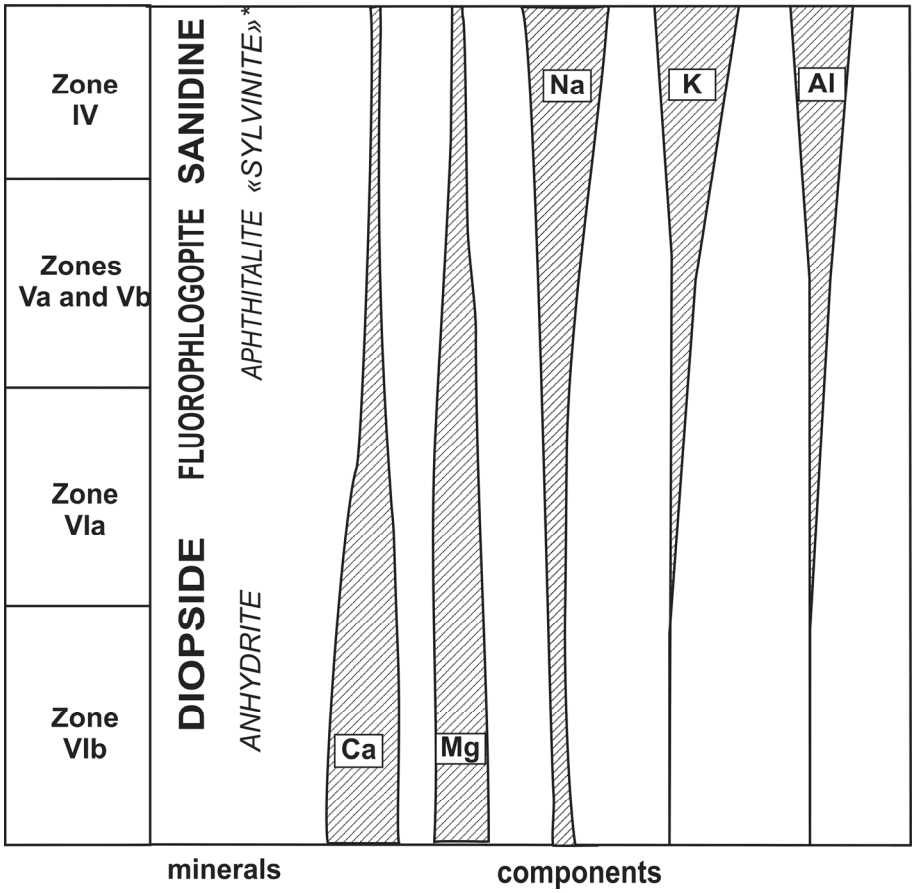

Figure. Distribution of the main species-defining lithophile components in silicates from different zones of the Arsenatnaya fumarole. The numbers of zones correspond to those in Table. The main silicate from each zone is given in boldtype and the main non-silicate mineral in italics.

All silicates there are hydrogen-free, including micas (fluorophlogopite and yanzhuminite) and amphiboles (potassic-fluoro-magnesio-arfvedsonite and potassic-fluoro-richterite). Additional anions in these minerals are F^- and admixed O^2 but not OH^-. This is due to the crystallization under the t > 500˚C and pressure close to atmospheric one.

Silicates, together with associated sublimate minerals belonging to other chemical classes, demonstrate an interesting zonation along the vertical section of the fumarole (Table). The gradual change of the main species-defining components in silicates (as well as major non-silicate minerals) from the deepest zones to the upper part of the Arsenatnaya fumarole is displayed on Figure. Full description of the zonation in the Arsenatnaya fumarole is reported by Pekov et al. (2018).

Mg and **Ca** are the main cations in minerals of deep zones VIa and VIb. These components occur in the most common silicates of these zones: diopside (the whole zone VI) and forsterite (zone VIb) as well as the major non-silicate minerals – anhydrite (the main calcium mineral in zone VI), As-bearing fluorapatite, svabite, calciojohillerite, johillerite, and berzeliite. Noteworthy, that at upper zones, including V and IV, calcium minerals are not essential. At the same time, magnesian minerals are traced up to zone IV. Thus, the main silicate of the upper part of zones VIa, Vb and Va is fluorophlogopite which can form nearly monomineral crusts and pods.

Alkali metals **Na** and **K** differ in behavior from one another. In deep zones, minerals with species-defining Na are common whereas almost no K minerals occur there. Na is fixed in pyroxenes (including aegirine), albite, and anorthoclase and in arsenates, namely calciojohillerite and berzeliite. K occurs here only as an impurity in haüyne, sodic feldspar and some arsenates. K content strongly increases to upper zones and becomes the species-defining component in crust-forming fluorophlogopite (zones Va and Vb), sanidine (zones Va and IV) and aphthitalite, langbeinite and

Table. Silicates and associated minerals in some mineralized zones* in the Arsenatnaya fumarole.

№	Zone	Silicates	Main associated minerals
IV	Polymineralic	**As-bearing sanidine**, **haüyne, sodalite**, fluorophlogopite, kalsilite, potassic-fluoro-magnesio-arfvedsonite, potassic-fluoro-richterite, yanzhuminite, diopside, litidionite, clinoenstatite, "fluoroeastonite"*	aphthitalite, methathenardite, cassiterite, johillerite, nickenichite, members of svabite-apatite series, hematite, tilasite, sylvite, halite, tenorite, pseudobrookite, corundum, anhydrite, tridymite
Va and Vb	Alluaudite-group minerals	**sanidine, fluorophlogopite,** haüyne, sodalite, leucite, diopside, nepheline	calciojohillerite, nickenichite, johillerite, paraberzeliite, hematite, tilasite, members of the svabite-fluorapatite series, cassiterite, pseudobrookite, alarsite, durangite, sylvite, tridymite
VIa	Anhydrite (upper part)	**diopside, fluorophlogopite,** K-Na feldspars, forsterite, haüyne	anhydrite, hematite, cassiterite, fluorapatite, magnesioferrite, tridymite
VIb	Anhydrite (lower part)	**diopside**, **forsterite**, andradite, enstatite, haüyne, Na-K feldspars, Mo- and W-bearing haüyne, titanite, celsian-anorthoclase	hematite, members of the svabite-fluorapatite series, anhydrite, tridymite, cristobalite

*Zones are marked in correspondence to the description given by Pekov et al. (2018).

*«Sylvinite» is a high-temperature solid solution halite NaCl – sylvite KCl.

sylvite (sulfate-rich zones). These zones also contain sodium feldspathoids: sodalite, haüyne and nepheline.

Behavior of **Al** resembles potassium one. Amount of Al gradually increases from zone VIb *via* VIa to V and IV. In relatively deep zones Al is mainly incorporated in fluorophlogopite. In upper zones sanidine (including the As-bearing variety) becomes the major mineral form of Al and different K-bearing feldspathoids (kalsilite, leucite, nepheline, haüyne) appear. It is interesting to note that alumina occurs mainly in the silicate phases with tetrahedral coordination of Al: tecto-aluminosilicates, magnesium micas and pyroxenes with Al substituting Si.

Trivalent **Fe** is an important component in minerals from all zones of the Arsenatnaya fumarole, and the main iron phase there is hematite. Silicates with Fe^{3+} as a species-defining component (esseneite, aegirine and andradite) are quite rare. However, impurity of trivalent Fe is incorporated almost in all studied silicates from this fumarole, regardless of the zone. Fe^{3+} substitutes Mg, Al, Ti and, rarely, Si.

Such distribution of the above-discussed components along the vertical section of the Arsenatnaya fumarole likely reflects the degree of their volatility in gas phase in temperature range 500 – 1000˚C. For instance, the calculated volatilities of these elements in gas of the Mount St. Helens volcano under t = 930˚C and p = 1 atm are as follows (concentrations are given in mole percent): 1.3 □ 10^{-10} for Ca, 2.2 □ 10^{-9} for Mg, 2.9 □ 10^{-8} for Al, 7.1 □ 10^{-5} for K and 2.0 □ 10^{-4} for Na (Symonds, Reed, 1993). The data presented by Zelenski et al. (2014) for the gases and aerosols from a lava tube window during the 2012-2013 effusive eruption of the Ploskiy Tolbachik basaltic volcano show that the average concentrations of Ca, Mg, Al, Na and K in gas are (ppm): 4.5, 0.9, 7.9, 224 and 150, respectively. The logarithms of enrichment factors that reflect the partition of these elements between gas and solid phases are as follows: 0.38 for Ca, 0.0 for Mg, 0.42 for Al, 2.37 for Na, and 2.55 for K.

In general, these data can explain the distribution of major species-defining lithophile components in sublimate minerals, both silicates and non-silicate phases, of the Arsenatnaya fumarole with the depth. The less volatile Ca and Mg are fixed in deep zones while more volatile K and Na in upper zones. Al, being less volatile in comparison with K and Na, can be mobilized from the wall rocks altered by high-temperature gas enriched by alkaline components. This can cause the appearance of mineral assemblages replacing a basalt scoria which consist mainly of aluminosilicates: sanidine, kalsilite, leucite, sodalite, and haüyne. The more plausible source of Si and mechanism of Si mobilization is seemed to be an erosion of wall rock with its further incorporation to gas phase. However, it is not excluded that part of Si could be carried by volcanic gas.

This work was supported by the Russian Science Foundation, grant no. 19-17-00050 (mineralogical studies), and the Russian Foundation for Basic Research, grant 18-05-00332 (structural studies of inosilicates).

References

Getahun A., Reed M.H., Symonds R. Mount St. Augustine volcano fumarole wall rock alteration: mineralogy, zoning, composition and numerical models of its formation process // Journal of Volcanology and Geothermal Research. 1996. Vol. 71. p. 73 – 107.

Naboko S.I., Glavatskikh S.F. Post-Eruptive Metasomatism and Ore Formation. Nauka Publishing, Moscow. 1983. pp 165. (in Russian)

Pekov I.V., Koshlyakova N.N., Zubkova N.V., Lykova I.S., Britvin S.N., Yapaskurt V.O., Agakhanov A.A., Shchipalkina N.V., Turchkova A.G., Sidorov E.G. Fumarolic arsenates – a special type of arsenic mineralization // European Journal of Mineralogy. 2018a. Vol. 30(2). p. 305-322.

Sharygin V.V, Kamenetsky V.S., Zhitova L.M., Belousov A.B., Abersteiner A. Copper-containing magnesioferrite in vesicular trachyandesite in a lava tube from the 2012-2013 eruption of the Tolbachik volcano, Kamchatka, Russia // Minerals. 2018. Vol. 8. paper 514.

Symonds R.B., Reed M.H. Calculation of multicomponent chemical equilibria in gas-solid-liquid systems: calculation methods, thermochemical data, and applications to studies of high-temperature volcanic gases with examples from Mount St. Helens // American Journal of Science. 1993. Vol. 293. p. 758–864.

Symonds R.B. Rose W.I., Reed M.H., Lichte F.E., Finnegan D.L. Volatilization, transport and sublimation of metallic and non-metallic elements in high temperature gases at Merapi Volcano, Indonesia // Geochemica et Cosmochimica Acta. 1987. Vol. 51. p. 2083-2101.

Tessalina S.G., Yudovskaya M.A., Chaplygin I.V., Birck J.L., Capmas F. Sources of unique rhenium enrichment in fumaroles and sulphides at Kudryavy volcano // Geochimica et Cosmochimica Acta. 2008. Vol. 72. p. 889-909.

Zelenski M., Malik N. and Taran Yu. Emissions of trace elements during the 2012–2013 effusive eruption of Tolbachik volcano, Kamchatka: enrichment factors, partition coefficients and aerosol contribution // Journal of Volcanology and Geothermal Research. 2014. Vol. 285. p. 136–149.

Vergasova, L.P. & Filatov, S.K. A study of volcanogenic exhalation mineralization // Journal of Volcanology and Seismology. 2016. Vol. 10. p. 71–85.

Co IN THE FLUIDS IN CONVERGENT PLATE SETTING

Simakin A.G.[1,2], Salova T.P.[1], Tutunnik O.A.[3]

[1]Korzhinsky Institute of Experimental Mineralogy of the Russian Academy of Sciences, Chernogolovka, Russia, simakin@iem.ac.ru

[2]Institute of Physics of the Earth RAS, Moscow, Russia

[3]Vernadsky Institute of Geochemistry and Analytical Chemistry of the Russian Academy of Sciences, Moscow, Russia

The red-ox state of magmas and fluids in the subduction zones can be seen from: 1) cumulates in the former magma chambers in the suture zones 2) xenoliths cumulates in active volcanoes 3) aerosols in the fluids of active volcanoes 4) composition and mineral zoning in the erupted volcanic rocks. Generally fluid of the subduction zones is oxidized with fO_2 in the range NNO+1-NNO+2.

At the moment of release during dehydration and decarbonatization reactions in subducting plate fluid contains predominantly oxidized components H_2O and CO_2 with high intrinsic oxygen fugacity (NNO+3÷4). These components react with iron bearing melts and fO_2 in the magma-fluid system is equilibrated at NNO+1÷2 level. Similarly, the fluid exsolved from the basic magma contains predominantly CO_2 and H_2O, since the reduced components such as H_2 and CO, have a much lower solubility. After and during exsolution, CO_2 and H_2O react with the melt and form the reduced components CO, H_2, COS and other.

Much more reduced state can be reached at the reaction of the olivine cumulates with CO_2-H_2O at the high subsolidus temperatures. As we have demonstrated with thermodynamic modeling and petrologic data (Simakin et al., 2019) at the upper crustal pressures (200-300 MPa) and T=900-950^oC oxygen fugacity can drop to CCO (near QFM-2) buffer level. Reaction of olivine with fluid proceeds through generation of the forsteritic olivine and spinel with the increased magnetite content. The progress of this reaction can be tracked by the evolution of the spinel composition in the xenoliths of magmatic cumulates probed in the Shiveluch volcano (Fig. 1).

Fluids in the mantle wedge and deep crust tend to be localized in the horizontal packages (deep reservoirs) and in the linear shear zones (fault zones), rather than being uniformly distributed. When porous fluids are crossed by the moving magma, they are activated (by the thermal and hydro-fracturing) and penetrate the magma. Thakurta et al. (2008) demonstrated that in Duke Island (Alaska) ultramafic intrusion of Ural-Alaska type, the initial fO_2 in magma was about NNO+1.5. At the solidification of this intrusion olivine cumulates formed while residual andesites erupted. The formation of sulfides with Ni and PGE was caused by the invasion of reduced C-S bearing crustal fluid associated with the decrease of fO_2 to QFM level. Involvement of the midcustal reduced fluid can be anticipated based on data on the zonality of olivines from basalt erupted 3600 BP in Shiveluch volcano (Gordeychik et al., 2018). The growth zones of olivine with sharply increasing content of P, Cr and Ni can be attributed to the magma-fluid interaction.

The importance of carbon monoxide as an active component of reduced carbonic fluid is confirmed by new experimental results on platinum solubility at different pressures (see Fig.2). The double-capsule technique was used (Simakin et al., 2016) while fluid of CO-CO_2 composition was generated at the thermal decomposition of MgC_2O_4. Platinum content in fluid traps was measured with electro-thermal atomic absorption spectrometry (ETAAS). Solubility estimates based on quartz glass and corundum ceramics fluid traps are close, with a difference in the range 25-15 %. Corundum is a denser phase than silica glass therefore concentrations in the trap are lower at the same porosity (Fig.2). Absolute value of solubility at P=200 MPa and T=950^oC is estimated to be 590±50 ppm. In accordance with preliminary data in the presence of water (and probably organic polar substances formed in the reduced conditions) solubility rises at the same PT to c.a. 0.6 wt.% of Pt. In accordance with our experimental data platinum presents in the fluid as $Pt_3(CO)_6$ or probably as anion (Chini complex) $Pt_3(CO)_6^{2-}$. More experimental data are required to develop a robust model for the formation of PGE deposits in layered ultramafic-mafic intrusions and other environments in which the reduced fluid with high carbon content (graphite bearing rocks) is involved.

This study was supported by RFBR grant № 18-05-00597.

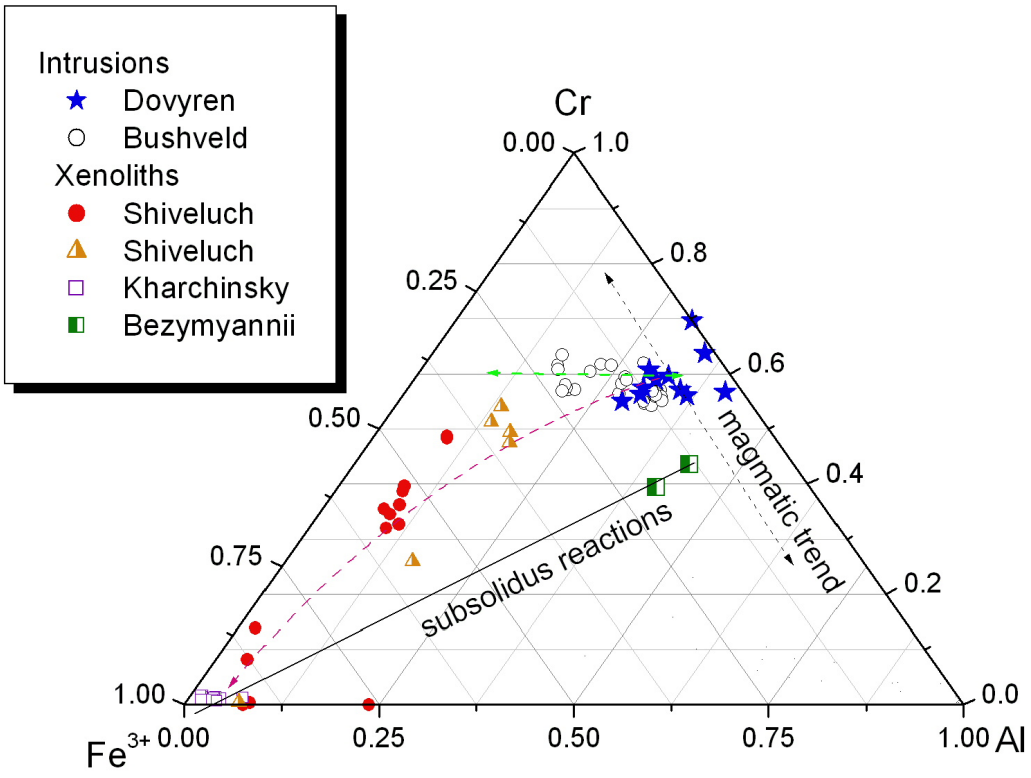

Figure 1. Composition of spinel from different magmatic settings: compositions along Cr-Al side follow magmatic crystallization trend; sequences directed to Fe^{3+} apex were formed at the fluid-cumulus interaction.

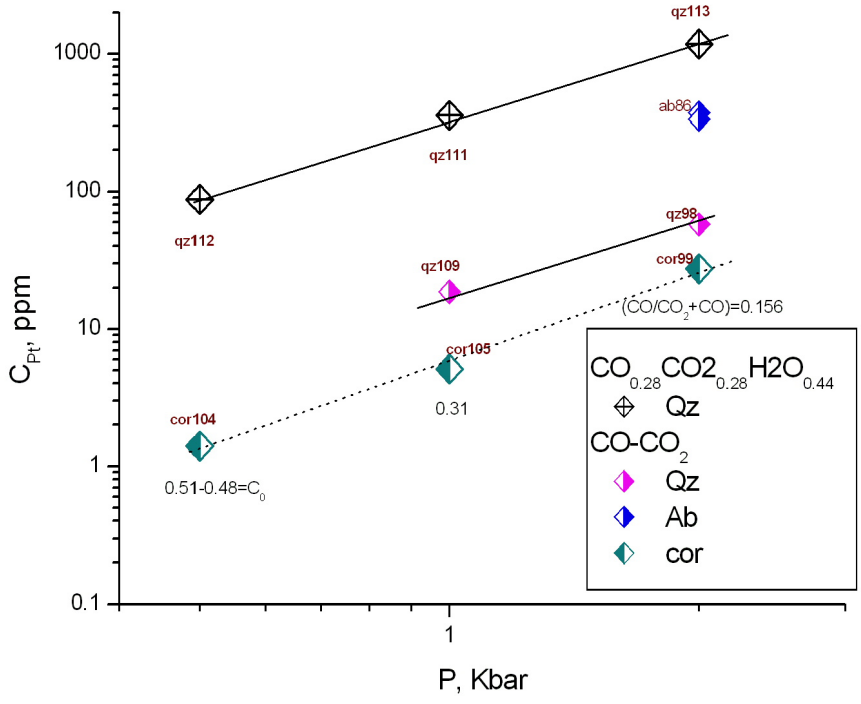

Figure 2. Dependence of the Pt content in the different fluid traps (quartz glass, albite glass and corundum ceramics) on pressure, T=950°C.

References

Gordeychik B., Churikova T., Kronz A., Sundermeyer C., Simakin A., Wörner G. Growth of, and diffusion in, olivine in ultra-fast ascending basalt magmas from Shiveluch volcano // Scientific Reports, 2018. Vol. 8(11775), pp. 1-15.

Simakin A.G.,. Salova T.P, Gabitov R.I. and Isaenko S.I. Dry CO_2–CO fluid as an important potential deep Earth solvent // Geofluids, 2016. Vol. 16, pp. 1043–1057.

Simakin A.G., Kislov E.V., Salova T.P., Shaposhnikova O.Yu., and Nekrasov A.N. Reduced CO2 Fluid as an Agent of Ore-Forming Processes: A Case Study of Dolomite-Replacement Skarns at the Yoko-Dovyren Massif // Petrology, 2019. Vol. 27(1), pp. 1–16.

Thakurta J., Ripley E.M. and Li C. Geochemical constraints on the origin of sulfide mineralization in the Duke Island Complex, southeastern Alaska // G3, 2008. Vol. 9(7), Q07003.

HISTORY OF DEVELOPMENT OF INTRUSIVE MAGMATISM IN THE URALIAN PLATINUM-BEARING BELT ON THE GROUNDS OF TO U-Pb DATING OF ZIRCONS FROM ROCKS, FORMING DIKES IN THE DUNITES OF KAMENUSHESKI MASSIF (MIDDLE URAL, RUSSIA)

Stepanov S.Yu.[1], Kutyrev A.V.[2], Lepekhina E.N.[3]

[1]Saint-Petersburg State University, Saint-Petersburg, Russia, Stepanov-1@yandex.ru
[2]Institute of Volanology and Seismology FEB RAS, Petropavlovsk-Kamchatsky
[3]A.P. Karpinsky Russian Geological Reserch Institute, Saint-Peterburg

Dikes of contrasting composition occur in the rocks of dunite-clinopyroxenite-gabbro intrusions along with the predominant rocks of the Uralian Platinum Belt, such as dunites, wherlites, clinopyroxenites, and gabbros. Hornblendites, gabbros, plagioaplites, and granites are among the rocks composing these dikes. The formation sequence of these dikes can be used to establish evolution patterns of intrusive magmatism, both within the Uralian Platinum belt and the Tagil island paleo-arc.

It is worth to be noted that the age of the dunite bodies, which are an integral part of the dunite-clinopyroxenite-gabbro intrusives, currently remains controversial (Efimov, 2009; Fershter et al., 2009; Anikina et al., 2012; Fershtater, 2013). And if isotope methods in most cases do not reliably determine the time beginning of the formation of dunite-clinopyroxenite-gabbro massifs, then the time of the end of their formation can be established with a high degree of confidence (Gottman et al., 2011). At the same time, the analysis of the formation sequence of different composition dikes can serve as a basis for assessing the evolution of intrusive magmatism within the Uralian Platinum belt.

The low degree of geologic certainty, the maximum possible number of various dike bodies (from wehrlites to granites) and the high degree of exposure of the Kamenushensky clinopyroxenite-dunite massif dunite “core” make this object most suitable for determining both relative and absolute age of dike bodies from among all massifs of Uralian Platinum belt. It is important to note that the evolution of intrusive magmatism within the Uralian Platinum belt and Tagil volcanic arc is studied in detail (Ivanov, 1998; Fershtater, 2013). This allows us to compare the results with already known facts. However, most researchers compare and correlate the results of their studies conducted for spatially separated geological bodies while the relationships between them are not clearly established. The results of our research, based on the presented geological data and, above all, an analysis of the intersecting relationships of geological bodies, allow for the first time for the Ural Platinum Belt to unambiguously characterize the sequence of different geological bodies formation, and subsequently to consider the evolution of intrusive magmatism using the example of a local geological object.

The relative age of dike and vein bodies in the dunites of the Kamenushensky massif was determined based on an analysis of their field relations. This became possible due to the high percentage of available polygons for geological observation. Clearly fixed and unambiguously interpreted spatial relationships of geological bodies within the dunite “core” of the Kamenushensky massif became a reliable basis for determining the age of rock formation using isotope methods. Such studies cannot be conducted for most massifs PBB due to either strong insufficient exposure and overlap with quaternary sediments, or weak distribution of dikes that do not intersect with each other.

Chromitites are the earliest veins in the dunites of the Kamenushensky massif, as in most zonal dunite-clinopyroxenite massifs. Some of them are syngenetic to the dunites and form vein-disseminated bodies, the other part forms epigenetic cutting veins (Zavaritsky, 1935). Chromitites are crossed by diopside veins (Stepanov et al., 2018). In turn, dunites containing clusters of chromite and diopside veinlets are crossed by a system of hornbendite and gabbro dikes. The most recent are dikes of biotite-containing granites, characterized by intersecting boundaries in relation to all the previously listed rocks. At the same time, the granites intruding caused the metasomatic processing in dunites with the formation of chlorite-actinolite alteration and the alteration of the gabbro to chlorite-epidote rock. In order to establish the upper age limit of intrusive magmatism within the dunite “core” of the Kamenushensky massif, it is advisable to examine in detail the hornblendites, gabbro, and granites composing the most recent dikes.

To solve the problems posed, zircons from gabbro-pegmatites, gornbendites and granites were studied. Zircon is widely distributed as an accessory mineral in all types of studied rocks. In dikes of gabbro-pegmatites, short-prismatic euhedral zircon grains were found, whose size may exceed 200 microns. Cathodoluminescence (CL) images reveal their course zonal and sectoral structure. Zircons are intergrown with pargasite and apatite, and, somewhat less often, they can be found separately from mafic minerals. Secondary inclusions of chlorite and epidote often occur along the cracks. Zircon from hornblendite dikes, in comparison with zircon from gabbro-pegmatite, is characterized by somewhat greater elongation and not so pronounced in the CL zonal and, especially, sectoral structure. At the same time, Hf zoning is a characteristic feature of hornblendite zircons. In the hornblende, zircon was found in accretion with albite, potassium-sodium feldspar and ilmenite. Zircons from granite dikes are characterized by a long prismatic appearance, weakly expressed, blunt-angled faces of a bipyramid, and the lack of zonal structure in CL, probably due to the extremely high concentrations of U and Th. Zircons grow together with titanite and quartz. Most rich in U zircons are partially metamict and host the inclusion of Ce-monazite, xenotime, and uraninite.

Thus, zircons from different types of rocks differ in morphological and anatomical features and a set of accompanying minerals found in the form of inclusions or accretions. In general, the investigated zircons differ in the number of impurity elements and, above all, in uranium and thorium. The zircons from gabbro-pegmatites are characterized by the lowest U contents: 30–206 g / t and Th: 7–130 g / t Th / U = 0.25–0.72. The content of U and Th in zircons from gornbendites is slightly higher than in zircon from gabbro-pegmatite - 25–573 and 12–256 g / t, respectively Th / U = 0.42–0.65. The highest U and Th contents among all the objects under consideration: 2,051–26,449 and 287–6,021 g / t, respectively, are inherent in zircons from granites and granite pegmatites. At the same time, Th / U ratios are the lowest, varying from which, as a rule, is characteristic of zircons from metamorphic and metasomatic rocks (Zircon, 2003).

The results of the U-Pb analysis of zircon are presented in the figure. The concordant U-Pb age, calculated on the base of 15 analytical points from 7 grains of zircons from gabbro-pegmatite from sample KR-7 (fig. a), was 418.3 ± 4.5 Ma (MSWD = 0.16). The concordant U-Pb age calculated on the base of 14 analytical points from 7 grains of zircons from hornblendites of sample KR-14 (fig. b) was 421.0 ± 2.4 Ma (MSWD = 0.97). Within the limits of errors in the determination of the age values, obtained for zircons from gabbro-pegmatites and hornblendites, is coincided. On the U-Pb diagram with concordia, 7 points of the isotopic composition of zircons from granites are located on concordia, and 9 points are located along the “reverse discordia” line (fig. c). Zircons from this sample, as described above, are characterized by extremely high concentrations of uranium. Williams and Hergt (2000) showed that in measurements on SIMS (SHRIMP) at concentrations of U over ~ 2500 ppm, the so-called “U-Pb matrix effect” occurs. This leads to a significant variation of isotopic ratios and, as a rule, overestimation of the $^{206}Pb/^{238}U$ ages. Thus, we believe that the U-Pb ages of 9 points with uranium concentrations above 3000 ppm are overestimated and do not accept them for calculations. At the same time, the weighted average $^{207}Pb/^{206}Pb$ age of zircons (fig. d), obtained over the entire set of measured points (n = 16) was 385.0 ± 6.3 Ma (MSWD = 0.96). The concordant U-Pb age, calculated by 7 points with the lowest concentrations of uranium (2051-3099 g / t), was 393.2 ± 2.5 Ma (MSWD = 0.109).

The age characteristics of rocks composing dunite-clinopyroxenite-gabbro complexes are widely discussed. The most controversial remains the question of the dunites formation time. The first isotope data on the age characteristics of ultramafic rocks were obtained in the study of zircons from the dunites of the Yudinskiy body, which is part of the Kytlym intrusion (Bea et al., 2001). At the same time, the ages obtained cover a wide range from the Archaean to the Upper Paleozoic. Further attempts (Malitch et al., 2009) of dating zircons from dunites, in general, did not allow us to reach a consensus on the formation time of the ultramafic part of the dunite-clinopyroxenite-gabbro series. However, if the age of the dunite-clinopyroxenite-gabbro intrusives formation remains the subject of discussion, then the time for the development of igneous rocks completion can be established with a high degree of confidence.

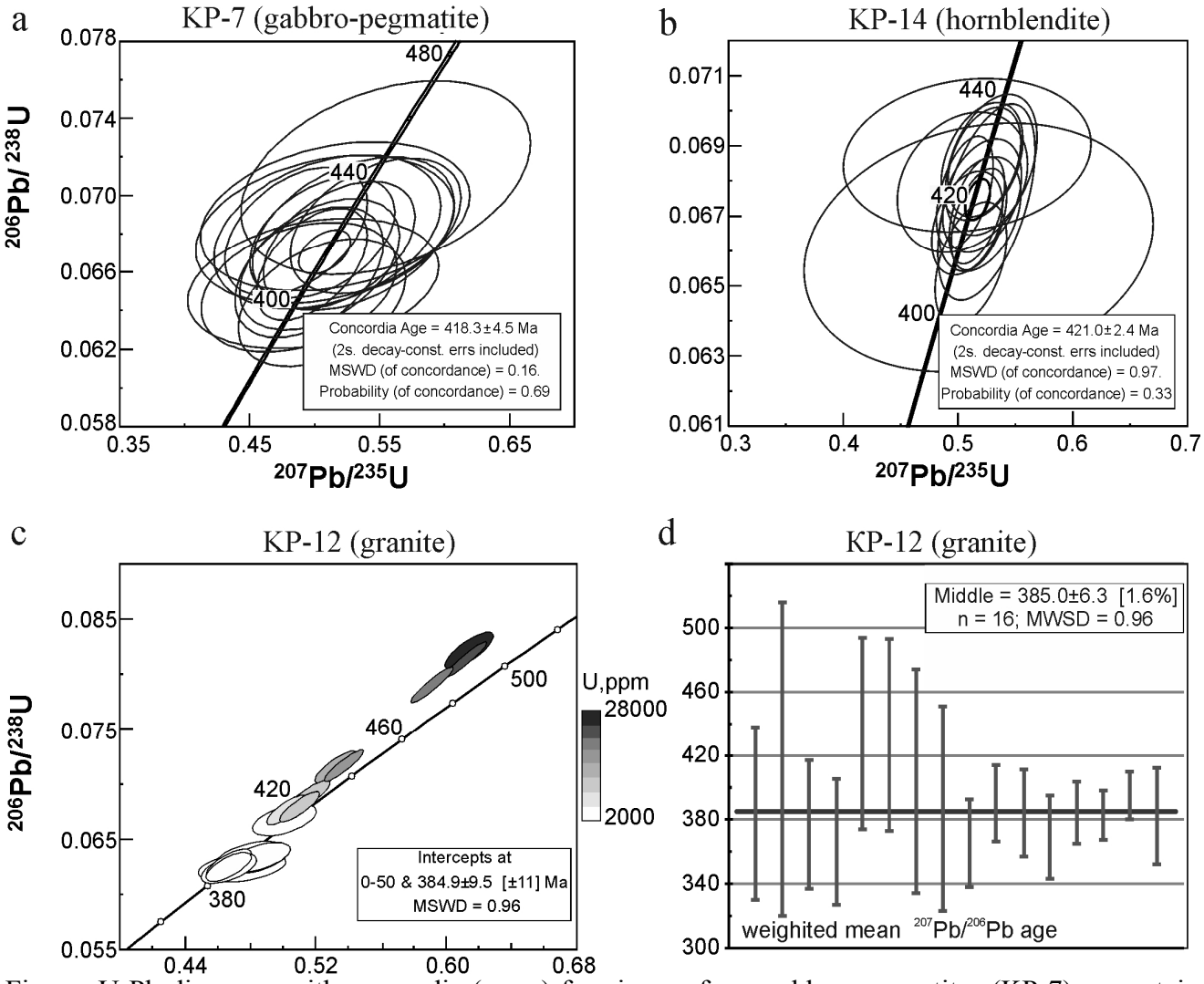

Figure. U-Pb diagrams with concordia (a – c) for zircons from gabbro-pegmatites (KP-7), mountain blendites (KP – 14) and granites (KP-12), and weighted average age of $^{207}Pb/^{206}Pb$ of zircons from granites (d).

In various sources, the upper age of ultramafic-mafic series formation, based on the study of the Svetloborsky dike complex (Ivanov, Kaleganov, 1993) and Kytlymsky (Pushkarev, Ronkin, 2014; Pushkarev et al., 2018) massifs can be assessed as Late Silurian. The results of our research are consistent with the data predecessors. However, it is important to emphasize that in the study of the dike complex in the dunite "core" of the Kamenushensky massif, Late Silurian age is characteristic both for gabbro-pegmatites, which are supposedly late differentiates of the dunite-clinopyroxenite-gabbro series, and for hornblendites, which likely are the differentiates of the gabbro series. For the latter, an age of 421 ± 2.4 Ma was obtained, which is close to the crystallization time of the residual melt, which forms when a gabbro series is formed in the gabbronorite intrusions (Bosch et al., 2006). It is this age that was adopted as the time for the formation of a gabbro (gabbronorite) complex as part of the Ural Platinum Belt (Anikina et al., 2010). Thus, the upper border of the dunite-clinopyroxene-gabbro series intrusion and the time of active development of the gabbro series is within the time span from 423.4 Ma to 413.5 Ma.

The completion of intrusive magmatism within the Tagil volcanic arc is associated with the introduction of the gabbro-diorite-granite Auerbach complex (Krasnobayev, Fershter, 2013). The age of 400–405 Ma is set for them (Fershter, 2013). A more ancient age is inherent in granites and other rocks of the leucogabbro-anorthosite-plagiogranite series, associated with the partial melting of previously formed gabbroids. Their formation fits into the time interval from 425 to 415 million years (Fershtater, 2013). By their geochemical parameters, the granites composing dikes in the dunites of the

Kamenushensky massif are like the anatectic granites of the Uralian Platinum Belt. According to zircon dating, they have an age of 384 ± 0.5 Ma. Thus, the processes of partial melting of gabbro and the formation of anatectic granites within the Uralian Platinum Belt did not end at 415 million years, as was assumed earlier, but continued throughout the entire period of the formation of the Tagil volcanic zone. These processes accompanied the transition from calc-alkaline island-arc magmatism to tholeiitic basaltic magmatism under back-arc spreading conditions, which culminated in the formation of riftogenic fine-grained amphibolite gabbro about 350 million years ago (Fershter, 2013). However, it is necessary to emphasize that zircons from granites, by the characteristics of their structure and composition and due to extremely high uranium contents and low uranium-thorium ratio can have a metasomatic nature (Zircon, 2003). The enrichment of zircons from granites with uranium can be associated with the influence of residual fluid accumulated during the differentiation of melts or the redistribution of a substance as a result of regional or contact metamorphism. The regularities of the structure of granitoid bodies in dunites, petrochemical and petrographic features of the studied granites (metasomatic transformations are not manifested), as well as the history of the geological development of the region, excludes the possibility of significant transformation processes of granites that could disturb the U-Pb system in zircons.

References

Anikina E.V., Alekseev A.V. Mineralogical and geochemical characteristics of gold-palladium mineralization in the Volkov gabbro-diorite massif (Ural Platinum-bearing Belt) // Lithosphere, 2010, № 5, p. 75 – 100 (In Russian).

Anikina E.V., Krasnobaev A.A., Rusin A.I., Busharina S.V., Kapitonov I.N., Lokhov K.I., Isotope-geochemical characteristics of zircon from dunite, clinopyroxenite and gabbro of the Ural Platinum-bearing Belt // Doklady Earth Scinces. 2012, V. 443, № 2, p. 513–516.

Gottman I.A., Pushkarev E.V., Kudryashov N.M. About the upper age boundary of the formation of dunites of the East – Habarninsky gabbro – ultramafic complex in the Southern Urals according to the U – Pb age of zircons from vein gornblenditov // Doklady Earth Scinces, 2011, vol. 438, No. 1, p. 539–597.

Efimov A.A. Platinum belt of the Urals: the current state of ideas about the geology, nature and history of the formation of a unique Russian object // Ultrabasite-basite complexes of folded regions and related fields, 2009, vol. 1, p. 176 – 179 (in Russian).

Ivanov K.S. The main features of the geological history (1.6–0.2 billion years) and the structure of the Urals. Ekaterinburg: IGG Ural Branch of the Russian Academy of Sciences, 1998. 252 p (in Russian).

Ivanov OK, Kaleganov B.A. // Reports of the Academy of Sciences, 1993, vol. 328, No. 6, p. 720-724 (in Russian).

Malich K.N., Efimov A.A., Ronkin Yu.L. Archean U-Pb isotope age of zircon dunites of the Nizhny Tagil massif (Ural Platinum Belt) // Doklady Earth Scinces, 2009, vol. 427 № 1, p. 851–855.

Stepanov S.Yu., Palamarchuk R.S., Khanin D.A., Varlamov D.A., Antonov A.V. The Distribution and form of finding the elements of the platinum group in the chromitites of the Svetloborsky, Veresoborsk and Kamenushensky clinopyroxenite-dunite massifs (Middle Urals) // Moscow University Bulletin. Series 4: geology. 2018, V. 73, №. 5, pp. 527–537.

Pushkarev E.V., Gottman I.A., Travin A.V., Yudin D.S. The age of the final stage of ultrabasic magmatism in the Ural Platinum Belt // Methods and geological results of studying isotopic geochronometric systems of minerals and rocks, 2018, p. 270 –273 (in Russian).

Pushkarev E.V., Ronkin, Yu.L., Yudin, DS, Travin, AV, Lepekhina, OP The formation time of nepheline tylaites in the Ural Platinum Belt: Sm – Nd–, Rb – Sr–, U – Pb–, 40Ar – 39Ar and K – Ar isotope datings and their limitations // Doklady Earth Scinces, 2014, vol. 455, № 1 , pp. 312–316.

Fershter G.B., Krasnobaev A.A., Bea F., Montero P., Levin V.Ya., Kholodnov V.V. Isotope-geochemical features and age of zircons from dunites of the Ural massifs of the platinum-bearing type, petrogenetic consequences // Petrology 2009, V. 17, № 5, pp. 539–558.

Fershter GB, Krasnobaev AA, Bea F., Montero P., Borodina N.S. Intrusive magmatism of the early stages of development of the Ural epiokeanic orogen: U-Pb geochronology (LA-ICP-MS, Nordsim, Shrinp-II), geochemistry, evolutionary laws // Geochemistry international, 2009, №. 2, pp. 143–162.

Fershter GB Paleozoic intrusive magmatism of the Middle and Southern Urals. Ekaterinburg: Due to the RIO UB RAS, 2013. 368 p. (in Russian)

Bea F., Fershtater G.B., Montero P., Whitehouse M., Levin V.Ya., Scarrow J.H., Austreim H. Pushkarev E.V. Recycling of continental crust into the mantle as revealed by Kytlym dunite zircons, Ural Mountains, Russia // Terra nova. 2001. P. 407-412.

Bosch D., Bruguier O., Efimov A.A., Krasnobayev A.A. (2006) U-Pb Silurian age for a gabbro of the Platinumbearing Belt of the Middle Urals (Russia): evidens for beginning of closure of the Uralian Ocean. In: Memoirs Geol. Soc. London, 32, 443-448.

Williams I.S., Hergt J.M. U-Pb dating of Tasmanian dolerites: a cautionary tale of SHRIMP analysis of high-U zircons // Beyond 2000: New Frontiers in Isotope Geoscience. Abstracts and Proceedings. Eds. J.D. Woodhead, J.M. Hergt, W.P. Noble. Lorne, 2000. P. 185-188.

Editors: John M. Hanchar, Paul W.O. Hoskin. Zircon // Reviews in Mineralogy and Geochemistry. Mineralogical Society of America. 2003. Vol. 53.

U-Pb GARNET AGES OF THE IJOLITES FROM KOLA ALKALINE PROVINCE MASSIFS

Stifeeva M.V., Salnikova E.B., Kotov A.B.

Institute of Precambrian Geology and Geochronology Russian Academy of Science, Saint-Petersburg, Russia, stifeeva.maria@yandex.ru

The dating of alkaline rocks and carbonatites is a rather complicated problem. These rocks contain a number of accessory minerals suitable for U-Th-Pb dating. However, most of these minerals are either very rare in alkaline rocks and carbonatites (e.g., zircon, calzirtite and thorianite), or susceptible to Pb loss, leading to low precision of isotopic measurements. Ca-garnet is common accessory mineral in alkaline rocks. The results of latest years studies demonstrated, that actinides and REE can substitute dodecahedral-coordinated cations. (Rák et al., 2011; Yudintsev et al., 2002). It's making Ca-garnet potential tool for U-Pb research.

One of the largest alkaline-ultramafic-carbonatite provinces (LIP) – Kola Alkaline Province. It's located in the Kola Peninsula, on the north-east part of Baltic Shield. The province is made up of agpaitic massifs, alkaline-ultramafic complexes with carbonatites, alkaline volcanics and enormous alkaline dykes. Most of the ultramafic, alkaline and carbonatite complexes is located within the Lapland-Kola-Belomorian collision zone. About twenty Paleozoic alkaline massifs, including two giant intrusions - Khibiny and Lovozero belong to this province. All of the massifs are a circular-concentric intrusions and comprise a series of ultramafic, alkaline and carbonatitic rocks. The main stage of alkaline magmatism in the Kola Peninsula occurred at ~375–385 Ma (Kramm et al., 1993, 1994; Arzamastsev, Wu, 2014).

Ca-garnet is a typical rock-forming mineral in ijolit-melteigite rocks series. We have studied garnet from pegmatoid ijolite of Vuoriyarvi massif, fine-grained ijolite and pegmatoid ijolite of Sallanlatva massif, pegmatoid ijolite of Salmagorskiy massif. All of the garnets samples represent a complex of solid solutions, dominated by andradite ($Ca_3Fe^{3+}{}_2Si_3O_{12}$), morimotoite ($Ca_3(Fe^{2+},Ti)Si_3O_{12}$) and schorlomite ($Ca_3Ti_2(Fe^{3+}{}_2,Si)O_{12}$); in minor parts by kimzeyite ($Ca_3Zr_2(Al_2Si)O_{12}$) and kalderite ($Mn_3Fe^{3+}{}_2Si_3O_{12}$). They form rhombic dodecahedral crystals of black or dark-brown color (light-brown in thin section) from 1 mm to 2 cm wide. The study of crystals with scanning electronic microscope don't found any mineral inclusions. Some of the garnet crystals (from Salmagora and from pegmatoid ijolite of Sallanlatva) are zoning: the abundance of Ti decrease from the core outward. The of Zr changing from 0.33 to 1.29 wt % (ZrO_2).

Garnets have high REE concentrations (from 5433 to 17595 ppm). The chondrite-normalized patterns for all samples shows convex-upward REE profiles and demonstrates enrichment in mid-range lanthanides. The garnet from Salmogorsky massif is different than others in low level of REE concentration (5433 ppm). Probably, the low REE abundances can be explained by the co-existence of these garnets with minerals capable of incorporating much higher levels of REE. The distribution of U is relatively uniform (7 – 10 ppm) and correlates with REE variations.

U-Pb ID-TIMS analyses were undertaken in the Institute of Precambrian Geology and Geochronology (IPGG) in St. Petersburg. Digestion of the garnets and Pb and U extractions were performed following a modified techniques of Krogh (Krogh et al., 1973), E. Horwitz et al. (Horwitz et al., 1992), and F. Corfu and T. Anderson (Corfu et al., 2001). The isotope analyses were performed using a TRITON TI multicollector mass spectrometer in static and dynamic (using an ion counter) modes. The analytical uncertainties in U/Pb ratios of the U and Pb concentrations were 0.5%, and the blanks were less than 10 pg for Pb and 1pg for U. The raw data were processed using PbDAT (Ludwig, 1989) and ISOPLOT (Ludwig, 2012). Common Pb correction was applied according to the model of Stacey and Kramers (Stacey et al., 1975). All errors are reported as 2σ.

For U-Pb study we hand-picked the most translucent and visibly homogeneous single-crystal fragments at 100-200 μm in size. The selected grains were then cleaned ultrasonically in purified water, and washed in a soft acidic bath. The latter treatment was performed for 20-30 minutes on a hot plate using a warm 8M – 3M HCl solution (DeWolf et al., 1996).

The garnet from Vuoriyarvi massif is characterized by relatively high concentration of U (4.8 – 8.0 ppm) and by a low common Pb (Pb_c/Pb_t = 0.5). The analytical data plot near the Concordia. The average $^{206}Pb/^{238}U$ age is at 373±2 Ma.

Two garnet samples from different rock types of Sallanlatva massif is characterized by relative high concentration of U (5.8 – 8.5 ppm) and by a low common Pb (Pb_c/Pb_t = 0.2 – 0.7). The garnets from fine-grained ijolite plot yield concordia age of is 375±2 Ma (MSWD = 0.0095). The concordia age of garnet from pegmatoid ijolite is at 373±6 Ma (MSWD = 0.08, Probability = 78%).

The garnet from Salmagorsky massif is characterized by U content ranging from 6.5 to 8.8 ppm and by a low common Pb (Pb_c/Pb_t = 0.3 – 0.4). The concordia age of this garnet is at 377±1 Ma (MSWD = 0.40, Probability = 53%).

U-Pb ID-TIMS ages obtained for garnets from three different massifs of the Kola Province (373-377 Ma) are in good agreement with earlier obtained garnet age data for calcite-amphobole-pyroxene pegmatite from the Afrikanda massif (377±3 Ma) (Salnikova et al., 2018). The studied garnets yield U-Pb age data of similar precision to those reported for well proven zircon, baddeleyite and perovskite. The U-Pb ID-TIMS ages demonstrate the advantages of calcic garnets for timing of alkaline-ultramafic-carbonatite intrusions and allow to shorten duration of the main stage of alkaline magmatism within the Kola Alkaline Province.

The study is supported by RFBR, grant 17-05-00912.

References

Rák, Zs., Ewing, R.C., Becker, U., 2011. Role of iron in the incorporation of uranium in ferric garnet matrices // Physical Review B84, 155128. 2011.

Yudintsev, S.V., Lapina, M.I., Ptashkin, A.G., Ioudintseva, T.S., Utsunomiya, S., Wang, L.M., Ewing, R.C. Accommodation of uranium into the garnet structure. // Materials Research Society Symposium Proceedings 713, 2002. JJ11.28. p. 1-4.

Kramm, U., Kogarko, L.N., Kononova, V.A., Vartiainen, H. The Kola Alkaline Province of the CIS and Finland: Precise Rb-Sr ages define 380-360 age range for all magmatism. // Lithos. 1993. Vol. 30, p. 33-44.

Kramm, U. Isotopic evidence for ijolite formation by fenitization: Sr–Nd data of ijolites from the type locality Iivaara, Finland.//Contrib. to Mineralogy and Petrology. 1994. Vol. 115, p. 279–286.

F. Y. Wu, A. A. Arzamastsev, R. H. Mitchell, Q. L. Li, J. Sun, Y. H. Yang, and R. C. Wang Emplacement age Sr-Nd isotopic composition of the Afrikanda alkaline ultramsfic complex, Kola Peninsula, Russia. // Chemical Geology. 2013. Vol. 353, p. 210–229.

Krogh, T.E. A low-contamination method for hydrothermal decomposition of zircon and extraction of U and Pb for isotopic age determination. // Geochimica et Cosmochimica Acta. 1973. Vol. 37, p. 485–494.

Horwitz, E. P., Dietz, M. L., Chiarizia, R., Diamondm H., Essling, A. M., Graczyk, D. Separation and preconcentration of uranium from acidic media by extraction chromatography. // Analitica Chimica Acta. 1992. Vol. 266, p. 25–37.

Corfu, F., Andersen, T. B. U–Pb ages of the Dalsfjord Complex, SW Norway and their bearing on the correlation of allochthonous crystalline segment of the Scandinavian Caledonides. // International Journal of Earth Science. 2002. Vol. 91, p. 955-963.

Ludwig, K. R., 1991. PbDat for MS-DOS, version 1.21 U.S. Geological Survey Open-File Report 88-542, 35 p.

Ludwig, K.R., 2003. Isoplot 3.70. A Geochronological Toolkit for Microsoft Excel //. Berkeley Geochronology Center Special Publications. 2003. Vol. 4, 70 p.

Stacey, J.S., Kramers, J.D. Approximation of terrestrial lead isotope evolution by a two-stage model. // Earth and Planetary Science Letters. 1975. Vol. 26, p. 207- 221.

DeWolf, C. P., Zeissler, C. J., Halliday, A. N., Mezger, K., and Essene, E. J. The role of inclusions in U-Pb and Sm-Nd garnet geochronology: Stepwise dissolution experiments and trace uranium mapping by fission track analysis. // Geochimica et Cosmochimica Acta. 1996. Vol. 60, p. 121–134.

Salnikova, E.B., Stifeeva, M.V., Chakhmouradian, A.R., Glebovitsky, V.A., Reguir, E.P. The U–Pb system in schorlomite from calcite–amphobole–pyroxene pegmatite of the Afrikanda complex (Kola Peninsula). // Doklady Earth Sciences. 2018. Vol. 478, p. 148–151.

LIQUID IMMISCIBILITY AS A FACTOR OF THE FORMATION OF STRATEGIC METAL ORES

Sokolov S.V.

Fedorovsky All-Russian Scientific-Research Institute of Mineral Resources, Moscow, Russia

In the national geological literature, liquid immiscibility – magmatic differentiation is regarded as a process of the separate of homogeneous magma into two (very rarely three) independent melts of different chemical composition, density and viscosity. Liquid immiscibility may sometimes be accompanied by the separation of a fluid phase of low density.

Evidence of the role of liquid immiscibility in the origin of rocks and ores is based on the following facts (Sokolov, 1994): 1) the existence, in nature, of associating compositionally contrasting rocks whose origin cannot be explained by the mechanism of crystallization differentiation, 2) the presence emulsion <<liquid-in-liquid>> textures in rocks, and 3) liquid immiscibility was detected in experiments with artificial systems similar in composition to natural magmatic systems at the same PT parameters. Note that the most unbiassed indication of the existence of this phenomenon is melt inclusions of the "liquid immiscibility" type in which traces of the separation of a liquid phases is seen under an optical microscope when microthermometric homogenization experiments are conducted (Roedder, 1984).

Numerous facts indicate that liquid immiscibility is widespread process and occurs in magmas of various composition during their magmatic differentiation. In mentioning the considerable participation of liquid immiscibility in petrogenesis, it should be emphasized that it plays a certain role in the redistribution and concentration of different metals (including strategic) in some separated melts.

The origin of ores of by means of liquid immiscibility was suggested many types of useful minerals, many of which are strategic raw materials. At the same time, experiments show that, unlike melts, solutions separated in relation to liquid immiscibility can only very rarely produce ores (Marakushev et al., 1994b).

Factors immediately affecting the onset and stabilization of liquid immiscibility can variously affect initial magmas of different composition. The preceding crystallization differentiation would contribute to the liquid immiscibility because brings them closer to lower temperature eutectic and enriches the melts in fluids that facilitate the onset of liquid immiscibility. Therefore, one of the main factors that control this process is likely volatile components (CO_2, H_2O, F, Cl, S, B) and alkalis.

A decrease in temperature favors the expansion of the field of stratification and stability of separated liquid phases. The ambiguity of the effect of pressure on the emergence and extent of manifestation of liquid immiscibility due to a dependence from the chemical composition with the initial magmas (rocks), temperature, as well as the common content and composition of fluid components and the relationship between them.

Without claiming completeness of the offered information, we present examples of ore-producing influence of the liquid immiscibility phenomenon for certain strategic metals (they are printed in bold) based on petrographic and mineralogical-geochemical studies, as well as on the results of experiments.

1. Nodular chromite ores, known in peridotite massifs of geosyncline areas in the USSR (Urals, Caucasus) and foreign countries (Bulgaria, Cuba, Pakistan), formed during the process of liquid differentiation of the **Cr**-bearing ultrabasic magma at significantly silicate and substantially oxide fractions (Pavlov et al., 1975).

2. In experiments on liquid differentiation of picrite magmas, basic and ultrabasic melts were produced, which captured **Cr** in different quantities (Marakushev et al., 1994a). Remarkable that, during this process, there were two types of ores of varying composition of **Cr** spinels and related **PGE**.

3. It should be emphasized that processes of liquid immiscibility have been involved in the formation of giant-scale deposits of strategic raw materials. Very large accumulations of **Cr** and **PGE (**principally, **Pt** and **Pd)** ores known in the rhythmic layering Bushveld intrusive. A.A. Marakushev and co-authors (1998) consider that the uniqueness of this massif "defines a specific magmatic

differentiation, because of which there were three types of fluid melts (sulfide-bearing chromitic and pyroxenitic, and hortonolite-dunitic)."

4. Another example are the exclusively large deposits of **Cu** and **Ni**, associated with massifs of basic rocks of the Norilsk area. They are represented by sulfide ores with a distinctly pronounced textures of liquid immiscibility type (Genkin et al., 1977). Emulsion impregnation of sulfides (pyrrhotite, troilit, pentlandit, cubanit, chalcopyrite) often forms of rounded and drop-similar accumulations in the picritic gabbro-dolerites.

5. E. Roedder (1979) cited numerous literary data on the results of experiments and petrographic observations indicating about separating from the basalt magmas of sulfide melts, which included industrial concentrations of **Cu** and **Ni**, as well as **Co** and Zn.

6. V.A. Zharikov with colleagues (1986) showed that the influence of various volatile on basalt magmas leads to separation of the diverse by composition of the salt melts (chloride, sulfide, carbonate, phosphate), that is largely determined by the content and ratio of F, CO_2, H_2O, Cl, S etc in fluid phase. These melts selectively accumulate strategic metals: for example, sulfide melt concentrated **Cu**, **Au**, **Ag**, **Ni** and **PGE**, and carbonate melt enriched in **Ta** and **Nb**.

7. It should be noted that a clear separation of metals occurs also between co-existing and differ on composition liquids also happened in silicic systems. For example, melting of trachyrhyolites from Central Mongolia was accompanied by separation from the initial melt enriched in fluids fraction of the fluoride-calcium composition. Silicate melt contained a few elevated amounts of **Pb**, Cs and Rb, whereas salt melt was enriched in **Zr**, **Nb**, **Ta**, **U**, Th, **HREE** and especially **Y** (Peretyazhko et al., 2018).

8. Quartz from F-granites of the rare-metal deposit Orlovskoe (Eastern Transbaikalia) contains melt inclusions of silicate composition with different content of Al, F, Na and K, which suggests heterogeneity (liquid immiscibility) of the parent melt (Badanina et al., 2018). It is remarkable that inclusion with markedly higher content of F have elevated concentrations of **Ta, Nb**, **Ti**, **W**, Zn, **Y** and **HREE**.

9. E.N. Gramenitsky and co-authors (2005) experimentally showed that Li-F granite magma breaks down into alumo-silicate liquid, which concentrate in Rb, **Zr**, Hf, **Nb**, **Ta**, Ga, **Ge**, and rich fluids salt liquid of alumo-fluoride composition enriched in **Li**, **REE**, **Y**, **Sc**, Th.

10. According to A. Müller and co-authors (2018), the formation of rare metal pegmatites in southern Norway took place with the participation of two coexisting alumo-silicate melts and equilibrium with them of fluid phase. Given data demonstrate the efficient distribution of metals between alkali-H_2O-poor fraction responsible for the formation of bulk pegmatites and F-H_2O-alkali-rich fraction which corresponds to the albite zone and is characterized by elevated contents of **Li**, Cs, Rb, **Ta**, **Nb**, **Ge**.

11. An unusual distribution of rare earth metals was determined in experiments on silicate-carbonate liquid immiscibility in the presence of CO_2 vapor (Wenlandt and Harrison, 1979). All lanthanides are mostly concentrated in the carbonate melt (i.e. in carbonatites), with enrichment coefficients of relative to silicate melt 2-3 for LREE and 5-8 for **HREE**.

Data presented above testify that deposits of the liquid immiscibility type (including large deposits) are genetically related to ultrabasic-basic magmatism, known for such strategic metals as **Cr**, **PGE**, **Cu**, **Ni**, **Co** (see §§ 1-6). Segregation processes shown in relation to the silicic rocks, pegmatites and carbonatites are characterized by other metallogeny of the strategic elements: **Zr**, **Li**, **Nb**, **Ta**, **REE_Y**, **Y**, **Sc**, **Ge** (see §§ 6-11).

References

Badanina E.V., Thomas R., Syritso L.F. Early stage of heterogenization of melt in rare metal granites of plumasitic type // XVIII All-Russian conference on thermobarogeochemistry. Moscow: 2018, p. 22-23. (in Russ).

Genkin A.D., Kovalenker V.A., Smirnov A.V., Muravitskaya G.N. Characteristics and genetic implications of mineral composition of impregnated sulfide ores on the Norilsk deposit // Geology of Ore Deposits. 1977, № 1, p. 24-38. (in Russ).

Gramenitsky E.N., Schekina T.I., Devyatova V.N. Differentiation of fluorine-containing granite and alkaline magmas and behaviour of ore elements according to experimental dada // In Proceedings of International (X All-Russian) Petrographic Conference. Volume 4. Metamorphism, cosmic, experimental and general issues of petrology. Apatity: KSC RAS. 2005, p. 83-85. (in Russ).

Marakushev A.A., Gramenitskiy E.N., N.I. Bezmen A.A. et al. Ore concentration processes in magmatic systems // In Experimental problems of geology. M.: Nauka, 1994a, p. 182-245. (in Russ).

Marakushev A.A., Shapovalov Yu.B, Glazovskaya L.I., Parfenova O.V. An Experimental Investigation of the Fluoride Extraction and the Problem of the Genesis of Rare Earth Metal Deposits // Geology of Ore Deposits. 1994b, № 4, p. 291-309. (in Russ).

Marakushev A.A., Paneyakh N.A., Rusinov V.L., Pertsev N.N., and Zoton I.A. Petrological Model of Formation of Giant Ore Deposits // Geology of Ore Deposits. 1998, № 3, p. 236-255. (in Russ).

Müller A., Spratt J., Thomas R., Williamson B.J., Seltmann R. Alkali-F-rich albite zones in evolved NYF pegmatites: the product of melt-melt ummiscibility // Canadian Mineralogist. 2018. Vol. 56, p. 657-687.

Pavlov N.V., Grigorieva I.I., Tsepin A.I. Chromite nodules as indicator of liquation in magmatic melt. // Proceedings of the USSR Academy of Sciences. Geological Series. 1975, № 11, p. 29-45. (in Russ).

Peretyazhko I.S., Savina E.A., Kotelnikov A.R., Suk N.I. Features of distribution of elements-impurities between fluoride-calcium and trachyrhyolitic immiscibility melts // In Proceedings of Russian Annual Seminar on Experimental Mineralogy, Petrology and Geochemistry. M.: GEOKHI RAS. 2018, p. 125-128. (in Russ).

Roedder E. Silicate liquid immiscibility in magmas // In The Evolution of the Igneous Rocks. Edited by H.S. Yoder, Jr. Princeton University Press, 1979, p. 15-57.

Roedder E. Fluid Inclusions. Reviews in Mineralogy. Vol. 12. 1984, 644 p.

Sokolov S.V. Melt inclusions in minerals as indicators of rocks and ores formation by liquid immiscibility // International Mineraljgical Association. 16th General Meeting 4-9 September 1994, Pisa, Italy. Abstracts, 1994, p. 387.

Wendlandt R.F., Harrison W.J. Rere earth partitioning between immiscible carbonate and silicate liquids and CO_2 vapor: results and implications for the formation of light rare earth-enriched rocks // Contrib. Mineral. and Petrol. 1979. Vol. 69, p. 409-419.

Zharikov V.A., Gorbachev N.S., Ishbulatov R.A. Fluid magmatic differentiation of the basic magmas // Geology and Geophysics. 1986. № 7, p. 35-40. (in Russ).

PARENTAL MAGMA OF UITKOMST MASSIF (BUSHVELD MAGMATIC PROVINCE): A STUDY OF OLIVINE-HOSTED INCLUSIONS

Solovova I.P.[1], Yudovskaya, M.A.[1,2], Zinovieva N.G.[3], Averin A.A.[4]

[1]Institute of Geology of Ore Deposits (IGEM) RAS, Moscow solovova@igem.ru

[2]School of Geosciences, University of Witwatersrand, Wits 2050, South Afric

[3]Moscow State University, Department of Geology, Moscow

[4]Frumkin Institute of Physical Chemistry and Electrochemistry RAS, Moscow

Layered intrusions have a complex structure and associate with large deposits of platinum group elements, Cr, V, and Ni. The Bushveld complex (2050 Ma) includes dyke-like and sill-like norite intrusions, layered mafic-ultramafic bodies, and associated silicic igneous rocks and carbonatites. The composition and genesis of parental Bushveld magmas are still disputable. Many researchers evaluated the possible composition of the parental magma using computer modeling. Our approach to this problem is based on the investigation of inclusions in minerals. This contribution reports the results of a study of inclusions in cumulus olivine (Fo_{90-91}) from ultramafic rocks in the central part of the Uitkomst massif, a small satellite intrusion of the Bushveld complex.

Inclusions were investigated in olivine from cumulus dunites. Rare muliphase crystallized inclusions were interpreted as primary melt inclusions (Fig. a-d). Sometimes, combined spinel + melt inclusions were observed. The silicate material of such inclusions at the boundary with the host olivine is meniscus-shaped, which indicates its initially liquid state. The inclusions contain daughter phases dominated by olivine and orthopyroxene. During heating experiments, melting of daughter phases was observed starting from 1000°C. Complete homogenization was not achieved, and a small gas bubble was retained even at the maximum experimental temperature of 1430°C.

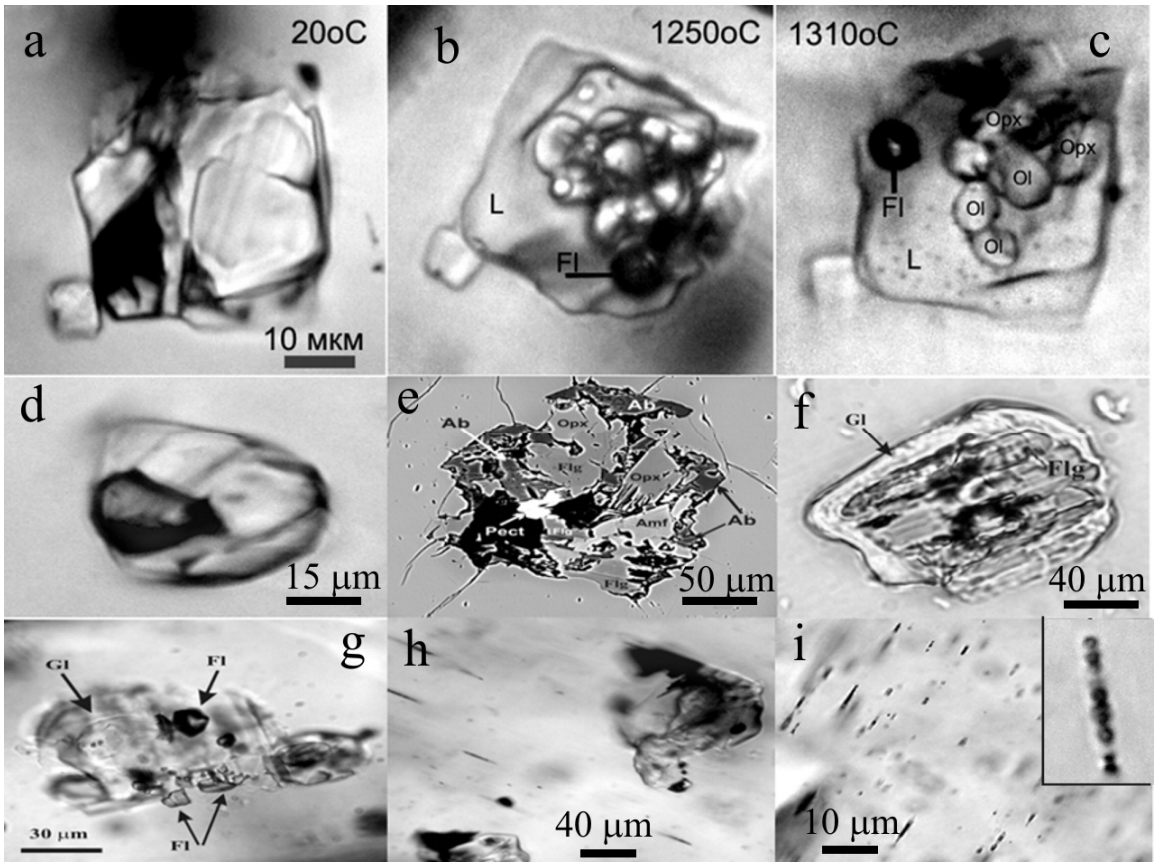

Figure. Photomicrographs of inclusions in olivine. a-d and f-i – transmitted-light, e – back-scattered electron image. a-d – primary melt inclusions at 20°C, 1250°C, 1310°C and 20°C, respectively. e-h – xenoliths of multimineral inclusions in olivine. f – xenolith surrounded by a rim of reactive glass. g – partly decrepitated xenolith. h-i – subparallel trails of the smallest fluid inclusions. h – the inset shows trail of fluid inclusions at 1200 magnification. L-melt, Fl – fluid, Gl – glass.

The compositions of the melt inclusions were determined using an electron microprobe and recalculated to equilibrium with the host olivine (Fo_{91}): 53–57 wt% SiO_2, <4.3 wt% CaO, and up to 2.9 wt% Na_2O+K_2O. The most primitive melt contains 20.5 wt% MgO and 12 wt% FeO.

Trace and volatile elements were analyzed by SIMS. Glasses from the heated melt inclusions contain 30–430 ppm H_2O. Melts with the highest MgO contents are characterized by low heavy rare earth element (HREE) contents, a steep REE distribution pattern (La_{PM}/Yb_{PM} up to 35.5), and the absence of a Eu anomaly. The low heavy REE contents indicate the retention of garnet in the residue. The relatively low contents of fluid-mobile large-ion lithophile elements (280 ppm Ba, 230 ppm Sr, 4 ppm Th) are consistent with the volatile-poor composition of the parental magma and the absence of primary fluid inclusions in minerals. The high-MgO magma is strongly enriched in Ni and V, which is of particular importance for determining the source of ore components. The correlation of Th/Zr with Nb/Zr indicates the occurrence of fluid metasomatism prior to the magma generation event (Yu et al., 2019).

The conditions of magma formation in the mantle were estimated using the olivine-orthopyroxene-melt thermobarometer of Girnis (2003). The obtained conditions of high-MgO melt formation are 1520°C and 1.8 GPa. The estimated composition and P–T parameters of melt generation indicate that the primary cumulus assemblage of the massif crystallized from a komatiite-like melt (Wilson, 2012; Yudovskaya et al., 2013).

In addition to the high-MgO inclusions, there are primary melt inclusions with 14–16 wt% MgO. These inclusions exhibit a negative Eu anomaly and high contents of H_2O (up to 2300 ppm) and fluid-mobile elements (Ba, Sr and Th). The strong correlation of $(La/Nb)_{PM}$ and $(Th/Ta)_{PM}$ indicates that the melt underwent mid-crustal contamination (Yu et al., 2019). This is supported by the presence of multimineral inclusions up to 300 □m in size in olivine (Fig. e-h), which were interpreted by us as crustal xenoliths. They are composed of orthopyroxene, Ca-amphibole (pargasite), phlogopite, albite, pectolite, Cl-apatite (up to 6 wt%), titanite, perovskite, rutile, ilmenite, sodalite and natrolite. These mineral aggregates are often surrounded by a reaction rim consisting of glass (Fig. f). Sometimes these xenoliths are partly decrepitated and are surrounded by small melt and fluid satellite inclusions (Fig. g), which indicates their post-entrapment heating. Olivine with such xenoliths contains numerous subparallel trails of tiny fluid inclusions (<1 μm) (Fig. h, i). The SIMS analysis of olivine with such inclusions showed up to 4000 ppm H_2O and 25 ppm Na, and its IR absorption spectrum exhibits a band at 3700-3750 cm^{-1}, which is characteristic of water. Single fluid inclusions of a negative crystal shape and up to 15 μm in size were occasionally found. Their Raman spectra showed that they are CH_4-dominated and contain N_2, H_2, graphite and a solid phase with OH groups.

The parental high-MgO melt is characterized by low CaO, TiO_2, H_2O and high SiO_2 and REE contents with LREE>HREE. This supports the hypothesis of a depleted harzburgitic source pre-enriched with metasomatic fluids. More evolved magmas (MgO<16 wt%) were affected by crustal contamination, which resulted in their enrichment in Na, Ca, H_2O and Cl.

This study was financially supported by the Russian Foundation for Basic Research (18-05-00291). The authors acknowledge partial support of Moscow State University (Program of Development).

References

Girnis A.V. Olivine-Orthopyroxene-Melt Equilibrium as a Thermobarometer for Mantle-Derived magmas // Petrology. 2003. Vol. 11 (2). p. 101-114.

Wilson A. A Chill Sequence to the Bushveld Complex: Insight into the First Stage of Emplacement and Implications for the Parental Magmas // J. Petrol. 2012. Vol. 53. p. 1123-1168.

Yu L., Fengyue S. F., Liang L., Li B., Peng B., Xua C., Li R., Wangd F., Shene D. Geochronology, geochemistry, and Sr–Nd–Hf isotopic compositions of mafic–ultramafic intrusions in the Niubiziliang Ni–(Cu) sulfide deposit, North Qaidam Orogenic Belt, NW China: Implications for magmatic source, geodynamic setting, and petrogenesis // Lithos. 2019. Vol. 326–327. p. 158–173.

Yudovskaya M. A., Kinnaird J. A., Sobolev A. V., Kuzmin D. V., Mcdonald I., Wilson A. H. Petrogenesis of the Lower Zone olivine-rich cumulates beneath the Platreef and their correlation with recognized occurrences in the Bushveld Complex // Econ. Geol. 2013. Vol. 108. p. 1923–1952.

LAMPROITOIDES OF THE MAGNITOGORSK MEAZONE (SOUTH URALS): PETROLOGIC-GEOCHEMICAL FEATURES AND GEODINAMIC CONDITIONS OF THEIR FORMATION

Surin T.N.

Federal State Budgetary Institution "A. P. Karpinsky Russian Geological Research Institute", Saint-Petersburg, Russia, Timofey_Surin@vsegei.ru

The Magnitogorsk megazone is one of the largest paleovolcanic submeridional belts of Southern Urals. It's an nothern branch of the Magnitogorsk-Mugojar ancient Island Arc system and is identified with Magnitogorsk Island Arc. This arc got through a long complicated history of development. Three distinctly expressed stages of its evolution may be described. The first stage is suboceanic (margin sea), it was displayed in Ordovician-Silurian. The second is the island arc stage, it took place in the mid Devonian and early Carboniferous. The third stage (collision and accretion) finishes the tectonic development of its region in the mid Carboniferous - Permian. The stabilization in subplatforms regime has taken place later on.

Lamproitoides were not known in the Urals until recently. For the first time they were found out in 1990 in the career of the Maleye Kuibas iron ore deposit during detailed geological maping of the Magnitogorsk ore area and later was defined as lamproites (Lukianova et al.,1992). At present inside the limits of the East-Magnitogorsk paleovolcanic belt about three tens of manifestations of lamproitoidic magmatism has already been revealed. They are introduced exclusively by subvertical dykes with visible thickness varying from 1 to 10 meters. According to the geochronologic data (K-Ar and Rb-Sr) its age is determined as mid Triassic - early Jurassic (197-240 millions years). Up to now the manifestations of Mezozoic magmatism in this section of the Urals were not known.

These rocks form the unified petrogenetic series, uniting the formations from an ultrabasic to a mediosilicic composition. Tthe dark-grey-brown-green colour, massive structure, the porphyritic texture and the microlites or glassy matrix are typical for them. The phenocrysts summary volume does not exceed 20 %, the size - from 0,3 to 2,5 mm. The phenocrysts are submitted olivine (1-10%), phlogopite (5-15%), clynopyroxene (1-10 %), less often leucite (to 5%). In the matrix the small-sized allocation phlogopite, diopside, enstatite, apatite, sanidine, richterite are defined. Olivine forms oval or wrong form of grains. The large phenocrysts contain the heaviest quantity MgO (Fo 95), in the small-sized crystalls MgO is less (Fo 88-89). Olivines do not contain CaO. Almost always olivine is superseded by serpentine and calspar. Phlogopite forms the plate-phenocrysts and small-sized scale and needle allocation in the matrix, making from 5 to 40 % the rocks volume. It is Ti-contains version (20-25% MgO, 0,7-4,0% TiO_2, 12-14,2% $A1_2O_3$, 6,6-10,5% K_2O) . The Ratio of aluminium and iron of the phlogopites is close to micas from lamproites of other regions. The tendency of reduction of Al_2O_3 content with growth of FeO, that is on the whole typically for lamproites, is observed. In phlogopite $A1_2O_3$and TiO_2 are connected by distinct negative dependence, that is more characteristic for rich-istonite phlogopites from kimberlites (Mitchell, 1985). With increase of TiO_2 in micas MgO is lowered sharply, thus from internal to external zones of phenocrystalls the MgO content decreases and TiO_2 increases that is typically for lamproites (Mitchell, 1985 and Jaques et al., 1986). Phlogopite is frequently replaced by chlorite. Clynopyroxene forms the prismatic microphenocrysts of the size to 0,5 mm and the microlites in the matrix. It is poor aluminium diopside (TiO_2 0,25-0,49%, $A1_2O_3$ 0,45-1,20%, FeOsum 3,20-4,20%, Na_2O (0,36-1,25%) and considerably less often Ti-augite (TiO_2 1,02-1,90%). In the endocontact zones of dykes the leucites pnenocrysts (size to 0,5 mm) possessing characteristic eight-coal cuts, are revealed. Leucite is usually replaced by sanidine, which contains the increased quantity Fe_2O_3 (0,4-2,5%), that is typically just for lamproites (Mitchell, 1985). Enstatite is rare, it is comparable with olivine (MgO 36,91%, FeOsum 3,79%) on the contents of iron. Amphibole is colourless Ti-richterite (TiO_2 2,60-5,30%, MgO 2,92-6,00%, CaO 2,62-15,01%, FeOsum 19,29-25,25%, Na_2O 4,44-12,41%, K_2O 0-0,15%).

According to mineralogical analysises the following accessory minerals were found: Cr-dyopside (0,9-1,56% Cr_2O_3), Cr-spinel (81-92 Cr/Cr+Al, 0,3-0,9% TiO_2, 0,1-0,6% MnO), garnets of pyrope-almandite-spessartite series, including very rare high-Cr pyrope (2,62-5,13% Cr_2O_3, 4,82-

6,10% CaO), Ti-magnetite (5,6-6,6% TiO_2) and Cr-magnetite (to 0,5% Cr_2O_3), rutile (0,4-0 > 6% FeO, 0,4-0,6% MgO), ilmenite (0,5-1,1% MnO), free Pb, Fe, Au, natural alloys Fe and Te, Mo and Pb, Au and Ag, Au and Cu, as well as sulfides: pyrite, chalcopyrite and sphalerite. Besides, according to the termochemical analyses, the presence in them of garnets (including pyrope), zircon, graphite were found.

Table 1. Average chemical and microelemenns composition of Magnitogorsk megazone lamproitoides (in terms of anhydrous basis).

Oxides, elements	1	2	3
SiO_2	42.021	47.812	52.689
TiO_2	1.111	1.110	1.008
Al_2O_3	0.798	9.936	10.422
Fe_2O_3	5.340	3.857	3.937
FeO	4.213	5.241	4.432
MnO	0.127	0.128	0.106
MgO	20.572	16.241	10.990
CaO	11.123	9.436	7.550
Na_2O	0.376	0.687	1.265
K_2O	4.006	3.956	5.986
P_2O5	1.315	1.596	1.616
N	2	20	6
Sr	806.5	1120	1431
Rb	140	102	111
Ba	1650	3600	8775
Th	9.3	10.8	18.7
U	4.9	3.7	6.4
Ta	1.2	0.4	0.6
Nb	16.6	11.3	10.5
Zr	239.5	275.5	345.3
Hf	4.5	6.2	6.6
Cs	5.0	3.4	4.1
Cr	945	819	712
Co	55.5	55.1	40.0
Ni	635	347	<100
Sc	19.5	13.8	20.3
Y	-	13	-
n	2	16	4

Note to the table. 1-3 – lamproitoides: 1 – ultrabasic composition (< 44 % SiO_2), 2 – basic composition (44 52 % SiO_2), 3 – medium composition, orendites (> 52 % SiO_2). N, n – number of analyzes.

Thus, according to the mineralogical criteria (Mitchell, 1985) the investigated rocks may be corresponded to lamproites. The minerals, typical for the formations of other types of alcaline-ultrabasic magmatism: plagioclase, nephelite, melilite, monticellite etc. are absent in them.The petrochemical peculirities of the rocks are typical for the lamproitic series. Their characteristic are: high summary alcaline at obvious prevalence K over Na (K_2O/Na_2O 4-12), high MgO (10-20 %) and P_2O_5 (0,8-2,0%) and low - Al_2O_3 (7-11%). On the distribution of the series of microelements they are

close to lamproites of other regions. The high contents Li (35-56), Ba (800-1500), Rb (90-180), Sr (570-1600), Cr (300-1000), V (110-170), Ni (200-900), Sc (10-30), Th (10-23), U (2-9) (ppm), indicate it (table 1). However, low contens of $Ti0_2$ (0,9-1,4%), Zr (150-350 ppm) and Nb (10-21 ppm) permit to speak about essential differences between them and "platforms" lamproites of Australia, Southern Africa, the USA, Greenland, Antarctic Continent, Northern Karelija.

The REE distribution (La 49-61 ppm, Ce 101-117 ppm at (La/Yb)N = 21,6-25,4) testifies to the benefit of it. The existence of small Eu-anomalies, probably, indicates to fractional differentiation processes. The adduced quantities are essentially below for the mentioned lamproitic provinces. Some mineralogical features of the rocks (low-Ti phlogopite, low-K richterite, absence of diamonds etc.) also are confirmed by these distinctions. The most close analogues of the East-Magnitogorsk belts rocks on the mineralogical and geochemical features are lamproitoides of Alger, Yugoslavia, Indonesia, Spain, Aldan, Kamchatka, regarded to "collision" type (Lamproites, 1991, Seliviorstov et al., 1994). The term "lamproitoides" was offerred for the similar rocks of Kamchatka, (Seliviorstov et al., 1994). It is interesting, that the increased contents of chalcophile elements are marked in Southern Urals lamproitoides: Cu 90-150, Zn 180-300, Co 34-42, Pb - to 66 (ppm), that, evidently, is a provincial feature of the Urals rocks. Possibly, it is explained by crusts contamination of the mantle magmas. The finds of garnets-pyralspites, typical for the formation of the "granulite-basite layer" earth crust and increased significance ($^{87}Sr/ ^{86}Sr$) = 0,70524-0,70593. also indicate to the certain role of contamination. PT-parameters evolution of initial melts (calculated by Simakov,S.G.: P=30-15 kbars, T=1416-1445°C) were defined according to many known geotermometers and geobarometers of investigated mineral paragenesises. Certainly, this pressure is far below than diamond subfacies of depth.

The represented data allow us to significantly clarify the mechanism of lamproitoides formation, summarized in previous work (Surin, 1999). Apparently, these are ultrabasic lamproitoides that have the closest composition to the initial melt. They are characterized by high mg-number and potassium content. According to modern concepts, lamproite magma is the result of partial melting of a metasomatically enriched mantle substrate represented by phlogopite-containing harzburgites or lherzolites under reduced (carbon–water buffer) conditions in the presence of a water enriched fluid (Mitchell, Bergman, 1991). It is the formation of phlogopite that is considered to be the most probable real expression of mantle metasomatism. The enrichment of the mantle source is also indicated by markedly increased of the primary isotope Sr relations in lamproitoides, although this value is significantly lower than in the platform diamondiferous lamproites. Calculations for different variations of olivine-spinel geothermobarometers indicate the following paragenesis formation parameters: P = 20-25 kbar, T = 1350-1400°C. This corresponds to the subsolidus region of spinel lherzolite (Surin, 1999). The primary melt, obviously, had a slightly lower temperature. A number of geochemical rock features, namely low content of elements with high-charged ions (titanium, zirconium, niobium, tantalum, hafnium), indicate the great role of water in petrogenesis. These elements have the least mobility in water and are characterized by the smallest value of affinity to the water fluid. These geochemical features are the key characteristics for all types of magma subduction geodynamic environments. Of all the formations belonging to the lamproite series, these features are fully inherent in the rocks of Aldan and the Mediterranean belt (Venturelli et al., 1991; Lamproites, 1991). In the observed case, the presence of phenocrysts of phlogopite indicates a large water saturation of the melt at an early stage of its evolution. Another important volatile component, probably present in the area of magma generation is carbon dioxide, which justifies the high temperature of the primordial melt. It has long been proven that the presence of CO_2 contributes to the increase of mantle peridotite solidus and smelting of unsaturated silica melts. The presence of a large amount of normative leucite in ultrabasic lamproitodes also indicates a specific role of CO_2 in generation of their melts, as in the well-studied system "kalsilite–forsterite–silica" peritectic point "forsterite + phlogopite + enstatite + melt" gradually shifts to ultrapotassic compositions as the concentration of carbon dioxide increases (Foley, 1992). However, it is clear that the content of free CO_2 in the magma generation area is quite low. Thus, the most likely mantle source for the primary melt lamproitoides is phlogopite peridotite subjected to fractional melting in the presence of a

substantially aqueous fluid with a markedly subordinate role of carbonic acid in its composition., In our case, obviously, the degree of melting should be sufficiently high. Crystallization of the lamproitoides melt occurs according to the scheme corresponding to the experimentally established phase relations in the presence of a substantially aqueous fluid (Fig.). When the melt is cooled and lifted, its crystallization begins near the place of its origin (point A) and olivine appears on the liquidus, to which phlogopite is added during the cooling phase. As temperatures and pressures decrease, the amount of olivine falls, and phlogopite increases due to the reaction "olivine + melt → phlogopite", which is confirmed by petrographic data. In case of melt retardation at depth (point B), the significant removal of olivine and phlogopite from the melt will lead to its depletion with potassium, rubidium, strontium, barium and refractory elements and, accordingly, enrichment with silicic acid, calcium, sodium and alumina. The decrease of temperature should lead to an increase in the fugacity of oxygen and fractionation of the oxide accessory phases (apatite, zircon, spinelides, etc.), as a result of which the residual melt is further depleted by elements with high-charged ions (zirconium, yttrium, heavy REE). The main phase of melt differentiation takes place in the hearth of the crust (segment C-D). When the C point is reached, the melt cooling and the significant removal of the load should lead to a significant saturation of the melt with carbon dioxide, resulting in an increase in its degree of polymerization and viscosity and a "delay" in the crust hearth. An increase in the role of CO_2 should also lead to an increase in the clinopyroxene crystallization field, i.e. its appearance at low pressures (see Fig. , large dotted line) and, accordingly, a significant role of clinopyroxene in the rock composition. The intrusion of lamproitoid melt into the upper parts of the crust (segment D-E) occured at low pressure conditions, and its crystallization ended as follows: olivine – magnesium biotite – clinopyroxene – leucite (sanidine) – titanomagnetite (ilmenite, sphen) – amphibole – magnetite. This series largely reflects the residual melt alkalinity increase and a significant rise in the activity of oxygen as it evolves. The formation of leucite and its replacement with sanidine occurs at the lowest pressures (below 5 kbar) due to the reaction "leucite + melt → sanidine". Obviously, the significant differentiation of high-alkaline and high-temperature melt in crustal conditions was accompanied by some assimilation of the crustal material. This is evidenced, in particular, by the presence of metamorphogenic garnet that, however, are quite rare.

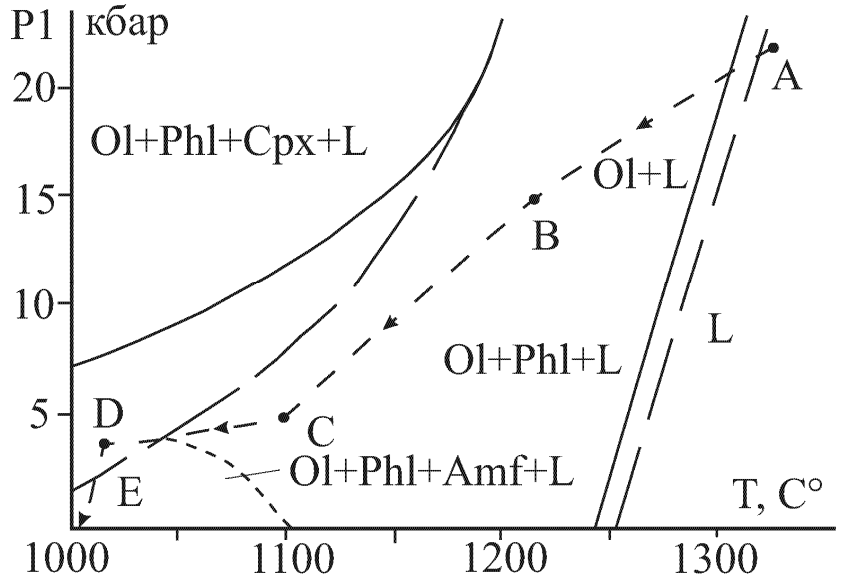

Figure. The phase PT-diagram for lamproitoid melt with the presence of aqueous fluid (Lamproites, 1991). O – olivine, Phl – phlogopite, Opx – orthopyroxene, Cpx – clinopyroxene, Amf-amphibole, L – melt. Dotted arrows indicate possible evolution paths of the lamproitoides melt in Magnitogorsk megazone. Explanations are provided in the text.

In view of geological conditions of lamproitoides' occurrences, (the Mezozoic activization of the Paleozoic fold belt with total cycle of development); it is suggested to allocate the rocks in the "postcollision" subtype. The research conducted does not allow us to consider these rocks as the primary source of the Urals' diamonds. The solution of aforementioned problem is to be found.

References

Foley S. 1992. Petrological characterization of the source components of potassic magmas: geochemical and experimental constraints. Lithos 28, 187-204.

Jaques, A.L., Lewis, J.D. and Smith, C.B. The kimberlites and lamproites of Western Australia. Perth: Geological Survey of Western Australia, 1986. 268 p.

Lamproites (Ed. O.A.Bogatikov and V.A.Kononova). M.: Nauka, 1991. 302 p. (in Russian).

Lukianova, L.I., Mareitchev, A.M., Maschak, I.M, Kuznetsov, G.P., Moseichuk, V.M., Petrov, V.I. and Shalaginov, V.E. (1992) The first finds of lamproiitic magmatism in the South Ural. Reports of Russian Academy of Sciences. 1992. V. 324. P. 1260-1264 (in Russian).

Mitchell R.H. A review of the mineralogy of lamproites. Transaction of Geology Society of South Africa. 1985. V. 88. P. 411-437.

Mitchell R.H., Bergman S.C. Petrology of lamproites. N. Y.: Plenum Publ. Co., 1991, 447 p.

Seliviorstov, V.A., Koloskov, A.V. and Chubarov, V.M. (1994) Potassic alkaline ultrabasic rocks of the Valaginskii Range, Eastern Kamchatka. Petrology. 1994. № 2. P. 197-213 (in Russian).

Surin T.N. Triassic lamproite and lamprophyre (kolymbaevkiy complex) of East-Magnitogorsk zone of the South Urals: mineralogy, geochemistry and petrogenesis. IG Ufa: UNC RAN, 1999. 115 p (in Russian).

Venturelli G., Capedri S., Barbieri M., Toscani L., Salvioli Mariani E., Zerbi M. The Jumilla lamproite revisited: a petrological oddity // Eur. J. Mineral. 1991. V. 3. P. 123-145.

MORPHOLOGY AND INTERNAL STRUCTURE OF PGE MINERALS FROM CHROMITITES OF ALKALINE-ULTRAMAFIC KONDYOR MASSIF (ALDAN SHIELD, RUSSIA)

Temnikov A.A., Petrov S.V., Stepanov S.Yu.

Saint-Petersburg State University, Saint-Petersburg, Russia, temnikov.alexander1998@mail.ru, petrov64@gmail.com, stepanov-1@yandex.ru

Kondyor is alkaline-ultramaphic massif of central type (Arkhangelskaia, Kats, 1959; Lazarenkov and other., 1992; Malitch, 1999). The central part of the massif consists of dunite, which has a complex structure, and the complexity appears in irregular alternation of rocks with different size of olivine grains. The main volume of platinum-bearing chromitites is located within transition contact of coarse-grained olivine and medium grained one (Stolyarov, 2002). A number of features like geochemical specifics of dunites, the character of the bedding and the structure of chromitite bodies, the prevalence of intermetallides among Pt-Fe-group minerals and the linkage between industrially significant placers and dunites allowe to compare clinopyroxene-dunite massifs of platinum-bearing Ural belt and ultrabasic part of ultrabasic-alkaline massif Kondyor (Efimov, Tavrin, 1978; Pushkarev and other., 2015; Tolstykh, 2018 and other).

Kondyor massif itself and chromium-platinum mineralization of placers associated with the massif are well studied. Nevertheless, there is still a number of discussional questions which requires additional investigations. One of the most difficult and problematic questions is the genesis of chromium-platinum mineralization. This question has been discussed since the discovery of the first platinum-bearing chromitites in the dunites of Nizhnetagilskiy massif (Zavaritskii, 1928; Betekhtin 1935). One of the methods which allows to understand a nature of chromite-platinum mineralization is the study of morphological features of mineral individuals using techniques developed and tested in the course of genetic mineralogy (Popov, 2011) and the teaching of onthogeny of minerals (Grigorev, 1961).

Interpretation of mineral individ's shapes and mechanisms of their intergrowth allow to determine the parageneses of minerals and then assume the geological processes of their formation. The aim of our investigations is the identification of genetic mechanisms of chromite-platinum ore-forming, based on analysis of genetic interrelationship between individs of platinum group minerals.

The gravitational concentrate of PGM from chromite schlieres of Kondyor Massif was studied. High concentration of Pt-Fe alloys was found in ores of area "Verhniy". Medium- and fine-grained dunites are exposed in the walls of quarry in this area , in which schlieres of massive chrome-spinels (30-80 cm in size and 2-10 cm in thickness), as well as disseminated chromite mineralization are found quite often. Large PGM aggregates are observed only in schlieres. Average concentration of platinum in schlieres is 200 g/t, in ore it is 3 g/t. Sample of chromite ores with total weight of 25 kg was selected for study. This sample was crushed up to 1 mm size of particles and then enriched on gravitational table. Obtained concentrate was separated into different fractions: non-magnetic, paramagnetic and magnetic. Morphology of PGM grains was explored using electron microscope JSM-6390LV (JEOL) with energy dispersive spectrometer (research center "Geoanalytic" IGG UrO RAS, analyst L.V. Leonova). The composition of PGM was studied in polished sections, using electron microscope Hitachi S-3400N equipped by energy dispersive attachment (research center "Geomodel", SPbSU, analyst V.V. Shilovskikh).

Predominance of Pt-Fe intermetallides in chromitites of dunites from Kondyor massif was determined. Composition of these intermetallides presents continuous row from isoferroplatinum Pt3Fe to ferrous platinum Pt2Fe, this fact is confirmed by other researches (Malitch, 1999. Malitch, Badanina, 2015; Tolstykh, 2018). Characteristics of interrelations between Pt-Fe minerals and chrome-spinels are different. During the investigations the inclusions of Pt-Fe intermetallides in chrome-spinels were observed. But the predominant amount of isoferroplatinum and ferrous platinum form complex intergrowth with chrome-spinels.. In flat sections such intergrowth look like the cementation of chrome-spinel grains by Pt-Fe intermetallides (fig. a). Apart from isoferroplatinum and ferrous platinum the most abundant among primary PGE minerals is cooperite, which forms idiomorphic

crystals sometimes in intergrowth with chrome- spinels.

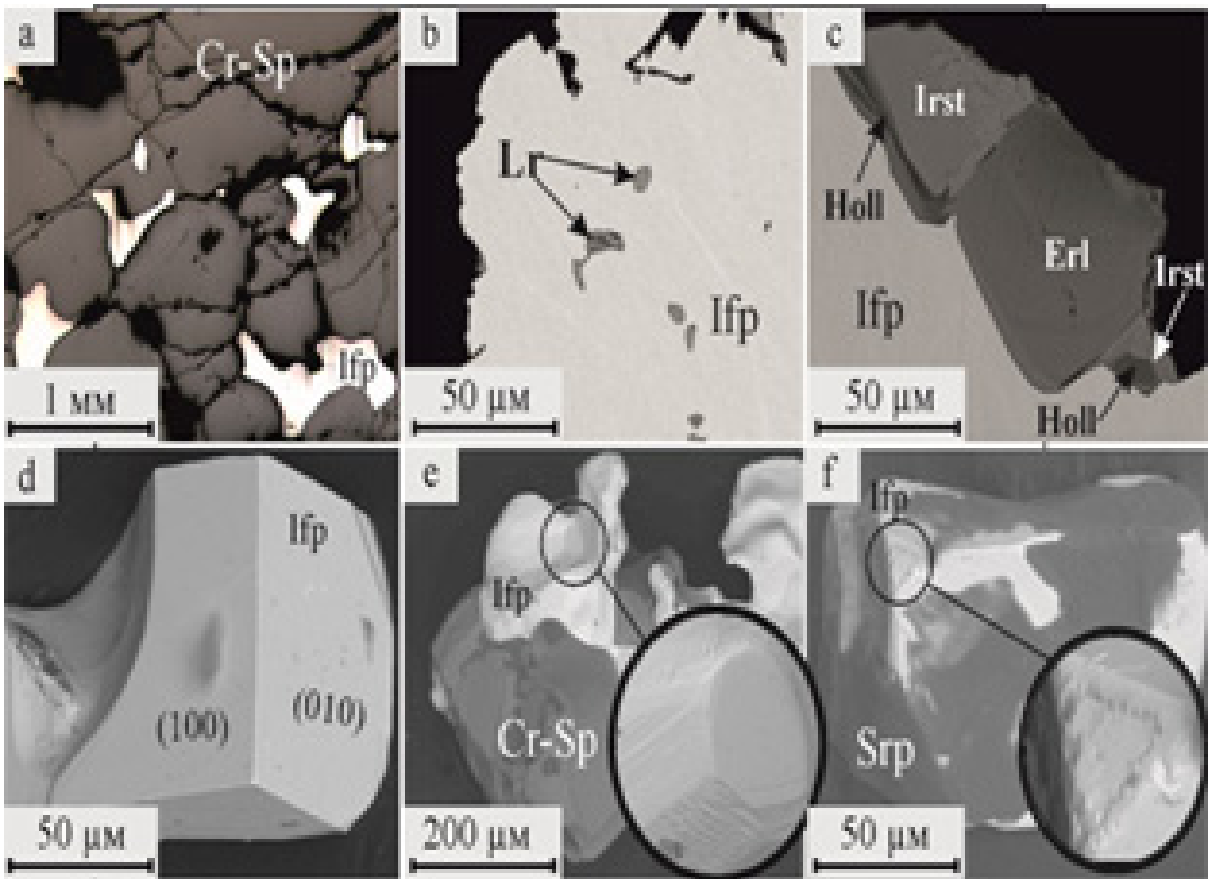

Figure. composition of aggregations and individs of Kondyor massif. Minerals: Cr-Sp – chrome spinel, Ifp – isoferroplatinum, Erl – erlichmanite, Irst – irarsite, Holl – hollingwortite

The common minerals as inclusions in Pt-Fe intermetallides are laurite, erlicmanite (fig. b), kashinite, bowieite and minerals of irarsite-hollingworthite isomorphic series. Sulphides of Os, Ru, Ir и Rh are typical inclusions in Pt-Fe intermetallides in chromitites of zonal massifs of Ural (Stepanov and other., 2017) and Koryak Mountains (Sidorov and other, 2012). According to research of chromite-platinum mineralization in zonal massifs of Ural (Begizov and other, 1976; Stepanov and other, 2018) irarsite-hollingworthite minerals are considered as secondary overlapping mineralisation. However specifics of location of irarsite-hollingworthite inclusions in Fe-Pt intermetallides in Kondyor massif and characteristics of intergrowth of these minerals with laurite and erlichmanite (fig. c) indicate the primary character of irarsite-hollingworthite in Kondyor chromitites. The majority of inclusions, especially grains of laurite-erlichmanite and irarsite-hollingworthite, have distinct zoning. The content of Rh in irarsite-hollingworthite increases from center to edges of crystal, opposite to Ir. So there are a lot of examples of cyclical zoning in samples. In laurite-erlichmanite Os increases from center to edges and cyclical zoning there is observed too.

Features of Pt-Fe intermetallides were investigated in detail for solving the problem of sequence of chrome-spinel and PGM crystallization. Less than 5% of total volume of Pt-Fe minerals in gravity concentrate are isoferroplatinum cubical crystals (fig. d). Cube faces of this crystals are partly developed. Apart from idiomorphic faces, the surfaces of co-growth and xenomorphic imprints are common. Most part of Pt-Fe intermetallides has induction surfaces, with minor imprint forms. Induction surfaces are the result of co-growth of chrome-spinels and intermetallides (fig. e). This surfaces are represented by different hatchings, where one part of hatchings corresponds to simple crystal forms of isoferroplatinum, another - to chrome-spinels and the third part of hatchings corresponds to compromise faces, which do not have rational crystallographic symbol Surfaces of dissolution are widely spread on faces of isoferroplatinum too (fig. f). Surfaces of dissolution are

mostly developed on crystals of platinum minerals, which are covered by serpentine aggregates.

An important feature of studied grains of platinum group minerals from chromitites from Kondyor massif is almost total absence of reaction rims which consist of tetraferroplatinum group minerals. Such grain rims are typical for platinum aggregates from zoned clinopyroxenite-dunite massifs located in folded regions (Stepanov, 2015; Tolstykh and other., 2011). The replacement of ferrous platinum by fine-grained tetraferriplatinum aggregate was detected only in occasional grains.

Common secondary minerals, which replace primary Pt-Fe intermetallides, cooperite and inclusions is them, are sulfides and sulfoarsenides and in a less degree arsenides of platinum group elements. Platarsite (PtAsS) was observed in rare fine metacrystals, replacing isoferroplatinum. Sperrylite (PtAs) forms metacrystals in isoferroplatinum and cooperite, often replacing these minerals on edges. Vysotskite (PdS) replacing isoferroplatinum too, forming complex aggregates, with average size less than 20 μm.

The analysis of the obtained results allows to conclude that, by analogy with the majority of chromite-platinum ore systems in zoned clynopyroxenite-dunite massifs of folded regions and inner parts of platforms the main amount of Pt-Fe intermetallides was formed together with chrome-spinel. These minerals form the primary paragenesis, which also contains Os, laurite, erlichmanite, kashinite, bowieite. Such mineral composition is common for chromitites of the majority of zoned clynopyroxenite-dunite massifs. A distinctive feature of the primary paragenesis of PGM of Kondyor massif is a prevalence of cooperite and minerals of isomorphic series irarsite-hollingworthite. The combination of the results of the analysis of the patterns of crystal faces and inner structure of mineral individuals allows to assume a magmatic origin of these minerals. It agrees with Tolstykh's results (2018). At the same time, it is important to note that in most cases formation of sulfoarsenides of Ir and Rh is connected to alteration of primary PGM as a result of serpentinization process. A prevalence of cooperite, irarsite and hollingworthite among minerals of the primary magmatic paragenesis is the evidence of unusually high activity of sulfur and arsenic in ore-forming process during the magmatic stage.

A limited occurence of metacrystals and pseudomorphs of secondary minerals, including tulameenite, tetraferroplatinum, ferronickelplatinum, makes a difference between Kondyor massif and Ural or Koryak zoned clinopyroxenite-dunite massifs of folding regions. A prevalence of tetraferroplatinum-group minerals among total amount of PGM from chromitites of Ural or Koryak zoned massifs is a result of their island arc origin, where the basic magmatism is accompanied by large amount of water fluids (Ivanov, 2011). Limited presence of secondary minerals can appear to be typomorphic sign of PGM association in chromitites from clinopyroxenite-dunite massifs formed in inner parts of platform.

References

Arkhangelskaya V.V., Katz A.G. Mezozoic magmatic rocks of eastern edge of Aldan Shield. (in Russian) // Sovetskaya geologia 1959. № 4. p. 67–82.

Begizov V.D., Zavyalov E.N., Khvostova V.P. Minerals of elrichmanite-laurite and hollingworthite-irarsite series from Ural placers. (in Russian) // Zapiski VMO. Saint-Petersburg: Gorniy institute, 1976, issue 2, p. 213-218.

Betekhtin A.G. Platinum and other minerals of platinum group. (in Russian) // Moscow: Pub. of Academy of Sciences of the Soviet Union. 1935. p.148.

Grigoryev D.P. Ontogeny of minerals. (in Russian) // Publishing house of Lvov University. 1961. p. 283.

Efimov A.A., Tavrin I.F. (in Russian) About genetic unity of platinum-bearing dunites of Ural Mountains and Aldan shield. // Doklady Akademii nauk SSSR. 1978. Vol. 243. № 4. p. 991-994.

Zavaritzkiy A.N. Primary platinum deposits of Ural mountains. (in Russian) // Pub. Of Geological Committie, 1928. p. 56.

Ivanov K.S. Genesis of Cr-Pt mineralization of Nizhnetagilskiy type (in Russian) // Doklady Akademii nauk , 2011. vol. 441. № 2. p. 224-226.

Lazarenkov V.G., Malich K.N., Sakhyanov L.O. Platinum mineralization of zonal ultramafic and

komatiite massifs. (in Russian) // Leningrad, Nedra, 1992. p. 217.

Malitch K.N. Platinoids of clinopyroxenite-dunite massifs of East Siberia (geochemistry, mineralogy, genesis). (in Russian) Saint Petersburg.: Pub. Map factory VSEGEI, 1999. p. 296.

Malitch K.N., Badanina I.Y. Iron-platinum alloys from chromitites of the Nizhny Tagil and Kondyor clinopyroxenite-dunite massifs (Russia) // Doklady Earth Sciences. 2015. T. 462. № 2. C. 634-637.

Popov V.A. Practical genetic mineralogy. (in Russian) // Yekaterinburg: IGG UrO RAS, 2011. p.167.

Pushkarev E.V., Kamenetsky V.S., Morozova A.V., Khiller V.V., Glavatskykh S.P., Rodemann T. Ontogeny of ore Cr-spinel and composition of inclusions as indicators of the pneumatolytic–hydrothermal origin of PGM-bearing chromitites from Kondyor massif, the Aldan Shield // Geology of Ore Deposits, 2015,vol. 57, № 5, p. 352-380.

Sidorov E.G., Kozlov A.P., Tolstykh N.D. Galmoenanskiy mafic-ultramafic massif and its platinum content (in Russian) // M.: Scientific World. 2012. p. 288.

Stolyarov S.A. Petrophysical zonality of central region of Kondyor and Nizhnetagilsky massifs and features of mineralization of platinoids (in Russian) // All-Russian science conference for students, aspirants and young specialists “Geologists of XXI century”. Saratov: SD EAGS, 2002. p. 120–123.

Stepanov S.Y. Comparative characteristics of platinum mineralization of Svetloborskiy, Veresovoborskiy and Nizhnetagilskiy dunite-clinopyroxenite intrusions (Middle Ural, Russia) (in Russian) // Novie dannye o mineralakh, 2015. № 50. p. 29–37.

Stepanov S.Y., Kozlov A.V., Malitch K.N., Badanina I.Y., Antonov A.V. Platinum group element mineralization of the Svetly Bor and Veresovy Bor clinopyroxenite–dunite massifs, Middle Urals, Russia // Geology of Ore Deposits. 2017. T. 59. № 3. C. 244-255.

Stepanov S.Y. Palamarchuk R.S., Varlamov D.A., Kozlov A.V., Hanin D.A., Antonov A.V. Minerals of platinum group from deluvial placer of Veresovka River, Veresovoborskiy clinopyroxenite-dunite massif (Middle Ural) (in Russian) // Zapiski RMO. 2018. Vol. 147. №5. p. 40 – 60.

Tolstykh N.D. Platinum mineralization of Kondyor and Inagli massifs. (in Russian) // Geospherniye issledovaniya. 2018. №1. p. 17–32.

N.D.Tolstykh, Yu.M.Telegin, A.P.Kozlov Platinum mineralization of the Svetloborsky and Kamenushinsky massifs (Urals Platinum Belt) // Russian Geology and Geophysics. Volume 52, Issue 6, June 2011, Pages 603-619.

VARIATIONS OF ALKALINITY AND OTHER GEOCHEMICAL CHARACTERISTICS OF MELTS IN KAMCHATKA: IMPLICATIONS TO THE GEODYNAMIC POSITION OF THE VOLCANIC CENTERS

Tolstykh M.L.[1], Volynets A.O.[2], Babansky A.D.[3]

[1]Vernadsky Institute of geochemistry and analytical chemistry RAS, Moscow, mashtol@mail.ru
[2]Institute of volcanology and seismology FEB RAS, Petropavlovsk-Kamchatsky 683006, Russia, a.volynets@gmail.com
[3]Institute of Geology of Ore Deposits, Petrography, Mineralogy and Geochemistry of Russian Academy of Sciences (IGEM RAS), Moscow, 119017

Kamchatka peninsula has a complicated geological history and structure. It includes active subduction processes manifested by the contemporary volcanoes of the Eastern volcanic front and Central Kamchatka Depression and also post-subduction volcanism (revealed as Holocene activity in the Sredinny Range). Post-subduction stage of evolution of this active continental margin is characterized by the involvement of the variably enriched sources to the magma generation process and by melts with increased alkalis and some groups of incoherent elements.

Influence of geodynamic position to the composition of the eruptive products is widely discussed in many petrological papers (Portnyagin et al., 2005, Churikova et al., 2007; Volynets et al., 2010; many others). This work is dedicated to the analyses of the data base of melt inclusions and glassy ash compositions (Naumov, 2010). Our goal was to reveal any variations in alkalinity and other geochemical characteristics of melts of Late Pleistocene volcanic rocks of the active subduction zone (Eastern volcanic front and Central Kamchatka Depression – EVF+CKD) and post-subduction environment (Sredinny Range, SR). We used our own thermobarogeochemical data (Naumov, 2008, Tolstykh, 2015, 2019) as well as other author's data (Auer 2009, Humphreys, 2008, Nekrylov, 2018, Plechova, 2011, Ponomareva, 2018, Portnyagin, 2005).

Given that Kamchatka melts are characterized by the bimodal distribution with minimum in andesitic area (basic and acid melts prevail), we have chosen data on melt inclusions of the contrast compositions: 1) basic MI in Ol, representing least differentiated varieties; and 2) naturally quenched dacitic-rhyolithic melt inclusions, which did not require experimental homogenization. Besides, we used data on the thin glassy tephra to characterize acid volcanism of the Southern Kamchatka (SK), because statistical comparison of the melt inclusions and glasses of the thin pyroclastic (Naumov, 2010) has shown that the difference in their composition is within the analytical error. Special attention is paid to the acid melts since their problems are less investigated.

Table 1 includes arithmetic averages for compositions of basaltic and dacite-rhyolithic melts formed in the EVF, CKD and SR.

Basic melts. Differences between EVF+CKD and SR melts in major element concentrations in most cases are within the standard deviation (table 1), but Mg# changes (0.6, 0.5 and 0.4 respectively), and alkalis ratio as well (K_2O/Na_2O in SR melts is 0.26, in EVF 0.22).

Difference in the microelement enrichment degree is more pronounced. SR melts are enriched by the LREE (La/Yb in the SR melt is at least 2 times higher than in the EVF melts); also, HFSE concentrations are substantially higher in them (Ba/Nb is 5 times lower than in the EVF melts). This ratio, as well as lowered Pb/Ce, records decreased subduction component amount in the melts of the SR (Peate, 2001). In general, SR melts characteristics allow us to suggest magma generation caused by the low degrees of melting of the enriched mantle (Volynets et al., 2010), while EVF is characterized by the high degrees of depleted mantle melting caused by the subduction fluid addition.

Acid melts. Differences in major elements are more pronounced here than for the basic melts. Similar to basic melts, acid melts of the SR are rather enriched by K_2O. Nevertheless, at detailed analyses we see that there are both middle-K (up to 5% K_2O) and low-K (less than 2.5% K_2O) melts present at Ichinsky volcano. CKD melts (for example of Shiveluch volcano) have relatively higher MgO. As for the incompatible elements, SR acid melts have the same features as basic ones – relative enrichment of the LREE, Nb, Th, low Ba/Nb, Zr/Nb.

Table 1. Average concentrations of major- and microelements in Kamchatka melts.

	1	σ	2	σ	3	σ	4	σ
N	152		34		51		37	
SiO_2	**49.17**	*1.80*	**49.28**	*1.47*	**72.68**	*2.64*	**73.19**	*2.33*
TiO_2	**1.02**	*0.25*	**1.48**	*0.31*	**0.26**	*0.08*	**0.24**	*0.10*
Al_2O_3	**16.30**	*1.73*	**17.69**	*1.94*	**12.46**	*0.80*	**12.67**	*1.09*
FeO	**8.22**	*1.56*	**9.05**	*1.95*	**1.29**	*0.41*	**1.08**	*0.47*
MnO	**0.12**	*0.04*	**0.10**	*0.05*	**0.08**	*0.05*	**0.05**	*0.03*
MgO	**8.18**	*2.55*	**6.48**	*1.12*	**0.32**	*0.16*	**0.22**	*0.10*
CaO	**11.57**	*1.90*	**9.92**	*1.96*	**1.15**	*0.49*	**0.86**	*0.45*
Na_2O	**3.08**	*0.75*	**3.70**	*0.34*	**4.37**	*0.52*	**3.41**	*0.48*
K_2O	**0.69**	*0.24*	**0.96**	*0.37*	**3.06**	*0.47*	**3.86**	*0.52*
Total	**98.34**		**98.66**		**95.57**		**95.58**	
La	**5.08**	*1.67*	**10.6**	*1.98*	**9.68**	*2.07*	**16.4**	*3.46*
Ce	**13.1**	*4.02*	**25.0**	*3.87*	**20.1**	*5.43*	**30.4**	*6.40*
Nd	**10.1**	*2.77*	**16.0**	*1.95*	**8.70**	*3.08*	**10.6**	*2.10*
Sm	**3.11**	*1.03*	**4.11**	*0.81*	**1.77**	*0.95*	**1.82**	*0.41*
Eu	**1.03**	*0.33*	**1.53**	*0.44*	**0.78**	*0.40*	**0.48**	*0.27*
Dy	**3.41**	*0.96*	**3.99**	*0.53*	**2.03**	*1.20*	**1.57**	*0.38*
Er	**2.24**	*0.73*	**2.53**	*0.65*	**1.54**	*0.88*	**1.2**	*0.32*
Yb	**2.12**	*0.74*	**1.90**	*0.41*	**1.63**	*0.93*	**1.46**	*0.31*
Sr	**317**	*78.8*	**545**	*79.8*	**135**	*88.3*	**145**	*119*
Ba	**240**	*93.2*	**233**	*152*	**632**	*151*	**946**	*161*
Zr	**67.5**	*18.7*	**122**	*24.4*	**173**	*70.3*	**106**	*40.9*
Hf	**2.11**	*0.63*	**3.01**	*0.55*	**2.71**	*1.45*	**3.16**	*0.90*
Nb	**1.61**	*0.57*	**7.48**	*2.17*	**3.61**	*1.59*	**11.1**	*2.83*
Th	**0.45**	*0.22*	**0.78**	*0.22*	**2.67**	*1.39*	**6.64**	*1.55*
U	**0.30**	*0.16*	**0.33**	*0.08*	**1.67**	*1.01*	**3.61**	*0.97*
Y	**20.8**	*5.83*	**22.1**	*2.39*	**8.54**	*6.29*	**9.31**	*2.48*
Pb	**2.35**	*1.91*	**2.24**	*1.06*	**3.34**	*0.67*	**6.23**	*1.14*
La/Yb	**2.40**		**5.55**		**5.95**		**11.3**	
Ba/Nb	**149**		**31.1**		**175**		**85.5**	
Ba/Th	**528**		**300**		**236**		**143**	
Pb/Ce	**0.18**		**0.09**		**0.17**		**0.20**	
Zr/Nb	**43.5**		**17.0**		**48.0**		**10.7**	

Notes. Melt inclusions in the minerals of volcanic rocks, 1, 3 – CKD and EVF; 2, 4 – SR. Basic melts were studied at volcanoes Klyuchevskoy, Tolbachik, Kamen (CKD), Karymsky, Zhupanovsky (EVF), Ichinsky, Akhtang, Kekuknaysky (SR). Acid melts were studied at Shiveluch (CKD), Karymsky (EVF), Ichinsky, Khangar (SR). Major elements in wt. %, microelements in ppm.

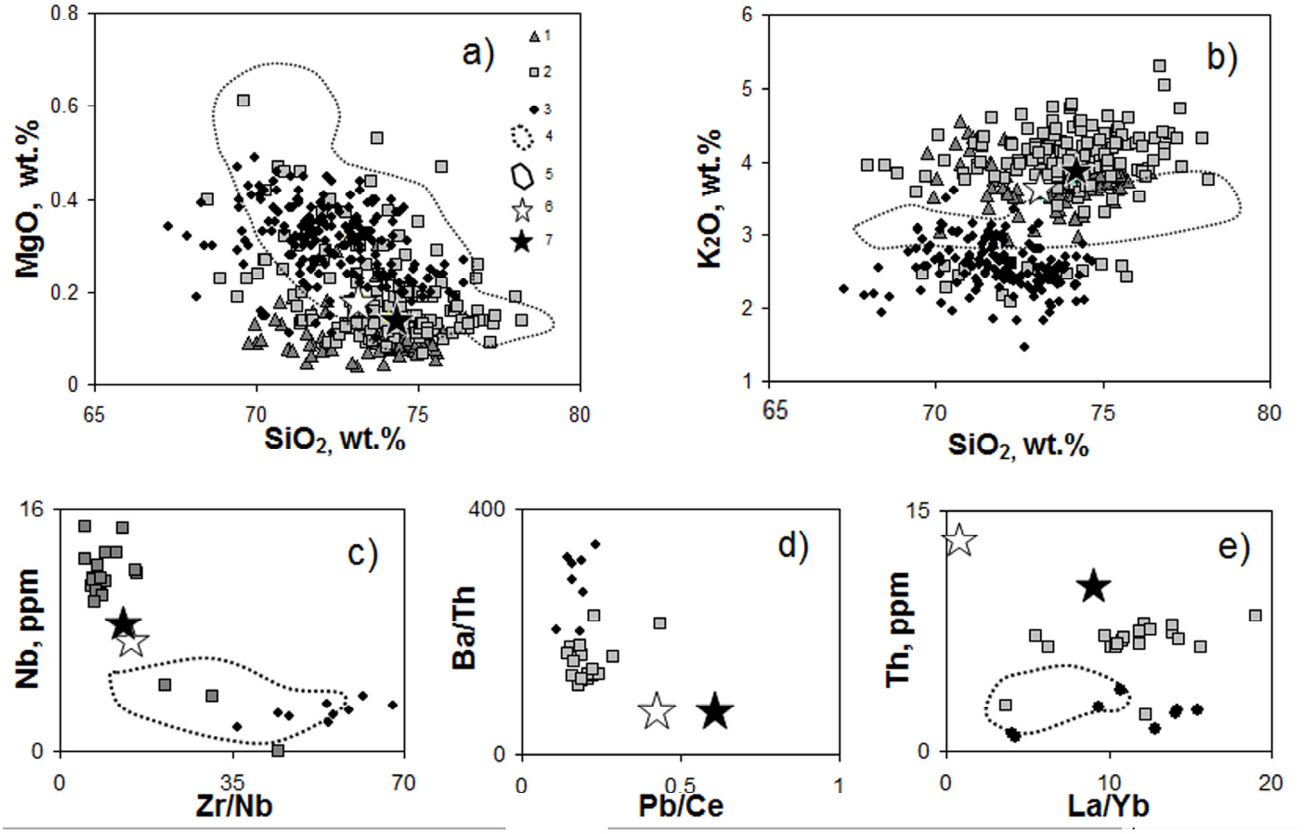

Figure. Binary diagrams for melts and restite acid glasses of the different volcanic structures of Kamchatka. 1 – Khangar volcano, SR; 2 – Ichinsky volcano, SR; 3 – Shiveluch volcano, CKD; 4, 5 – CKD and SK compositions, respectively; 6, 7 – average compositions of melts of the island arc and active continental margins, respectively, by (Naumov et al., 2019).

Therefore, basic melts of the subduction and post-subduction stages indeed differ by the concentrations and ratios of alkalis (with K_2O predominant relative to Na_2O in the SR), and concentrations of Nb, Th, LREE. It is likely that these characteristics may be caused by the melting of phlogopite-bearing metasomatized mantle. These characteristics of the basic melts are inherited by the acid melts. Probably dacitic melts may be genetically connected to the basic melts, which is indirectly confirmed by the decreased HREE and MREE concentrations in the dacitic melts relative to basic; these elements are usually concentrated in amphiboles.

Thus, increased potassium content together with the relative enrichment of Th, HREE and LREE in melts may be considered as a marker of the certain subduction environments.

This work is performed in accordance with research theme № 0137-2019-0014 GEOKHI RAS, financial support by RFBR grants № 17-05-00112, № 18-05-00224a.

References

Auer S.L., Bindeman I., Wallace P., Ponomareva V.V., Portnyagin M. The Origin of Hydrous, high-δ18O voluminous volcanism: Diverse Oxygen Isotope Values and High Magmatic Water Contents within the Volcanic Record of Klyuchevskoy Volcano, Kamchatka, Russia // Contributions to Mineralogy and Petrology. 2009. Vol. 157. pp. 209-230.

Churikova T., Wőrner G., Mironov N., and Kronz A. Volatile (S, Cl and F) and fluid mobile trace element compositions in melt inclusions: Implications for variable fluid sources across the Kamchatka arc//Contributions to Mineralogy and Petrology. 2007. Vol. 154. N 2. pp. 217–239.

Humphreys M.C.S, Blundy J.D., Sparks R.S. J. Shallow-level decompression crystallisation and deep magma supply at Shiveluch Volcano // Contrib. Mineral. Petrol. 2008. Vol. 155. pp. 45-61.

Naumov V.B., Tolstykh M.L., Grib E.N., Leonov V.L., Kononkova N.N. Chemical Composition. Volatile Components, and Trace Elements in Melts of the Karymskiy Volcanic Center, Kamchatka, and Golovnina Volcano, Kunashir island: Evidence from Inclusion in Minerals // Petrology. 2008. Vol. 16, No. 1, pp. 3–20.

Naumov V.B., Kovalenko V.I., Dorofeeva V.A. and others. Average composition of magmatic melts of the main geodynamic settings according to the study of melt inclusions in minerals and quenching glasses of rocks // Geochemistry Int. 2010. Vol. 12. pp. 1266-1288.

Nekrylov N.A., Popov D.V., Plechov P.Y., Shcherbakov V.D., Danyushevsky L.V. Garnet-pyroxenite-derived end-member magma type in Kamchatka: evidence from composition of olivine and olivine-hosted melt inclusions in Holocene rocks of Kekuknaisky volcano // Petrology. 2018. Vol. 26, N.4.pp. 329-350.

Peate D.W. U-series Isotope Data on Lau Basin Glasses: the Role of Subduction-related Fluids during Melt Generation in Back-arc Basins // Journal of Petrology. 2001. Vol. 42. N. 8. pp. 1449–1470.

Plechova A.A., Portnyagin M.V. and Bazanova L.I. The Origin and Evolution of the Parental Magmas of Frontal Volcanoes in Kamchatka: Evidence from Magmatic Inclusions in Olivine from Zhupanovsky Volcano // Geochemistry International. 2011. Vol. 49. N 8. pp. 787-812.

Ponomareva V., Bubenshchikova N., Portnyagin M., Zelenin E., Derkachev A., Gorbarenko S., Garbe-Schönberg D. and Bindeman I. Large-magnitude Pauzhetka caldera-forming eruption in Kamchatka: Astrochronologic age, composition and tephra dispersal // Journal of Volcanology and Geothermal Research. 2018. Vol. 366. pp. 1-12.

Portnyagin M., Hoernle K., Avdeiko G., Hauff F., Werner R., Bindeman I., Uspensky V., Garbe-Schonberg D. Transition from arc to oceanic magmatism at the Kamchatka-Aleutian junction // Geology. 2005. Vol. 33. Pp 25–28.

Portnyagin M.V., Mironov N.L., Matveev S.V., Plechov P.Y. Petrology of avachites, high-magnesian basalts of Avachinsky Volcano, Kamchatka: II. Melt inclusions in olivine // Petrology. 2005. Vol. 13. N. 4. P. 322-351.

Tolstykh M.L., Pevzner M.M., Naumov V.B., Babansky A.D., Kononkova N.N. Types of parental melts of pyroclastic rocks of various structural–age complexes of the Shiveluch volcanic massif, Kamchatka: Evidence from inclusions in minerals // Petrology. 2015. V. 23. I. 5. Pp. 480–517.

Tolstykh M.L., Pevzner M.M., Naumov V.B., Babansky A.D. The Characteristic of Acid Melts which Formed Tephra of Pleistocene-Holocene Eruptions of Ichinsky Volcano, Kamchatka (Results of Melt Inclusions Study) // Geokhimia. 2019. Vol 64. N 3. pp. 237-262.

Volynets A., Churikova T., Woerner G., Gordeychik B., Layer P. Mafic Late Miocene - Quaternary volcanic rocks in the Kamchatka back arc region: implications for subduction geometry and slab history at the Pacific-Aleutian junction // Contrib. Mineral. Petrol. 2010. Vol. 159. N 5. Pp. 659-687.

GEOCHEMICAL CHARACTERISTICS OF ALKALINE PICRITES OF RARE-METAL-RARE-EARTH ORE FIELDS (MIDDLE TIMAN, RUSSIA)

Udoratina O.V.[1,2], Kulikova K.V.[1,3], Varlamov D.A.[4], Shmakova A.M.[1]

[1]IG Komi SC UB RAS, Syktyvkar, Russia, udoratina@geo.komisc.ru

[2]Tomsk State University, Tomsk, Russia

[3]Syktyvkar State University, Syktyvkar, Russia, fopolina1@yandex.ru

4IEM RAS, Chernogolovka, Russia, dima@iem.ac.ru

Intrusive structures, composing Chetlassky complex of subalkaline ultrabasic rocks, carbonatites, phenites and vein rocks, are developed within the Chetlassky Kamen in Middle Timan. Generally, the ultrabasites compose dike bodies marking faults with NE strike. The dikes break metaterrigenous structures of Late Riphean Chetlasskaya (Svetlinskaya, Novobobrovskaya, Vizingskaya formations) and Bystrinskaya (Rochugskaya, Paunskaya, Pavyugskaya formations) series. The absolute age of the rocks is Late Riphean ~ 600±15(30) Ma. Here in Middle Timan in the upper reaches of the Mezen, Svetlaya, Kosyu rivers we know complex rare metal–rare earth occurrences Kosyu, Oktyabrskoye, Novobobrovskoye, Mezenskoye, Shchugorskoe and others. Rare metal–rare earth mineralization is confined to vein Chetlassky complex and developed in albite-aegirine phenites on quartz sandstones and the dike rocks proper, as well as in veins (quartz-feldspar-goethite, quartz-feldspar-carbonate with hematite). Ore minerals: columbite, rarer pyrochlore, rare-earth carbonates, monazite, xenotime, Nb-rich rutile and wide range of other rare-metal and REE minerals.

Many published and archive papers were devoted to the study of ultrabasic rocks of Chetlassky Kamen in connection with the search for Timan primary diamond sources: Yu.P. Ivensen (1964), V.G. Cherny (1972), I.P. Ilupin (1990), E.V. Francesson (1983), V.I. Stepanenko (1979–1982, 1987), I.A. Malakhov (1985) and many others authors. Recently they were the subject of papers by A.B. Makeev et al. (2008, 2009), I.V. Nedosekova et al. (2011, 2013, 2017), O.V. Udoratina (2014). However, only few works are devoted to the geochemical characteristics of the rocks, only ultrabasic rocks of the Kosyu ore field are well characterized (Nedosekova et al., 2011).

Below we present new geochemical data on the dike bodies within the ore fields: Kosyu (A/15, KO3/15, 3052/3, MT16-41ц), Novobobrovskoye (A14-1), Oktyabrskoe (836), Nizhne-Mezenskoe (AH-4M). The data on the content of rare earth elements are obtained by ICP MS at the VSEGEI Central Laboratory (St. Petersburg). The chemical composition of the minerals was studied at the Geonauka Common Use Center (Syktyvkar). The minerals were studied at IEM RAS (Chernogolovka) on digital scanning electron microscope Tescan VEGA-II XMU with energy-dispersive spectrometer (EDS) INCA Energy 450.

The features of the mineral, petrographic and petrochemical composition of ultrabasic rocks within the studied ore fields reflect a complex and non-permanent composition of magma, and the rocks are also often saturated with various xenoliths of enclosing rocks, altered by alkaline processes and disintegrated in the oxidation zone. The terms of these ultrabasic rocks vary – lamprophyres, alkaline picrites, kimpicrites, elicites – indicate that the rocks are derived from mantle carbonate-rich magma.

These are olivine-pyroxene rocks with biotite (phlogopite) with amphiboles, chlorite, carbonate (dolomite, siderite), potassium feldspar, plagioclase, epidote and zoisite, zeolites, ore magnetite, pyrite, and accessory apatite and zircon. Pyroxene is represented by augite, in altered varieties – by aegirine; and amphibole (hastingsite, tremolite). But often the rocks are completely altered by subsequent fenitization processes and located in the oxidation zone, turning into a friable, lumpy mass that is hard to classify.

The least altered rocks are from the Kosyu site. Thin dike bodies (outcrop A/15, central part of the ore field), exposed by surface mine workings (ditch, KO3/15, 3 km down the Kosyu River from central part of the ore field) are petrographically medium-grained black and dark green alkaline picrites often saturated with a large volume of xenoliths of enclosing rocks (quartzitic sandstones). In thin sections, there is an irregular granular hypidiomorphic structure with elements of poikilite. Composition: phlogopite, olivine, clinopyroxene, hornblende, titanomagnetite, apatite, glass. Large (3-

4 mm) flakes of phlogopite and amphibole grains are either in intergrowths with olivine (0.5-1 mm) and clinopyroxene (0.5-0.8 mm), or contain their poikilite inclusions. Olivine is pseudomorphically substituted by talc. Devitrified glass is developed between crystalline phases.

Sample 3052/3 was taken from the outcrops on the left bank of the Kosyu River in the central part of the ore zone. Pycrite-like rocks with a brecciated structure with xenoliths of quartzite-sandstones (Figure 1) – black and green rocks, saturated by a large volume of strongly modified fragments of enclosing rocks of various sizes from fine-grained to gravel. Interclastic cement is represented by albite with abundant needle apatite, single zonal clinopyroxenes (Aeg-Aug) with amphiboles rims and «druzite» clinopyroxene shells, sulphides (chalcopyrite and pyrite), magnetite, and titanite. Debris have predominantly albite cores (often with quartz and calcite) and pyroxene-amphibole shells. The mineral composition of the shells – aggregate of lamellar aegirine-augite, alkaline amphiboles, calcite, zonal apatites, titanites (sometimes niobium-enriched up to 3.5% Nb_2O_5), sulfides, single relict chrome-spinellides. Allanite-epidote aggregates were detected in the shells of altered xenoliths, the microprobe analysis of which showed the presence of central allanite zones significantly enriched in chromium (up to 13 wt % Cr_2O_3 – Varlamov et.al.(2019)).

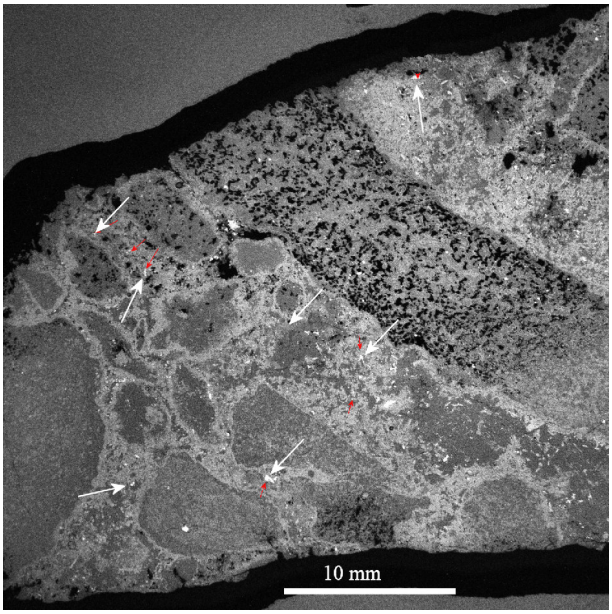

Figure 1. Altered xenoliths in picrite-like breccias, sample 3052/3. White arrows – extremely high-Cr allanites.

Sample MT16-41ц from central part of the ore field drilled by a borehole near puff-up A (carbonatite bunch), the rock contain abyssal xenolite (MT16-41). The rocks are represented by friable material with preserved fragments of gravel size of light green color. In the plates (bulk material), microprobe studies record the following minerals – pyroxene, phlogopite, epidote, and abundant amount of chlorite. In preserved lumps, albite-aegirine rocks with Th monazite are observed.

The dike rocks of the Novobobrovsky ore field (borehole material A14, sample A14/1), black porphyritic, phenocrysts of phlogopite are distinguished. The rock is composed of porphyritic phenocrysts of potassium feldspar (2-4 mm) and a fine-grained mass of quartz- potassium feldspar grains (80-100 microns), with dispersed abundant ore mineralization.

Dike within the Oktyabrskoe ore field, sample 836 (collection by V.I. Stepanenko). The rock is composed of a uniformly-grained (0.8-1 mm) mass of hypidiomorphic potassium feldspar grains and biotite flakes.

The dike rocks of the Nizhne-Mezensky site from the ditch-opened area of Anomaly 4, sample AH4-M – full crystalline, ferriferous ultrabasic green rocks. The rock has a clastic texture, a newly formed lepidoblast structure, and relics of the poikilite structure are preserved in the areas. Composition: talc, serpentine, chlorite, amphibole, magnetite, pikotit. The pseudomorphically talc-substituted small (0.5-0.6 mm) grains of olivine are found in large serpentinite secretions.

Table 1. Chemical composition of rocks.

	A/15	**3052/3**	**KO3/15**	**MT16-41ц-1**	**A14/1**	**836**	**AH4-M**
SiO_2	40.2	54.9	39.0	35.3	51.3	46.3	38.64
TiO_2	1.6	1.0	1.3	1.9	1.4	2.4	1.2
Al_2O_3	11.5	9.2	10.5	9.6	11.0	16.0	13.89
Fe_2O_3	3.0	4.0	4.7	9.2	18.8	7.1	10.73
FeO	6.3	2.1	4.0	0.8	0	6.1	2.98
MnO	0.2	0.1	0.2	0.2	1.3	0.1	0.19
CaO	13.3	10.5	16.5	10.6	**1.9**	**0.3**	**4.42**
MgO	13.7	1.2	14.2	18.0	**0.5**	**6.2**	**16.43**
K_2O	2.5	0.4	3.3	1.2	**8.1**	**5.4**	**0.54**
Na_2O	1.4	4.7	0.5	0.2	0.6	0.5	0.25
P_2O_5	0.5	0.4	0.6	0.6	0.8	0.2	0.28
LOI	4.4	1.7	4.1	11.1	4.2	9.5	10.62
Total	99.2	98.1	99.3	98.9	100.0	100.1	100.01
H_2O	0.4	0.3	0.6	5.4	0.7	0.5	0.34
CO_2	2.1	0.6	1.3	0.8	0.1	0.7	0.54
Be	1.5	1.8	1.6	1.7	4.6	3.3	1.8
V	203.0	191.0	241.0	212.0	148.0	295.0	224.0
Cr	661.0	446.0	617.0	713.0	648.0	**1010.0**	**2510.0**
Co	52.7	31.3	47.8	54.0	40.4	68.7	81.3
Ni	228.0	99.7	171.0	382.0	99.6	319.0	**658.0**
Cu	36.2	93.2	38.6	63.8	46.3	201.0	45.7
Zn	56.8	49.5	58.3	73.2	**634.0**	**3010.0**	**146.0**
Ga	13.4	13.5	12.5	15.2	87.3	20.8	18.0
Rb	113.0	6.3	128.0	62.0	156.0	140.0	20.5
Sr	994.0	286.0	943.0	173.0	271.0	31.1	153.0
Y	21.1	18.5	16.3	24.5	94.0	39.7	28.0
Zr	120.0	163.0	113.0	257.0	178.0	151.0	145.0
Nb	92.8	66.7	113.0	124.0	**1160.0**	98.1	93.7
Ba	991.0	508.0	1600.0	1160.0	976.0	592.0	348.0
La	103	69.3	96.8	107.0	**947.0**	81.6	111.0
Ce	171.0	123.0	170.0	178.0	**1820.0**	158.0	182.0
Pr	18.2	13.4	17.8	19.1	259.0	18.9	19.8
Nd	60.1	47.1	60.7	67.7	**1190.0**	74.0	70.1
Sm	8.3	7.3	8.3	10.5	230.0	13.8	11.0
Eu	2.4	1.8	2.6	3.2	46.7	3.9	2.9
Gd	8.0	5.4	7.1	8.2	97.5	13.2	8.6
Tb	1.0	0.7	0.9	1.1	7.5	1.7	1.1
Dy	4.4	3.6	3.9	5.3	24.3	8.3	5.7
Ho	0.9	0.7	0.7	0.9	3.6	1.4	1.0
Er	2.0	1.8	1.5	2.3	9.3	3.6	2.6
Tm	0.3	0.3	0.2	0.3	1.2	0.5	0.4
Yb	1.6	1.5	1.2	1.8	8.4	3.4	2.0
Lu	0.3	0.3	0.2	0.3	1.4	0.5	0.3
Hf	2.5	4.2	2.3	6.6	5.8	4.0	3.5
Ta	4.2	3.8	5.4	6.0	16.5	5.7	6.3
Pb	5.3	9.8	17.7	8.7	**3570.0**	**2590.0**	6.9
Th	15.9	11.8	13.7	18.2	**960.0**	15.8	14.6
U	2.6	2.0	2.9	1.6	22.9	7.8	2.7

The chemical composition strongly depends on the secondary alterations of the rocks. Petrochemically, the rocks are divided into groups according to the chemical composition in ore fields, as a rule, these are potassium rocks. The K_2O content in the ultrabasic rocks in the ore fields varies (wt %, Table 1) Kosyu 0.4–3.0, Novobobrovskoye 8.0, Nizhne-Mezenskoe 1.0, Oktyabrskoe 5.0. Generally, more high potassium rocks are less magnesian. Total concentrations of REE in the studied rocks vary (table): Kosyu 276-405 ppm, Novobobrovsk 4646 ppm, Nizhne Mezensky 419 ppm, Oktyabrskoe 383 ppm. Geochemically, the differences are very large and the content of Nb, La, Ce, Nd Th, and Zn, Pb increases by an order of magnitude in the most phenitized dike rocks, which is associated with the development of mineralization - columbite, Th-monazite, zinc and lead sulfides/carbonates.

This work was supported by the project AAAA-A17-117121270035-0. The study of elemental composition was partially supported by the Government of the Russian Federation (project 14.Y26.31.0012).

References

Nedosekova I.L., Udoratina O.V., Vladykin N.V., Pribavkin S.V., Gulyaeva T.Ya. Petrochemistry and geochemistry of dike ultrabasites and carbonatites of the Chetlas complex (Middle Timan) // Yearbook 2010, IGG UB RAS, No. 158, 2011, p. 122-130. (in Russian).

Varlamov D.A., Ermolaeva V.N., Chukanov N.V., Yanchev S., Vigasina M.F., Plechov p.Yu. New data in epidote supergoup mineralogy: unusual chemical compositions, typochemistry, Raman Spectroscopy // Russian Mineralogy Society Proceedings, 2019, 148(1), 79-99 DOI: 10.30695/zrmo/2019.1481.07 (in Russian).

EXPERIMENTAL CONSTRAINTS ON THE FORMATION OF RARE METAL ORE DEPOSITS IN CARBONATITE DERIVATIVES OF NEPHELINITIC MAGMA

Veksler I.V. [1,2]

[1] *German Research Centre for Geosciences, GFZ, Telegrafenberg, 14473 Potsdam, Germany*

[2] *V.S. Sobolev Institute of Geology and Mineralogy, Siberian Branch of Russian Academy of Sciences, pr. Akad Koptyuga, 3, Novosibirsk, 630090, Russia*

Carbonatites, a group of rare igneous rocks with the modal content of magmatic carbonates no less than 50 percent, are known for extremely high concentrations of rare earth elements (REE), Nb and some other rare metals. Carbonatites and the products of their surface weathering constitute the main, if not the only, source of REE and Nb for the world economy. The majority of known to date ore-bearing carbonatitic complexes represent a close association of carbonatites with a broad range of silica-undersaturated ultramafic-alkaline igneous rocks. This association is believed to result from extensive differentiation of a parental carbonated basanitic-nephelinitic magma of the mantle origin. The magmatic differentiation is driven by fractional crystallization and silicate-carbonate liquid immiscibility, whereas hydrothermal processes may play a significant role at the post-magmatic stage. The concentrations of rare metals increase several thousand times during partial melting in the mantle source and subsequent differentiation of nephelinitic magma. For example, average concentrations of Nb and La in nephelinites according to the GEOROC database (http://georoc.mpch-mainz.gwdg.de/georoc/) exceed the mantle values 150-180 times; average concentrations of these elements in carbonatites are 2000-4000 times greater than in the mantle (Woolley and Kempe, 1989) and concentrations in the ores usually further increase by a factor of 2 or 3. Such extensive enrichment is hard to achieve even in carefully designed technological processes. However, concentrations and resources of rare metals vary broadly from one carbonatitic complex to another and a satisfactory explanation for the causes of those variations currently does not exist. In the database of 527 presently known carbonatite occurrences compiled by Wolley and Kjarsgaard (2008) commercial exploration or proven economic resources of rare metal ores have been reported in 45 cases. Thus, the enrichment process of rare metals in carbonatites reaches the economically sufficient level approximately once in a dozen carbonatite occurrences.

Carbonatitic melts can be produced directly in the mantle by very low degrees of partial melting (0.03-0.3%) of carbonated peridotite or eclogite (Foley et al., 2009; Hammouda et al., 2009; Dasgupta and Hirschmann, 2010; Dasdupta et al., 2004; Kiseeva et al., 2013) but here we consider only derivative, residual carbonatites associated with foiditic and nephelinitic rocks at crustal pressures below 1 GPa. The total mass of carbonatite that can be produced from a volume of basanitic-nephelinitic magma is limited by CO_2 solubility in silicate melts which at 1 GPa does not exceed a few weight percent and exponentially decreases by about two orders of magnitude with further decrease in pressure (Blank and Brooker, 1994; Brooker et al. 2001). When the saturation is reached, CO_2 exsolves into low density C-O-H fluid phase and/or into immiscible carbonatite melt. Cotectic crystallization of silicates together with carbonates from a single homogenous melt has been experimentally demonstrated in some synthetic systems, e.g., CaO-MgO-SiO_2-CO_2 (Huang and Wyllie, 1976) but in those few experimental studies on multicomponent, geologically relevant compositions that have been published so far crystallization of carbonates is always preceded by liquid immiscibility (Kjarsgaard, 1998, Kjarsgaard et al., 1995; Weidendorfer et al., 2017).

According to experimental and petrochemical data, nephelinitic magmas that evolve towards liquid immiscibility and can produce significant volumes of carbonatite are strongly silica-undersaturated and alkali-rich. In terms of the (Na_2O+K_2O)-Al_2O_3-SiO_2 relationships, the initial compositions of carbonatite-generating magma should be on the silica-undersaturated (phonolitic) side of the feldspar thermal barrier and the magma should from the start contain large amounts of carbonate component, preferably close to CO_2 saturation (Weidendorfer et al., 2016; Schmidt and Weidendorfer, 2018). High initial concentrations of REE, Nb and other strongly incompatible lithophile elements in the parental magma are due to low degrees of partial melting (around 1 wt.%) in an enriched, metasomatized mantle source (Schmidt and Weidendorfer, 2018). Fractional crystallization of major

rock-forming silicates results in further rare metal enrichment, and drives the evolving magma towards CO_2 saturation and silicate-carbonate liquid immiscibility. However, when immiscibility is reached, some of the key ore-forming rare metals do not concentrate in immiscible carbonatite but partition to the silicate melt. Liquid-liquid distribution of individual elements is traditionally quantified by Nernst distribution coefficients (*D*), which are calculated as mass ratios of an element concentration in immiscible carbonate melt to the concentration of the same element in the conjugate silicate melt. Distribution coefficients of individual elements are complex functions of pressure, temperature and activities of all the major components in immiscible melts. For example, experimentally determined *D* values for REE vary broadly from 0.1 to 0.9 in anhydrous systems at 0.1-1.7 GPa and from 0.8 to 40 in H_2O-bearing compositions at 1.7-3 GPa (Martin et al, 2012, 2013; Veksler et al. 1998, 2012). However, the *D* values for Nb and other high field strength elements (HFSE) such as Ti, Zr, Hf, Ta, U and Th in all the experiments are below 1 as the elements concentrate in the silicate conjugate melt. One has to conclude that the apparent enrichment of ore-bearing carbonatites in Nb, Ti, Zr, U and Th cannot be caused by liquid immiscibility itself. And the same is true for REE if nephelinitic magma is anhydrous and immiscibility takes place at a pressure below 1 GPa.

In view of the above-listed experimental constraints, rare metal enrichment and ore formation in a shallow-level nephelinite-carbonatite plutonic complex could follow the following scenario. The starting point is the parental nephelinitic magma intruding to a crustal magma chamber. As mentioned above, the parental magma composition should be strongly silica-undersaturated, alkali-rich and carbonate-rich. After the emplacement, the parental magma evolves by fractional crystallization of early liquidus minerals (some combination of olivine, clinopyroxene, melilite, nepheline, leucite, etc.) towards carbonate saturation and silicate-carbonate liquid immiscibility, which is likely to start at around 1000-1100 °C. At the start of immiscibility, the immiscible carbonatite melt has been shown to be predominantly calcitic with the sum of Na_2O and K_2O at about 4-8 wt.% and SiO_2 at about 5-10 wt.% (Kjarsgaard, 1998; Weidendorfer et al., 2017). Notably, mineral assemblages precipitating prior to liquid immiscibiliy may include accessory minerals, e.g., perovskite and apatite that can host large amounts of REE, Nb and other rare metals. Fractionation of the accessories could slow down, or even stop rare metal accumulation in the melt and decrease the chances for significant rare metal deposits in carbonatite. Furthermore, economic rare metal deposits are unlikely to form in immiscible carbonatite if it is mechanically separated (e.g., by gravity) from the conjugate silicate melt and earlier formed cumulates because, as pointed out above, the immiscible carbonatite melt is depleted in Nb, other HFSE and possibly also in REE, especially the heavy REE. However, if the immiscible melts do not physically separate and continue to react with each other and earlier formed cumulates, silicate melt is expected to reach its solidus at about 700 °C and immiscible carbonatite would remain in the system as the only liquid phase. The degree of crystallization of the parental magma at this stage should be around 95% or higher. According to Kjarsgaard (1998), calcite crystallization starts at 900-960 °C and it should drive the composition of carbonatite melt towards alkali enrichment and, finally, to carbonatite solidus at about 500-520 °C. Final composition of the residual, near-solidus carbonatite melt should be similar to those of natrocarbonatite lava at the Oldoinyo Lengai volcano in Tanzania (Kjarsgard et al. 1995; Weidendorfer et al., 2017). Natrocarbonatite melts are known to be very mobile and reactive. Therefore, they may be capable of remobilizing rare metals from earlier formed cumulates and may cause numerous dissolution-precipitation reactions. Earlier hosts of rare metals may be replaced by new minerals, e.g., perovskite by pyrochlore.

Late stages of magma evolution, e.a., between the silicate and carbonate solidi, remain practically unexplored by experimental studies. Little is known about solubilities of rare metals in evolved carbonatite melts, the magmatic stability of key ore-forming minerals such as bastnaesite and pyrochlore, the conditions for and the products of replacement reactions between ore-forming minerals. These are urgent topics for future experiments.

This project is supported by RSF grant № 19-17-00013.

References

Blank, J.G. and Brooker R.A (1994). Experimental studies of carbon dioxide in silicate melts: solubility, speciation and stable isotope behavior. Reviews in Mineralogy and Geochemistry, 30: 157-186.

Brooker, R.A., Kohn, S.C., Holloway, J.R. and McMillan, P.F. (2001). Structural controls on the solubility of CO2 in silicate melts: part I: bulk solubility data. Chemical Geology, 174: 225-239.

Dasgupta, R., and Hirschmann, M.M. (2010). The deep carbon cycle and melting in Earth's interior. Earth and Planetary Science Letters, 298: 1-13.

Dasgupta, R., Hirschmann, M.M. and Withers, A.C. (2004). Deep global cycling of carbon constrained by the solidus of anhydrous, carbonated eclogite under upper mantle conditions. Earth and Planetary Science Letters, 227: 73-85.

Foley S.F., Yaxley G.M., Rosenthal A., Buhre S., Kiseeva E.S., Rapp R.P. and Jacob D.E. (2009). The composition of near-solidus melts of peridotite in the presence of CO_2 and H_2O between 40 and 60 kbar. Lithos 112: 274–283.

Hammouda T., Moine B.N., Devidal J.L. and Vincent C. (2009) Trace element partitioning during partial melting of carbonated eclogites. Physics of the Earth and Planetary Interiors 174: 60–69.

Huang W.-L. and Wyllie, P.J. (1976). Melting relationships in the systems CaO–CO_2 and MgO–CO_2 to 36 kilobars. Geochimica et Cosmochimica Acta 40: 129–132.

Kiseeva, E.S., Litasov, K.D., Yaxley, G.M., Ohtani, E. and Kamenetsky, V.S. (2013). Melting and phase relations of carbonated eclogite at 9–21 GPa and the petrogenesis of alkali-rich melts in the deep mantle. Journal of Petrology, 54: 1555-1583.

Kjarsgaard, B.A. (1998). Phase relations of a carbonated high-CaO nephelinite at 0.2 and 0.5 GPa. Journal of Petrology 39: 2061-2075.

Kjarsgaard, B.A., Hamilton, D.L., and Peterson, T.D. (1995). Peralkaline nephelinite/carbonatite liquid immiscibility: comparison of phase compositions in experiments and natural lavas from Oldoinyo Lengai. In Carbonatite Volcanism (pp. 163-190). Springer, Berlin, Heidelberg.

Martin L.H.J., Schmidt M.W., Hannes B., Mattsson H.B., Ulmer P., Hametner K. and Günther D. (2012). Element partitioning between immiscible carbonatite–kamafugite melts with application to the Italian ultrapotassic suite. Chemical Geology 320-321: 96–112.

Martin L.H.J., Schmidt M.W., Mattson H.B. and Guenther D. (2013). Element partitioning between immiscible carbonatite and silicate melts from dry and H_2O-bearing systems at 1 - 3 GPa. Journal of Petrology 54: 2301 - 2338.

Schmidt, M.W. and Weidendorfer, D. (2018). Carbonatites in oceanic hotspots. Geology, 46: 435-438.

Veksler I.V., Petibon C., Jenner G., Dorfman A.M., Dingwell D.B. (1998). Trace element partitioning in immiscible silicate and carbonate liquid systems: an initial experimental study using a centrifuge autoclave. Journal of Petrology 39: 2095-2104.

Veksler I.V., Dorfman A.M., Dulski P., Kamenetsky V.S., Danyushevsky L.V., Jeffries T., Dingwell D.B. (2012). Partitioning of elements between silicate melt and immiscible fluoride, chloride, carbonate, phosphate and sulfate melts with implications to the origin of natrocarbonatite. Geochimica et Cosmochimica Acta 79: 20-40.

Weidendorfer, D., Schmidt, M. W. and Mattsson, H. B. (2017). A common origin of carbonatite magmas. Geology 45: 507-510.

Woolley A.R. and Kempe D.R.C. (1989). Carbonatites: nomenclature, average chemical compositions, and element distribution. In: Carbonatites: Genesis and Evolution (Bell, K., ed.). Unwin-Hyman, London, 1-14.

Wooley A.R. and Kjarsgaard B.A. (2008). Carbonatite occurrences of the world: map and database. Geological survey of Canada. Open file, 5796(1).

GEOCHEMISTRY AND Lu-Hf ISOTOPIC – GEOCHEMICAL SYSTEMATICS OF THE NEOARCHAEAN PERALKALINE GRANITES OF THE KEIVY MEGABLOK, KOLA PENINSULA

Vetrin V.R.[1,3], Belousova E.A.[2], Kremenetskiy A.A.[3]

[1]Geological Institute KSC RAS, Apatity, Russia, vetrin@geoksc.apatity.ru

[2]Macquarie University, Sydney, Australia, elena.belousova@mq.edu.au

[3]Institute of Mineralogy, Geochemistry and Crystal Chemistry of Rare Elements, Moscow, Russia, nauka@imgre.ru

In the central part of the Kola Peninsula, subalkaline and peralkaline granites, granosyenites, quartz syenites, nepheline and alkaline syenites form the Neoarchaean alkaline province with an area of more than 2500 km^2. In the study of the Keivy structure, the discrepancy between the Palaeoproterozoic rock dating, determined when studying a number of isotopic systems (K-Ar, Sm-Nd, U-Pb), and the Archaean age of rocks and minerals was shown. The reason for this discrepancy is assumed to be the temperature and fluid effects of Proterozoic magmatism and metamorphism, which caused the rearrangement of isotopic systems (Vetrin et al., 1999; 2014). An effective geochemical criterion for the melt nature of crustal, mantle or mantle-crustal genesis that are less susceptible to the influence of the temperature factor, is the isotopic composition of Hf in zircon. On this basis, we have carried out a study of the rock geochemistry and Lu-Hf isotopic composition of zircon from sub-alkaline and peralkaline granites of the Keivy megablock. The origin of the initial melts of granites is supposed to be a result of melting metasomatically altered rocks of the lower crust when mantle basic magmas were introduced into it with the subsequent differentiation of palingenetic silicic melts.

The chemical composition of the rocks was determined at the Geological Institute KSC RAS (Apatity), the concentration of rare elements - at the FGBU IMGRE (Moscow) using the ICP-MS method in an Elan 6100 DRC equipment with determination errors of rare and rare earth elements not exceeding 5–7%. The Hf isotopic composition in zircon from the crystals dated in SHRIMP II (Vetrin, Rodionov, 2009) was determined at Macquarie University, Sydney, Australia, by the method of laser ablation according to the procedure described by Griffin et al. (2000). The calculation of the model age was performed using a two-stage model with an average value of $^{176}Lu/^{177}Hf = 0.015$ for the crust as a whole.

The subalkaline granites of the Kuksha massif dated at 2673 ± 10 Ma, the peralkaline granites of the White Tundra (2674 ± 10 Ma) and the Ponoy massif (2666 ± 10 Ma) were studied. Granites pertain to potassic, alkaline-calcic and high-ferruginous rocks under-saturated by aluminum and containing elevated concentrations of large-ionic, high-charged and rare-earth elements. According to these criteria, they meet A_2-type granites (Eby, 1992), formed in post-orogenic or anorogenic tectonic settings. In the ratio diagrams of SiO_2 and rock-forming oxide concentrations, points of the granite compositions form uniform trends with a decrease in the contents of Al_2O_3, FeO*, MgO, CaO, Ba, Sr, P and Ti and an increase in the concentrations of K, Na, Rb, Cs, Th, U, Zr, Hf and REE. Changes in major and minor elements in granites were probably due to the varying degree of crystallization differentiation of similar in composition initial melts with removal of Fe-Mg silicates, magnetite, Ti and P-containing phases, such as ilmenite, titanite and apatite, as well as fractionation of plagioclase causing a decrease of Ca and Al concentrations in the melt. Modelling of the mineral balance (Cabero et al., 2012) using the composition of minerals from peralkaline granite samples of the White Tundra massif shows that a change in the composition of the main elements with increasing SiO_2 concentration from 70.65% to 75.6% is consistent with the fractionation of mineral associations comprising 48% amphibole, 38% aegirine, 12% albite and 2% ilmenite. The amount of restite, corresponding to the sub-alkaline gabbro in chemical composition, is estimated at 18%.

The two-stage model age of $T_{Hf}(DM)^c$ for all studied zircon crystals is 2.92–3.28 billion years. The initial $^{176}Hf/^{177}Hf$ ratios of the crystals central parts are within 0.281004–0.281175, and the zircon composition points form a field in the area of the age trend of the evolution of a homogeneous chondrite reservoir (CHUR, Fig. 1). Most of the points are located in the fields of zircon compositions

from plagiogneisses of the Kola Superdeep Well, eclogites from the southern Kola Peninsula, and garnet granulites of the lower crust. According to geochemical and isotopic-geochemical data for all previously studied zircons from these rocks, the basic composition of protoliths is assumed (Mints et al., 2010; Vetrin et al., 2016). The Hf_i value in the shells of zircon crystals is set at 0.281234–0.281308, which exceeds the Hf_i value in the Neoarchaean crystal nuclei by 0.001–0.003 and corresponds to the increment of this value in the zircon during the development of the crust with $^{176}Lu/^{177}Hf = 0.015$ under a closed system. The points of the shell composition are located in the fields of leucogranite compositions of southern Finland and porphyry granites of the northern Baltic Shield, the crystallization of which is assumed to be from the melts formed during the introduction of mantle rocks of basic composition in the rocks of the lower crust. The fractionation coefficient $f_{Lu}=[(^{176}Lu/^{177}Hf)_{sam.}/^{176}Lu/^{177}Hf)^0_{CHUR}]-1$ in all studied zircons has negative values and varies from -0.925 to -0.987. The average values of the fractionation coefficient in zircon have similar values in subalkaline granites (f_{Lu} = -0.974) and peralkaline granites of the White Tundra (-0.970) and the Ponoy massif (-0.968). These data determine the formation of the initial melts of all massifs mainly due to the crust substance depleted in Lu and enriched in Hf as compared to chondrite. Granites of all massifs have high concentrations of K, Rb, Cs, Th, U, Zr, Hf, REE and elevated values of the Y/Nb (1.9–2.5) and Yb/Ta (3.4–3.7) ratios, which are characteristic of granites formed with the use of crustal sources (Eby, 1990). By the value of the ratio Th/U=5.7, granites are comparable with the rocks of the lower crust (6.0; Rudnick, Gao, 2003), which is confirmed by the characteristics of the Lu-Hf isotopic composition of zircon from the rocks considered.

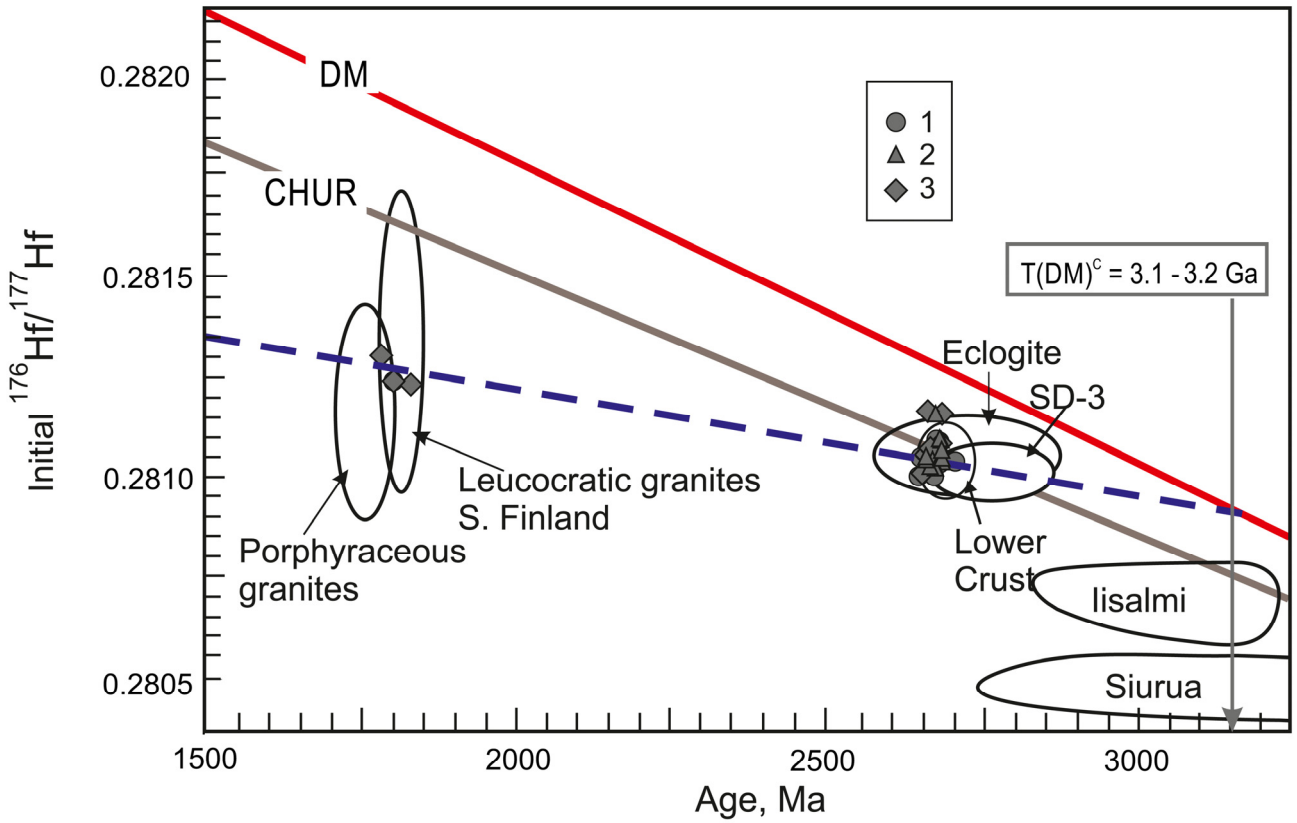

Figure 1. Initial isotopic ratios $^{176}Hf/^{177}Hf$ in zircon from granites. Composition fields are after Vetrin et al. (2014; 2016). The dotted line shows the trend of the crust evolution dated at 3.1–3.2 billion years with $^{176}Lu/^{177}Hf$= 0.015. 1- zircon from subalkaline granites, 2, 3- zircon from peralkaline granites of the White Tundra and Ponoy massifs.

Rocks of the lower crust within the Keivy megablock are not known. Possible analogues of the lower crust of this structure can be Meso-Neoarchaean rocks of the basic composition studied in the southern Kola Peninsula and containing vein bodies of plagiogranites dated at 2.87-2.78 billion years (Mints et al., 2010). Unlike the Belomorsky mobile belt, the lower crust of the Keivy megablock in

Neoarchaean was probably subjected to alkaline metasomatism, which caused a wide development of alkaline metasomatites in the rocks of the upper crust (Belolipetsky et al. 1980).

The study of the geology and petrology of peralkaline granite massifs on the Kola Peninsula indicates a close age and spatial conjugacy of basic and alkaline magmatism (Batieva, 1976). Peralkaline granites contain xenoliths of the basic rocks - gabbrodiabase, gabbro and gabbronorite, which correlate in composition and age with the rocks of the dike complex in the massif environment. It can be assumed that basic magmas provided thermal energy for partial melting of the lower crust with formation of intermediate and silicic melts, which were a mixture of melting derivatives mainly of basic and felsic materials.

The concentrations of these components in zircon were determined using the two-component mixing model. The calculations were performed using the formula $Xb=(\varepsilon Hf^{f} - \varepsilon Hf^{r})Hf_f /[\varepsilon Hf^{r}(Hf_b - Hf_f) - (\varepsilon Hf^{b}Hf_b - \varepsilon Hf^{f}Hf_f)] \times 100$, where Xb is the concentration of the basic component, %, εHf^{f}, εHf^{b}, εHf^{r} - Hf epsilon for felsic, basic and test samples, Hf_f, Hf_b - Hf concentrations in zircon from felsic and basic rocks. Zircon of Mesoarchaean gabbro – protoliths of Fe-Ti eclogites from the southern Kola Peninsula with $\varepsilon Hf_{(2670)}= 5.65$ was taken as the basic component in calculations, and zircon from vein plagiogranite in eclogites with $\varepsilon Hf_{(2670)}= -3.55$ was taken as the felsic component (Mintz et al., 2010). The Hf concentrations were taken 0.61% and 1.28% for zircon from basalts and granitoids, respectively (Belousova et al., 2002). The content of the basic component in the studied zircon crystals, and, accordingly, in the initial melts, varies from 14% to 89% with the highest frequency of occurrence from 30% to 70%.

In addition to the lower crust components, the mantle component in the amount of 3–7% was established in the composition of the alkaline granites in the Ponoy massif, which was recorded in the composition of helium isolated from accessory ilmenite during annealing of primary fluid inclusions. It is assumed that the fluid trapped during granite crystallization was formed by mixing radiogenic helium of the crust with the juvenile isotope ^{3}He evacuated from the mantle rocks of basic composition, which caused the lower crust melting in the ratio ~ (14-42): 1 (Vetrin et al., 2003).

These data suggest that about 2.7 billion years ago, the asthenospheric diapir (asthenolith) floated to the basement of the Keivy megablock lithospheric mantle, causing its melting with formation of basic melts represented by rocks of dike series in the upper crust and xenoliths in granites. During the asthenolith rise, the fluid flow that accompanied and passed ahead of it, produced prior to melting a metasomatic change (alkaline metasomatism) in the lithospheric mantle and crustal rocks above, with their enrichment in alkalies and rare elements. When high-temperature basic melts intruded into the lower crust basement, metasomatically altered lower crustal rocks melted. The generated silicic melts to a large extent could inherit the nature of the lower crust enriched in microelements, which is transmitted to intra-plate A-type granites (Frost, Frost, 2011). During the ascent to the upper crust, the palingenetic lower crust melts changed their composition in the process of fractional crystallization with the formation of more silicic subalkaline and peralkaline compositions.

The studies were carried out at research subject № 0226-2019-0052 and with the support of the Russian Foundation for Basic Research (Grant 16-05-00756a) and Government Contract No. 13/17-1.

References

Batieva I. D. Petrology of Alkaline Granitoids of the Kola Peninsula. L.: Nauka. 1976. 224 p. (In Russian).

Belolipetsky A.P., Gaskelberg V.G., Gaskelberg L.A., Antonyuk E.S., Ilyin Yu.I. Geology and Geochemistry of Metamorphic Complexes of the Early Precambrian of the Kola Peninsula. L.: Nauka. 1980. 240 p. (In Russian).

Belousova E.A., Griffin W.L., O'Reilly S.Y., Fisher N.I. Igneous Zircon: Trace Element Composition as an Indicator of Source Rock Type // Contrib. Mineral. Petrol. 2002. V.143. P. 602–622.

Cabero M.T., Mecoleta S., Lopez-Moro F.J. OPTIMASBA: A Microsoft Excel Workbook to Optimise the Mass-Balance Modelling Applied to Magmatic Differentiation Processes and Subsolidus Overprints // Computers & Geosciences. 2012. V. 42**.** P. 206–211.

Eby G.N. Chemical Subdivision of the A-Type Granitoids: Petrogenetic and Tectonic Implication // Geology. 1992**.** V. 20. P. 641–644.

Frost C.D., Frost B.R On Ferroan (A-Type) Granitoids: their Compositional Variability and Modes of Origin // J. Petrol. 2011. V**.** 52. 39–53.

Griffin W.L., Pearson N.J., Belousova E., Jackson S.E., O'Reilly S.Y., van Achterberg E., Shee S.R. The Hf Isotope Composition of Cratonic Mantle: LAM-MC-ICPMS Analysis of Zircon Megacrysts in Kimberlites. Geochim. Cosmochim. Acta. 2000. V. 64. P. 133–147.

Mints M.V., Belousova E.A., Konilov A.N., Natapov L.M., Shchipansky A.A., Griffin W.L., O'Reilly S.Y., Dokukina K.A., Kaulina T.V. Mesoarchean Subduction Processes: 2.87 Ga Eclogites from the Kola Peninsula, Russia. Geology. 2010. Vol. 38. № 8. P. 739–742.

Rudnick R.L., Gao S. Composition of the Continental Crust. Treasure on Geochemistry. Oxford: Elsevier-Pergamon. 2003. V. 3. P. 1–64.

Vetrin V.R., Kamensky I.L., Bayanova T.B., Timmerman M., Belyatskii B.V., Levskii L.K., Balashov Yu.A. Melanocratic Nodules in Alkaline Granites of the Ponoiskii Massif, Kola Peninsula: a Clue to Petrogenesis // Geochem**.** Int. 1999. V.37. P. 1061–1072.

Vetrin V. R., Kamenskii I.L., Ikorskii S.V., Gannibal M.A. Juvenile Helium in Archean Enderbites and Alkaline Granites of the Kola Peninsula // Geochemistry Int. 2003. V. 41. № 7. P. 631-636.

Vetrin V.R., Rodionov N.V. Geology and Geochronology of Neoarchean Anorogenic Magmatism of the Keivy Structure, Kola Peninsula // Petrology. 2009. V. 17. № 6. P. 537–557.

Vetrin V.R., Skublov S.G., Balashov Yu.A., Lyalina L.M., Rodionov N.V. Time of Formation and Genesis of Yttrium-Zirconium Mineralization in the Sakharjok Massif, Kola Peninsula // Geol. Ore Deposits. 2014. V. 56. № 8. P. 603–616.

Vetrin V.R., Belousova E.A., Chupin V. P. Trace Element Composition and Lu-Hf Isotope Systematics of Zircon from Plagiogneisses of the Kola Superdeep Well: Contribution of a Paleoarchean Crust in Mesoarchean Metavolcanic Rocks // Geochem. Int. V. 54. 2016. № 1. P. 92–111.

Vetrin V.R., Belousova E.A., Kremenetskiy A.A. Lu-Hf Isotopic Systematics of Zircon from Lower Crustal Xenoliths in the Belomorian Mobile Belt // Geol. Ore Deposits. 2018. V. 60. № 7. P. 568 - 577.

HORNBLENDITE XENOLITHS FROM DEVONIAN VOLCANIC ROCKS OF THE PRIPYAT RIFT (BELARUS): PETROGRAPHY, GEOCHEMISTRY AND T-P DATA

Volkova G.D.[1], Yutkina E.V.[2], Nosova A.A.[2], Sazonova L.V.[1], Kuz'menkova O.F.[3], Laptsevich A.G.[3], Tikhomirova Y.S.[4]

[1]Moscow State University, Moscow, Russia, earlinndrow@gmail.com

[2]Institute of Geology of Ore Deposits, Petrography, Mineralogy and Geochemistry, Moscow, Russia, eyutkina@gmail.com

[3]Institute of Geology, Republican Unitary Enterprise "Scientific-Production Center for Geology", Minsk, Belarus

[4]Vernadsky Institute of Geochemistry and Analytical Chemistry of Russian Academy of Sciences, Moscow, Russia, y.s.tikhomirova@gmail.com

Devonian igneous rocks from the Pripyat rift contain xenoliths, which in general can be divided into two groups: (1) crustal basement xenoliths (biotite-garnet gneisses, garnet-clinopyroxene plagiogneisses, metagabbroids and granites), and (2) hornblendite xenoliths. We studied hornblendite xenoliths in the host rocks from boreholes in the area of the Zlobin field (the Pripyat rift marginal zone), the Uvarovichi paleovolcanoes area (intermediate rift zone) and the Gomel Structural Dam (axial rift zone). Similar hornblendite xenoliths from the Zlobin field have been already studied by (Markwick et al., 2001) and yielded 381 ± 2 Ma $^{40}Ar/^{39}Ar$ plateau age. Host rocks of xenoliths are alkaline ultramafic lamprophyres, alkaline picrites, picrobasalts, alkaline basalts and trachytes (Volkova et al., 2017).

After petrographic study of rock samples in thin sections, five least altered and most representative hornblendite xenoliths were chosen for further research. They were analyzed for major elements by XRF at the Institute of the Geology of Ore Deposits, Petrography, Mineralogy, and Geochemistry (IGEM RAS) on a PW-2400 (Philips Analytical B.V.) spectrometer. The analyses were accurate to 1–5% for elements whose concentrations were > 0.5 wt. % and no worse than 12 % for elements in concentrations of 0.5 wt. %. Trace elements were analyzed by ICP-MS at the Institute of Problems of Technologies of Microelectronics and Extrapure Materials, Russian Academy of Sciences. The samples were decomposed in acids in an autoclave. The chemical yield during decomposition was controlled by adding ^{161}Dy, ^{146}Nd and ^{174}Yb. Analysis accuracy was controlled by measurements of the GSP-2 standard. Minerals were analyzed in thin sections on a JEOL JSM-6480LV scanning electron microscope with energy-dispersive spectrometer INCA Energy 350 at the Laboratory of Local Analytical Methods, Geology Department, Moscow State University, and at the Laboratory for the Analysis of Minerals at IGEM RAS on an JXA-8200 (JEOL) microprobe equipped with five wave-dispersive and one energy-dispersive spectrometers. Sr and Nd isotopic compositions were analysed at the Laboratory of Isotopic Geochemistry and Geochronology at the Vernadsky Institute of Geochemistry and Analytical Chemistry of Russian Academy of Sciences (GEOKHI RAS) by Y.S. Tikhomirova on a Triton multicollector thermal ionisation mass spectrometer. Sr compositions were corrected for isotopic fractionation by normalising to $^{88}Sr/^{86}Sr = 8.375209$, according to the exponential law. The accuracy and reproducibility of Sr isotopic measurements were monitored using the SRM-987 standard (the average $^{87}Sr/^{86}Sr$ ratio 0.710244 ± 8). Nd compositions were corrected for isotopic fractionation by normalising to $^{146}Nd/^{144}Nd = 0.7219$, according to the exponential law. The accuracy and reproducibility of Nd isotopic measurements were monitored using the JNdi-1 standard (the average $^{143}Nd/^{144}Nd$ ratio 0.512107 ± 8).

Hornblendite xenoliths (samples 15Bl-699/410 and 15Bl-712/371) from the diatremes of the Zlobin field (Krasnitskaya and Knyazhinskaya pipes in the Gadilovichskiy cluster area) are inequigranular fine to coarse grained subhedral igneous rocks with massive rock fabric. They consist of amphibole (as the sole major mineral), accessory titanomagnetite, ilmenite, rutile, apatite, sulfides, and barite, secondary chlorite and carbonates. Compositionally the amphiboles are strongly zoned pargasite and magnesio-hastingsite with Mg# ($Mg/[Mg+Fe^{2+}]$) is 0.58-0.75.

The hornblendite xenolith (sample 15Bl-57d/354) from the Uvarovichi paleovolcanoes area (the South-Uvarovichskaya pipe) is inequigranular fine to medium grained subhedral igneous rock with

massive rock fabric, consisting of amphibole (85 %), biotite (10 %), garnet (5 %) and K-feldspar relics, accessory apatite, spinel, rutile, sulfides and secondary chlorite. Amphiboles are slightly zoned pargasite (Mg# = 0.71-0.79). Biotite forms anhedral and subhedral unzoned grains with 17.7-18.9 wt. % of Al_2O_3, 4-5 wt. % TiO_2, 4.2-7.6 wt. % BaO, and Mg# = 0.64-0.68. They are moderately altered by diaphthoritic veins. Garnet is presented by slightly zoned anhedral relics up to 1 mm in size, surrounded by fibrous chlorite and K-feldspar relics (up to 0.5 mm), which are surrounded by radiate-fibrous chlorite as well. The garnets consist of 38-45 % almandine, 36-44 % pyrope, 15-19 % grossular, 1-3 % spessartine, 0-1 % andradite, and contain also up to 0.1 wt. % TiO_2 and minor amounts of Cr_2O_3.

Hornblendite xenoliths (samples 15Bl-75d/323 and 15Bl-105/343) from the Gomel Structural Dam (the boreholes 75d and 105) are inequigranular fine to medium grained subhedral igneous rocks with massive or linear rock fabrics. The sample 15Bl-105/343 consists of amphibole (85 %), clinopyroxene (35 %), biotite and phlogopite (5 % micas altogether), accessory titanite, apatite, pyrrhotite, chalcopyrite, titanomagnetite and ilmenite, any secondary minerals are nearly absent. Amphiboles (Mg# = 0.51-0.73) are zoned Ti-pargasite and Ti-magnesio-hastingsite. They often contain clinopyroxene, biotite, titanomagnetite, apatite, sulfide and titanite inclusions. Clinopyroxenes are strongly zoned (core, intermediate zones and rims) diopsides, containing inclusions of titanomagnetite and ilmenite. Biotite (Mg# = 0.64-0.68) forms subhedral grains up to 1 mm in length, containing 4.0-4.4 wt. % TiO_2, 0.3-1.9 wt. % BaO. They are moderately altered by diaphthoritic veins. Phlogopite grains constitute a rounded agglomerate up to 1.5 mm in size. They have Mg# = 0.77-0.79 and contain 3.0-3.2 wt. % TiO_2 and up to 0.5 wt. % BaO. The sample 15Bl-75d/323 consists of amphibole (as the sole major mineral), accessory apatite, titanite, rutile, titanomagnetite, pyrrhotite, secondary calcite and chlorite. Amphibole grains (Mg# = 0.43-0.50, occasionally 0.60) constitute linear fabric of this rock, they are partly zoned pargasite, ferroan pargasite, hastingsite and magnesio-hastingsite.

Table 1. Major elements compositions of hornblendite xenoliths.

Sample	15Bl-699/410	15Bl-712/371	15Bl-57d/354	15Bl-75d/323	15Bl-105/343
SiO_2	39.98	38.46	38.73	34.04	38.76
TiO_2	2.29	3.23	1.95	3.47	3.70
Al_2O_3	10.76	9.81	13.49	11.70	7.81
FeO_{total}	16.72	20.53	14.97	22.11	18.80
MnO	0.16	0.15	0.17	0.32	0.23
MgO	13.49	12.49	13.71	8.67	10.22
CaO	8.73	8.21	9.67	10.47	14.40
Na_2O	2.88	2.52	2.12	2.05	2.23
K_2O	1.34	1.50	1.23	1.11	0.78
P_2O_5	0.12	0.03	0.53	1.83	1.20
S	0.12	0.19	0.27	0.05	0.05
LOI	3.17	2.66	2.65	3.85	1.38
Total	99.76	99.78	99.49	99.67	99.56

Our T-P estimations by single-amphibole thermobarometric equations (Ridolfi, Renzulli, 2012) give values in the range of 1015-1020 ºC and 12.6-13.5 kbar, 1005-1036 ºC and 11.1-14.8 kbar, 1034-1060 ºC and 12.4-14.3 kbar for the samples 15Bl-57d/354, 15Bl-75d/323, 15Bl-105/343 correspondingly. These equations give ± 23.5 °C uncertainty for temperature and ± 11.5% for pressure (Ridolfi, Renzulli, 2012). We also applied clinopyroxene-liquid thermometer (Putirka, 2008) and barometer (Neave, Putirka, 2017) to the sample 15Bl-105/343, using the whole rock composition as a nominal liquid composition. It gave values spanning 1175-1249 °C and 4.1-8.0 kbar for the clinopyroxene interior parts (core and intermediate zone). For the clinopyroxene rims adjoining

amphibole grains values are 1274-1299 °C and 10.9-12.6 kbar. However, there are doubts in the validity of these estimations seeing that the true liquid composition of that rock is unknown. The temperature uncertainty of clinopyroxene-liquid thermometer is ±52-60 °C (Putirka, 2008); the pressure uncertainty of clinopyroxene-liquid barometer is ±1.4 kbar (Neave, Putirka, 2017). There is no T-P estimations for the hornblendite xenoliths from the Zlobin field as their amphiboles are not eligible for the above mentioned single-amphibole thermobarometer due to chemical features (they don't correspond to calibration amphiboles).

The chemical compositions for major elements in hornblendite xenoliths is given in the Table 1. The hornblendite xenolith from the Uvarovichi paleovolcanoes area (sample 15Bl-57d/354), which contains garnet relics, is the most rich in Mg and has minimum amounts of TiO_2 and FeO_{total}, while the sample 15Bl-75d/323 from the Gomel Structural Dam is the most rich in FeO_{total} and has minimum amounts of MgO and SiO_2.

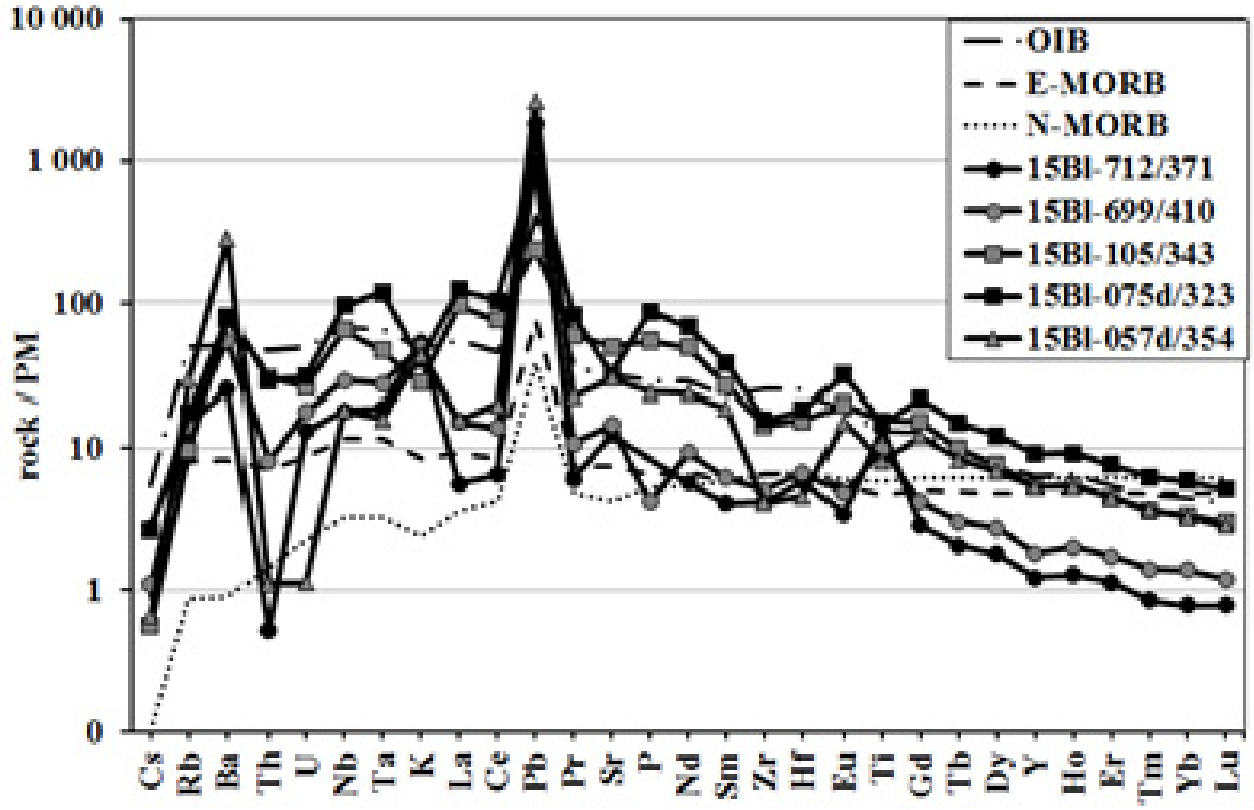

Figure 1. PM-normalized trace elements diagram for hornblendite xenoliths.

Trace elements and REE patterns (Fig. 1) show that the Zlobin field xenoliths are the least enriched in the most incompatible elements, the Gomel Structural Dam xenoliths are the most enriched, and the Uvarovichi paleovolcanoes area xenolith is intermediate between them. The trace elements patterns of the Gomel Structural Dam xenoliths compared to N-MORB, E-MORB and OIB (Sun, McDonough, 1989) resemble OIB pattern most of all (as the host rocks) and even a little more enriched. They have Th, U, K, Sr, Zr, Hf, Ti negative anomalies and Ba, Nb, Ta, Pb, P positive anomalies. Their REE patterns are smooth and a little more enriched than OIB ((La/Yb)n are 21 and 28.2 for the samples 15Bl-75d/323 and 15Bl-105/343 correspondingly). The trace elements pattern of the Uvarovichi paleovolcanoes area xenolith is located between OIB and N-MORB. It has strong Ba, K, Pb positive anomalies and Th, U, Zr, Hf, Ti negative anomalies, its REE pattern follows the Gomel Structural Dam xenoliths patterns for HREE, and decreasing and less enriched for LREE ((La/Yb)n is 4.8). The trace elements patterns of the Zlobin field xenoliths resemble OIB pattern, but much more depleted. They have prominent Rb, Ba, K, Pb, Sr, Hf, Ti positive anomalies and Th negative anomaly. Their REE patterns are smooth and resembling depleted OIB pattern (in shape) ((La/Yb)n are 11 and 7.2 for the samples 15Bl-699/410 and 15Bl-712/371 correspondingly). Compared to the host rocks

trace elements patterns, the Gomel Structural Dam xenoliths patterns roughly follow the host rocks patterns, the Uvarovichi paleovolcanoes area xenolith pattern deviates from them, and the Zlobin field xenoliths patterns are markedly different, more depleted and often have opposite anomalies.

Measured $^{87}Sr/^{86}Sr$ and $^{143}Nd/^{144}Nd$ ratios for the sample 15Bl-712/371 are 0.704218 and 0.512377 respectively, ε_{Nd}(381 Ma) is -2.0, T_{DM} model age is 1.4 Ga. For the sample 15Bl-75d/323 measured $^{87}Sr/^{86}Sr$ and $^{143}Nd/^{144}Nd$ ratios are 0.704351 and 0.512234, ε_{Nd}(381 Ma) is -3.3, T_{DM} model age is 1.2 Ga. For the sample 15Bl-105/343 measured $^{87}Sr/^{86}Sr$ and $^{143}Nd/^{144}Nd$ ratios are 0.703832 and 0.512386, ε_{Nd}(381 Ma) is -0.3, T_{DM} model age is 1.0 Ga. Hornblendite xenoliths and host rocks (data from Wilson, Lyashkevich, 1996; Marckwick et al., 2001; Pervov et al., 2004; Mikhailov et al., 2011) fall in the same area on a ε_{Nd} vs. ε_{Sr} diagram. It is close to BSE (bulk silicate Earth).

Therefore, according to our data hornblendite xenoliths are related to their host rocks. Previous researches (Marckwick et al, 2001) came to this conclusion for hornblendite xenoliths from the Zlobin field, noting that they might be derived from an earlier flux of alkaline lamprophyre magma as cumulates. Our samples from the Zlobin field may represent cumulates from parent magmas for host rocks as well. The sample from the Uvarovichi paleovolcanoes area could be either cumulate or residue due to high Mg-content and garnet relics. Samples from the Gomel Structural Dam were probably formed from a derivative magma generated from a host rocks parent magma, because their trace elements patterns coincide quite well.

The study was carried out according to the projects No. 17-05-00534 and 18-55-00006.

References

Neave D.A., Putirka K.D. A new clinopyroxene-liquid barometer, and implications for magma storage pressures under Icelandic rift zones // American Mineralogist, Vol. 102, 2017, pp. 777–794.

Markwick A.L.W., Downes M., Veretennikov M. The lower crust of SE Belarus: petrological, geophysical and geochemical constraints from xenoliths // Tectonophysics, № 339, 2001, pp. 215-237.

Mikhailov N.D., Laptsevich A.G., Vladykin N.V. Sr and Nd isotopic composition of Devonian alkali igneous rocks of Belarus // Lithosphere, 2 (35), 2011, pp. 113-122 (in Russian).

Pervov V.A., Nikitin E.A., Levsky L.K. Ultramafic alkaline volcanic rocks of the Zhlobin field (Belarus): sources and evolution of magmas // Petrology 12, 2004, pp. 354–373 (in Russian).

Putirka K.D. Thermometers and barometers for volcanic systems // Reviews in Mineralogy and Geochemistry, 69, 2008, pp. 61–120.

Ridolfi F., Renzulli A. Calcic amphiboles in calc-alkaline and alkaline magmas: thermobarometric and chemometric empirical equations valid up to 1,130 °C and 2.2 GPa // Contributions to Mineralogy and Petrology, 2012, 163, pp. 877–895, DOI: 10.1007/s00410-011-0704-6.

Sun S.S., McDonough W.F. Chemical and isotopic systematics of oceanic basalts: implications for mantle composition and processes // Magmatism in the Oceanic Basins. Geological society special publication, 42, 1989, pp. 313-345.

Volkova G.D., Yutkina E.V., Sazonova L.V., Kondrashov I.A. Petrochemical features of Devonian volcanic rocks from the north-western part of the Pripyat-Dnieper-Donets Rift System (Belarus): rocks typification and their genetic aspects // New in the knowledge of oregenesis processes: 7th Russian scientific school for young researchers, Moscow, 13-17 November 2017, Conference abstracts – digital data, IGEM RAS, 2017, pp. 78-81 (in Russian).

Wilson M., Lyashkevich Z.M. Magmatism and geodynamics of rifting of the Pripyat-Dnieper-Donets rift, East European Platform // Tectonophysics, v. 268, 1-4, 1996, pp. 65-81.

GEOLOGICAL AND GEOPHYSICAL CONSTRAINTS ON THE STRUCTURE OF THE TAJNO MAGMATIC STRUCTURE UNDER COVER (NE POLAND)

Wiszniewska J., Petecki Z., Dymowski W.
Polish Geological Institute, ul. Rakowiecka 4, 00-975 Warsaw, Poland,
janina.wiszniewska@pgi.gov.pl

INTRODUCTION. The Tajno Massif is located in north-eastern part of Poland, south from Mezoproterozoic beltiform Mazury Complex, under 600 m cover of Mesozoic–Cenozoic strata. An extensive geophysical investigations (magnetic and gravimetric surveys) have defined pronounced magnetic and gravity highs, covering an area of Tajno 12 sq. km. Two other alkaline intrusions were discovered by deep drillings along E-W extension from the Tajno intrusion: the Ełk alkaline syenite massif, and the Pisz gabbro-syenite intrusion. This intrusions have been recently dated by different methods that gave well constrained emplacement age of 354–345 Ma. for the hidden alkaline and carbonatite province in NE Poland (Demaiffe et al. 2013).

GEOLOGY AND GEOPHYSICS. The first boreholes on the Tajno area have shown the relationship between the geophysical anomalies and alkaline ultramafic rocks in the hidden basement. Several methods of the magnetic and gravity field transformations have been applied, among them the reduction to the pole, and analytical downward continuation of the magnetic anomaly (Fig. 1), and bandpass filtering of the gravity anomaly (Fig. 1).

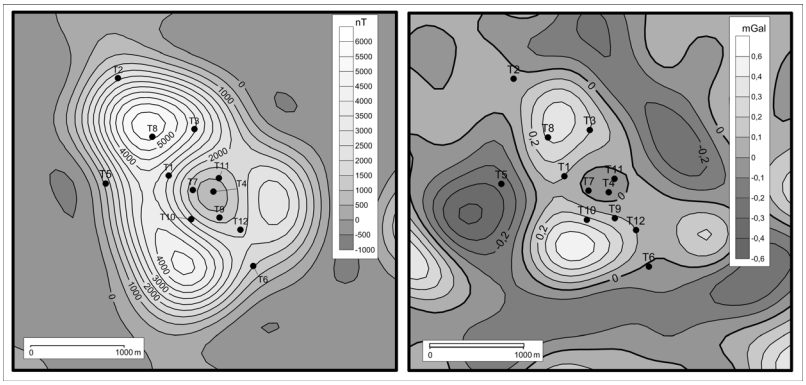

Fig. 1 a) The reduced to the pole magnetic anomalies downward continued to the depth of 600 m below observation surface: b) the residual (bandpass filtered) gravity anomalies.

The transformed anomalies indicate the segmentation of the Tajno massif indicating presence of several distinct contrasts of the value of magnetic and density properties indicating significant petrological differentiation of the massif rocks. Both, magnetic and gravity anomalies are subdivided into two main two elements i.e. the zone of positive gravity and magnetic anomalies and the local drop of the gravity and magnetic values. This local drop of the gravity and magnetic values is very strongly manifested in the magnetic field (Fig. 1) while in the gravity field image it is much weaker (Fig. 2). The local magnetic low forms a closed, rounded anomaly about 0.75 km in diameter. This centrally located area of low values of the magnetic and gravity fields indicating the rocks of weak magnetic properties and lower density occur in the central part of the massif. The boreholes situated within the local magnetic low (Fig. 1) reviled the presence of carbonatite pipe. These drillings penetrated a crater of paleovulcano filled with chimney breccia and pyroclastic materials. The crater-facies are characterized by a weaker magnetic properties in comparison with surrounding rocks of the massif.

The sub-platform alkaline-carbonatite Tajno massif is characterized by great lithological and structural variability of rocks. The main, oldest plutonic rocks are fenitized ijolites, surrounded and intruded by microperthite syenite, malignite and nepheline syenite (Krystkiewicz, Krzemiński, 1992). Cumulate pyroxenite is playing the essential role in the composition of the intrusion. Metasomatized pyroxenite were also formed due to alkaline metasomathosis. Dikes of variable composition e.g. melanephelinite, nephelinite, phonotephrite, tephriphonolite, phonolite, trachyte, and tinguaite are

crosscutting the entire complex. The central part of this structure is built of pyroclastic and volcanic rocks of the chimney breccia, cemented by carbonatites.

PETROGRAPHY. Three stages of carbonatite intrusions were distinguished in the Tajno massif (Ryka, 1992). Carbonatites of the first stage are brecciated and kept only as fragments in the chimney diatrema breccia. Carbonatites of the II stage are appearing most profusely and they are very heterogeneous. They contain titanite and amphibole and usually display in form of veins of a few cm into even 1 meter thickness or binders cementing blocks of pyroxenite. Many other rocks within the breccia pipe were subjected by metasomatosis. Carbonatite veins and breccia binder of the stage III are clearly post-kinematic. Most of carbonatites from the Tajno intrusion are calcio-carbonatite, containing calcite and fluorspar mainly.

GEOCHEMISTRY OF SEDIMENTARY COVER. Sedimentary cover consists mainly of clastic rocks. Lower part is composed of the weathered crystalline basement sediments: breccias, gravels or different mixed sandstones, mudstones and claystones of the Lower Triassic or Middle to Upper Jurassic terrestrial and marine rocks.

The aim of the geochemical study of sedimentary cover over alkaline massif was to detect of geochemical footprints of ore mineralization, especially REE enrichments near the contact of magmatic with sedimentary rocks. 18 samples from 2 wells (Tajno-3 and Tajno-11) were tested by ICP-MS method. Visible enrichment of LREE in 2 testing boreholes T-3 and T-11 were documented. The study assessed the processes of vertical geochemical dispersion through cover, to determine traces of elements penetrated sedimentary cover.

This idea is the most important challenge facing mineral exploration today.

Acknowlegdement: The research was financed from Polish Geological Institute-National Research Institute grant no. 61.6701.1801.00.0.

References

Ryka W., 1992 – Geology of the Tajno massif carbonatites. Prace Panstwowego Instytutu Geologicznego Warszawa, 139, 43-77.

Ryka W., 1994. Geology of the Elk syenite massif, NE Poland. Prace Państwowego Instytutu Geologicznego Warszawa, 144, 85-120.

Krystkiewicz E., Krzemiński L. 1992 – Petrology of the alkaline-ultrabasic Tajno massif. In: Ryka W. (Ed), Geology of the Tajno Massif (NE Poland), Prace Państwowego Instytutu Geologicznego Warszawa, 139, 19-36.

Demaiffe D., Wiszniewska J., Krzeminska E., Williams I. S., Stein. H., Brassinnes S., Ohnenstetter D., Deloule E. 2013- A hidden alkaline and carbonatite province of Early Carboniferous age in NE Poland: U-Pb zircon and Re-Os sulphide geochronology. The Journal of Geology, 2013, volume 121, p. 91–104, DOI: 10.1086/668674.

MELILITE-OLIVINE NEPHELINITES AND OLIVINE NEPHELINITES OF MT. TABAAT (MAKHTESH RAMON, ISRAEL): GEOLOGICAL, PETROGRAPHICAL, GEOCHEMICAL FEATURES, AND LIKELY ORIGIN

Yudalevich Z.[1], Vapnik Ye.[1], Samoilov V.[1], Vishniakova M.D.[2]

[1]Department of Geological and Environmental Sciences, Ben-Gurion University of the Negev, P.O.B. 653, Bear-Sheva, 84105 Israel; zinovi@bgu.ac.il, vapnik@bgu.ac.il*, samoilov@bgu.ac.il*

[2]A.N. Zavaritsky Institute of Geology and Geochemistry, Urals Branch of RAS, 15 Akad. Vonsovsky st., Ekaterinburg, 62016 Russia; vishniakova@igg.uran.ru

Magmatic rocks with rock-forming melilite belong to very rare type of silica undersaturated rocks (melilitite clan). The melilitite clan makes up about one volume percent of all magmatic rocks known in the Earth. Mitchell (1996, 2001) and Woolley et al. (1996) made geological overview of such rock outcrops and their petrogeochemical classification. The present report describes the new discovery of melilitic rocks in the sub-volcanic body of Mt. Tabaat (Makhtesh Ramon, Israel).

The main geological-petrographic and petrochemical data on age, composition and geodynamic mode of magma formation in Makhtesh Ramon are reported in numerous publications (Eyal et al., 1996; Vapnik, 2005; Samoilov, Vapnik, 2005; Vapnik et al., 2007; Yudalevich et al., 2014; Fershtater et al., 2016; Fershtater, Yudalevich, 2017; Yudalevich, Vapnik, 2018).

The region is located on the Levant, at continental border restricted by the East Mediterranean on the west and Dead Sea Transform Fault on the east. The Precambrian crystalline basement is overlain by thick sequence of mainly Mesozoic and Cenozoic sedimentary layers. There are several erosion cirques in this area; Makhtesh Ramon is deepest and longest (about 45 km) one. The cirque locates on a big anticline, having gently sloping north and steep dipping south limbs. The anticline formed due to Syrian folding event, which occurred during collision of African and Arabian plates and development of Late-Cretaceous Alpine-Himalayan mountain belt.

Triassic alkali basalts of the Saharonim Formation and two Early Cretaceous associations characterize the magmatism of Makhtesh Ramon. The layer of Aptian conglomerates of the Arod Formation divides the alkali basalts of Early Cretaceous age into bimodal PreArodcgl alkali gabbro-syenite and continuous PostArodcgl alkali olivine-basalt – basanite-nephelinite series of magmatism (Yudalevich et al., 2014).

Magmatic rocks of Makhtesh Ramon region are related to within plate continental magmatism and belong to the same OIB-like alkaline geochemical type. It is nevertheless surprising that rocks show petrochemical and geochemical similarity with post shield (bimodal association) and post-erosional (continuous association) series of Hawaii.

PostArodcgl series is most complicated according to its geological features, composition, spectrum and quantity of mantle (lherzolite, wehrlite, websterite, clinopyroxenite) and deep crustal (gabbro norite) xenoliths. Rocks also includes numerous products of xenoliths disintegration: mega- and xenocrysts (Yudalevich, Vapnik, 2018). The series is most completely exposed in the Western part of Makhtesh Ramon. This area is comparable to epicenter of Aptian-Albian magmatism. The intensity of magmatism decreases in the Central and Eastern parts of Makhtesh Ramon.

PostArodcgl series is amalgamated from different types of bodies and rocks showing diverse composition. It is composed of eleven volcanic flows with total thickness of 230 m and thickness of separate flows between 5.5 and 41 m. It includes interlayers of carbonate-bearing tuffs, tuffs and subvolcanic bodies (necks, dykes, stocks, sills, laccoliths- and loppoliths-like bodies, vents with accompanied tuffo-breccia, lapilli- and ash tuffs, explosion pipes). Some of subvolcanic bodies are up to 900 x 1500 m in size. The following rock types are common: olivine basalts, microgabbros, basanites, and nephelinites, including melilite- and analcimite-bearing units. Volcanic glass is common in the rock matrix and, in some cases, the matrix completely glassy. The rocks are black, and show porphyritic texture. Olivine, clinopyroxene, and plagioclase are common phenocrysts in olivine basalts; in nephelinites these are olivine, clinopyroxene, and rarely melilite. Phenocrysts quantity is between 5 and 34 % but commonly between 15 and 25 %.

Subvolcanic body of Mt Tabaat belongs to PostArodcgl series. It has oval shape, 800 x 600 m; its cross-section is similar to conical steep dipping concentric zonal body with olivine-melanephelinites in the border zone and olivine-melilite-nephelinites in the central zone. The host rocks are pyroclastic- and lapilli-tuffs, volcanic and subvolcanic olivine basalts.

Olivine phenocrysts are common for nephelinites in the border zone. Nephelinite rock matrix is composed of clinopyroxene and titanomagnetite microliths, intergranular nepheline, zeolite, and/or calcite, and minerals of smectite group (mainly saponite). Water-bearing phases including analcime, plagioclase, and nepheline are filling amygdules, and gradually transform into leucocratic rock matrix. Nephelinite part of subvolcanic body of Mt. Tabaat has spotty texture of matrix, which caused by deferent ratios of leucocratic and melanocratic components.

Phenocrysts of olivine with subordinate quantity of clinopyroxene (1.0-1.5 %) are characteristic for rocks in the intermediate zone. The matrix is mainly composed of clinopyroxene, nepheline and titanomagnetite, with minor intergranular melilite and Ba-enriched phlogopite. In comparison to the rocks of the border zone, the quantity of zeolite-plagioclase amygdules is significantly reduced.

Melilite nephelinites of the central zone are distinguished by steady presence of melilite both as phenocrysts and as fine-grained matrix crystals. Prismatic-shaped melilite phenocrysts are up to 0.25 x 0.9 mm in size; melilite in the matrix is often subjected to pseudomorphic replacement by high aluminum zeolite. Rocks show increased quantity of clinopyroxene phenocrysts (up to 10.2 %); quantity of Ba-enriched phlogopite in the matrix is growing. Ball-like pegmatoid segregations of meltigite-ijolite compositions are distinctive. Segregations are up to 3-4 cm in diameter and filled with nepheline, melilite, clinopyroxene (aegirine, aegirine-augite, titanaugite, augite), zeolite with subordinate olivine, biotite, amphibole (arfvedsonite, riebeckite, ferrogastingsite), and ilmenite.

Radial prismatic columns are characteristic feature of Mt. Tabaat subvolcanic body. Prism dipping angle is between 5 and 45º and mainly directed to the contact with host rocks. Rarely prisms show horizontal position. Prisms at the contact are commonly flattened whereas prism faces show concave-curved pattern. Diameter of prisms is changing at contact quenching zone from 7-10 to 20-30 cm; in the central part of body diameter of prisms up to 1.0-1.2 m; their length in some cases is 40-45 m. Prisms commonly are wavelike curved. Prismatic jointing is faded to the central part of the body. Gradual changing of prismatic columns is accompanied by gradual changing of some external characteristic of rocks, which make possible to distinguish different types of rocks in the field. Black and very dense cryptocrystalline nephelinites with leucocratic segregations up to 3-5 mm are characteristic for the quenching zone. The zone thickness is between 7 and 11 m; the diameter of prismatic columns is between 20 and 30 cm. Grey-black microcrystalline melilite-free and melilite-bearing nephelinite compose the intermediate zone (the thickness is between 3.0 and 5.0 m). Diameter of prismatic columns here is between 30 and 70 cm. Dark grey microcrystalline melilite nephelinite with lumpy potato-like cleavage, without prismatic jointing, comprises the central part of subvolcanic body.

The transition between different types of nephelinites occurs at very shot interval (a few centimeters). In some cases, the border between two types of rocks is observed in thin section as a line dividing two adjacent rocks with noticeably different size of grains. Any features typical for contacts/interactions between two magmatic impulses separated in time are absent. The contacts between border and intermediate zones are always oriented parallel to the contact with host rock.

Rocks composing different zones of Mt. Tabaat subvolcanic body show similar modal compositions. Olivine (phenocrysts mainly) and titanomagnetite (matrix exclusively) contents are constant, 10 and 12 %, respectively. Quantity of clinopyroxene is decreasing from the border zone (52.3 %) to intermediate zone (47.6 %) and then to central zone (37.9 %). Two microscopically different units of nephelinites were determined in the intermediate zone: melilite-free and melilite-bearing nephelinites. The first one is adjacent to border zone, the second one - to central zone.

Major rock forming components of different rock types of Mt. Tabaat subvolcanic body show quite similar concentrations (Table 1). Nevertheless, there is a trend of magma evolution (Figure 1) and the data recalculated to the normative mineral composition revealed marked variations. Orthoclase and albite always present in nephelinites of the border zone (up to 12.6 % together), whereas they are

completely absent in melilite-bearing nephelinites of the intermediate zone and melilite nephelinite of the central zone. Melilite-bearing nephelinites and melilite nephelinites show the presence of normative leucite (4.31-6.53 %) and larnite (0.38-8.37 %). Both leucite and larnite are absent in the border zone, whereas larnite content is 0.38-2.34 % and 4.79-8.37 % in melilite-bearing nephelinites and melilite nephelinites, respectively.

Table 1. Mean major element composition of Mt. Tabaat olivine-melanephelinite rocks and their normative mineral compositions.

Rock type	1	2	3	4	5	Norm	1	2	3	4	5
Mean	8	5	5	9							
SiO_2	40.64	40.54	39.79	37.70	39.68	or	6.50	6.62	-	-	1.13
TiO_2	2.59	2.70	2.53	2.18	2.50	ab	2.13	2.35	-	-	-
Al_2O_3	12.47	12.40	11.68	11.59	12.03	an	13.76	13.78	11.96	11.52	12.72
Fe_2O_3	13.11	13.16	13.74	14.16	13.54	lc	-	-	5.75	5.56	4.54
MnO	0.22	0.21	0.23	0.26	0.23	ne	16.22	15.83	16.59	16.91	17.01
MgO	10.41	10.68	11.37	11.09	10.89	di	31.72	30.91	34.14	24.53	34.85
CaO	12.34	12.07	13.02	14.26	12.92	ol	12.47	13.05	14.47	17.98	12.13
Na_2O	3.79	3.73	3.62	3.69	3.71	mt	7.41	7.48	7.25	7.48	8.03
K_2O	1.10	1.12	1.24	1.20	1.17	il	4.92	5.13	4.81	4.14	4.75
P_2O_5	1.17	1.11	1.14	1.20	1.16	ap	2.71	2.57	2.64	2.78	2.69
LOI	2.40	2.03	1.50	2.30		ln	-	-	0.76	6.43	-
Total		100.24	99.75	99.86	99.63						
Mg*	0.64	0.65	0.66	0.67	0.65	An%	86.57	85.44	100	100	100
Al_2O_3/TiO_2	4.76	4.58	4.61	4.80							
Na_2O/K_2O	3.48	3.38	3.00	3.05							
CaO/Na_2O	3.27	3.24	3.60	3.95							
CaO/Al_2O_3	0.99	0.98	1.12	1.22							
CaO/MgO	1.18	1.13	1.15	1.30							

Note: 1 – cryptocrystalline to microcrystalline olivine nephelinite, border zone; 2 – microcrystalline melilite-free olivine nephelinite rock, intermediate zone; 3 – melilite-bearing olivine nephelinite, intermediate zone; 4 – melilite-nephelinite, central zone; 5 – calculated composition of parent magma. Mg* - magnesium rock content; An% - anorthite content of plagioclase.

Among numerous magmatic bodies of Maktesh Ramon Mt. Tabaat is a single subvolcanic body which rock matrix is deficient in glass. This feature and the absence of contact metamorphism of host rocks suggest magma crystallization in a closed adiabatic system.

Petrographic variations of compositions and character of rock contacts propose rocks crystallization from the single portion of magma. Mt. Tabaat intrusion is quenched at the contact with host lava flows. Olivine nephelinites are enriched in amygdules and segregations filled in by analcime, zeolites, calcite and saponites. Consequently, rock mineralogical content testify that magma was enrichment in volatiles.

Based on the obtained data the following scheme of melilite nephelinite formation may be suggested:

Quenching of border zone with rapid crystallization of olivine nephelinite from undercooling melt. Non-equilibrium character of rock crystallization is likely imitated by rock spotty matrix with different ratio of melanocratic and leucocratic minerals.

Dissipation of heat and volatiles into the intermediate and central zones of subvolcanic body. Continued increased pressure of volatiles that accompanied melt crystallization is revealed in deformed pattern of prismatic columns.

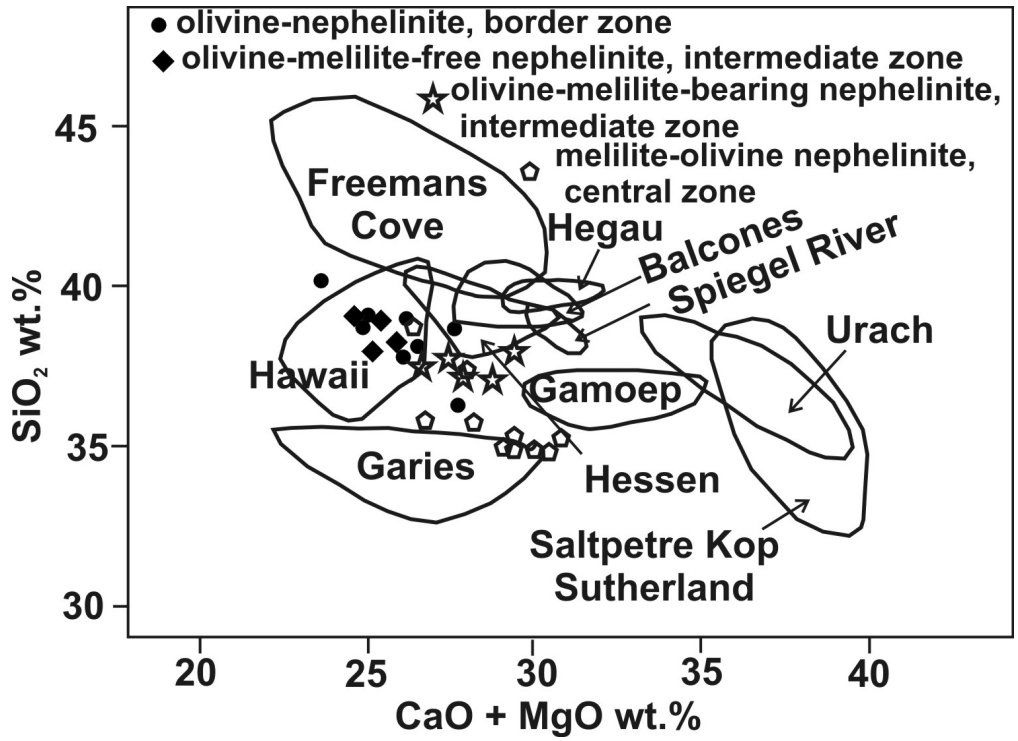

Figure 1. CaO + MgO versus SiO_2 for mililitites and melilite nephelinites (according to Mitchell, 2001) supplemented by data on Mt. Tabaat subvolcanic body.

Due to increased temperature and fluid pressure the cotectic crystallization of olivine-clinopyroxene displaced into the crystallization field (or to the peritectic? point) of olivine-clinopyroxene-melilite.

Decreasing temperature accompanied by increasing fluid pressure provides the crystallization of pegmatoid segregations of meltigite-ijolite and pseudomorphic replacement of melilite by zeolite.

Composition of the parent magma of Mt. Tabaat subvolcanic body was calculated as average composition of rocks normalized according to the areal distributions of border, intermediate, and central zones (Table 1). The parent magma corresponds to olivine melanephelinite with normative leucite, and An_{100}. Such magma composition indicates the potential possibility of melilite crystallization from the melt.

References

Eyal M., Becker A., Samoilov V. Mt. Arod – an Early Cretaceous basanitic volcano with a fossil lava lake // Israel Journal of Earth Sciences. 1996. Vol. 45. p. 31-38.

Fershtater G.B., Yudalevich Z.A., Khiller V.V. Xenoliths in alkaline basaltoids of Makhtesh Ramon (Negev, Israel) as indicator of mantle metasomatism and magma genesis // Lithosphere. 2016. Vol. 3. p. 5-26. (In Russian).

Fershtater G., Yudalevich Z. Mantle metasomatism and magma formation in continental lithosphere: Data on xenoliths in alkali basalts from the Makhtesh Ramon, Negev desert, Israel // Petrology. 2017. Vol. 25. p. 181-205.

Mitchell R.H. The Melilitite clan // In Undersaturated Alkaline Rocks: Mineralogy, Petrogenesis, and Economic Potential, Edited by R.H. Mitchell. 1996. Mineralogical Association of Canada, Short Course Series. 1996. Vol. 24. pp. 123-152.

Mitchell R. H. The classification of melilitite clan // In Alkaline Magmatism and Problems of Mantle Sources, Edited by N.V. Vladykin. Irkutsk, 2001, pp. 120-157.

Samoilov V., Vapnik Ye. Fractional crystallization – the determining factor in the origin of thephrite-basanite-nephelinite rock suite: evidence from western Makhtesh Ramon, Israel // Neues Jahrbuch für Mineralogie – Abhandlungen. 2007. Vol. 184 (2). p. 181-195.

Vapnik Ye. Melt and fluid inclusions and thermobarometry of mantle xenoliths in Makhtesh Ramon, Israel // Israel Journal of Earth Sciences. 2005. Vol. 54. p. 15-28.

Vapnik Ye., Sharygin V., Samoilov V., Yudalevich Z. The petrogenesis of basic and ultrabasic alkaline rocks of western Makhtesh Ramon, Israel: melt and fluid inclusion study // International Journal of Earth Sciences. 2007. Vol. 96. p. 663-684.

Woolley A.R. Classification of lamprophyres, lamproites kimberlites, and kalsilitic, melilitic, and leucitic rocks // The Canadian Mineralogist. 1996. Vol. 34. p. 175-186.

Yudalevich Z.A., Fershtater G.B., Eyal M. Magmatism of Makhtesh Ramon: geology, geochemistry, petrogenesis (Natural reserve of Har ha-Negev, Israel) // Lithosphere. 2014. Vol. 3. p. 70-92. (In Russian).

Yudalevich Z., Vapnik Ye. Xenocrysts and megacrysts of alkali olivine-basalt-basanite-nephelinite association Makhtesh Ramon (Israel): interaction with transporting magmas and morphological adjustment // Lithosphere. 2018. Vol. 18 (5). p. 718-742. (In Russian).

SPATIO-TEMPORAL EVOLUTION OF DEVONIAN MAGMATISM IN THE PRIPYAT-DNIEPER-DONETS RIFT ZONE (PDDR): PETROLOGICAL FEATURES OF SOURCES AND EVOLUTION MODEL OF THE PRIPYAT RIFT

Yutkina E.V.[1], Nosova A.A.[1], Sazonova L.V.[2], Volkova G.D.[2], Kargin A.V.[1], Kuz'menkova O.F.[3], Laptsevich A.G.[3], Lebedeva N.M.[1], Kondrashov I.A.[1]

[1]IGEM RAS, Russia, eyutkina@gmail.com

[2]Lomonosov Moscow State University, Russia, sazonovalv52@mail.ru

[3]Institute of Geology, Republican Unitary Enterprise "Scientific-Production Center for Geology", Minsk, Belarus

The Pripyat-Dnieper-Donetsk rift zone (PDDR) is the largest structure of the southwestern part of the East European Platform (EEP). PDDR is characterized by the presence of extensive Late Paleozoic magmatism and include the Pripyat Trough and its framing (the Northern Pripyat shoulder, including the Zhlobin saddle), the Dnieper-Donets rift, the Donbass-Azov junction zone, Eastern Azov segment and the north-eastern part of the Voronezh Crystalline Massif (VCM). Magmatism of large rift zones is usually characterized by a variety of melt sources and mechanisms of their evolution: primary mantle melts change composition due to interaction with mantle peridotites, fractional crystallization, mixing with new portions of mantle melts and crustal magmas, and assimilation of the crustal rocks (Wilson, 1989). These processes produce a variety of igneous rocks of both effusive and intrusive facies, localized in rift zones. The Pripyat-Dnieper-Donets rift zone is a typical example of extremely diverse magmatism. In this zone, represented alkaline ultrabasic rocks (kimberlite, ultramafic lamprophyres, alkaline picrites), alkaline effusives (nephelinites, leicitites, melilitites), tholeiitic basalts, acidic volcanics (Wilson, Lyashkevich, 1996 ; Pervov, 2004; Geology ..., 2001; Kimberlite ..., 1978; Yutkina et al., 2004, 2017; Shumlyanskyy et al. 2010; Sazonova et al., 2019 (in print)).

The nature of the Paleozoic intraplate EEP magmatism is widely discussed at the present time. Along with plume models (Kusznir et al, 1996; Wilson, Lyashkevich, 1996, and others), the theory is being considered that the EEP Devonian rifts can be linked to back-arc processes (Sorohtin, Sorohtin, 2006; Lyngsie, etc., 2007). But now there are more signs that the Devonian intraplate magmatism of the EEP was associated with large-scale shifts in the lithosphere in response to relative plate movement and platform rotation (Chalot-Prat et al, 2007, McCann et al., 2003). That is, this magmatism is initiated not so much by extension due the plume ascent, as by compression associated with the processes of subduction or collision along the edges of cratons. This conclusion was also made by us in (Nosova et al., 2019, this review).

It should be noted that recent studies of ours point to significant differences in the degree and type of magmatic manifestations in different segments of the PDDR. This is obviously due to the structure of the Precambrian basement under them and the strong heterogeneity of the lithosphere. A similar opinion was previously expressed earlier (Schipansky, Bogdanova, 1996). The fact of the presence of kimberlite manifestations in the PDDR, similar to the kimberlite manifestations in the northern part of the EEP in the Arkhangelsk diamondiferous province, but unlike the latter sharply limited (in scale and location) only confirms our assumptions. At the same time, as such, kimberlites were found only in the Eastern Azov region (4 tubes and dike), on the southeastern flank of the rift zone, while at the north-western end in the peripheral part of the PDDR (Zhlobin saddle of the Pripyat rift) compared with the Eastern Azov kimberlites, but only kimberlite-like manifestations of alkaline ultrabasic lamprophyres of the orangeite type (Volkova et al., 2018, Nosova et al., 2019, in this review). Such a sharp difference in the kimberlite magmatism of the two largest EEP rift structures, in our opinion, is obviously related to the different geodynamic conditions of rifting. So, for the White Sea rift system (which also includes AAP) in the north of the platform, the expansion mechanism of this magmatism became mainly expansion conditions, and for the PDDR in the south EEP was dominated by compression conditions (Nosova et al., 2019, in this review).

The studied igneous rocks of PDDR were derived from magmatic sources that had different petrological features. For the northeastern part of the VCM reveal a clear sign of crustal contribution in

their source. We suggest also the contribution of the Early Precambrian upper crustal material of the VCM to initial melt and melting of the garnet-containing metabasites (Yutkina et al., 2017). The metasomatized spinel-bearing peridotites from the upper lithospheric mantle can be taken as possible sources for VCM basalts. The VCR volcanics were probably derived by melting of a network of hornblendite/amphibole-pyroxenite veins in the peridotite protolith or the amphibolized cumulate in the underplating zone (Yutkina et al., 2017).

The Eastern Azov segment (southwestern part of the PDDR) represents the junction area of the Early Precambrian rocks of the Ukrainian Shield and the Paleozoic sedimentary and volcanogenic rocks of the Donbass. Rift processes (graben formation, magmatism) in the Eastern Azov segment manifested themselves in several phases during the late Devonian - early Carboniferous (eiffel - visa). As the Devonian Association of the Eastern Azov segment was formed, there was a decrease in the depth of the mantle source, and the association was formed by various mantle levels melting. An important feature of the Eastern Azov magmatic rocks is a very high content of Ti (up to 7.3 wt.% TiO_2) in the most highly Mg# (0.48–0.65) and deepest (CaO/Al_2O_3> 0.8) melts. These melts form the lavas of picrobasalts and carbonat-bearing lamprophyre (with the primary carbonate) dikes. Petrographic observations do not show cumulus structures and obvious signs of ilmenite accumulation in rocks containing elevated concentrations of Ti, mainly lamprophyre dykes, whereas in the case of high contents of Ti cumulus nature (such as ore pyroxenite), similar structures are clearly observed. Petrographic and geochemical characteristics of rocks suggest that high Ti contents are not the result of its accumulation during the melts fractionation but took place in the primary melt. Since the melting of ordinary peridotite cannot provide such high TiO_2 contents (Prytulak and Elliot, 2007), it is necessary to assume an additional source of Ti for the primary melting. We can be considered as an additional source of titanium: (1) melting of eclogite fragments in an uplifting plume (for example, Kamenetsky et al., 2012) or (2) the contribution of partial melts of Ti-Fe oxides from gabbro in the composition of the stagnating surface in the pathway of uplifting plume, as assumed in the model (Bai et al ., 2014).

The magmatites of the Eastern Azov region studied by us (Sazonova et al., 2019, in press) have a certain similarity in the trace elements distribution for the earliest clinopyroxene phenocrist from gabbroids and clinopyroxene from mantle metasomatite of phlogopite-ilmenite-clinopyroxene (PIC type) composition (Fitzpayne et al., 2018 and references in this work). Such metasomatized peridotites are likely to be formed from carbonate-silicate kimberlite melts (Fitzpayne et al., 2018). The main difference between our clinopyroxenes and clinopyroxenes of the PIC is the presence of a negative Zr-Hf anomaly in the Eastern Azov clinopyroxenes. For the PIC clinopyroxenes take place a positive Zr-Hf anomaly. The first melts of low degrees of melting from carbonated peridotites have a substantially carbonate composition. They are depleted with Zr and Hf (Dasgupta et al., 2009). Therefore, the restit from this melt will be enriched with these elements. In this case, there is a positive Zr-Hf anomaly in clinopyroxenes, which are preserved in the mantle restite. Thus, we compared the geochemical features of the early phenocrysts of clinopyroxenes from the Eastern Azov gabbroids and clinopyroxenes from ilmenite-containing mantle metasomatites and assume that the ultra-high-Ti primary melts for carbonate-bearing lamprophyres of the Eastern Azov segment were carbonated ilmenite-containing peridotites or perhaps also phlogopite-containing (PIC type).

The rocks from Pripyat segment of the PDDR (Zhlobin saddle, Pripyat trough, Gomel structural dam) and their sources were previously discussed in (Veretennikov et al., 2001; Pervov et al., 2004; Volkova et al., 2018). It has been shown that these volcanics have a rather heterogeneous isotopic and geochemical characteristics, which suggests lithosphere heterogeneity and, hence, several types of sources. The studied rocks can be divided into several groups. Alkaline ultramafic lamprophyres by rift margin with low SiO_2, K_20, Na_2O, Al_2O_3 and high MgO and Fe_2O_3 are first group. The rocks from intermediate and axial rift parts included two groups: high-Na and high-K. All of the rocks enriched in trace elements. The most enriched rocks are located at intermediate part of the rift. The rift margin magmatites show the lower degrees of enrichment. The axial rift zone rocks are intermediate position by the degrees of trace elements enrichment. Values of (Gd/Yb)n and (La/Yb)n ratios for most studied rocks show that its sources were in the melting zone of garnet peridotites. On the other hand, we can

see that these sources were on different depths and have varied degrees of enrichment. Also, the LREE enrichment as well as the presence of crustal xenoliths (Markwick et al., 2001 and our data) in the many magmatites indicate to crustal contamination of primary melts. The possible sources of Pripyat rift rocks were discussed in (Pervov et al., 2004) previously. It was shown that the sources of these volcanics could be both enriched (EM1-type) mantle and depleted (DM), as well as PREMA-source.

According to our data, there is little variety of rocks compositions at the rift margin. More varied magmatites compositions are observed in intermediate and axial parts of the rift. The zoning of sources by depth within one territory can be explained that they were formed here during several evolution stages of the rift (Figure). Perhaps, alkaline ultramafic rocks from intermediate and axial rift parts were formed during the pre-rift and/or initial rift stage when lithospheric thickness was big enough. Basalts and other similar volcanic rocks from the same parts could have formed from more depleted sources during later stages of the rift evolution. The asthenosphere has already ascended thereat. The lithospheric thickness decreased. Therefore, rocks sources were less deep and have geochemical parameters like as depleted mantle. Thus, we trace lateral and depth geochemical zoning for the Pripyat rift rocks with a change in the enrichment degrees of them mantle sources and see the influence of lithospheric metasomatism and crustal contamination.

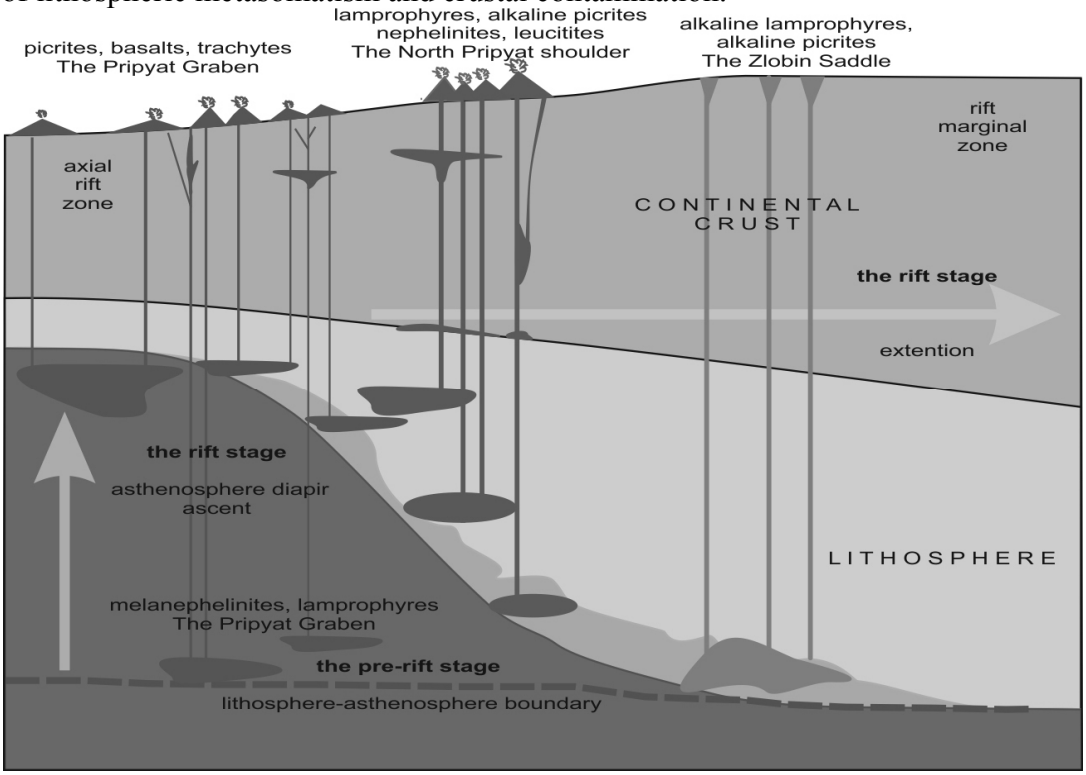

Figure. Diagram of the rift evolution in the Pripyat segment of the PDDR.

This study was financially supported by the Russian Foundation for Basic Research, projects nos. 17-05-00534 and 18-55-00006.

References

Bai Z.-J. Zhong H., Li C., Zhu W.-G., et al. Contrasting parental magma compositions for the Hongge and Panzhihua magmatic Fe-Ti-V oxide deposits, Emeishan large igneous province, SW China // Econ. Geol. 2014. V. 109. P. 1763–1785.

Chalot-Prat, F., Tikhomirov, P., Saintot, A. Late Devonian and Triassic basalts from the southern continental margin of the East European Platform, tracers of a single heterogeneous lithospheric mantle source. Journal of Earth System Science, Volume 116, Issue 6, pp.469-495.

Dasgupta R., Hirschmann M.M., McDonough W.F., et al. Trace element partitioning between garnet lherzolite and carbonatite at 6.6 and 8.6 GPa with applications to the geochemistry of the mantle and of mantle-derived melts // Chem. Geol. 2009. V. 262. № 1–2. P. 57–77.

Fitzpayne A., Giuliani A., Hergt J., et al. New geochemical constraints on the origins of MARID and PIC rocks: Implications for mantle metasomatism and mantle-derived potassic magmatism // Lithos. 2018. V. 318–319. P. 478–493.

Geologiya Belarusi (Geology of Belarus) Makhnach, A.S., Ed., Minsk: Inst. Geol. Nauk NAN Belarus, 2001.

Kamenetsky V.S., Chung S.-L., Kamenetsky M.B., et al. Picrites from the Emeishan Large Igneous Province, SW China: a compositional continuum in primitive magmas and their respective mantle sources // J. Petrol. 2012. V. 53. № 10. P. 2095-2113.

Kimberlitovye porody Priazov'ya (Kimberlite Rocks of the Azov Region), Kononova, V.A., Ed., Moscow: Nauka, 1978.

Kusznir N.J., Kovkhuto A., Stephenson R.A. Syn-rift evolution of the Pripyat Trough: constraints from structural and stratigraphic modeling // Tectonophysics. 1996. V. 268. Iss. 1-4. P. 221-236.

Lyngsie S.B., Thybo H., and Lang R. Rifting and lower crustal reflectivity: A case study of the intracratonic Dniepr-Donets rift zone, Ukraine, J. Geophys. Res., 2007, vol. 112, no. 12, pp. 124-142.

Markwick A.J.W., Downes H., and Veretennikov N., The Lower Crust of S.E. Belarus: Petrological, Geophysical and Geochemical Constraints from Xenoliths, Tectonophysics. 339. 215–237 (2001).

Mccann, T., Saintot, A., Chalot-Prat, et al. Evolution of the southern margin of the Donbas (Ukraine) from Devonian to Early Carboniferous times. Geological Society, London, Special Publications, 2003. V. 208(1). P. 117–135.

Nosova A.A., Kuz'menkova O.F., Kargin A.V. et al. Alkaline magmatism of the Devonian rift systems of the East European platform: age, geochemistry, tectonic setting of the Pripyat-Dnieper-Donets rift and the Arkhangelsk-Kola province comparison (in this review).

Pervov V.A., Nikitin E.A., Levsky L.K. Ultramafic alkaline volcanic rocks of the Zhlobin field (Belarus): Sources and evolution of magmas // Petrology. 2004. V. 12. № 4. P. 312-329.

Prytulak J; Elliott T.R. TiO_2 enrichment in ocean island basalts // Earth and Planet. Science Lett. 2007. V. 263 (3-4). P. 388 – 403.

Sazonova L.V., Nosova A.A., Yutkina E.V.et al. Genesis and evolution of mantle melts of the Devonian mafic-ultramafic rocks from the Eastern Azov (the Dnieper-Donets rift, Ukraine): evidence from geochemistry of the clinopyroxene // Petrology. 2019 (in press)

Shchipansky A.A., Bogdanova S.V. The Sarmatian crustal segment: Precambrian correlation between the Voronezh Massif and the Ukrainian Shield across the Dniepr-Donets Aulacogen // Tectonophysics/ 1996. V. 268. № 1-4. P. 109-125.

Shumlyanskyy L.V., Billström K., Tsymbal S.N., Bogdanova S.V. On the nature of the kimberlites of the Eastern Azov area, Ukraine: Isotopic (U-Pb, Hf zircon and Sr, Nd, Pb rock data) evidence for a depleted mantle origin and subsequent crustal contamination. XXVII international conference Geochemistry of Alkaline rocks. 2010.

Sorokhtin O.G., Sorokhtin, N.O. Subduction mechanism of diamond origin // Geologiya i poleznye iskopaemye mirovogo okeana (Geology and Mineral Resources of the Ocean). 2006. V. 1. P. 5-36.

Torsvik T.H., Steinbergerd B., Gurnise M., Gainab G. Plate tectonic and net lithosphere rotation over the past 150 My // Earth Planet. Sci. Lett. 2010. V. 291. Iss. 1-4. P. 106-112.

Volkova G.D., Yutkina E.V., Nosova A.A. et al. Geochemistry and some genetic aspects of Devonian alkaline igneous rocks from the Pripyat rift (southwestern part of the East European Craton) // Geophysical Research Abstracts. EGU2018. Vol. 20. P. 207.

Wilson M. Igneous Petrogenesis. London: Unwin Hyman, 1989. 466 p.

Wilson, M. and Lyashkevich, Z.M., Magmatism and the geodynamics of rifting of the Pripyat–Dnieper–Donets rift, East European platform, Tectonophysics,1996, vol. 268, № 1–4, P. 65–81.

Yutkina E.V., Kononova V.A., Bogatikov O.A. et al. Kimberlites of Eastern Priazov'e (Ukraine) and geochemical characteristics of their sources // Petrology. 2004. V. 12. № 2. P. 134-148.

Yutkina E.V., Nosova A.A., Sazonova L.V. et al. Devonian volcanic rocks of the Voronezh crystalline massif, East European Platform: the evolution of melts and features of crustal contamination // Petrology. 2017. V. 25. № 3. P. 241-271.

LOMONOSOVITE MELTING AT 1 ATM EXPERIMENTS AND PROBLEM OF PHOSPHATE-SILICATE LIQUATION

Zaitsev V.A.
GEOKHI RAS, Moscow

Agpaitic rocks are characterize high diversity titanium minerals rather than in usual for other magmatic rocks accessories titanomagnetite, ilmenite and titanite. Obliviously, titanium minerals are sensitive indications for agpaitic rocks petrogenesis, but experimental data about their stability are too limited.

One of the most important titanium minerals of agpaitic rocks is lomonosovite $Na_4Ti_4(Si_2O_7)_2O_4 \cdot 2Na_3PO_4$, belongings to the seidozerite-nacaphite polysomatic serie (titanosilicate analogs of mica) (Egorov-Tismenko, 1998) The crystal structures of lomonosovite is a combination of a titanium silicate block of composition $Na_4Ti_4(Si_2O_7)_2O_4$ with intermediate block which is a framework of Na polyhedra and P tetrahedra which gives $2[Na_3(PO)_4]$ p.f.u. (Belov et al., 1977). The aim of experiments was to provide experimental data on lomonosovite melting to estimate the temperature limit of it's stability.

The starting material was natural lomonosovite from the pegmatite, located in Koashva mine (Khibina massif, Kola Peninsula), kindly provided by I.V. Pekov. Lomoniosovite is sharply zoned: main part of lomonosovite with 3.5 wt % Nb2O5 contains minor inclusions of Nb-rich (10.5 wt%) lomonosovite. The composition of both variety of lomonosovite are listed in table 1.

Experiment in an open platinum crucible was carried out in the vertical electric microfurnace with Pt heater made by L.D. Krigman. Melting was determined by visual observation using Olympus BX-51 microscope.

The quenching experiments were carried out with pulverized material, welded in Pt ampoules, which were held in vertical electric furnaces with Ni–Cr heater and then quenched in iced water. The duration of runs was 7 hours. The temperature was measured by a Pt–Rh thermocouple. Quenched run products were examined under the microscope in immersion oils preparates, and later with the electron micrprobe Camebax microbeam (in GEOKHI RAS, analyst V.G. Senin).

The experiment with visual observation showed that the first droplets of liquid appeared at 820°C and intense melting occurs at 866° the liquid becomes mobile and flows down from the crystals.

The quenching experimental products contained reflects of lomonosovite, glass, inhomogeneous phosphate globules, perovskite solid solution and freudenbergite-like phase.

Lomonosovite relicts was found in the products of experiments at 800 and 820°C "from below" together with minor amount of titanosilicate glass.

After quenching from 870°C, the experimental products consisted of glass, phosphate globules and two titanates (see table 2). One titanate forms prismatic crystals up to 25*5 mkm and is chemically similar to freidenbergite. The other titanate forms isometric crystals up to 7 mkm and was chemically identified as the pervskite solid solution. In products of an experiments at 945°C and higher temperatures titanates were not observed, only silicate glass and phosphate globules present.

The phosphate globules formed at 870 and 945°C are rounded or oval. Individual globules are 8-30 mkm in diameter, sometimes they form chains and dendrite-like forms up to 200 mkm long, but coalescence structures into bigger globules was not fund. Globules consist from the thin-grain mixture. Compositions of this mixture present in the table.

Compositions of mixture, composing globules are variable because of phase proportions. The two last analyses in the table with the lowest titanium and silica contents and highest content of Ca, Mg are close to the $Na(Ca,Mg,Mn,Fe)PO_4$. Other analyses show higher contents of titanium and silica, and in the same time are similar or even higher in P2O5 content. This implies that they cannot be mixtures of this phosphate and a silicate glass, similar with surrounded one, but represent composition of phosphate liquid. A comparison of the compositions of phosphate and silicate material shows that the phosphate melt is enriched in Ca, Mg and Mn and depleted in Fe, Ti and Nb.

In experiments at 1025, 1040 and 1060°C, only brown glass of the lomonosovite composition present.

Table. Composition of starting material and representative composition of crystal phases after experiments.

	Lomonosovite *	High-Nb zone of lomonosovite*	Fraidenbergite **	Perovskite solid solution*	Phosphate material						
n	3	3	2	3							
T°C	Starting material		870	870	870	870	870	870	955	955	955
Na_2O	28.62	27.19	8.03	14.82	13.17	10.35	9.22	12.03	11.79	13.6	11.26
MgO	0.25	0.45	0.94	0.01	1.49	1.25	1.83	1.97	1.72	2.93	2.48
Al_2O3	0.00	0.00	0.03	0.01	0.14	0.5	0.17	0.32	0.13	0.22	0.31
SiO_2	24.08	23.53	1.17	2.06	9.71	7.25	8.64	5.17	6.44	2.72	3.15
P_2O_5	14.06	13.48	0.37	0.57	33.43	40.38	33.54	35.05	42.39	35.97	30.14
CaO	1.19	1.62	0.22	7.59	8.47	8.55	10.16	10.93	8.37	16.56	12.53
TiO2	26.87	19.42	76.05	19.70	7.45	3.98	2.29	1.84	4.15	1.66	1.33
MnO	0.78	1.85	2.34	0.22	3.82	3.51	5.56	6.56	4.86	5.88	5.97
FeO	1.29	2.52	10.14	0.38	0.89	0.81	2.83	3.05	1.93	3.13	3.09
Nb_2O_5	3.52	10.55	2.01	52.82	2.57	1.22	0.73	0.31	1.1	0.27	0.2
Total	100.67	100.60	101.27	98.18	81.14	77.8	74.97	77.23	82.88	82.94	70.46

Note: analyst V.G. Senin. *Average of 3 analyses, **Average of 2 analyses.

The experimental data show that lomonosovite incongruently melts between 820 and 866 °C with the formation of perovskite-lueshite solid solution, freidenbergite and immiscible liquids phosphate and titanosilicate silicate liquidus.

Forming of two immiscible liquids is quite unusual type of incongruent melting. It is supposed, that silicate-salt liquid immiscibility can be important during late stages of alkaline magma evolution (Kogarko, 1977). Lage amount of experimentally data about silicate-phosphate liquid immiscibility were obrainded in the last part of XX and fistf years of XXI centurte, mainly in connection with promlem of apatite deposit genesis, cheramics syntesys, and pyrometalurical applications.

Despite the fact that the problem of the genesis of apatite deposits was one of the main motives for the study of phosphate-silicate liquation, the experimental data did not become the last argument in the discussion about it. Several researchers treat experimental results as confirmation of liquation hypothesis (for e.g. Marakushev, Suk, 1993) whereas others (for e.g. Kogarko, 1990) consider experimental data disproving their this hypothesis. Aspect of acid-base interaction was never considered during this discussion. As a first approximation, the acid-base interaction in an alumosilicate melt may be presented as interaction between net-forming oxides and modifier oxides of alkali and bivalent cations. It was shown that the degree of melt polymerization is the key factor to discuss silicate melt immiscibility (Bogaerts, Schmidt, 2006).

Like the silicate thertahedra, in silicate melts and glasses, phosphoric tetrahedra in phosphate melts and glasses link through covalent bridging oxygens to form various phosphate anions and may be classified using the Qi terminology. So, acid-base interaction conception may be used for phosphate melts as well as for alumosilicate ones.

Synthesis of published experimental data in fig. 1 shows well correspondence of co-existing melts acidity in terms $\Sigma n*Me^{n+}/(Si+Al)$ and $\Sigma n*Me^{n+}/P$ for all systems with low concentration of Ti and Nb. Orthophosphate melts were obtained in equilibrium with silicate melts with $\Sigma n*Me^{n+}/(Si+Al)$ ratio 1/2 (similar with nepheline composition), while metaphosphate melts were obtained in equilibrium with gaplogranite melt, depolymerized silicate melts may be in equilibrium with salyty melts with $\Sigma n*Me^{n+}/P > 3$.

Titanosilicate glasses formed in experiments by lomonosovite incongruent melting show much higher $\Sigma nMe^{n+}/(Si+Al)$ ratio than it might be expected form composition of phosphate globules. This

fact demonstrates that titanium and niobium instead of they are mostly five- or six- coordinated (Fancns, 1997) play in highly alkaline melts the role of acid glass-forming components.

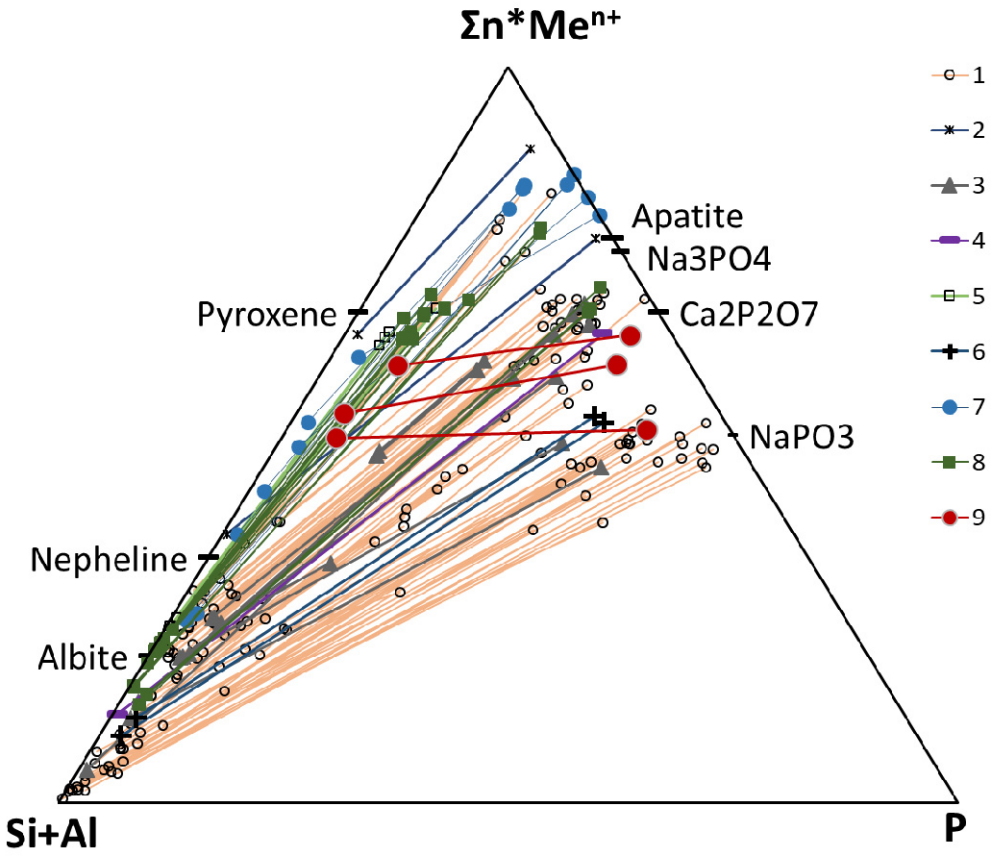

Fig. 1. Coexisting silicate and phosphate melts in experimentally studied silicate-phosphate sistems.
1- Khibina massif model systems (Marakushev, Suk, 1993, Suk, 2015), 2- Phosphate and silicate inclusions in apatite and pyroxene from the nelsonites and jotunites (Kozłowski, Wiszniewska, 2003), 3- Ne-Q-Ca2P2O7 + NaF (Krigman et al., 2004), 4- Apatite+silicate melt, (Prowatke, Klemme 2006), 5- Fo–Or–SiO_2–CaO–MgO–TiO_2–P_2O_5 (Bogaerts, Schmidt, 2006) 6-Gaplogranite+H_2O+P_2O_5 (Veksler et al., 2012), 7- REEPO4-SiO2-NaF-Nb2O5-Fe2O3- modelling the Tomtor ore melting (Delitsyn, 2015-2018), 8- Ryolite-Fayalite-magnetite-apatite mix, modelling Kiruna-type or iron oxide-apatite (IOA) deposits (Hou et al., 2018) 9- Lomonosovite incongruente melting, new data.

It is obvious that orthophosphate (apatite) crystallization from the phosphate melt with $\Sigma n*Me^{n+}/P > 3$ must result in progressive incensement of $\Sigma n*Me^{n+}/P$ ratio, so this melts might me crystallize as apatite-carbonate etc. mixtures.

Orthophosphate crystallization from the phosphate melt with $\Sigma n*Me^{n+}/P < 3$ (which may be originally in equilibrium with the nepheline- syenite melt) will result in $\Sigma n*Me^{n+}/P$ ratio decrease (melt enrich in phosphorus and became the more and more acid). There are two possible geochemical result of this evolution:

1) Crystallization of evolved phosphate melt as in a closed system toward the polyphosphate including eutectic.

2) Re-equilibration (reactions) of evolved phosphate melt with products of silicate melt crystallization.

The first situation must be consider in the liquation models of Khibina apatite ore deposits. If one believe that phosphate melt was separated from the nepheline-syenite melt, segregated in the large-scale body and then crystallized, he must expect that crystallization of this melt will result in formation of pyro- or metaphosphate-bearing paragenesies. However, no one condensed phosphate was found in

Khibina apatite ores. This is the new evident contra the liquation hypotheses of Khibina apatite ore formation.

The second situation must be consider if salty melt was not effectively segregate from silicate one, e.g. if liquation take place during the interstitial crystallization. In this case, spatial movement of these immiscible liquids can be responsible for the non-uniform distribution of phosphate in the rocks. In the same time, acid phosphate melt will be the active agent of reactions with silicate melt and early formed minerals. For example, L.N. Kogarko and co-authors (2002) reported seven reactions between loparite with late magmatic melt, corresponding secondary minerals associations, replacing loparite. Each of these associations contain phosphates and silicophosphates. The fact that phosphates and phosphosilicates are the mandatory part of pseudomorphoses after loparite shows that phosphate melt play an important role in the late magmatic processes of loparite replacement. These reactions can be summarized as

$(Me^{+},Me^{2+})PO_{4-n} + NaF + SiO_2 + (Na,REE)TiO_3 \rightarrow (Me^{+},Me^{2+})_{3-5}(PO_4)_{1-3}(F)_{1-0} + Na_xTi_ySi_zO_{x/2+2y+2z}$

where $(Me^{+},Me^{2+})PO_{4-n} + NaF$ – components of salty melt, SiO_2 – component of silicate melt $(Me^{+},Me^{2+})_{3-5}(PO_4)_{1-3}(F)_{1-0}$ – orthophosphate as secondary mineral or part of silicophosphate - $Na_xTi_ySi_zO_{x/2+2y+2z}$ - titanosilicate mineral.

So, we can conclude that the review of experimental data show that, correspondence between acidity (polimerisation degree) of immiscible silicate and phosphate melts is an important constrain into the possible models of phosphate melt petrological fate. Silicate-phosphate liquation found in the lomonosovite incongruent melting could be considered as a model of silicate-salt liquation in the late-magmatic stage of agpaitic system of Lovozero massif.

References

Belov, N.V., Gavrilova, G.S., Solov'eva, L.P., and Khalilov, A.D. (1977) Refined structure of lomonosovite. Soviet Physics – Doklady: 22: 422-424.

Bogaerts M. Schmidt M. W. Experiments on silicate melt immiscibility in the system Fe2SiO4–KAlSi3O8–SiO2–CaO–MgO–TiO2–P2O5 and implications for natural magmas//Contrib Mineral Petrol (2006) 152:257–274.

Delitsyn L. M. Distribution of niobium and lanthane between two non-mixed melts in the system LaPO4 – SiO2 – NaF – Nb2O5 – Fe2O3 // Reports of Academy of Sciences, 2017, 477, No. 3, p. 307–312.

Delitsyn L. M., Batenin V. M., Magazin L. O., Borodina T. I. Coexistence of Immiscible Liquid Phases in the LaPO4–SiO2–NaF–Nb2O5 System//Doklady Akademii Nauk, 2018, Vol. 480, No. 4, pp. 433–438.

Delitsyn L.M., Melentyev G.B., Tolstov A.V., Magazina L.O., Samonov A.E. Technological problems of Tomtor and their solution // Rare earths. 2015. № 2 (5). Pp. 164–179.

Egorov-Tismenko Yu. K. On the seidozerite-nacaphite polysomatic series of minerals - Titanium silicate analogs of mica// Crystallography Reports 1998 43(2):271-277.

Fancns F., 1997 Coordination of Ti4*in silicate glasses: A high-resolution XANES spectroscopy studyat theTi K edg American Mineralogist, 82, pp. 36-43.

Hou, T., Charlier, B., Holtz, F., Veksler, I., Zhang, Z., Thomas, R., & Namur, O. (2018). Immiscible hydrous Fe-Ca-P melt and the origin of iron oxide-apatite ore deposits. Nature communications, 9(1), 1415. doi:10.1038/s41467-018-03761-4.

Kogarko L.N. Problems of agpaitic magmas genesis// Moscow, Nauka 1977, 225 p. (in russ.).

Kogarko L.N., Williams C.T., Wooley A.R. Chemical evolution and petrogenetic implications of loparite in the layered, agpaitic Lovozero complex, kola Peninsula, Russia. // Mineralogy and Petrology 2002, 74, pp. 1-24.

Kozłowski A., Wiszniewska J. B. Phosphate and silicate inclusions in apatite and pyroxene from the Precambrian nelsonites and jotunites of NE Poland//ARCHIWUM MINERALOGICZNE T. LIV, 2003 , 5-21.

Krigman L.D., Dorfman A.M., Senin V.G., Dingwell D.B. The solubility of phosphorus in the Na-Ca-Al-Si-O-F system melts // Electronic Scientific Information Journal “Herald of the Department of Earth Sciences RAS”. 2004. URL: http://www.scgis.ru/russian/cp1251/h_dgggms/1-2004/informbul-1_2004/term-37e.pdf.

Suk N.I. 2015 liquid immiscibility in alkaline magmatic systems (experimental studies) Dr.Sci. thesis.

Veksler I., Dorfman A.M., Dulski P., Kamenetsky V.S., Danyushevsky L.V., Jeffries T., Dingwell D.B. (2012): Partitioning of elements between silicate melt and immiscible fluoride, chloride, carbonate, phosphate and sulfate melts, with implications to the origin of natrocarbonatite. - Geochimica et Cosmochimica Acta, 79, 15, p. 20-40. DOI 10.1016/j.gca.2011.11.035.

ESTIMATIONS OF SULFIDES FORMATION TEMPERATURES OF CARBONATITE ROCK SERIES VUORIYARVI MASSIF (KOLA PENINSULA)

Zaitsev V.A., Sorokhtina N.V., Kononkova N.N.
Vernadsky Institute, Moscow, Russia, alkaline@geokhi.ru

Sulfide–bearing intrusive carbonatites may be potential source of noble metals (Gavrilenko et al., 2002; Bulakh et al., 1998; Rudashevsky et al., 1995). For example average concentration of Au and Ag in Vuoriyarvi pyroxenites are 1.1 ppm and 120 ppm, in sulfide-bearing phoscorites - 1 ppm and 400 ppm, in calcite carbonatite – 0.7 ppm and 95 ppm, in sulfide-bearing calcite-dolomite carbonatite – 2.6 ppm and 500 ppm respectively (Gavrilenko et al., 2002).

The Vuoriyarvi alkaline-ultramafic intrusion is one of the twenty Paleozoic massifs of Kola-Karelian Alkaline Provinces and located in the west part of the Murmansk region. The massif is intruded Archean granite gneisses and formed concentrically zoned body (20 km^2) of pipe-like shape. The massif consists of several rock types magmatic and hydrothermal genesis (Afanasiev, 2011). Olivinites (relics), pyroxenites, including ore-pyroxenites and titanomagnetite-perovskite ores and foidolites, mainly ijolites was formed consecutively. Two multistage stockworks of dykes and veins of phoscorites and carbonatites crosscut the ultramafic rocks in Tukhtavara and Neskevara areas.

Table. Composition (wt.%) of chalcogenides from carbonatite rock series of the Vuoriyarvi massif.

	Magnetite-tetraferriphlogopite phoscorite					Calcite-dolomite carbonatite						
	Po	Py	Sp	Cp		Po	Mrc	Cp	Ga			Hes
	Min-max	Core	Av.	Low-S	Min-max High-S	Min-max	Core	Min-max	Av. Core	Av. Rim	Av. Rim, Hg-bearing	Av.
Fe	59.32-60.15	46.23	10.17	30.76	29.9-30.56	58.7-60.14	46.02	30.33-30.73	0.07	0.19	0.57	0.10
Co	0.1-0.16	0.06	0.07	0.06	0.01-0.08	0.07-0.12	0.10	0.02-0.05	0.04	0.03	0.01	0.02
Ni	0.04-0.09	0.05	0.01	0	0-0.04	0.02-0.08	0.06	up to 0.02	0.03	0.03	0.03	0.01
Zn	0.01-0.21	0	51.80	0.24	0.22-1.38	0.06	0.01	0.02-0.12	0.05	0.09	0.05	0.04
Cd	0.03	0	2.24	0	up to 0.12	0	0	0	0	0	0	0
Mn	0.05	0	0.08	0	up to 0.05	up to 0.11	0.02	up to 0.04	0.02	0.03	0.07	0.01
Cu	0.1-0.13	0.02	0.14	34.6	32.95-33.81	0.05-0.13	0.01	34.08-34.8	0.08	1.20	0.13	0.02
Pb	0.02-0.29	0.07	0.12	0.23	0.04-0.2	0.06-0.28	0.23	up to 0.16	81.15	79.41	80.67	0.20
Ag	0.05	0.08	0.07	0.12	0.08-0.16	0.05-0.1	0.01	0.05-0.07	0.70	0.35	0.36	63.26
Hg	0	0	0	0	0	up to 1.09	1.23	0	0	0	1.38	up to 1.08
Au	0	0	0	0	0	0	0	0.88-1.43	0.10	0.27	0.84	0
Bi	0	0	0	0	0	0.04-0.22	0.09	up to 0.09	1.68	1.55	1.78	0.03
S	39.06-40.29	52.91	33.18	34.49	34.8-35.1	38.06-39.41	50.93	33.62-34.07	12.88	12.47	12.51	0.10
Te	0	0	0	0	0	0	0	0	0.14	0.11	0.15	37.37
∑		99.42	97.80	100.5			98.61		96.84	95.27	98.46	101.51

Mimerals: pyrrhotite (Po), pyrite (Py), chalcopyrite (Cp), markasite (Mrc), sphalerite (Sp), galena (Ga) and hessite (Hes) Av. – average

There are three stages of formation of carbonatite series rocks characterizing of a typical silicate and carbonate minerals, such as forsterite, diopside, phlogopite or tetraferriphlogopite, magnesio-arfvedsonite, calcite, dolomite (Karchevsky, Moutte, 2004). Temperature of carbonatite formation was estimated by the melt inclusions homogenization for phoscorites are 760-915°C, for synchronous with them calcite carbonatites - 710-740°C, homogenization of fluid inclusions from the rocks shows 320-

440 and 200-400°C, respectively. The formation pressures for inclusions in phoscorites was estimated as 3.4–4.0 kbar. Homogenization temperatures of melt inclusions in the dolomite-calcite carbonatite are 550-580°C (Sokolov, 2005). Pyrrhotite, pentlandite and cobaltepentlandite are earliest sulfides of the phoscorites and carbonatites; molybdenite, pyrite, galena, sphalerite, millerite, chalcocite, bornite, chalcopyrite, covellite, tetrahedrite, bournonite, jamsonite, boulangerite, marcasite, zigenite, violarite are formed later (Shpachenko, 2012).

The aim of this study is estimate conditions of sulfide associations in dolomitized magnetite-tetraferriphlogopite phoscorite and calcite-dolomite carbonatite from Neskevara area.

Irregularly shaped pyrrhotite grains, crystals of sphalerite with exsolution inclusions of chalcopyrite and chalcopyrite with minor pyrite overgrow on pyrrhotite (Fig.1a,b) represent the sulfide mineralization in phoscorite. The calcite-dolomite carbonatite consist of grains of pyrrhotite, chalcopyrite, and galena in calcite matrix and pyrrhotite is often replaced by marcasite (Fig.1c). Galena contain micro inclusions of hessite, first discovered by A.K. Shpachenko (Shpachenko, Savchenko, 2004). The compositions of sulfides from both rocks types are given in the table.

Pyrrhotite composition from phoscorite vary from $Fe_{0.84}S$ to $Fe_{0.88}S$, that correspond to 444-624°C on the "solvus" diagram (Osadchii, Chareev, 2006). Pyrrhotite content from 0.1 to 0.16 wt.% Co and from 0.04 to 0.09wt.% Ni. Concentration of Ni in pyrrhotite shows positive correlation with Fe. Distribution of Ni between pyrrhotite and pyrite correspond to temperature 458-532°C by the Bezmen N.I. geothermometr (Bezmen et al., 1975), so the most iron-rich pyrrhotite might be in equilibrium with pyrite by Ni content. In the same time the most iron-rich pyrrhotite are enriched by Cu (up to 0.13 wt%).

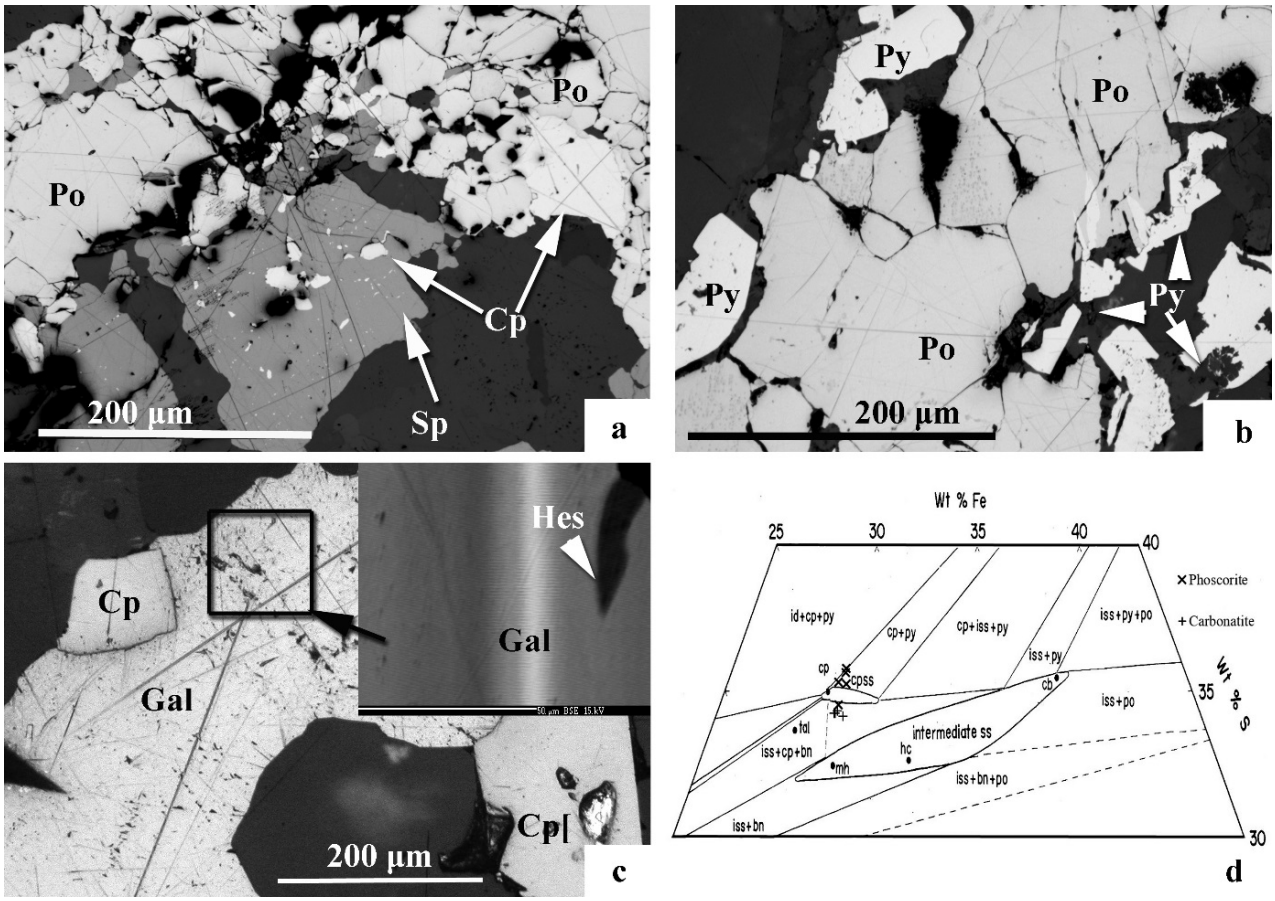

Figure 1. Microstructural features of polyphaser sulphide segregations: a - sphalerite (Sp) with exsolution inclusions of chalcopyrite (Cp), b – replacement pyrrhotite (Po) by pyrite (Py), magnetite-tetraferriphlogopite phoscorite, sample VU-430-120; c – sequential crystallization of chalcopyrite and galena (Ga) with hessite ionclution (Hes), calcite-dolomite carbonatite, sample 447/265, Optical and BSE images; d – projection of chalcopyrite composition to the part of Cu-Fe-S phase diagram at 350°C (Sugaki et al., 1975).

The pyrrhotite composition from calcite-dolomite carbonatite vary from $Fe_{0.87}S$ to $Fe_{0.90}S$. In the most cases, the compositions of mineral correspond to temperatures of equilibrium with pyrite (403-424°C). In the same time the Fe-richest compositions are clearly was not in equilibrium with pyrite. The minor elements content are vary: Ni (0.02-0.08 wt.%), Co (0.07-0.12) and Cu (up to 0.13 wt%).

A generalization of experimental data on sulfide equilibria shows that pyrrhotite formed in equilibrium with the intermediate solid solution (ISS) and/or bornite at temperatures above 500°C, content more 1% wt. of Cu, at 350°C - 0.6wt. % Cu, and at 300 - 0.3 wt.% Cu (Wiggins, Craig, 1980, Sugaki et al., 1975). Pyrrhotite in equilibrium with pyrite and chalcopyrite may contain only 0.1wt.% Cu (Sugaki et al., 1975). Thus, the low copper content in pyrrhotite indicates that in both cases Cu-bearing phases was not formed during the pyrrhotite crystallization.

Sphalerite grains with chalcopyrite exsolutions from phoscorite contents from 9.46 to 11.16 wt.% Fe, 2.05 - 2.42 wt.% Cd, up to 0.19 wt.% Cu, 0.08 wt.% Co and up to 0.12% Ag. Pressure estimation by sphalerite with pyrrhopite and pyrite geobarometer (Lusk, Ford, 1978) is from 0.53 to 2.20 kbar. However, fluid inclusions evident about higher pressure (Sokolov, 2005). It is show that sphalerite was not in equilibrium with pyrite, but only with pyrrhotite. The solubility of CuS in sphalerite was described as geothermometer for sphalerite + pyrrhotite + pyrite + ISS; it was shown that solubility of CuS in sphalerite, coexisting with pyrrhotite is higher than in sphalerite, coexisting with of pyrrhotite and pyrite (Hutchison, Scott, 1981). The solubility of CuS in sphalerite according to geothermometer allow to estimate lower limit of chalcopyrite exsolution formation as 470-550°C.

Chalcopyrite was found as exsolution inclusions in sphalerite and in intergrowths with pyrrhotite in the phoscorite. Most compositions of chalcopyrite are slightly enriched in S relatively ideal $CuFeS_2$ and correspond to chalcopyrite associated with pyrite at the Cu-Fe-S diagram for 350°C (Fig.1d). Only one analysis fall into the low-sulfur part of chalcopyrite field, corresponding to association with ISS and bornite. In a contrast, most of chalcopyrite from the calcite-dolomite carbonatite correspond low-sulfur chalcopyrite.

It is very important that chalcopyrite-pyrrhotite association may be stable only below 335°C, above this temperature pyrite+ISS paragenesis is stable (Raghavan, 2004). At 300°C only the Fe-rich chalcopyrite may be stable with S-rich pyrrhotite, while observes compositions of chalcopyrite are rich in copper (Fig.1d). Absence of pyrite or ISS zone between chalcopyrite and pyrrhotite evident that chalcopyrite crystalize blow the 335°C.

Analyzes of galena demonstrate the enrichment of the central parts with Ag, and the marginal ones with Cu and Au (Table). In addition, in the marginal parts there are areas enriched with Hg and Au, but not with Cu and Ag. Inclusions of hessite were detected in galena of calcite-dolomite carbonatites, containing 0.86-0.18 wt.% Ag, 0.28-0.09 wt.% Te, 1.71-2.0 wt.% Bi. Hessite contains 0.05-0.31 wt% Pb. Blachnik and Gather (1978) studied PbTe-Ag_2Te system and found that β-Ag_2Te highly capable in PbTe transforms into Pb-free α-Ag2Te, and PbTe at 140±2°C. Therefore, low concentration of Pb in hessite evident that dissolution of galena was at or below 140°C.

Our data demonstrate long history crystallization of chalcogenides in Vuorijarvi carbonatite rock series. Early sulfide phases were pyrrhotite, crystallizing at ~624°C and sphalerite with exsolution inclusions of chalcopyrite, forming at 470-550°C. Probably at the same temperature (458-532°C) pyrite was formed. The most grains of chalcopyrite was crystalized below the 330°C. Temperature of galena crystallization is unknown; we only know that dissolution of hessite was at or below 140°C.

Interesting that in spite of chalcopyrite abundance in rocks, at the temperatures >350°C pyrrhotite was unsaturated in copper. It does mean that CuS was added into rock for chalcopyrite formation. Source of additional copper is unclear.

This work is supported by RFBR grant № 18-05-00590.

References

Afanasyev B.V. Mineral resources of alkaline ultrabasic massifs of the Kola Peninsula. // SPb: Windrose publishing house. 2011. 224.

Bezmen N.I., Tikhomirova V.I. Kosogova V.P. Pyrite-pyrrhotite geothermometer: Partition of nickel and cobalt//Geokhimiya. 1975. 5. 700-714 (in russian).

Bulakh A.G., Rudashevsky N.S., Karchevsky P.I. Gold, silver, sulphides and rare earth minerals in carbonatites of the Loolekop deposit (RSA) // Zapiski Vserossiiskogo Mineralogicheskogo Obchestva. 1998. 3. 45-53. (in russian).

Gavrilenko B.V., Shpachenko A.K., Skiba V.I., Balaganskaya E.G., Vursiy G.L. Distribution of noble metals in rocks, ores and concentrates of apatite-bearing intrusive complexes of the Karelian-Kola region // Geology and mineral resource of the Kola Peninsula. 2. Apatity: KSC RAS. 2002. 48-63.

Hutchison, M. N., & Scott, S. D. (). Sphalerite geobarometry in the Cu-Fe-Zn-S system. // Economic Geology. 1981. 76(1). 143–153.

Karchevsky P. I., Moutte J. The phoscorite - carbonatite complex o Vuoriyarvi, northern Karelia / In Phoscorites and Carbonatites from Mantle to Mine. The Key Example of the Kola Alkaline Province. (Wall F. Zaitsev A.N. Eds). UK. London.: Mineralogical Society. 10.163-199.

Lusk J., Bray D. M. Phase relations and the electrochemical determination of sulfur fugacity for selected reactions in the Cu–Fe–S and Fe–S systems at 1 bar and temperatures between 185 and 460° C. // Chemical Geology. 2002. 192. 227–248.

Lusk J., Ford C.E. Experimental extension of the sphalerite geobarometer to 10 kbar. // Am. Min. 1978. 63. 516-519.

Osadchii E.G., Chareev D.A. Thermodynamic studies of pyrrhotite–pyrite equilibria in the Ag–Fe–S system by solid-state galvanic cell technique at 518–723 K and total pressure of 1 atm// Geochimica et Cosmochimica Acta. 2006. 70. 5617–5633.

Raghavan V. Cu-Fe-S (Copper-Iron-Sulfur)// Journal of Phase Equilibria and Diffusion. 2004. 25. 5. 450–454.

Rudashevsky N.S., Knauf V.V., Krasnova N.I., Rudashevsky V.N. Platinum and gold-silver mineralization in ores and carbonatites of alkaline-ultrabasic cjmplex (Kovdor massif, Russia) // Zapiski Vserossiiskogo Mineralogicheskogo Obchestva. 1995. 5. 1-15. (in russian).

Shpachenko A.K., Savchenko E.Ea. Tellurium and bismuth minerals in carbonatites and alkaline rocks of Kola alkaline province // Geology and mineral resources of the European Northeast of Russia. II. Proceedings of the XIV Geological Congress of Komi Republic. Syktyvkar. Geoprint. 2004. 244-246. (in russian)

Shpachenko A.K. Sulfide minerals of alkaline-ultrabasic with carbonatites massifs of the Kola Peninsula. // Proceedings of the Fersman scientific session IX of GI KSC RAS. 2012. 316-318.

Sokolov S.V. Physic-chemical conditions of formation of mineralization in rocks of the carbonatite series // Exploration and protection of mineral resources. 2005. 4. 29-32.

Sugaki A., Shima H., Kitakaze A., Harada H. Isothermal phase relations in the system Cu-Fe-S under hydrothermal conditions at 350°C and 300°C. // Economic Geology. 1975. 70(4). 806-823.

Wiggins L.B., Craig J. R. Reconnaissance of the Cu-Fe-Zn-S System' Sphalerite Phase Relationships // Economic Geology. 1980. 75. 742-751.

PROSPECTING CRITERIA FOR OFF-SET APATITE-NEPHELINE DEPOSITS IN THE KHIBINY MASSIF AREA

Zhirov D.V.

Geological Institute of the Kola Science Centre RAS, Apatity, Russia, zhirov@geoksc.apatity.ru

Huge mineral areas and structures, which the Khibiny alkaline massif (KM) surely refers to, are primary sources of both world-class, and numerous minor deposits. Most of them have been studied in detail according to adopted prospecting techniques based on a certain set of ore-controlling criteria. Commonly, the total fertility of a mineralized area is constrained by the final amount of deposits. However, there are some cases, when changing of prospecting techniques provided new discoveries in well-studied ore areas, e.g. PGE deposits in the Monchepluton (Russian Federation, Kola region), Cu-Ni deposits at deep horizons of the Sudbury complex (Canada), etc.

All of the Khibiny pluton deposits have been discovered and prospected within one ore-control structure of an ijolite-urtite arc (IUA) or in cone-like intrusions of a foidolite complex. This ring-like structure is fairly well-studied along its strike and at the depth of up to 1.5-2 km. All of its major deposits and occurrences have been detected. At the same time, a critical mass of new data and results of geological-geophysical and tectonic-physical research has been accumulated. It allows taking a fresh look at the genesis of deposits and applying previously disregarded structural control criteria of their distribution and morphology. There is a sufficient background to elaborate a new prospecting model of the ore bodies and deposits genesis that will highlight new promising areas. Furthermore, the suggested model will not reject previously adopted concepts, but supplement and specify them.

Which previously disregarded criteria can significantly supplement existing and well-tested indicators? First, it is the visco-elastic and plicated tectonics of foidolites and, in particular, ore bodies. Most of researchers indicated their distribution and occurrence in all deposits (Onokhin, 1975; Kamenev, 1987, etc.). However, scientists did not pay it much of attention, because, first of all, their actual impact on the occurrence and scale of ore bodies is minimal. At the same time, visco-elastic shifts, common and drag folds, ore flowing in and over voids and niches, multi-stage brecciation of ores and host rocks with frequent direct and divers geological relations indicate an intensive non-disjunctive tectonics. A half of 8-9 industrial ore types (the main types are mottled, banded, lenticular-banded, block, net-like, massive, brecciated; apatite-titanium and apatite-bearing urtites are secondary) have distinct traces of visco-elastic deformations, while in the rest ore types they occur sporadically. We can explain the lack of attention to this feature by a minor impact of elastic deformations on the geometry, occurrence and scale of ore bodies, since all of them are confined to the inner part of ore bodies and usually do not spread beyond their boundaries. Thus, they hardly make any change in setting conditions or linear parameters of ore bodies. The visco-elastic tectonics properly explains the genesis of “drag folds” that were repeatedly recorded and described at deposits in the southern part of the group. Their formation was caused not by the shift of the hanging wall of country rocks (Onokhin, 1975), but by the brake of a flowing elastic ore at this wall.

The visco-elastic flow is important, since the ore can flow and redistribute from areas of its primary bedding to a new place. A vertical zoning of ore bodies occurs in result of such an overflow. In near-surface (by-contact) areas, ore bodies are characterized by a high thickness (horizontal and true), high representativeness of rich ore varieties and flattening. Sometimes ore bodies lie over mountain tops, producing a “cap”, i.e. a sub-horizontal swelling (thickening), an overflow of country rocks on the surface. It can be possibly explained by the flowable extruding, overflow and filling of the weakened zone with the ore in a by-contact apical part of the massif. It could be facilitated by the multi-stage magmatism, when there were numerous injections along a cone-like fault and each subsequent portion of the mantle destroyed (like a hydraulic fracturing) and extended the surface of the fault (i.e. the Main cone-like fault). As a result, a swell occurred in the previously formed interface area of alkaline rocks and host crystalline and/or sedimentary rocks. The elastic ore was extruded to the interface with the gravity of the overlying suite and, possibly, with the crystallization forces. Then, the ore filled in lenticular “voids and traps” both in the near-surface area, and at the depth (Fig. 1). Relics of such “caps” are known to be in the “Ijolite Spur” (20-25 m to 40 m of the vertical thickness

of rich ores, in average) and in the “Nagorny”-Yuksporr area (1-5 to 48 m). Such formations are likely to be typical of most known deposits; they seem to be much thicker (up to 100-150 m) and mainly consist of rich ore varieties (banded, massive, lenticular-banded, brecciated). These “caps” were eroded in the major part of IUA during the Mesozoic-Cenozoic evolution of KM. As for some other areas, there are specific settings that predetermine the preservation of these “caps”.

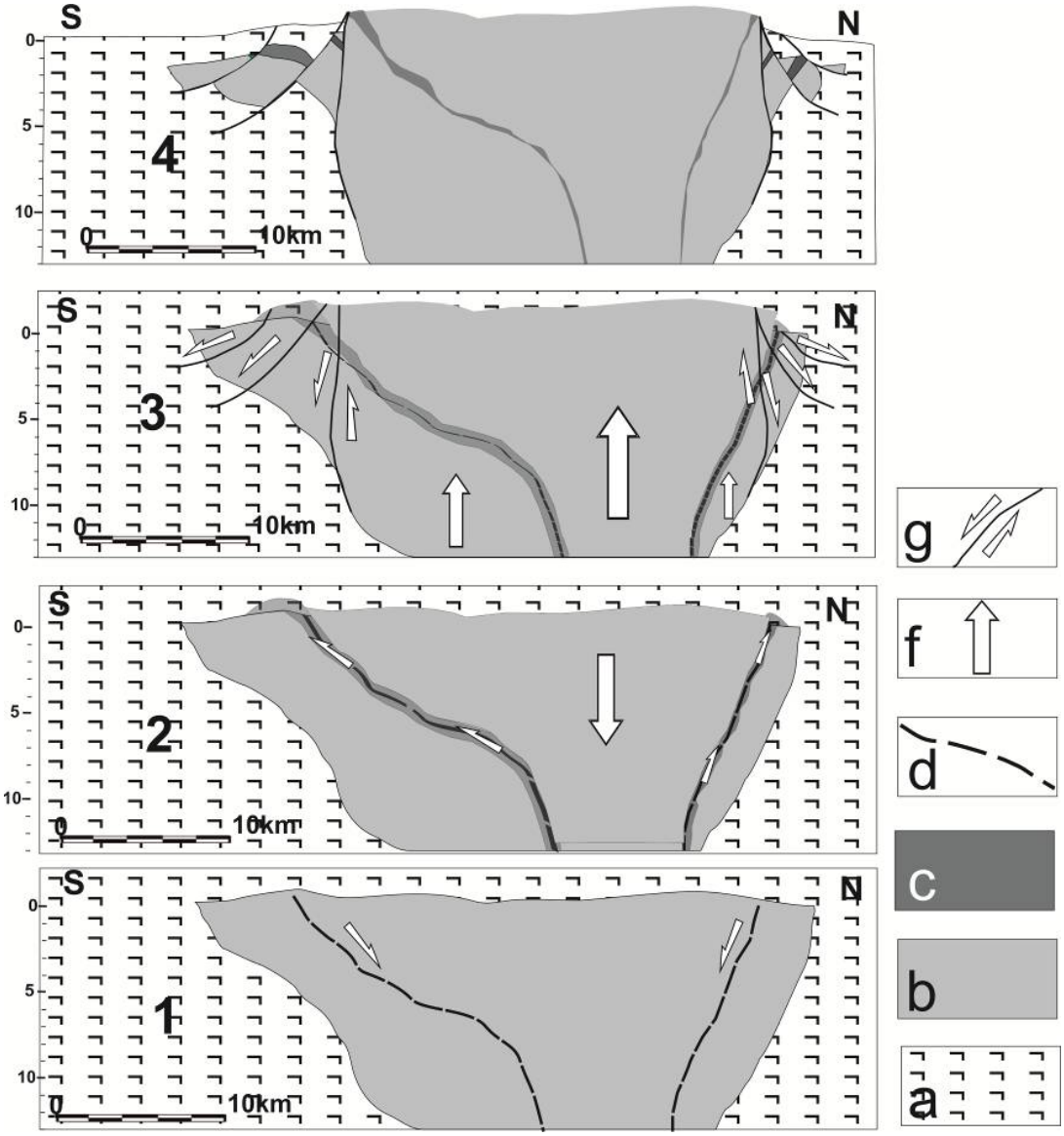

Fig. 1 - Basic scheme of the off-set deposits formation in the Khibiny: 1 – phase of formation of a layered alkaline intrusion (lopolith); 2 – phase of formation of a ring (cone-like) fault and foidolite intrusions; 3 – phase of an intensive flowable posterior (protrusive) uplift of the central part of the Khibin; 4 – approximate location of off-set “separated” blocks with ore-bearing foidolites. Legend: a - host rocks, b - alkaline rocks, c- foidolite complex, d - ring (cone-like) fault, f - direction of the rock massif displacement, g - kinematics of the “pseudo-fault” structures.

The next important criterion is a peculiar nature of the pluton tectonics, which was detected during our tectonic-physical research in 2012-2018 (Zhirov et al., 2016; Zhirov & Zhirova, 2018). It is defined that there was an intensive posterior protrusive uplift of KM in the time span of the lower Mesozoic (upper Triassic) to the Pleistocene. This uplift was associated with a split and destruction of by-contact marginal parts and origination of “pseudo-fault” structures (Fig. 2). A pseudo-fault occurs as a classic fault with a steep, up to diagonal, dip of the displacement surface; however, it was produced not by a downward shift of the hanging wall, but by an uplift of the footwall (the central core of KM). Favorable conditions for a dropping of the most fertile near-surface parts and their further

preservation at the primary bedding site occurred in the areas, where IUA was close to the outer margin of the pluton (eastern, south-eastern and north-eastern parts). The central part of the massif was uplifted, exhumed, eroded and weathered.

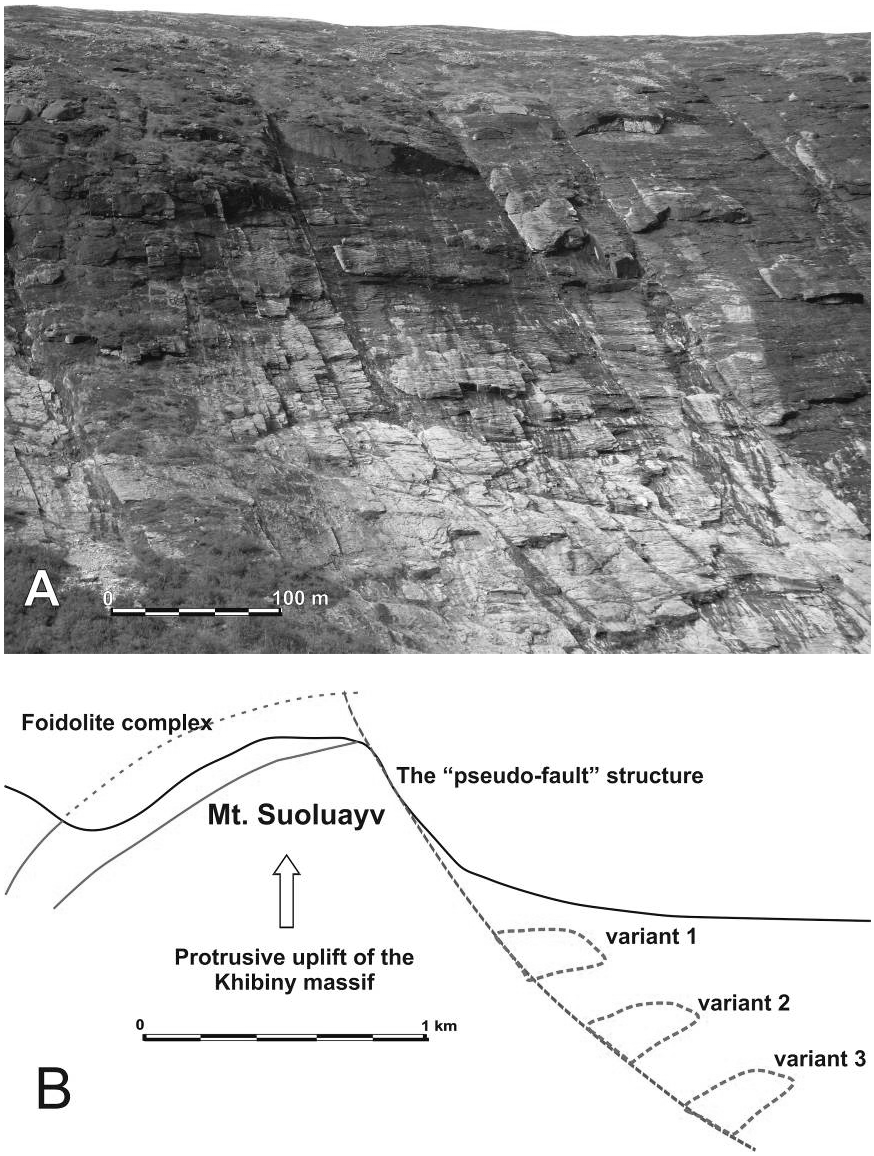

Fig. 2 - "Pseudo-fault" structure of the Mt. Suoluayv (Eastern part of Khibiny massif). A - photo of eastern slope of the Mt. Suoluayv. B - schematic section with variants of foidolite complex locations.

Numerous step-like and unitary "pseudo-faults" with a total visible shift of 300 to 500 m are easily defined in the contemporary KM landscape. Their surface has distinct traces of the fault kynematics. One of such sites occurs at the eastern slope of Mt. Suoluayv, where the visibly exposed part of the "pseudo-fault" is at least 3 km extent and at least 370 m fall length. It is estimated to be at least 4.5 km along the strike and up to 1 km and even more along the dip. It is also characterized by a gradual change in the dip angle from 55-65º at the top of the plateau to 35-45º at the bottom. In this area the complex of ore-control foidolites flattens as it approaches the contemporary surface of the plateau-like mountain. However, the thickest swelled part is cut and left in the buried part. Therefore, the potentially most productive "cup" occurred at the primary bedding site. Thus, we have tectonically justified preconditions for off-set ores prospecting.

The following criteria should be considered, while geometrizing an area promising for "buried" off-set apatite-nepheline ores: 1) actual shift along the pseudo-fault is at least 450-500 m; it can be up to 1.0-1.2 km at maximum (the maximal height of the Khibiny above the surrounding landscape,

taking into account an approximate estimation of the eroded part of the "cap" near the Rasvumchorr Plateau and Apatite Cirque deposits); 2) uplift of the central part of KM with the concurrent slip of its marginal parts was associated with both vertical, and horizontal shifts; it provides a horizontal displacement exceeding the vertical one 1.2-1.5 times, while an average angle of the displacement surface descent is 35-45º. According to these ideas, the most promising area is to the south-east and to the east of Mt. Suoluayv at the horizontal distance of 100-200 m from its bottom to the middle of Umbozero Lake (1.5-1.8 km), inclusive. The estimated depth of occurrence of the roof pendant of ore-control foidolite complex varies from 200-500 m to 950-1000 m from the day surface, depending on the selected estimation of an absolute value of the shift. The most probable depth of undercutting of the IUA roof is expected to be 250-350 m.

The potential of off-set ores can be estimated based on an average content of P_2O_5 and representativeness of the Oleniy Ruchey and Nyorpakhk deposits in the host foidolite complex. Volume ratio of ores and host foidolites varies from 0.01 to 0.34 (0.12 in average), while an average amount of the ore in geometrized bodies of the deposits is 13-15% P_2O_5. If we take a pseudo-fault length along the eastern and south-eastern slope of Mt. Suoluayv of 4.2-4.4 km (up to the Nyorpakhk deposit), a vertical thickness of the "cap" of 150 m with an average estimated width of the collapsed part of the plateau top of 300-400 m as baseline data, we get 25-29 mln m^3 of estimated forecast resources, or 75-95 mln tons of the ore with an average content of 13-15% P_2O_5. Certainly, at this stage the model cannot take into account all possible criteria that complicate or, on the contrary, simplify the assessment. Therefore, it is necessary to make at least one pilot prospecting profile from several boreholes with a drill depth of 500-800 m in order to test the suggested model.

The research is carried out in the framework of the section "Innovative technologies and methods of collecting, calibrating and analysis of geological-geophysical data for efficient and safe prospecting of deep-seated horizons of strategic mineral deposits" of the planned scientific research project No. 0226-2019-0053.

References

Cu-Ni ores of Pechenga. (Ed. N.P. Lavyorov) - M.: GEOS, 1999.- 236 p.

Mitrofanov F.P. et al. The Kola PGE Province: new data. In: Platinum of Russia. Book 1. Moscow, JSC «Geoinformark» 1999, p. 43-52

Fersman A.E. The challenging issue of the Khibiny and Lovozero tundras. / Priroda, No. 5. 1929.

Kupletsky B.M. Geological structure of the Kukisvumchorr, according to research data of 1930 // Khibiny apatites. V. 2. L.: GONTI, Lenkhimsector, 1932. P. 392-395.

Kamenev E.A. Geology and structure of the Koashva apatite deposit. - L., «Nedra», 1975. 128 p.

Kamenev E.A. Search, prospecting and geological-industrial estimation of the Khibiny-type apatite deposits (Methodological basis). - L.: Nedra, 1987. - 188 p.

Zak S.I., Kamenev E.A., Minakov F.V., Armand A.L., Mikheichev A.S., Petersilye I.A. The Khibiny alkaline massif. - L., «Nedra», 1972. 176 p.

New apatite deposits in the Khibiny / Ed. by E.A. Kamenev, D.A. Mineeva (IMGRE, Sevzalgeologiya, MGRI). - M., Nedra, 1982. 182 p.

Geology of ore areas of the Murmansk region. (Ed. by F.P. Mitrofanov, N.I. Bichuk). Authors: Pozhilenko V.I., Gavrilenko B.V., Zhirov D.V., Zhabin S.V. – Apatity: Publ. by Kola Science Centre RAS, 2002. - 359 p.

Zhirov D.V., Zhirova A.M. Neotectonics of the Khibiny alkaline massif / Conference Proceedings SGEM-2018, Albena (Bulgaria) 30 June-09 July, 2018. - 2018. Issue 1.1 Science and Technology in Geology, Exploration and Mining. P. 355-362

Zhirov D.V., Sim L.A., Marinin A.V. Reconstruction of paleo-stress states in the southern part of the Khibiny pluton (eastern Fennoscandian Shield) / Proceedings of the Conference "Topical issues of the dynamic geology in studying platform areas", Moscow, MSU, 24-26 May, 2016. - M: "Pero" Publ. House, 2016. P. 39-44.

VELOCITIES AND DENSITIES OF ROCKS OF THE KHIBINY MASSIF AND ITS FRAMING

Zhirova A.M.
Geological Institute KSC RAS, anzhelaz@geoksc.apatity.ru

In geophysical studies and processing of the results of these studies, in particular by seismic tomography method, physical parameters of rocks of the studied object are necessary. Data of the physical properties of rocks is required at all stages of tomographic research: at the stage of construction of initial velocity model, which is the basic for further calculations; when interpreting the results of building a three-dimensional seismic model. Therefore, for research of structure of the Khibiny massif and its framing, the generalization and systematization of heterogeneous materials of the properties of rocks, and includes primary and resulting data of the massif rocks and its surrounding rocks (Atlas of physical properties..., 1975; Galdin, 1977; Ignatieva, 1967; Petrophysics of crystalline..., 1982; Distribution and correlation..., 1981; Seismic studies..., 1987). The approximation function, which is a logarithmic function of the velocity dependence on density, is determined. The function is necessary both for the conversion velocity to density, and for the inverse procedure at the stage of building a complex geophysical model of the massif and its framing.

Velocity of rocks of the Khibiny massif and its framing

The velocity of the rocks of the Khibiny massif were studied during the whole period of the research of the region. Laboratory measurements on rock samples of the Khibiny massif were carried out by the method of liquid saturation (Dortman, Magid, 1968). Elastic parameters were determined, as a rule, on samples prepared from unweathered, intact rocks. Measurement of physical constants, including the elastic properties, on the rock samples also carried out in the area of the "Kukisvumchorr" Geophysical Observatory (Tyuremnov, Zubarev, 1979). The researched rocks formed the walls of the underground mine of this Observatory. Reseaches of the elastic characteristics of rocks based on seismic works were carried out by the laboratory of the Geological Institute of the Kola Branch of the Academy of Sciences of the USSR (Ivanov, Pavlovsky, 1983).

Detailed seismic studies were carried out in the rocks at a level of 0.252 km of the Kirovsk mine within the Khibiny massif. Profiling was performed by the system of reversed related time-distance plots of waves. The length of the time-distance plots corresponded to 0.3 ÷ 0.5 km. Such a small length determines the accuracy and detail of the resulting velocites. The physical parameters of the rocks of the Khibiny massif were also obtained based on the research of boreholes by the method of acoustic logging (Golubev, 1976).

Based on the compilation and analysis of data on the elastic properties of rocks of the Khibiny massif and its framing, diagrams of the values of the velocity of longitudinal waves of rocks are constructed, one of which is shown in Figure 1 and displays the average values of the velocities for each of the complexes. Among the rocks of the massif, it was found that the foidoliths are characterized by the highest values of the elastic wave velocities (on average, 6.03 km/s). Nepheline syenites have the lowest velocities: for the khibinite the value is 4.85 km/s and for the foyaite the value is 5.06 km/s.

Petrophysical properties of rocks depend on mineralogical composition. For the rocks enclosing the ore body (ristschorrite, ijolite-urtite, juvite, malignity) within the Khibiny massif observed changes in the physical properties depending on the amount of mafic minerals (pyroxene, titanomagnetite, sphene). Among the rocks of the framing of the massif, the lowest values correspond to the complex of the granodiorites-tonalites and tonalites-gneisses, while the highest values correspond to the alkaline ultramafite, peridotite of the layered Intrusive complexes and volcanites of the Imandra-Varzuga.

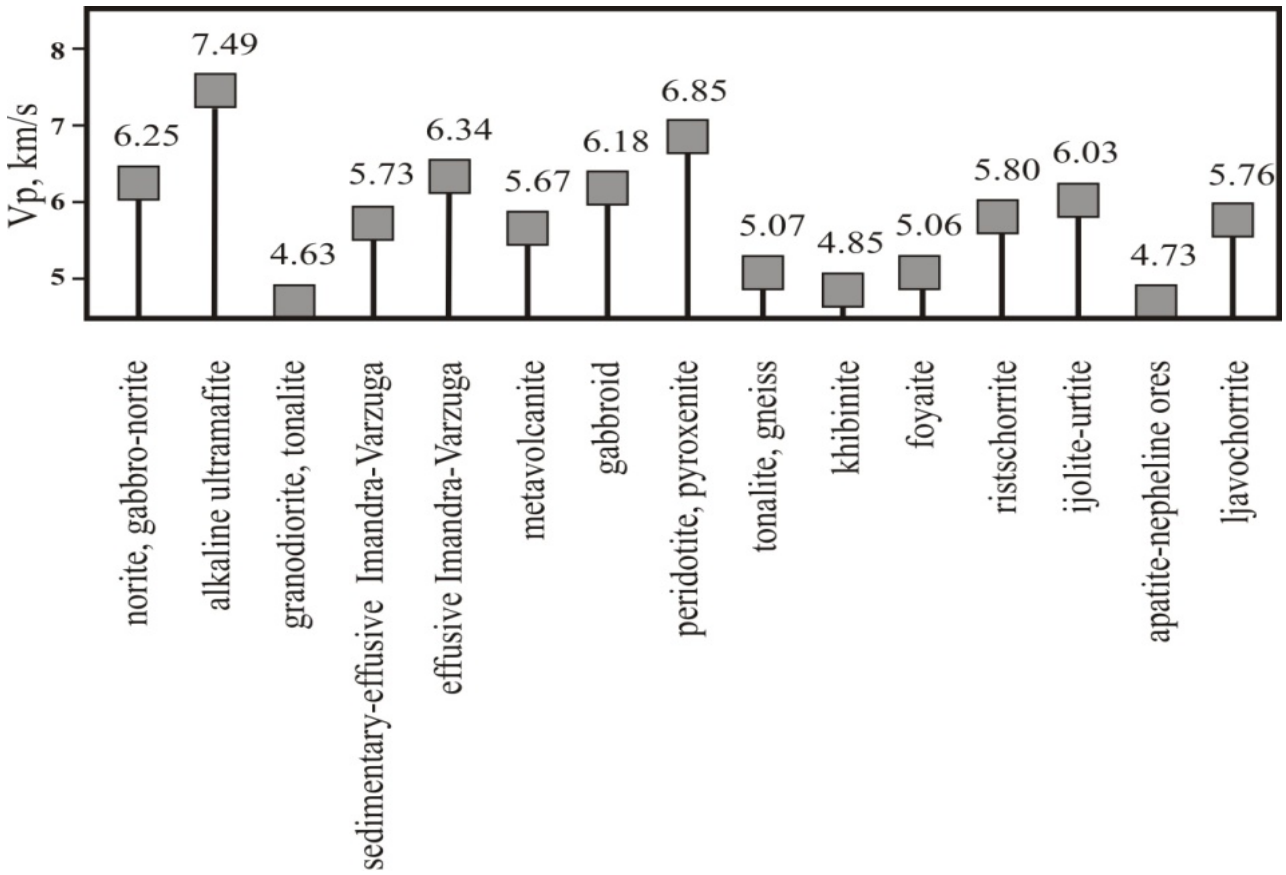

Fig. 1. Diagram of average velocities of rocks of Khibiny massif and the complexes of rocks surrounding massif.

Density of rocks of the Khibiny massif and its framing

The density of rocks and ores of the Khibiny massif and its framing, were studied by researchers on the basis of various methods, primarily petrophysical method (Ignatieva, 1967; Tyuremnov, Zubarev, 1979; Shablinsky, Kaverzneva, 1965 and other). According to the researches, the khibinites, ristschorrites and foyaits, which constitute more than 90% of the Khibiny pluton, have a density of 2.64 g/cm^3. The density of the ultrabasic foidolites is higher. According to averaged data, based on the results of different authors the average density of the urtites is 2.79 g/cm^3. The average density of the ijolites is 2.87 g/cm^3. N.A. Kaverzneva, G.N. Shablinsky and T.S. Ignatieva found close relationship is between the petrographic composition of rocks and their density. The density change is directly proportional to the percentage content of non-ferrous minerals in the rock. For ores, the mineralogical composition is determined by the content of apatite, nepheline and pyroxene, but because the variations in the content of pyroxene in ores are insignificant (2.6 ÷ 7.0%), the change in the physical characteristics of the ores is mainly determined by the variation in the content of apatite (Atlas of physical properties ..., 1975). The increase in the foidolite density is explained by the presence of significant amounts of iron oxides and other heavy minerals in these rocks. There is a clear dependence of the increase in density on the increase in the content of heavy dark minerals for the ijolite-urtites. I.A.Turchaninov and R.V. Medvedev (Atlas of Physical Properties ..., 1975) performed a quantitative assessment of the relation between the mineral composition and density of rocks. They point out high correlation coefficient between density and pyroxene content (0.91) for the urtites and ijolites. Rocks enclosing the massif are non-uniform in density. The complex of granodiorites, tonalites, Archaean plagiogranites adjacent to the Khibiny massif from the North has a density of 2.67 g/cm^3. The base complex of biotite gneisses, amphibole- and pyroxene-biotite gneisses, migmatites, tonalites, gneisses, developed south of the Proterozoic rocks of the Imandra-Varzuga, has a density of 2.72 g/cm^3. According to several thousand samples of rocks calculated (Shablinsky, Kaverzneva, 1965) the average density of rocks of the Khibiny massif (2.67 g/cm^3) and the average density of rocks of the effusive-sedimentary layer surrounding the massif from the West and South (2.94 g/cm^3). Based

on petrophysical researches by different authors, the average values of the density of rocks of the Imandra-Varzuga complex is 2.91 g/cm^3 for effusive rocks and 2.90 g/cm^3 for sedimentary-effusive rocks. As for the contrast in density of rocks of the border zone of the Khibiny massif and enclosing rocks, the khibinits and the complex of granodiorites and tonalites have similar density values (2.64 g/cm^3 and 2.67 g/cm^3). The contrast of rocks from the southwest is 0.273 g/cm^3. The lowest values of density has: a) the granodiorites, tonalites (2.67 g/cm^3); b) complex of the base (2.72 g/cm^3); c) the mica paragneisses, garnet-mica paragneisses, slates, conglomerates (2.72 g/cm^3), located in the south-east of the region of research. Based on the collection and analysis of the materials, a table of the density of the rocks and ores of the massif and its framing was compiled (table 1).

Table 1. Density properties of rocks of the Khibiny massif and rocks containing the Khibiny massif.

№	Rock	Density, g/cm ^{3}
1	norite, gabbro-norite	2,91
2	alkaline ultramafite	2,98
3	granodiorite, tonalite	2,67
4	sedimentary-effusive Imandra-Varzuga	2,9
5	effusive Imandra-Varzuga	2,91
6	metavolcanite	2,81
7	gabbroid	2,92
8	peridotite, pyroxenite	3,01
9	tonalite, gneiss	2,72
10	enderbite	2,76
11	paragneiss, slate	2,72
12	orthogneiss, paragneiss	2,87
13	Kolvitsa granulite	2,89
14	enderbite, granodiorite	2,82
15	khibinite	2,64
16	ristschorrite	2,64
17	foyaite	2,64
18	lujavrite	2,65
19	muvite	2,69
20	urtite	2,79
21	ijolite	2,87
22	apatite-nepheline ores	3,02
23	melteigite	3,16

Relationship between velocity and density

Based on the analysis of the physical properties of the rocks of the Khibiny massif and the rocks corresponding to the surrounding rocks, collected on the results of various studies, the logarithmic dependence of the velocity on the density of rocks is determined. For the rocks of the massif, it was found that for the nepheline syenites (ristschorrites, khibinites, foyaites, lyavochorrites) there is a higher resolution in velocity than in density. And for foidolites (ijolites, urtites, melteigites, lyavochorrites), the opposite is true: with small variations in velocity, the density differentiation is significant. Therefore, the density resolution is more characteristic of foidoliths. Features of the nature of the dependence of velocity on density rocks is a confirmation of the possibility of integration such methods as gravimetry and seismometry.

Work is performed under the topic of the scientific research project No. 0226-2019-0053.

References

Atlas of the physical properties of minerals and rocks of the Khibiny deposits / Turchaninov I.A., Volarovich M.P., Bondarenko A.T. and others. Ed. Turchaninov I.A. L .: Science, 1975. 72 p.

Galdin N.E. Physical properties of deep metamorphic and igneous rocks under high pressures and temperatures. M.: Nedra, 1977. 127 p.

Golubev A.A. Results of ultrasonic researches of rocks of different composition on the Kola Peninsula // Petrophysical characteristics of the Soviet part of the Baltic Shield. Apatity: Kola Branch of the USSR Academy of Sciences USSR, 1976. P. 76-80.

Dortman N. B., Magid M. S. New data on the elastic wave velocity in crystalline rocks and its dependence on humidity. Geology. 1968. No. 5. P. 123-129.

Ivanov G.A., Pavlovsky V.I. Possibility of using the anisotropy of the velocities of longitudinal and transverse waves to estimate the stress state of rocks using the example of the Monchegorsk ore region // Exploration Geophysics. 1983. Issue. 96. Pp. 22-24.

Ignatieva T.S. Physical properties of rocks and ores of apatite deposits // Experience of using radioactive and other physico-chemical methods in the search and exploration of ores of non-radioactive elements. L .: Nedra, 1967. Pp. 112-123.

Petrophysics of crystalline rocks of the ore districts of the Kola Peninsula / Tyuremnov V. A., Galichanina L. D., Kazeblin P. L. and others. Ed. Pavlovsky V. I. L.: Nauka, 1982. 119 p.

Distribution and correlation of indicators of physical properties of rocks: Ref. guide / Protodyakonov M.M., Teder R.I., Ilnitskaya E.I. and others. Ed. Melnikov N.V. M .: Nedra, 1981. 190 p.

Seismic researches in the mines of the Khibiny massif / Pavlovsky V.I., Ivanov G.A., Rubinraut S.I., Berman B.I. Ed. Epinatyev A.M. Apatity: Kola Branch of the USSR Academy of Sciences, 1987. 82 p.

Tyuremnov V.A., Zubarev A.I. Geological and geophysical conditions of the underground part of the «Kukisvumchorr» geophysical observatory // Seismic and geodynamic researches in the north-east of the Baltic shield. Apatity: Kola Branch of the USSR Academy of Sciences, 1979. Pp. 92-96.

Shablinsky G.N., Kaverzneva N.A. On the application of geophysical methods to search for apatite ores // Exploration and protection of mineral resources. 1965. №9. Pp. 32-35.

NEW DATA ON THE CRYSTAL CHEMISTRY OF LAYERED TITANOSILICATES FROM THE ALKALINE MASSIFS OF THE KOLA PENINSULA

Zolotarev A.A.[1], Krivovichev S.V.[1,2], Zhitova E.S.[1,3], Selivanova E.A.[2], Lyalina L.M.[2], Panikorovskii T.L.[2], Yakovenchuk V.N.[2], Pakhomovsky Y.A.[2], Savchenko Ye.E.[2], Ivanyuk G.Yu.[2]

[1]Saint-Petersburg State University, Saint-Petersburg, Russia, a.zolotarev@spbu.ru

[2]Federal Research Center, Kola Science Center, RAS, Apatity, Russia

[3]Institute of Volcanology and Seismology FEB RAS , Petropavlovsk-Kamchatsky, Russia

Titanosilicates constitute an important group of minerals that have found many applications as materials. Of particular interest are layered titanosilicates of the seidozerite supergroup that currently contains more than forty-five mineral species (Sokolova and Cámara, 2017). These species are usually rare accessory minerals of alkaline rocks: carbonatites and nepheline syenites (and associated pegmatites) and occur mainly in alkaline massifs such as those occurring in Kola peninsula, Russia. The variety of mineral species in this family is associated with a wide range of variation of structural modules and different schemes of cation-anion substitution, which in turn is determined by the structural and chemical complexity of these minerals. Belov and Organova (1962) were the first who considered the crystal chemistry of several minerals of the current murmanite group of seidozerite supergroup (Sokolova and Cámara, 2017). Belov (1976) and Pyatenko et al. (1976) made further generalizations and called minerals with a "seidozerite block" (= TS block, (Sokolova, 2006)) and astrophyllite-group minerals titanosilicate analogues of micas. The modular approach to these minerals has been developed by Egorov-Tismenko and Sokolova (1987, 1990) who described a homologous series of Ti-analogues of micas and Ferraris (1997, 2008) who named those minerals heterophyllosilicates and described them as a polysomatic series. In contrast to having all TS-block minerals qualitatively under one series (homologous and/or polysomatic), Sokolova (2006) quantitatively divided TS-block minerals into four groups based on the content of Ti, topology and stereochemistry of the TS block.

Here we represent the new data of crystal chemical studies of several layered titanosilicates (heterophyllosilicates) including determination of structural changes under increasing temperature for some of them.

Crystal structure of shkatulkalite. Shkatulkalite, $Na_{10}MnTi_3Nb_3(Si_2O_7)_6(OH)_2F{\cdot}12H_2O$, was described by Menshikov et al. (1996) from the pegmatite "Shkatulka" of the Lovozero alkaline massif, Kola Peninsula, Russia. In their review on the seidozerite-supergroup minerals, Sokolova and Cámara (2017) pointed out that shkatulkalite is a potential member of the supergroup, but the final assignment of the mineral to a particular group remained unclear, due to the fact that its crystal structure was unknown until now. Menshikov et al. (1996) established that the mineral is monoclinic, a = 5.468(9), b = 7.18(1), c = 31.1(1) Å, β = 94.0(2)°, V = 1218(8) Å^3, Z = 1, and commented on the proximity of the a and b parameters of shkatulkalite to those typical for other known Ti and Nb sorosilicates. However, due to the poor quality of single-crystal X-ray diffraction data, the structure of the mineral could not be solved at the time. Németh et al. (2005) investigated syntactic intergrowths of epistolite, murmanite and shkatulkalite and reported on the absence of the $l = 2n + 1$ reflections for the latter mineral, pointing out that its c parameter is halved with respect to the value of 31.1 Å reported by Menshikov et al. (1996). Later shkatulkalite was described in nepheline syenites of the alkaline sill of St. Amable, Quebec, Canada (Horvath et al., 1998). Horvath et al. (1998) noted that the shkatulkalite is visually indistinguishable from vuonnemite and epistolite found in the same voids. At the same time, Menshikov et al. (1996) pointed out that shkatulkalite sometimes forms pseudomorphs after vuonnemite and thus can be considered as a transformation mineral species (Khomyakov, A. P. 1996; 2008), i.e. mineral species that forms as a result of a secondary transformation of a primary proto-phase. The crystal structure of shkatulkalite has been solved by us recently for firs time (Zolotarev et al., 2018). The mineral is monoclinic, $P2/m$, a = 5.4638(19), b = 7.161(3), c = 15.573(6) Å, β = 95.750(9)°, V = 606.3(4) Å^3, R_1 = 0.080. The crystal structure is based upon the *HOH* blocks consisting of one octahedral (*O*) sheet sandwiched between two heteropolyhedral (*H*) sheets. The *Na* and *Ti* sites are located within the *O* sheet. The *H* sheets are formed by *Nb* octahedra and Si_2O_7 groups

New mineral batievaite-(Y). Batievaite-(Y), $Y_2Ca_2Ti[Si_2O_7]_2(OH)_2(H_2O)_4$, is a new mineral found in nepheline syenite pegmatite in the Sakharjok alkaline massif, Western Keivy, Kola Peninsula, Russia (Lyalina et al., 2016). The crystal structure of batievaite-(Y) is similar to the structures of hainite and götzenite (Atencio et al. 1999; Bulakh and Kapustin 1973; Cannillo et al. 1972), which belong to the rosenbuschite group (Christiansen et al. 2003). The crystal structures of minerals of this group are based upon HOH blocks: the H-layer is a heteropolyhedral layer composed of *M1*On and *M3*On polyhedra (n=6–8) linked to Si_2O_7 groups. The O-layer is an octahedral layer containing the *M2*, *M4*, *M5* cation sites. Details on the distribution of cations over the *M1, M2, M3, M4, M5* sites in minerals of the rosenbuschite group were discussed by Christiansen et al. (2003). The structure of batievaite-(Y) differs from that of hainite in the composition of the O-layer. In batievaite-(Y), *M4* site is predominantly vacant, with only 39 % total occupancy by Na and H_2O molecules. The crystal structure of batievaite-(Y) contains two mixed anion positions: *X8* (OH, F) and *X9* (H_2O, F). It is noteworthy that the cation (*M2*, *M4*) and anion (*X9*) positions in the structure are partially occupied by H_2O molecules, which is possible because of the vacancies present in the O-layers. The presence of hydroxyl groups in the *X8* site and H_2O molecules in the *X9* site results in the overall shift of the Y^{3+} and Ca^{2+} cations away from these sites in order to satisfy their bond-valence requirements by formation bonds to other anions. As a consequence, the γ angle of batievaite-(Y) changes compared to that of hainite (from ca. 101° to 96.6°, respectively), whereas the *a* and *b* parameters are shrinking. The observed shrinkage is accompanied by considerable re-arrangement of the layer formed by the *M1* and *M3* polyhedra. The *M1* site in batievaite-(Y) is preferentially occupied by Y^{3+} and has a sevenfold coordination, which distinguishes it from the octahedral (sixfold) coordination of the *M1* site in hainite which is dominantly occupied by Ca. These changes are associated with a change in the coordination of the *M3* site, which, in hainite, has a coordination number 6 or 7 and is fully occupied by Ca. In the case of batievaite-(Y), the coordination number of the *M3* site is increased to 7 and 8. Therefore, the crystal structure of batievaite-(Y) can be considered as consisting of two basic blocks: Na-deficient O-layers, typical for such TS-block minerals as mosandrite (Bellezza et al. 2009; Sokolova and Hawthorne 2013) and layers of *M1–M3* polyhedra similar to the layers of Ca polyhedra in tobermorite (Merlino et al. 1999). The *M1–M3* polyhedral layer is surrounded by Si_2O_7 groups thus forming H layer. Thus, batievaite-(Y) can be considered as a Na-deficient Y-analogue of hainite $Na_2Ca_4(Y,REE)Ti[Si_2O_7]_2OF_3$, or a cation-deficient analogue of fogoite-(Y), $Na_3Ca_2Y_2Ti(Si_2O_7)_2OF_3$ - a new Y-rich mineral of the rosenbuschite group recently described by Cámara et al. (2017).

High-temperature behavior of layered titanosilicates. Recently we found that the astrophyllite, $K_2NaFe_7^{2+}Ti_2(Si_4O_{12})_2O_2(OH)_4F$, undergo iron oxidation deprotonation at T ~ 500 ºC and transform into high-temperature oxidized modifications stable at room conditions (Zhitova et al. 2017a). The crystal structures of the minerals of the astrophyllite supergroup are based upon HOH blocks, where the O-layer consists of edge-sharing octahedra occupied by Fe, Mg, Na and Mn (cation sites *M1-4*) and H-layers are heteropolyhedral layers constructed from $[Si_4O_{12}]^{8-}$ astrophyllite-type ribbons and *D*-centered octahedra (DO_6) or DO_5 pyramids, *D* = Ti, Nb and Zr. Adjacent HOH blocks are connected through interlayer alkali and alkaline-earth cations: K, Na, Ca, Sr and Ba (see: Sokolova et al. 2017b,

and references therein). High-temperature study of astrophyllite reveal the occurrence of a phase transformation due to the thermal iron oxidation coupled with deprotonation according to the scheme $Fe^{2+} + OH^- \rightarrow Fe^{3+} + O^{2-} + ½H_2 \uparrow$, and defluorination according to the scheme $Fe^{2+} + F^- \rightarrow Fe^{3+} + O^{2-}$. Thermal behavior of astrophyllite in the 25–475 °C temperature range can be described as a volume thermal expansion with maximal coefficient of thermal expansion in the direction perpendicular to the plane of the HOH layers. In contrast, the HT (high-temperature) phase experiences a strong contraction in the 600–775 °C temperature range, again in the direction perpendicular to the plane of the HOH layers.

Lobanovite, $K_2Na(Fe^{2+}_4Mg_2Na)Ti_2(Si_4O_{12})_2O_2(OH)_4$, is also a member of the astrophyllite supergroup (Sokolova et al., 2017a). Lobanovite is structurally and chemically related to astrophyllite but contains five-coordinated Ti in contrast to astrophyllite where Ti is six-coordinated. Our study revealed that lobanovite also undergoes temperature-induced irreversible iron oxidation and transformation into high-temperature phase associated with the contraction of unit-cell parameters similar to astrophyllite. The striking feature of lobanovite is that the octahedral layers before and after high temperature treatment have different cation site occupancies. The study revealed that, in lobanovite, iron oxidation-deprotonation process triggers cation rearrangement occurring mainly in the octahedral layers (*M1-4* sites) by exchange of the Fe^{3+} and Mg^{2+} cations between *M2* and *M3* and *M4* sites. We suppose that the cation migration is governed by the tendency of the structure to preserve the bond-valence sum associated with the apical oxygen atom of the TiO_5 square pyramid. The observed $Fe^{3+} \leftrightarrow Mg^{2+}$ exchange coupled with the oxidation and deprotonation reactions reinforces stability of the oxidized modification governed by local ordering mechanism.

As well as astrophyllite bafertisite $Ba_2Fe^{2+}_4Ti_2(Si_2O_7)_2O_2(OH)_2F_2$ experiences temperature-induced iron oxidation coupled with deprotonation registered at temperature above 450 ◦C (Zhitova et al. 2017b). However, in the case of bafertisite, the complete iron oxidation does not result in the formation of a stoichiometric (charge-balanced) high-temperature phase as it was observed for astrophyllite. The crystal structure of bafertisite contain complex layers consisting of octahedral sheets (O) formed by MO_6 octahedra (*M* = Fe, Mn, Zr, Na) and sandwiched between two heteropolyhedral sheets (H) formed by Si_2O_7 groups linked by TiO_6 octahedra. Unlike to astrophyllite in bafertisite the HOH blocks are separated by the layers of Ba atoms (Cámara et al., 2016), whereas, in astrophyllite, adjacent HOH blocks are connected via corner sharing of two Ti□6 (□ = F, OH, O) octahedra, i.e. formation of the Ti-□-Ti linkage along the direction of layer stacking. In addition, bafertisite and astrophyllite are different in the topology of the octahedral layers.

The oxidation of iron for all minerals is confirmed by: DTA/TG, Mössbauer spectroscopy, IR spectroscopy, electron microprobe analysis, reduction of the *M*–O interatomic distances, distortion indices of the MO_6 octahedra and $D\varphi_{5\text{-}6}$ polyhedra.

The study was supported by the Foundation of the President of the Russian Federation (grant Nsh-3079.2018.5). The X-ray diffraction studies were performed in the X-ray Diffraction Resource Centre of St. Petersburg State University. The chemical analytical studies were done in "Geomodel" Resource Centre of St. Petersburg State University and Geological Institute, Kola Science Centre, Russian Academy of Sciences.

References

Atencio D, Coutinho J.M.V, Ulbrich M.N.C., Vlach S.R.F., Rastsvetaeva R.K., Pushcharovsky D.Y. Hainite from Poços de Caldas, Minas Gerais, Brazil. Can. Mineral. 1999. 37. 91–98.

Bellezza M., Merlino S., Perchiazzi N. Mosandrite: structural and crystal-chemical relationships with rinkite. Can. Mineral. 2009. 47. 897–908.

Belov N.V. Essays on structural mineralogy. Nedra, Moscow, 1976. 344 p. (in Russian).

Belov N. V., Organova N. I. Crystal chemistry and mineralogy of the lomonosovite group in the light of the crystal structure of lomonosovite. Geokhimiya. 1962. 1. 4–13.

Bulakh A.G., Kapustin Y.L. Götzenite from alkaline rocks of Turii Peninsula (Kola Peninsula). Zap. Vsesoiuznogo Mineral. Obshch. 1973. 102. 464–466 (in Russian).

Bussen I. V., Denisov A. P., Zabavnikova N. I., Kozyreva L. V., Menshikov Y. P., Lipatova E.A. Vuonnemite, a new mineral. Zap. Vses. Mineral. Obshch. 1973. 102. 423-426 (in Russian).

Cámara F., Sokolova E., Abdu Y.A., Pautov L.A. From structure topology to chemical composition. XIX. Titanium silicates: Revision of the crystal structure and chemical formula of bafertisite $Ba_2Fe^{2+}{}_4Ti_2(Si_2O_7)_2O_2(OH)_2F_2$, A Group-II TS-block mineral. The Canadian Mineralogist. 2016. 54. 49-63.

Cámara F., Sokolova E., Abdu Y.A., Hawthorne F.C., Charrier T., Dorcet V., Carpentier J.F. Fogoite-(Y), $Na_3Ca_2Y_2Ti(Si_2O_7)_2OF_3$, a group I TS-block mineral from the Lagoa do Fogo, the Fogo volcano, São Miguel Island, the Azores: Description and crystal structure. Mineralogical Magazine. 2017. 81. 369-381.

Cannillo E., Mazzi F., Rossi G. Crystal structure of götzenite. Sov. Phys. Crystallogr. 1972. 16. 1026–1030.

Christiansen C.C., Johnsen O., Makovicky E. Crystal chemistry of the rosenbuschite group. Can. Mineral. 2003. 41. 1203–1224.

Egorov-Tismenko Yu. K.. Sokolova E. V. Comparative crystal chemistry of a group of titanium silicate analogues of mica. In: Comparative Crystal Chemistry, Moscow State University, Moscow, Russia, 1987. pp. 96-106 (in Russian).

Egorov-Tismenko Yu. K., Sokolova E. V. Homologous series seidozerite-nacaphite. Mineral. Zh. 1990. 12. 4. 40–49 (in Russian).

Ercit T. S., Cooper M. A., Hawthorne F. C. The crystal structure of vuonnemite, $Na_{11}Ti^{4+}Nb_2(Si_2O_7)_2(PO_4)_2O_3(F,OH)$, a phosphate-bearing sorosilicate of the lomonosovite group. Can. Mineral. 1998. 37. 1311-1320.

Ferraris G. Polysomatism as a tool for correlating properties and structure. In Modular Aspects of Minerals; Merlino, S., Ed.; Eötvös University Press, Budapest, Hungary. 1997. pp. 275-295.

Ferraris G. Modular structures - the paradigmatic case of heterophyllosilicates. Z. Kristallogr. 2008. 223. 76-84.

Horvath L., Pfenniger-Horvath E., Gault R. A., Tarasoff P. Mineralogy of the Saint-Amable Sill, Varennes and Saint- Amable, Quebec. Miner. Rec. 1998. 29. 83-118.

Khomyakov A. P. Transformation mineral species and their use in paleomineralogical reconstructions. 30th Int. Geol. Congr. Abstr.; Beijing, China. 1996. Vol. 2/3. p. 450.

Khomyakov A. P. The largest source of minerals with unique structure and properties. Minerals as Advanced Materials I. Krivovichev S.V. Ed. Springer. Germany. 2008. p. 71-77.

Khomyakov A. P., Yushkin N. P. The principle of inheritance in crystallogenesis. Dokl. Akad. Nauk SSSR 1981. 256. 1229-1233.

Lyalina L.M., Zolotarev A.A., Selivanova E.A., Savchenko Y.E., Krivovichev S.V., Mikhailova Y.A., Kadyrova G.I., Zozulya D.R. Batievaite-(Y), $Y_2Ca_2Ti[Si_2O_7]_2(OH)_2(H_2O)_4$, a new mineral from nepheline syenite pegmatite in the Sakharjok massif, Kola Peninsula, Russia. Mineralogy and Petrology. 2016. 110. 895-904.

Menshikov Y. P., Khomyakov A. P., Polezhaeva L. I., Rastsvetaeva R. K. Shkatulkalite – $Na_{10}MnTi_3Nb_3(Si_2O_7)_6(OH)_2F{\cdot}12H_2O$ a new mineral. Zap. Vseross. Mineral. Obshch. 1996. 125(1). 120-126 (in Russian).

Merlino S., Bonaccorsi E., Armbruster T. Tobermorites: their real structure and order–disorder (OD) character. Am. Mineral. 1999. 84.1613–1621.

Németh P., Ferraris G., Radnóczi G., Ageeva O. A. TEM and X-ray study of syntactic intergrowths of epistolite, murmanite and shkatulkalite. Can. Mineral. 2005. 43. 973-987.

Pyatenko Yu.A., Voronkov A.A. and Pudovkina Z.V. Mineralogical crystal chemistry of titanium. Nauka, Moscow 1976. 155p. (in Russian).

Sokolova E., Hawthorne F. C. The crystal chemistry of epistolite. Can. Mineral. 2004. 42. 797-806.

Sokolova E. From structure topology to chemical composition. I. Structural hierarchy and stereochemistry in titanium disilicate minerals. Can. Mineral. 2006. 44. 1273–1330.

Sokolova E., Hawthorne F.C. From structure topology to chemical composition. XIV. Titaniumsilicates: refinement of the crystal structureand revision of the chemical formula of

mosandrite, $(Ca_3REE)[(H_2O)_2Ca_{0.5}\square_{0.5}]Ti(Si_2O_7)_2(OH)_2(H_2O)_2$, a Group-I mineral from the Saga mine, Morje, Porsgrunn, Norway. Mineral Mag. 2013. 77. 6. 2753–2771.

Sokolova E., Cámara F. The seidozerite supergroup of TS-block minerals: nomenclature and classification, with change of the following names: rinkite to rinkite-(Ce), mosandrite to mosandrite-(Ce), hainite to hainite-(Y) and innelite-1T to innelite-1A. Mineral. Mag. 2017. 81. 1457-1484.

Sokolova E., Cámara F., Hawthorne F.C., Cirotti M. The astrophyllite supergroup: nomenclature and classification. Mineralogical Magazine. 2017a. 81. 143-150.

Sokolova E., Cámara F., Hawthorne F.C., Semenov E.I., Cirotti M. Lobanovite $K_2Na(Fe^{2+}{}_4Mg_2Na)Ti_2(Si_4O_{12})_2O_2(OH)_4$, a new mineral of astrophyllite supergroup and its relation to magnesioastrophyllite. Mineralogical Magazine. 2017b. 81. 175-182.

Zhitova E.S., Krivovichev S.V., Hawthorne F.C., Krzhizhanovskaya M.G., Zolotarev A.A., Abdu Ya.A., Yakovenchuk V.N., Pakhomovsky Ya.A., Goncharov A.G. High-temperature behavior of astrophyllite, $K_2NaFe_7^{2+}Ti_2(Si_4O_{12})_2O_2(OH)_4F$: a combined X-ray diffraction and Mössbauer spectroscopic study. Physics and Chemistry of Minerals. 2017a. 44. 595-613.

Zhitova E.S., Zolotarev A.A., Krivovichev S.V., Goncharov A.G., Gabdrakhmanova F.A., Vladykin N.V., Krzhizhanovskaya M.G., Shilovskikh V.V., Vlasenko N.S. and Zolotarev A.A. Temperature-induced iron oxidation in bafertisite $Ba_2Fe^{2+}{}_4Ti_2(Si_2O_7)_2O_2(OH)_2F_2$: X-ray diffraction and Mössbauer spectroscopy study. Hyperfine interactions. 2017b. 238. 96.

Zolotarev Jr. A.A., Selivanova E.A., Krivovichev S.V., Savchenko Y.E., Panikorovskii T.L., Lyalina L.M., Pautov L.A., Yakovenchuk V.N. Shkatulkalite, a rare mineral from the Lovozero massif, Kola Peninsula: A re-investigation. Minerals. 2018. 8. 303.

FORMATION OF ZEOLITE GROUP MINERALS IN SILICOCARBONATITE: CASE STUDY FROM BREIVIKBOTN, NORTHERN NORWAY

Zozulya D.R.[1], Kullerud K.[2,3], Ravna E.K.[2]

[1]Geological Institute, Kola Science Centre, Apatity, Russia
[2]Department of Geology, University of Tromsø, Tromsø, Norway
[3]Norwegian Mining Museum, Kongsberg, Norway

Alkaline rocks and carbonatites represent less than 1% of all igneous rocks of the Earth's crust. However, the petrogenesis of these rocks is particularly interesting, in part due to their great variability and in part because they are economically important, containing most of the global reserves of, for example, the rare earth elements (REE), zirconium, niobium and phosphorus (apatite). Experimental data (Wyllie, Tuttle, 1960), field observations (Elliot et al., 2018) and fluid inclusion studies (Andersen, 1986; Morogan, Lindblom, 1995) show that carbonatite melt contains the significant amounts of volatiles: H_2O (principal phase), CO_2, F, Cl, S. Fluid-saturated carbonatitic magma releases volatiles into separate fluid during late- and post-magmatic stages while pressure sharply decreases. The fluid reacts with country rocks, forming brecciation and vast fenitization halos, and causes the alteration of carbonatitic rocks itself. Among cations, carbonatitic fluid contains mainly Na and minor K, Ca, Fe in different proportions. Late-stage silicification is also observed in a number of carbonatite complexes (Heinrich, 1966). In this paper new mineralogical data on the Breivikbotn carbonatite occurrence are presented and possible late-, post-crystallization processes are proposed. The occurrence is remarkable for the high zeolite content, thereby suggesting a new mineral commodity from carbonatite complexes.

Breivikbotn alkaline-carbonatite complex consists of silicocarbonatite, melteigite and pyroxenite, with nepheline and aplitic syenites, interpreted as the products of fenitization. It occurs as a deformed, 2 km long and 500 m wide sill. The silicocarbonatite shows a rare mineral association. It is a massive rock of porphyritic texture with hypidiomorphic, lesser idiomorphic phenocrysts of garnet, pyroxene and sporadic biotite laths. The groundmass is medium and coarse grained and composed of carbonate, pyroxene, amphibole and zeolite. The mineral content is variable and consists of carbonate (20-50 vol. %), amphibole (5-20 vol. %), pyroxene (5-20 vol. %), zeolite group minerals (5-30 vol. %), garnet (0-30 vol. %). Minor and accessory minerals are apatite (1-3 vol. %), titanite (1-5 vol. %), allanite, magnetite, zircon, pyrite, pyrrhotite, chalcopyrite, scheelite, celestine, barite, and baddeleyite. Occasionally, accessory interstitial quartz is observed. Calcite, titanite and pyroxene (Di_{36-46} Acm_{22-37} Hd_{14-21}) are primarily magmatic minerals. Amphibole of hastingsitic composition has formed after pyroxene at a late-magmatic stage. Poikilitic garnet (Ti-bearing andradite) has inclusions of all primary minerals, amphibole and zeolites, and presumably crystallized metasomatically during a late metamorphic event (Caledonian orogeny).

Whole rock chemical compositions of the silicocarbonatite differs from the global average of calciocarbonatites by elevated silica, aluminium, sodium and iron, but show comparable contents of trace elements (REE, Sr, Ba). The spatial proximity of carbonatite and alkaline ultramafic rock (melteigite), the presence of silicate minerals in carbonatite together with the trace element distributions indicate that the carbonatite was derived from crystal fractionation of a parental carbonated foidite magma (Zozulya et al., 2018).

Clusters of zeolite group minerals (ZGM) have a stubby rectangular or equant rounded (roughly hexagonal) form, up to 2-3 mm in diameter (Fig. 1a). Most clusters are composed of natrolite and gonnardite; natrolite often occurs in the central parts of gonnardite aggregates, and it is inferred that natrolite is the earliest phase (Fig. 1b, c.).

Natrolite forms colorless, white, smooth anhedral grains of 1-2 mm size. The average chemical composition of natrolite is $Na_{1.98}Ca_{0.03}Si_{3.01}Al_{1.98}O_{10}\cdot 2H_2O$ (Table 4), which is very close to the stoichiometric formula $(Na_2(Si_3Al_2)O_{10}\cdot 2H_2O$, IMA-list 09-2017). The Si/(Si+Al) ratio varies from 0.57 to 0.65, while sodium is in the range 1.81-2.22 apfu and calcium does not exceed 0.1 apfu.

Gonnardite occurs as colorless, uneven, cracky aggregates up to 1-3 mm size, the individual grains are anhedral and 100-500 μm in diameter. The average composition of gonnardite is calculated

as $(Na_{1.57}Ca_{0.38})_{2.05}(Si_{2.67}Al_{2.38})_{5.05}O_{10}\cdot 3H_2O$, which is close the stoichiometric formula $((Na,Ca)_2(Si,Al)_5O_{10}\cdot 3H_2O$, IMA-list 09-2017). The Si/(Si+Al) ratio varies from 0.52 to 0.54, while Na/(Na+Ca) from 0.76 to 0.85.

Thomsonite-(Ca) forms colorless and white rectangular grains. It is irregularly zoned, and in BSE images characterized by brighter and darker zones (Fig. 1d). The mineral appears as partly fibrous. The average composition is $Na_{1.13}Ca_{1.7}(Al_{4.98}Si_{5.1})O_{20}\cdot 6H_2O$, which is close to ideal formula $(NaCa_2(Al_5Si_5)O_{20}\cdot 6H_2O$, IMA-list 09-2017). The mineral is characterized by elevated Sr content (0.02 – 0.34 apfu, with average 0.09 apfu). The Sr content may vary within a single crystal as indicated by the brighter and darker zones in BSE images (Fig. 1d). The Si/(Si+Al) ratio varies from 0.49 to 0.52, while Na/(Na+Ca+Sr) varies from 0.34 to 0.42.

Overall, the ZGM of Breivikbotn carbonatite shows successively increasing Ca, Si and Al content from natrolite, via gonnardite to thomsonite-(Ca).

In some natrolite-gonnardite clusters, water-absent Na-Al silicates with chemical compositions close to nepheline were found (Zozulya et al., 2018). These compositions in combination with the textural appearance of the natrolite-gonnardite aggregates suggest that the aggregates are pseudomorphs after nepheline. Thomsonite-(Ca) can also be inferred as an alteration product of nepheline. The water-absent nepheline-like mineral is characterized by compositions corresponding to $Na_{0.53\text{-}0.7}Ca_{0.01\text{-}0.16}Al_{1.07\text{-}1.24}Si_{1.06\text{-}1.22}O_4$, which is somewhat different from the stoichiometric formula of nepheline, with lower Na and higher Ca. We suggest that the mineral initially crystallized as nepheline from a carbonatite magma, and subsequently underwent alteration in a high-Ca environment. Nepheline is an unusual and rare mineral in classic carbonatite complexes world-wide. Nevertheless nepheline-bearing carbonatites have been reported from a number of carbonatite localities; e.g. Laacher See, Germany and Alnø, Sweden (Heinrich, 1966)), Fen (Andersen, 1988) in Norway, Chilwa Island and Kangankunde, Malawi (Garson, 1966), Budeda Hill and Homa Bay, Uganda (King, 1966), Dicker Willem, Namibia (Cooper, Reid, 1998), and in Ilmeny–Vishnevogorsky, Urals, Russia (Nedosekova et al., 2013). In addition, other carbonatites contain natrolite, analcime or cancrinite, formed by breakdown of nepheline; e.g. Oka, Canada (Treiman, Essene, 1985); Legetet Hills, Kenya, Nachendezwaya, Tanzania, Tororo and Bukusu, Uganda (all summarized by Heinrich (1966)). On the basis of this distribution, and the petrographic and mineralogical evidence for the above described localities, it is possible to infer that nepheline-bearing carbonatites are often associated with the "nephelenitic-clan" rather than with the "melilititic-clan" carbonatites (using the terminology of Mitchell (2005).

Because of the alkalic and volatile-rich character, the silicocarbonatite resulted in the significant fenitization that can be observed at the Breivikbotn outcrops (see above). Moreover, the presence of late-magmatic amphibole and biotite suggests that the silicocarbonatite magma contained sufficient water to produce voluminous hydrothermal fluids during late stages of crystallization. Such deuteric fluids would be able to alter the primary mineral assemblage producing the abundant water-bearing phases that can be observed. The metasomatic alteration can be considered to be the result of autometasomatism, or subsolidus process, in which early magmatic phases reacted with their own residual fluids to form a suite of low-temperature minerals such as natrolite, gonnardite, and thomsonite. Experimental studies, quantitative estimates and field observations indicate that natrolite-type and thomsonite-type zeolites formed in the temperature range of 100-200 °C (Gottardi, 1989).

Petrographic studies have shown that ZGM could be the products of nepheline alteration. Several reactions for nepheline alteration at successive enrichment of H_2O, CaO Al_2O_3 and SiO_2 in hydrothermal fluid might be possible:

$$2NaAlSiO_4(Ne) + SiO_2(aq) + 2H_2O(aq) = Na_2(Si_3Al_2)O_{10}\cdot 2H_2O\ (Ntr)$$

$$NaAlSiO_4(Ne) + SiO_2(aq) + CaO(aq) + Al_2O_3(aq) + 3H_2O(aq) = (Na,Ca)_2(Si,Al)_5O_{10}\cdot 3H_2O\ (Gonn)$$

$$NaAlSiO_4(Ne) + 4SiO_2(aq) + 2CaO(aq) + 2Al_2O_3(aq) + 6H_2O(aq) = NaCa_2(Al_5Si_5)O_{20}\cdot 6H_2O\ (Toms)$$

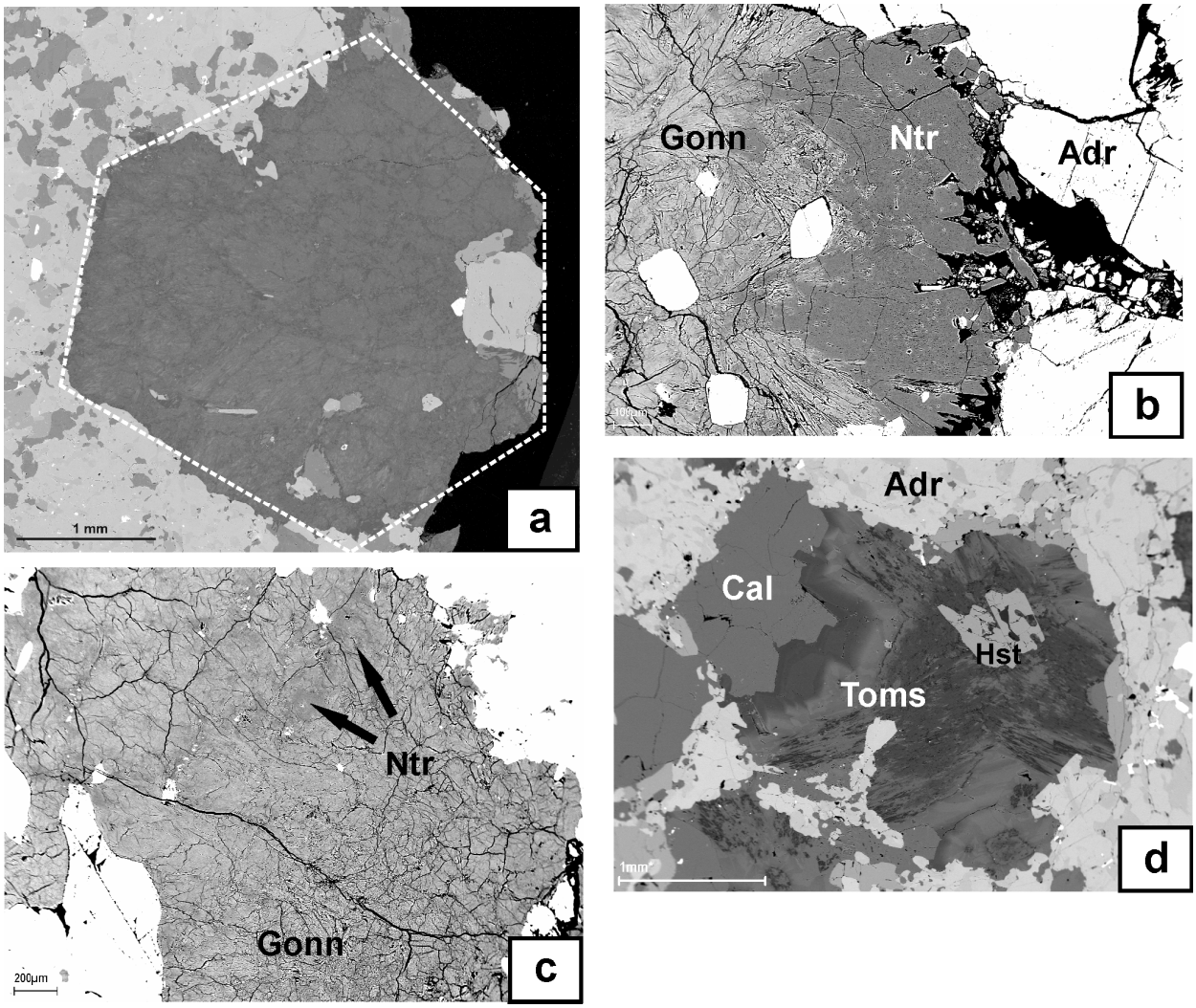

Fig. 1. BSE images showing the morphology and internal textures of zeolite group minerals: (a) roughly hexagonal habit of zeolite aggregate; (b) intergrowths and aggregates of natrolite and gonnardite; (c) "shadow"-type domains of natrolite (dark-gray) in gonnardite (light-gray), illustrating the early crystallization of natrolite relative to gonnardite (XRPD of the sample indicated a mix of both minerals); (d) zonal structure of thomsonite-(Ca) with low (dark gray) and high (gray) Sr content. Ntr – natrolite, Toms – thomsonite-(Ca), Gonn – gonnardite, Adr – andradite, Cal – calcite, Hst - hastingsite.

Textural evidence for replacements of natrolite by gonnardite is supported by the successive enrichment of the fluid phase by H_2O, CaO, Al_2O_3 and SiO_2 according to following reaction:

$$Na_2(Si_3Al_2)O_{10}\cdot 2H_2O\ (Ntr) + 2SiO_2(aq) + 2CaO(aq) + 2Al_2O_3(aq) + 4H_2O(aq) = 2(Na,Ca)_2(Si,Al)_5O_{10}\cdot 3H_2O\ (Gonn)$$

The alteration of nepheline to zeolite group minerals progressed through several steps: (1) "altered nepheline", (2) natrolite, (3) gonnardite , and (4) Sr-rich thomsonite-(Ca). The main prerequisites for zeolite formation in the carbonatite complex were (1) silicocarbonatite composition of the parent magma and crystallization of nepheline, (2) fractional crystallization of primary magmas leading to fluid enrichment of residual melts/hydrothermal solutions, (3) extensive fluid alteration of the rock at late- and post-magmatic stages.

Although, most economically important zeolite deposits are confined to volcanic (glasses, tuffs) beds and have the mineral content of 50-80 vol. % (Marantos et al., 2011), the zeolites from carbonatite complexes can be regarded as promising by-products to their traditional mineral commodities.

This work was supported by Russian Ministry of Education and Science, grant № 0226-2019-0053.

References

Andersen T. Magmatic fluids in the Fen carbonatite complex, S.E. Norway. Evidence of mid-crustal fractionation from solid and fluid inclusions in apatite // Contributions to Mineralogy and Petrology. 1986. Vol. 93. p. 491-503.

Andersen T. Evolution of peralkaline calcite carbonatite magma in the Fen complex, southeast Norway // Lithos. 1988. Vol. 22. p. 99-112.

Cooper A.F., Reid D.L. Nepheline sovites as parental magmas in carbonatite complexes: Evidence from Dicker Willem, southwest Namibia // Journal of Petrology. 1998. Vol. 39. p. 2123-2136.

Elliott H.A.L., Wall F., Chakhmouradian A.R., Siegfried P.R., Dahlgren S., Weatherly S., Finch A.A., Marks M.A.W., Dowman E., Deady E. Fenites associated with carbonatite complexes: A review // Ore Geology Reviews. 2018. Vol. 93. p. 38-59.

Garson M.S. Carbonatites in Malawi // In Carbonatites, Edited by O.F. Tuttle and J. Gittins. Interscience, New York, 1966, pp. 33–71.

Gottardi G. The genesis of zeolites // European Journal of Mineralogy. 1989. Vol. 1. p. 479-487.

Heinrich E.W. The Geology of Carbonatites // Rand McNally, Chicago, 1966; p. 555.

King B.C., Sutherland D.S. The carbonatite complexes of Eastern Uganda // In Carbonatites, Edited by O.F. Tuttle and J. Gittins. Interscience, New York, 1966, pp. 73–126.

Marantos I., Christidis G.E., Ulmanu M. Zeolite formation and deposits // In Natural Zeolites Handbook. Bentham Science Publishers Ltd, 2011, pp. 19-36.

Mitchell R.H. Carbonatites and carbonatites and carbonatites // Canadian Mineralogist 2005. Vol. 43. p. 2049-2068.

Morogan V., Lindblom S. Volatiles associated with the alkaline-carbonatite magmatism at Alno, Sweden: a study of fluid and solid inclusions in minerals the Lingarsholmen ring complex // Contributions to Mineralogy and Petrology. 1995. Vol. 122. p. 262-274.

Nedosekova I.L., Belousova E.A., Sharygin V.V., Belyatsky B.V., Bayanova T.B. Origin and evolution of the Ilmeny-Vishnevogorsky carbonatites (Urals, Russia): Insights from trace-element compositions, and Rb-Sr, Sm-Nd, U-Pb, Lu-Hf isotope data // Mineralogy and Petrology. 2013. Vol. 107. p. 101-123.

Treiman A.H., Essene E.J. The Oka carbonatite complex, Quebec - geology and evidence for silicate-carbonate liquid immiscibility // American Mineralogist. 1985. Vol. 70. p. 1101-1113.

Wyllie P.J., Tuttle O.F. The system CaO-CO_2-H_2O and the origin of carbonatites // Journal of Petrology. 1960. Vol. 1. p. 1-96.

Zozulya D., Kullerud K., Ravna E.K., Savchenko Ye.E., Selivanova E.A., Timofeeva M.G. Mineralogical and geochemical constraints on magma evolution and late-stage crystallization history of the Breivikbotn silicocarbonatite, Seiland igneous province in Northern Norway: prerequisites for zeolite deposits in carbonatite complexes // Minerals. 2018. Vol. 8(11). p. 537.

NATURAL EVIDENCE FOR ECLOGITE-CARBONATITE-DIAMOND CONNECTION IN UHP ENVIRONMENT FROM TØNSVIKA OCCURRENCE, NORTHERN NORWAY

Zozulya D.[1], Ravna E.K.[2], Janak M.[3], Kullerud K.[2,4]

[1]Geological Institute, Kola Science Centre, 184209 Apatity, Russia
[2]Department of Geology, University of Tromsø, N-9037 Tromsø, Norway
[3]Earth Science Institute, Slovak Academy of Sciences, Bratislava, Slovak Republic
[4]Norwegian Mining Museum, N-3616 Kongsberg, Norway

The genesis of carbonatite melts by partial melting of mantle rocks (peridotites and eclogites) is one of the most common assumptions of the origin of carbonatites. There is a number of experimental studies and numerical models confirming this process of carbonatite origin (Dasgupta et al., 2004; Yaxley, Brey, 2004; Kiseeva et al., 2012; etc.). Carbonatization and metasomatism of sublithospheric mantle are also considered as important mechanisms of formation of diamondiferous kimberlites and lamproites; single occurrences of diamondiferous carbonatites are also known. Finally, there are numerous finds of diamondiferous eclogites both within orogenic belts and in the form of mantle xenoliths from explosion pipes and dikes of ultrabasic rocks. The above observations suggest a genetic link between eclogites, carbonatites and diamondiferous rocks. The Tønsvika occurrence in Northern Norway (Tromsø area) is the only known natural object (laboratory), where all components of the system "eclogite-carbonatite-diamond" are identified and it is possible to study the deep segment of the global carbon cycle in field.

The Tønsvika carbonatite occurs in the Scandinavian Caledonides and represents a series of veins and dikes in the host complex of eclogites (including carbonated and metasomatized eclogites), garnet clinopyroxenites and glimmerites, as well as garnet-phengite gneisses and marbles (Ravna et al., 2017). Diamonds were found in garnet-kyanite-phengite gneisses (Janak et al., 2013). The carbonatite has a massive texture and shows the following mineral content: Mg-Fe-calcite (50-90 %) ± Fe-dolomite + almandine-grossular-pyrope garnet + Cr-diopside ± omphacite + phlogopite; secondary and accessory minerals: apatite, rutile, ilmenite, allanite, titanite, zircon, monazite. Veins (up to 10 cm thickness) of almost monomineralic carbonate rocks are less common. In all cases silicacarbonatite and carbonatite have sharp intrusive contacts with the host rocks, and there is an intense fenitization along the contacts by late K-bearing fluids with the formation of phlogopite.

U-Pb ages of zircon and titanite from the carbonatite fall into time span of 452-455 Ma (Ravna et al., 2017) and coincide within the error with the age of the host eclogites (452.1 ± 1.7 Ma). Chondrite-normalized patterns of incompatible elements and REE are similar to those of typical carbonatites and the carbonatite shows significantly higher concentrations of REE than the associated marbles (Ravna et al., 2017).

The contents and ratios of some rare elements are very informative for determining the tectonic setting of carbonatite complexes. The dominant majority of the World's carbonatites is formed in withinplate environment, in particular in continental rifts. These carbonatites are characterized by high concentrations of LIL (especially Sr and Ba) and HFS elements (mean values for Zr, Nb, Hf and Ta are 256.4, 308.9, 4.3 and 8.9 ppm, respectively (Chakhmouradian, 2006)). Carbonatites formed in subduction and collision environments have high contents of LIL and much lower contents of HFS elements. The following data are provided for the Eden Lake complex (Chakhmouradian et al., 2008): 47-98 ppm for Zr, 4.0 for Nb, 1.5–2.4 for Hf, and 0.2 for Ta. For the Tønsvika carbonatite, we obtained the following HFSE concentrations (Zr varies from 26 to 460 ppm (mean 114 ppm); Nb: 1-31 ppm (18 ppm); Hf: 0-7.7 ppm (2.5 ppm); Ta: 0.5–2.0 ppm (1.2 ppm)). Because the contents of HFS elements in carbonatites have significant variations, the "canonical" ratios Zr/Nb, Zr/Hf, Nb/Ta were used to establish the initial characteristics. Average carbonatite (withinplate) has the following average values Zr/Nb = 0.8, Zr/Hf = 60, Nb/Ta = 35 (Chakhmouradian, 2006). For the Tønsvika carbonatite these values (Zr/Nb = 18, Zr/Hf = 42 and Nb/Ta = 18) are significantly different, but are similar to those for subduction and collision related carbonatites (Eden Lake, Canada (Chakhmouradian et al., 2008); Italy (Stoppa, Wooley, 1997; D'orazio et al., 2007); North China (Xu et al., 2010); Antarctica (Hagen-Peter, Cottle, 2016); NE China (Ying et al., 2004); SW China (Hou et al., 2006); Tien Shan,

Uzbekistan (Lapin et al., 2002)). Analysis of the distribution of these ratios can have petrogenetic significance. The Tønsvika carbonatite has Zr/Nb- and Nb/Ta-ratios, close to primitive mantle ratios. Together with low HFSE, this indicates that the mantle source in our case was not metasomatized before melting, which is typical for intraplate carbonatites. Thus, we can assume that the carbonatite melt of Tønsvika formed by direct partial melting of either mantle lherzolites ("magnesium" carbonate melts) or eclogites ("calcium" carbonate melts). The mineral composition of the Tønsvika carbonatite (see above) points toward an "eclogite" substrate.

Sr–Nd isotopic studies of the Tønsvika rocks showed the following results: silicocarbonatite has $^{87}Sr/^{86}Sr$ ratios of 0.705–0.708 for □Nd= -1 to -2 for, similar to the marbles; the carbonatite has similar initial Sr isotope ratios, but more negative values of □Nd (-3.3); the eclogite has the most radiogenic Sr ratios (0.708–0.710) and unradiogenic Nd ratios (-2.4 to -3.3); carbonated and metasomatized eclogites have initial strontium ratios similar to the carbonatites, but diametrically different □Nd (non-radiogenic and radiogenic values, respectively). The similar initial strontium ratios for the carbonatite and for the carbonated and metasomatized eclogite indicate that they are genetically linked. Comparison of the initial isotopic ratios of Sr and Nd of the Tønsvika carbonatites with carbonatites from different tectonic environments shows that the studied carbonatite is similar to the carbonatites from collision and subduction settings (Figure).

Calculations of P-T parameters showed that carbonatites were formed at a pressure of 3.2–3.6 GPa and a temperature of 970-1100 °C (Ravna et al., 2017). The data of experiments on melting of anhydrous carbonated eclogite (Dasgupta et al., 2004; Yaxley, Brey, 2004; Kiseeva et al., 2012) show that the carbonatite solidus can vary over a significant temperature and pressure range (1000 – 1300°C; 4 – 5 GPa). All these parameters exceed the values of the" hot " subducted slab. However, a significant decrease in the melting point of the eclogite to form a carbonatite melt can be achieved by adding Na_2O, H_2O and F to the system, as shown by experimental data (Yaxley, Brey, 2004; Kiseeva et al., 2012; Jago, Gittins, 1991).

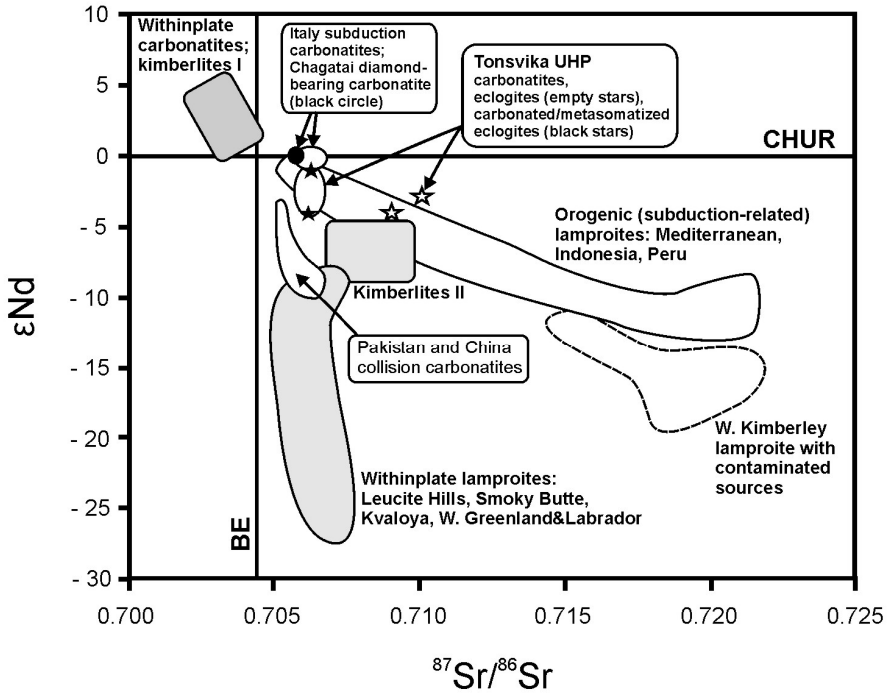

Figure. Diagram $^{87}Sr/^{86}Sr$ *vs* □Nd for the Tønsvika carbonatites and eclogites in comparison with published data for withinplate carbonatites, kimberlites 1 and 2, withinplate and orogenic lamproites, and carbonatites in subduction and collisional settings (Italy (D ' Orazio et al., 2007; Rosatelli et al., 2007), Pakistan (Tilton et al., 1998), China (Himalayas) (Hou et al., 2006), diamond-bearing carbonatites of Chagatai (Tien Shan) (Lapin et al., 2002; Moore et al., 2009)).

Since the Tønsvika carbonatite contains significant amounts of phlogopite and fluorapatite, it can be assumed that the presence of F, P_2O_5, K_2O and H_2O could play a significant role in lowering the solidus of the source rocks (carbonated eclogite) to temperatures characteristic for subducted slabs. Another important source of water may be the reaction of CH_4-bearing fluids from deep mantle horizons with oxygen from the subducted slab:

$$CH_4 + O_2 \rightarrow 2H_2O + C,$$

as suggested by Foley (2011). This reaction can be used to explain the origin of diamonds at the Tønsvika locality. Diamond-bearing kyanite-phengite gneisses were formed under conditions of 3.2-3.6 GPa at temperatures of 750-800°C (Janak et al., 2013). Along with the possible obvious decrease in temperature in the system, the presence of reduced carbon is necessary for the formation of diamond. In addition to the external (deep) source of carbon, carbonates of the deposit itself can be another important source of carbon. Experimental and field studies (Tao et al., 2018) revealed that the formation of graphite and light hydrocarbons in carbonated eclogites can be through the reduction of carbonate due to the low fugacity of oxygen (~FMQ - 2.5 log). In this case, the main condition for the redox reaction is the presence of Fe component in the carbonate, and in general the reaction can be represented as:

$$3FeCO_3 + H_2O \rightarrow Fe_3O_4 + 3CO_2 + H_2.$$

It should be noted that the Tønsvika carbonates show corresponding to Mg-Fe-calcite and Fe-dolomite, and magnetite is a common accessory mineral. The relationship of other Fe-Ti oxides, rutile and ilmenite, may also indicate a relative decrease in the oxygen fugacity in the late stages of the carbonatite melt crystallization. A characteristic feature of Fe-Ti oxides in the Tønsvika carbonatite is a later crystallization of ilmenite relative to rutile, ase ilmenite forms reaction rims on rutile. This reaction takes place with the absorption of oxygen:

$$2Fe+2TiO_2+ O_2 \rightarrow 2FeTiO_3.$$

Moreover, the formation of ilmenite on rutile can occur with the decomposition of water and the release of hydrogen into the system:

$$Fe+TiO_2+H_2O \rightarrow FeTiO_3+H_2.$$

Thus, during the late stages of crystallization of the carbonatite in Tønsvika there was a change to reducing conditions, which together with favorable P-T conditions led to crystallization of diamond.

Similar isotopic ratios of Nd and Sr in eclogites, carbonatites and lamproites (including diamondiferous ones) from subduction environments (see Figure) also indicate their paragenetic relationship and integrated role in the deep carbon cycle. Whether carbonate or water is the main metasomatic agent could be the controlling factor during formation of “carbonatite-diamond” and “lamproite-diamond” systems.

This work was supported by Russian Ministry of Education and Science, grant № 0226-2019-0053.

References

Chakhmouradian A.R. High-field-strength elements in carbonatitic rocks: Geochemistry, crystal chemistry and significance for constraining the sources of carbonatites // Chemical Geology. 2006. Vol. 235(12). p. 138-160.

Chakhmouradian A.R., Mumin A.H., Demény A., Elliott B. Postorogenic carbonatites at Eden Lake, Trans-Hudson Orogen (northern Manitoba, Canada): Geological setting, mineralogy and geochemistry // Lithos. Vol. 2008. 103(3-4). p. 503-526.

Dasgupta R., Hirschmann M.M., Withers A.C. Deep global cycling of carbon constrained by the solidus of anhydrous carbonated eclogite under upper mantle conditions // Earth and Planetary Science Letters. 2004. Vol. 227. p. 73-85.

D’Orazio M., Innocenti F., Tonarini S., Doglioni C. Carbonatites in a subduction system: The Pleistocene alvikites from Mt. Vulture (southern Italy) // Lithos. 2007. Vol. 98. p. 313-334.

Foley S. A reappraisal of redox melting in the Earth’s mantle as a function of tectonic setting and time // Journal of Petrology. 2011. Vol. 52. p. 1363-1391.

Hagen-Peter G., Cottle J.M. Synchronous alkaline and subalkaline magmatism during the late Neoproterozoic–early Paleozoic Ross orogeny, Antarctica: Insights into magmatic sources and processes within a continental arc // Lithos. 2016. Vol. 262. p. 677-698.

Hou Z., Tian S., Yuan Z., Xie Y., Yin S., Yi L., Fei H., Yang Z. The Himalayan collision zone carbonatites in western Sichuan, SW China: Petrogenesis, mantle source and tectonic implication // Earth and planetary Science Letters. 2006. Vol. 244. p. 234-250.

Jago B.C., Gittins J. The role of fluorine in carbonatite magma evolution // Nature. 1991. 349. p. 56-58.

Janák M., Ravna E.J.K., Kullerud K., Yoshida K., Milovsky R., Hirajima T. Discovery of diamond in the Tromsø Nappe, Scandinavian Caledonides (N. Norway) // Journal of Metamorphic Geology. 2013. Vol. 31. p. 691-703.

Kiseeva E.S., Yaxley G.M., Hermann J., Litasov K.D., Rosenthal A., Kamenetsky V.S. An experimental study of carbonated eclogite at 3.5-5.5 GPa – Implications for silicate and carbonate metasomatism in the cratonic mantle // Journal of Petrology. 2012. Vol. 53. p. 727-759.

Lapin A.V., Divaev F.K., Kostityn Yu.A. Petrochemical interpretation of carbonatite-like rocks from the Chagatai Complex of the Tien Shan with application to the problem of diamond potential // Petrology. 2005. Vol. 13(5). p. 499–511.

Moore K.R., Wall F., Divaev F.K., Savatenkov V.M. Mingling of carbonate and silicate magmas under turbulent flow conditions: Evidence from rock textures and mineral chemistry in sub-volcanic carbonatite dykes, Chagatai, Uzbekistan // Lithos. 2009. Vol. 110. p. 65–82.

Ravna E.K., Zozulya D., Kullerud K., Corfu F., Nabelek P.I., Janak M., Slagstad T., Davidsen B., Selbekk R.S., Schertl H.-P. Deep-seated carbonatite intrusion and metasomatism in the UHP Tromsø nappe, Northern Scandinavian Caledonides – A natural example of generation of carbonatite from carbonated eclogite. Journal of Petrology, 2017. Vol. 58(12). p. 2403–2428.

Rosatelli G., Wall F., Stoppa F. Calcio-carbonatite melts and metasomatism in the mantle beneath Mt. Vulture (Southern Italy) // Lithos. 2007. Vol. 99. p. 229-248.

Stoppa F., Woolley A.R. The Italian carbonatites: Field occurrence, petrology and regional significance // Mineralogy and Petrology. 1997. Vol. 59. p. 43-67.

Tao R., Zhang L., Tian M., Zhu J., Liu X., Liu J., Höfer H.E., Stagno V., Fei Y. Formation of abiotic hydrocarbon from reduction of carbonate in subduction zones: Constraints from petrological observation and experimental simulation // Geochimica et Cosmochimica Acta. 2018. Vol. 239. p. 390-408.

Tilton G.R., Bryge J.G., Mateen A. Pb-Sr-Nd isotope data from 30 and 300 Ma collision zone carbonatites in Northwest Pakistan // Journal of Petrology. 1998. Vol. 39. p. 1865-1874.

Xu C., Kynicky J., Chakhmouradian A.R., Qi L., Song W. A unique Mo deposit associated with carbonatites in the Qinling orogenic belt, central China // Lithos. 2010. Vol. 118. p. 50-60.

Yaxley G.M., Brey G.P. Phase relations of carbonate-bearing eclogite assemblages from 2.5 to 5.5 GPa: implications for petrogenesis of carbonatites // Contributions to Mineralogy and Petrology. 2004. Vol. 146. p. 606-619.

Ying J., Zhou X., Zhang H. Geochemical and isotopic investigation of the Laiwu-Zibo carbonatites from western Shandong Province, China, and implications for their petrogenesis and enriched mantle source // Lithos. 2004. Vol. 75. p. 413-426.

CRYSTAL CHEMISTRY OF Ag-EXCHANGED FORMS OF ELPIDITE

Zubkova N.V.[1], Nikolova R.P.[2], Chukanov N.V.[3], Kostov V.V.[2], Pekov I.V.[1], Varlamov D.A.[3,4]

[1]Moscow State University, Moscow, Russia, n.v.zubkova@gmail.com

[2]Institute of Mineralogy and Crystallography, Bulgarian Academy of Sciences, Sofia, 1113, Bulgaria, vkytin@abv.bg

[3]Institute of Problems of Chemical Physics, Russian Academy of Sciences, 142432 Chernogolovka, Moscow region, Russia, chukanov@icp.ac.ru

[4]Institute of Experimental Mineralogy, Russian Academy of Sciences, 142432 Chernogolovka, Moscow region, Russia, dima@iem.ac.ru

Zeolite-like microporous zirconosilicates with heteropolyhedral frameworks (i.e. frameworks formed by SiO_4 tetrahedra and ZrO_6 octahedra) characterized by the general formula $[Zr_mSi_nO_{3m+2n}]^{-2m}$ attract much attention due to their wide application in chemical technologies as ionites, high-selectivity sorbents, catalysts, ion conductors, etc. Many of these compounds have natural analogues and some of them are able to form deposits which are of a special interest as the resources of zeolite-like material of such type. Elpidite, ideally $Na_2ZrSi_6O_{15}\cdot 3H_2O$, is one of the brightest examples of such minerals. This mineral is characterized by ion-exchanged properties which occur in both laboratory conditions (Turchkova et al., 2006; Grigor'eva et al., 2011) and in nature (Salvi, Williams-Jones, 2001). The crystal structure of elpidite is based on a heteropolyhedral framework consisting of double Si_6O_{15} chains (ribbons) and isolated ZrO_6 octahedra. Zeolite cavities are occupied by Na+ cations (usually with minor Ca^{2+} and K^+ admixtures) and H2O molecules (Cannillo et al., 1973). Previously we reported the crystal structures of the product of elpidite dehydration in laboratory conditions, $Na_2ZrSi_6O_{15}$, (Zubkova et al., 2011), Rb-exchanged forms of elpidite $Na_{1.58}Rb_{0.20}H_{0.22}Zr[Si_6O_{15}]\cdot 2.69H_2O$ and $Rb_{1.78}Na_{0.06}H_{0.16}Zr[Si_6O_{15}]\cdot 0.90H_2O$ (obtained at 90 and 150°C, respectively) and K-exchanged forms $K_{1.78}Na_{0.16}H_{0.06}Zr[Si_6O_{15}]\cdot 0.85H_2O$ and $K_{1.84}Na_{0.11}H_{0.05}Zr[Si_6O_{15}]\cdot 0.91H_2O$ (obtained at 90 and 150°C, respectively) (Grigor'eva et al., 2011). For the dehydration product of elpidite and its K-exchanged form obtained at 90 and 150°C and Rb-exchanged forms obtained at 150°C, doubling of the unit cell in comparison with the initial elpidite and space group *Cmce* were revealed. Here we report chemical and structural data for Ag-exchanged elpidite samples from a low-temperature hydrothermal association at Mount Alluaiv in the Lovozero alkaline massif (Kola Peninsula, Russia) (I) and from an alkaline granite pegmatite in the Khan Bogdo massif (Mongolia) (II) and crystal chemistry of the Ag-exchanged samples.

Hydrothermal exchange reactions for I and II were carried out in Teflon-lined steel autoclaves that had about 10-ml capacity. In a typical synthesis 0.05g of elpidite crystals were mixed with 5 ml 1M $AgNO_3$ solution placed in the autoclave and heated for 3 days at 90°C. The products were carefully washed free from entrained salts and dried at 60°C before further investigations. The averaged chemical data for I resulted in the empirical formula $Ag_{1.8}Na_{0.30}Zr_{1.10}Si_6O_{15}\cdot nH_2O$, and electron microprobe analyses of II revealed two zones with the composition $Ag_{2.05}Ca_{0.03}Na_{0.03}Zr_{1.02}Si_{5.94}O_{15}\cdot nH_2O$ and $Ag_{1.25}Ca_{0.375}Na_{0.05}Zr_{1.00}Si_{5.99}O_{15}\cdot nH_2O$.

Both samples were studied using single-crystal XRD technique. The unit cell parameters (Table 1) are close to those obtained for the dehydration product of elpidite and its K- (90 and 150°C) and Rb-exchanged (150°C) forms. The structures were solved and refined in the frames of the space group *Cmce* to final R_{hkl} values 0.0483 for 1200 unique reflections with $I>2\sigma(I)$ for I and 0.0517 for 1707 unique reflections with $I>2\sigma(I)$ for II.

Both structures (Figure) retain the heteropolyhedral framework of elpidite consisting of double chains of SiO_4 tetrahedra, which are linked by isolated ZrO_6 octahedra. At the same time evident distortions of the heteropolyhedral framework (ZrO_6 octahedra in the heteropolyhedral framework are significantly twisted relative to each other) and the arrangement of extra-framework cations revealed in the studied samples result in the doubling of the *a* parameter of the unit cell. In both Ag-exchanged samples extra-framework cations show a high degree of disorder: there are eight Ag sites in I and five

Ag sites in II; all of them are characterized by partial occupancy. There are two main extra-framework sites in both structures which have similar coordinates and are characterized by the site occupancy factors (s.o.f.) of 0.78 (Ag1) and o.78 (Ag2) (I) and 0.49 (Ag1) and 0.74 (Ag2) (II) [in both cases Ag scattering curve was used]. In the sample I both sites are further split occupying sub-sites close to the main ones with very low s.o.f. In the sample II only the Ag(1) site is characterized by further splitting. The position of Ag(1) site in I and II is not similar but close to the most highly occupied Rb site in the Rb-exchanged form (150°C) and to the most highly occupied K site in both K-exchanged forms of elpidite (90 and 150°C). In K- and Rb-exchanged forms of elpidite this site is closer to H_2O molecule position in the initial elpidite but not to Na(2) whereas in both Ag-exchanged samples this Ag(1) site is something intermediate between H_2O molecule position and the Na(2) site in initial elpidite. Moreover, the Ag(1) site in both structures corresponds to one of the Na sites [Na(1)] in the product of elpidite dehydration in which this site is additionally split and also corresponds to the intermediate position between H_2O molecule site and the Na(2) site in initial elpidite. The Ag(2) site in I and II corresponds to the Na(1) site in initial elpidite. It is important to note that this site retains only small amounts of Na in the structures of K- and Rb-exchanged forms of elpidite but is not occupied by the exchanged K or Rb cations. It was supposed that the zeolitic cavity that includes this Na(1) site at the center of an eight-fold polyhedron does not have enough space to accommodate cations larger in size than Na (Grigor'eva et al., 2011). In the case of Ag^+ this site could host exchanged silver cations.

Table 1. Some crystallographic data for elpidite and its laboratory-modified forms.

	Sp.gr., Z	*a* (Å)	*b* (Å)	*c* (Å)	*V* (Å^3)	Ref.
Elpidite	*Pbcm* 4	7.14(2)	14.68(1)	14.65(1)	1535.5	Cannillo et al., 1973
Dehydr.	*Cmca* 8	14.0899(1)	14.4983(1)	14.3490(1)	2931.23(4)	Zubkova et al., 2011
K-exch. (90°C)	*Cmca* 8	14.054(3)	14.308(3)	14.553(3)	2926.4(11)	Grigor'eva et al., 2011
K-exch. (150°C)	*Cmca* 8	14.037(3)	14.266(3)	14.552(3)	2914.1(11)	Grigor'eva et al., 2011
Rb-exch. (90°C)	*Pbcm* 4	7.1280(10)	14.644(3)	14.642(3)	1528.4(5)	Grigor'eva et al., 2011
Rb-exch. (150°C)	*Cmca* 8	14.2999(12)	14.4408(15)	14.7690(12)	3049.8(5)	Grigor'eva et al., 2011
Ag-exch. I	*Cmca* 8	14.1755(7)	14.6306(9)	14.2896(7)	2963.6(3)	This work
Ag-exch. II	*Cmca* 8	14.1411(5)	14.5948(4)	14.3035(5)	2952.04(17)	This work

Thus, elpidite from both Lovozero and Khan Bogdo demonstrates high exchange capacity to Ag^+. The cation exchange is accompanied by the significant distortion of the heteropolyhedral framework that results in the doubling of the *a* parameter of the unit cell and the change in symmetry from space group *Pbcm* (characteristic to the initial elpidite) to *Cmce*. Similar structural transformations were found earlier for the product of thermal dehydration of elpidite and for its K- and Rb-exchanged forms. At the same time, the mechanism of exchange of Na^+ for Ag^+ in elpidite apparently differs from that in the case of K^+ and Rb^+ exchange where large exchanged cations incorporate to the site formerly occupied by H_2O molecule in the most voluminous zeolitic cavity rather than the proper site of the Na^+ cation. Thus the filling by exchanged K and Rb cations preferentially H_2O molecules sites explains the drastic decrease in the water content in K- and Rb-exchanged forms of elpidite. Unlike, exchanged Ag^+ cations preferably occupy the sites that are closer to the Na sites in the initial elpidite and correspond to the Na sites in the product of elpidite dehydration. This results in the higher in comparison with K- and Rb-exchanged forms of elpidite water content in the Ag-exchanged forms: 2.42 H_2O p.f.u. for I and 2.24 H_2O p.f.u. for II (possible water "admixture" at Ag sites was not taken into account).

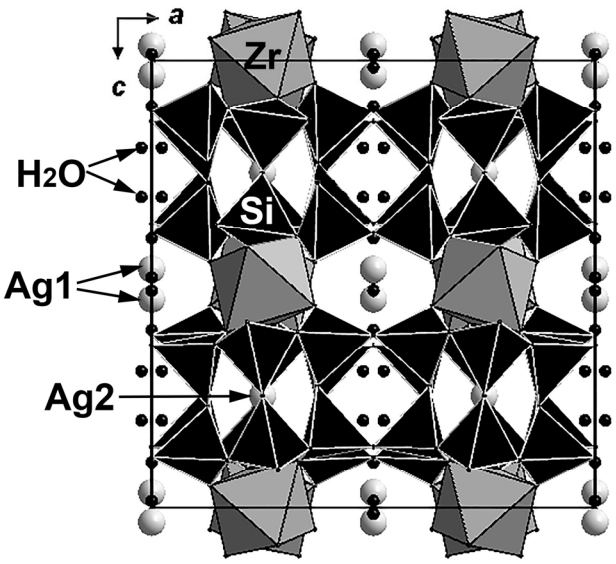

Figure. The crystal structure of Ag-exchanged elpidite. Only the main Ag sites are shown. The unit cell is outlined.

Infrared spectrum of I contains six distinct bands of O–H stretching vibrations (at 3605, 3551, 3507, 3453, 3360 and 3262 cm^{-1}) and three bands of H–O–H bending vibrations (at 1650, 1637 and 1610 cm^{-1}), which indicates the presence of three nonequivalent water molecules in this sample. Bands of H_2O in the IR spectrum of II are broad and consist of numerous overlapping components which reflects chemical inhomogeneity of this sample.

This work was supported by Russian Foundation for Basic Research, grant 18-55-18003 and by the National Science Fund of Bulgaria under contract No. DNTS/Russia 02/8 from 15.06.2018.

References

Cannillo E., Rossi G., Ungaretti L. The crystal structure of elpidite // American Mineralogist. 1973. Vol. 58. p.106–109.

Grigor'eva A.A., Zubkova N.V., Pekov I.V., Kolitsch U., Pushcharovsky D.Yu., Vigasina M.F., Giester G., Đorđevic T., Tillmanns E., Chukanov N.V. Crystal chemistry of elpidite from Khan Bogdo (Mongolia) and its K- and Rb-exchanged forms // Crystallography Reports. 2011. Vol. 56(5). p. 832–841.

Salvi S., Williams-Jones A.E. Zirconosilicate phase relations in the Strange Lake (Lac Brisson) Pluton, Quebec-Labrador, Canada // American Mineralogist. 2001. Vol. 13. p. 355-363.

Turchkova A.G., Pekov I.V., Bryzgalov, I.A. Cation-exchange properties of natural zeolite-like sodium zirconosilicates: an experimental study in aqueous solutions at 80–90°C and 1 atm. 19th General Meet. of IMA, Kobe, 2006, p. 280.

Zubkova N.V., Ksenofontov D.A., Kabalov Yu.K., Chukanov N.V., Nedel'ko V.V. Dehydration-induced structural transformations of the microporous zirconosilicate elpidite // Inorganic Materials. 2011. Vol. 47(5). p. 506–512.

DIAMONDS AND THEIR MINERAL INCLUSIONS FROM THE TOLBACHIK VOLCANO, KAMCHATKA

Kaminsky F.V.[1], Wirth R.[2], Schreiber A.[2], Shilobreeva S.N.[1], Sevastyanov V.S.[1], Saraykin V.V.[1], Karpov G.A.[3], Anikin L.P.[3], Galimov E.M.[1]

[1]Vernadsky Institute of Geochemistry and Analytical Chemistry, Russian Academy of Sciences, Moscow, Russia, kaminsky@geokhi.ru

[2]Helmholtz Centre Potsdam, Potsdam, Germany

[3]Institute of Volcanology and Seismology, Russian Academy of Sciences, Petropavlovsk–Kamchatskii, Russia

Approximately 700 diamond crystals were identified in volcanic (mainly pyroclastic) rocks of the Tolbachik volcano, Kamchatka, Russia. They were studied with the use of SIMS, scanning and transmission electron microscopy and utilization of electron energy loss spectrometry and electron diffraction. Diamonds have cube-octahedral shape and extremely homogeneous internal structure.

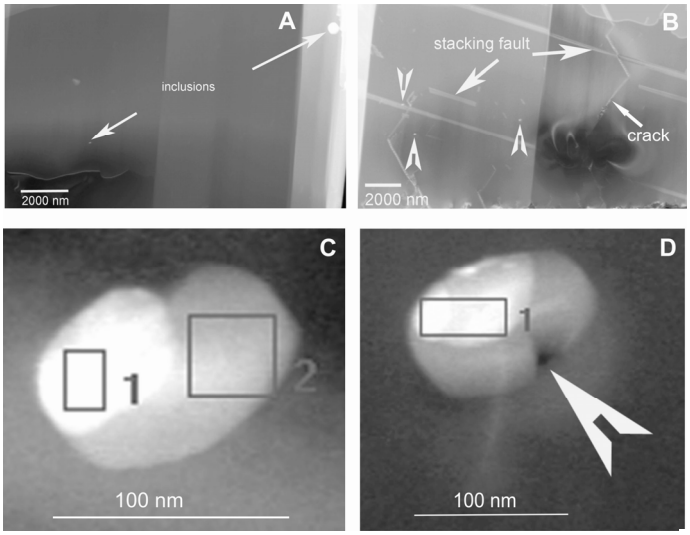

Most elements have concentrations 3-4 orders of magnitude less than chondritic values. Besides N and H, only Si, F, and Cl are relatively elevated, that is caused by their concentrations in micro- and nanoinclusions. Two groups of impurity elements are distinguished by a character of their distribution within the diamond. First group, N and H, the most common structural impurities in diamond, are distributed homogeneously. All other elements (Cl, F, O, S, Si, Al, Ca, and K) form local concentrations, implying the existence of inclusions, causing high concentrations of these elements.

Mineral inclusions in the studied diamonds are 70-450 nm in size, round- or oval-shaped grains. They are represented by two mineral groups: Mn-Ni alloys and silicides, with wide variations of concentrations for each group. Alloys vary in stoichiometry from MnNi to Mn_2Ni, with a minor admixture of Si from 0 to 5.20-5.60 at.%. Silicides, usually coexisting with alloys, vary in composition from $(Mn,Ni)_4Si$ to $(Mn,Ni)_5Si_2$ and Mn_5Si_2, and further to MnSi, forming pure Mn-silicides. Mineral inclusion grains have nano-sized pores that contain a fluid or a gas phase (F and O).

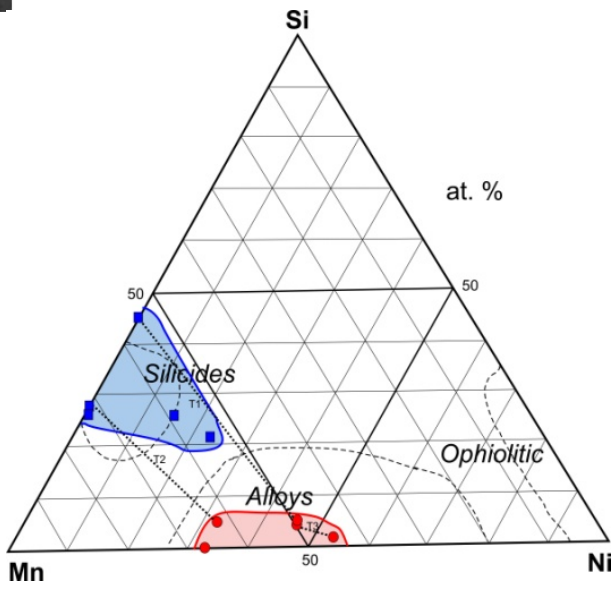

Geological, geochemical and mineralogical data confirm the natural origin of studied Tolbachik diamonds possibly as a result of the cavitation synthesis or chemical vapor deposition (CVD) mechanism at the explosive stage of the eruption.

NEOARCHEAN ALKALINE GRANITE HISTORY AS AN EXAMPLE OF TITANITE U-PB SIMS SHRIMP DATING

Lepekhina E.N.[1], Rodionov N.V.[1], Belyatsky B.V.[1], Antonov A.V.[1], Arzamastsev A.A.[2,3], Sergeev S.A.[1,3]

[1]Karpinsky Geological Institute, CIR, Saint-Petersburg, Russia, nickolay_rodionov@vsegei.ru
[2]Institute for Precambrian Geology & Geochronology, RAS, Saint-Petersburg, Russia, arz1998@yahoo.com
[3]Saint-Petersburg State University, Institute of Earth Sciences, Saint-Petersburg, Russia

The Baltic Shield is one of the world's largest provinces of alkaline granites, which are outcropped on the area ca 2500 km^2 and are confined to the Keivy segment of the Kola fold system. The alkaline granites are represented by 6 large massifs and numerous veins of amazonite pegmatites associating with minor massifs of alkaline and nepheline syenites. The geology, petrology, geochemistry and geochronology of alkaline granitoids, have been studied for the last 50 years in detail (Batieva, 1978; Mitrofanov et al., 2000; Bayanova, 2004; Vetrin, 2018). According to the modern concept, neoarchean anorogenic granitoid magmatism within the Keivy structure includes three series of mantle-source rocks of different origin, but close in time of formation: subalkaline gabbro-labradorite-latite-monzonite-granites, plagiomicrocline granites and alkaline aegerine-arfvedsonite granites, linked to the Late Archaean mantle plume (Vetrin, Rodionov, 2009; Vetrin, 2018).

However, geological history of alkaline granite magmatism remains unsolved. In particular, the alkaline granites postdate subalkaline latite-monzonite rocks, which were separated in time from alkaline granites by intrusion of plagiomicrocline granites (Vetrin, Rodionov, 2009), whereas the U-Pb zircon age estimations indicate either the inverse accordance or the coincidence for the spatial alignment of genetically different series. For example, the U-Pb zircon age of the aegerine-arfvedsonite granite of the Ponoy massif is of 2751±40 Ma, ID-TIMS (Bayanova, 2004), confirmed by the Sm-Nd isochron, while the SIMS SHRIMP-II U-Pb zircon data vary from 2666 to 1802 Ma. However, similar rocks of the White Tundry massif U-Pb zircon SIMS SHRIMP-II age is of 2671±11 Ma (Vetrin et al., 1999; Vetrin, Rodionov, 2009). Taking into account some mobility of the zircon U-Pb system during crystallization in fluid-saturated alkaline granitoid melts, we tried to estimate the age of crystallization using the titanite U-Pb system which was successful in dating of the similar rocks (Frost et al., 2000; Piccoli et al., 2000; McLeod et al., 2011; Kohn, 2017; Rodionov et al., 2018).

We have studied 10 titanite samples from three alkaline granitoids massifs from the Keivy structure – Western Keivy, Ponoy and White Tundry, collected by I.D. Batieva during field works in 1956-1967. Titanites are represented by light-colored yellow-brown irregular-shaped fragments of crystals ca 400-500 microns and more. Microinclusions of zircon, apatite, rutile, ilmenite, allanite and rock-forming minerals are normal. Sometimes it has clear oscillatory or sectorial growth zoning, mainly due to variations of light REE and Y. Some tracks of grain partial recrystallization on crystal faces are noted.

The U/Pb ratios in titanite were measured using microprobe SHRIMP-II at the CIR VSEGEI (St.-Petersburg) employing OLT1 titanite grains of 1015 My old as a reference material (Kennedy et al., 2010). Details of the analytical technique are similar to (Rodionov et al., 2018). All studied titanites were characterized by variations of the uranium content within 10-100 ppm range, whereas the Th/U ratio varied from 0,1 to 13, and the proportion of non-radiogenic Pb ranged from 0.1 to 70%. Nevertheless, after correction on non-radiogenic Pb, based on the measured ^{204}Pb, all calculated U-Pb ages turned out to be concordant within the error limits. The calculated ages and characteristics of the U-Pb isotope system of studied titanites from alkaline granites are presented in the Table 1 and Figure below.

Obviously, the resulting dispersion of ages reflects the poly-stage formation of titanite on the massifs studied. The closing temperature of the titanite U-Pb system (Kohn, 2017) is comparable to the crystallization temperature of granite melts (600-800 °C), which allow U-Pb age of titanite to fit with the primary crystallization of alkaline granite massifs at 2710 Ma, (Ponoy and Western Keivy massifs).

.Table 1. U-Pb isotope systematics of studied titanite from Keivy alkaline granites

№	sample	rock type, massive	titanite characteristics	U-Pb SIMS SHRIMP data, Ma (analyses)
1	1086/57	amazonite pegmatite, Lentjavr Lake (*1753±13 Ma* published data)*	40-60% $Pb_{comm,}$ [U]: 10-30, Th/U: 1.2-2.7	**1852±30** (n=19)
2	35/63A	alkaline granite, conact zone, White Tundry massif (*2674±10**)	20-50% Pb_{comm} [U]: 10-20, Th/U: 4.5-7.4	**2485±48** (n=21) **2636±110** zircon inclusion in titanite **2460 Ma**
3	79/56	alkaline granite, Ponoy massif (*2666±10**)	0.3-1.0/1-13 %Pb_{comm} [U]: 60-100/15-130, Th/U: 6-13/0.02-0.1	**2710.7±7.2** (n=20) **1750±11** (n=18) zircon inclusion in titanite **2470 Ma**
4	1/57	alkaline granite, Western Keivy massif (*2674±6**)	1-1.9% Pb_{comm} [U]: 40-80, Th/U: 5-7.3	**2794.6±9.0** (n=15) **2709±12** (n=5)
5	148/69	subalkaline granite, augite-lepidomelane granodiorite, Koutyng massif	0.2-4.0% Pb_{comm} [U]: 20-260, Th/U: 0.4-2.6	**2650.5±7.0** (n=21)
6	1110/57	aenigmatite alkaline granite, Kulijock massif	50-70% Pb_{comm} [U]: 20-40, Th/U: 1.4-2.2	$T^{206/238}$=**1739±39** T_{conc}=**1720±25** (n=15)
7	143/69	subalkaline granite, Yokanga massif, lepidomelane-ferrohastingsite granite (*2800±30*, 2653±8**)	0.6-9.4% Pb_{comm} [U]: 20-150, Th/U: 0.3-1.8	**2674.4±7.4** (n=24) zircon inclusion in titanite **2628 Ma**
8	2/57	alkaline granite, aenigmatite-aegirine-arfvedsonite granite, Western Keivy massif	50-80% Pb_{comm} [U]: 20-40, Th/U: 1.3-1.9	**1769±28** (n=17) zircon inclusion in titanite **1760 Ma**
9	281	amazonite granite, Western Keivy massif, Tapperuaive Mountain	60-70% Pb_{comm} [U]: 15-45, Th/U: 1.2-2.7	**1825±18** (n=22)
10	282	alkaline granite, Western Keivy massif, Tapperuaive Mountain	60-70% Pb_{comm} [U]: 10-40, Th/U: 1.2-1.8	**1820±19** (n=20)

The formation of lepidomelane-ferrohastingsite granites of satellite relatively small bodies (Yokanga and Koutyng massifs) occurred at 2650-2670 Ma, whereas the pegmatite veins of amazonite granites, completed the magmatic stage of the granite succession, formed at 1850-1820 Ma. The ultimate titanite, both in the Ponoy and Western Keivy massifs, was formed at about 1750 Ma, which reflects the influence of the tectonic-metamorphic Paleoproterozoic event widespread on the Kola Peninsula. All ages obtained using the U-Pb titanite system are well-known for Keivy alkaline granites and are in agreement with previous U-Pb zircon ages (Bayanova, 2004; Vetrin et al., 1999), as well as with our SIMS age of zircon inclusions found in titanite (Table). It should be noted that the U-Pb systematics of titanite from the White Tundry massif differs sharply from the other studied samples. This may be explaned by the hybride origin of granites when melt is intruded into the host gneisses (Batieva, 1976). In this case U-Pb system of titanite becomes unstable, and the ages vary from 2485 to 2630 Ma for individual titanite grains.

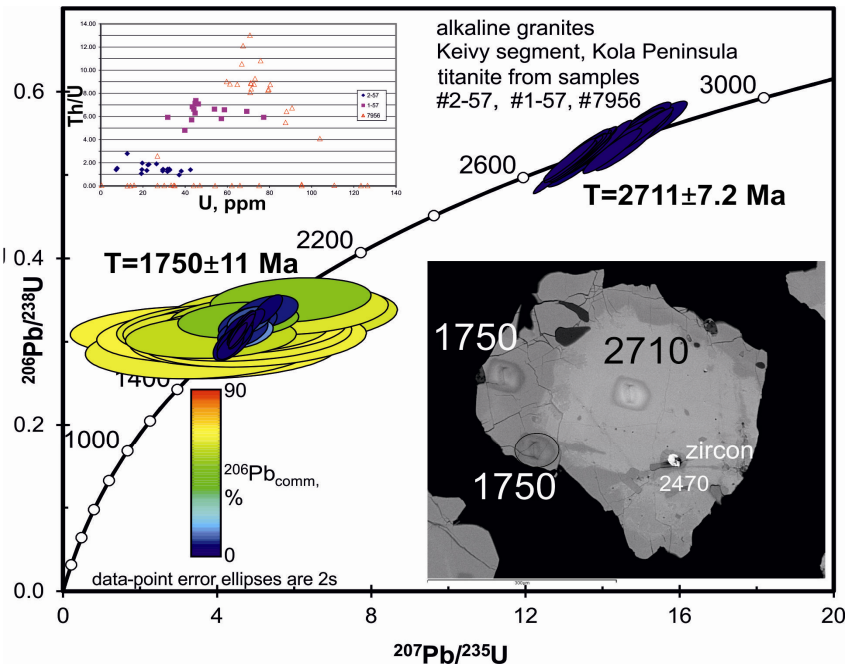

Figure. U-Pb concordia diagram for titanites from alkaline granite of Keivy, Kola peninsula, with BSE image of complex titanite grain with zircon inclusion.

This work was done as a part of CIR works under the project of «Thematic and methodic works within 2018-2020 aimed in development of laboratory and analytical methods» supported by the State Geological Survey subsidy.

References

Aleinikoff J.N., Wintsch R.P., Fanning C.M., Dorais M.J. U-Pb geochronology of zircon and polygenetic titanite from the Glastonbury Complex, Connecticut, USA: an integrated SEM, EMPA, TIMS, and SHRIMP study // Chemical Geology. 2002. Vol. 188. p. 125-147.

Batieva I.D. Petrology of alkaline granitoids of the Kola Peninsula // Nauka, Leningrad, 1976, 224 p. (in Russian)

Bayanova T.B. Age of the reference geological complexes of the Kola region and duration of magmatic processes // Nauka, S.-Petersburg, 2004, 174 p. (in Russian)

Frost B.R., Chamberlain K.R., Schumacher J.C. Sphene (titanite): phase relations and role as a geochronometer // Chemical Geology. 2000. Vol. 172. p. 131-148.

Kennedy A.K., Kamo S.L., Nasdala L., Timms N.E. Grenville skarn titanite: potential reference material for SIMS U-Th-Pb analysis // The Canadian Mineralogist. 2010. Vol. 48. p. 1423-1443.

Kohn M.J. Titanite petrochronology // Reviews in Mineralogy & Geochemistry. 2017. Vol. 83. p. 419-441.

McLeod G.W., Dempster T.J., Faithfull J.W. Deciphering magma-mixing Processes using zoned titanite from the Ross of Mull granite, Scotland // Journal of Petrology. 2011. Vol. 51(1). p. 55-82.

Mitrofanov F.P., Zozulya D.R., Bayanova T.B., Levkovich N.V. The world's oldest anorogenic alkaline granitic magmatism in the Keivy structure of the Baltic Schield // Doklady of Earthy Sciences. 2000. Vol. 374. p. 1145-1148.

Piccoli P., Candela P., Rivers M. Interpreting magmatic processes from accessory phases: titanite - a small-scale recorder of large-scale processes // Transactions of the Royal Society of Edinburgh: Earth Sciences. 2000. Vol. 91. p. 257-267.

Rodionov N.V., Lepekhina E.N., Antonov A.V., Kapitonov I.N., Balashova Yu.S., Belyatsky B.V., Arzamastsev A.A., Sergeev S.A. U-Pb SHRIMP-II ages of titanite and timing constrains of apatite-nepheline mineralization in Khibiny and Lovozero alkaline massifs (Kola Peninsula) // Russian Geology and Geophysics. 2018. Vol. 59. p. 962-974.

Stearns M.A., Cottle J.M., Hacker B.R., Kylander-Clark A.R.C. Extracting thermal histories from the near-rim zoning in titanite using coupled U-Pb and trace-element depth profiles by single-shot laser-ablation split stream (SS-LASS) ICP-MS // Chemical Geology. 2016. Vol. 422. p. 13-24.

Vetrin V.R., Kamenskii I.L., Baynova T.B., Timmerman M., Belyatsky B.V., Levsky L.K., Balashov Yu.A. Melanocratic nodules in alkaline granites of the Ponoiskii Massif, Kola Peninsula: a clue to petrogenesis // Geochemistry International. 1999. Vol. 37. p. 1061-1072.

Vetrin V.R., Rodionov N.V. Geology and geochronology of Neoarchean anorogenic magmatism of the Keivy structure, Kola Peninsula // Petrology. 2009. Vol. 17 (6). p. 537-557.

Vetrin V.R. Isotope-geochemical systematics (Sm-Nd, Lu-Hf) of Neoarchean subalkaline and alkaline rocks of the Keivy structure (Kola Peninsula): their age and genetic relations // Zapiski RMO. 2018. Pt. CXLVII. N4. p. 1-13 (in Russian).

“Magmatism of the Earth and related strategic metal deposits”

Proceedings of International Conference

Saint Petersburg State University, 23-23 May 2019.

Компьютерная вёрстка: В.Н. Ермолаева
Оформление обложки: В.А. Зайцев

Отпечатано в типографии ООО "Супервэйв Групп".
193149, Ленинградская область, Всеволожский район, п. Красная Заря 15,
телефон: (812) 325-99-96, факс: (812) 315-04-62
www.superwave.ru
Тираж 120 экз.